Novel Monomer and Polymer Syntheses Involving Elemental Sulfur and Sulfur-Containing Functional Groups

Zur Erlangung des akademischen Grades eines

DOKTORS DER NATURWISSENSCHAFTEN

(Dr. rer. nat.)

von der KIT-Fakultät für Chemie und Biowissenschaften

des Karlsruher Instituts für Technologie (KIT)

genehmigte

DISSERTATION

von

M.Sc. Peter Conen

aus Trier

1. Referent: Prof. Dr. Michael A. R. Meier

2. Referent: Prof. Dr. Joachim Podlech

Tag der mündlichen Prüfung: 11.12.2025

Für meine Eltern,

Anja und Ralf Conen

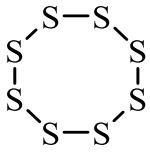

One ring to rule them all.

Declaration of Authorship

Die vorliegende Arbeit wurde von Januar 2023 bis November 2025 unter Anleitung von Prof. Dr. Michael A. R. Meier am Institut für Organische Chemie (IOC) des Karlsruher Instituts für Technologie (KIT) angefertigt.

Erklärung

Hiermit versichere ich, dass ich die Arbeit selbstständig angefertigt, nur die angegebenen Quellen und Hilfsmittel benutzt und mich keiner unzulässigen Hilfe Dritter bedient habe. Insbesondere habe ich wörtlich oder sinngemäß aus anderen Werken übernommene Inhalte als solche kenntlich gemacht. Die Satzung des Karlsruher Instituts für Technologie (KIT) zur Sicherung guter wissenschaftlicher Praxis habe ich beachtet. Des Weiteren erkläre ich, dass ich mich derzeit in keinem laufenden Promotionsverfahren befinde und auch keine vorausgegangenen Promotionsversuche unternommen habe. Die elektronische Version der Arbeit stimmt mit der schriftlichen Version überein und die Primärdaten sind gemäß Abs. A (6) der Regeln zur Sicherung guter wissenschaftlicher Praxis beim Institut abgegeben und archiviert.

Karlsruhe, den 19.01.2026

_____

Peter Conen

Danksagung

Viele Personen haben mich auf dem Weg zu meiner Promotion begleitet, unterstützt und inspiriert, und damit erheblich zum Erfolg dieser Arbeit beigetragen. All jenen Personen möchte ich an dieser Stelle meinen Dank aussprechen.

Zuallererst gilt mein Dank dir, Mike, für die Aufnahme in die Gruppe, nicht nur zur Promotion, sondern auch schon davor zu allen anderen Abschlussarbeiten sowie zahlreichen Hiwis. Ich bin sehr dankbar für das Vertrauen, das du mir in all der Zeit entgegengebracht hast, sowie für deine stets offene Tür sowohl für fachliche, als auch für überfachliche Gespräche. Besonders die zahlreichen morgendlichen Kaffeerunden im Büro werden mir in warmer Erinnerung bleiben, und stehen für mich symbolisch für die tolle Atmosphäre, die du in der Gruppe geschaffen hast.

Weiterhin danke ich dem „Karlsruhe House of Young Scientists“ (KHYS) für die finanzielle Unterstützung meiner Promotion im Rahmen der „Landesgraduiertenförderung“.

Selbstverständlich danke ich auch allen aktuellen und ehemaligen Mitgliedern des Arbeitskreises, die die guten Tage noch besser und die schlechten Tage erträglicher gemacht haben, sowohl innerhalb als auch außerhalb des Labors.

Besonders hervorzuheben sind hier meine langjährigen Laborkollegen und guten Freunde Luis und Timo. Danke euch beiden für die stets produktiven fachlichen Diskussionen, die zahlreichen Business-Lunches und Feierabend-Arzneien, die gemeinsame Beschallung des IOCs mit allen erdenklichen Arten von „Musik“, und alles was wir sonst so gemeinsam erlebt haben. Ich hätte mir keine besseren Laborpartner als euch beide vorstellen können.

Ein weiterer Dank gilt der vorherigen IOC-Generation, Maxi, Roman und Michi. Ich bin überaus dankbar, euch während meines Studiums über den Weg gelaufen zu sein. Nicht nur die Zeit, die ich mit euch im Labor als Hiwi/Bachelor/OCF/nochmal Hiwi verbracht habe, sondern auch darüber hinaus im Campingstuhl, auf dem Rennrad und bei „The Crew“-Abenden weiß ich sehr zu schätzen. Ihr drei habt mich in vielerlei Hinsicht fachlich und persönlich geprägt, und ich bin froh euch als Freunde gewonnen zu haben.

Der Rest des Arbeitskreises darf natürlich nicht unerwähnt bleiben. Henni ist ein anständiger Junge, ich kenne ihn jahrelang. Danke dir für all die gemeinsamen Erlebnisse schon während des Studiums, und die Fahrten zum SC. Clara, danke besonders für dein stets offenes Ohr, für die Betreuungsentlastung beim Reviewschreiben, sowie für deine gnadenlosen Korrekturen. Sandra, danke dir für den Krawallkaffee am Morgen, die gemeinsamen Pack Openings und die vielen tollen Memes. Leon, danke für die hervorragende Führung des Tiny Stores, sowie das gemeinsame Radeln und Duellieren. Qianyu, danke für deinen herrlich trockenen Humor und

die gute Zeit in Groningen. Celeste, thank you for all the good times we shared. Bohni, danke dir für deine Hilfsbereitschaft und die tolle Zeit in den USA. Luca Narducci, thank you for your positive attitude even in difficult times and for enriching my vocabulary with words such as "munnezz". Simon, ich bin froh das Labor mit gutem Gewissen in deine Hände übergeben zu können. Danke besonders für die vielen Chemdles und für Banger wie „Tübingen warum bist du so hügelig". Luca Holzhauer, du bist ein würdiger Nachfolger für meinen Laborplatz. Danke dir für Kaffee im einen Büro am Morgen und schwere Arbeit im anderen Büro am Abend. Danke darüber hinaus an Francesca, Nichollas, Federico, Anja und Jonas.

Ein weiterer Dank gilt meinen fleißigen Laborhelfern, allen voran meinen beiden Azubis Sophia und Silas. Eure Unterstützung im Labor war für mich unbezahlbar, und es ist schwer vorstellbar was ich ohne euch alleine zustande gebracht hätte. Ganz besonders danke ich auch meinem Hiwi/Bachelor Flo. Ich bin sehr stolz auf deine Leistungen, und danke dir für deine häufigen spontanen Besuche im Lab, für unseren gemeinsamen Lieblingsvogel, den spontanen Poolabend in Brettne sowie für die (Dauer)leihgabe deiner JBL Extreme. Ramon, auf deine Entwicklung bin ich ebenso stolz. Deine einmalige Arbeitsweise und nüchterner Humor waren sowohl während deines Vertiefers als auch deiner Masterarbeit stets eine Bereicherung, und ich wünsche dir, nie wieder an Thioessigsäure riechen zu müssen. Max, dir möchte ich hiermit auch für die gute Zusammenarbeit deinen vollen Einsatz im Endspurt meiner Promotion danken. Ich hoffe, dass die Malle-Playlist hat dich nicht zu sehr traumatisiert und deine Nase hat sich vom Willgerodt-Kindler-Aroma erholt hat. Ich wünsche euch allen weiterhin alles Gute für eure weitere Laufbahn und hoffe, dass ich euch auch das eine oder andere mit auf den Weg geben konnte.

Einen besonderen Dank möchte ich auch an meine Kommilitonen aussprechen, die mich während des Studiums und der Promotion begleitet haben, besonders an Aleo, Caro, Andi (besonders für den Karibikurlaub), Henni, Patrick, David, Tilman und Domi. Dank euch werde ich mich immer gerne an die vielen Jahre am KIT zurückerinnern.

An dieser Stelle möchte ich mich auch bei den zahlreichen Personen bedanken, die durch Mithilfe in Form von Analytik oder Materialien zum Erfolg meiner Promotion beigetragen haben. Besonders zu nennen sind in diesem Zusammenhang Dr. Andreas Rapp, Lara Hirsch, Angelika Mösle, Richard von Budberg, Birgit Huber, Klara Urbschat und Dr. Jonas Wenzel. Nicht zuletzt danke ich der Paulaner Brauerei, deren koffeinhaltiges Erfrischungsgetränk der Treibstoff war, der mich durch sämtliche Phasen meiner Promotion mit Kraft versorgt hat.

Außerdem möchte ich nochmal Clara, Sandra, Luis, Timo, Henni und Leon für das Korrekturlesen dieser Arbeit danken.

Zu guter Letzt danke ich aus tiefstem Herzen meiner Familie für die bedingungslose Unterstützung und den Rückhalt in schwierigen Zeiten – ganz besonders meinen Eltern Anja und Ralf, meiner Schwester Helena, sowie meinen Großeltern Anneliese und Winfried, Agnes und Rudolf. Ohne euch hätte ich diesen Weg nicht beschreiten können, und ich bin euch unendlich dankbar, dass ihr immer an mich geglaubt habt.

Abstract

A newly discovered sulfur-mediated olefination reaction of *N*-tosylhydrazones (NTHs), which entails the formation of olefins *via* homocoupling of two NTH alkylidene units, was investigated in terms of its synthetic scope. The reaction proved to be highly effective for the homocoupling of aromatic NTHs, enabling the successful synthesis of symmetrical tetraarylethylene (TAE) derivatives in yields between 83% and 99%. Mechanistic studies further enabled the development of a cross-coupling variant that uses a stoichiometric thioketone as the coupling partner, thus allowing the selective synthesis of olefins comprising different alkylidene units with an additional tolerance for aliphatic NTH substrates. Diverse alkylidene-cross-coupled olefins could thus be obtained in yields ranging between 56% and 99%. In comparison to established methods for the synthesis of highly substituted olefins, such as the McMurry coupling or transition-metal-catalyzed cross-couplings, the developed methodologies stand out due to their reliance on cheap, metal-free reagents and short reaction times while exhibiting similar product yields and a complementary substrate scope.

The sulfur-mediated alkylidene-homocoupling was subsequently transferred to bifunctional substrates. In this context, further optimization studies revealed that the homocoupling can be successfully conducted at lower temperatures down to 70 °C while employing argon atmosphere, reaching full NTH conversion within 16 hours. The newly optimized homocoupling conditions allowed the successful polymerization of eight different bifunctional NTHs to their corresponding polyarylene(1,2-diarylvinylene)s (PAV-DAs), achieving yields up to 88% and number average molecular weights up to 26.9 kg mol^{-1}. All obtained homopolymers were characterized with respect to their thermal and optical properties, generally exhibiting very high glass transition temperatures (175-256 °C) and decomposition temperatures (430-541 °C), as well as characteristic aggregation-induced emission (AIE) properties. Additionally, two copolymers were successfully synthesized and their thermal and optical properties could be tuned *via* copolymerization. Compared to literature-described synthesis protocols of PAV-DAs, the herein investigated method stands out due to it use of bench-stable substrates while simultaneously exhibiting similar or superior yields and molecular weights.

In another project, a novel method for the synthesis of renewable polythiols from unsaturated triglycerides was established. The method involved initial gallium bromide-catalyzed

deoxygenation of the triglyceride ester functions to ethers with tetramethyldisiloxane (TMDS), followed by thiol-ene addition of thioacetic acid and subsequent alcoholysis of the resulting thioesters. Three different polythiols were thus synthesized in overall yields of 58-73% from two different kinds of sunflower oils, as well as a synthetic triglyceride based on bio-based 10-undecenoic acid. In due course, new insights were gained on previously unreported side reactions of the ester deoxygenation, which lead to the formation of higher molecular weight species *via* intermolecular homocoupling. Furthermore, a new method for the separation of the polysiloxane side products of the reduction *via* alkaline hydrolysis was established. The viability of the synthesized polythiols as crosslinkers for the synthesis of polymeric networks was exemplarily demonstrated by the synthesis of model materials using radical thiol-ene chemistry, as well as nucleophilic addition to isothiocyanates. All reaction steps were optimized with regard to the principles of Green Chemistry as far as feasible.

A further project focused on the application of levulinic acid as a renewable platform for the synthesis of novel sulfur-containing polymers. The general synthetic strategy entailed a two-step polymer synthesis by sequential conversion of the carboxy function and the keto function of levulinic acid each with bifunctional substrates. For the transformation of the keto group, the Willgerodt-Kindler (WK) reaction was employed, in which aliphatic ketones react with amines and elemental sulfur under formation of terminal thioamides. Initially, the viability of various levulinic acid derivatives as substrates for the WK reaction was studied in model reactions with monofunctional amines. In this context, secondary levulinamides were identified as suitable substrates, selectively reacting with secondary amines and elemental sulfur under formation of a monothioglutaramide. The gained insights were subsequently transferred to a bifunctional levulinamide, successfully yielding a poly(monothioglutaramide) in a yield of 94% and with a number average molecular weight of 11.1 kg mol^{-1}.

Kurzzusammenfassung

Eine neu entdeckte schwefelvermittelte Olefinierung von N-Tosylhydrazonen (NTHs), die zur Bildung von Olefinen durch Homokupplung zweier Alkyliden-Einheiten des NTH führt, wurde hinsichtlich ihres Substratspektrums untersucht. Die Reaktion eignete sich sehr gut zur Homokupplung aromatischer NTHs und erlaubte so die Synthese symmetrischer Tetraarylethylen-Derivate (TAEs) in Ausbeuten zwischen 83 und 99%. Die Aufklärung des Mechanismus der Reaktion ermöglichte zudem die Entwicklung einer Kreuzkupplungs-Variante der Reaktion unter Verwendung stöchiometrischer Mengen eines Thioketons als Kupplungspartner, und erlaubte so die selektive Synthese von Olefinen unterschiedlicher Alkylideneinheiten. Hierbei wurden zusätzlich aliphatische NTH-Substrate toleriert. Somit konnten verschiedene alkyliden-kreuzgekuppelte Olefine in Ausbeuten von 56-99% erhalten werden. Die entwickelten Syntheseprotokolle zeichnen sich im Vergleich zu etablierten Methoden zur Synthese hoch substituierter Olefine, wie beispielsweise der McMurry-Reaktion oder übergangsmetallkatalysierten Kreuzkupplungen, durch kurze Reaktionszeiten und die Verwendung kostengünstiger, metallfreier Reagenzien, bei vergleichbaren Ausbeuten und komplementärem Substratspektrum aus.

Zudem wurde die schwefelvermittelte Alkyliden-Homokupplung auf bifunktionelle Substrate übertragen. In diesem Zuge zeigten weitere Optimierungsstudien zur Homokupplung, dass die Reaktion auch bei tieferen Temperaturen bis 70 °C unter Argonatmosphäre innerhalb von 16 Stunden vollständig abläuft. Unter den neu optimierten Homokupplungsbedingungen konnten acht verschiedene bifunktionelle NTHs zu den entsprechenden Polyarylen(1,2-diarylvinylen)en (PAV-DAs) polymerisiert werden. Dabei wurden Ausbeuten bis zu 88% und zahlenmittlere Molekulargewichte bis zu 26.9 kg mol^{-1} erhalten. Alle Homopolymere wurden bezüglich ihrer thermischen und optischen Eigenschaften charakterisiert und wiesen allgemein sehr hohe Glasübergangstemperaturen (175-263 °C) und Zersetzungstemperaturen (430-541 °C), sowie charakteristische aggregationsinduzierte Emission (AIE) auf. Weiterhin konnten erfolgreich zwei Copolymere hergestellt werden, deren thermische und optische Eigenschaften durch die Copolymerisation gut eingestellt werden konnten. In Vergleich zu literaturbekannten Synthesen von PAV-DAs zeichnet sich die hier untersuchte Methode durch einfacher zu handhabende Materialien bei gleichzeitig ähnlichen oder besseren Ausbeuten und Molekulargewichten aus.

In einem weiteren Projekt wurde eine neue Methode zur Synthese nachwachsender Polythiole aus ungesättigten Triglyceriden etabliert. Die Methode beinhaltet zunächst die Galliumbromid-katalysierte Desoxygenierung der Triglycerid-Esterfunktionen zu Ethern mit Tetramethyldisiloxan (TMDS), gefolgt von Thiol-En-Addition von Thioessigsäure und Umesterung der resultierenden Thioester. Auf diese Weise konnten drei verschiedene Polythiole aus zwei Arten von natürlichen Sonnenblumenölen, sowie einem synthetischen Triglycerid aus biobasierter 10-Undecensäure, in Ausbeuten von 58-73% hergestellt werden. Im Zuge der Synthese wurden neue Erkenntnisse über zuvor unbekannte Nebenreaktionen der Ester-Desoxygenierung, die zur Bildung höhermolekularer Spezies durch Homokupplung führen, gewonnen, sowie eine neue Methode zur Abtrennung der Polysiloxan-Nebenprodukte durch alkalische Hydrolyse etabliert. Die Eignung der synthetisierten Polythiole zur Synthese polymerer Netzwerke wurde exemplarisch durch die Synthese von Modellmaterialien durch Thiol-En-Chemie und nucleophile Addition an Isothiocyanate bestätigt. Alle Reaktionsschritte wurden soweit möglich unter Berücksichtigung der Prinzipien der Grünen Chemie optimiert.

Ein weiteres Projekt zielte auf die Anwendung von Lävulinsäure als erneuerbare Plattform für die Synthese neuer schwefelhaltiger Polymere ab. Dabei wurde eine zweistufige Synthesestrategie verfolgt, die die aufeinanderfolgende Reaktion der Carboxyfunktion und der Ketofunktion von Lävulinsäure jeweils mit bifunktionellen Substraten beinhaltet. Zur Umwandlung der Ketofunktion wurde die Willgerodt-Kindler-Reaktion (WK-Reaktion) verwendet, in welcher aliphatische Ketone mit Aminen und elementarem Schwefel zu terminalen Thioamiden umgesetzt werden. Zunächst wurde die Eignung verschiedener Lävulinsäurederivate als Substrate für WK-Reaktionen mittels Modellreaktionen mit monofunktionalen Aminen untersucht. Dabei wurden sekundäre Lävulinamide als geeignete Substrate identifiziert, die selektiv mit sekundären Aminen und Schwefel zu den entsprechenden Monothioglutaramiden reagieren. Die Erkenntnisse wurden anschließend auf ein bifunktionelles Lävulinamid übertragen, sodass erfolgreich ein Poly(monothioglutaramid) in einer Ausbeute von 94% und einem zahlenmittleren Molekulargewicht von 11.1 kg/mol erhalten werden konnte.

Table of Contents

1 Introduction

The chemical industry provides humanity with critical goods such as fertilizers, polymers, or pharmaceuticals, and has thus played a major role in the development of modern civilization as we know it. In this context, it derives its main feedstock from fossil resources such as natural gas or petroleum, which are not renewable within the timeframe they are currently being consumed in. Consequently, the chemical sector contributes significantly to greenhouse gas emissions and fossil resource depletion, the exhaustion of oil already being expected to occur within the current century. Furthermore, modern society currently operates on linear production-consumption patterns, leading to major problems in global waste management and environmental pollution.[1–6]

In the face of these existential threats, a transition of all industrial sectors, including the chemical industry, to more sustainable production models that focus not only on the use of renewable resources, but also on the valorization of waste materials, is inevitable. The concepts of Green Chemistry have emerged as part of general social and political efforts in response to these issues, in order to promote more sustainable practices in the chemical sector.[7–11]

Elemental sulfur is an example of an underutilized byproduct of the chemical industry, currently being a waste stream of petroleum refining that is generated in greater amounts than the market can consume. Hence, large amounts of sulfur have accumulated, thus currently not only representing a cheaply available waste material, but also posing significant hazards for fires and environmental pollution due to its indefinite storage.[12–15] These circumstances have recently inspired increasing research efforts aimed at directly implementing elemental sulfur into novel chemical processes. For instance, elemental sulfur has gained interest as a versatile reactant or reagent in organic synthesis, as well as a raw material for the production of functional polymers that have shown promise for applications in fields such as waste water treatment or energy storage.[16–18] Beyond the direct utilization of elemental sulfur, sulfur-containing compounds such as thiols have gained attention due to their highly selective reactivities, rendering them powerful tools for more sustainable and efficient synthetic strategies.[19]

As such, it is the main objective of this work to investigate novel synthetic procedures that involve the direct use of elemental sulfur or derived compounds, both in organic and polymer chemistry. In this context, this study seeks to contribute to the development of novel synthesis methods for new functional compounds and materials, which are essential for continued technological progress. Furthermore, the use of renewable resources is simultaneously investigated, aiming to further improve the sustainability of all developed procedures.

2 Theoretical Background

2.1 Green Chemistry and Sustainability

In the early 1970s, the dangers posed to humanity by uncontrolled growth, climate change as well as the depletion of planetary resources have received increasing recognition and concern in global politics, leading to political initiatives aimed towards meeting these challenges.[20,21] The Brundtland Report, officially titled "Our Common Future", was issued in 1987 by the World Commission on Environment and Development of the United Nations and established the concept of a "sustainable development" as the necessary response to these threats, defining it as "meeting the needs of the present without compromising the ability of future generations to meet their own needs".[22] Continued efforts have since led to the formulation of major global action plans, such as the Agenda 21 in 1992 and the UN Sustainable Development Goals in 2015, as well as international contracts such as the Paris Agreement.[23,24] Furthermore, public awareness on matters of sustainability has increased, especially concerning the environment, as expressed by the emergence of global movements such as "Fridays for Future".[25]

The chemical industry is a major contributing factor to global warming, environmental pollution and resource depletion.[26] It is responsible for roughly 5% of global carbon dioxide emissions, ranking it third among industrial sectors. Furthermore, it represents the largest consumer of fossil resources, not only as a source of energy, but as the primary feedstock for the production of bulk and fine chemicals as well as polymers.[1–6] Polymer production in particular is still subject to strong annual growth, driven by the rise of single-use "throw-away" plastic products, which further contributes to increasing problems in waste management and plastic pollution.[27–29] At the same time, the chemical industry has been instrumental to human welfare, playing an essential role in ensuring food supply, combating disease, and providing the materials necessary for technological progress.

As part of the general movement towards more sustainability, the ideas of *Green Chemistry* emerged in the early 1990s, aimed at promoting the necessary transitions in the chemical sector. The introduction of the *Twelve Principles of Green Chemistry* by Paul Anastas and John Warner in 1998 marks the first major conceptualization as a set of guidelines (Table 1).[7,8] Green Chemistry was herein defined as the "design of chemical products and processes the reduce or eliminate the use and generation of hazardous substances", considering the entire life-cycle.

The Twelve Principles of Green Chemistry are intended to function as a coherent design philosophy for the development of new synthetic methods and target compounds.

Table 1: The Twelve Principles of Green Chemistry in their original wording as formulated by Anastas and Warner.[7]

	Principles of Green Chemistry
1	**Waste Prevention**: It is better to prevent waste than to treat or clean up waste after it is formed.
2	**Atom Economy**: Synthetic methods should be designed to maximize the incorporation of all materials used in the process into the final product.
3	**Less Hazardous Synthesis**: Wherever practicable, synthetic methodologies should be designed to use and generate substances that possess little or no toxicity to human health and the environment.
4	**Safer Chemicals**: Chemical Products should be designed to preserve efficacy of function while reducing toxicity.
5	**Safer Auxiliary Substances**: The use of auxiliary substances (*e.g.* solvents, separation agents) should be made unnecessary wherever possible and innocuous when used.
6	**Energy Efficiency**: Energy requirements should be recognized for their environmental and economic impacts and should be minimized.
7	**Renewable Feedstock**: A raw material or feedstock should be renewable rather than depleting, wherever technically and economically practicable.
8	**Reduce Derivatives**: Unnecessary derivatization (blocking group, protection/deprotection, temporary modification of physical/chemical processes) should be avoided wherever possible.
9	**Catalysis**: Catalytic reagents (as selective as possible) are superior to stoichiometric reagents.
10	**Design for Degradability**: Chemical products should be designed so that at the end of their function they do not persist in the environment and break down into innocuous degradation products.
11	**Real-Time Analysis**: Analytical methodologies need to be further developed to allow for real-time, in-process monitoring, and control prior to the formation of hazardous substances.
12	**Safer Methods**: Substances and the form of a substance used in a chemical process should be chosen so as to minimize the potential for chemical accidents, including releases, explosions, and fires.

Green Chemistry has since evolved into an independent branch of research with a dedicated scientific community. Following the launch of the journal "Green Chemistry" by the Royal Society of Chemistry in 1999, all major publishers in the chemistry field now offer their own range of journals with their main focus on innovations in sustainable chemistry.[30] Furthermore, the main ideas of Green Chemistry have seen translations into other related fields, such as the Twelve Principles of Green Engineering, and received numerous contemporary interpretations and reformulations under consideration of more modern concepts such as circular economy, as well as socioeconomic aspects.[9–11,31,32]

In the following sections, numerous theoretical and practical tools for the application of the concepts of Green and Sustainable Chemistry will be presented.

2.1.1 Assessing Sustainability

One of the most fundamental values of Green Chemistry is its focus on waste prevention in favor of waste treatment and disposal, both from an ecological and an economical point of view. Several metrics have been established in order to allow chemists to assess and compare different processes in terms of their tendency to generate waste.[33,34] The oldest such concept is called atom economy (AE) or atom efficiency, first established by Barry Trost in 1991.[35] AE is a dimensionless number that reflects the percentage of reactant mass that is incorporated into the final product under consideration of their stoichiometric factors (Equation 1).

$$AE = \frac{M(product)}{\sum_i M_i(reactants)} \qquad (1)$$

In an ideal reaction, all reactant atoms are incorporated into the final product, corresponding to an AE equal to one. Notably, AE only considers the starting materials of a reaction in ideal stoichiometric ratio, without including solvents, catalysts or any other reagents. Furthermore, it does not consider the actual isolated yield of the product or the possible formation of byproducts. Still, AE is a very useful indicator for preliminary assessment of a chemical reaction, since it can be calculated prior to performing any synthetic work. Some reaction types, such as elimination or substitution reactions, inherently possess lower atom economy due to the inevitable formation of byproducts, *i.e.* waste. Addition reactions or rearrangements often possess a perfect atom economy of 100 %, making them generally superior choices for early-stage synthesis design.[7,35–37] Since AE is an idealized concept that does not consider any

practical circumstances, other complementary metrics have been established for better assessing sustainability in more realistic scenarios.

One such metric is the environmental factor, often abbreviated to E-factor.[38,39] The concept was first proposed by Roger Sheldon in 1992, and is defined as the mass of waste produced by a chemical process per mass of obtained product (Equation 2). A lower E-factor thus signifies that less waste is generated, with the ideal value being zero.

$$E = \frac{m(waste)}{m(product)} \qquad (2)$$

In contrast to AE, the E-factor considers the product yield, as well as all other materials involved throughout a chemical process, including solvents, catalysts, or byproducts, and is thus better suited for sustainability assessment at a later stage of the design process. The E-factor is a very useful and commonly employed metric in the chemical and pharmaceutical industries, since it can be easily calculated without much additional effort by simply considering the mass of purchased materials for a particular process.

The more synthetic steps are involved in an industrial production chain, the higher the value of its E-factor, since the generated waste adds up across all stages. Sheldon *et al.* have used industrial data to compile typical E-factor ranges for products of different industrial segments, ranging from near zero for petrochemicals that are obtained directly from oil refining to values between 25-100 for pharmaceutical products.[39] However, substances of the latter category can easily reach values larger by several orders of magnitude. For instance, recombinant insulin has been reported to have an E-factor of 50000.[34] These values highlight the urgency for transition towards circularity in the chemical industry.

Several circumstances complicate the comparability of different processes by their E-factors. For instance, the original definition states that water should not be included into the calculation. The reasoning for this was that water is used in more different capacities than other substances, for instance as coolant or cleaning agent, so that its inclusion will disproportionately distort the values and thus compromise the reliability of the concept.[39] However, since the treatment of aqueous waste is especially energy-intensive due to the high heat capacity of water, and thus not at all unproblematic, modern interpretations of the E-factor encourage the consideration of water usage.[40] Another important matter is the usage and recycling of solvents, since solvent loss is generally the most impactful contributing factor to waste generation. Especially in academic research, solvent recycling is often not investigated, and thus often no data for solvent recovery is available. In such cases, it has often been assumed that 90% of solvents were

recovered when calculating E-factors. Recently, Roger Sheldon has referred to this practice as "overoptimistic", since efficient solvent recycling is often impeded by cross-contaminations, particularly for multi-step syntheses.[39]

In response to these issues, it has been proposed to redefine the concept of the E-factor into two values, called the simple E-factor (sEF, Equation 3) and the complete E-factor (cEF, Equation 4).[39,41]

$$sEF = \frac{m(reactants) + m(reagents) - m(product)}{m(product)} \quad (3)$$

$$cEF = \frac{m(reactants) + m(reagents) + m(solvents, water) - m(product)}{m(product)} \quad (4)$$

The sEF considers only the reactants and reagents and thus shows similarities to AE in terms of its applicability. The cEF additionally includes solvents and water without accounting for possible recycling, and can hence be considered the "worst-case" E-factor. The true value of the E-factor will range between those of sEF and cEF.

Several similar, alternative metrics to AE and the E-factor have been proposed and applied. A noteworthy example due to its broad usage in the pharmaceutical industry is called process mass intensity (PMI), which is defined as the total mass of all materials divided by the total mass of waste (Equation 5), thus equaling the value of the E-factor plus one.[42,43] Hence, PMI essentially serves the same purpose as the E-factor, and arguments in favor of either metric are mostly of philosophical nature than of scientific importance.[39,43]

$$PMI = \frac{m(materials)}{m(product)} = E + 1 \quad (5)$$

Together, AE and the E-factor allow for effective, early and late stage assessment of reactions in terms of their mass efficiency. Other important aspects of sustainability, for instance the environmental impact of the involved raw or waste materials, are more abstract and not as easily quantified. Several approaches have been proposed to reflect these matters in comparable numbers, which generally involve assigning different scores to certain substances depending on their toxicity or recyclability. A number of different concepts describe the assignment of an "unfriendliness" or "potential environmental impact" value to each material, for instance depending on their hazard statements, and using that value as an additional factor for waste assessment metrics.[44,45] Phan *et al.* have reported a penalty point system that rates a process

with a score from 0 to 100 after answering a series of yes-or-no questions concerning the characteristics of the involved substances and methods.[46] The C-Factor, suggested by Christensen *et al.*, quantifies the amount of carbon dioxide emissions per mass of a particular product, and is thus an indicator for a substance's impact on global warming.[47,48]

The most in-depth way of evaluating environmental impact and hazards associated with a process or product is called life cycle assessment (LCA).[49,50] So called "cradle-to-grave" LCA considers all aspects of a substance's existence, including the acquisition of the required raw materials, its manufacture, distribution, use and disposal. Material and energy streams are identified and evaluated in terms of their impact in several relevant categories, for instance climate change, ozone depletion, fossil depletion, water eutrophication or land use, among others. LCA methods have been internationally standardized and are widely applied in industry.[51,52] Since LCA requires a significant amount of data concerning material flows, it is considered very time consuming and often impossible at early stages of development due to a lack of data. It is therefore more suited for optimizing and evaluating already established processes.

2.1.2 Sustainable Reaction Design in Practice

As already briefly mentioned in the previous section, certain types of chemical reactions inherently generate less waste than others and are thus generally superior choices for a more sustainable process. For instance, as directly stated in the original formulation of the Twelve Principles of Green Chemistry, reactions that involve catalytic reagents are more sustainable than those that rely on stoichiometric reagents. Substituting stoichiometric reagents with catalysts not only reduces the amount of waste *per se*, catalytic reactions also often enable highly selective transformations with fewer undesired byproducts.[53,54] The field of biocatalysis is particularly attractive in the context of a sustainable chemical industry, since enzymes are generally considered non-toxic, renewable as well as highly efficient and selective under mild reaction conditions.[55–57]

Multicomponent reactions (MCRs) are reactions where three or more starting materials are converted selectively into a single product. MCRs typically exhibit near-perfect atom economy, often proceed under mild conditions and allow the synthesis of complex scaffolds in a low number of steps. This makes them useful tools for instance in the research and synthesis of pharmaceutical ingredients. Noteworthy examples for MCRs are for instance the Passerini reaction or the Willgerodt-Kindler reaction, the latter of which will be discussed in more detail a section 2.3.3.[58–60]

The concept of click chemistry was proposed by Sharpless *et al.* and encompasses a set of chemical reactions that fulfil certain criteria that make them generally applicable in various settings. Click reactions should possess modular character with a wide synthetic scope and proceed selectively under simple conditions with high yields. Furthermore, the starting materials for click reactions should be readily available and the products should be simple to isolate without the need for elaborate or waste-intensive workup techniques. The development of click chemistry and biorthogonal chemistry have been laureated with the Nobel Prize in Chemistry 2022 to Bertozzi, Meldal and Sharpless.[61] Notable well known click reactions are the copper-catalyzed azide-alkyne cycloaddition or the thiol-ene reaction, the latter of which will be introduced in more detail in a chapter 2.4.2. It has to be noted that although click reactions exhibit many of the desired qualities for a Green Chemistry approach, certain hazards are often associated with the materials due to the high thermodynamic driving forces required for such reactions. For instance, organic azides are often toxic *per se* or can lead to the formation of toxic and explosive compounds.[62] This illustrates that compromises are often inevitable for the design of more sustainable chemical processes and an overall evaluation is always necessary.

Optimally, chemical reactions should proceed at ambient temperature and pressure without the need for additional heating or cooling, however this is not possible in practice for all transformations. Still, several alternative external reaction conditions have been established that can potentially enable more energy-efficient and simultaneously more effective syntheses. For instance, microwave irradiation has been successfully employed in some cases as more efficient methods of energy transfer than conventional heating, while simultaneously producing higher product yields.[63,64] The field of photochemistry uses light as a source of energy and thus bears great potential for more sustainable processes. The development of photocatalysts that enable the direct usage of sunlight is especially promising in this regard, rendering the light source essentially waste-free.[65–67]

The use of solvents is also generally undesirable, yet unavoidable in many cases. Solvents are typically the largest contributors to the overall waste of a process, and many commonly used solvents are associated with environmental, health and safety concerns.[68] The pharmaceutical company GlaxoSmithKline (GSK) has pioneered the compilation of solvent selection guides, which are convenient tools for assessing and comparing different commonly used solvents based on LCA. Solvent selection guides assign scores to all listed solvents in different categories concerning waste, environmental and health hazards and physical safety, allowing for quick assessment of potential issues associated with particular solvents and identifying potential replacements.[69] Supercritical fluids or ionic liquids are frequently suggested as

sustainable alternative solvents. For instance, supercritical carbon dioxide is already industrially established for the decaffeination of coffee.[70–72]

In summary, the concepts of Green Chemistry have emerged as part of a global movement towards more sustainability in the face of threats such as resource depletion and climate change. The key values are expressed in the Twelve Principles of Green Chemistry, and numerous metrics and tools have been established to assist chemists in implementing the philosophy into the design of the chemical processes of the future. While progress towards more sustainability has undoubtedly been made, the transition from linear production patterns based on fossil resources towards a sustainable, circular chemical industry is still at its early stages and becoming increasingly urgent.

2.2 Renewable Resources

As stated in section 2.1, non-renewable fossil resources are still the primary feedstock for global energy supply, transportation fuels, as well as the industrial production of fine chemicals and polymers. The eventual transition towards the use of renewable resources in all sectors is without alternative and thus one of the most pressing challenges of the 21st century. Biomass represents the most abundant source of renewable carbon on earth and is thus the most promising feedstock for the defossilization of the chemical industry.[3] Approximately 170 billion tons of biomass are generated on earth *per annum*, only 3.5% of which is currently utilized by humanity in the form of food, construction materials or energy carriers.[73] The main components are polysaccharides, mainly cellulose, chitin and hemicellulose, as well as lignin, which comprise 95% of the total biomass. Cellulose, hemicellulose and lignin are often collectively referred to as "lignocellulosic biomass". The remaining 5% consist mainly of plant oils and terpenes, as well as other biomolecules such as proteins, alkaloids and nucleic acids (Figure 1).

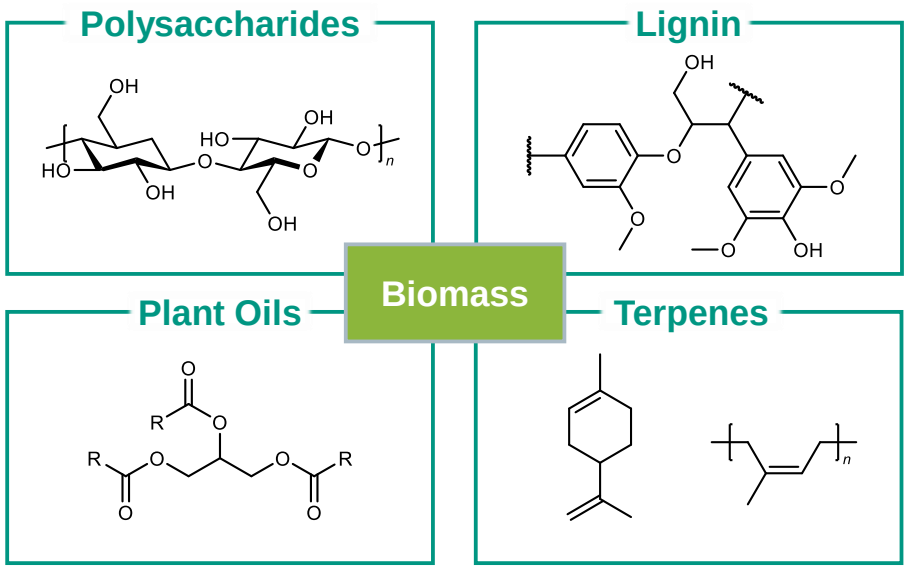

Figure 1: Representative structures of the main components of biomass.[73]

Due to the large available amounts, the sole reliance on biomass for covering the global needs for energy carriers and chemical products is feasible in theory.[56,73] However, in comparison to fossil resources consisting mainly of non-functional hydrocarbons, biomass is a comparatively highly functionalized and heterogeneous feedstock. Hence, its incorporation into existing industrial infrastructure for the synthesis of fine chemicals and polymers is not straightforward and requires the design of new processes that also have to be economically and socially sustainable.[48,74,75] In the following section, several approaches for the use of renewable feedstocks for the synthesis of fine chemicals and polymers will be discussed.

2.2.1 Lignocellulosic Biomass

Lignocellulosic biomass is the main constituent of plants and consists of cellulose (35-50%), hemicellulose (20-35%) and lignin (10-25%), with the exact composition depending on the source.[76] Cellulose is a linear polysaccharide consisting exclusively of poly-*(D)*-glucopyranose units, connected *via* 1,4-β-glycosidic bonds (Figure 1, top left). Hemicellulose is a collective term for all other plant-derived polysaccharides comprising other sugars, for instance pentoses such as xylose or arabinose, and other hexoses including galactose and mannose.[77] Lignin is a complex, heterogeneous network consisting of phenylpropane units, which are crosslinked either *via* C-C or C-O bonds (Figure 1 top right).

Cellulose in particular has a rich history of applications in the chemical industry. The development of methods to solubilize cellulose *via* a derivatizing approach, such as the viscose process, has enabled the processing of cellulose into films and fibers.[78] Cellulose esters such as cellulose nitrate (celluloid) and cellulose acetate are thermoplastic polymers that have seen successful applications as plastics or textile fibers, among others. However, with a few exceptions such as cigarette filters, cellulose esters have been replaced by cheaper, fossil-based polymers in some instances.[79,80] Still, the depletion of fossil resources and the desirable properties of cellulose-based polymeric materials can potentially render them economically attractive again in the future, also for commodity applications. Current applications include, for instance, membranes, fibers or pharmaceutical formulations. Today, research is focused on more sustainable methods for cellulose derivatization, for instance using switchable ionic liquids.[81–85]

In contrast to cellulose and hemicellulose, lignin is still considered a waste product, since it does not yet have many major industrial applications. It is still generated in large amounts since the production of cellulose requires the complete separation of the lignin content from lignocellulosic biomass. Most of the lignin waste is incinerated for energy recovery, and only a very small amount is further processed and used in the production of surfactants, adhesives or fine chemicals such as vanillin.[86,87] As the only major renewable source of aromatic compounds and currently also a waste product, sustainable modification of lignin for its direct use in the production of platform chemicals and polymeric materials is also a matter of current research.[88,89]

Due to the ready availability of carbohydrates in lignocellulosic biomass, significant research efforts have been directed towards their use for the production of value-added platform chemicals that can replace the basic chemicals currently provided by the petrochemical refining of fossil feedstocks. This concept is called “biorefinery”, and many approaches have emerged

that either generate the same basic chemicals currently obtained from oil and gas (so called drop-in solutions), or supply functional alternatives.[48,90–92]

A notable example for a biorefinery is the synthesis of bioethanol *via* fermentation of low molecular weight sugars, which is already performed on large scale and used for instance as a fuel additive. The fermentation substrates are currently mostly obtained from food crops such as sugar cane (1st generation bioethanol). Since this feedstock competes with food production and is thus critical in terms of social sustainability, the valorization of cellulose and hemicellulose is being developed as an alternative in this context, since they can for instance be sourced from agricultural wastes (2nd generation bioethanol).[93–95]

The catalytic dehydration of bioethanol into bio-ethylene is considered as a potential drop-in solution for a bio-based chemical industry. Ethylene is currently the single most produced organic chemical in the world and thus one of the most important commodities for the chemical industry, being the basis for the production of fine chemicals such as higher olefins, ethylene glycol or styrene, as well as polymers such as polyethylene. A potential industrial implementation of biosourced ethylene could thus take advantage of existing industrial infrastructure and value chains (Scheme 1).[96–98] Another relevant drop-in process is the so-called biomass gasification, which entails the generation of syngas (a mixture of carbon monoxide and hydrogen) *via* oxidation of biomass at high temperatures. Syngas is an important precursor for the industrial synthesis of chemicals such as methanol or acetic acid.[99–101]

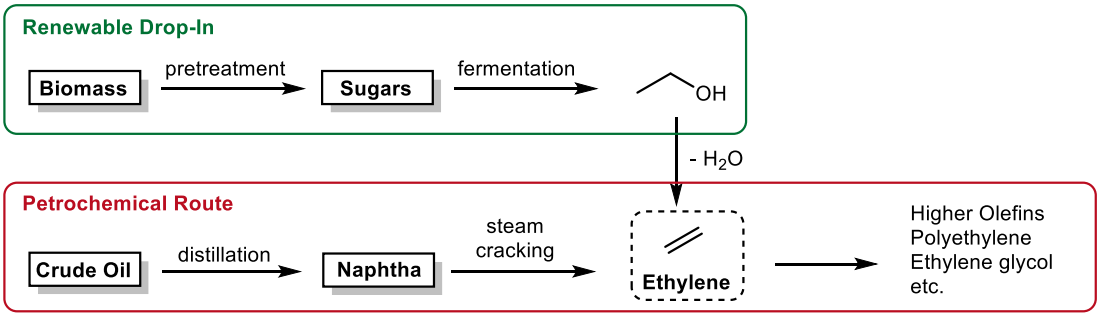

Scheme 1: Illustration of the renewable drop-in of bioethylene obtained from fermentation of biomass into the existing petrochemical value chain. [96–98]

Besides drop-in solutions, chemical transformations of lignocellulosic biomass offer access to several alternative platform chemicals, providing potential functional substitutes for established compounds. The United States Department of Energy has identified several promising bio-based platform chemicals, which are accessible on industrial scale from carbohydrates *via* targeted fermentation or simple chemical reactions such as hydrolysis.[75,102]

An example of such a platform chemical is 5-hydroxymethylfurfural (HMF), which can be obtained *via* acid-catalyzed dehydration of monosaccharides such as glucose.[103,104] A potential use of HMF is its further oxidation to furan-2,5-dicarboxylic acid (FDCA). FDCA is widely

regarded as a functional alternative to terephthalic acid for the production of polyesters. For instance, polyethylene furanoate (PEF), a polyester of FDCA with ethylene glycol, represents a renewable alternative to polyethylene terephthalate (PET), which also exhibits superior mechanical properties and better biodegradability.[105–107]

Further acidic hydrolysis of HMF can yield levulinic acid (LA), which has been identified as another valuable precursor for a variety of different chemicals. For instance, LA can be further converted to γ-valerolactone (GVL) or 2-methyltetrahydrofuran (MeTHF), which are considered valuable biofuel additives, as well as renewable solvents for organic synthesis. Further potential downstream products of LA include pyrrolidones, which see use as polar aprotic solvents, or diphenolic acid, a potential more benign substitute for bisphenol A, among many others.[108–110]

A representative diagram for the generation and further processing of HMF is depicted in Scheme 2.

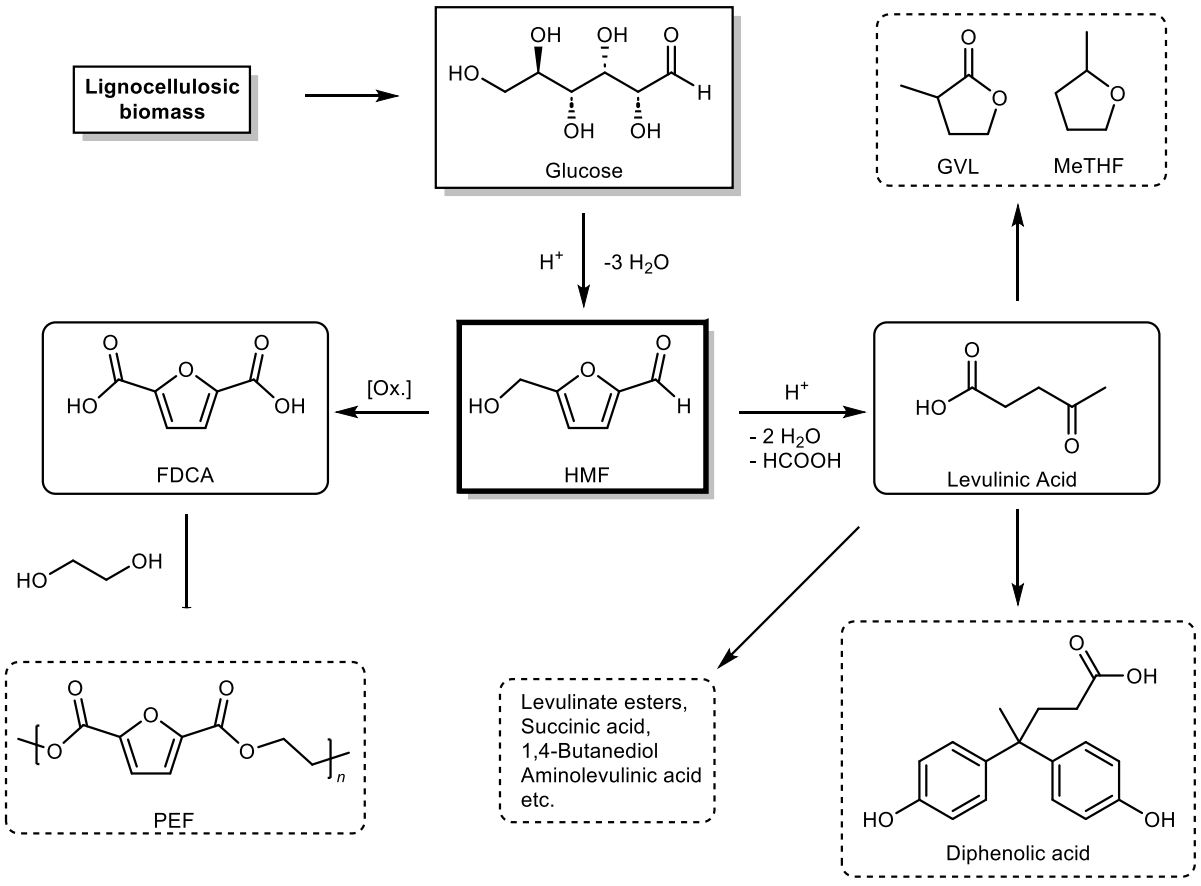

Scheme 2: Schematic representation of of HMF synthesis via hydrolysis of glucose from biomass, as well as its further processing to FDCA and LA, along with further downstream products.[108–110]

2.2.2 Plant Oils

Plant oils consist of triglycerides, *i.e.* triesters of glycerol and fatty acids, and represent another important class of renewable feedstock from biomass (Figure 1, bottom left). “Fatty acid” is a comprehensive term for long-chain aliphatic carboxylic acids, often containing an even number of carbon atoms, with numerous different fatty acids being found in naturally occurring fats and oils. Many fatty acids contain carbon-carbon double bonds in their aliphatic chains, and are thus often classified into saturated fatty acids (SFA) and unsaturated fatty acids, the latter frequently being further subdivided into monounsaturated fatty acids (MUFA) and polyunsaturated fatty acids (PUFA). Several naturally occurring fatty acids contain additional functionalities, such as hydroxy functions or, more rarely, epoxide or cyclopropane moieties. The fatty acid signature of naturally occurring oils and fats strongly influences their physical and chemical properties and depends on a variety of factors such as the original plant or crop, the season and the growth conditions. Table 2 presents an assortment of notable fatty acids together with a representative oil known for containing the respective fatty acid in significant amounts.[111–114]

Table 2: Names and structures of several relevant fatty acids, as well as a representative oil containing the respective acids.[111–114]

Fatty Acid	Occurrence / %	Structure
Lauric acid (C12)	Palm Kernel Oil (50%)	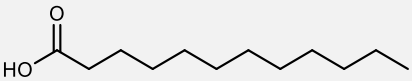
Palmitic acid (C16)	Palm Oil (46%)	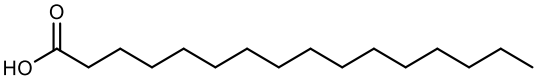
Oleic acid (C18:1)	High Oleic Sunflower Oil (>85%)	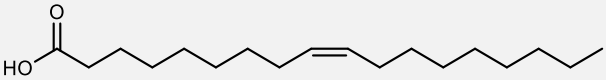
Erucic acid (C22:1)	High Erucic Rapeseed Oil (20-54%)	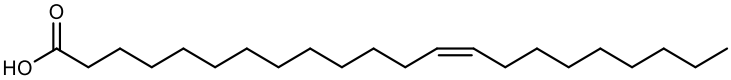
Linoleic acid (C18:2)	Sunflower Oil (61%)	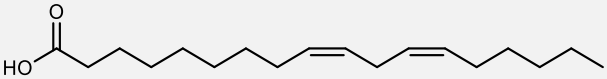
Linolenic acid (C18:3)	Linseed Oil (52%)	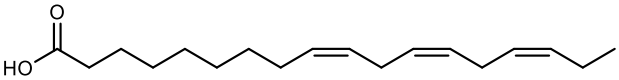
Ricinoleic acid (C18:1)	Castor Oil (88-90%)	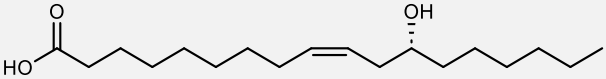

Despite only constituting a comparably low percentage of biomass, plant oils are currently the most used renewable feedstock in the chemical industry, seeing usage for the production of cosmetic products, lubricants or surfactants, among others.[112,115,116]

Most industrially practiced oleochemistry is conducted at the carbonyl function of triglycerides or fatty acids. For instance, transesterification of triglycerides with methanol yields fatty acid methyl esters (FAMEs) and glycerol.[117,118] FAMEs see common usage as biodiesel, while glycerol can serve as a platform for the production of a variety of commodity chemicals. A notable example is epichlorohydrin (ECH), a widely used precursor for epoxy resins that has traditionally been synthesized from fossil-based propylene.[119]

Hydrolysis of triglycerides yields free fatty acids, which can for instance be further converted to fatty alcohols by catalytic hydrogenation. Particularly fatty alcohols derived from shorter, saturated fatty acids such as lauric acid, which occurs in palm kernel oil or coconut oil, are commonly applied in the production of surfactants.[112,120,121]

The presence of double bonds in unsaturated fatty acids gives rise to further possibilities for the synthesis of fine chemicals or polymers, some of which are already industrially established.

For instance, oil drying refers to the oxidative gelation of plant oils to yield solid resins. On a chemical level, oil drying is a radical process, mediated by airborne oxygen, that leads to the crosslinking of polyunsaturated fatty acids such as linoleic or linolenic acids.[122,123] After initial radical formation *via* H-abstraction in their highly reactive bis(allylic) positions and subsequent hydroperoxide formation, intermolecular crosslinking occurs by the formation of alkyl, ether or peroxide linkages, leading to the formation of a polymeric network. Oil drying processes are for instance the operating principles of historical oil paints based on linseed oil, more modern paints and varnishes based on alkyd resins (fatty acid-modified glyceryl polyesters), as well as polymeric materials such as linoleum.[124–126] Linoleum rose to significance as a material for floor covering, but has been mostly edged from the market by cheaper alternatives such as polyvinyl chloride (PVC).[127]

Epoxidation of the double bonds in unsaturated fatty acids / triglycerides is also conducted on industrial scale. The introduction of highly electrophilic epoxide moieties provides many opportunities for further functionalization. Epoxidized vegetable oils themselves can for instance be used for the formulation of renewable epoxy resins with curing agents such as anhydrides or amines.[128,129] Ring-opening reactions of the epoxide moiety also allow the further modification of epoxidized oils for other applications.[130] For instance, Chrisholm *et al*. reported the synthesis of cyclic carbonates from epoxidized soybean oil and their subsequent aminolysis to yield renewable non-isocyanate polyurethane (NIPU) networks (Scheme 3).[131]

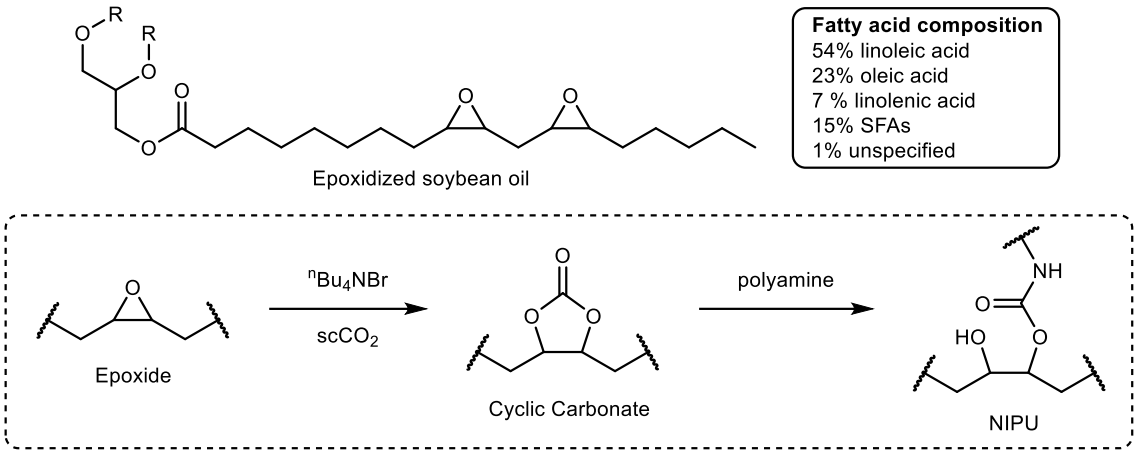

Scheme 3: Synthesis of a NIPU network from epoxidized soybean oil, reported by Chrisholm et al [131]

Oxidative cleavage of fatty acids is another prevalent strategy for the synthesis of commodity chemicals and monomers. Most notably, ozonolysis of oleic acid is a relevant process, yielding pelargonic acid and azelaic acid, the latter of which sees application in the pharmaceutical industry or as monomer for polycondensations.[132–134] Due to the high energy demand of ozonolysis as well as the hazards associated with ozone, more benign cleavage methods have been investigated and ozonolysis is no longer common in industrial oleochemistry.[135] For instance, Behr *et al*. reported a ruthenium-catalyzed oxidative cleavage of methyl oleate with hydrogen peroxide. Meier *et al.* recently employed the method directly to high oleic sunflower oil (HOSO), obtaining the tricarboxylic acid glyceryl triazelate, which was subsequently used for the synthesis of polymeric networks.[136–138]

Due to the additional hydroxy function, ricinoleic acid, derived from castor oil, provides very unique possibilities for further applications in fine chemical or polymer synthesis. For example, the pyrolysis of methyl ricinoleate is an industrially established process that results in the selective formation of methyl-10-undecenoate and heptanal *via* an intramolecular Alder-Ene reaction, the former of which can be hydrolyzed to 10-undecenoic acid (UA) (Scheme 4).[113] UA is a very useful building block due to its terminal double bond and carboxy function, which has seen wide application in the synthesis of polymeric materials.[139] A relevant industrial process involving UA is the production of Nylon 11, which is distributed by the company Arkema under the brand name Rilsan already for decades. The synthesis involves radical anti-Markovnikov hydrobromination of UA, followed by nucleophilic substitution with ammonia, yielding 11-aminoundecanoic acid, which is then subjected to polycondensation (Scheme 4).[140] Beyond applications for the synthesis of platform chemicals, castor oil itself can be considered a naturally occurring polyol and has accordingly found use in the synthesis of polymer networks such as polyurethanes or polythiourethanes.[141]

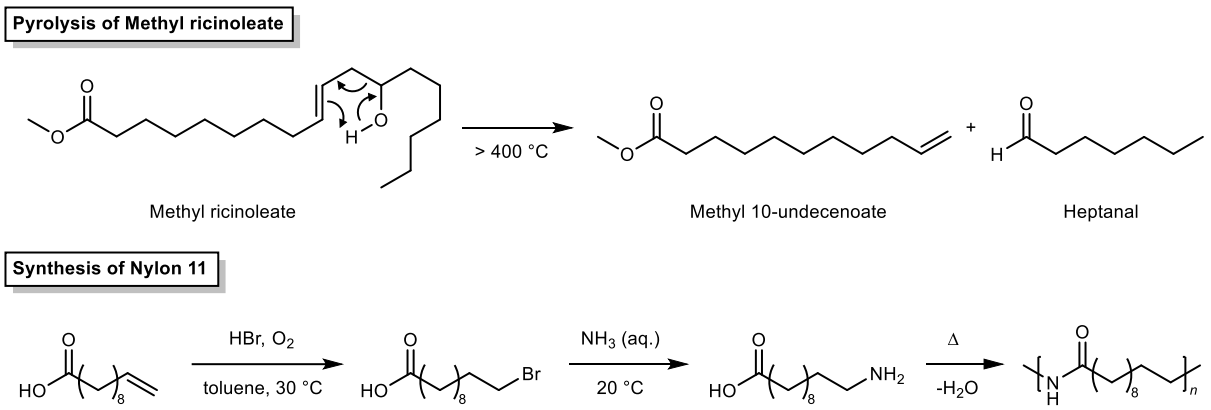

Scheme 4: Pyrolysis of methyl ricinoleate to yield methyl 10-undecenoate and heptanal (top) and synthesis of Nylon 11 from 10-undecenoic acid (bottom).[113]

Olefin metathesis, laureated with the 2005 Nobel Prize in Chemistry, is another noteworthy example of alkene chemistry and has seen application to unsaturated triglycerides and fatty acids.[142] For instance, the efficient self-metathesis of polyunsaturated C18-FAMEs such as methyl linolenate has been described to yield interesting products such as α,ω-diesters, which could be successfully employed for polyester synthesis. Another interesting self-metathesis product is 1,4-cyclohexadiene, which itself has been utilized for the synthesis of polymers such as polycarbonates or polyesters.[143,144] Other olefin metathesis approaches, such as ethenolysis or cross-metathesis with alkenes such as acrylates, have also been reported, both for fatty acids and vegetable oils.[145,146]

Overall, the potential of renewable feedstocks such as lignocellulosic biomass and plant oils for the chemical industry has been highlighted by a variety of successful developments in biorefinery concepts and direct valorization of the feedstocks for polymer synthesis, providing alternative access to currently fossil-based commodities, as well as functional alternatives. Processes involving other sources of renewable carbon, such as terpenes from biomass or also carbon dioxide, have also shown potential in this regard.[74,147,148] Future developments are aimed at further improving their socioeconomic viability, in order to promote the transition to a more sustainable chemical industry.

2.3 Chemistry of Elemental Sulfur

Disclaimer

Parts of this chapter are based on a published literature review by the author of this thesis. Text and figures are partially reproduced, edited and extended from this article, which is licensed for re-use under Creative Commons CC-BY-NC:[149]

P. Conen, M. A. R. Meier "Reactivities and mechanisms in organic reactions involving activation of elemental sulfur under basic conditions" *Tetrahedron Chem* **2024**, *11*, 100086. https://doi.org/10.1016/j.tchem.2024.100086

Sulfur has been known to humanity for millennia, with its early uses including gunpowder production and as a topical treatment for infections.[150,151] Today, with its global market volume consistently exceeding 80 million tons *per annum* since 2020, elemental sulfur is one of the most produced chemicals in the world.[152] However, more than 90% of the annually produced sulfur is not the result of a targeted production, but instead generated as a byproduct of petroleum refining.[12–14] Natural oil and sour gas contain considerable amounts of sulfur species, the sulfur content generally ranging between 0.1-6 weight%.[153] The removal of sulfur containing species is critical in order to counteract sulfur oxide emissions and catalyst poisoning in downstream processes.[154,155] The recovery of sulfur from petroleum is achieved *via* catalytic conversion of sulfur-containing compounds into hydrogen sulfide, followed by the Claus Process, which involves partial catalytic oxidation of hydrogen sulfide to sulfur dioxide and subsequent symproportionation into elemental sulfur (Scheme 5).[153,156,157]

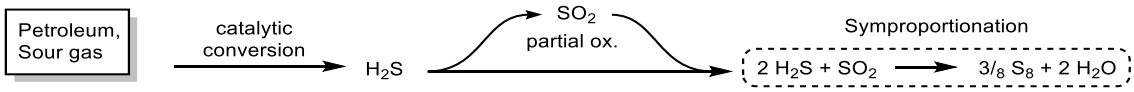

Scheme 5: Schematic representation of the Claus process.[153,156,157]

The main industrial sink for elemental sulfur is sulfuric acid synthesis, with further uses being rubber production or alkali metal-sulfur batteries.[12,158,159] Despite this, the large inflow of sulfur from the petrochemical industry has exceeded its demand in recent times. Excess sulfur is constantly accumulating in designated deposits, not only representing an unutilized resource, but also posing significant hazards for fires and environmental pollution.[12,15,160,161] These circumstances, in combination with the knowledge that sulfur-containing materials show promising application possibilities, have recently served as new inspiration for scientists to explore novel applications for elemental sulfur in chemistry and material sciences. As a cheaply available waste material and a non-toxic, non-odorous and generally storage-stable solid at ambient conditions, sulfur exhibits highly desirable properties as a raw material for novel processes, in line with the principles more sustainable chemistry. In addition to these convenient

characteristics, sulfur possesses great potential as a versatile reagent in chemical synthesis. In the following chapters, the basic chemical properties of sulfur, as well as several applications in organic and polymer chemistry will be presented.

2.3.1 Basic Physical and Chemical Properties of Sulfur

Sulfur chemistry is characterized by the high variety of possible oxidation states, ranging from -II to +VI. As the heavier homologue of oxygen in Group 16 of the periodic table, sulfur-containing variants of many oxygen-containing functional groups are well known.[162–165] In contrast to oxygen, however, sulfur more readily forms stable bonds with itself. The average S-S-bond dissociation energy is valued at 265 kJ mol^{-1}, making it the third most stable homoatomic single bond, only surpassed by H-H and C-C bonds.[166,167] The tendency of sulfur to form double bonds is significantly lower than that of oxygen.[164] Instead, sulfur is known for its tendency to form chains and cycles. In fact, elemental sulfur has the largest known number of solid allotropes, comprising cyclic modifications with 6-20 S-atoms, as well as phases consisting of polymeric sulfur chains. Additionally, a great number of polysulfur cations, anions and radicals have been described.[164]

The only thermodynamically stable modification is the orthorhombic α-sulfur, which consists of cyclic, crown-shaped S_8 molecules of D_{4d} symmetry, forming the characteristic yellow crystals that are commonly associated with sulfur.[168] Above 96 °C, a phase transition to β-sulfur occurs, which is a monoclinic modification also consisting of S_8 cycles. The melting point of β-sulfur is reached at roughly 120 °C. In liquid sulfur, S_8 rings are still the predominant species, however an equilibrium with other S_x ring sizes is established. At 159 °C, an entropy-driven homolytic ring-opening polymerization occurs, resulting in the formation of biradical polymeric sulfur chains comprising up to 10^5 S-atoms, which is accompanied by a color change from yellow to deep red, as well as a drastic viscosity increase of the melt.[164,169]. Further heating results in gradual depolymerization until the boiling point is reached at 444 °C.

The physical solubility of S_8 is generally very poor, especially at low temperatures. The very notable exception is carbon disulfide, which dissolves roughly 25 wt% of elemental sulfur even at ambient temperature and pressure.[170] Moderate solubility of elemental sulfur has been reported for non-polar solvents such as toluene, *p*-xylene, chlorobenzene and cyclohexane, with toluene being the most effective solvent among them, dissolving approximately 2.8 wt% sulfur at 30 °C. Generally, sulfur solubility increases with rising temperature. The presence of ions drastically decreases the physical solubility.[171,172] It has been reported that in solutions of elemental sulfur in polar solvents, like methanol or acetone, an equilibrium is established in

which ~1% of the dissolved sulfur is present as smaller S_7 and S_6 cycles. The solubility of S_8 can be further be drastically enhanced by the addition of surfactants such as cetyltrimethylammonium bromide.[173]

2.3.2 Interactions of Elemental Sulfur with Bases

While the S_8 molecule is chemically inert towards many chemicals at standard conditions, it shows much higher reactivity towards basic compounds. The interaction of sulfur with bases is accompanied by a chemical transformation of S_8, typically associated with the formation of polysulfide anions and/or sulfur-centered radicals. As a very classic example, elemental sulfur rapidly dissolves in aqueous solutions of ammonium sulfide and other inorganic sulfides (Scheme 6). The resulting yellowish-brown solutions comprise polysulfide dianions $[S_n]^{2-}$ of variable chain lengths, with their ratio depending on the pH.[174,175] Mechanistically, it has been suggested that the sulfur dissolution is initiated by the nucleophilic attack of a bisulfide ion SH^- on the S_8 ring, resulting in the formation of the nonasulfide dianion S_9^{2-}, followed by the rapid establishment of an equilibrium with polysulfide dianions of variable chain lengths *via* continuous nucleophilic substitution of sulfur atoms within the polysulfide chains.

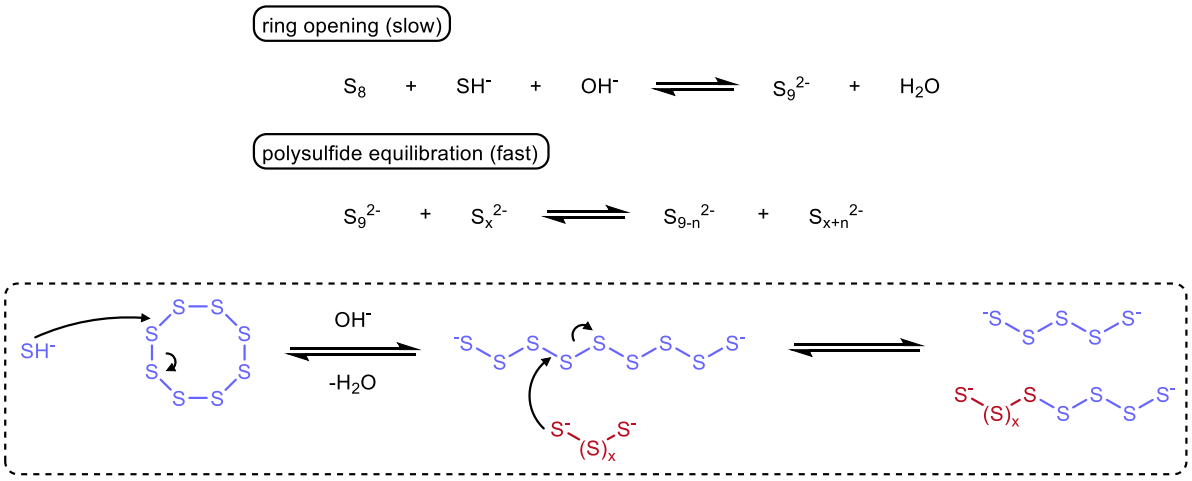

Scheme 6: Reported mechanism for the dissolution of elemental sulfur in aqueous sulfide solutions, entailing initial nonasulfide formation followed by polysulfide equilibration.[149]

In addition to their equilibrium with each other and with *cyclo*-S_8, polysulfide dianions also exist in an equilibrium with corresponding radical monoanions, resulting from the homolytic scission of a central S-S-bond.[165,167] The most well-known is the deep-blue trisulfide radical anion $S_3^{\bullet-}$, which also occurs naturally in several minerals such as lapis lazuli or ultramarines, granting them their characteristic blue color.[176] Although the formation of blue colorations associated with the interaction of sulfur and bases or solutions of polysulfide salts had been observed numerous times before, the nature of the $S_3^{\bullet-}$ as the underlying species was first

characterized by Chivers *et al.* in 1972 in solutions of alkali polysulfides in hexamethylphosphoramide (HMPA).[177–181] Other polysulfide radical anions are the disulfide and tetrasulfide radical anions $S_2^{\bullet-}$ and $S_4^{\bullet-}$., which are observed less frequently than $S_3^{\bullet-}$.[167] The equilibrium between the dianions and monoanions is known to depend on several factors such as temperature, solvent polarity, or the nature of the corresponding cations. [167,182–184]

In organic reactions involving elemental sulfur and bases (see chapter 2.3.3), the $S_3^{\bullet-}$ radical anion has been frequently observed spectroscopically using its characteristic UV/Vis, electron paramagnetic resonance (EPR) and Raman signals, and is thus often suggested as an intermediate in such reactions. Its observation is frequently associated with the presence of oxygen-centered bases such as hydroxides, alkoxides and carbonates, as well as polar aprotic solvents such as dimethyl sulfoxide (DMSO) or *N*,*N*-dimethylformamide (DMF).[167,185–188]

Nitrogen-centered bases such as ammonia and amines also display characteristic interactions with elemental sulfur. Solutions of elemental sulfur in liquid ammonia are highly complex systems that have been controversially discussed and thoroughly investigated using Raman, UV/Vis, EPR and nuclear magnetic resonance (NMR) spectroscopies.[189–192] The main sulfur species detected within these solutions are the hexasulfide dianion S_6^{2-}, in temperature- and concentration-dependent equilibrium with its corresponding radical monoanion $S_3^{\bullet-}$, as well as several sulfur-nitrogen anions, namely the cyclic S_7N^-, and the open-chain species S_4N^- and S_3N^-.[191] The presence of shorter-chain aminopolysulfides, such as NH_2S^- and $NH_2S_2^-$ has been suggested as well.[193] Physically dissolved S_8 was not detected.[190] Chivers *et al.* have suggested mechanisms for the dissolution of sulfur in liquid ammonia (Scheme 7).[190,194,195]

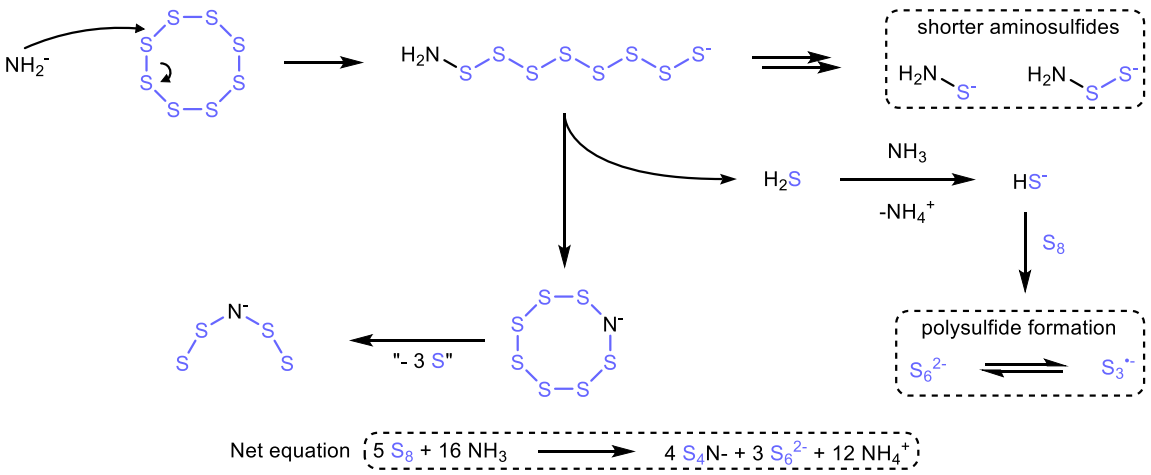

Scheme 7: Proposed mechanisms for the dissolution of elemental sulfur in liquid ammonia.[149]

After initial ring-opening of S_8 by amide anions or ammonia, H_2S extrusion is suggested to form the cyclic heptasulfurimide anion S_7N^-, which is known to further decompose into S_4N^-. The generation of H_2S results in the subsequent formation of polysulfide anions in analogy to the mechanism presented in Scheme 6.

In a similar fashion to ammonia, amines also react with elemental sulfur to form complex systems involving polysulfides and nitrogen-sulfur species.

The formation of ionic species in sulfur solutions in primary and secondary amines was confirmed *via* electrical conductivity measurements performed by Davis *et al.*, reporting an increase in conductivity upon sulfur dissolution which correlated well with amine basicity and was impeded by increasing steric hindrance. The presence of both polysulfide dianions and the corresponding radicals in such systems was later confirmed spectroscopically.[196–199] An NMR study conducted by Ozin *et al.* upon a solution of elemental sulfur in *n*-octylamine found that the amine proton resonance is shifted downfield as a function of the sulfur content, indicating an increasing degree of positive charge at the nitrogen center.[200]

Overall, these observations suggest the initial formation of ammonium aminopolysulfides by nucleophilic ring opening followed by the deprotonation of the resulting zwitterion. Furthermore, it has been suggested that the aminopolysulfide anions can further react to polythiobisamines and polysulfide dianions by nucleophilic attack of another amine molecule. Polythiobisamines have been detected in mass spectrometry (MS) measurements conducted by Nicolaou *et al.*[201] Illustrative mechanisms are depicted in Scheme 8. It was noted that all steps are generally reversible, since elemental sulfur could be quantitatively recovered upon evaporation of the amines from fresh solutions. Irreversible formation of thioamide side products by oxidation of the amine α-methylene protons was only observed upon aging.

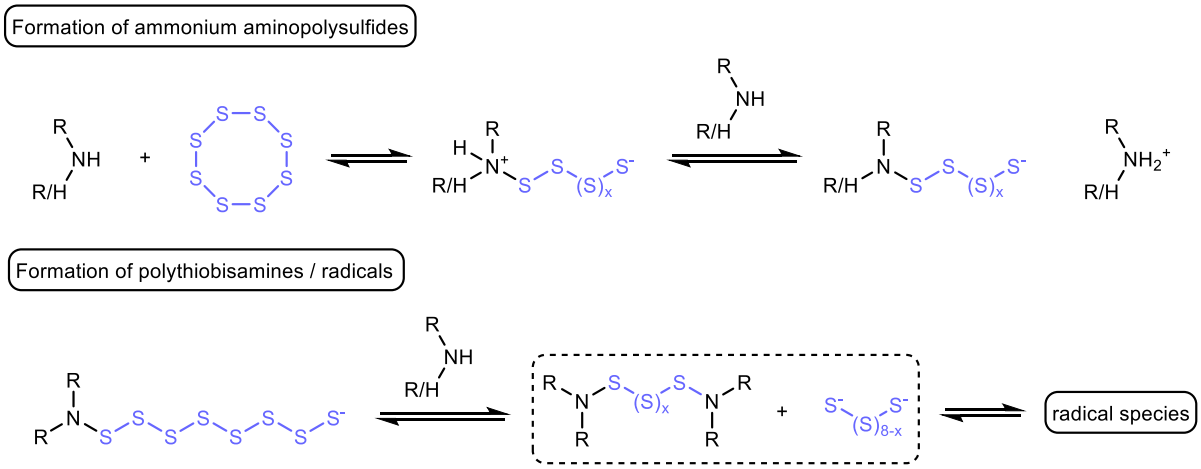

Scheme 8: Formation of ammonium aminopolysulfides (top) and subsequent formation of polythiobisamines and polysulfides and their equilibrium with radicals (bottom), as postulated by Davis (see Ref [196]) and Hodgson (see Ref [197]).[149]

In contrast to primary and secondary amines, solutions of elemental sulfur in tertiary amines did not result in measurable conductivity increases or radical formation in the investigations of Davis and Hodgson.[196,197] It was thus concluded that the interactions of tris(alkylamines) and elemental sulfur do not result in opening of the S_8 ring, but instead merely in the formation of a charge-transfer complex. While no further fundamental investigations on the interaction of

sulfur with tris(alkylamines) like NEt_3 were conducted since, a recent density functional theory (DFT) study has confirmed the exergonic formation of a stable zwitterion from the strong guanidine-base 7-methyl-1,5,7-triazabicyclo[4.4.0]dec-5-ene (MTBD) and sulfur, suggesting that ring opening can also be effected by some tertiary amines (Scheme 9).[202] As will become apparent in section 2.3.3, tertiary amines are often observed to catalyze organic reactions with elemental sulfur, suggesting some degree of interaction that results in sulfur activation.

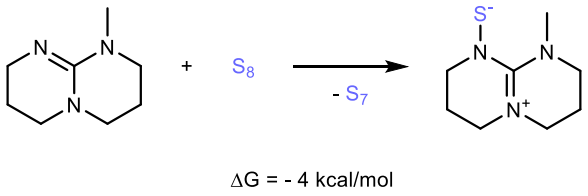

Scheme 9: Formation of a stable zwitterion from the guanidine base MTBD and elemental sulfur.[202]

Several nucleophiles are irreversibly oxidized by elemental sulfur under formation of thermodynamically stable products *via* incorporation of sulfur atoms, which drive the reaction by being removed from the equilibria. A representative example is the reaction of cyanide with elemental sulfur under formation of thiocyanate, which has been subject of extensive mechanistic studies.[203–205] A recent computational study by Champagne *et al.* revealed a great degree of complexity in the mechanism of this seemingly simple reaction.[205] The initial step of heterolytic S_8 ring opening by the cyanide ion under formation of an octathiocyanate ion, is followed by a complex equilibrium of different nucleophilic reactions, leading to the formation of polythiocyanates of different chain lengths, as well as other sulfur allotropes. Two main pathways that lead to the formation of the monosulfurized thiocyanate ion were identified. The first is unimolecular decomposition of a polysulfide, which results in the formation of thiocyanate and a smaller sulfur allotrope (Scheme 10 top) The second pathway is called polysulfide scrambling and entails the intermolecular nucleophilic attack of polysulfides upon each other, forming thiocyanate and a longer polythiocyanate (Scheme 10 bottom). The nucleophilic attack occurs most favorably at the sulfur atom furthest from the negative terminus not bonded to a heteroatom (the S^2 position), which was identified as the most electrophilic site of the polysulfide chain. Furthermore, the sulfur allotropes that form during unimolecular cyclization can themselves be nucleophilically attacked by other polysulfides, leasing to the formation of polythiocyanates of increased chain length. The prevalence of these pathways is generally dependent on the polysulfide chain length. For instance, unimolecular decompositions occur more readily for longer polysulfides, while scrambling is the more prevalent decomposition pathway for shorter polysulfides. It can be expected that the reactions of other nucleophiles with S_8 also involve the described pathways, however the exact influence of each is expected to be highly individual to the nucleophile.

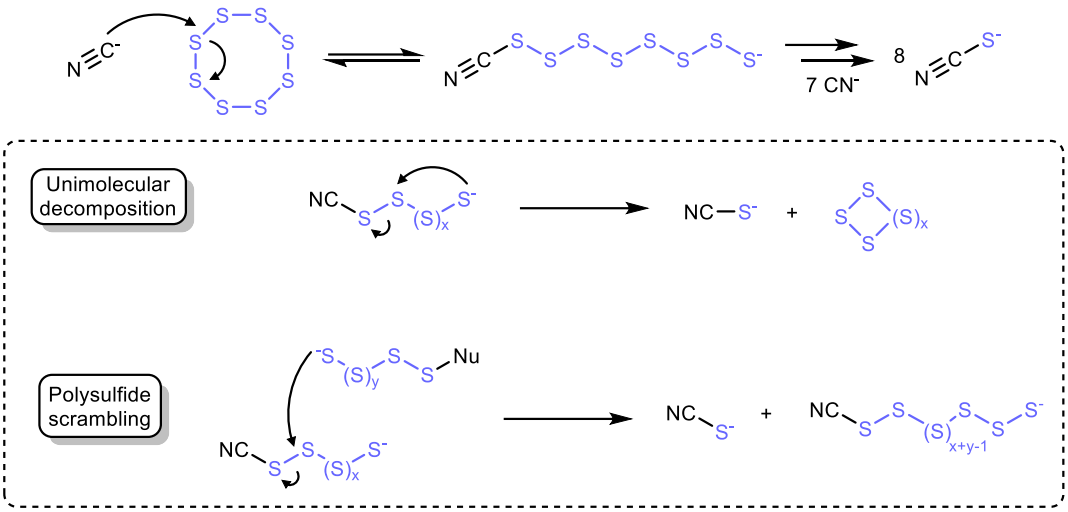

Scheme 10: Unimolecular decomposition (top) and polysulfide scrambling (bottom) as the two main mechanisms for the formation of thiocyanate ions during the reaction of cyanide with sulfur.[149]

2.3.3 Organic Reactions Involving Elemental Sulfur

In the previous section, a number of studies have been presented that have investigated the fundamental interactions of elemental sulfur with bases. It was generally found that bases effect a nucleophilic ring opening of the *cyclo*-S_8 molecule, leading to complex equilibria of sulfur anions, radicals, and sulfur-heteroatom species, which enable elemental sulfur to participate in irreversible chemical reactions such as the sulfurization of cyanide. Indeed, the presence of basic compounds as sulfur activators is frequently utilized in organic reactions involving elemental sulfur. A variety of different interesting reactivities of elemental sulfur in organic reactions has been observed, which will be presented in the following section.

2.3.3.1 Thiol oxidation

Thiols are known to be easily oxidized by elemental sulfur in the presence of bases. In the absence of other reactants, this oxidation leads to the formation of bis(alkyl)polysulfides and hydrogen sulfide.[206–208] The mechanism for thiol oxidation suggested by Vineyard entails initial deprotonation of the thiol, followed by nucleophilic attack on S_8, leading to the formation of an alkyl nonasulfide (Scheme 11). Nucleophilic attack of another thiolate at any point of the sulfur chain leads to the formation of the bis(alkyl)polysulfide and a polysulfide dianion, which is eventually further degraded into hydrogen sulfide.

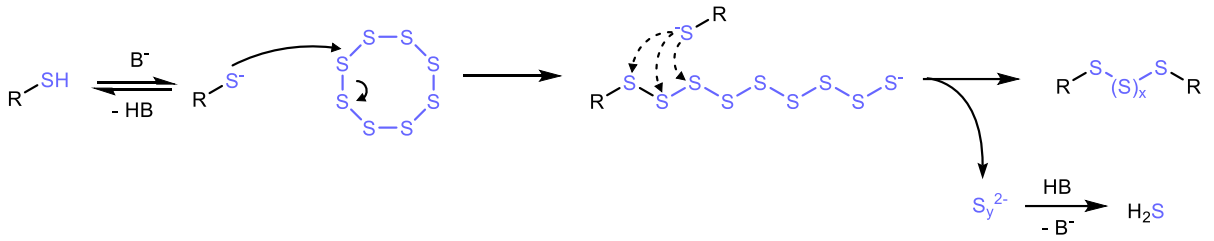

Scheme 11: Proposed mechanism of the oxidation of thiols with elemental sulfur, proposed by Vineyard in Ref. [208].

The length of the sulfur chain in the bis(alkyl) polysulfide product increases with steric hindrance of the thiol and the used equivalents of sulfur and decreases with increasing and deprotonation efficiency, *i.e.* the difference in pK_a of thiol and base. For instance, primary thiols generally form disulfides with stoichiometric amounts of sulfur, while tertiary thiols generate tetrasulfides as the main products.[207] The oxidation of dithiols frequently results in the formation of cyclic polysulfides.[209–211]

2.3.3.2 Oxidation of imines / enamines

A very commonly observed reactivity in organic reactions involving elemental sulfur is the oxidation of imines / enamines by incorporation of sulfur atoms. The Willgerodt-Kindler (WK) reaction, perhaps the oldest organic reaction involving elemental sulfur, is a very typical example of this archetype, first reported by Kindler in 1923 based on an earlier report of Willgerodt in 1889. The "classic" WK reaction is a multicomponent reaction of an araliphatic ketone, a primary or secondary amine and elemental sulfur, yielding a terminal thioamide. The most peculiar feature of this reaction is the migration of the functional group to the end of the aliphatic chain. Notably, many other substrates such as aldehydes or alkynes, among others, form thioamides under similar conditions, which is also sometimes classified as a WK reaction. [60,212,213]

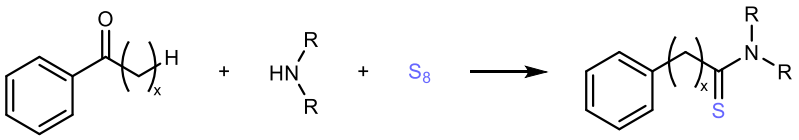

Scheme 12: The "classic" WK reaction of an araliphatic ketone with a secondary amine and sulfur, yielding a terminal thioamide under migration of the functional group.[149]

Despite its long history, the mechanism of this interesting reaction is still not unambiguously clarified. The most widely accepted mechanism was suggested by Carmack *et al*, who performed extensive experimental studies on this reaction (Scheme 13).[214,215]

The initial step of the reaction is the condensation of ketone and amine to form an enamine. The enamine then undergoes sulfur-catalyzed isomerization along the aliphatic chain. The nature of the catalytically active sulfur species could not be determined, although it was found

that many different sulfur sources, such as elemental sulfur, sodium tetrasulfide or dithiobis(morpholine) were equally effective at mediating the transformation. It was suggested that the isomerization proceeds *via* reversible α-thiolation of the enamine by the active sulfur species, yielding an α-thioiminium compound, which is proposed to be in equilibrium with a thiirenium species through intramolecular ring closure under elimination of amine. The isomerization proceeds *via* subsequent ring opening of the thiirenium species by nucleophilic attack of the amine at either carbon atom in its three-membered ring, either regenerating the original α-thioiminium species, or producing its isomeric form.

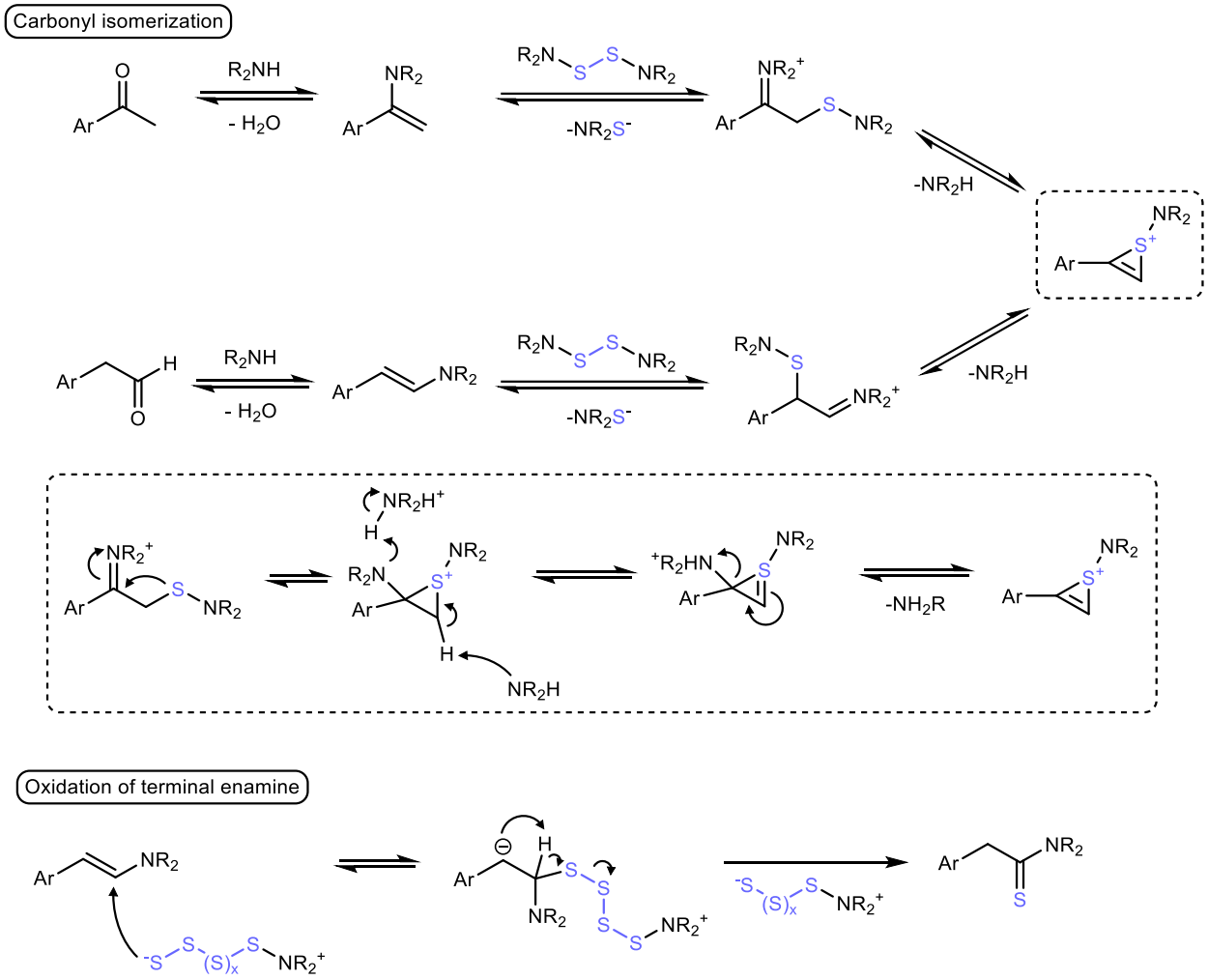

Scheme 13: The Carmack mechanism of the Willgerodt-Kindler isomerization and oxidation of the terminal enamine. (see Ref. [214]).

The mechanism is schematically depicted in Scheme 13 using a dithiobisamine as the catalytically active sulfur species. The reaction is driven by the irreversible oxidation of the terminal enamine to a thioamide, thus removing it from the isomerization equilibrium. It was postulated that this oxidation proceeds *via* nucleophilic attack of an anionic polysulfide on the electrophilic iminium carbon atom. Subsequently, a proton shift to the α-position, which is only possible for the terminal species, followed by extrusion of a shortened polysulfide generates the thioamide (Scheme 13).[214,215]

Other mechanisms have been suggested, although none sufficiently explain the isomerization of the functional group along the aliphatic chain.[149,216,217] A recent review on the chemistry of the trisulfide radical anion has noted that radical mechanisms for the WK reaction have not been sufficiently considered, and has suggested a possible involvement of radicals in the pathways, referring to the detection of such species in sulfur solutions of amines.[188] WK-like transformations are frequently reported in combination with other reactivities. For instance, Nguyen *et al.* reported the synthesis of oxazoles from acetophenones and *o*-aminophenols, which involves initial WK reaction of the aromatic amino function with acetophenone, yielding a thioamide, which then undergoes condensation with the *o*-hydroxy group to yield the oxazole under elimination of hydrogen sulfide (Scheme 14). *N*-methylpiperidine (NMPip) was used as an auxiliary base due to the low basicity of aromatic amines.[218]

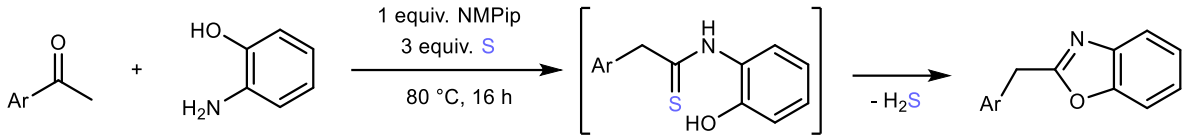

Scheme 14: Willgerodt-Kindler reaction for the synthesis of oxazoles, reported by Nguyen et al.[218].

Depending on the substrates, other interesting reactions can occur in competition to the WK reaction. In 2007, Neckers *et al.* reported a one-pot synthesis of 2-aminobenzothiophenes from 2-chloro-5-nitroacetophenone. Biehl *et al.* performed the same reaction under microwave conditions and suggested a mechanism for the transformation, involving WK-type formation of a terminal thioamide from the acetophenone, followed by cyclization *via* S_NAr of the chloride substituent by the thiocarbonyl sulfur (Scheme 15, upper pathway).[219,220] However, in 2010, Androsov *et al.* found that the products of the reaction had been incorrectly characterized, reporting that the synthesis had yielded the corresponding 3-aminobenzothiophenes instead.[221] It was suggested that enamine reacts with sulfur to form a thiolate in α-position by reaction with elemental sulfur, which quickly undergoes intramolecular S_NAr in favor of the Willgerodt-Kindler isomerization, thus yielding the 3-substituted product (Scheme 15, lower pathway).

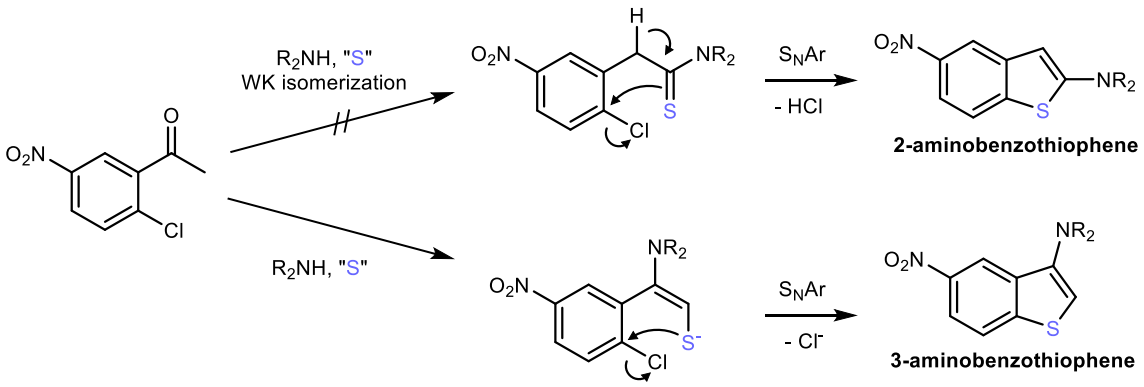

Scheme 15: Synthesis of aminobenzothiophenes, reported by Neckers et al., Biehl et al. and Androsov et al., and the postulated mechanistic intermediates leading to either isomer. Reportedly, only the 3-substituted product is formed.[219–221]

The Asinger reaction, a multicomponent reaction of aliphatic ketones, ammonia and elemental sulfur to generate thiazolines, is another noteworthy example for a reaction which reportedly involves the α-thiolation of imines / enamines (Scheme 16).[222,223]

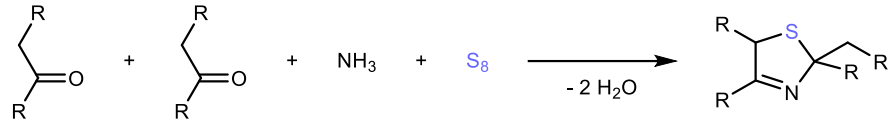

Scheme 16: Schematic representation of the Asinger reaction.[149]

2.3.3.3 Oxidations of activated C-H positions

In many organic transformations involving base-activated elemental sulfur, oxidative transformations at the α-positions of electron withdrawing groups are observed. In most cases, this entails the effective replacement of an H substituent with a thiol function. If the β-position bears H-atoms, the formation of α,β-unsaturated compounds by elimination of hydrogen sulfide is also frequently reported. In some cases, further conversion of the α-thiol to an α-thione is suggested as well. The substrates for such reactions include for instance the α- and vinylogous positions of carbonyl or cyano functions, as well as benzylic positions.

A typical example is the Gewald reaction, first reported in 1966, which is one of the most well-known organic reaction involving elemental sulfur. In its most prevalent form, it is a base-catalyzed three-component reaction between enolizable carbonyl compounds, α-acidic nitriles and elemental sulfur, yielding 2-aminothiophenes under mild conditions. The scope of the nitrile component of the Gewald three-component reaction includes highly C-H acidic nitriles such as dicyanomethane, α-cyanoesters, α-cyanoketones or α-cyanocarboxamides.[224,225] The proposed mechanism entails the initial Knoevenagel condensation of the carbonyl component and the nitrile. The resulting Knoevenagel product is then deprotonated by the base in the γ-position and then thiolated by nucleophilic attack on S_8 and elimination of S_7. The final step is the cyclization by intramolecular nucleophilic attack of the thiolate on the nitrile group, yielding an imine, which tautomerizes to the final product under aromatization (Scheme 17). This pathway has recently been confirmed as the most favorable by computational investigations conducted by Champagne *et al.* [224–226]

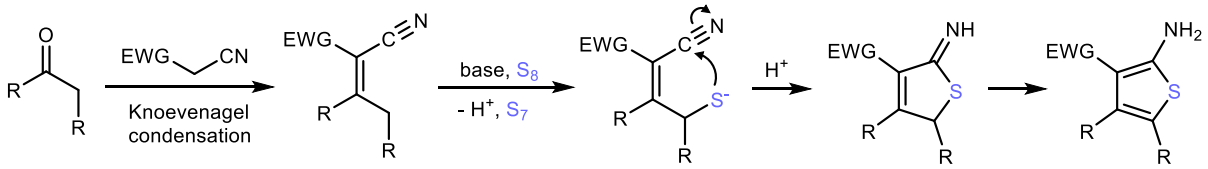

Scheme 17: Mechanism of the Gewald reaction.[224–226]

Enolates are often proposed to nucleophilically attack elemental sulfur, leading to the formation of α-mercaptocarbonyl compounds, which then undergo further reactions. For instance, Nguyen *et al.* reported a series of Gewald-type syntheses of 5-acylaminothiophenes using chalcones, nitriles and elemental sulfur. In these reactions, Michael addition of the cyano component to the chalcone was reported as the first step. Notably, the Michael adduct obtained in these cases are essentially the α,β-saturated equivalent of a Knoevenagel product obtained during a "regular" Gewald reaction. Still, 2-aminothiophenes are obtained as products, indicating that an additional oxidation step must take place under release of hydrogen sulfide.[227,228]

Mechanistically, all reports propose the formation of an enolate by deprotonation of the Michael adduct and its subsequent attack on elemental sulfur, forming a thiolate in the α-position of the carbonyl group. This is followed by intramolecular nucleophilic attack onto the cyano function similarly to the Gewald reaction, yielding a dihydrothiophene in this case. Oxidation to the final product is postulated by another deprotonation/thiolation sequence at the α-position of the carbonyl function, followed by elimination of hydrogen sulfide, driven by aromatization (Scheme 18).[227,228] Several variations of this reaction using different C-H-acidic compounds have been reported, yielding a variety of different products such as pyridinethiones, cyanothiophenes or furans. These reactions are generally suggested to proceed *via* similar pathways, involving deprotonation of the substrates, followed by thiolation with elemental sulfur and subsequent cyclizations / oxidations.[229–235]

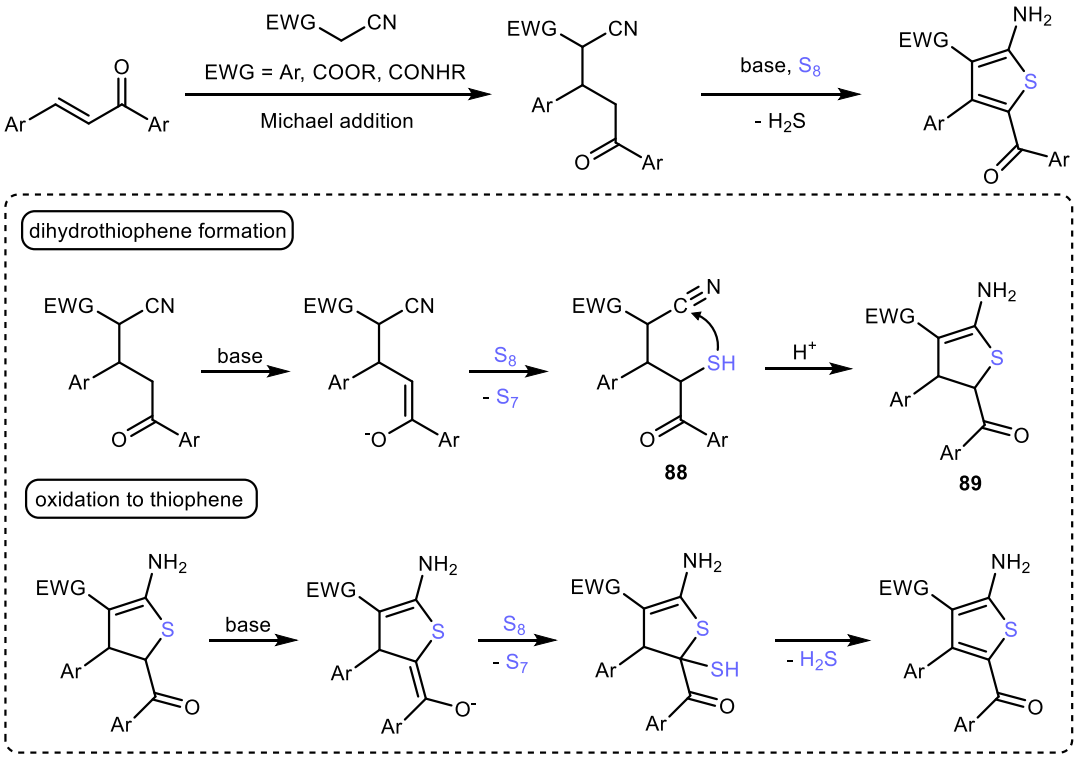

Scheme 18: Proposed mechanism for the oxidative Gewald reaction of Michael adducts of cyano compounds and chalcones, reported by Nguyen et al.. [227,228]

The benzylic position possesses characteristic properties compared to other sp^3-carbon positions due to its increased capacity to stabilize radicals, carbocations and carbanions. In many cases, it has been observed that benzylic positions react readily with activated sulfur, resulting in the formation of thiocarbonyl functions.

Numerous reports feature the oxidative homocoupling of benzylic amines in the presence of elemental sulfur, forming *N*-substituted thioamides.[236–238] Nguyen *et al.* report the selective oxidative homocoupling of benzylamine to *N*-benzylthiobenzamide at temperatures of 110 °C, achieving almost full conversion after 16 hours (Scheme 19, reaction 1).[238] Using 2-phenethylamine instead, they also observed formation of the corresponding homocoupled thioamide, although higher temperatures of 150 °C were required, illustrating the particular reactivity of the benzylic position (Scheme 19, reaction 2). Due to these different reactivities, a synthetically useful cross-coupling between benzylamines and non-benzylic amines could be established, providing access to a wide range of thioamides (Scheme 19, reaction 3). It was noted that benzylic amines bearing electron-withdrawing substituents reacted more efficiently.

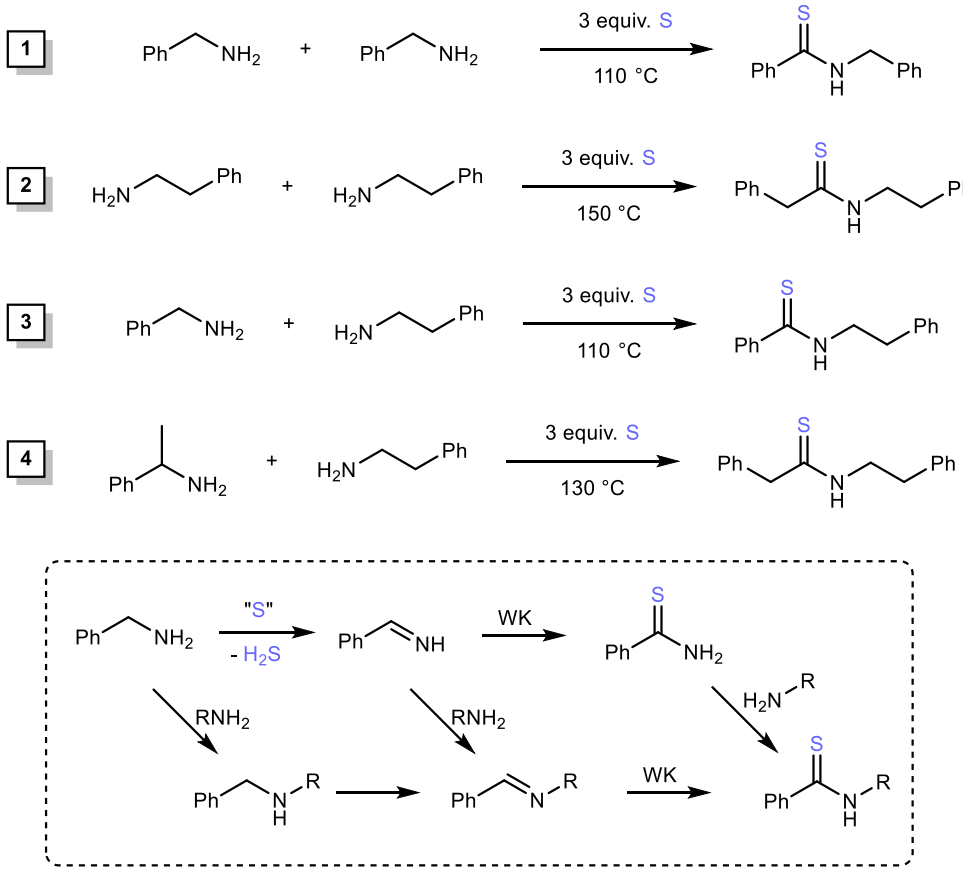

Scheme 19: Oxidative coupling of amines to thioamides, reported by Nguyen et al.., along with suggested pathways that lead to the products.[238]

A mechanism was proposed, suggesting oxidation of benzylamine to benzylideneimine as the first step. From the imine, two main pathways to the product were proposed, the first involving oxidation of the imine to the corresponding thioamide, followed by trans-thioamidation,

yielding the final product. The second pathway involves alkylation of the imine, followed by oxidation to the final thioamide. Earlier reports suggest initial homocondensation of the amines to the corresponding secondary amines under release of ammonia (Scheme 19).[236,237] Interestingly, 1-phenethylamine yielded the same 2-phenylthioacetamides obtained when 2-phenethylamine was used, indicating an intermediate Willgerodt-Kindler rearrangement under the reaction conditions and confirming the involvement of imines in the pathway (Scheme 19, reaction 4).[238]

Wang and Wei *et al.* provided further insight into the oxidation of benzylic amines by elemental sulfur, suggesting the involvement of radicals when the reaction is carried out in amide-based solvents such as DMF or *N*,*N*-dimethylpropyleneurea (DMPU). It was reported that radical anions can be formed from the interactions of amide solvents and sulfur or sulfide salts at elevated temperatures of 90 °C, also forming trisulfide radical anions (Scheme 20). The radical pathway was further underlined by control experiments with radical scavengers.

It was suggested that benzylic amines are oxidized to the imine by radical H-abstraction, forming a benzyl radical, followed by single-electron-transfer, yielding the imine. DFT calculations further reinforced the particular character of the benzylic position, indicating that radical H-abstraction is exergonic for benzylic substrates. For non-benzylic positions, it was found that radical formation is both endergonic and kinetically disfavored *via* a higher activation barrier.[239] Furthermore, the involvement of the $S_3^{\bullet-}$ in the Willgerodt-Kindler oxidation of imines to thioamides was suggested in this report.

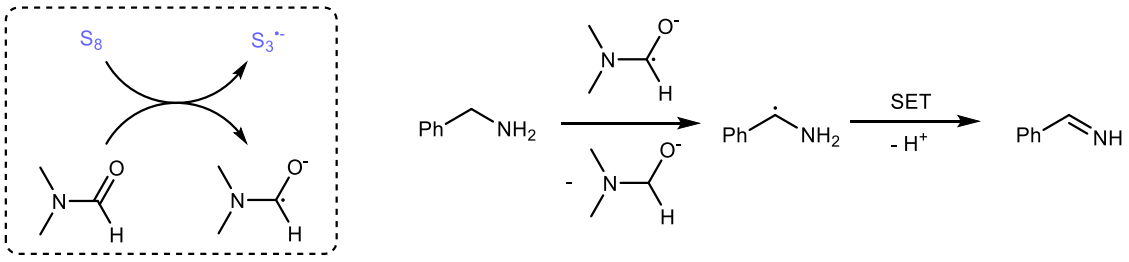

Scheme 20: Radical mechanism for the benzylic oxidation of amines to imines, suggested by Wei et al. in Ref. [239].

Benzylic positions activated by electron-withdrawing substituents, for examples those present in picoline derivatives, benzyl halides or phenylacetonitriles, are especially readily oxidized by elemental sulfur, with synthetically useful transformations reported for such substrates in numerous instances.[240–244]

2.3.3.4 Oxidation of Alkenes and Alkynes

Several oxidative transformations of alkenes and alkynes in the presence of base-activated elemental sulfur have been described. Alkynes are known to undergo WK-like transformations

under similar conditions as ketones or aldehydes, similarly leading to terminal thioamides. Carmack *et al.* reported that terminal aliphatic and aromatic alkynes react with morpholine and sulfur under WK conditions, yielding the corresponding terminal thiomorpholides.[245,246] It was proposed that the electron-rich triple bond reacts with morpholine octasulfide, forming the same thiirenium intermediate that is proposed as part of the mechanism of the Willgerodt-Kindler reaction of ketones (compare Scheme 13), thus producing the thioamide in an analogous mechanism (Scheme 21).[214]

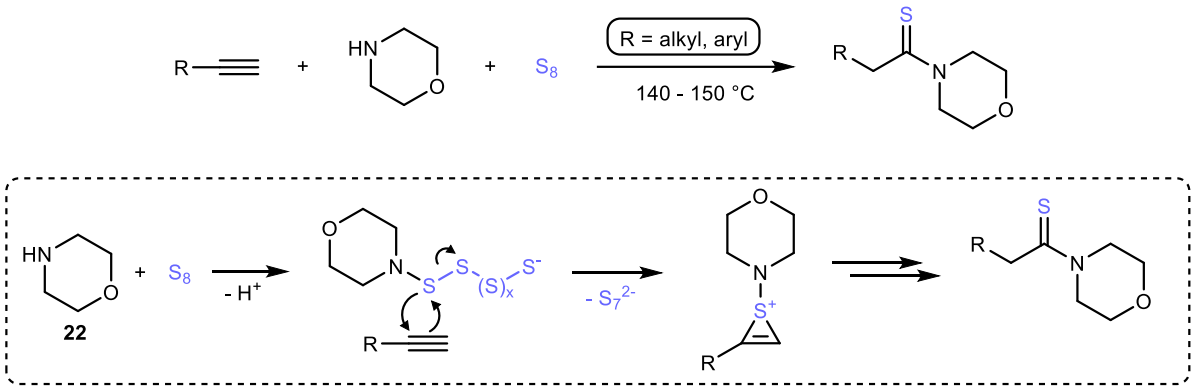

Scheme 21: Mechanism for the synthesis of thioamides from alkynes, proposed by Carmack et al. in Ref. [214].

Nguyen *et al.* further elaborated the synthetic methodology of the alkyne-WK reaction, achieving the reaction at significantly lower temperatures of 60 °C for a wide range of primary and secondary aliphatic and aromatic amines.[247,248] Interestingly, also internal alkynes were demonstrated to react to terminal thioamides, indicating that a WK isomerization is also possible with alkynes as the original substrates. Control experiments further indicated that in the absence of either reactant, no reaction occurred, suggesting that hydroamination or thiolation of the alkyne are not involved in the pathway.

Lei *et al.* reported that conjugated diynes, such as diphenyldiacetylene, react with elemental sulfur and KO^{t}Bu already at room temperature in DMF, forming 2,5-disubstituted thiophenes.[249] It was concluded by the authors that the trisulfide radical anion $S_3^{\bullet-}$ was the key intermediate in this transformation, being detected in EPR studies. The reaction was completely inhibited by radical scavengers such as tetramethylpiperidinoxyl (TEMPO). The involvement of $S_3^{\bullet-}$ was further evidenced by a similar synthesis using potassium sulfide in DMF as the sulfur source.[250] Experiments with deuterated solvents further confirmed that the hydrogen substituents of the thiophene ring are incorporated *via* H-abstraction from solvent molecules. Lei *et al.* proposed a mechanism involving the addition of $S_3^{\bullet-}$ to one of the triple bonds, followed by H-abstraction from the solvent, yielding an enethiolate. This is followed by nucleophilic 5-endo-dig ring closure with the other triple bond, yielding a thiophene anion, which is protonated by solvent molecules, yielding the thiophene product (Scheme 22).

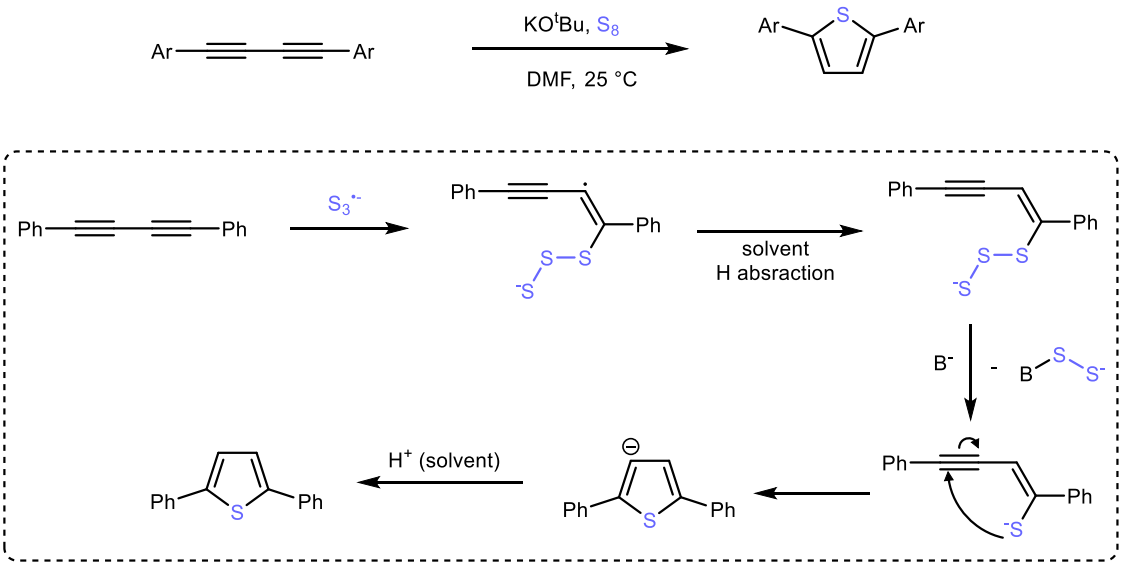

*Scheme 22: Synthesis of 2,5-disubstituted thiophenes **180** from conjugated diynes **179**, reported by Lei et al. in Ref. [249].*

Another interesting reaction from a mechanistic point of view is the formation of 1,4-dithiins from ynones in the presence of potassium carbonate and elemental sulfur at temperatures as low as 0 °C, reported by Kong and Li (Scheme 23).[251] It was observed that both 2,5- and 2,6-homosubstituted dithiins were generated, with the 2,5-isomers being the clear main products, especially when conducting the reaction at low temperatures, producing isomeric ratios up to 10:1. Both organic and inorganic bases were effective for the transformation.

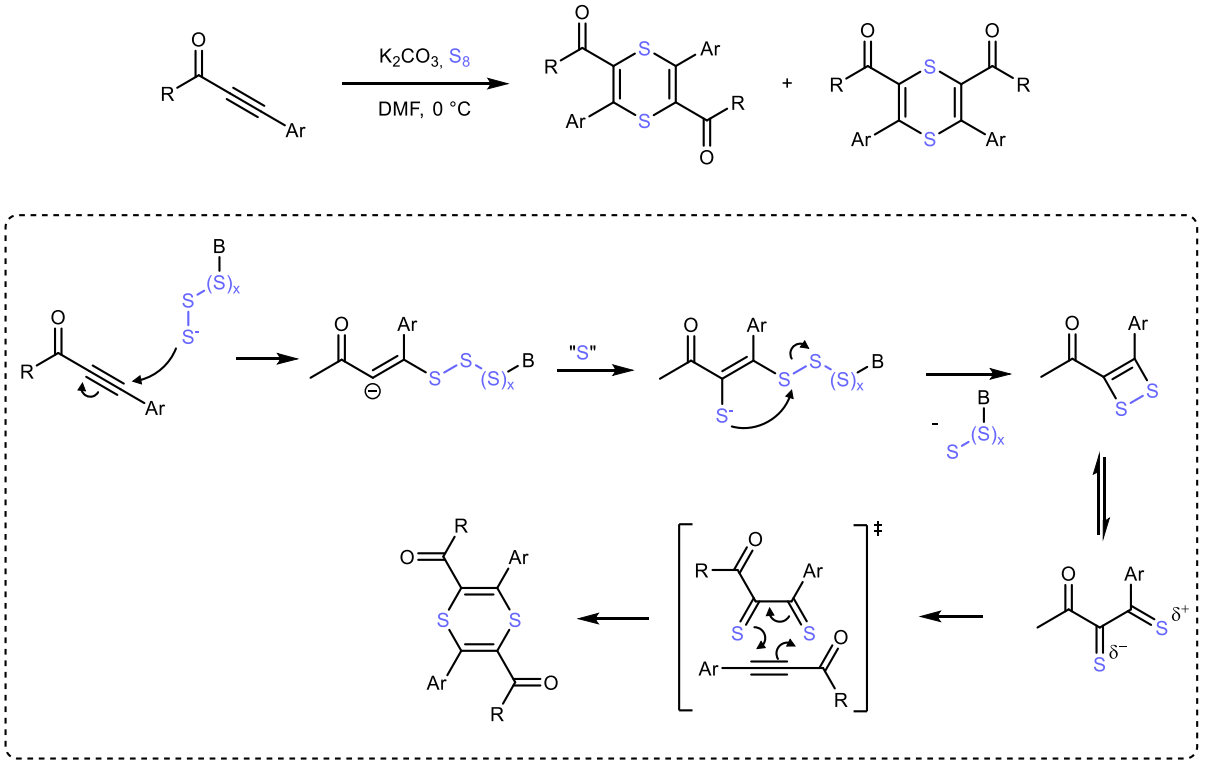

Scheme 23: Proposed mechanism for the formation of 1,4-dithiins from ynones, reported by Kong and Li in Ref. [251]. The postulation of dithiete intermediate is based on a previous observation by Nakayama et al.. from Ref. [252].

The mechanistic postulate involves the formation of a 1,2-dithiete intermediate *via* nucleophilic Michael addition of a polysulfide, generated form sulfur and base, to the ynone, followed by further thiolation of the resulting carbanion and ring-closure (Scheme 23). The suggestion of a dithiete intermediate was based on earlier reports by Nakayama *et al.* on stable dithietes, formed from sterically hindered alkynes such as bis(*tert*-butyl)acetylene and elemental sulfur at very high temperatures.[252,253] The dithiete intermediate is proposed to be in equilibrium with its open dithione form, which can undergo a hetero-Diels-Alder reaction with another alkyne, yielding the final dithiin product. The preferred formation of the 2,5-isomer was attributed to electronic reasons.

Terminal alkenes such as styrenes reportedly also react in WK-type reactions to form terminal thioamides, although the reaction requires higher temperatures and is accompanied by hydrogen sulfide evolution due to the additional oxidation step.[245,246] Darabi *et al.* compared the reactivity of several substrates under Willgerodt-Kindler conditions, and found that styrenes generally give lower yields than the corresponding alkynes or acetophenones.[254]

A series of highly interesting reactions involving the cleavage of carbon-carbon multiple bonds have been reported. Xu and Liu *et al.* found that the reaction of phenylacetylenes or styrenes with formamides in the presence of a large excess of sulfur and potassium phosphate yielded thiobenzamides, resulting from the cleavage of the alkyne triple bond or alkene double bond (Scheme 24, top).[255] It was found that also internal alkynes/alkenes could undergo the cleavage reaction, yielding thioamides derived from both alkylidyne/alkylidene fragments. Control experiments involving terminal alkynes revealed that using amines instead of formamides did not lead to cleavage and the expected Willgerodt-Kindler product, a phenylthioacetamide, was generated.

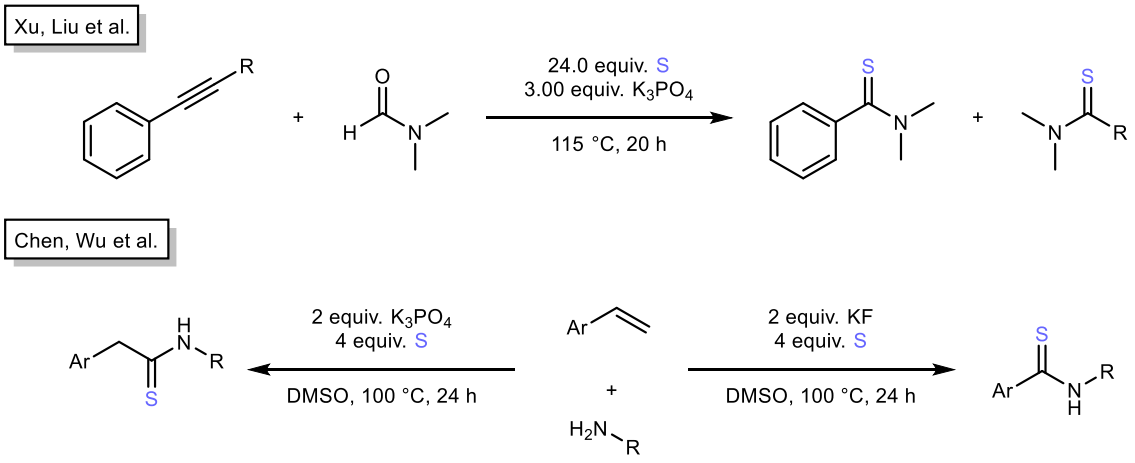

Scheme 24: Cleavage thioamidation reactions reported by Xiu, Liu et al. (top) and Chen, Wu et al. (bottom). [255],[256]

The cleavage of alkenes was also observed by Chen and Wu *et al.* in their report on the thioamidation of styrenes with amines (Scheme 24, bottom).[256] They found that the cleavage reaction competes with the expected thioamide formation, depending on the used base. While using K_3PO_4 resulted in complete selectivity towards the uncleaved product, the use of KF exclusively yielded the cleaved thioamide. Other bases produced mixtures of both. No comment on the exact nature of the generated byproduct resulting from the cleavage has been made. Furthermore, the authors noted that the reasons for the chemoselectivity exerted by the bases remained unclear.

2.3.3.5 Carbene thionation

Carbenes are generally transient species with high electrophilic character due to the electron sextet at the carbon center. Reactions of carbenes with elemental sulfur result in the formation of C=S double bonds.

Carbon monoxide possesses carbenoid character at its carbon atom, making it susceptible to nucleophilic attack. Mizuno *et al.* published a series of reports involving the *in situ* reaction of carbon monoxide with elemental sulfur under basic conditions, forming carbonyl sulfide COS or chemically equivalent species.[257–261] It was for instance reported that primary amines react with sulfur and carbon monoxide under formation of ammonium thiocarbamates.

Isocyanides are isoelectronic with carbon monoxide and thus possess the same characteristic amphiphilic character at their carbenoid carbon atoms. Lipp *et al.* discovered that isocyanides and sulfur react with amines or hydrazines, forming thioureas and thiosemicarbazides, respectively.[262] Al-Mourabit *et al.* further optimized the reaction and suggested several possible pathways. The most likely mechanism involves the activation of elemental sulfur by the amine and subsequent nucleophilic attack of the formed polysulfide on the isocyanide carbon. Elimination of a shortened polysulfide species results in the formation of an intermediate isothiocyanate, which undergoes rapid nucleophilic addition with the amine (Scheme 25).[263,264]

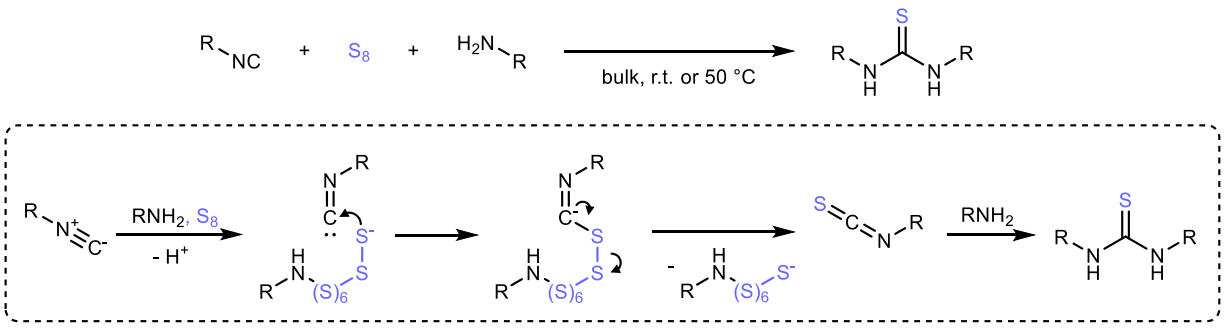

Scheme 25: Possible pathway for the synthesis of thioureas from isocyanides, amines and sulfur.[263,264]

The formation of an intermediate isothiocyanate in the pathway is evidenced by multiple reports of isothiocyanate syntheses from isocyanides and sulfur/base in the absence of nucleophilic compounds that can undergo follow-up reactions with the isothiocyanate. Ábrányi-Balogh *et al.* have reported a synthesis of thiourethanes from isocyanides, alcohols and elemental sulfur using sodium hydride as the activating base. In the absence of alcohol, isothiocyanates were the sole products. No reaction occurred in the additional absence of base (Scheme 26).[265] Meier *et al.* found that isothiocyanates could be efficiently synthesized form isocyanides and sulfur using catalytic amounts of organobases under mild conditions (Scheme 26). It was found that higher basicity correlated with the catalytic effect of the base, 1,8-diazabicyclo[5.4.0]-undec-7-ene (DBU) being the most effective among the examined catalysts in loadings as low as 2 mol%.[266] These reports indicate that the activation of elemental sulfur with bases is crucial for the formation of isothiocyanates form isocyanides under mild conditions. Still, there have been reports of the synthesis of isothiocyanates from isocyanides and sulfur without any basic additives, albeit requiring higher temperatures and longer reaction times (Scheme 26).[267,268] It has been proposed that this case, the isocyanide reacts as a carbon-centered nucleophile at elevated temperatures.

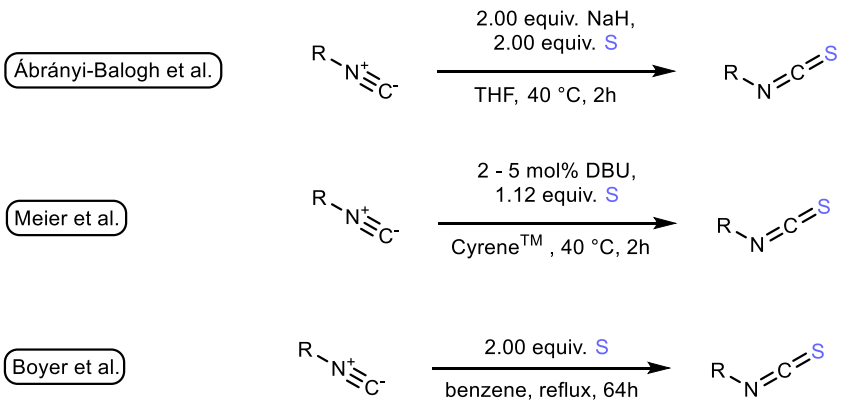

Scheme 26: Reported syntheses of isothiocyanates from isocyanides and elemental sulfur.[265–267]

2.3.3.6 Reductions

While elemental sulfur generally acts as an oxidizing agent in most organic reactions, a range of sulfur-mediated reduction reactions have been reported as well. Several reports feature the reduction of nitroarenes to the corresponding anilines. Oae *et al.* reduced nitrobenzene and other nitroarenes with elemental sulfur in amine solvents.[269] It was suggested by the authors that the amine solvent acts as a cooxidant, being oxidized to the corresponding imine (Scheme 27). The potential involvement of radicals in the mechanism was suggested.

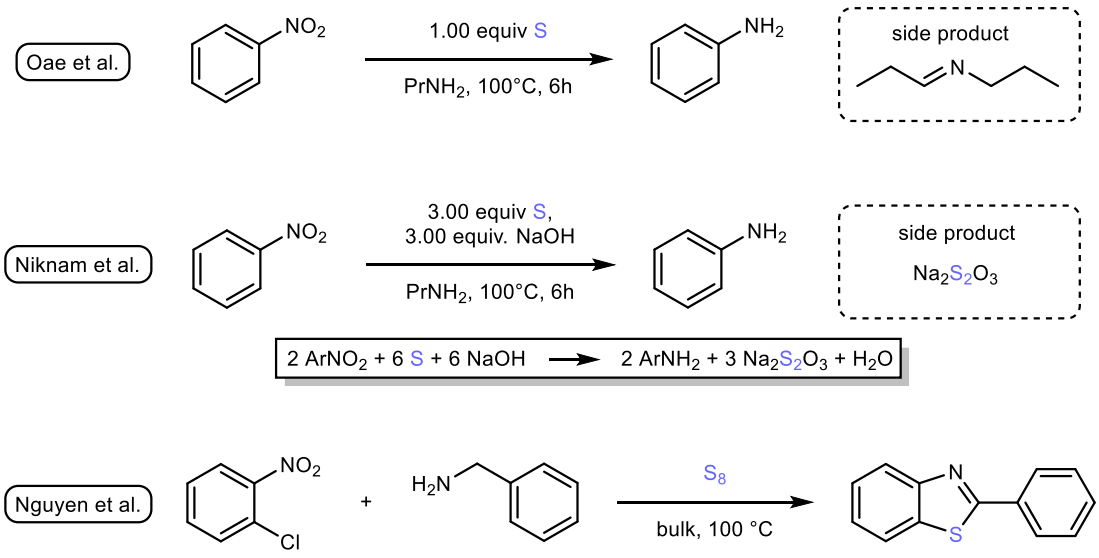

Scheme 27: Reduction of nitroarenes to anilines with elemental sulfur, reported by Oae et al. (top) and Niknam et al. (middle) and nitro-redox coupling of o-halonitrobenzenes and benzylamines reported by Nguyen et al. (bottom).[269–272]

Niknam *et al.* reported the reduction of nitroarenes with elemental sulfur, mediated by NaOH, and identified thiosulfate anions as the oxidized sulfur species. A stoichiometry for the reaction was proposed, indicating that a threefold excess of sulfur and hydroxide base is necessary (Scheme 27).[270,271] The reduction of nitroarenes to anilines with elemental sulfur is presumably closely related to the Zinin reduction, which instead uses sodium sulfide or polysulfides as the reducing agents. The mechanism for the reduction is proposed to proceed in stepwise fashion *via* intermediate nitrosoarenes and arylhydroxylamines, with the initial reduction of the nitroarene being the rate-determining step.[273]

Synthetic applications of the reduction of nitroarenes were elaborated by Nguyen *et al.* by combining this reactivity with other typical reactivities associated with elemental sulfur. For instance, a reported nitro-redox coupling of *o*-halonitrobenzenes with benzylamines combines the nitro reduction with the transamination and benzylic oxidation of benzylamines, yielding benzothiazoles as the products. (Scheme 27).[272]

The above presented examples highlight the great versatility of elemental sulfur as a reagent in organic reactions. However, there is still a large degree of diversity and ambiguity in the suggested mechanistic pathways of these reactions, even for similar transformations. The mechanisms of long-established reactions such as the Willgerodt-Kindler reactions which has been known for decades, have not been unambiguously clarified. Clearly, further investigations are necessary in order to fully understand and unlock the potential of elemental sulfur in organic synthesis.

2.3.4 Elemental Sulfur in Polymer Synthesis

Like in organic synthesis, elemental sulfur is part of long-established processes in the production of polymeric materials. In recent times, its nature as a cheaply available waste material and the problems associated with its long-term storage have inspired research on new possible applications of sulfur in the context of polymer and material science. The presence of sulfur-containing functional groups in polymers can induce interesting and useful properties like self-healing, metal ion binding or unique electronic and optical properties.[18,158,274–277] Vulcanization is a noteworthy example of an industrially relevant process that uses elemental sulfur, mainly being used for the manufacture of car tires. Its discovery is attributed to Charles Goodyear in 1839.[278] Vulcanization entails the crosslinking of different unsaturated rubbers with sulfur bridges, natural rubber mainly consisting of linear polyisoprene units, increasing the thermal and chemical resistance of the material and inducing characteristic elasticity.[279] Typically, vulcanized rubbers contain approximately 2 weight% sulfur.[276] Vulcanization is considered to proceed most likely *via* a radical mechanism, involving thermally induced homolytic sulfur ring opening.[280] The crosslinking occurs by radical H-abstraction in the allylic position, where sulfur atoms are subsequently incorporated and undergo radical addition to a double bond of another unsaturated polymer chain (illustrated Scheme 28 for polyisoprene).[281,282] The use of activators, such as metal oxides, amines or several sulfur-containing organic molecules such as thiurams, accelerate the otherwise very slow vulcanization process, allowing it to proceed at lower temperatures.[281,283]

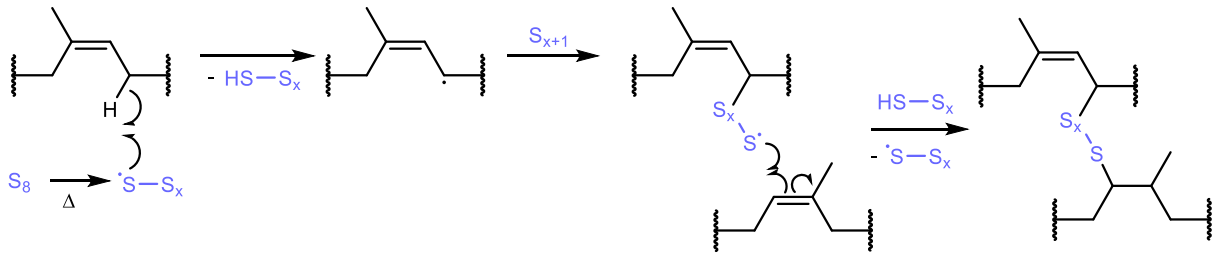

Scheme 28: Exemplary radical mechanism for the sulfur crosslinking of polyisoprene during vulcanization.[281,282]

So-called “inverse vulcanization” (IV) is another, more recently emerging method for the synthesis of polymeric materials using elemental sulfur, first reported by Pyun *et al.* in 2013.[17,284] IV entails the crosslinking of polymeric sulfur chains with olefins, thus effectively swapping the roles and the stoichiometries of sulfur and alkene as compared to “regular” vulcanization (Scheme 29). The formation of biradical polysulfur chains occurs *via* homolytic S_8 ring opening when exposing elemental sulfur to temperatures higher than 159 °C. In the original report, 1,3-diisopropenylbenzene (DIB) was used as the comonomer, and the polymerization was conducted by simple mixing of both components in the desired ratio and

heating the mixture to 185 °C, with vitrification of the melt observed already after 5 minutes. It was found that, in contrast to polymeric sulfur which is unstable when cooled to ambient conditions and slowly reverts to orthorhombic S_8, the materials obtained *via* IV were stable against this degradation. IV is thus generally very simple to operate, and allows the effective synthesis of materials with very high sulfur contents around 90 weight%. Furthermore, the properties of the materials could be easily tuned by adjusting the monomer ratio.

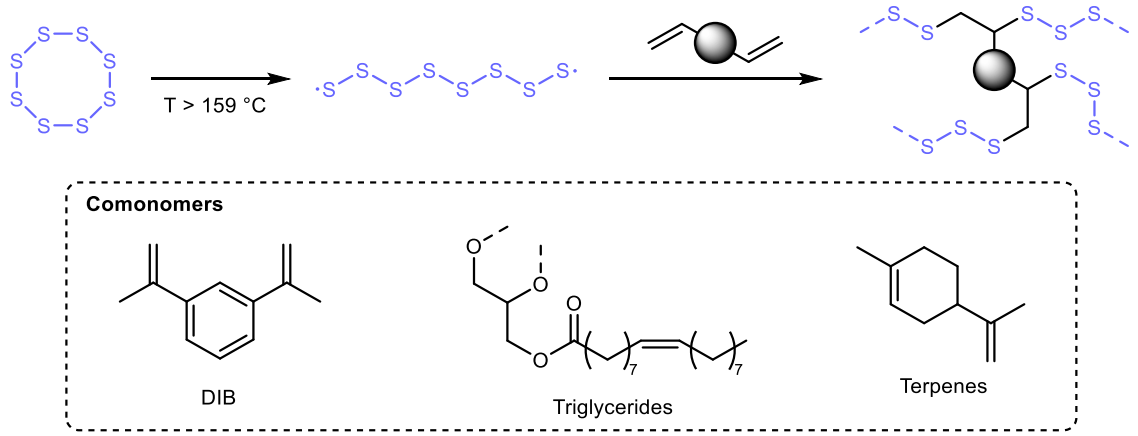

Scheme 29: Schematic representation of inverse vulcanization.

The required high temperatures narrow the scope of viable comonomers and lead to undesired side reactions such as hydrogen sulfide formation and thermal monomer degradation. Several catalytic approaches have been developed that allow IV to be conducted at lower temperatures and enable the incorporation of a wider range of comonomers. For instance, akin to their frequent usage in organic synthesis (see section 2.3.3), the use of amines can promote the activation of elemental sulfur and accelerate the IV process.[285] Pyun *et al.* reported a significant acceleration of the IV of styrene by adding 1 mol% of 4-aminostyrene as additional comonomer, allowing the polymerization to proceed already at 110 °C.[286] Hasell *et al.* reported the use of several metal *N*,*N*-diethyldithiocarbamates as effective catalysts for IV, allowing the use of previously unreactive methacrylates as crosslinkers at a temperature of 135 °C.[287] More recently, photoinduced or mechanochemical IV methods have been reported to proceed at room temperature, which enabled the copolymerization of sulfur with gaseous olefins such as isoprene.[288,289]

As already mentioned in section 2.2, carbon-carbon double bonds are a very common functionality found in renewable feedstock. As such, numerous bio-derived crosslinkers have been used in the synthesis of IV materials. For instance, Chalker *et al.* reported the direct use of several plant oils containing unsaturated fatty acids such as canola oil and castor oil, or even recycled cooking oils, as IV comonomers.[276,290,291] Terpenes, such as limonene, are another readily available renewable source of olefins and have similarly been employed in IV.[292] Other prominent renewable feedstocks, such as cellulose or lignin, do not inherently contain alkene

functions, but can be made accessible to IV polymerization *via* functionalization with double bond-containing moieties.[293,294] For instance, Meier *et al.* reported the synthesis and subsequent IV of fatty acid cellulose esters.[293]

Due to their unique and tunable properties, materials synthesized *via* IV have shown several promising application possibilities. The high sulfur content equips IV materials with high refractive indices and infrared transparency, enabling potential application in infrared (IR) optics, for instance as lenses for thermal imaging.[17,295] Furthermore, IV materials have been suggested as possible replacement for elemental sulfur in Li-S batteries due to similar performance and improved cycle stability.[159,296] Possible applications in water purification have been demonstrated as well, with numerous studies reporting the removal of toxic metal ions such as Hg^{2+} from aqueous solutions.[290,293]

Overall, the IV methodology exhibits high atom economy, can effectively utilize abundant and benign waste materials as well as renewable feedstock and generally does not requiring the use of auxiliary substances. The recent advances made in enabling milder reaction conditions, combined with the useful properties the products, make IV a highly promising procedure in the context of sustainable chemistry.[277,297]

Other strategies to use elemental sulfur for the synthesis of polymeric materials involve nucleophilic reactions which generate polysulfide nucleophiles as the active species when elemental sulfur is employed as an additional comonomer, thus leading to the formation of sulfur chains during the polymerization. For instance, Penczeck *et al.* investigated the anionic polymerization of thiiranes in the presence of elemental sulfur. It was found that elemental sulfur could be efficiently copolymerized with the thiiranes, yielding polysulfide linkages in the final polymer in addition to the thioether groups resulting from the thiirane homopolymerization (Scheme 30, top).[298–300]

Mutlu *et al.* reported the synthesis of polydithiocarbonates in a DBU-mediated polycondensation of dithiols with carbonyldiimidazole (CDI).[301] When conducting the polymerization in the presence of elemental sulfur, polymers with a higher sulfur content were obtained, where sulfur was incorporated *via* its interaction with the thiolate anions formed by deprotonation of the dithiol monomers (Scheme 30, bottom).

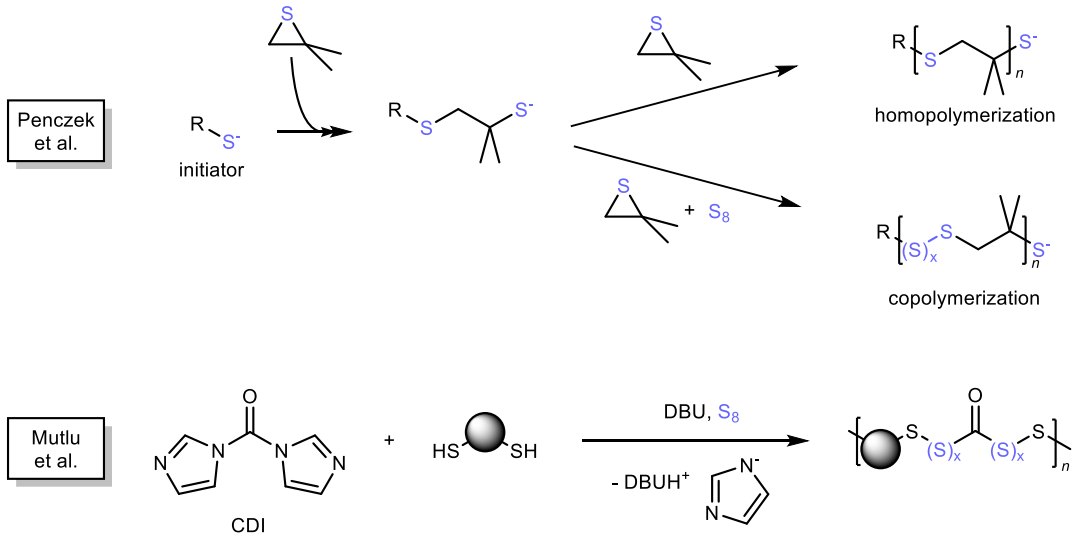

Scheme 30: Copolymerization of elemental sulfur in nucleophilic polymerization reactions, reported by Penczek et al. (top) and Mutlu et al. (bottom).[299,301]

Plajer *et al.* reported the sequence-selective lithium-catalyzed terpolymerization of elemental sulfur with epoxides and carbon disulfide or thioanhydrides, where sulfur is incorporated into the polymer backbone by interaction with a thiolate nucleophile formed *via* a lithium-mediated S-O-exchange during the polymerization (Scheme 31).[302,303]

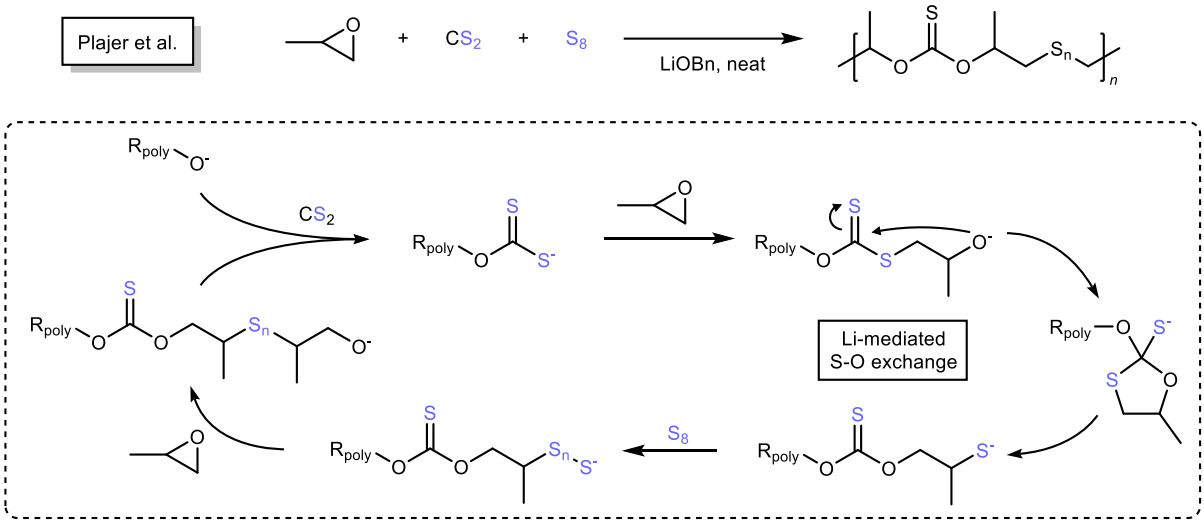

Scheme 31: Mechanism for the terpolymerization of elemental sulfur, carbon disulfide and propylene oxide, reported by Plajer et al.[302]

Elemental sulfur can also be utilized in polymer synthesis by transferring the synthesis protocols of organic reactions involving elemental sulfur (see chapter 2.3.3) to bifunctional substrates. In contrast to strategies such as IV, such multicomponent polymerization (MCPs) allow the synthesis of sulfur-containing polymers with tailored functional groups.

For instance, polythioamides (PTAs) were synthesized using several different Willgerodt-Kindler type polycondensations of difunctional amines, elemental sulfur and a variety of different reactants. Kanbara *et al.* reported the synthesis of a range of PTAs from aromatic

dialdehydes in DMF at 115 °C, using both primary and secondary amines and obtaining polymers with number average molecular weights (M_n) up to 38.2 kg mol^{-1} (Scheme 32, top).[304,305]

Tang *et al.* reported several PTAs syntheses from difunctional alkynes or arylacetic acids (Scheme 32 middle).[306–308] Alkynes were found to undergo polymerization at 90 °C without the need for additional catalysts. The highest molecular weights were achieved using pyridine as the solvent.[306] With electron-deficient alkynes, the polymerization proceeded already at room temperature in some cases.[307] The decarboxylative synthesis of PTAs from bifunctional arylacetic acids required the use of potassium carbonate as auxiliary base and proceeded best at 100 °C in DMSO.[308]

Chen *et al.* reported the synthesis of PTAs by homocoupling oxidation of benzylamines without any additional starting material (Scheme 32 bottom).[309]

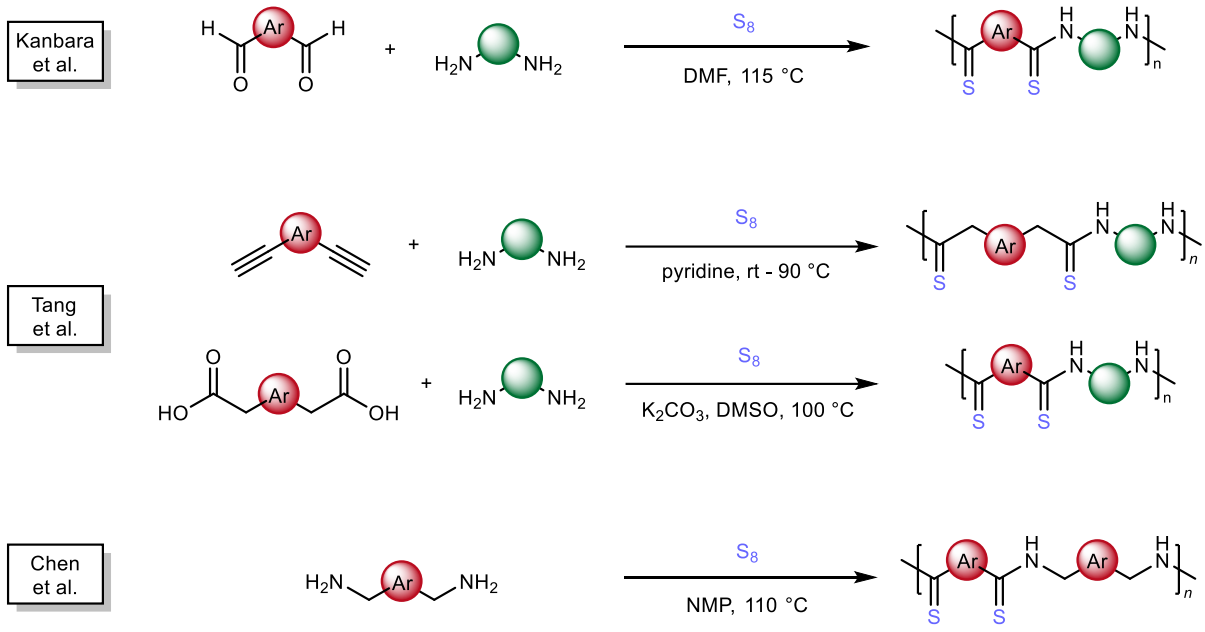

Scheme 32: Polythioamide syntheses reported by the groups of Kanbara (top), Tang (middle) and Chem (bottom).[305–309]

PTAs were demonstrated to exhibit several interesting and unique properties and application possibilities. For instance, Tang *et al.* found several of their synthesized PTA to exhibit solid-state fluorescence, despite the absence of conventional fluorophores in the backbone. This phenomenon has been attributed to clustering-induced emission, a behavior observed also for other polymer classes containing polar, electron-rich functional groups.[306,310] Furthermore, Tang *et al.* reported very high extraction efficiency for Au^{3+} ions from aqueous solutions for PTAs even in the presence of other ions, demonstrating potential application for gold recovery from electronic waste.[308]

Other sulfur-MCPs are based on the *in situ* formation of isothiocyanates from isocyanides and sulfur and subsequent nucleophilic addition (compare Scheme 26). Tang *et al.* reported the used

of sulfur and difunctional isocyanides for the synthesis of polythioureas (PTUs) and polythionocarbamates (PTCs) with difunctional amines and alcohols, respectively (Scheme 33, top).[311,312] While the reaction with amines proceeded without any additional reagents at room temperature, the use of alcohols required stoichiometric amounts of sodium hydride and temperatures of 55 °C to enable both sulfur activation for the generation of the isothiocyanate and nucleophilic addition of the alcohol. Meier *et al.* later demonstrated that the synthesis of PTUs is also feasible with catalytic amounts of DBU.[141] Similarly to PTAs, PTUs and PTCs are both effective materials for metal ion extraction from aqueous solution with particular affinity for Ag^+ and Hg^{2+}. Tang *et al.* demonstrated that the incorporation of a tetraarylethylene (TAE) moiety into the polymer backbone, which shows increased fluorescence upon aggregation (see section 2.5) and can thus serve as a fluorescent sensor for these metal ions since the fluorescence is only turned on upon metal complexation.[311,312]

Meier *et al.* reported the synthesis of polythiosemicarbazones by condensation of dialdehydes with difunctional polythiosemicarbazides, the latter of which were obtained in an MCR of diisocyanides, sulfur and hydrazine (Scheme 33). The obtained polymers were successfully used for the fabrication of water-permeable membranes which showed high efficiency for the complexation of Ag^+ from aqueous solution.[313,314]

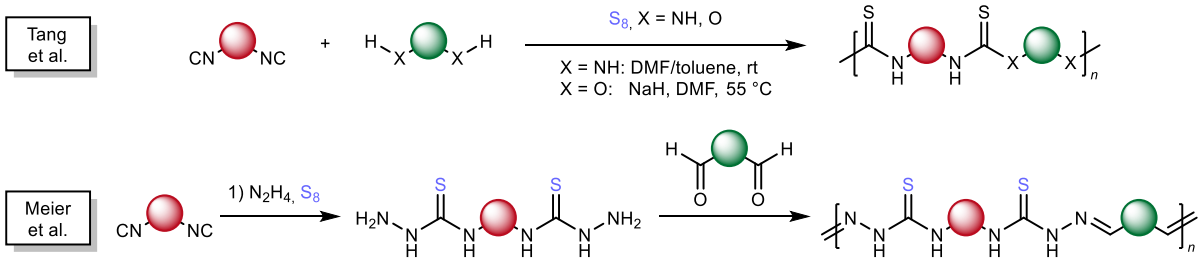

Scheme 33: Multicomponent polymerizations based on sulfur and isocyanides, reported by Tang et al. and Meier et al.[311–313]

The synthesis of sulfur-containing polymers by harnessing the potential of the many reported organic reactions involving sulfur remains a topic of current investigation, with many interesting new polymerization approaches and polymer classes being continuously reported.[315,316]

Overall, elemental sulfur has proven to be a highly versatile reagent in both organic and polymer synthesis. Driven by the issues caused by current industrial overproduction as well as its benign and desirable characteristics as a raw material, research on new synthetic processes involving elemental sulfur remains important and interesting. Sulfur-containing polymers in particular possess a range of highly interesting properties and are widely considered to have great potential as alternative materials in the context of sustainability and Green Chemistry.

2.4 Thiols in Polymer Chemistry

Thiols (also called mercaptans) are the sulfur-containing analogues of alcohols. However, since the S-H bond is much weaker than the O-H bond, thiols show significant differences in their chemical properties. Thiols are generally several orders of magnitude more acidic than alcohols (*e.g.* pK_a(EtOH) = 16 and pK_a(EtSH) = 10.5 in water)[317] and the resulting thiolate anions are very potent, soft nucleophiles. Furthermore, the S-H bond easily undergoes homolytic cleavage, triggered by common radical initiators, airborne oxygen or light. The resulting thiyl radicals are highly electrophilic and for instance readily undergo addition reactions to electron-rich sites, such as carbon-carbon π-bonds. Thiol chemistry often proceeds under mild conditions with short reaction times and high yields, while exhibiting perfect atom economy. For these reasons, thiols are often associated with the concepts of click chemistry, and are considered powerful tools for sustainable chemistry. Additionally, these characteristics make thiol-related reactions viable reactions for the synthesis of polymers. In the following chapter, several applications of thiol-related reactions will be presented, mostly focusing on the synthesis of monomers and polymers.

2.4.1 Nucleophilic Reactions of Thiols

The strong nucleophilic character of thiolate anions enables efficient reactions with a variety of electrophilic functional groups, such as epoxides, iso(thio)cyanates or Michael acceptors. Usually, nucleophilic thiol chemistry requires the use of a basic catalyst in order to ensure efficient deprotonation of the thiols and thus a high concentration of active thiolate ions.

Thiols efficiently add to epoxides under formation of β-hydroxythioethers. The addition generally proceeds under mild conditions with high regioselectively at the less sterically hindered site of the epoxide. In comparison to other epoxy curing agents like amines or anhydrides, thiols often exhibit rapid curing at ambient temperature, which is useful for instance for adhesive applications.[318–322] Khan *et al.* reported the synthesis of thermoset materials from polyfunctional thiols and glycidyl ethers using 1 mol% of DBU as the basic catalyst. Fast gelation times between one and 25 minutes were achieved under solvent-free conditions at room temperature. Furthermore, it was possible to achieve photochemical control over the reaction by using a photolabile DBU ketoprofen salt. In this form, the catalyst is inactive unless irradiated with ultraviolet light, releasing free DBU by decarboxylation of the ketoprofen carboxylate anion and thus initiating the reaction (Scheme 34).[323]

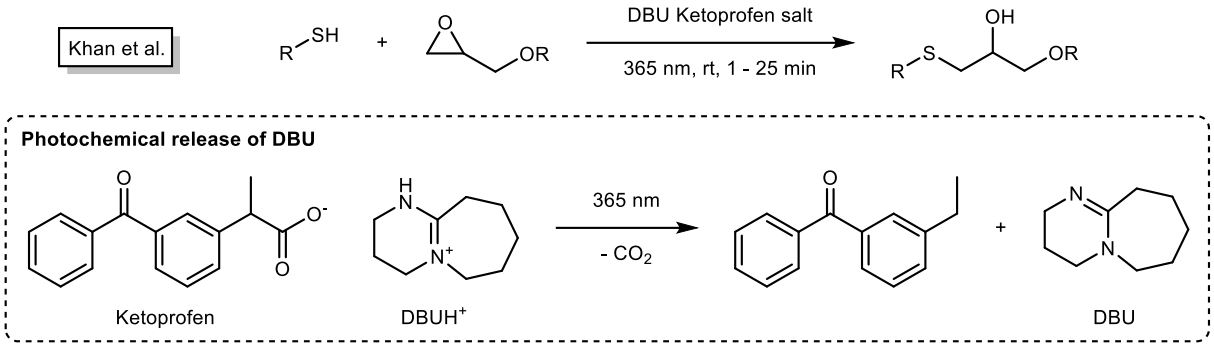

Scheme 34: Photochemically triggered Thiol-epoxy polymerization reported by Khan et al..[323]

The base-catalyzed nucleophilic addition of thiols to isocyanates or isothiocyanates has also been employed in polymer synthesis. The resulting (di)thiourethane functionalities are noteworthy because their formation is reversible, with the equilibrium shifting back to the reactants at elevated temperature. As an illustrative example, Endo *et al.* reported the synthesis of polydithiourethanes from aliphatic diisothiocyanates and dithiols at 50 °C, catalyzed by triethylamine. The resulting dithiourethanes could be partially depolymerized at 150 °C and subsequently repolymerized by addition of fresh catalyst (Scheme 35).[324]

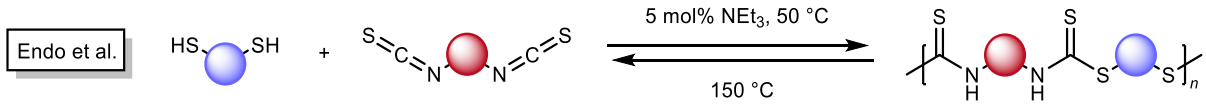

Scheme 35: Synthesis and depolymerization of dithiourethanes, reported by Endo et al..[324]

Functional groups exhibiting this kind of dynamic behavior are particularly interesting for the synthesis of crosslinked polymers, since their presence can allow for effective reprocessing of the materials. Commonly used thermosetting polymers generally lack this property, impeding their recycling and thus contributing to waste formation. Polymer networks with dynamic properties are commonly referred to as covalent adaptable networks (CANs), and are considered promising candidates for more sustainable polymeric materials.[325] Yang *et al.* produced thiolourethane networks by crosslinking isocyanate-terminated polyurethane oligomers with polythiols, catalyzed by the amidine-base 1,5-diazabicyclo[4.3.0]non-5-ene (DBN). Due to the dynamic nature of the thiolourethane functions, the networks showed excellent self-healing capabilities and reprocessibility at elevated temperature.[326] Photocontrollable strategies by light-induced catalyst activation have also been reported for the reaction of thiols with isocyanates.[327]

The thia-Michael addition, *i.e.* the nucleophilic addition of thiols to electron-deficient olefins or alkynes, also sees common usage.[328–330] Commonly used Michael acceptor motifs are for instance vinyl sulfones, α,β-unsaturated carbonyl compounds such as acrylic and methacrylic acid derivatives or maleimides.[331]. Meier *et al.* used the thia-Michael reaction for the synthesis of sulfone-functionalized polycaprolactones by ring-opening polymerization (ROP). The

monomers were synthesized by thia-Michael addition of thiols to cyclohex-2-enone, followed by Baeyer-Villiger oxidation with Oxone, which generated the caprolactone while simultaneously oxidizing the thioether functions to sulfones. Variation of the used thiols allowed for efficient property adjustment (Scheme 36). Notably, the starting cyclohex-2-enone could be obtained *via* oxidation of 1,4-cyclohexadiene, a self-metathesis product of polyunsaturated fatty acids (compare section 2.2.2).[332] Thia-Michael products also show dynamic behavior at high temperatures or in the presence of strong bases, making them potentially interesting moieties for CANs.[329]

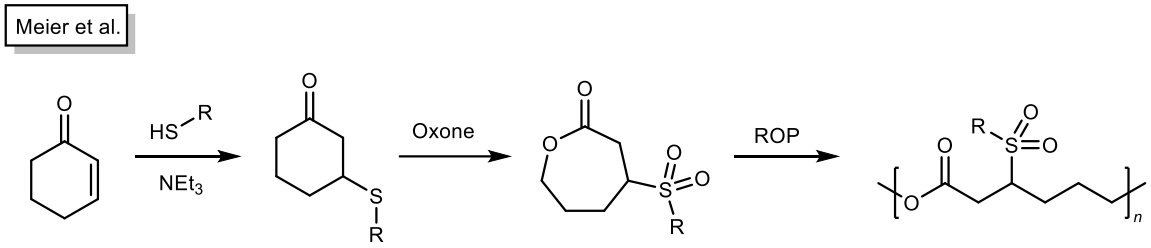

Scheme 36: Synthesis of a sulfone-functionalized polycaprolactones via sequential thia-Michael addition, Baeyer-Villiger oxidation and ROP, reported by Meier et al.[332]

2.4.2 Radical Reactions of Thiols

Radical reactions of thiols, particularly the radical addition of thiols to olefins known as the radical thiol-ene reaction, are also well-established and see widespread usage. Radical thiol-ene reactions were first reported at the beginning of the 20th century and have since evolved into a widely used tool in polymer chemistry, as well as in other scientific fields.[19,333–335] Notably, the nucleophilic thia-Michael addition of thiols to electron-deficient olefins is also considered a thiol-ene reaction. In this work, any use of the term "thiol-ene reaction" without further specification will always be in reference to the radical reaction.

The thiol-ene reaction proceeds *via* a classic radical chain reaction mechanism, involving initial radical formation, followed by propagation and chain transfer (Scheme 37). Initiation of the reaction by homolytic cleavage of the weak S-H bonds can be effected by the addition of radical initiators such as dibenzoyl peroxide (DBPO) or dimethoxyphenylacetophenone (DMPA), as well as *via* irradiation with ultraviolet light.[334,336] Airborne oxygen can likewise serve as radical initiator.[337] Furthermore, self-initiation by formation of a ground-state charge-transfer complex between olefin and thiol, resulting in additional weakening of the S-H bond, has also been reported.[338] The regioselectivity of the thiyl radical addition to the olefin is generally determined by the stability of the resulting carbon-centered radical. Hence, thiol-ene reactions generally result in the formation of the anti-Markovnikov products.

Notably, the propagation step can be reversible, as evidenced by reports of the fast stereoisomerization of *(Z)*-olefins to less reactive *(E)*-olefins in the presence of thiols. It has been noted that in the case of terminal olefins, as well as olefins bearing radical-stabilizing groups such as aromatic substituents, the reversibility of the radical addition is less pronounced and instead more often observed for internal alkenes.[339,340]

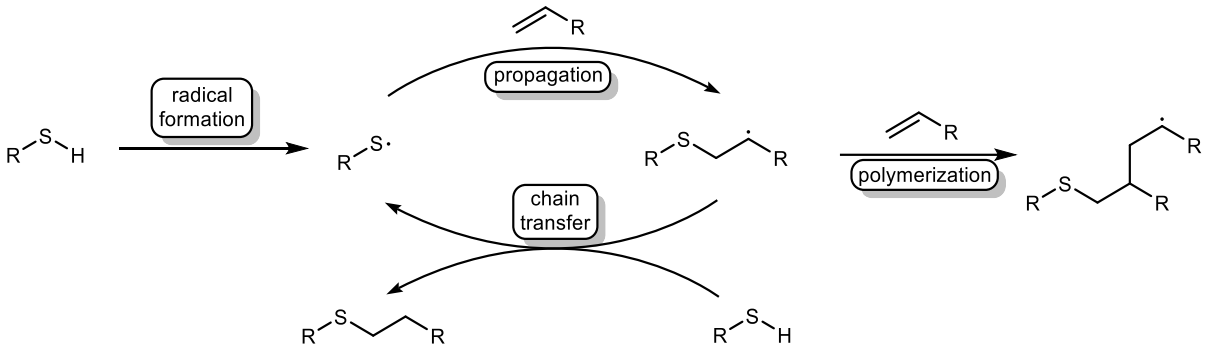

Scheme 37: Mechanism of the radical thiol-ene reaction.[334]

The chain transfer step is generally the rate-determining step of the thiol-ene reaction. In the case of well-stabilized radicals and thiols, resulting in slow chain transfer, radical homopolymerization can become a relevant side reaction, which has for instance been observed for acrylates.[341]

Electron-rich or strained olefins such as vinyl ethers or norbornenes tend to react more efficiently. Similarly, thiols bearing electron-withdrawing substituents, leading to further polarization of the S-H bond, are more effective due to faster rates of initiation and chain transfer. For instance, derivatives of 3-mercaptopropionic acid generally show faster reaction rates than simple aliphatic thiols. Steric hindrance of both olefin and thiol also play an important role. Internal and 1,1-disubstituted alkenes are less efficient due to slower thiyl addition and a more pronounced reversibility, often not reaching full conversion in thiol-ene reactions. Furthermore, an increasing degree of substitution of the thiol also slows the reaction.[336,340–342] The overall reaction kinetics thus depends on the H-donor capacity of the thiol, steric hindrance of both olefin and thiol, as well as the stability of the intermediate carbon-centered radical, and can thus vary strongly for each individual reaction.

Thiol-ene reactions proceed efficiently under mild conditions in many solvents, including water, and possess a very high tolerance towards other functional groups. For instance, they see substantial use in surface modification, photolithography or protein immobilization.[343–346] Notably, their insensitivity to water renders thiol-ene reactions promising for potential biomedical applications.[347]

Thiol-ene strategies have further been identified as particularly effective for the synthesis of polymer networks and coatings. This is due to their high conversion rates, as well as their step-

growth polymerization character leading to high monomer conversion before the gel point is reached, thus resulting in exceptionally homogeneous networks and reduced shrinkage stress.[19,345]

Since carbon-carbon double bonds frequently occur in renewable feedstock such as terpenes or vegetable oils, thiol-ene strategies have been widely employed especially for the synthesis of monomers and polymers materials from renewable resources (see chapter 2.2).

The thiol-ene reaction can be employed directly as the polymerization strategy for polymer synthesis. For instance, Meier *et al.* reported a thiol-ene approach for the synthesis of renewable NIPUs. Herein, a bis(vinyl)-urethane monomer was obtained *via* Lossen rearrangement from 10-undecenoyl hydroxamic acid and allyl alcohol. Subsequent photochemical thiol-ene polymerization with a range of dithiols yielded NIPUs with M_n up to 26.6 kDa (Scheme 38).[348] Numerous syntheses of polymer networks from renewable feedstock were reported as well.[349–353]

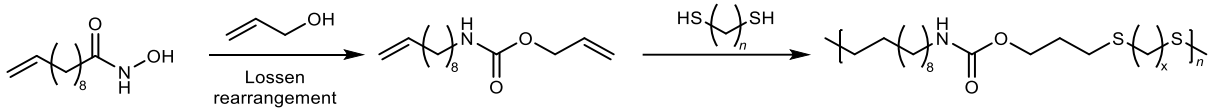

Scheme 38: Synthesis of linear NIPUs via thiol-ene polymerization, reported by Meier et al. [348]

Reineke *et al.* described the synthesis of suitable polyfunctional alkene monomers from terpene alcohols and subsequent photopolymerization *via* thiol-ene reaction using commercially available polythiols.[352]

Beyond being a polymerization method itself, thiol-ene chemistry is also a powerful tool to install other moieties into target compounds, taking advantage of its orthogonality with many other functional groups. For instance, amine functionalities can be installed by thiol-ene addition of cysteamine. Using this stragegy, Rios *et al.* reported the synthesis of a polyamine from canola oil and subsequently employed it for the synthesis of renewable NIPUs *via* aminolysis of cyclic carbonates (Scheme 39).[354] Similar strategies have been utilized for other vegetable oils such as high oleic sunflower oil (HOSO).[89]

Other moieties that can be incorporated into olefins *via* thiol-ene addition of suitable functional thiols include carboxylic acids, alcohols, vicinal diols or aromatics, among others.[355]

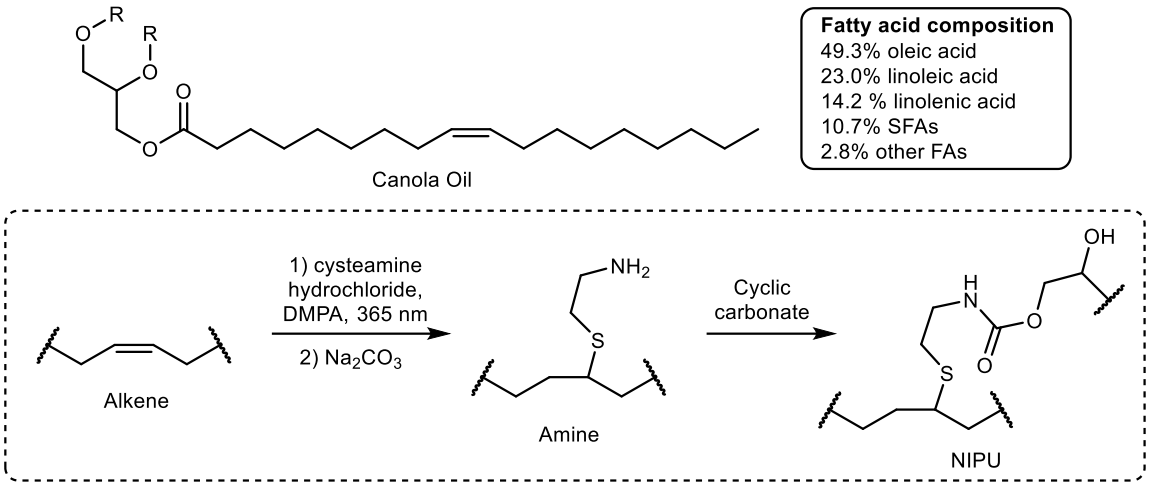

Scheme 39: Functionalization of canola oil with cysteamine and subsequent use for NIPU synthesis, reported by Rios et al.[354]

Although not as widespread as the thiol-ene reaction, alkynes can also undergo radical additions of thiols *via* a similar mechanism, known as the thiol-yne reaction.[356,357] In this case, the initial addition product is a vinyl sulfide, which is typically more reactive towards another radical thiol addition than the original alkyne, ultimately resulting in the formation of a 1,2-bis(thioether).[358] Hence, thiol-yne reactions are for instance useful for the preparation of polymer networks with exceptionally high crosslinking density and sulfur content. Furthermore, as demonstrated by Meier *et al.*, linear polymers can be obtained from the thiol-yne polymerization of difunctional thiols with monofunctional alkynes such as propargyl alcohol (Scheme 40).[359]

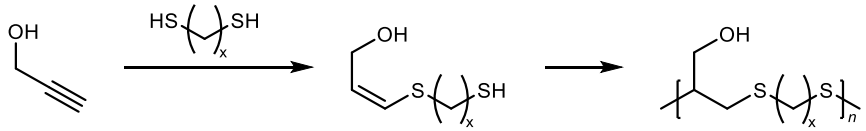

Scheme 40: Thiol-yne polymerization of propargyl alcohol and dithiols, reported by Meier et al.[359]

The various different reactivities of thiols, both nucleophilic and radical, can compromise their general applicability and thus the "click" character of thiol-related reactions. Notably, especially low molecular weight thiols often possess strong odor, exhibit toxicity and suffer from poor shelf-life due to their instability against air oxidation. Thiols must thus be handled mindfully and their applicability must be evaluated for each case individually.[19,333] In spite of this, thiol chemistry offers a multitude of powerful strategies not only for polymer synthesis, but also in other scientific fields, and will undoubtedly continue to play an important role in future research.

2.5 Tetraarylethylenes and Related Polymers

Tetraarylethylenes (TAEs) are a class of highly substituted olefins that are particularly noteworthy since they often show an interesting luminescence behavior, known as aggregation-induced emission (AIE).[360] AIE-active compounds exhibit strong solid-state luminescence, which is a highly advantageous property for real-world applications of organic luminophores. The polymeric derivatives of TAEs, known as polyarylene(1,2-diarylvinylene)s (PAV-DAs), share the AIE properties of their monomeric counterparts, and possess several further interesting traits due to their conjugated polymeric character.[361] In the following section, several applications of TPEs and PAV-DAs (Scheme 41), as well as the most common methods for their synthesis, will be presented.

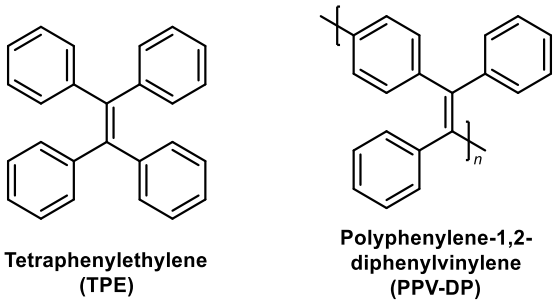

Scheme 41: Structures of tetraphenylethylene (TPE) and polyphenylene-1,2-diphenylvinylene (PPV-DP).

2.5.1 Aggregation-Induced Emission

AIE refers to the property of a luminescent compound to exhibit stronger emission in aggregated states, *i.e.* bulk solids or nanoparticles, than in solvated states. AIE is thus the opposite of the typical behavior of emissive compounds, which generally show aggregation-caused quenching (ACQ), *i.e.* a strong luminescence in solution that diminishes with increasing aggregation.[362,363]

The discovery of the AIE phenomenon is attributed to Tang *et al.* in 2001, who first noticed the behavior during their investigations of the compound 1-methyl-1,2,3,4,5-pentaphenylsilole. It was observed that a solution of the compound was not fluorescent, however a spot of the solution on a silica plate turned strongly emissive after complete evaporation of the solvent. In due course, it was found that the addition of an antisolvent to a solution of the compound, resulting in the formation of nanoscale precipitates, was similarly accompanied by a strong increase in fluorescence intensity.[364] Since the discovery of the phenomenon, AIE properties have been observed for many other compound classes, most notably TPE and its derivatives.[360,365] Figure 2 illustrates a qualitative comparison of the fluorescence behavior of

tetrahydrofuran (THF) solutions of fluorescein, a conventional ACQ-fluorophore, and an AIE-active TPE derivative with increasing amounts of the antisolvent water, demonstrating the contrasting emission behavior.

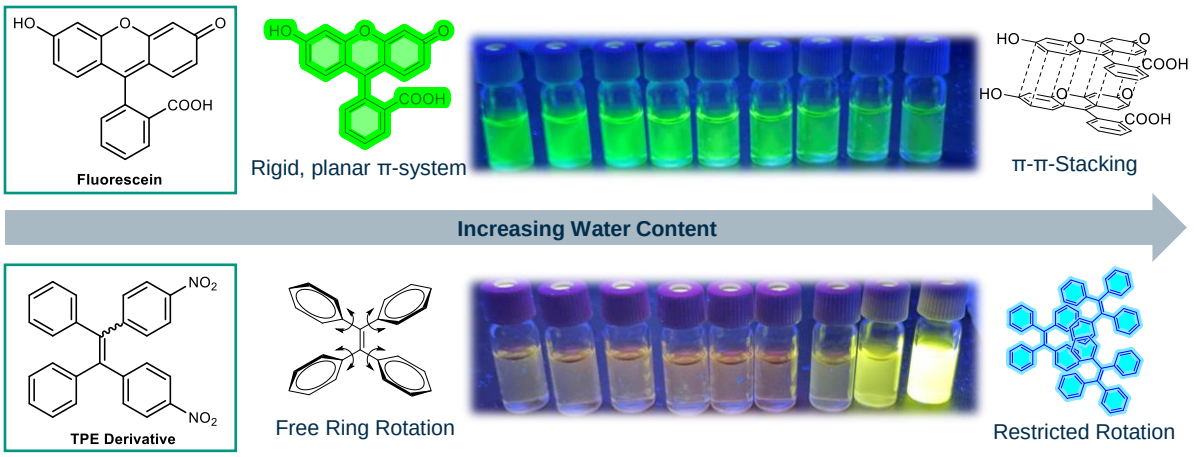

Figure 2: Qualitative comparison of the fluorescence behavior of THF solutions of fluorescein (top) and a TPE derivative (bottom) with increasing water content. Images were taken by the author of this thesis.

The underlying mechanisms for the occurrence of AIE are still a matter of discussion. AIE is typically attributed to the restriction of intramolecular motions upon increasing aggregation. For instance, in the case of TPE, the free rotation of the phenyl substituents connected to the central olefinic carbon atoms in solution provides a pathway for non-radiative relaxation in the solvated state. In aggregated states however, these rotational modes are restricted and the TPE molecule is fixed in a propeller-like shape, turning on its fluorescence.[366,367] At the same time, the non-planar shape of TPE impedes π-π-stacking in condensed phases, which is often the cause of ACQ effects in conventional luminophores due to their typically rigid, planar π-systems.[368–372]

2.5.2 Design and applications of AIE-active compounds

Since the discovery of AIE, the design of new AIE-active luminophores for real-world applications has been continuously researched due to their inherent suitability for solid-state usage. The development of functional AIE-active compounds often entails the tailoring of the desired properties by introduction of further functional groups into typical AIE-active building blocks such as TPE. Notably, the design of polymeric materials with AIE properties has also been extensively investigated in this regard, because polymeric materials can offer several additional benefits, such as improved mechanical properties and processability, as well as easier property adjustment. Polymers can either intrinsically show AIE properties due to their structure, as is the case for PAV-DAs or several other conjugated polymers, or AIE properties

can be bestowed by incorporating AIE-active moieties into the polymer backbone or side chains.[373–378]

A notable example for an application of luminescent compounds are optoelectronic devices such as organic light-emitting diodes (OLEDs), which see wide application in smartphone or television displays. OLEDs are multilayer devices based on electroluminescence, generating light by application of an external voltage that results in the formation and decay of excitons in the emissive layer. The emissive layer is typically a thin film of a host material doped with the emitting luminophore. As such, the typical ACQ behavior of conventional organic emitters is a substantial issue for OLED technology since it lowers the quantum yield and red-shifts the emission wavelength.[379–381] While ACQ effects can be somewhat mitigated, for instance by the presence of sterically demanding groups, AIE-active emitters intrinsically benefit from existing in aggregated states and are thus advantageous for OLED applications. The introduction of AIE properties into OLED luminophores by incorporation of TPE units has shown promise, and the viability of numerous AIE-active emitters on the basis of TPE scaffolds with emission wavelengths across the entire visible spectrum for application in OLEDs has been demonstrated.[360,381–384] The structure of a blue OLED emitter, reported by Duan, Ge *et al.*, is depicted in Scheme 42.[385,386] Similarly, viable designs of OLEDs and other optoelectronic devices such as solar concentrators based on polymeric AIE emitters, including PAV-DAs, have been reported.[375,387–389]

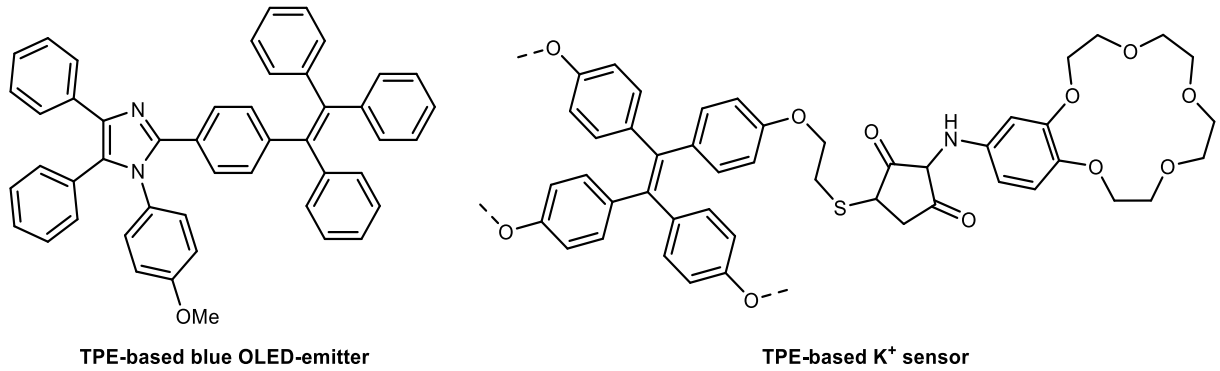

Scheme 42: Structures of a TPE-based blue emitter for OLEDs, reported by Duan, Ge et al.. (left) and a TPE-based fluorescent sencor for the detection of potassium ions, reported by Zhang, Liu et al. (right).[385,390]

Another major application for AIE-active compounds is the design of optical probes. TPE derivatives have been used as templates for the design of luminescent sensors for an exceptional variety of stimuli, for example as chemical probes for metal ions or biologically relevant compounds, or physical sensors that can be responsive to changes in physical parameters such as temperature or pH.[362,391–393] The general operating principle of such sensors is the functionalization of TPE with sensitive moieties, whose response to the relevant stimulus will

cause an activation of the AIE fluorescence, for instance by the formation of cross-linked networks, or by precipitation.

As a simple example for an ion-sensitive fluorescent probe, Zhang, Liu *et al.* reported a selective sensor for potassium ions based on a TPE scaffold bearing 15-crown-5 moieties, which form a sandwich complex with K^+ (Scheme 42). Hence, the presence of potassium ions effects the formation of a crosslinked network, turning on the AIE fluorescence. Selective detection of K^+ was possible even in the presence of a range of other metal ions.[390]

An instance of a polymeric sensor based on TPE was provided by Tang *et al.*, who synthesized AIE-active polythioureas *via* a multicomponent polymerization described in a previous chapter (compare Scheme 33) using a TPE-diisocyanide as a monomer, thus incorporating TPE units into the polymeric backbone. Due to the metal coordination properties of the thiourea moieties combined with the AIE properties, the resulting polythiourea was demonstrated to serve as an efficient fluorescent sensor for Hg^{2+} ions.[311]

PAV-DAs are known as polymers of intrinsic microporosity, granting them very high specific surface areas. This enables potential application as optical sensors that operate based on fluorescence quenching due to the adsorption of gases or vapors. For instance, applications of PAV-DA derivatives for the detection of oxygen or nitroaromatic compounds have been reported, which could play an important role in the fast and sensitive detection of explosives.[394–398]

AIE-active materials have further seen use in a variety of biomedical applications. AIE emitters are advantageous for usage in biological settings since organic fluorophores are often water-insoluble and thus susceptible to ACQ effects. Furthermore, several AIE compounds based on TPE have shown excellent biocompatibility, and potential uses for cellular and tissue imaging, as well theranostics or drug delivery have been demonstrated.[399–403]

2.5.3 Synthesis of TAEs and PAV-DAs

The synthesis of highly substituted olefins such as TPE derivatives is generally met with challenges due to the substantial steric demand of the substituents surrounding the carbon-carbon double bond.[404] The resulting high activation barriers render common methods for olefin synthesis, such as the Wittig or Horner-Wadsworth-Emmons olefinations, highly ineffective. Instead, the synthesis of TPE derivatives has to resort to strong thermodynamic driving forces, which can often be provided by strategies involving metallic or metalorganic reagents.

The most common method for the synthesis of TPE derivatives is the McMurry coupling of two carbonyl compounds using low-valent titanium (Scheme 43). The driving force of the reaction is the formation of strong titanium oxygen bonds.[391,405–407] In practice, low-valent titanium is generated *in situ* from Ti sources such as $TiCl_4$ or $TiCl_3$ and a reducing agent such as lithium aluminium hydride or metallic zinc. McMurry couplings are usually carried out in refluxing ether solvents such as THF or dimethoxyethane (DME).[406] The McMurry coupling is most effective for the synthesis of symmetrical TPE derivatives. The use of unsymmetrically substituted ketones results in the formation of isomeric mixtures, with slight preference for the *(E)*-isomer if one of the substituents is more sterically demanding than the other.[405,406] Despite this, successful unsymmetrical TPE synthesis *via* McMurry coupling and subsequent purification of the stereoisomers has been reported, for instance *via* different crystallization behavior of the isomers, or *via* chromatographic methods if the polarity difference of the stereoisomers was sufficient to allow effective separation.[408] The McMurry coupling is generally ineffective in achieving selective alkylidene-cross coupling of two different ketones, since the homocoupled products will also be generated, leading to lower yields, more waste and more complicated workup.[407,409]

Another strategy that has seen use for the synthesis of TPEs is the Knoevenagel-type condensation of aromatic ketones with lithiated diarylmethanes, first reported by Rathore *et al.* (Scheme 43). This method provides effective access to cross-coupled TPEs, but suffers from poor general applicability due to the use of highly reactive organolithium reagents. Furthermore, isomeric mixtures of the *(E)* and *(Z)*-TPEs will be generated in the case of unsymmetrical starting materials. [391,405,410–412]

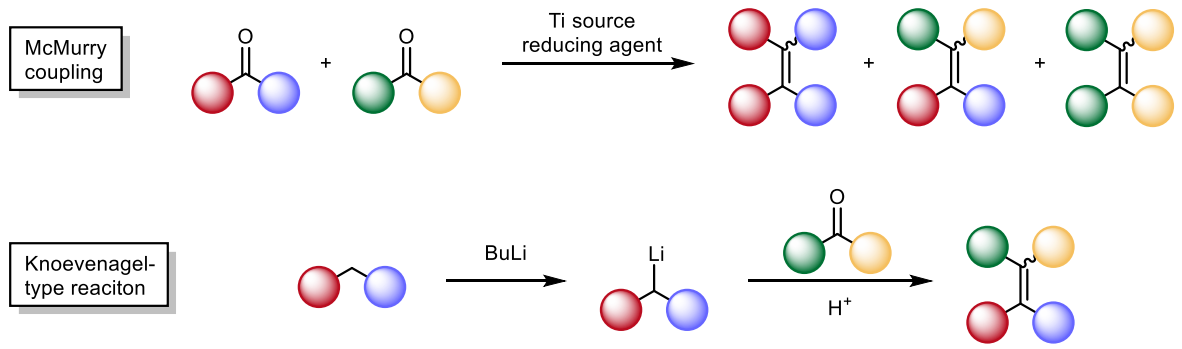

Scheme 43: TPE synthesis via McMurry coupling (top) and Knoevenagel-type condensation of lithiated diarylmethanes and ketones (bottom). The differently colored spheres represent differently substituted aryl moieties.

Transition-catalyzed cross-coupling (TMCC) reactions offer another very powerful strategy for the synthesis of highly substituted alkenes such as TPEs. The use of TMCCs for TPE synthesis requires an already existing alkene scaffold, either as the electrophilic component of the reaction, for instance as a vinyl halide, or as the nucleophilic component as an organometallic

vinyl compound. Many efficient strategies have emerged that can allow a very high degree of control over both the regio- and stereochemical outcome of the reactions.

For instance, Larock *et al.* reported a palladium-catalyzed three-component TPE synthesis from bis(aryl)alkynes, aryl iodides and arylboronic acids (Scheme 44). The reaction proceeds by initial *syn*-carbometalation of the alkyne, yielding a vinylboronate *in situ*, followed by Suzuki-Miyaura cross-coupling to yield the final TPE product. The *syn*-character of the carbometalation makes the reaction highly stereospecific. However, poor carbometalation regioselectivity was observed for unsymmetrically substituted alkynes.[413,414]

Tobrman *et al.* presented an interesting modular strategy for the regio- and stereoselective synthesis of TPE derivatives (Scheme 44). Starting from an α-dibromoacetophenone, the initial step entails the synthesis of a corresponding enol phosphate. The two bromo-substituents and the phosphate substituent could then serve as the leaving groups for three consecutive TMCCs, with full regioselectivity achievable by optimization of the catalyst system.[415]

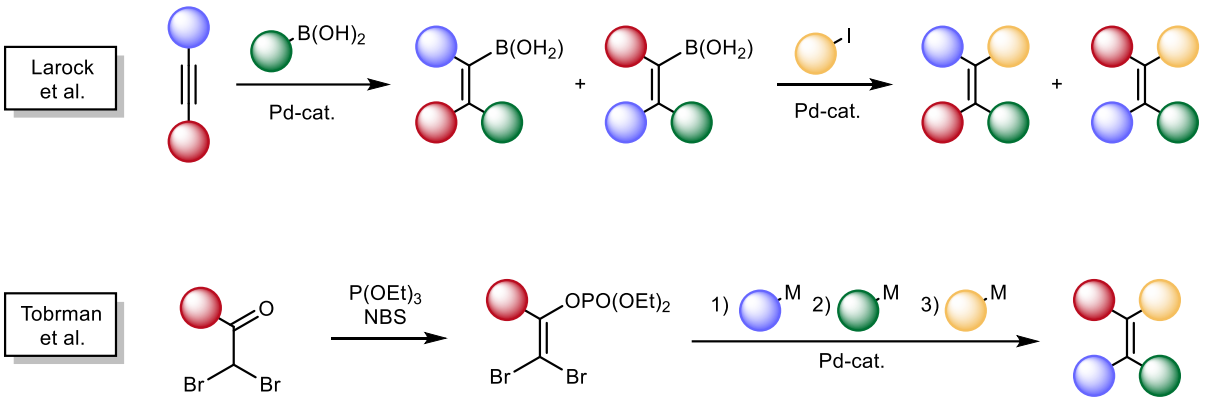

Scheme 44: TPE syntheses based on TMCCs, reported by Larock et al.. (top) and Tobrman et al.. (bottom). The colored spheres represent differently substituted aryl moieties.[414,415]

Many other methods for stereo- and regioselective TPE synthesis involving TMCCs have been reported. The main drawback of these reactions is the need for expensive catalysts, as well as often elaborate synthesis of the starting materials.[404,405]

PAV-DAs being the polymeric derivatives of TPEs, their synthesis can be achieved by transfer of the established synthetic procedures for TPE synthesis towards bifunctional reactants. As such, the McMurry coupling of bifunctional ketones, as well as methods based on TMCCs of bifunctional substrates, have been reported.[416–418] However, reports on PAV-DA syntheses are generally scarce, and in contrast to TPEs, McMurry coupling and TMCCs are not the most established method for their synthesis. The most recent examples for the synthesis of PAV-DAs were provided by Scherf *et al.*, utilizing a reductive polyolefination of *gem*-dichlorides with metallic reducing agents such as cobalt octacarbonyl. *gem*-Dichlorides were obtained from the respective carbonyl compounds *via* reaction with PCl_5. Previously, the use of other reducing agents, such as chromium(II) species, had been reported as well.[395,396,419–421] No comments

were made on the stereoselectivity of the reductive polyolefination of *gem*-dichlorides, however a report on PAV-DA synthesis *via* McMurry coupling states that statistical isomeric mixtures were obtained in that case, suggesting the same for the other method.[417]

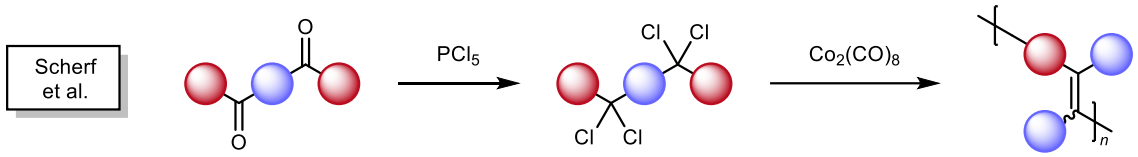

Scheme 45: Synthesis of PAV-DAs via reductive polyolefination of gem-dichlorides with cobalt octacarbonyl, reported by Scherf et al..[395,396]

In conclusion, AIE-active compounds and polymers such as TPEs and PAV-DAs have been shown to bear great potential for many useful applications, including bioimaging and the manufacture of optoelectronic devices and fluorescent sensors. A variety of synthetic methods has been established to access TPE derivatives, some allowing for very high degrees of control over regio- and stereoselectivity.

3 Aims

The pressing challenges of resource depletion, global warming and the accumulation of waste in the environment necessitate the development of novel, more sustainable synthetic strategies that rely on renewable resources and contribute to a more responsible waste management. At the same time, the development of novel functional compounds and polymers is key for technological progress.

This work aims to develop new synthetic methodologies involving the use of elemental sulfur and sulfur-containing functional groups, focusing on the synthesis of polymeric materials. In this context, the principles of Green Chemistry are utilized as a guiding framework in order to ensure improved sustainability of all developed procedures as far as feasible. Overall, this work comprises four different projects, which are illustrated in Scheme 46:

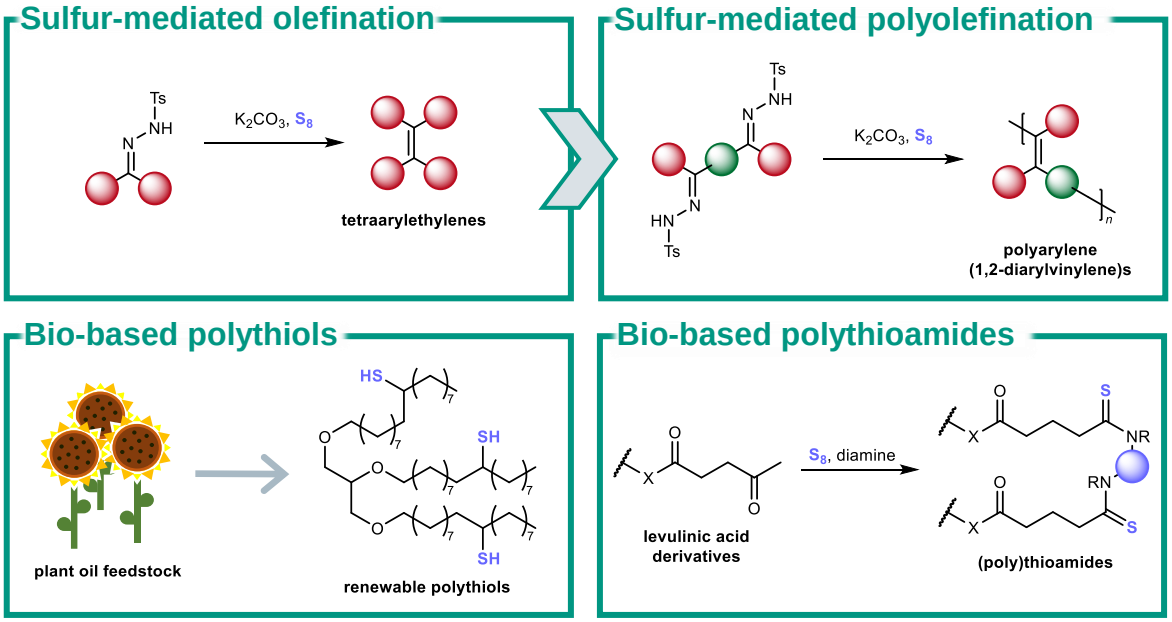

Scheme 46: Schematic representation of the four main projects of this work.

The first two projects focus on understanding and harnessing the reactivity of elemental sulfur in a newly discovered organic reaction. In this context, the initial project aimed to investigate a novel sulfur-mediated olefination reaction of *N*-tosylhydrazones. The method had previously been shown to serve as an efficient access to tetraarylethylene derivatives, which see widespread usage in the design of luminescent materials for various applications due to their aggregation-induced emission properties. After mechanistic insights on the reaction had been gained in a previous study, the synthetic scope of the methods was to be elaborated in the context of this work.

In the second, related project, the olefination reaction investigated in the first project was to be extended towards bifunctional substrates in order to potentially enable the synthesis of polymeric tetraarylethylene derivatives, namely polyarylene(1,2-diarylvinylene)s (PAV-DAs). The remaining projects are focused on the synthesis of more sustainable polymeric materials using sulfur chemistry and renewable resources.

As such, a third project was aimed at developing a strategy to synthesize polythiols from renewable vegetable oils such as sunflower oil. The thiol synthesis was then to be optimized under consideration of the principles of Green Chemistry. Subsequently, the polythiols were to be applied as crosslinkers for the synthesis of novel polymer networks *via* radical thiol-ene chemistry, as well as nucleophilic addition reactions. For the latter strategy, the use of isothiocyanates was envisioned as comonomers, also being derived from elemental sulfur.

Finally, the fourth project investigated in the context of this work was to evaluate the viability of the Willgerodt-Kindler reaction, a long-established organic reaction involving elemental sulfur, for the synthesis of bio-based polythioamides from levulinic acid, a renewable platform chemical derived from lignocellulosic biomass.

4 Results and Discussion

4.1 Synthesis of Olefins by Sulfur-mediated Olefination

Disclaimer

The results described in this chapter are based on a previous publication by the author of this thesis. Text and figures are partially reproduced, edited and extended from this article, which is licensed for re-use under Creative Commons CC BY 4.0:[422]

P. Conen, R. Nickisch, M. A. R. Meier, Synthesis of highly substituted alkenes by sulfur-mediated olefination of N-tosylhydrazones, *Commun. Chem.* **2023**, *6*, 255. https://doi.org/10.1038/s42004-023-01058-2

The original discovery of the olefination reaction and the optimization of the conditions were made by Roman Nickisch as part of his dissertation.[423] The author of this thesis performed the associated experiments as a research assistant under the supervision of R. Nickisch.

The mechanistic investigations on the olefination reaction were performed by the author of this thesis as part of his master thesis.[424] The synthetic methodology and synthetic scope of the homocoupling and cross-coupling olefinations, although also partially described in the master thesis, were re-evaluated, further elaborated and expanded as part of the research for this thesis. Compounds that were synthesized out of the context of this work are indicated in the discussion and the Experimental Section.

The author of this thesis planned and evaluated the herein described experiments and wrote the original draft of the publication.

Silas Leidenheimer performed several syntheses related to this project as part of his apprenticeship under co-supervision of the author. Maya Ludwig performed several syntheses related to this project as part of the "Organisch-Chemisches Fortgeschrittenenpraktikum" under supervision of the author.

Abstract

Tetraphenylethylenes are well-known for their aggregation-induced emission (AIE) properties. The synthesis of TPE derivatives, as well as other highly substituted olefins, generally requires the use of hazardous reagents, such as metalorganic compounds, to overcome the high activation energies caused by the sterically congested double bond. Herein, an efficient and metal-free procedure for the synthesis of tetraarylethylenes (TAEs) in excellent yields *via* alkylidene-homocoupling of *N*-tosylhydrazones (NTHs), derived from readily available benzophenones, is presented. The method relies only on cheap and benign additives, *i.e.* elemental sulfur and potassium carbonate, and easily competes with other established procedures in terms of scope, yield and practicability. Based on mechanistic insights gained in a preceding study, a modified method, which allows for selective alkylidene-cross-coupling, generating a broader scope of olefins in good yields, is described as well.

4.1.1 Discovery and Initial Optimizations

Disclaimer

The results described in this chapter are part of the dissertation of Roman Nickisch and were thus not obtained in the context of this work.[423]
They are briefly summarized for better contextualization of the project and for the sake of completeness.

The olefination reaction described in this project was discovered by Roman Nickisch as part of his PhD research as part of studies on the reactivity of carbenoid structures with elemental sulfur to form thiocarbonyl moieties (see chapter 2.3.3.5).[423] In this context, it was originally intended to investigate a potential synthetic access to thioketones by the reaction of elemental sulfur with carbenes generated *in situ via* the base-induced decomposition of *N*-tosylhydrazones. NTHs are well-established in organic synthesis, for instance as the substrates for the Bamford-Stevens reaction, and are known to decompose into diazo compounds / carbenes under basic conditions in aprotic solvents (Scheme 47, top).[425,426]
NTH **1a**, derived from 4,4'-dimethoxybenzophenone, was thus prepared and reacted with sodium hydride and elemental sulfur at 130 °C in DMSO (Scheme 47). However, characterization of the isolated product revealed that not the expected thioketone, but instead tetraarylethylene **2a** had formed, resulting from the homocoupling of the alkylidene moieties of **1a**. TAE **2a** was obtained in a yield of 92%, indicating a highly selective reaction. The expected thioketone **3a** could not be isolated or detected spectroscopically, however the visual observation of a blue coloration during workup, which is the reported color of **3a**, indicated its formation in trace amounts.[422]

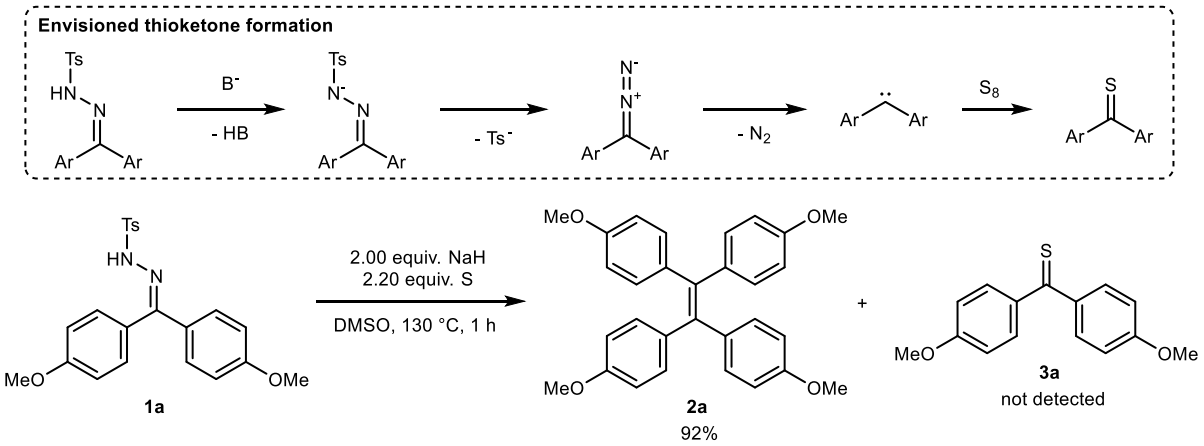

*Scheme 47: Mechanism of the envisioned thioketone formation (top) and the practically observed formation of TAE **2a** from NTH **1a** in the presence of sodium hydride and elemental sulfur.*[423]

Despite the lack of formation of the intended product, the selective generation of TAE **2a** served as motivation for further investigations on the newly discovered homocoupling, with the new

goal of establishing the reaction as a potential alternative to other commonly employed methods for TAE synthesis, such as the McMurry coupling or TMCCs (see section 2.5.3).

After optimization of the reaction conditions, carrying out the reaction in DMSO at 100 °C was found to result in full conversion of **1a** after 30 minutes using 2.00 equivalents of atomic sulfur and 1.20 equiv. of potassium carbonate, leading to an isolated yield of 99% of TPE **2a** (Scheme 48).

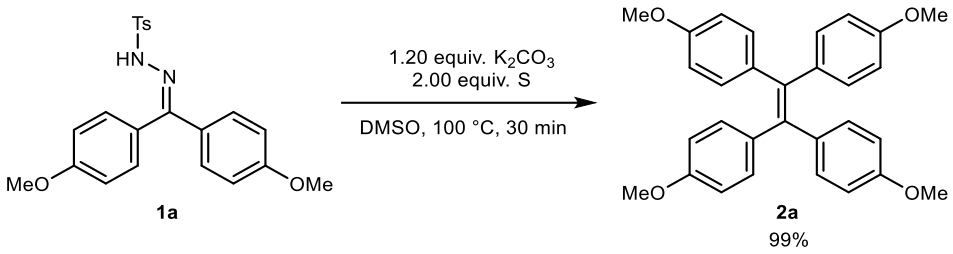

*Scheme 48: Optimized conditions for the synthesis of TAE **2** from NTH **1** via sulfur-mediated homocoupling.*[422,423]

4.1.2 Mechanistic Study

Disclaimer

The results described in this chapter are part of the master thesis of the author and were thus not obtained in the context of this work.
They are briefly summarized for the sake of completeness.

In order to elucidate the mechanism of the homocoupling reaction, plausible pathways were considered and control experiments were developed. The mechanistic study was performed using the alkylidene-homocoupling of **1a** to **2a** under the optimized reaction conditions as the model reaction (compare Scheme 48).

The results of the performed test reactions showed that both elemental sulfur and the base are crucial for selective formation of TAEs from NTHs. Thus, the occurrence of Wanzlick-type carbene dimerization as part of the pathway was ruled out and the original assumption of a potential formation of thioketone **3a** from the NTH **1a** was re-evaluated (compare Scheme 47, top). Thioketones and diazo compounds are known to react in a [4+2]cycloaddition known as the Barton-Kellogg reaction, forming a 1,3,4-thiadiazoline, which readily decomposes into a thiirane *via* nitrogen elimination and recyclization of the intermediate sulfur ylide (Scheme 49).[427–429] Barton-Kellogg reactions are themselves frequently used reactions for the synthesis of highly congested alkenes, but have not seen widespread application in the synthesis of TPE derivatives. In Barton-Kellogg reactions, the use of a desulfurization agent is often necessary to achieve the synthesis of the alkene from the thiirane. This is usually achieved using a

stoichiometric reagent such as for instance triphenylphosphine, which reduces the thiirane to the olefin under formation of triphenylphosphine sulfide.

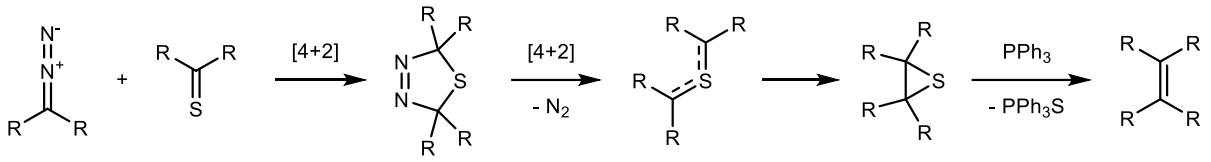

Scheme 49: Barton-Kellogg reaction of a diazo compound and a thioketone, forming a thiirane, followed by desulfurization of the thiirane to an alkene with triphenylphosphine.[427–429]

The possibility of the occurrence of an *in situ* Barton-Kellogg reaction as part of the mechanism present homocoupling reaction was investigated by synthesizing the associated intermediates, *i.e.* diazo compound, thioketone and thiirane, and investigating their general behavior under the homocoupling conditions. It was found that an *in situ* Barton-Kellogg-type formation of a thiirane from NTHs and thioketones is possible under the employed reaction conditions. Furthermore, quantitative desulfurization of the thiirane into the olefin product under the homocoupling conditions was observed.

Based on the obtained insights, a plausible reaction mechanism for the alkylidene-homocoupling of NTHs was proposed (Scheme 50).[424] The initial step of the reaction is a base-induced decomposition of the reactant NTH in similar fashion to established reactions, such as the Bamford-Stevens reaction, resulting in the formation of a carbene, which then yields a thioketone by reaction with elemental sulfur. Wanzlick dimerization of the carbene was excluded as a possible pathway for alkene formation under the utilized conditions.

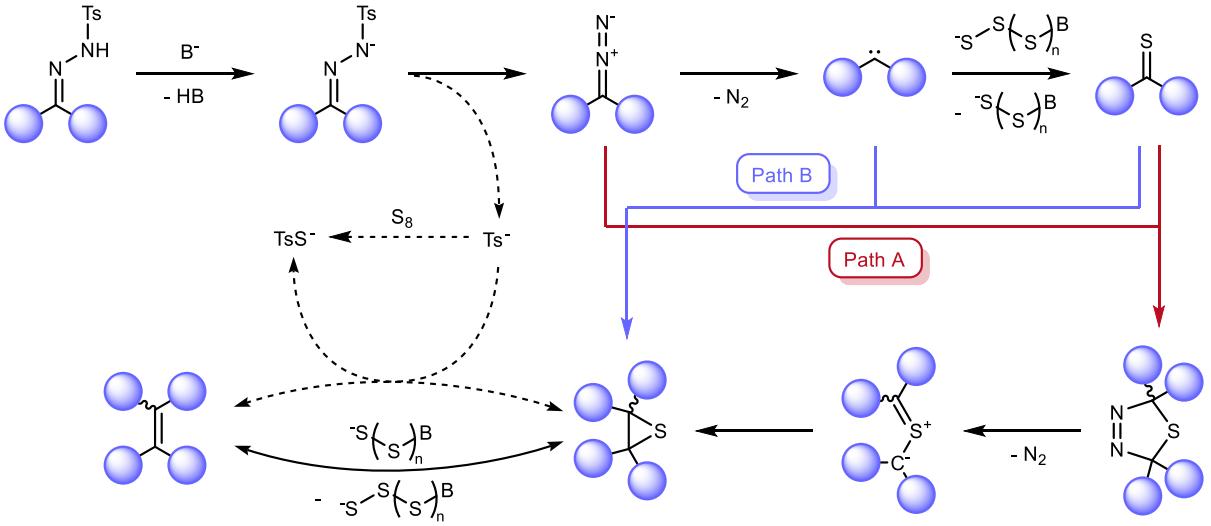

Scheme 50: Proposed mechanistic pathways for the herein described alkylidene-homocoupling of NTHs.[422]

The coupling step of the reaction is the formation of a thiirane *via* reaction of the *in situ* generated thioketone with a prior intermediate. For instance, the already described Barton-Kellogg cycloaddition with the diazo intermediate would result in the eventual formation of a thiirane after nitrogen elimination and recyclization (Scheme 50, path A). Direct reaction of the

carbene intermediate with the thioketone is also conceivable, providing a direct pathway to the thiirane (Scheme 50, path B).[430] The final step is the reductive desulfurization of the thiirane to the final product. It was found that the *p*-toluenesulfinate ion, which is eliminated from the NTH in the initial step of the reaction, can serve as a stoichiometric desulfurization agent, forming *p*-toluenethiosulfonate as the byproduct.

However, it was also observed that the thiirane is more efficiently desulfurized in the presence of both base and elemental sulfur. While this kind of reactivity was not previously known in this manner, the desulfurization of aromatic thiiranes with catalytic amounts of strong nucleophiles such as thiophenoxide has been reported.[431] Regarding the frequently suggested formation of nucleophilic polysulfide species from elemental sulfur in the presence of activating bases, such a mechanism is also conceivable in this case (compare chapter 2.3.2). It is assumed that the reaction is driven by the energy gain due to extended π-conjugation by the formation of the double bond. Notably, the utilized reaction conditions of an *O*-centered base in an aprotic solvent have been frequently reported to favor the formation of sulfur-centered radicals such as $S_3^{\bullet-}$.[149,188] Hence, a radical mechanism for the final desulfurization is also plausible.

4.1.3 Homocoupling Scope

Disclaimer

Several products described in this chapter were synthesized as part of the master thesis of the author and were thus not obtained in the context of this work. The respective compounds are indicated in the discussion and the Experimental Section (chapter 6.3.1).

In order to investigate the feasibility of the alkylidene-homocoupling for a wider scope of substrates, a range of additional NTHs **1b**-**1l** was synthesized and subjected to the optimized homocoupling conditions.

NTH synthesis was performed by condensation of the respective carbonyl compounds **4a**-**4l** with tosyl hydrazide in ethanol. NTHs were obtained between 33% and quantitative yield (Scheme 51). All required carbonyl compounds with the exception of **4c**, **4d**, **4f** and **4j** were obtained commercially. **4c** was synthesized *via* Friedel-Crafts acylation of bromobenzene with 4-bromobenzoyl chloride in the presence of aluminium chloride, while **4d**, which is not accessible *via* electrophilic aromatic substitution reactions, was instead accessed *via* benzylic oxidation of 4,4-dinitrodiphenylmethane, using potassium permanganate under phase transfer catalysis.[432–434] The experimental details are available in section 6.3.1.1. **4f** and **4j** were obtained during the preceding master thesis of the author and thus not synthesized as part of this work.[424]

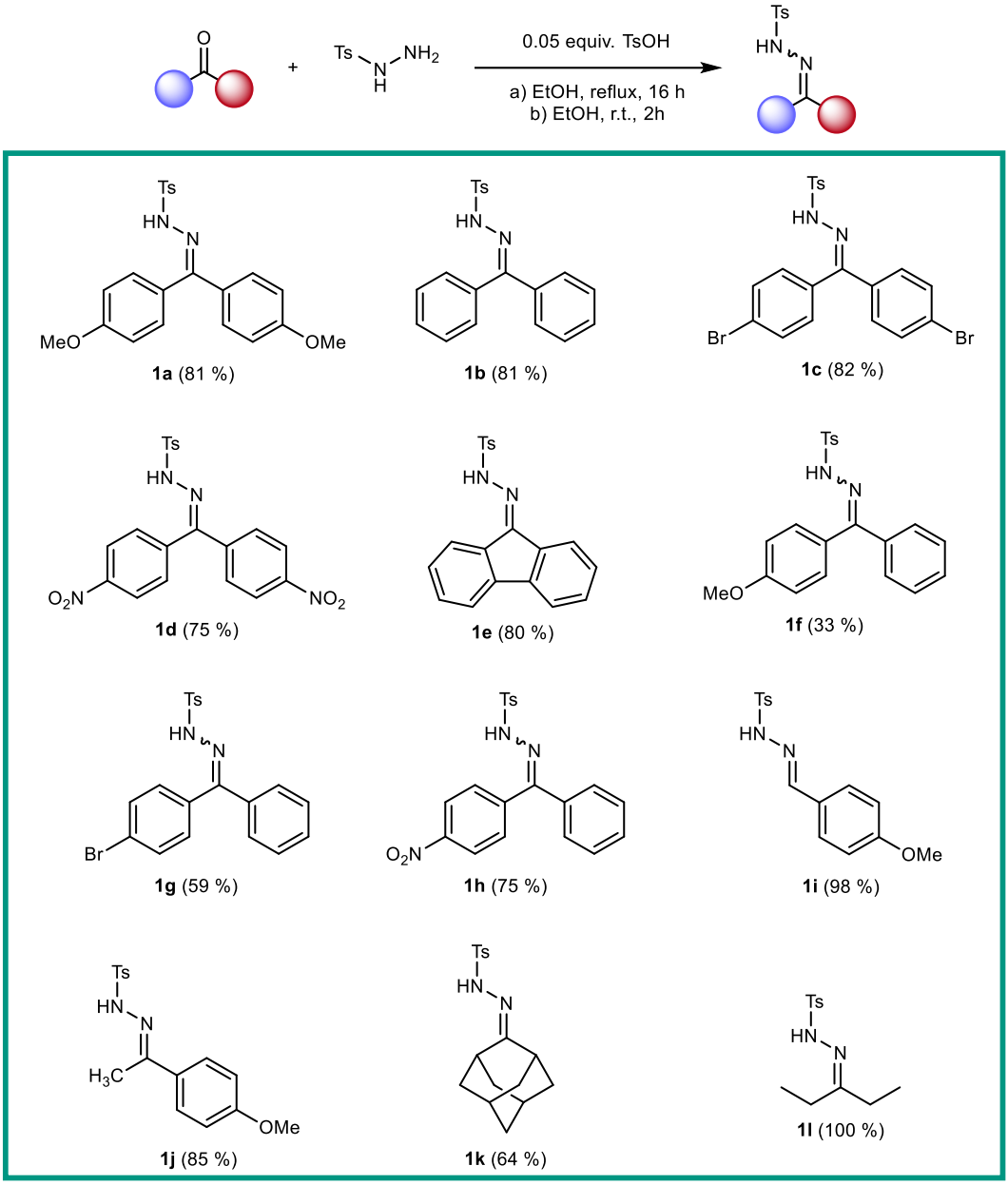

*Scheme 51: Scope of the investigated NTHs. **1i**, **1j** and **1l** were prepared according to conditions b, all others were prepared according to conditions a. **1e**, **1f**, **1g**, **1i**, **1j** and **1k** were synthesized during the master thesis of the author.*[424]

The synthesis of aromatic NTHs from benzophenone derivatives required heating of the reaction mixture overnight in the presence of catalytic amounts of *p*-toluenesulfonic acid. Aliphatic ketones and aldehydes reacted efficiently with tosyl hydrazide under ambient conditions without the need for heating or acidic catalysis. NTHs **1e-1g** and **1i-1j** were synthesized prior to this work.[424]

The benzophenone-derived NTHs **1a-1h** were all found to undergo smooth homocoupling, yielding their corresponding TPE derivatives **2a-2h** in good yields ranging from 80 to 99% (Scheme 52). This demonstrates a high tolerance of the method for generating both electron-rich and electron-poor, condensed cyclic, as well as synthetically useful di- or tetrahalogenated and -nitrated TPE derivatives.

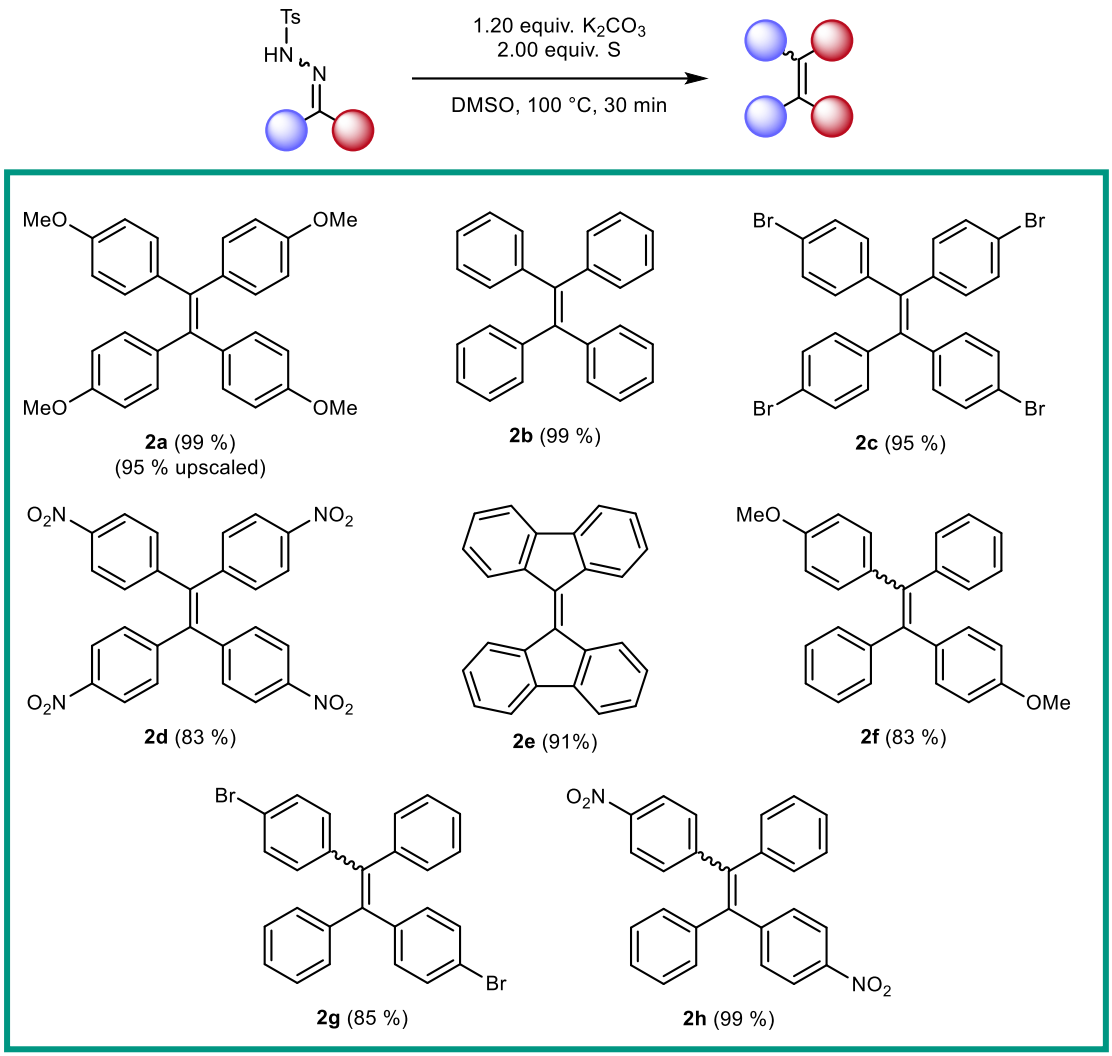

*Scheme 52: Synthetic scope of the homocoupling of NTHs. Compounds **2f** and **2g** were synthesized during the master thesis of the author.*[424]

The successful homocoupling of nitro-bearing substrates to TPEs **2d** and **2h** is particularly noteworthy, since it is out of scope for the commonly used McMurry coupling due to the instability of the nitro function against reducing agents.[406]

In similar fashion to the McMurry reaction, the homocoupling of unsymmetrically substituted NTHs **1f**-**1h** resulted in a near-statistical mixture of the respective *(E)*- and *(Z)*-isomers of the corresponding TAEs **2f**-**2h**. The homocoupling of aldehyde-based NTH **1i** and aliphatic NTHs **1j-1l** was investigated in the master thesis prior to this work.[424] It was found that these substrates did not undergo selective alkylidene-homocoupling, instead producing mixtures consisting of numerous different products as apparent by the appearance of various signals in the methoxy-region of the crude ^{1}H-NMR spectra. In the cases of **1i** and **1j**, the homocoupling products could be qualitatively detected *via* gas chromatography / mass spectrometry (GC-MS). However, due to the complicated nature of the product mixtures, no further workup and analysis were undertaken, The homocoupling method was thus deemed not feasible for NTHs derived

from aldehydes and aliphatic compounds, and not further investigated in the context of this work.[424]

Interestingly, all prepared TPE derivatives, except for **2e**, exhibited their characteristic solid-state-fluorescence behavior, known as aggregation-induced emission (AIE).

The homocoupling of **1a** to **2a** could be successfully upscaled to a gram scale (5 mmol), with the product **2a** being obtained in a yield of 95% in this case.

Furthermore, a one-pot-procedure, combining the NTH synthesis and the homocoupling, was attempted. Herein, the crude NTH **1a** was used in the subsequent homocoupling without purification, allowing the isolation of TPE **2a** in a good yield of 85% in relation to ketone **4a**. This is slightly superior compared to the two-step approach with intermediate isolation of NTH **1a**, which exhibits a combined yield of 81%.

In comparison, the synthesis of the TPE derivatives **2a**–**2h** from their respective ketones **4a**-**4h** *via* a McMurry coupling has been reported several times with yields generally ranging from 70-99%.[435–439] The typically applied reaction conditions employ overstoichiometric amounts of titanium reagents and a reducing agent such as zinc under inert atmosphere. Workup is generally performed *via* extraction and subsequent column chromatography.

When considering a combination of both the NTH synthesis as well as the homocoupling, the herein presented method achieves combined yields of 28% to 85% in relation to the respective ketones, and was further shown to be feasible without the purification of the NTH. While these yields are generally slightly lower than those of the McMurry reaction, the presented homocoupling comes with the advantages of a complementary substrate scope, lower cost and easier operability due to not requiring excessive amounts of metallic reagents, extensive workup and inert conditions. These advantages illustrate that the presented procedure can potentially serve as a viable addition to the repertoire of synthetic methods to access TPE derivatives.

4.1.4 Cross-Coupling

Disclaimer

Several products described in this chapter were synthesized as part of the master thesis of the author and were thus not obtained in the context of this work. The respective compounds are indicated in the discussion and the Experimental Section (chapter 6.3.1).

The mechanistic study of the homocoupling reaction described in section 4.1.2 provided evidence for the *in situ* formation of a thioketone as part of the mechanism.[424] The homocoupling was also shown to proceed when using the thioketone as an additional stoichiometric reactant. Therefore, using thioketones and NTHs bearing different substituents,

the synthesis of cross-coupled TPEs was attempted. The general feasibility of this cross-coupling approach was already demonstrated in the preceding master thesis.[424]

Thioketones **3a**-**3c** were synthesized from the respective carbonyl compounds **4a**-**4c** by thionation using Lawesson's reagent, and obtained in yields of 70-94% (see section 6.3.1.4).

For the cross-coupling, thioketones and NTHs were reacted only with potassium carbonate in order to prevent the competing NTH homocoupling. The thioketone component was used in a very slight excess of 1.02 equivalents. Elemental sulfur was added after 30 minutes of reaction time and the reaction was continued for another 30 minutes in order to ensure complete thiirane desulfurization. Thus, sulfur was only used in its capacity as desulfurization agent in this cross-coupling approach. Essentially, this kind of reaction protocol can be considered an upgraded Barton-Kellogg reaction, since it does not require the handling of a diazo compound, instead generating it *in situ* from the corresponding NTH, and further demonstrates a new method for thiirane desulfurization.

The cross-coupling method also proved to be highly viable for the synthesis of TPE derivatives, as shown by successful coupling of thioketone **3a** with a range of benzophenone-derived NTHs **1a**-**1c**, yielding the cross-coupled TPEs **5a**–**5c** in good yields ranging from 79 to 85% (Scheme 53). Similar to the homocoupling method, the compatibility of the cross-coupling procedure with NTHs bearing electron-donating and electron-withdrawing functional groups, particularly the easily reducible nitro group, was confirmed.

Similarly, thioketones **3b** and **3c** were efficiently cross-coupled with NTHs **1a** and **1b**, yielding TPE derivatives **5g**–**5i** in good yields (82-95%). Notably, TPE derivative **5b** could be successfully synthesized both from **3a** and **1c** as well as **3c** and **1a**, illustrating the flexibility of the method from both the NTH and thioketone sides.

Akin to the TPE derivatives accessed *via* the homocoupling route, compounds **5a**-**5c** and **5g**-**5i** exhibited the expected AIE behavior.

Additionally, it was found that the aliphatic and aldehyde-derived NTHs **1i**, **1j** and **1l**, which did not undergo selective alkylidene-homocoupling, could be successfully cross-coupled with thioketone **3a**, yielding compounds **5d**–**5f** in moderate to excellent yields (56-93%). Thus, the successful introduction of alkyl substituents expands the scope of the alkylidene-cross-coupling to a wider range of highly substituted alkenes beyond TPEs.

It has to be noted that the thioketones used in this work were synthesized and stored under an inert atmosphere (see section 6.3.1.4). However, they were found to be sufficiently stable towards air and moisture to perform the cross-coupling reactions without an inert atmosphere, maintaining the feasible and simple reaction set-up.

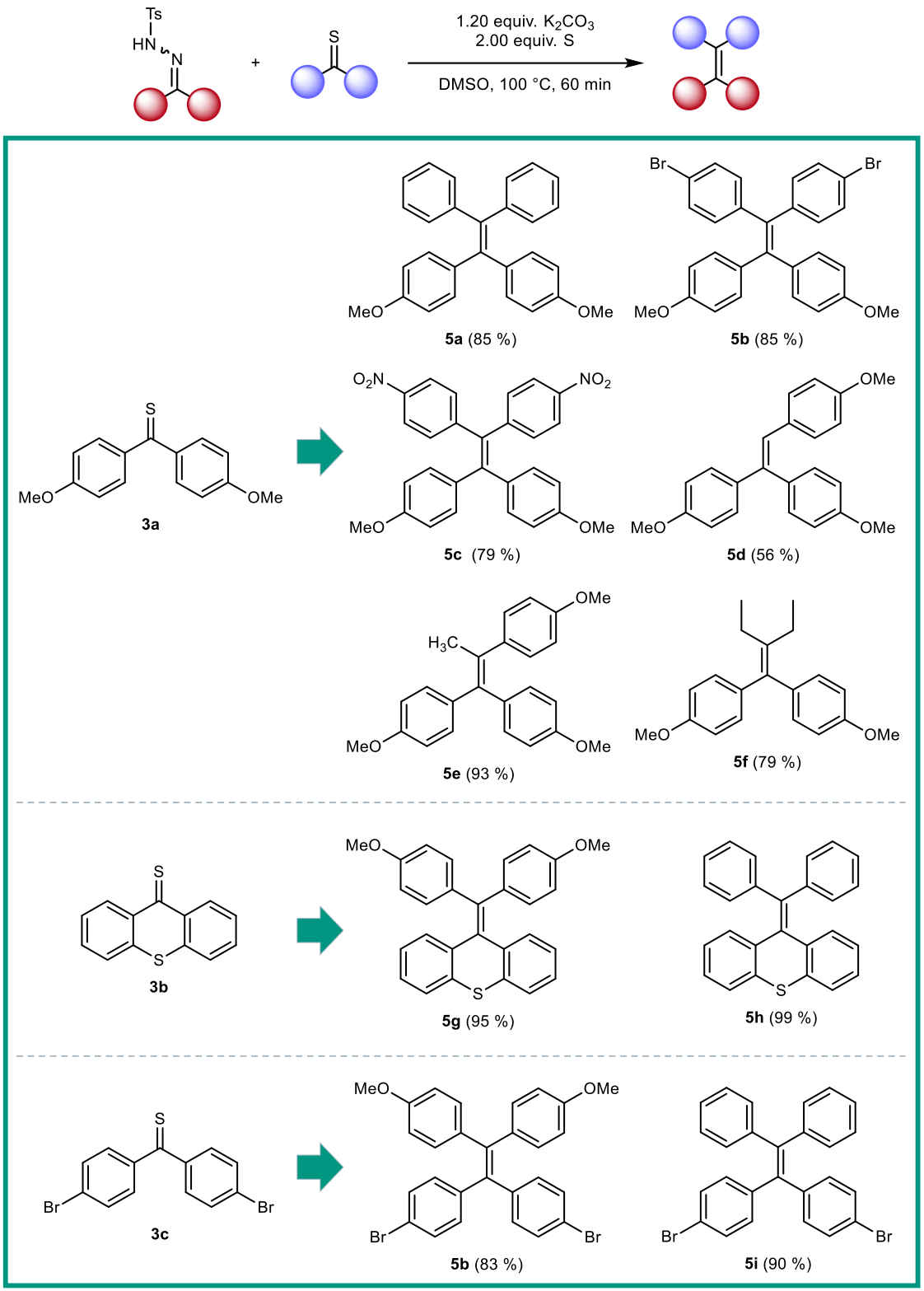

*Scheme 53: Synthetic Scope of the herein investigated cross-coupling of NTHs with thioketones. Compound **5d** was synthesized during the master thesis of the author.*[424]

In comparison to other prevalent synthetic routes toward unsymmetrical alkenes comprising different alkylidene moieties (see section 2.5.3), the herein described method can be more efficient and feasible.[404] For instance, the utility of the McMurry coupling of two different benzophenone derivatives is greatly hindered by the competing homocoupling reaction. This

results in the formation of statistical mixtures of all possible products, greatly complicating the workup and leading to low yields.[409,439]

Due to the infeasibility of the McMurry coupling, significantly more elaborate methods, often involving multiple reaction steps are required for a selective synthesis of alkylidene-cross-coupled alkenes, frequently relying on transition-metal-catalyzed cross-couplings (compare section 2.5.3). The herein presented method for the synthesis of alkylidene-cross-coupled alkenes poses a similar synthetic effort, since the preparations of NTH and thioketone as well as the subsequent coupling require three reaction steps. Still, all steps are carried out without the need for overly hazardous and expensive (organo)metallic reagents.

4.1.5 Summary

Two methods for the synthesis of highly substituted alkenes *via* olefination of *N*-tosylhydrazones (NTHs) were established. The first method entails a sulfur-mediated alkylidene-homocoupling of aromatic NTHs and was shown to effectively generate a range of TPE derivatives with different substituents. Compared to classic approaches like McMurry reactions or transition-metal-catalyzed cross-couplings, this two-step reaction can be advantageous in terms of feasibility (easy reaction setup, cheap and benign additives, less elaborate work-up, tolerance of reduction-labile functional groups). Additionally, the possibility to perform both reaction steps in a one-pot approach further adds to the viability of the procedure. However, the method showed low selectivity for aliphatic and aldehyde-derived substrates. The second method uses a thioketone as an additional starting material, which enables the synthesis of alkylidene-cross-coupled alkenes with an additional tolerance for aliphatic and H-substituents, while maintaining similar benefits as its homocoupling pendant in comparison to alternative procedures. The cross-coupling method can be considered a variation to the already established Barton-Kellogg reaction, since it entails the *in situ* generation of the required diazo compounds. Both methods were shown to be viable alternatives to other established procedures often used to access TSAs, particularly TPE derivatives, which are interesting target molecules due to their aggregation-induced fluorescence properties. The synthetically useful scope of both methods paired with the high obtained yields and the operative simplicity potentially makes the showcased reactions a viable addition to the toolbox for the synthesis of highly substituted double bonds.

4.2 Synthesis of Conjugated Polymers by Sulfur-mediated Polyolefination

Disclaimer

The results described in this chapter are based on a previous publication by the author of this thesis. Text and figures are partially reproduced, edited and extended from this article, which is licensed for re-use under Creative Commons CC BY 4.0:[440]

P. Conen, F. J. O. Niedermaier, S. Abou El Mirate, M. A. R. Meier, A Novel Synthesis Strategy for Poly(Arylene-Vinylene) Derivatives by Elemental Sulfur-Mediated Polyolefination, *Macromol. Rapid Commun.* **2025**, 2500166. https://doi.org/10.1002/marc.202500166

The author of this thesis planned, performed and evaluated the herein described experiments and wrote the original draft of the publication.

Florian J. O. Niedermaier performed the major part of the investigations on monomer synthesis and polymerization conditions of the model substrate as part of his bachelor thesis under co-supervision of the author. Sophia Abou El Mirate performed a major part of syntheses related to the polymerization scope of this project as part of her apprenticeship under co-supervision of the author. Philipp Mehr performed several syntheses related to this project as part of the "Organisch-Chemisches Fortgeschrittenenpraktikum" under supervision of the author.

Abstract

Herein, a new synthetic access to poly(arylene-1,2-diarylvinylene) (PAV-DA) derivatives by a novel polyolefination of bifunctional *N*-tosylhydrazones using base-activated elemental sulfur is presented. PAV-DAs are particularly interesting due to their aggregation-induced emission (AIE) properties, resulting in high solid-state photoluminescence quantum yields. The presented procedure allowed the successful synthesis of 8 homopolymers and 2 copolymers with different arylene backbones and aryl side chains from easily accessible monomers, not requiring the use of expensive or highly hazardous materials. The polymers were obtained in good yields and number average molecular weights up to 26.9 kDa. Thermal analysis revealed exceptionally high thermal stability with degradation temperatures as high as 541 °C and glass transition temperatures of up to 263 °C. Furthermore, it was found that the polymer properties were readily adjustable *via* copolymerization.

4.2.1 Context

As discussed in chapter 2.5, AIE-active compounds such as TAEs have seen a plethora of potential uses, including as physical and chemical sensors, in bioimaging or in the manufacture of optoelectronic devices.[363,381,441–444] In this context, polymeric materials with AIE properties have similarly been thoroughly researched due to their superior processability and mechanical properties compared to small molecules.[373–378] The linear polymeric counterparts of TAEs, poly(arylene-1,2-diarylvinylenes) (PAV-DAs), also possess high photoluminescence quantum yields in the solid state, and have been shown to exhibit additional interesting properties such as intrinsic microporosity. As such, several potential applications of PAV-DAs as optical sensors or in organic electronics have been reported.[387–389,394–398]

However, most of the currently established methods for the synthesis of PAV-DAs suffer from severe drawbacks such as the need for highly toxic or unstable materials, as well as expensive catalysts, significantly compromising their practicability. For instance, the currently most prevalent synthesis method for PAV-DAs is the conversion of diketones into bis(*gem*-dichlorides), followed by a reductive polyolefination using metal-based reducing agents such as chromium(II) salts or cobalt octacarbonyl (see Scheme 45).[395,396,419–421] Other methods to synthesize PAV-DAs are described in section 2.5.3.

In the previous section, a novel sulfur-mediated homocoupling reaction of aromatic NTHs was presented, providing an efficient synthetic access to TPE derivatives. In this chapter, the applicability of this method towards bifunctional NTHs was investigated in order to provide a novel alternative access towards of PAV-DAs that does not rely on expensive and/or highly hazardous materials such as cobalt octacarbonyl (Scheme 54).

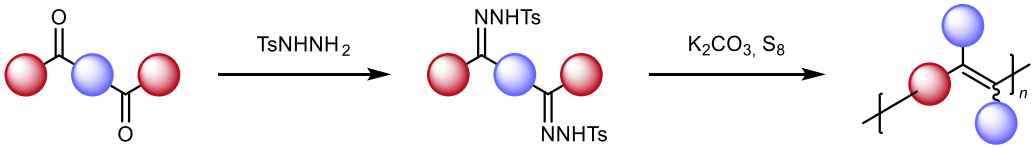

Scheme 54: Envisioned synthesis strategy for PAV-DAs by sulfur-mediated polyolefination.[440]

4.2.2 Monomer Synthesis

First, a methoxy-substituted model monomer **7a** was prepared from diketone **6a**, allowing for easy monitoring of all steps *via* ^{1}H NMR spectroscopy. The corresponding diketone **6a** was synthesized according to a slightly adapted literature procedure *via* Friedel-Crafts acylation of anisole with commercially available terephthaloyl chloride in the presence of $AlCl_3$, obtaining **6a** in a yield of 84% (see section 6.3.2.1).[445]

For the synthesis of the bifunctional NTH **7a** from diketone **6a**, the previously used procedure for monoketones was initially attempted (compare Scheme 51), using a slight excess of tosyl hydrazide and catalytic *p*-toluenesulfonic acid (10 mol%) in refluxing ethanol.[422] However, conversion of **6a** remained incomplete, even after extending the reaction time to 72 hours (see Experimental Section, Supplementary Figure 71). Gratifyingly, it was found that switching the solvent to toluene instead of ethanol resulted in complete conversion of **6a** after 16 hours, yielding monomer **6a** in a yield of 78% (Scheme 55). Notably, no formation of monosubstituted NTH, resulting from the condensation of only one of the two carbonyl groups of **6a**, was observed. It is expected that the electron-withdrawing character of the installed tosylhydrazone moiety after the first substitution activates the second carbonyl group, so that the second condensation proceeds at a higher rate. Furthermore, ^{1}H NMR indicated the formation of only one of the three possible stereoisomers of **7a**, greatly simplifying the workup of the reaction, which could be performed by simple filtration and washing. **7a** could hence be synthesized in an overall yield of 66% from cheap and commercially available starting materials in an efficient two-step process without requiring any elaborate workup methods.

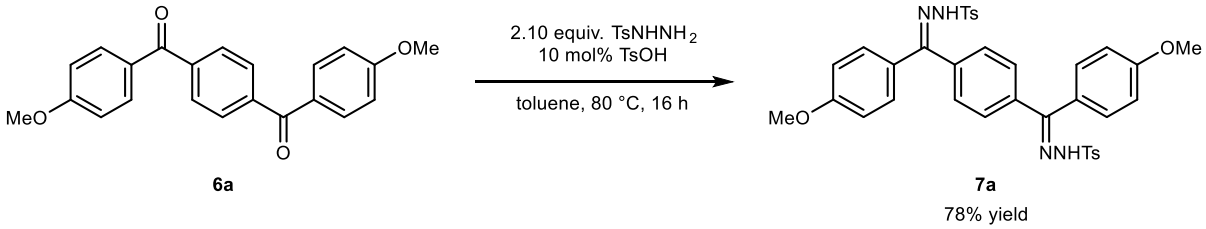

*Scheme 55: Synthesis of model monomer 7**a** from the corresponding diketone **6a**.*[440]

4.2.3 Optimization of Polymerization Conditions

4.2.3.1 Initial Experiments and Workup optimization

The initial polymerization attempt was conducted under the optimized homocoupling conditions described in the previous chapter, adapted for a bifunctional substrate (compare Scheme 48). Accordingly, **7a** was reacted with 2.40 equivalents of potassium carbonate in the presence of 4.00 equivalents of atomic elemental sulfur. The reaction was conducted at 100 °C under air atmosphere in deuterated dimethyl sulfoxide (DMSO-d_6) (c(**7a**) = 0.25 M) and the progress of the polymerization was followed *via* ^{1}H-NMR spectroscopy. Full conversion of **7a** was observed after 30 minutes, as apparent by the disappearance of its N-H resonance at 10.45 ppm. Furthermore, the emergence of broad signals in both the aromatic and methoxy spectral regions indicated the successful formation of polymer **P1** (Scheme 56).

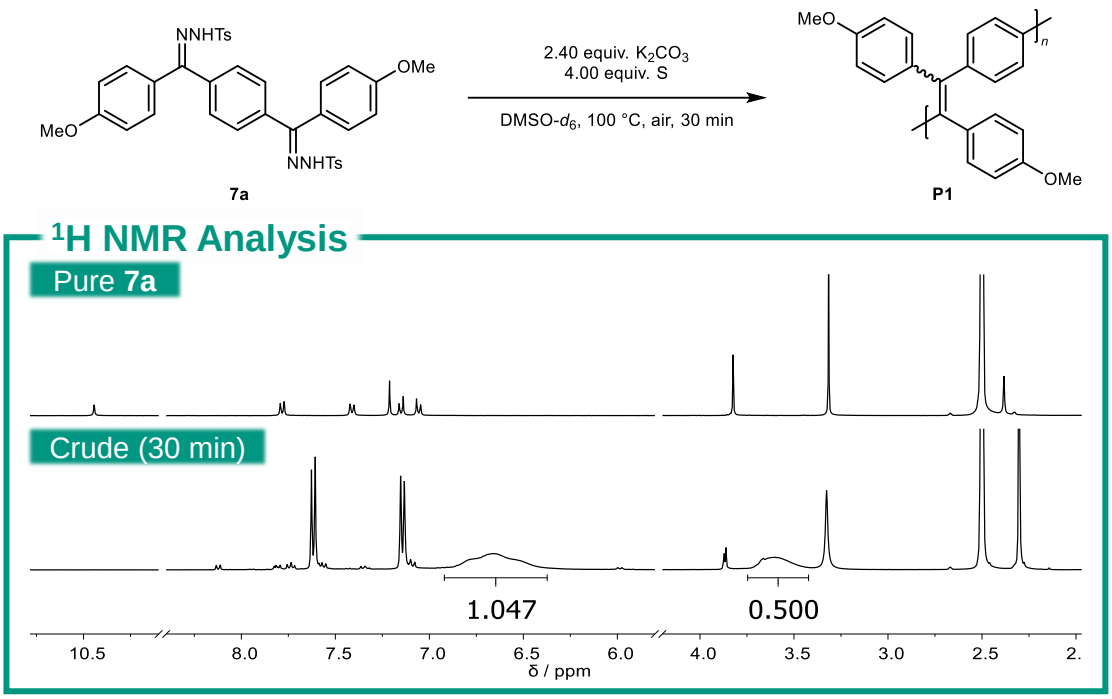

*Scheme 56: Reaction conditions employed for the initial synthesis of **P1** (top) and ^{1}H NMR spectra of **7a** and the crude reaction mixture of the first polymerization after 30 minutes (bottom).*[440]

In order to isolate the product, the reaction mixture was diluted with dichloromethane (DCM), filtered over celite, concentrated *in vacuo* and precipitated into cold MeOH, yielding **P1** as a dirty yellow powder. Size exclusion chromatography (SEC) measurements indicated a number average molecular weight M_n of 6.0 kDa and a dispersity $Đ$ of 2.08. However, the obtained yield exceeded 100 %, which was attributed to the presence of residual elemental sulfur in the product. This was confirmed *via* differential scanning calorimetry (DSC), revealing an endothermic peak around 120 °C, corresponding to the melting temperature of sulfur (see Experimental Section, Supplementary Figure 100). Hence, the workup procedure was further optimized before continuing to optimize the polymerization conditions. First, DCM was substituted with chloroform, which was found to be a superior solvent for the polymer. Furthermore, the chloroform phase was subjected to additional washing steps with sodium sulfite solution and water in order to more efficiently remove elemental sulfur. With the optimized workup method, **P1** could be isolated in a yield of 46%, now as a bright yellow powder. In this instance, the successful removal of sulfur was confirmed by the absence of a melting peak in the DSC measurement and further underlined by elemental analysis (see section 6.3.2.3). Furthermore, as expected, **P1** exhibited yellowish-green AIE fluorescence under irradiation with ultraviolet light.

After establishing a workup method, further optimizations of the reaction conditions were attempted. Interestingly, it was found that increasing the reaction temperature up to 140 °C led to a decrease of the number average molecular weight of **P1**, while also exhibiting

unsatisfactorily low yields (Table 4, entries 3-4 in Section 4.2.3.3). It was thus assumed that higher molecular weight polymers can be obtained at lower reaction temperatures. However, in the original optimization study of the monofunctional olefination reaction of **1a** (see section 4.1.1), temperatures below 100 °C had been dismissed as not feasible and not further investigated due to incomplete conversion of the starting materials even after prolonged reaction times.[422,423] Hence, further studies were needed in order to examine the applicability of lower reaction temperatures to the olefination reaction, especially since the temperature studies in the previous work were still conducted using NaH instead K_2CO_3.[422,423]

4.2.3.2 Further optimization studies of the monofunctional homoolefination

Further optimization studies using the monofunctional NTH **1a** as a suitable model for **7a**, were thus performed (Table 3). It was found that the olefination still proceeded well at 90 °C, with full conversion of **1a** reached after 30 minutes (Table 3, entry 2). At 80 °C, 93% conversion were achieved after 90 minutes, which increased to 99% after 3 hours (Table 3, entry 3). The reaction was simultaneously attempted at 80 °C using vacuum-dried reagents, flame-dried glassware and an argon atmosphere, achieving 99% conversion after 90 minutes, with full conversion after 3 hours (Table 3, entry 4). Generally, fewer unidentifiable signals were observed in the crude NMR spectra of the experiments conducted under inert atmosphere, indicating fewer side reactions, which is of significant importance to the efficiency of step-growth polymerizations. Hence, inert atmosphere was used from this point onward. However, it has to be noted that, as described in chapter 4.1, an inert atmosphere is not required for efficient olefination of monofunctional NTHs at 100 °C.

The reaction could similarly be conducted at 70 °C with **1a** being fully converted after 16 hours. At 60 °C, complete conversion of **1a** was not achieved even after 72 hours (Table 3, entries 5-6). Since the rate-determining step of the olefination reaction is the initial base-induced decomposition of the NTH into a diazo compound, it was speculated that substitution of the tosyl group of **1a** with a better leaving group could potentially allow for the reaction temperature to be lowered even further.[422] This can be achieved using more sterically demanding sulfonyl moieties like the triisopropylbenzenesulfonyl (trisyl) moiety or electron-deficient groups such as nitrobenzenesulfonyl (nosyl) or trifluoromethylbenezenesulfonyl (triftosyl) moieties.[426,446] For instance, triftosylhydrazones have been reported to readily decompose at temperatures as low as -40 °C.[447]

*Table 3: Temperature screening reactions using monofunctional sulfonylhydrazones **1a** and **8a**. The reactions were conducted in DMSO-d_6 (0.5 M) using 1.20 equiv. K_2CO_3 and 2.00 equiv. S.*[440]

Entry	Substrate	T / °C	Atm.	Solvent	Base	t / h	Conversion/ %
1	**1a**	100	Air	DMSO	K_2CO_3	0.5	Full
2	**1a**	90	Air	DMSO	K_2CO_3	0.5	Full
3	**1a**	80	Air	DMSO	K_2CO_3	1.5	93
						3	99
4	**1a**	80	Argon	DMSO	K_2CO_3	0.5	90
						1.5	99
						3	Full
5	**1a**	70	Argon	DMSO	K_2CO_3	2	64
						4	85
						16	Full
6	**1a**	60	Argon	DMSO	K_2CO_3	4	45
						23	94
						72	98
7	**10a**	70	Argon	DMSO	K_2CO_3	0,5	36
						1	57
						2	92
						4	93
						16	Full
8	**10a**	60	Argon	DMSO	K_2CO_3	4	51
						23	99
						48	Full
9	**1a**	80	Argon	Ethylene glycol	K_2CO_3	0,5	36
10	**1a**	80	Argon	Triglyme	K_2CO_3	0,5	0
11	**1a**	80	Argon	MeCN	K_2CO_3	0,5	0
12	**1a**	80	Argon	DMC	K_2CO_3	0,5	0
13	**1a**	80	Argon	2-methyl-THF	K_2CO_3	0,5	0
14	**10a**	70	Argon	DMSO	Cs_2CO_3	1	54
15	**10a**	70	Argon	DMSO	K_3PO_4	1	30
16	**10a**	70	Argon	DMSO	KO^tBu	1	51
17	**10a**	70	Argon	DMSO	NaOMe	1	35

Hence, hydrazides bearing *p*-nosyl, trisyl and *o*-nosyl moieties were synthesized from the commercially available sulfonyl chlorides and hydrazine according to literature procedures (see section 6.3.2.3). The hydrazides were subsequently reacted with 4,4'-dimethoxybenzophenone **4a** in order to generate the corresponding sulfonylhydrazones (Scheme 57).[448] *p*-Nosylhydrazone **8a** could be generated in a yield of 92%, albeit an excess of nosyl hydrazide had to be used due to its competing thermal decomposition into the corresponding sulfinic acid. Using *o*-nosyl hydrazide resulted in the formation of an insoluble mass, while in the case of trisyl hydrazide, benzophenone **4a** was recovered unreacted. Hence, thermal decomposition of the activated hydrazides presumably prevents the condensation with the benzophenone. It was thus concluded that the mismatch of low electrophilicity of aromatic ketones and the thermal instability of trisyl and *o*-nosyl hydrazides rendered a synthesis of the corresponding hydrazones **8b** and **8c** unfeasible, and no further investigations were conducted.

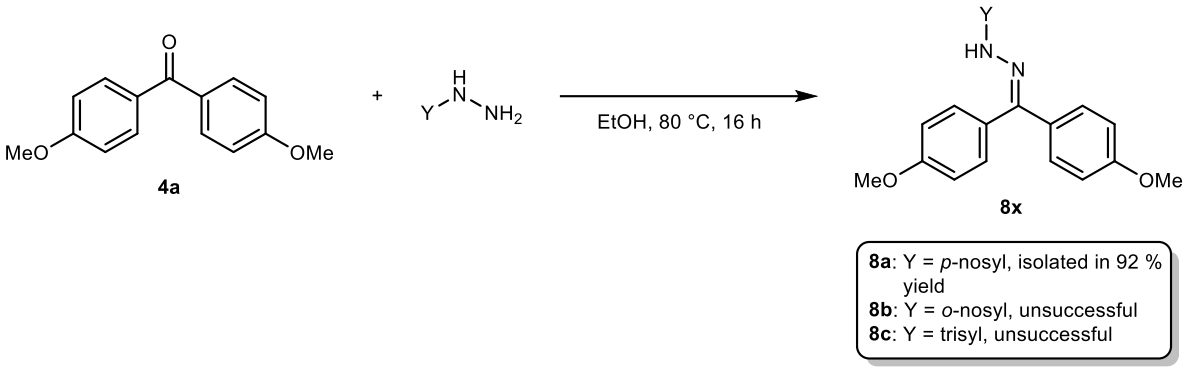

*Scheme 57: Synthesis attempts of differently substituted hydrazones. Only p-nosylhydrazone **8a** could be successfully isolated.[440]*

As anticipated, *p*-nosylhydrazone **8a** was indeed found to undergo the olefination reaction at a slightly higher rate than tosylhydrazone **1a** (Table 3, entries 7-8). It was possible to achieve full conversion of **8a** at 60 °C within 48 hours. Further complementary optimization experiments using different bases and solvents were conducted, however none were found to be as efficient as the already used potassium carbonate / DMSO system (Table 3, entries 10-17).

In order to be able to conduct the polymerization at 60 °C, it was attempted to synthesize the bifunctional *p*-nosylhydrazone **7a'** from **6a**. Unfortunately, it was observed that the thermal decomposition of *p*-nosyl hydrazide was more significant in this case. Using 3 equiv. of nosyl hydrazide, only 38% of **6a** were converted into **7a'** after 8 hours, while the remaining hydrazide had fully decomposed (see section 6.3.2.3). It was assumed that the low solubility of **6a** is responsible for slowing down the hydrazone condensation compared to the thermal decomposition of the hydrazide. Due to these complications, it was opted to not further follow this approach and to instead maintain tosylhydrazone **7a** as the monomer of choice because of its easier accessibility and commercial availability of tosyl hydrazide,

4.2.3.3 Polymerization under optimized conditions

As shown in Table 3, the sulfur-mediated olefination of monofunctional NTH **1a** could be conducted at 70 °C under inert conditions at the cost of a somewhat longer reaction time but the gain of fewer side reactions. These findings were subsequently applied to the polymerization of **7a**.

The beneficial effect of inert conditions and pre-dried reagents was apparent when repeating the polymerization at 100 °C, furnishing **P1** with an increased number average molecular weight of 7.8 kDa (Table 4, entry 5), as compared to the 6.3 kDa obtained under air atmosphere without prior drying (Table 4, entry 2). Furthermore, as expected, it was found that conducting the polymerization at lower temperatures indeed resulted in a further increase of the molecular weight of **P1** (Table 4, entries 7-9), reaching a maximum M_n of 16.4 kDa at a reaction temperature of 70 °C. Finally, it was found that variation of the amount of solvent had only marginal effect on the efficiency of the polymerization (Table 4, entries 8 and 10-11). Notably however, increasing the concentration to 0.5 M resulted in a very heterogeneous reaction mixture and stirring difficulties. For this reason, no further optimizations of the stoichiometric ratios of the reactants, *i.e.* using more sulfur and/or base, were attempted.

*Table 4: Optimization experiments for the polymerization of **7a** to **P1**. The reactions were conducted in DMSO under inert conditions using 2.40 equiv. K_2CO_3 and 4.00 equiv. S. The reaction times were adapted based on the screenings in Table 1.*[440]

Entry	Temp. / °C	Yield	Atm.	M_n / g mol^{-1}	M_w / g mol^{-1}	Đ	Comments
1	100	>100%	Air	5960	12400	2.08	No optimized workup
2	100	46%	Air	6250	12300	1.93	
3	120	28%	Air	5270	9500	1.80	
4	140	48%	Air	4130	11200	2.70	
5	100	40%	Inert	7800	16600	2.12	
6	120	42%	Inert	7500	17500	2.33	
7	90	60%	Inert	8800	20000	2.28	
8	80	64%	Inert	10800	24800	2.30	
9	70	76%	Inert	16400	34200	2.11	
10	80	72%	Inert	10700	24100	2.25	c = 0.5 M
11	80	74%	Inert	10400	21300	2.05	c = 0.125 M

4.2.4 Polymerization Scope and Characterization

After establishing an optimized polymerization method, the synthetic scope of the procedure was investigated. Thus, a range of diketones **6b** – **6h**, comprising a structural variety of aryl substituents and arylene backbones, were synthesized in similar fashion to **6a** *via* Friedel-Crafts acylation and obtained in yields between 37% and 83 %. Subsequently, the diketones were converted to their respective bis(NTH) monomers **7b** – **7h**. In all cases, both the ketone and NTH syntheses could be carried out using the same general protocols used for the synthesis of **7a**, providing generally good yields and pure products. Merely in the case of **7h**, slightly lower yields were observed, which assumedly is due to the solubilizing effect of the *tert*-butyl substituents, resulting in increased product losses during washing steps. All synthetic details are found in sections 6.3.2.1 and 6.3.2.2.

The synthesized bis(NTH)s were subsequently subjected to the optimized polymerization conditions (Scheme 58). In all cases, ^{1}H NMR spectroscopy confirmed full monomer conversion after 24 hours, and subsequently the products **P2** – **P8** could be isolated using the previously described workup procedure, obtaining yields between 24% and 86% (Table 5). All polymers were fully characterized using ^{1}H and ^{13}C NMR spectroscopy. Exemplarily, full characterization of **P1** is shown in Figure 3. SEC measurements revealed number average molecular weights between 9.0 kDa and 26.9 kDa and dispersities around 2.00, as is expected for step-growth polymerizations. The only exception is **P7**, which exhibited a very low molecular weight (M_n = 1.7 kDa), a high dispersity of 4.97, and a low product yield of merely 24%. Contrarily, **P2** was obtained with a high number average molecular weight of 26.2 kDa, which significantly outperforms other recently reported methods. For instance, Scherf *et al.* obtained **P2** with an M_n of 8.3 kDa using a reductive polyolefination with cobalt octacarbonyl (yield 61%).[395,449] Older reports for the synthesis of **P2** feature even lower molecular weights.[416,450] For polymers **P3** – **P8**, similar molecular weights and yields to those in literature were generally achieved.[395,396,416,449] It is however noteworthy that in all cases, except for **P7**, more narrow dispersities around 2 were obtained, while for instance for **P5** and **P8** only highly disperse polymers ($Đ$ ~ 5) have been reported.[395,396]

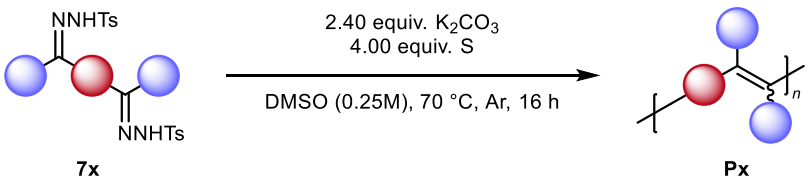

7x **Px**

*Scheme 58: Employed polymerization conditions for the synthesis of polymers **P1**-**P8**.*[440]

*Table 5: Structural scope of the polyolefination and characterization of the obtained poly(arylene-vinylene)s **P1-P8**.*[440]

Polymer			**Yield**	M_n / g mol^{-1}	**Đ**	$T_{d.5\%}$ / °C	T_g / °C
P1 (from **7a**)	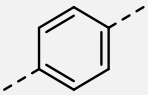	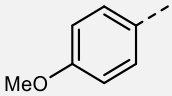	76%	16200	2.11	457	227
P2 (from **7b**)	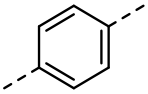	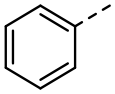	60%	26900	1.86	541	256
P3 (from **7c**)	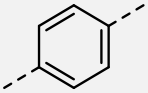	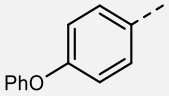	76%	14700	1.90	516	155
P4 (from **7d**)	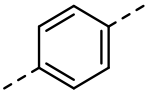	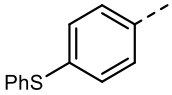	88%	12500	2.23	471	161
P5 (from **7e**)	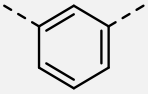	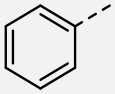	47%	10300	2.01	538	194
P6 (from **7f**)	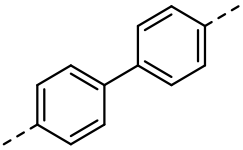	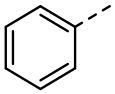	74%	9300	1.61	535	263
P7 (from **7g**)	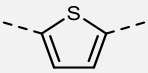	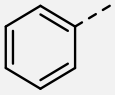	24%	1670	4.97	430	n.o.[a]
P8 (from **7h**)	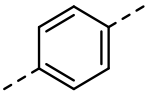	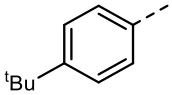	73%	14900	2.19	514	175

a) not observed due to very low molecular weight.

Notably, the polyolefination reaction can result in the formation of both *(E)*- and *(Z)*-configured double bonds. However, it was unfortunately not possible to gain any insights on the isomeric ratio in our obtained polymers with any of the employed methods. For instance, due to poor resolution in the ^{1}H and ^{13}C NMR spectra, experiments such as nuclear Overhauser enhancement spectroscopy (NOESY) were not feasible for structural characterization. While there is generally little or no mention of the isomeric distribution of PAV-DAs synthesized *via* polyolefination reactions in recent literature reports, a paper published by Feast *et al*. in 1999 claims that PAV-DA derivatives synthesized *via* McMurry coupling possess a near-equal ratio of *(E)*- and *(Z)*-double bonds.[395,396,417] Since statistical isomeric mixtures have also been observed for the olefination of unsymmetrically substituted monofunctional NTHs **1f-1h** in chapter 4.1.3, it is tentatively assumed that the same also applies to for the present case.[422]

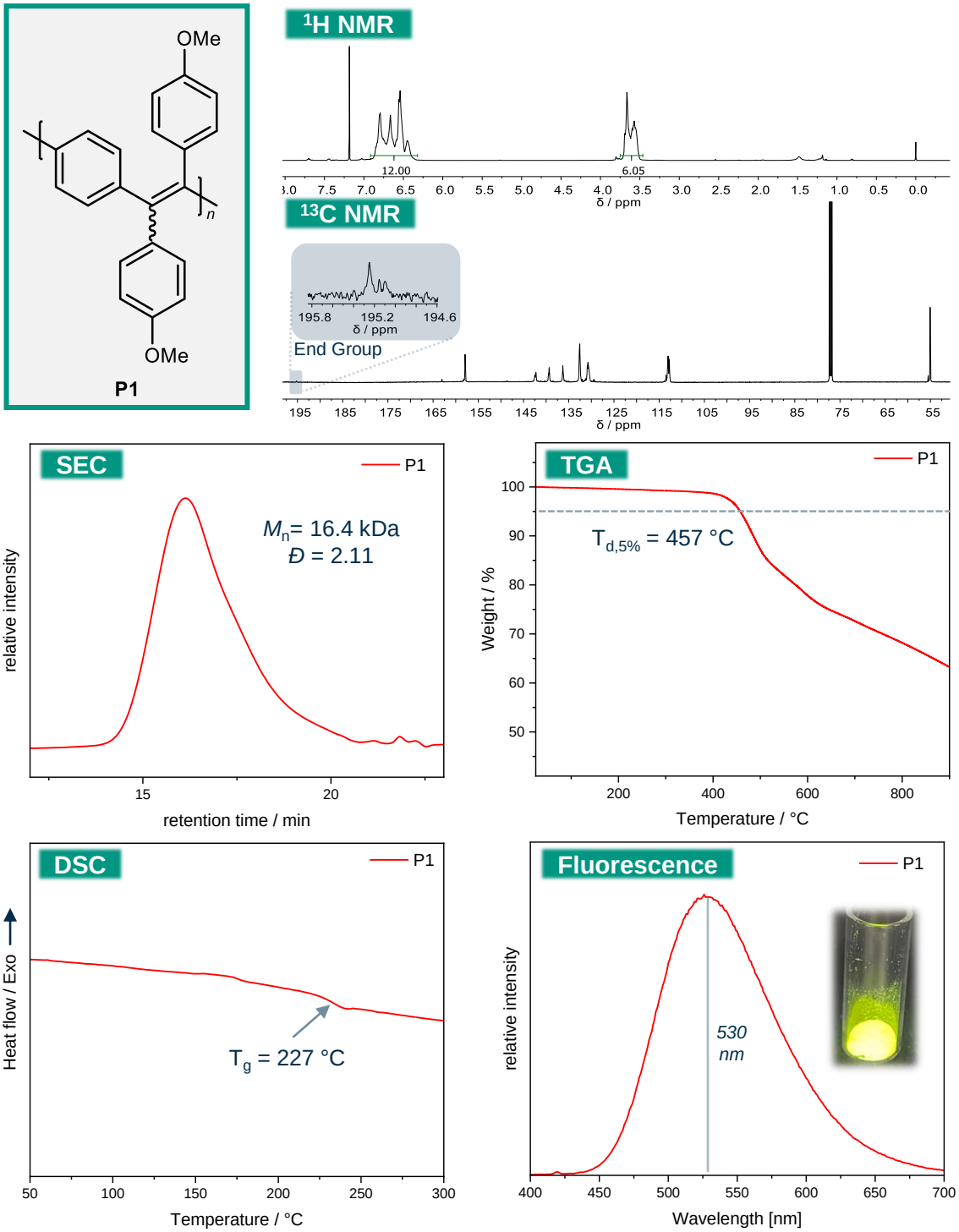

*Figure 3: Characterization of polymer **P1**, including ^{1}H and ^{13}C NMR, SEC, TGA, DSC and Fluorescence.*[440]

The thermal properties of all polymers were examined using thermogravimetric analysis (TGA) and DSC (see Figure 3 for exemplary data for **P1**).

TGA measurements showed significant thermal stability of all polymers, as shown by the very high degradation temperatures ($T_{d,5\%}$, temperature at which 5% weight loss was detected) in the range between 430 °C and 538 °C. The high thermal stability most likely stems from the aromatic character of the polymers. DSC measurements revealed very high glass transition temperatures for the synthesized polymers, ranging from 155 °C for **P3** to 263 °C for **P6**. It was

generally observed that the presence of additional substituents on the phenyl side chains lowered the T_g (for instance **P3**, **P4**, **P8**), while the polymers bearing unsubstituted phenyl side chains exhibit the highest glass transition temperatures (**P2**, **P6**). For **P7**, no glass transition temperature could be detected, possibly due to its low degree of polymerization. Furthermore, DSC measurements confirmed the successful removal of elemental sulfur from all polymers due to the absence of endothermic melting peak around 120 °C.

As anticipated, most of the synthesized polymers exhibited characteristic AIE fluorescence under UV irradiation, being non-emissive in solution but highly emissive in aggregated states. Most polymers were obtained as yellow solids and exhibited yellowish-green fluorescence with emission maxima between 513 and 531 nm. The exceptions were **P5** and **P7**, the former being an off-white solid with a blue fluorescence at 473 nm, and the latter being a dark red solid and non-emissive both in solution and in the solid state.

In order to determine the nature of the polymer end groups, a ^{13}C NMR study (see Figure 3) of a sample of **P1** sample revealed a low-intensity resonance at 195 ppm, which is indicative of a carbonyl function (the carbonyl resonance of the corresponding diketone **6a** is at 194 ppm). This is easily explained considering the postulated polymerization mechanism (compare Scheme 50). The reaction proceeds *via* a diazo intermediate, which subsequently reacts to a thioketone with elemental sulfur, as recently explained in the literature.[149,422] The thioketone subsequently reacts with a prior intermediate of the reaction mechanism to form a thiirane, which represents the growth step of the polymerization. Nearing complete conversion of the NTH, it is expected that once no more diazo compound is being generated, residual thioketone that cannot react further, remains as the polymer end group. Subsequently, due to the aqueous workup conditions, the thiocarbonyl functions are hydrolyzed to carbonyl functions, which were observed in ^{13}C NMR.

Next, the synthesis of copolymers was attempted by mixing monomers **7a** and **7b** (**CP1**) as well as **7a** and **7e** (**CP2**), respectively, in equal stoichiometric ratios (Scheme 59). Both copolymers could be successfully isolated as yellow solids, underlining the versatility of polymer design using the newly established synthetic procedure.

The structure of **CP1** could be confirmed *via* the correct ratio of aromatic and methoxy protons in the ^1H NMR spectrum, **CP2** showed overlaying peaks in the aromatic region due to the chemically very similar structure of the monomer units. Furthermore, the success of the copolymerizations was indicated by SEC analysis, showing high molecular weights (M_n (**CP1**) = 19.2 kDa, M_n (**CP2**) = 15.1 kDa) and dispersities around 2.00.

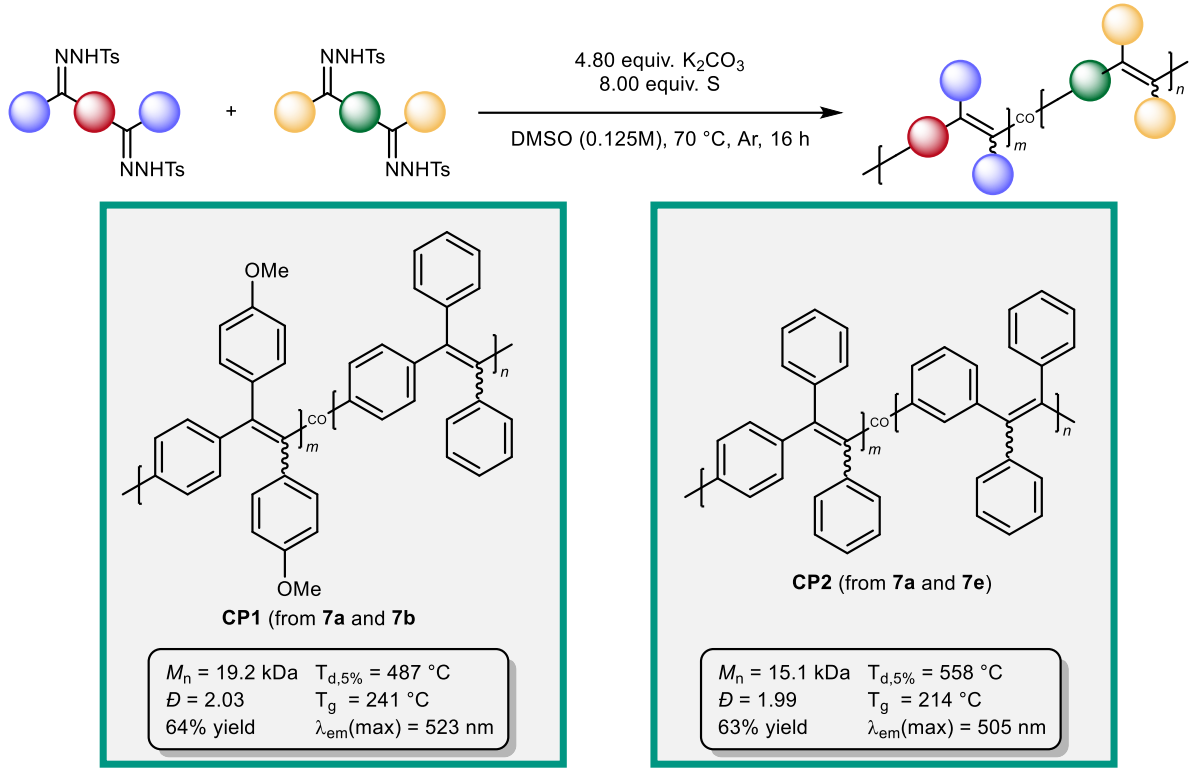

*Scheme 59: Synthesis and characterization of copolymers **CP1** and **CP2**.*[440]

The copolymers share the already observed characteristics of the homopolymers, *i.e.* high thermal stability, high glass transition temperatures, as well as AIE fluorescence. The emission maxima of **CP1** and **CP2** were observed between those of the respective homopolymers. This is particularly noticeable for **CP2**, which exhibits greenish blue fluorescence at 505 nm (Figure 4). The same trend was observable for the glass transition temperatures of the copolymers with respect to the homopolymers, with **CP1** exhibiting a T_g of 241 °C (227 °C and 256 °C for **P1** and **P2**, respectively), and **CP2** showing a glass transition at 214 °C (256 °C and 194 °C for **P2** and **P5**, respectively). These results show that a straightforward copolymerization allows for an easy property adjustment.

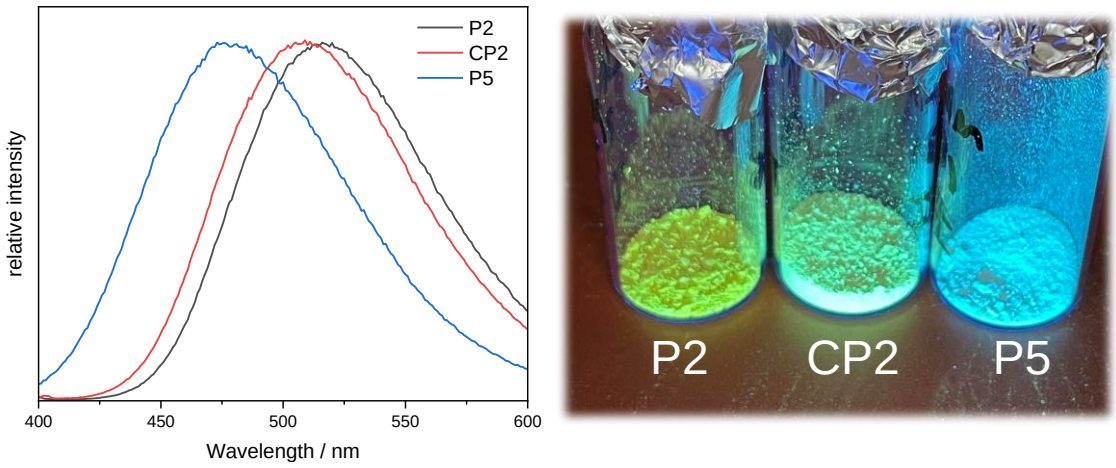

*Figure 4: Comparison of the fluorescence spectra of copolymer **CP2** and the respective homopolymers **P2** and **P5**.*[440]

4.2.5 Summary

In this study, a new strategy to access poly(arylene-1,2-diarylvinylene) (PAV-DA) derivatives *via* an elemental sulfur-mediated polyolefination of bifunctional *N*-tosylhydrazones was presented. The monomers were easily accessible in good yields by a simple two-step procedure *via* Friedel-Crafts acylation and subsequent hydrazone condensation with commercially available tosyl hydrazide. Eight homopolymers comprising different arylene backbones and aryl side chains were successfully obtained in good yields, exhibiting high molecular weights (M_n up to 26.4 kDa). The new polyolefination has proven advantageous compared to established literature procedures, providing superior yields and molecular weights for several examples, while also being significantly more practicable due its bench-stable reagents and lack of expensive or overly hazardous materials. All synthesized polymers were fully characterized using ^{1}H and ^{13}C NMR spectroscopy, IR spectroscopy, SEC, TGA, DSC and fluorescence spectroscopy, revealing interesting characteristics such as AIE fluorescence and exceptional thermal stability. Furthermore, two PAV-DA copolymers were successfully synthesized, allowing for easy adjustment of the desired polymer properties and thus greatly increasing the feasibility of the new procedure. In light of the promising application possibilities of AIE-active polymers such as PAV-DAs, the newly enhanced accessibility of these interesting materials may hopefully incentivize further studies on their properties and potential applications.

4.3 Synthesis and Application of Vegetable Oil-based Polythiols

Disclaimer

The results described in this chapter are based on an accepted article by the author of this thesis. Text and figures are partially reproduced, edited and extended from this article:[451]

P. Conen, F. C. M. Scheelje, R. Häusl, M. A. R. Meier, Synthesis of Novel Vegetable Oil-derived Polythiols and their Thermosets, *ACS Sustainable Chem. Eng.* **2025**, accepted. https://doi.org/10.1021/acssuschemeng.5c10328

Parts of the investigations on side reactions of the herein described ester deoxygenation are published in another article. Text and figures are partially reproduced, edited and extended from this article with permission from the Royal Society of Chemistry:[452]

L. J. Bartlewski, P. Conen, Q. Cai, M. Bürk, D. Armspach, M. A. R. Meier, A more sustainable two-step synthesis of alkylated β-cyclodextrin *via* acetylation and $GaBr_3$-catalyzed reduction, *RSC Sustainability* **2025**, *3*, 4126-4136. https://doi.org/10.1039/D5SU00590F

The author of this thesis planned, performed and evaluated the herein described experiments and wrote the original draft of publication [451]. The author further drafted a section in publication [452] concerning the ester deoxygenation side reaction in collaboration with Leon J. Bartlewski. Clara Scheelje assisted the author in planning and evaluating the experiments and co-supervised the students involved in this project. Ramon Häusl performed the initial optimizations of the reaction conditions of the polythiol synthesis from as part of his "Vertiefungspraktikum" under co-supervision of the author and Clara Scheelje. Mathilde Bourcier assisted with the further optimizations of the polythiol synthesis as part of an internship under co-supervision of the author and Clara Scheelje.

Abstract

Due to the looming depletion of fossil resources, the use of renewable raw materials for the development of new chemical products processes has received increasing attention. Herein, a novel synthetic method for the synthesis of renewable polythiols from vegetable oils is presented. Two types of sunflower oils with different fatty acid composition, as well as a triglyceride prepared from the bio-based platform chemical 10-undecenoic acid, were used as starting materials. The three-step synthesis protocol involves catalytic reduction of the triglyceride ester moieties to ethers, followed by conversion of the carbon-carbon double bonds of the fatty acid substituents to thiols *via* thiol-ene addition of thioacetic acid and subsequent alcoholysis. Polythiols were obtained in overall yields ranging from 58-73% and their feasibility for applications as crosslinkers in the synthesis of polymeric networks was exemplarily demonstrated. Furthermore, all synthetic steps were optimized considering the principles of Green Chemistry as far as feasible, relying on bulk syntheses, simple reaction setups and workup methods, as well as mostly benign and cheap materials.

4.3.1 Context and Synthetic Strategy

The chemistry of thiols was introduced in section 2.4, and the particular utility of thiol-related reactions, such as the radical thiol-ene reaction, for the synthesis of polymeric networks was highlighted. The synthesis of polymeric networks using thiol chemistry commonly involves the use of commercially available polythiols, which are derived from fossil feedstock. Frequently used examples for commercially available polythiols are trimethylolpropane trimercaptopropionate (TMPMP) or pentaerythritol tetramercaptopropionate (PETMP), which are synthesized by esterification of the respective polyols with 3-mercaptopropionic acid (MPA).[453–455] The industrial production of MPA involves the thia-Michael addition of sodium hydrosulfide to acrylonitrile, which is a highly toxic compound derived from fossil-based propylene (Scheme 60).[456–458]

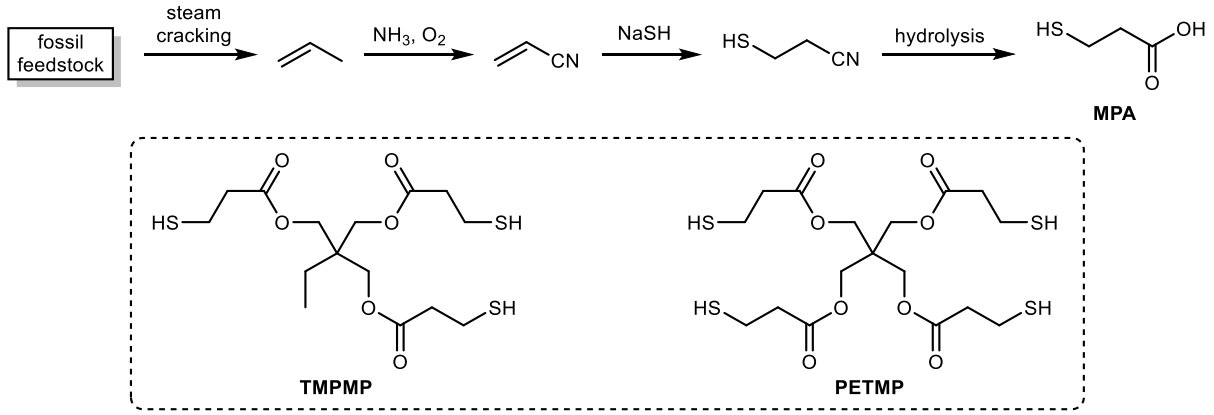

Scheme 60: Synthesis of MPA from fossil feedstocks and the structure of the derived commerically available polythiols TMPMP and PETMP. [453–458]

Meanwhile, only few instances of bio-based polythiols have been reported, especially such with more than two thiol moieties per molecule. Polythiols have for example been synthesized from terpene feedstock, including limonene-derived dithiol **LDT** or squalene-derived hexathiol **SHT**, and have has seen applications for the synthesis of various polymeric materials (Scheme 61).[348,459–463] Furthermore, a small number of publications describe the use of "mercaptanized soybean oils" (MSOs), which were prepared using hydrogen sulfide and soybean oil (representative structure in Scheme 61). MSOs have also been employed for the synthesis of polymer networks or other polyfunctional monomers, mainly *via* nucleophilic addition reactions.[464–467] However, MSOs contain residual unsaturation due to incomplete double bond conversion in their synthesis, and have been demonstrated to be unsuitable for radical thiol-ene chemistry because of intramolecular thiol-ene additions.[353,468]

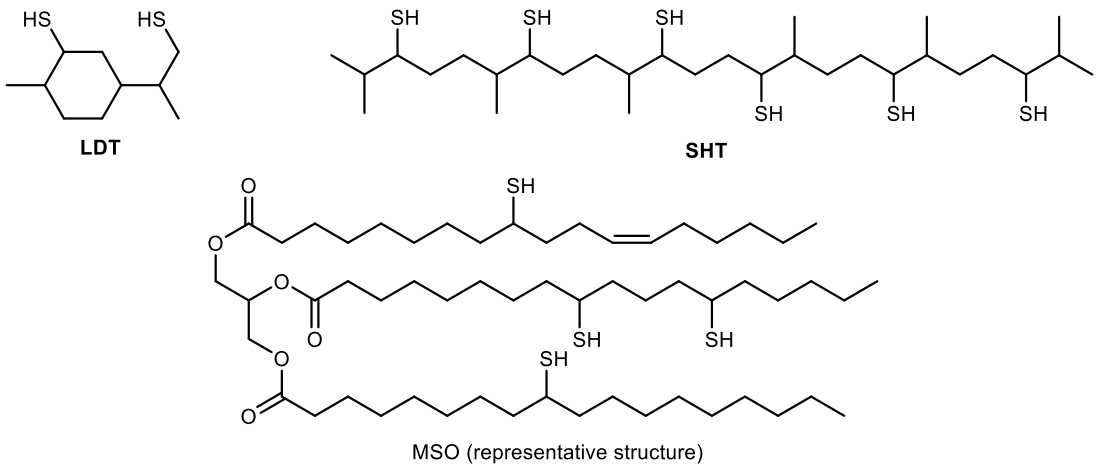

Scheme 61: Representative structures of reported bio-based polythiols.[451,462,466]

This project also aims to synthesize renewable polythiols from unsaturated triglycerides found in vegetable oils, by converting the carbon-carbon double bonds into thiol moieties. Thiols are generally accessible from olefins by thiol-ene addition of hydrogen sulfide or a chemically equivalent compound. As mentioned, MSOs are for instance synthesized by the direct thiol-ene addition of hydrogen sulfide to the carbon-carbon double bonds of soybean oil, which contains large amounts of PUFAs such as linoleic acid (Scheme 61).[464–467] However, the direct use of H_2S in thiol-ene additions suffers from several severe drawbacks. H_2S has a higher bond dissociation energy compared to other sulfhydryl compounds. Accordingly, the thiol products are more reactive than H_2S, resulting in the inevitable formation of thioether side products in (Scheme 62, top).[334,353,456,468] Furthermore, H_2S is more challenging to handle on smaller scales due to its volatility and high toxicity. An alternative method uses thiocarboxylic acids, such as thioacetic acid (HSAc), instead of H_2S, thus yielding a thioester upon thiol-ene addition to the olefin, which is converted to a thiol *via* subsequent transesterification (Scheme 62, bottom). Despite the necessity of an additional synthetic step, this method is generally preferred due to improved reactivity and selectivity along with lowered toxicity, and is frequently used in literature for the synthesis of thiols from renewable feedstock.[348,456,459,460,469]

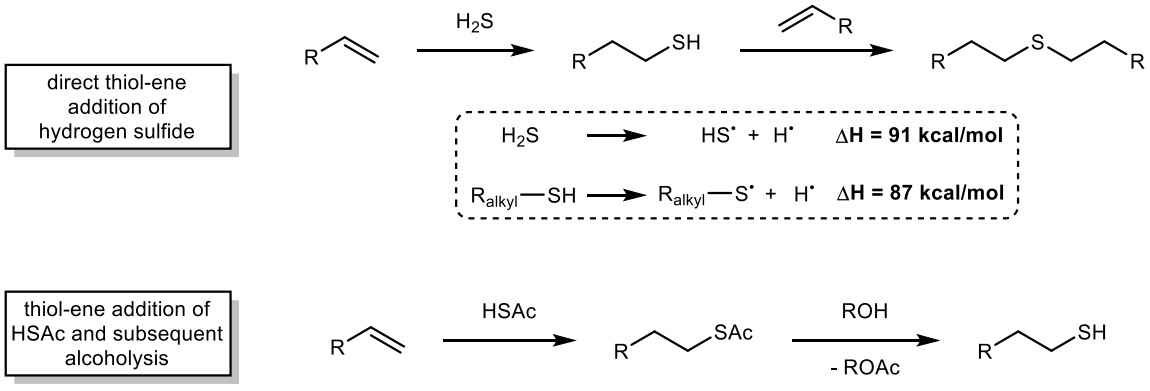

Scheme 62: Thiol synthesis from olefins via direct thiol-ene addition of H_2S and competing thioether formation (top), as well as by addition of HSAc and subsequent alcoholysis (bottom).[334,336]

However, this strategy is not directly applicable to plant oils, since the final alcoholysis step would also result in triglyceride transesterification. Hence, in order to unlock the potential of this method of thiol synthesis for triglycerides, it is necessary to first render the ester functionalities unreactive towards transesterification, while simultaneously maintaining the polyfunctional character of the oil.

In order to achieve this, the ester groups can be converted to ethers *via* a gallium bromide-catalyzed deoxygenation with silanes. This method has already been applied in the context of more sustainable synthesis in previous reports, *e.g.* for the synthesis of renewable (poly)ethers.[470–473] The glyceryl triethers obtained *via* triglyceride deoxygenation can subsequently undergo thiol-ene addition of HSAc, followed by transesterification, without degradation of the trifunctional backbone. The envisioned three-step synthesis strategy for polythiols from vegetable oils is depicted in Scheme 63.

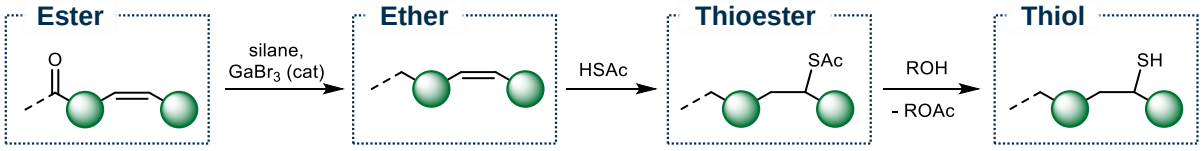

Scheme 63: Synthesis strategy for obtaining thiols from unsaturated fatty esters, involving ester deoxygenation followed by acetylthiolation and transesterification.[451]

4.3.2 Substrate Synthesis and Characterization

High Oleic Sunflower Oil (**HOSO**) was selected as main substrate due to its easy commercial availability and high content of monounsaturated oleic acid and low content of polyunsaturated fatty acids (PUFAs) and saturated fatty acids (SFAs). Despite the lower amount of double bonds per molecule in **HOSO**, monounsaturated fatty acids (MUFAs) are generally more suitable for thiol-ene functionalization than PUFAs, since the formation of stabilized bis(allyl) radicals in PUFAs impedes radical reactions. Indeed, incomplete conversions of polyunsaturated linoleic and linolenic fatty acid derivatives in thiol-ene reactions are frequently reported.[474,475] Complete double bond conversion is crucial in order to prevent intramolecular thiol-ene reactions of the synthesized thiols, thus ensuring their viability for the synthesis of polymeric networks. Still, it was decided to also employ "regular" high linoleic sunflower oil (**HLSO**) in this study in order to test the viability of the synthesis strategy for acids with high PUFA content, potentially enabling the synthesis of thiols with higher functionality per molecule. The fatty acid compositions of the **HOSO** and **HLSO** used in this study were determined using ^{1}H NMR spectroscopy according to the method of Herrera *et al*. (Table 6).[476]

*Table 6: Calculated fatty acid contents of **HOSO** and **HLSO**, determined via 1H NMR. [476]*

Entry	Oil	SFA content / %	MUFA content / %	PUFA content / %
1	**HOSO**	8.6	89.7	1.7
2	**HLSO**	12.6	29.8	57.6

As a complementary triglyceride substrate, glyceryl triundecenoate (**GTU**) was selected. **GTU** is derived from 10-undecenoic acid (UA), a major bio-based platform chemical produced on industrial scale *via* the pyrolysis of castor oil (see section 2.2.2) .[113,139,477–479] In comparison to **HOSO** and other naturally occurring triglycerides, **GTU** contains terminal double bonds, thus allowing the selective synthesis of primary thiols due to the anti-Markovnikov character of radical thiol-ene additions.

Although **GTU** does not occur naturally and is not commercially available, Rios *et al*. recently described its direct synthesis from UA and glycerol, enabling the synthesis of **GTU** in 91% yield (see section 6.3.3.1).[480] Representative structures for the three triglyceride substrates used in this work are depicted Scheme 64. For simplicity, oleate and linoleate will be used as the representative moieties for **HOSO** and **HLSO**, respectively, in graphical illustrations and chemical equations.

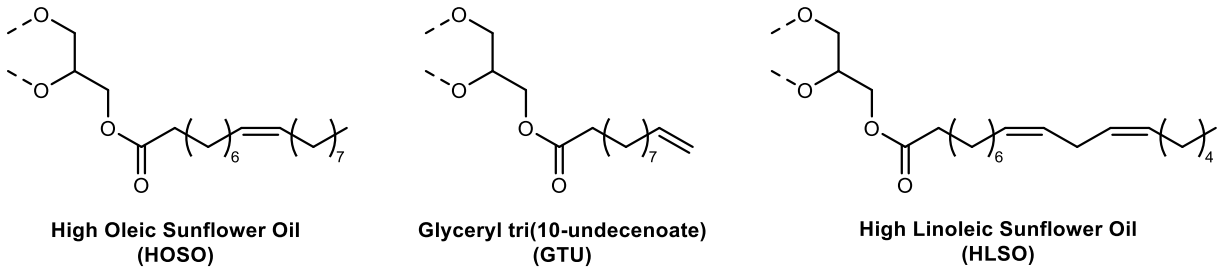

*Scheme 64: Representative structures of **HOSO**, **GTU** and **HLSO**.*

4.3.3 Ester Deoxygenation

4.3.3.1 Synthesis and Workup

The deoxygenative reduction of esters to ethers using silanes was first reported by Sakai *et al*. using triethylsilane (TES) as the reductant and $InBr_3$ as the catalyst.[481] Biermann *et al*. further optimized the reduction and extended the substrate scope to triglycerides (including **HOSO** and **GTU**), revealing that the use of tetramethyldisiloxane (TMDS) / $GaBr_3$ instead of TES / $InBr_3$ was more effective and resulted in fewer undesirable side reactions, such as overreduction under the formation of alcohols and/or silyl ethers. Furthermore, with TMDS being a cheap and non-

toxic side product of the silicon industry, its use is more in line with the principles of Green Chemistry.[470,471]

The reduction of **HOSO** to its respective triether **9a** was thus conducted by applying the reported conditions of Biermann *et al*., employing 1 mol% of $GaBr_3$ and 1.10 equiv. of TMDS respectively per ester function under bulk conditions.[471] Due to its sensitivity to moisture, $GaBr_3$ was added to the reaction vessel inside an inert gas box and the vessel was subsequently closed with a septum. **HOSO** was then added over the septum using a syringe. Afterwards, TMDS was added dropwise to the reaction mixture over the course of 2 hours using a syringe pump while cooling with a water bath. After complete addition, the mixture was stirred at room temperature. The progress was followed *via* ^{1}H NMR by observing the signal assigned to the ester α-methylene protons at 2.31 ppm, indicating 94% conversion after 3 hours (marked in red in Scheme 65). Full conversion, indicated by the absence of any discernible ester signal, was reached after subsequent heating to 60 °C for one additional hour (Scheme 65, middle spectrum).

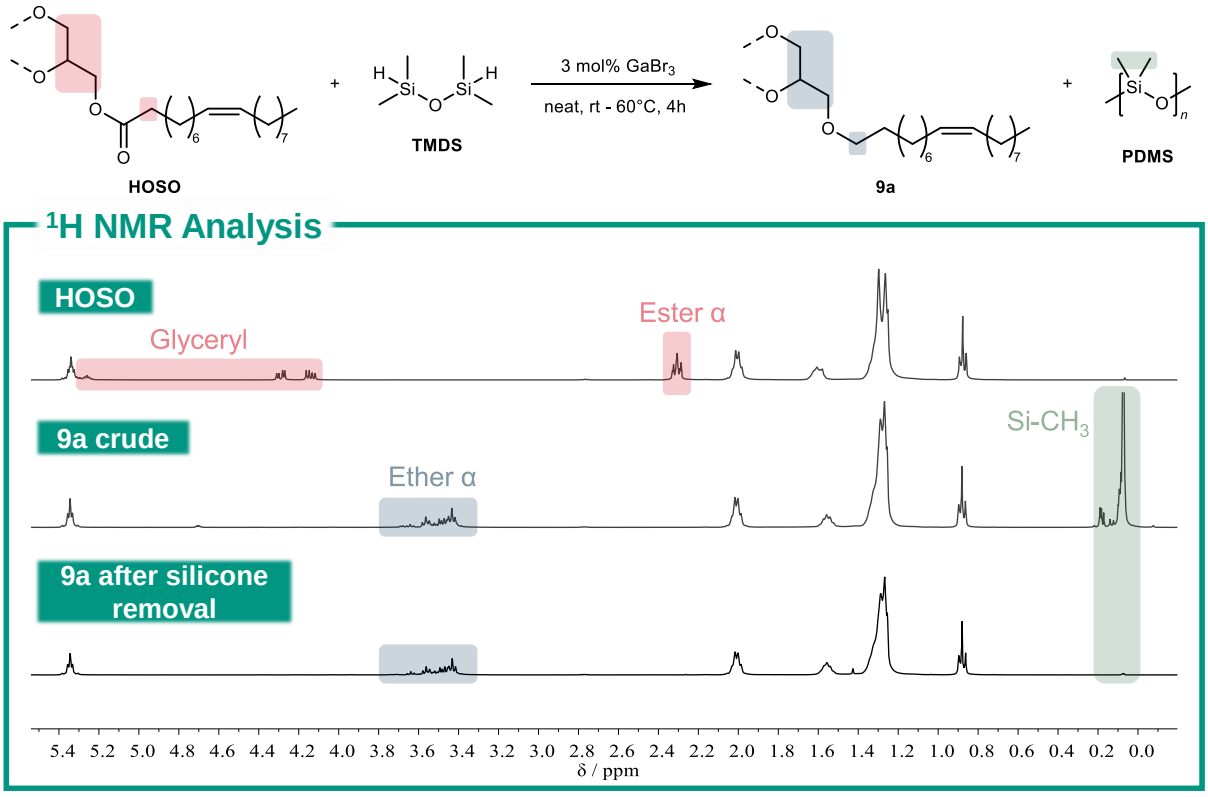

*Scheme 65: $GaBr_3$-catalyzed deoxygenation of HOSO with TMDS and comparison of the ^{1}H NMR spectra (in $CDCl_3$) of **HOSO** (top), the crude reduction mixture at full ester conversion (middle) and the isolated product **1a** after silicone removal (bottom).[451]*

Notably, it was found that increasing the amount of TMDS to 1.5 equiv. per ester function allows the reaction to proceed to completion within 4 hours at room temperature, thus eliminating the need for additional heating. However, it was decided that the benefit of using less starting material and thus generating less waste outweighs the energy saved by not having

to heat the reaction mixture. Hence the use of 1.10 equiv. of TMDS was maintained in the optimized reduction conditions.

The subsequent isolation of pure products has proven difficult in past instances due to the formation of polydimethylsiloxane (PDMS) byproducts. While lower molecular weight ethers have been successfully purified *via* distillation in literature reports, this method was not applicable to triether **9a** due to insufficient volatility.[470] Biermann *et al*. reported that by simply extracting the crude reduction mixture with acetone, which is reportedly not miscible with the HOSO-derived triether **9a**, it was possible to completely remove PDMS and isolate a product mixture containing 80% triether **9a** and 20% oleyl and glyceryl silyl ethers bearing oligo-dimethylsiloxane substituents of different lengths in a combined yield of 93%.[471]

Unfortunately, it was not possible reproduce these findings to the same effect in this study. While acetone washing generally resulted in the successful separation of the majority of silicone species from the crude reduction mixture of **9a**, inconsistent silicone removal and significant product losses were encountered across different reaction batches. In order to compare the effectiveness of silicone removal across different reduction batches, the value of silicone removal efficiency (SRE) was defined as described in Equation 6.

$$SRE = \left(1 - \frac{I\,(Si - CH_3)}{4 \cdot I\,(fatty\ CH_3)}\right) \cdot 100\% \qquad (6)$$

I(Si-CH_3) and I(fatty CH_3) represent the respective integrals obtained from the ^{1}H NMR spectra of the purified products (see section 6.3.3.3). This calculation of SRE assumes perfect stoichiometry between TMDS and ester functions, not considering the excess of TMDS that is used in practice, since only a stoichiometric amount of TMDS will react to a polymeric silicone and the remaining, unreacted TMDS can be separated under reduced pressure.

Figure 5 depicts the ^{1}H NMR spectra of a reduction reaction (scale of 18.7 g **HOSO**) that was washed a total of 4 times with acetone (20 mL each), illustrating the removal of silicone species with each washing. After 4 washing steps, an SRE of 83% was achieved, with only a very slight SRE increase between the third and fourth washing steps. Furthermore, significant yield losses were observed since the triether product **9a** was found to be partially soluble in acetone, with only 7 g of crude product remaining after the washing. Generally, product yields obtained *via* acetone washing ranged between 17 wt% and 45 wt% of used triglyceride, with SRE ranging between 55-96%. In due course, it was observed that acetone washing was not applicable to GTU-derived triether **10a**, which was found to be fully miscible with acetone. Thus, due to achieving only incomplete and inconsistent silicone removal along with poor general applicability to all substrates, other strategies for silicone removal were investigated.

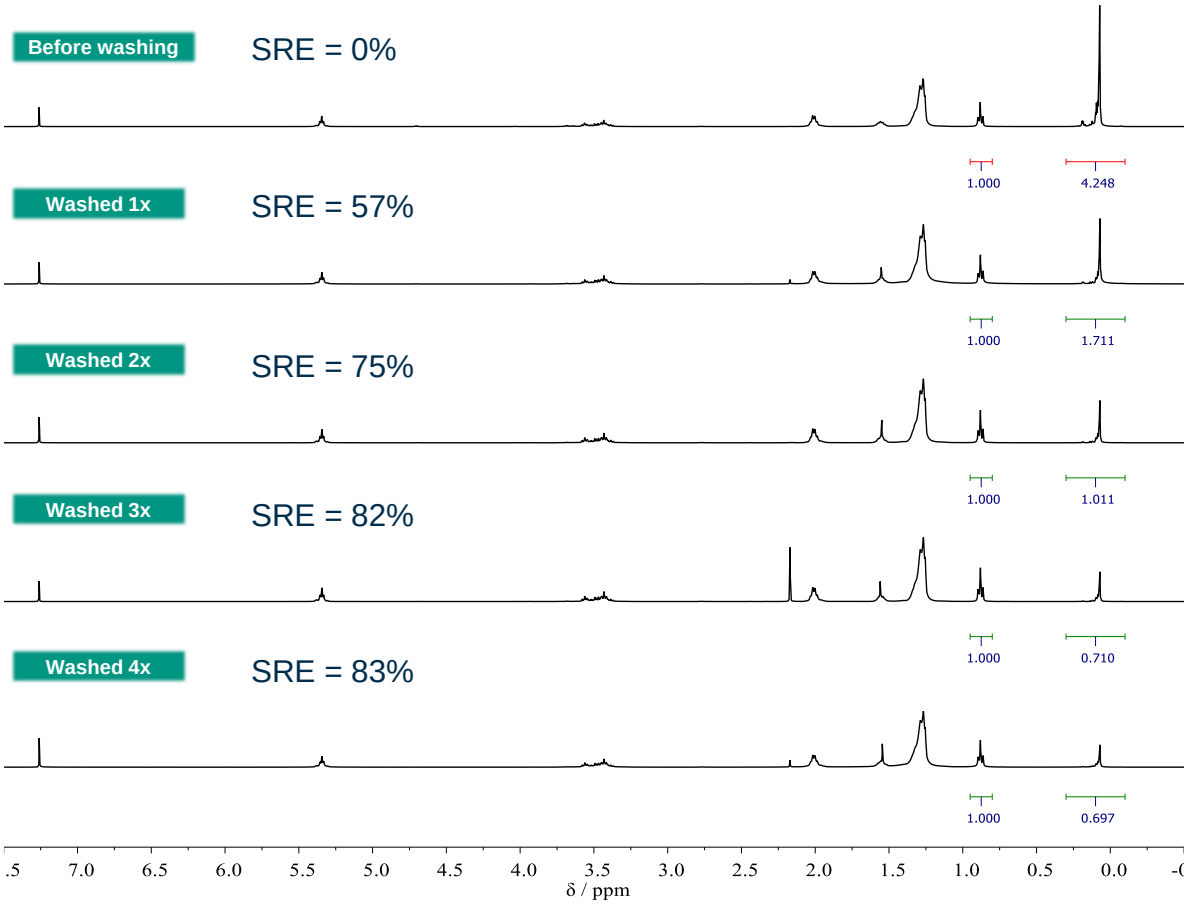

*Figure 5: Stacked ^{1}H NMR spectra obtained during attempted silicone removal from the crude reduction mixture of **1a** via acetone washing.*[451]

Column chromatography has been utilized for the removal of silicone byproducts in literature reports, however, it proved ineffective for the workup of triether **9a**, resulting in a product yield of 62 % with an SRE of 67%.[481] Due to the similar polarity of the ether products and polysiloxanes, along with the highly waste-intensive nature of column chromatography, this workup method was not further investigated.

An alternative workup approach based on the chemical degradation of silicones under basic conditions was subsequently devised. Örn *et al*. reported successful depolymerization of PDMS under alkaline conditions into water-soluble products such as dimethylsilanediol.[482–484] Inspired by this, the crude reduction mixture was treated with aqueous NaOH (5 equiv. NaOH per Si, 5 vol% EtOH), stirred at 100 °C overnight, and the phases were separated. ^{1}H NMR spectroscopy of the resulting product indicated an SRE of 83% (Table 7, entry 1). Afterwards, further attempts at optimization were conducted, revealing that the presence of EtOH, which reportedly acts as a cosolvent for the immiscible oil, was absolutely necessary for successful silicone removal (Table 7, entry 3).[484] A lower NaOH concentration of 2.5 M resulted in a slightly more effective removal of 90 % after 16 hours (Table 7, entry 4). Interestingly, prolonging the reaction time did not meaningfully impact the SRE (Table 7, entry 5). Conducting the workup at a lower temperature of 80 °C resulted in no measurable silicone

removal (Table 7, entry 6). Finally, increasing the amount of EtOH led to a further slight SRE increase to 91% (Table 7, entry 7). Although it was unfortunately not possible to achieve complete removal of silicones in a single workup step under any of the employed conditions, it was found that by separating the product and performing a second treatment with fresh NaOH, the silicones could be completely removed to the point where no respective signal was distinguishable in the NMR (Scheme 65).

*Table 7: Optimization of silicone removal from **9a** via aqueous hydrolysis with NaOH.[451]*

Entry	equiv. NaOH[a)]	c(NaOH) / M	φ(EtOH) / vol%	t / h	T / °C	SRE / %
1	5	5	5	16	100	83
2	10	5	5	16	100	76
3	5	5	0	16	100	25
4	5	2.5	5	16	100	90
5	5	2.5	5	72	100	87
6	5	2.5	5	16	80	0
7	5	2.5	10	16	100	91

a) equivalents of NaOH per atomic Si.

Notably, potential further optimizations of this silicone removal approach have not yet been fully investigated in the context of this study. Possibly, the amount and concentration of NaOH solution could be further decreased, which would contribute to less overall waste and thus improve the sustainability of the procedure. However, due to the successful removal of all silicone species, it was prioritized to continue with the next steps of the polythiol synthesis.

The optimized reduction and silicone removal protocols allowed for the successful synthesis of silicone-free **1a** in a yield of 76%. The established methods were directly transferrable to the other substrates **GTU** (triether **10a**) and **HLSO** (triether **11a**), similarly resulting in full reduction of all ester functionalities and complete silicone removal, yielding the respective triethers in yields of 64% (**10a**) and 83% (**11a**).

4.3.3.2 Investigation of Side Reactions

In order to investigate potential degradation of the triglyceride backbone during synthesis and workup, SEC analysis of the isolated triethers was conducted. The SEC traces of **GTU** and the thereof derived triether **10a** after silicone removal are depicted in Figure 6. Compared to **GTU**, **10a** exhibits additional signals both at lower and higher retention times compared to the main signal.

The emergence of signals at higher retention times can be attributed to overreduction, a series of side reactions that result in the formation of alcohol or silyl ether side products under cleavage of the ether bonds. Overreductions are well documented in literature reports and are an inevitable consequence of the applied synthesis strategy.[470,471,473,481] However, as indicated by the low intensity of the associated signals, the amount of overreduction is low and not expected to have a major impact on the applicability of the thiol as a crosslinking agent.

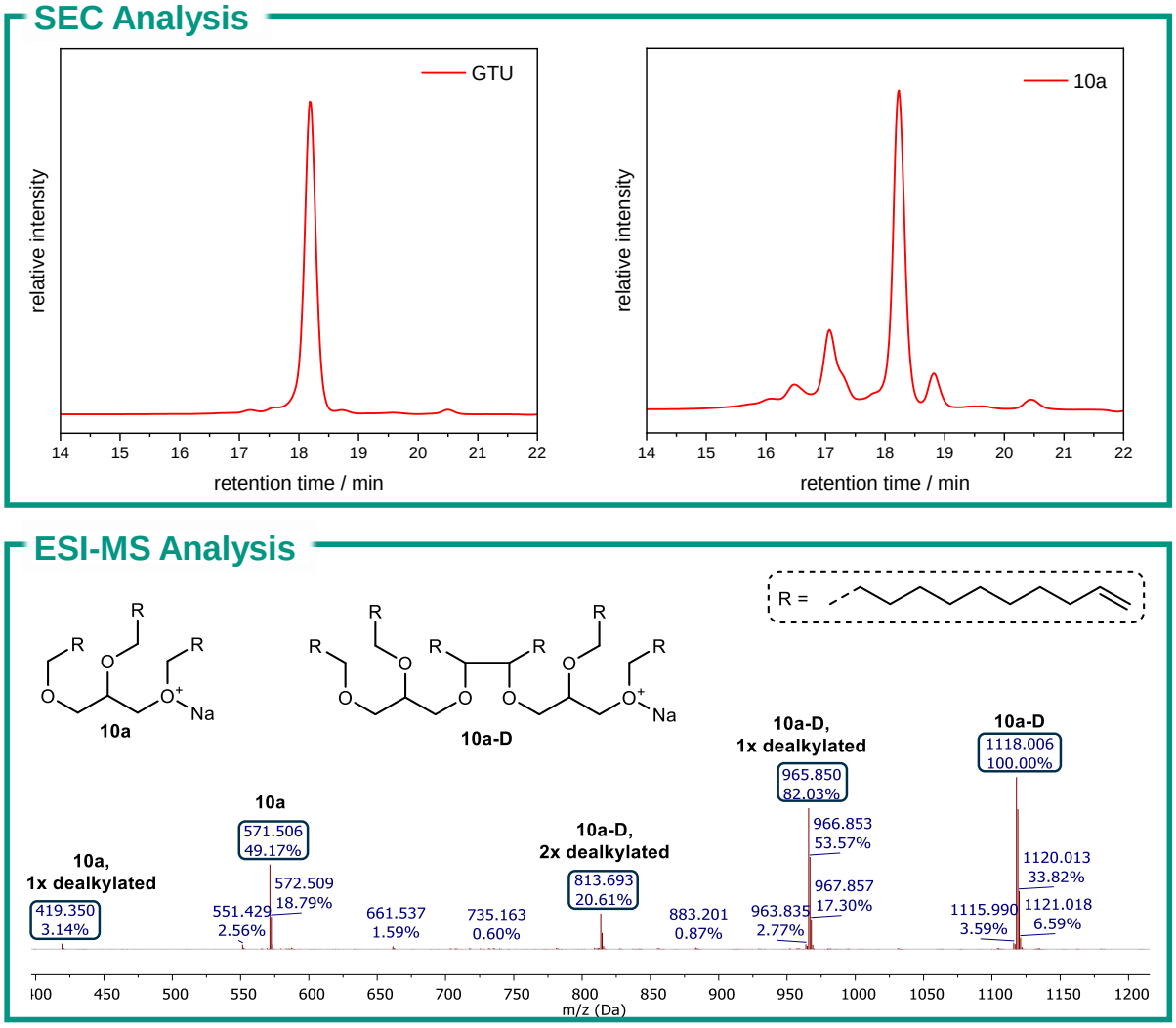

*Figure 6: SEC analysis (top) and ESI-MS analysis (bottom) of triether **10a**, confirming the occurrence of slight overreduction and intermolecular homocoupling as side reactions of the ester deoxygenation.[451]*

The emergence of signals at lower retention times indicates the formation of higher molecular weight species during the reduction, which cannot be explained by any of the literature-documented side reactions. In order to gain further insights, ESI-MS analysis of triether **10a** was conducted (Figure 6, bottom). The mass spectrum reveals the expected $[M+Na]^+$ signals for the product **10a** at *m/z* = 571.507, as well as an overreduction product at *m/z* = 419.350, which corresponds to **10a** with one ether function replaced by an alcohol function.

However, several signals at higher *m/z* than the main product are visible as well. The signal at *m/z* = 1118.006 corresponds to the calculated $[M+Na]^+$ signal of a product dimer **10a-D**,

comprising the mass of two molecules of **10a** minus two hydrogen atoms. The structure of **10a-D** depicted in Figure 6 is a representative structure that would fit the detected *m/z* signal, however the exact location of the covalent bond between the two **10a** molecules is hypothetical and has not been confirmed experimentally. The additional *m/z* signals visible in the mass spectrum at 965.850 and 813.697 correspond to overreduction products of the dimer **10a-D**, with one and two alkoxy functions replaced by hydroxy functions, respectively.

The presence and assignment of these signals serve as strong evidence for the occurrence of a previously unreported intermolecular coupling as a side reaction of the $GaBr_3$-catalyzed reduction of esters to ethers. Notably, in a recent report by Meier *et al*. on the $GaBr_3$-catalyzed reduction of acetylated cyclodextrins to ethylated cyclodextrins, higher molecular weight species were also detected in the SEC traces after the reduction.[452] Hence, the occurrence of the coupling is not due to the presence of carbon-carbon double bonds in triether **10a** and must thus be mechanistically related to the reduction itself. While the mechanism of the ester deoxygenation has not yet been fully clarified, a postulated pathway suggested by Sakai *et al.* involves the formation of intermediate α-oxy radicals (Scheme 66).[485] Radical-radical recombination could for instance serve as a pathway for the formation of the detected side products, especially due to potentially high radical concentration as a result of the employed bulk conditions. Still, the exact mechanism of the formation of these coupled species remains unconfirmed and no further studies were performed as part of this project. Further insights could be gained in future studies by utilizing simpler model substrates, allowing for potential isolation and characterization of the coupled side products.

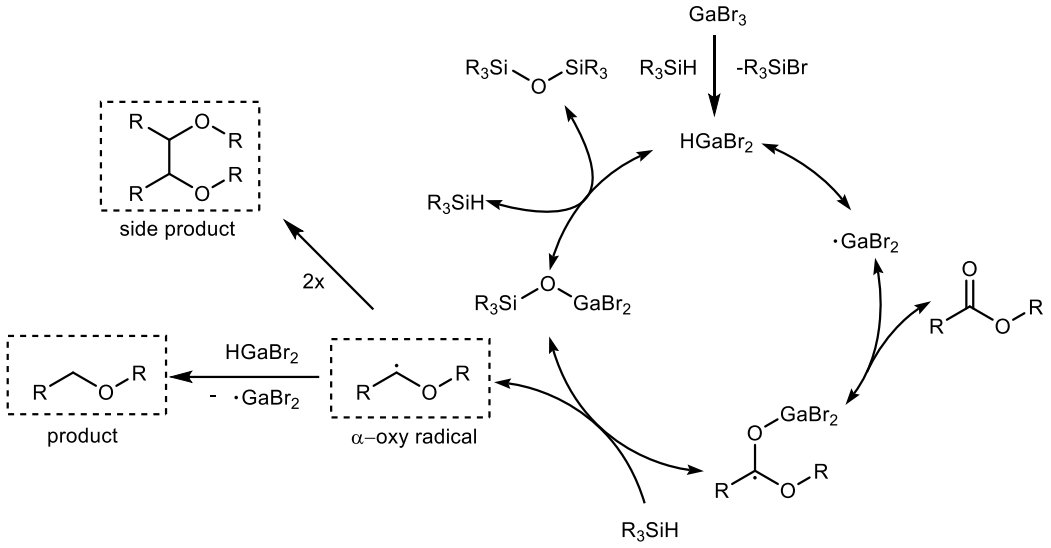

Scheme 66: Reaction mechanism of the $GaBr_3$-catalyzed reduction of esters to ethers with silanes, postulated by Sakai et al., as well as the potential formation of side products by radical-radical recombination.[452,485]

The occurrence of both lower and higher molecular weight species was also confirmed for the other triethers **9a** and **11a** via SEC analysis (see section 6.3.3.2). Notably, the presence of these

higher molecular weight side products in the reduced triglycerides is not problematic for the subsequent synthesis steps and envisioned application of the products as crosslinkers for thermoset resins. It can actually be expected to somewhat counterbalance the presence of lower molecular weight species formed by overreduction.

In summary, all three triglyceride substrates successfully underwent deoxygenative reduction to their respective triethers. Furthermore, a novel strategy for the removal of silicone byproducts *via* alkaline hydrolysis was established. Silicone-free triether products were obtained in yields ranging from 64-83%.

4.3.4 Acetylthiolation

After successful reduction of the ester moieties and removal of the silicone byproducts, the subsequent step of the polythiol synthesis was the thiol-ene addition of thioacetic acid to the double bonds of the triethers. Mutlu *et al*. previously described the reaction on methyl oleate with 3 equiv. of thioacetic acid while irradiating with a UV lamp for 26 hours.[469] The conditions were adapted for **HOSO**-derived triether **9a** (10 equiv. HSAc, corresponding to 3.3 equiv. per double bond). In the initial attempt, ^{1}H NMR indicated 74% double bond conversion after 72 hours of irradiation. Subsequently, the product was isolated by vacuum-drying and the reaction was performed a second time with fresh HSAc, slightly increasing the double bond conversion to 83%, which did not increase any further when attempting the reaction a third time (see section 6.3.3.4). In another synthesis attempt, the HSAc was purified by distillation before the reaction, which was found to significantly impact conversion and yield. By using freshly distilled HSAc, complete double bond conversion was achieved already after 3 hours without the need for UV irradiation. Presumably, airborne oxygen acted as a radical initiator in this case.

After full conversion of the double bonds, the thioester product **9b** was isolated in quantitative yield by distilling the excess HSAc under reduced pressure (Scheme 67). Notably, the thiol-ene addition of HSAc to oleyl chains results in the formation of a statistical mixture of 9- and 10-acetylthiolated products. For simplicity, only one regioisomer is used in subsequent graphical representations.

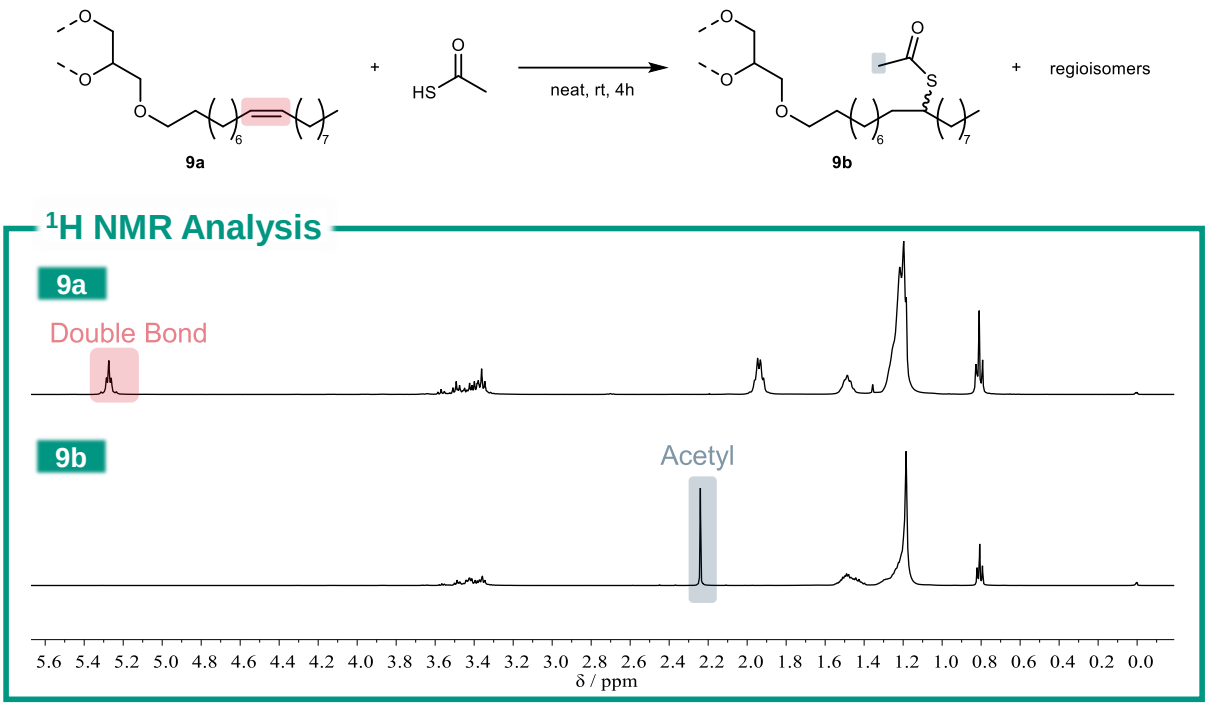

*Scheme 67: Acetylthiolation of triether **9a** with thioacetic acid (top) and comparison of the ^{1}H NMR spectra (in $CDCl_3$) of triether **9a** and tri(thioester) **9b** (bottom).*[451]

The underlying reasons for the large impact of pre-distilling HSAc prior to its use remain unclarified. Comparison of the ^{1}H NMR spectra of HSAc before and after the distillation reveals the successful removal of some minor, unidentified contaminants by distillation (see section 6.3.3.4). Reportedly, thermal decomposition of HSAc can result in the formation of species such as COS, methanethiol, H_2S, acetic (thio)anhydride or ketene.[486,487] It is however unclear which of these species, or others, form upon aging of thioacetic acid under ambient conditions. In literature reports using HSAc, distillation prior to its utilization is also frequently performed, however no comments are made related to the necessity of the distillation.[488–491] No further investigations on this matter were conducted in the present study beyond the practical evidence that distillation of HSAc is beneficial and essential for full double bond conversion in the acetylthiolation of **9a**. It is assumed that non-volatile contaminants are formed upon aging of HSAc, which can potentially act as chain transfer agents in radical chain reactions, resulting in the formation of stabilized radicals and thus slowing the overall reaction rate.

The established acetylthiolation protocol could be successfully transferred to the **GTU**-derived triether **10a**, achieving full conversion already after 1 hour due to the higher reactivity of terminal double bonds. As expected, only the primary thioester **10b** product was regioselectively formed in this case.

In the case of the triether **11a** derived from **HLSO**, it was unfortunately not possible to achieve full double bond conversion. A conversion of 92% was observed after 22 hours, which did not increase further even after prolonging the reaction time and performing a second run with fresh

HSAc and under UV irradiation. It is assumed that the incomplete conversion is a consequence of the high content of PUFAs, which are known to be less reactive in radical additions than MUFAs due to the possible formation of stabilized bisallylic radicals.[474,475]
Overall, the **HOSO**- and **GTU**-derived triethers **9a** and **10a** reacted efficiently with distilled thioacetic acid under mild conditions without the need for additional solvents, initiators or external conditions (heating or pressure). In the case of triether **11a**, a maximum conversion of 92% was achieved. The products **9b**-**11b** could be isolated by simply separating, and thus recovering, excess HSAc under reduced pressure.

4.3.5 Alcoholysis

The final synthesis step involves the alcoholysis of the synthesized thioesters **9b**-**11b** to obtain the respective thiols **9c**-**11c**. The initial conditions were again adapted from the work of Mutlu *et al*., who used excess methanol (20 equiv.) and 0.10 equiv. of 1,5,7-triazabicyclo[4.4.0]dec-5-ene (TBD) for the transesterification of a thioester derived from methyl oleate.[469] Unfortunately, the adapted conditions were not feasible for the transesterification of **HOSO**-derived thioester **9b**, since it was not soluble in MeOH, leaving **9b** completely unreacted after refluxing for 24 hours (Table 8, entry 1). To address the poor solubility, *n*-propanol was used instead of methanol, since it was found to be the lowest molecular weight alcohol that is fully miscible with **9b**. The TBD-catalyzed transesterification of **9b** with PrOH (10 equiv.) was successful, reaching full conversion after 16 hours at 80 °C (Table 8, entry 2). However, ^{1}H NMR analysis indicated a small amount of disulfide formation *via* oxidation of the thiol. (see section 6.3.3.5) Other possible transesterification catalysts were thus investigated, including a variety of inorganic acids and bases, as well as other organic bases (Table 8, entries 3-9). Among the examined catalysts, sulfuric acid was found to efficiently catalyze the alcoholysis, also resulting in full conversion after 16 hours, without any discernible disulfide formation (Table 8, entry 3). All other investigated catalysts either yielded incomplete conversion after 16 hours or were completely inactive. Hence, sulfuric acid was selected as the optimal catalyst. Further screening revealed that reducing the catalyst loading to 3 mol% still resulted in complete transesterification after 16 hours (Table 8, entries 10-11). Polythiol **9c** was isolated after the transesterification by removing remaining PrOH and PrOAc *in vacuo*. Subsequent washing of the crude reaction mixture with sodium bicarbonate yielded **9c** in a yield of 94% (Scheme 68), corresponding to an overall yield of 71% across all three synthesis steps.

*Table 8: Results of the optimization study of the transesterification of thioester **9b** to thiol **9c**.*[451]

Entry	Catalyst	Cat. loading / mol%	Alcohol (equiv.)	Conversion (16h) / %
1	TBD	30	MeOH (60)	0[a)]
2	TBD	30	PrOH (10)	100[b)]
3	H_2SO_4	30	PrOH (10)	100
4	HOAc	30	PrOH (10)	0
5	Pyridine	30	PrOH (10)	0
6	NEt_3	30	PrOH (10)	0
7	DBU	30	PrOH (10)	91[b)]
8	KOH	30	PrOH (10)	0
9	H_3PO_4	30	PrOH (10)	31
10	H_2SO_4	10	PrOH (10)	100
11	H_2SO_4	3	PrOH (10)	100

a) Sample was taken after 24 hours.

b) Disulfide formation *via* thiol oxidation was detected in the ^{1}H NMR spectra.

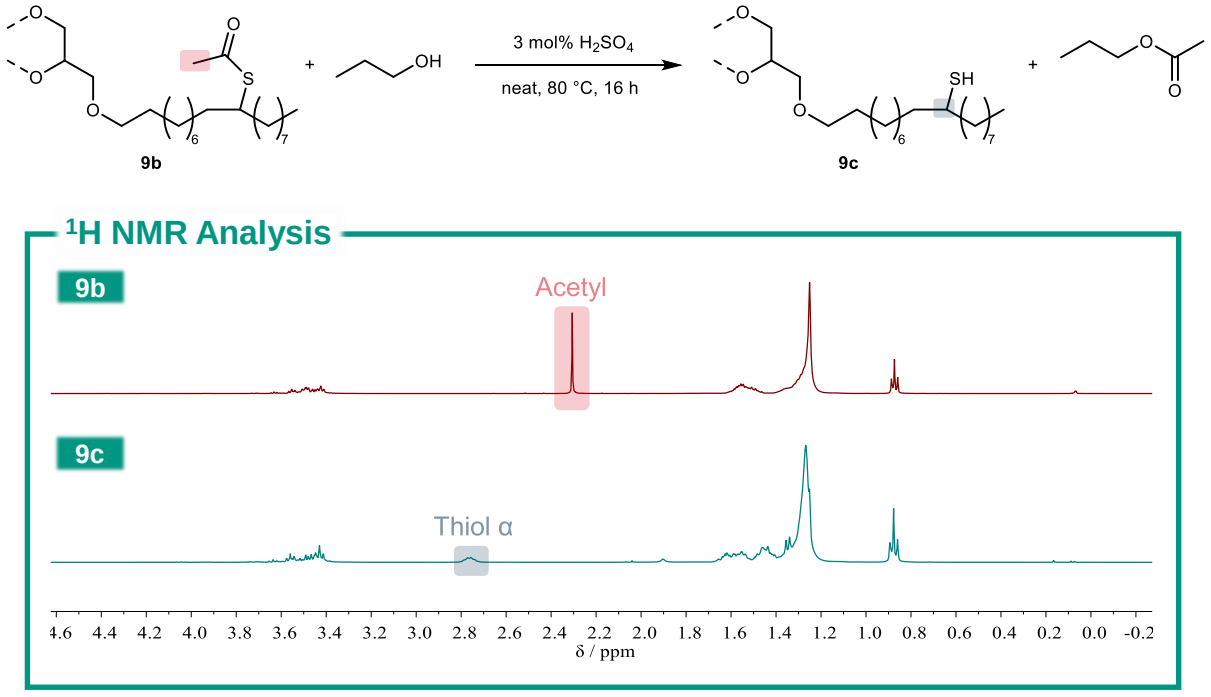

*Scheme 68: Transesterification of thioester **9b** with PrOH (top) and comparison of the ^{1}H NMR spectra (in $CDCl_3$) of thioester **9b** and thiol **9c** (bottom).*[451]

The optimized transesterification protocol was transferrable to the other substrates **10b** and **11b**, yielding the corresponding thiols **10c** and **11c** in 91% and 95% yield, respectively. All polythiols were obtained as viscous, yellow liquids with a mildly unpleasant odor.

Notably, due to the occurrence of overreduction and homocoupling side reactions during the deoxygenation step, the obtained polythiol products represent a mixture of thiols of different

functionality per molecule. It is unfortunately not feasible to exactly quantify the average number of thiol functions per molecule or the variance of the product distribution, since full separation and characterization of all side products would be required. However, by comparing the average number of double bonds per molecule of the triglyceride substrates, it can be assumed that the average functionality increases qualitatively in the order **9c** < **10c** < **11c**. For further application in polymer synthesis, the amount of thiol functions per mass (mmol SH / g) was determined *via* quantitative ^{1}H NMR (see section 6.3.3.7). The results of the polythiol synthesis are summarized in Table 9.

Table 9: Summarized results of polythiol synthesis, including overall yield across all 3 synthetic steps and amount of thiol functions per gram.[451]

Entry	Polythiol	Overall yield / %	Thiol functions / mmol SH g^{-1}
1	**9c**	71	2.99
2	**10c**	58	4.46
3	**11c**	73	3.51

4.3.6 Synthesis of Polymer Networks

In order to demonstrate the suitability of the newly synthesized polythiols for thermoset synthesis, polymerizations *via* thiol-ene chemistry as well as *via* nucleophilic addition to isothiocyanates were investigated.

For the synthesis of thiol-ene networks, a photoinitiated approach was adopted.[351,459] 1,7-Octadiene (**OD**) was initially selected as the model polyene comonomer. Thiols **9c** and **10c** were thus mixed in equal stoichiometry of functional groups with **OD** and 1 mol% of DMPA was added (Table 10, entries 1-2). After dissolution of the photoinitiator, the mixtures were cast into molds and irradiated overnight at a wavelength of 365 nm. Solidification of the mixtures after irradiation served as first indicator of successful crosslinking. This was further underlined by IR spectroscopy, revealing near-complete disappearance of the δ_{oop}(C=C-H) vibration band of the terminal alkene function at 909 cm^{-1} (shown for **10c** in Scheme 69). Analysis of the gel fraction (GF) revealed a low GF of merely 61% for **9c+OD**, while **10c+OD** exhibited a high GF of >99%. This can be explained by the lower reactivity of secondary thiols and the lower SH functionality of **9c**. Due to the low GF of **9c+OD**, it was decided to attempt a polymerization using GTU as a trifunctional comonomer instead of the difunctional **OD**. In this case, the resulting thermoset **9c+GTU** exhibited a GF of 98%, indicating a significantly higher degree of crosslinking (Table 10, entry 3). Still, a small amount of residual terminal alkene functions was observed in the IR spectrum of the network. **10c+GTU** produced a highly crosslinked

material with a GF >99% and full double bond conversion according to the IR spectrum (Table 10, entry 4). Polymerization of the HLSO-derived polythiol **11c** with GTU unfortunately did not result in the formation of a solid material (Table 10, entry 5). Unsuccessful curing is further evidenced by a high-intensity alkene vibration in the IR spectrum of the cured mixture (see section 6.3.3.7). This can presumably be attributed to intramolecular additions to the residual double bonds present in **11c**, as reported in literature for the use of MSOs, highlighting the importance of full double bond functionalization when synthesizing thiols from vegetable oils.[353,468]

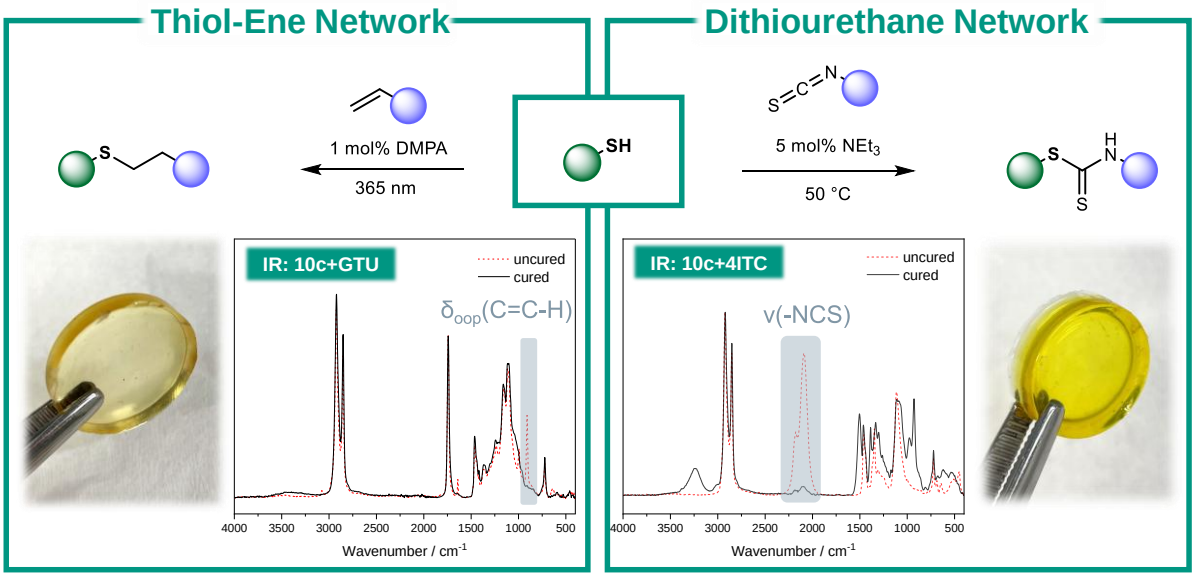

Scheme 69: IR spectra and pictures of polymer networks formed via thiol-ene reaction (left) and nucleophilic addition (right).[451]

As a complementary polymerization strategy, the nucleophilic addition of thiols to isothiocyanates (ITCs), resulting in the formation of dithiourethanes, was attempted. The model comonomer 1,4-butanediisothiocyanate (**4ITC**) was synthesized from the respective diamine using more sustainable synthesis protocols described by Meier *et al.*[266,492] For the polymerization, conditions reported by Endo *et al*. were adapted, *i.e*. the reaction was performed at 50 °C using 5 mol% triethylamine as a catalyst.[324]

After curing overnight, solidified materials were obtained for all polythiols and subsequently characterized using IR spectroscopy (Table 10, entries 6-8). Successful polymerization was indicated by the near-complete disappearance of the isothiocyanate vibration bands between 2250 and 2000 cm^{-1} along with the emergence of N-H signals at 3250 and 1500 cm^{-1} (Scheme 69). Notably, the HOSO-derived dithiourethane network **9c+4ITC** exhibited an increased GF of 89% as compared to **9c+OD**, demonstrating the usability of thiol **9c** for the formation of polymeric networks also with difunctional comonomers. The respective dithiourethane polymers of the other two polythiols **10c** and **11c** exhibited GFs >99%. Notably, this illustrates

that thiol **11c**, derived from PUFA-rich **HLSO**, can be successfully employed for thermoset synthesis *via* nucleophilic thiol chemistry even without complete double bond conversion during its synthesis.

Table 10: Characterization of the synthesized polymer networks in terms of gel fraction (GF), glass transition temperature (T_g), decomposition temperature ($T_{d,5\%}$), Young's modulus (E), ultimate tensile strength (σ_{max}) and elongation at break (ε_{max}).[451]

Entry	Material	GF / %	T_g / °C	$T_{d,5\%}$ / °C	E / MPa	σ_{max} / MPa	ε_{max} / %
1	**9c**+OD	61	n.a.	n.a.	n.a.	n.a.	n.a.
2	**10c**+OD	>99	-9	356	n.a.	n.a.	n.a.
3	**9c**+GTU	98	-36	345	2.39±0.52	0.44±0.10	21.7±1.55
4	**10c**+GTU	>99	-8	359	9.41±0.98	1.36±0.23	18.7±1.00
5	**11c**+GTU	0	n.a.	n.a.	n.a.	n.a.	n.a.
6	**9c**+4ITC	89	-28	224	n.a.	n.a.	n.a.
7	**10c**+4ITC	>99	-11	214	7.51±0.59	1.84±0.22	35.8±2.39
8	**11c**+4ITC	>99	1	232	7.04±0.39	1.83±0.15	31.6±0.17

The obtained materials, excluding **9c+OD** and **11c+GTU** due to insufficient cross-linking, were further investigated in terms of their mechanical and thermal properties (see Table 10). Glass transitions were observed in the range between -36 and 1 °C. Generally, the value of the glass transition temperature correlated well with the used thiol. The thermosets derived from **10c** (Table 10, entries 4 and 7) generally exhibited higher T_g than the corresponding materials derived from **9c** (Table 10, entries 3 and 6) due to the absence of dangling alkyl chains. The polydithiourethane synthesized from **11c** (Table 10, entry 8) showed the highest measured T_g, presumably since polythiol **11c** possesses the highest average thiol functionality per molecule and thiourethane formation is not impeded by residual PUFA moieties, in contrast to thiol-ene chemistry as discussed above. Thermogravimetric analysis (TGA) revealed single-step thermal degradations with onset temperatures between 345 and 359 °C for all thiol-ene networks. The dithiourethane polymers showed two-step degradations starting at temperatures between 214 °C and 232 °C. The mechanical properties of the polymers were also characterized for some materials using tensile strength measurements. All synthesized materials exhibited soft, rubber-like properties, with Young's moduli between 2.39 and 9.41 MPa, maximum stress ranging from 0.44 to 1.84 MPa, and elongations at break between 18.7% and 35.8%.

4.3.7 Summary and Outlook

In summary, a new synthetic strategy to access polythiols from renewable triglyceride feedstock was established. As substrates, commercially available vegetable oils **HOSO** and **HLSO** were used, as well as the synthetic triglyceride **GTU**, which was accessed in one step from bio-based 10-undecenoic acid and glycerol. The synthetic strategy involves the initial $GaBr_3$-catalyzed deoxygenation of the ester functions to ether functions with TMDS, followed by thiol-ene addition of excess thioacetic acid and acid-catalyzed alcoholysis of the resulting thioester with *n*-propanol, yielding the polythiols in overall yields ranging from 58-73%.

Novel insights on the $GaBr_3$-catalyzed ester deoxygenation with silanes were gained. The occurrence of previously unreported side reactions, which result in intramolecular homocoupling, was discovered. Furthermore, a novel method for the separation of silicone byproducts formed during the reduction *via* hydrolysis using aqueous NaOH has been described.

The applicability of the synthesized polythiols for the synthesis of polymer networks was exemplarily demonstrated by the synthesis of polymeric materials using thiol-ene chemistry and nucleophilic addition to isothiocyanates.

The newly established synthesis protocol relies almost exclusively on cheap and benign materials and does not require the use of additional solvents or elaborate and waste-intensive workup methods such as column chromatography. The only utilized substance that is classified as toxic according to GHS, thioacetic acid, still represents an easy to handle alternative to other substances commonly employed in the synthesis of thiols, such as hydrogen sulfide or thiourea. Hence, the method is overall in good agreement with the principles of Green Chemistry.

Future studies could be aimed at attempting to further optimize the synthesis of thiols for PUFA-rich feedstocks, for instance by investigating other conditions for the acetylthiolation with HSAc, or by attempting to remove the residual double-bond functionalities after thioester synthesis *via* hydrogenation. Furthermore, as already mentioned, further investigations on the nature of the homocoupling products formed during the reductions could be performed.

4.4 Synthesis of Bio-based Polythioamides *via* the Willgerodt-Kindler Reaction

Disclaimer

The author of this thesis planned and evaluated the herein described experiments. Maximilian L. Schmitt performed the model reactions and monomer and polymer syntheses as part of his bachelor thesis under co-supervision of the author. Sophia Abou el Mirate performed several syntheses related to this project as part of her apprenticeship under co-supervision of the author.

Abstract

Levulinic acid (LA) is regarded as one of the most relevant bio-based platform chemicals, being easily accessible *via* the acidic hydrolysis of hexoses, which are abundantly available from biomass.

In this project, the utilization of LA as a renewable platform for the synthesis of novel sulfur-containing monomers and polymers was investigated. The general synthetic strategy involves a two-step polymer synthesis by converting both the carboxy function and the keto function of LA each with difunctional comonomers. For the conversion of the keto function, the Willgerodt-Kindler reaction was utilized, which involves the formation of terminal thioamides from aliphatic ketones, amines, and elemental sulfur.

Willgerodt-Kindler reactions were initially investigated using model reactions with monofunctional amines and elemental sulfur for a variety of LA derivatives, including the free acid, levulinate esters, and levulinamides, Among the utilized substrates, it was found that a levulinamide derived from piperidine most efficiently underwent the Willgerodt-Kindler reaction with piperidine and sulfur, selectively yielding the corresponding monothioglutaramide in good yield.

The gained insights were subsequently transferred to a bifunctional levulinamide derived from piperazine, which was successfully converted in a Willgerodt-Kindler polymerization with piperazine and sulfur, yielding a poly(monothioglutaramide).

4.4.1 Context and Project Outline

The "biorefinery" concept, which entails the valorization of biomass for the synthesis of valuable platform chemicals for the chemical industry, was introduced in chapter 2.2.1. Carbohydrates represent the most abundant substance class in biomass, and are thus expected to play a significant role in the transition of the chemical industry towards the utilization of renewable feedstock. In 2004, the United States Department of Energy has devised a set of criteria for assessing the viability of carbohydrate-based compounds as potential industrial platform chemicals, leading to the identification of a list of suitable compounds and compound classes. These "top ten chemical opportunities from biorefinery carbohydrates" include ethanol, polyols such as glycerol, sorbitol, and xylitol, "biohydrocarbons" such as isoprene, furan derivatives, as well as carboxylic acids like lactic acid, hydroxypropionic acid, succinic acid, and levulinic acid.[75]

Among these compounds, levulinic acid (LA) stands out due to its bifunctional character, bearing both a carboxylic acid moiety and an aliphatic keto function. LA can be obtained in good yields on industrial scale from the acidic hydrolysis of hexoses such as glucose, with direct application of cellulose or lignocellulosic biomass also having been reported. Sajid and Zhao *et al*. have recently reviewed processes for the synthesis of LA from a variety of different feedstocks with different catalyst systems, reporting LA yields of up to 90%.[109] The acid-catalyzed formation of LA from hexoses is commonly accepted to involve isomerization of the hexoses to fructose, subsequently yielding HMF *via* elimination of water. HMF is unstable under acidic conditions and further converts to LA under rehydration and elimination of formic acid (Scheme 70 for the example of glucose).[109,110,493]

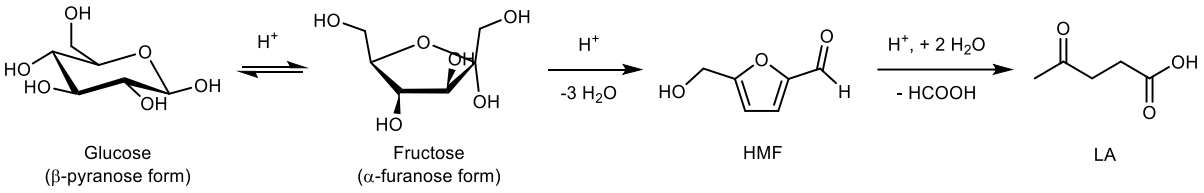

Scheme 70: Schematic illustration of the formation of LA from glucose.

In this project, LA is utilized as a readily available, renewable raw material for the synthesis of more sustainable polymeric materials. Specifically, the synthesis of polythioamides is envisioned by taking advantage of the presence of an aliphatic keto function in LA, which makes it a potential substrate for the Willgerodt-Kindler reaction.

The WK reaction yields terminal thioamides by conversion of aliphatic ketones with elemental sulfur and amines. As extensively discussed in section 2.3, elemental sulfur is currently a major waste product of the petrochemical industry with extensive recent research on its utilization in

value-added products, promoting its utilization for more sustainable processes. Since polymer synthesis is the main focus of the present project, the use of diamines is required. Diamines are currently still mostly produced from fossil feedstock involving hazardous chemicals. For instance, 1,6-hexanediamine is industrially produced *via* hydrogenation of adiponitrile, which is accessed from hydrogen cyanide and fossil-based butadiene. However, biomass-based processes for the synthesis of aliphatic diamines have been developed, for instance *via* bacterial fermentation, and show potential for the eventual replacement of the established fossil-based routes.[494,495]

Two strategies for the synthesis of polythioamides from LA are possible and were investigated in this project. The first strategy involves conducting the WK reaction using free LA, yielding an α,ω-dicarboxylic acid, which can subsequently be polymerized *via* polycondensation, for instance with diols to yield polyesters, or with diamines to yield polyamides (Scheme 71, top path). The second strategy inverts these steps by first converting the carboxy function of LA with a diol or diamine to yield an α,ω-bis(acetyl) monomer, which is then polymerized in a poly-WK reaction (Scheme 71, bottom path).

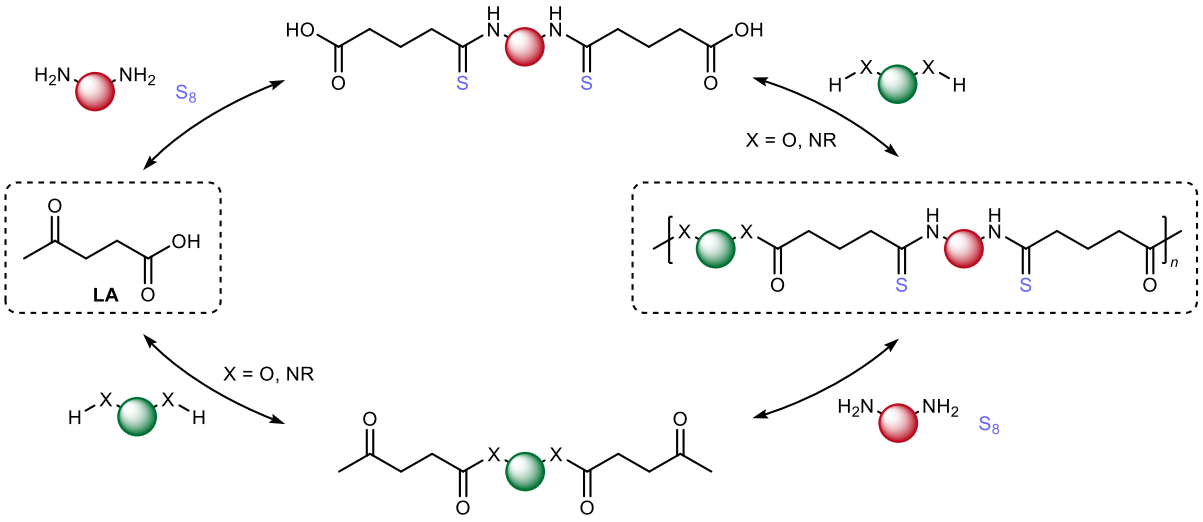

Scheme 71: Illustration of the possible strategies for polymer synthesis from LA, either by intial WK reaction and subsequent polycondensation (top path) or conversion of the carboxyfunction with a difunctional compound and subsequent poly-WK reaction (bottom path).

4.4.2 WK Reactions of LA Derivatives with Monofunctional Substrates

Prior to performing any polymerization attempts, WK reactions of LA and LA derivatives using monofunctional amines were investigated, allowing for easier reaction monitoring, for instance *via* spectroscopic methods. Test reactions were carried out using piperidine as a model secondary amine due to its frequent use in related literature.[60,215] Furthermore, experiments using benzylamine as a model for primary amines were conducted.

4.4.2.1 WK Reactions of Free Levulinic Acid

In the initial test reaction, free LA was reacted with 3.00 equiv. of piperidine and 2.00 equiv. of atomic elemental sulfur at 100 °C under neat conditions (reaction **T1-A**). Additionally, a control experiment in the absence of elemental sulfur was conducted in order to investigate potential side reactions of the substrates under the employed conditions unrelated to elemental sulfur (reaction **T1-A**). The progress of the reactions was monitored *via* ^{1}H NMR spectroscopy. The resulting spectra after a reaction time of 18 hours, along with a t_0 spectrum of the mixture before heating the reaction are depicted in Scheme 72.

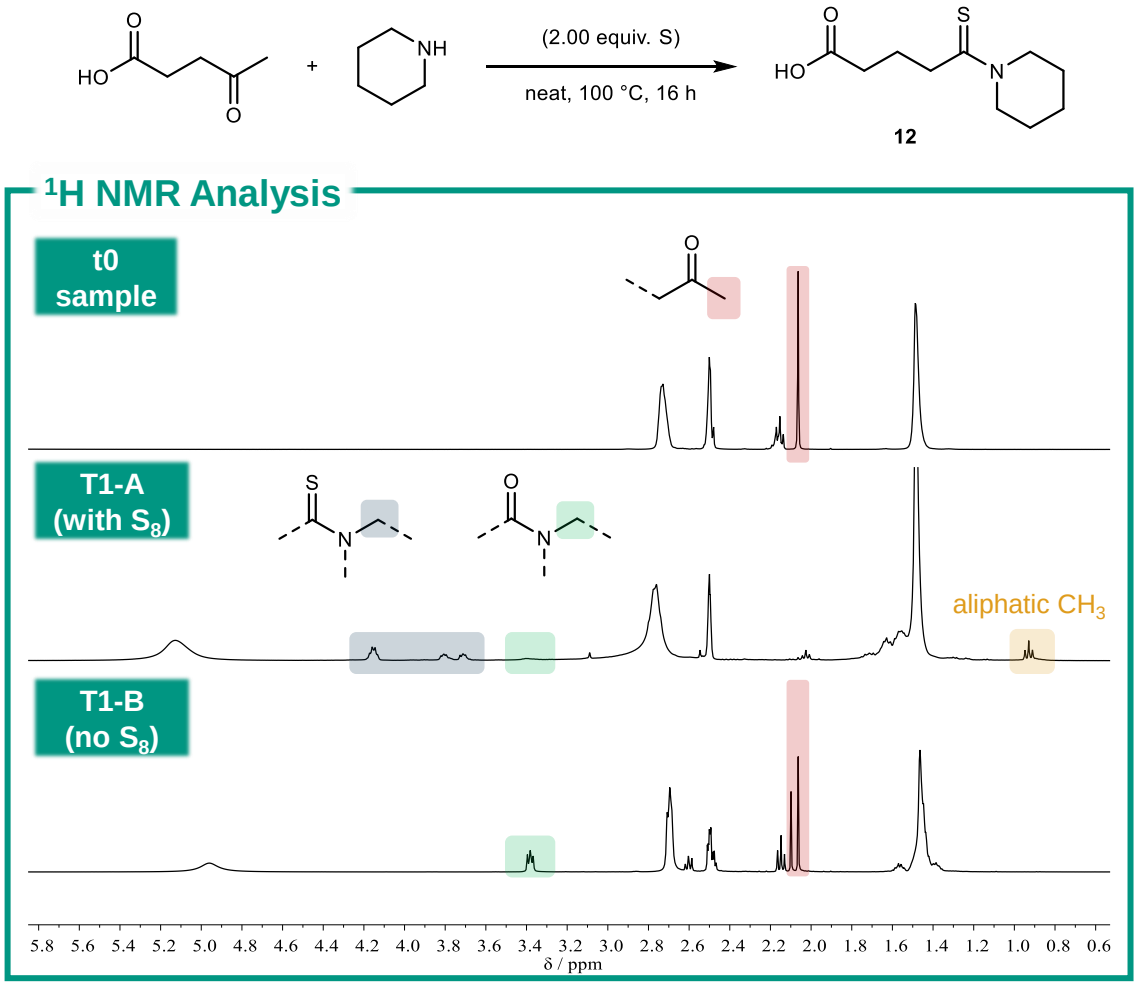

*Scheme 72: ^{1}H NMR screening (DMSO-d_6) of the reaction of levulinic acid with piperidine, both in the presence (**T1-A**) and absence of sulfur (**T1-B**). Only the desired ω-carboxythioamide **12** is depicted in the reaction equation.*

The spectrum of reaction **T1-A** (Scheme 72, middle spectrum) depicts full conversion of LA after 16 hours, as illustrated by the complete disappearance of the singlet at 2.06 ppm, corresponding to the ketone α-methyl group of LA (marked in red in Scheme 72). Furthermore, the emergence of resonances between 3.60 and 4.20 ppm is indicative of the successful formation of thioamides (marked in blue in Scheme 72). This spectral range is characteristic for

the resonance of the methylene protons in α-position to the nitrogen atom for aliphatic thioamides derived from piperidine, as confirmed by comparison with literature spectra.[496] However, the control experiment **T1-B**, which was conducted in the absence of sulfur, indicates the occurrence of a side reaction, as apparent by the emergence of new signals in the ketone α-methyl region, as well as at 3.38 ppm. The newly emerging signals could be attributed to the formation of levulinamide **13**, resulting from the condensation of amine and carboxylic acid (Scheme 73, top). Compound **13** was synthesized at a later stage of this work and confirmed that the newly emerged signals at 3.38 ppm correspond the the α-methylene protons of the amide **13** (marked in green in Scheme 72). Integration revealed that after 18 hours at 100 °C, already 41% of LA had reacted to the amide. The same signal is also slightly visible in the spectrum of test reaction **T1-A**, indicating that the amidation also takes place in this case. Furthermore, it is to be expected that the levulinamide **13** can also react in a WK reaction, forming monothioglutaramide **14** (Scheme 73, bottom).

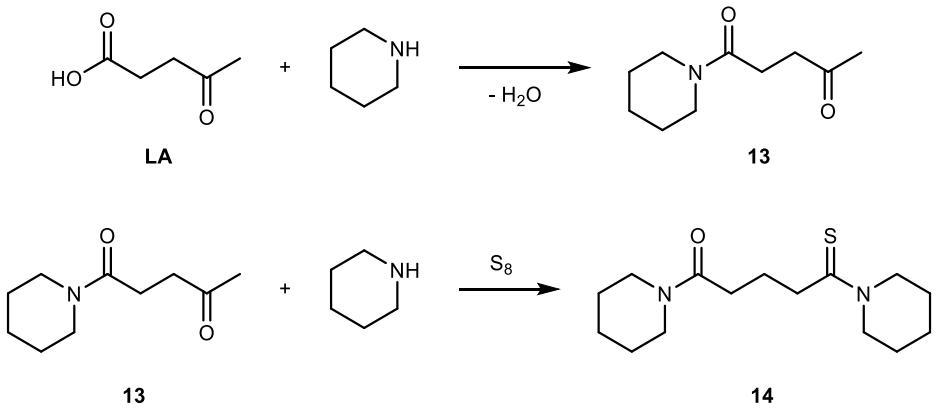

*Scheme 73: Observed side reactions of the WK reaction of LA with piperidine, involving condensation of LA and piperidine into levulinamide **13** (top), as well as follow-up WK reaction of **13**, yielding monothioglutaramide **14** (bottom).*

Another peculiar observation is the emergence of a triplet at 0.93 ppm in the spectrum of reaction **T1-A** (marked in yellow in Scheme 72). This is a characteristic signal range and shape for aliphatic methyl groups, which are however neither present in the expected thioamide product **12**, nor in any of the identified side products (Scheme 73). A possible explanation for the emergence of the methyl protons is based on a report by Takemoto *et al.*, who described the decarboxylative thioamidation of α-ketoacids with amines and sulfur, occurring already at room temperature (Scheme 74, top).[497] Considering the mechanism of the WK reaction, which involves the isomerization of the keto functionality across the entire length of the aliphatic chain, the formation of an α-ketoacid in the equilibrium is conceivable in the present case, which could subsequently lead to the formation of thiobutyramide **15** under decarboxylation (Scheme 74, bottom).

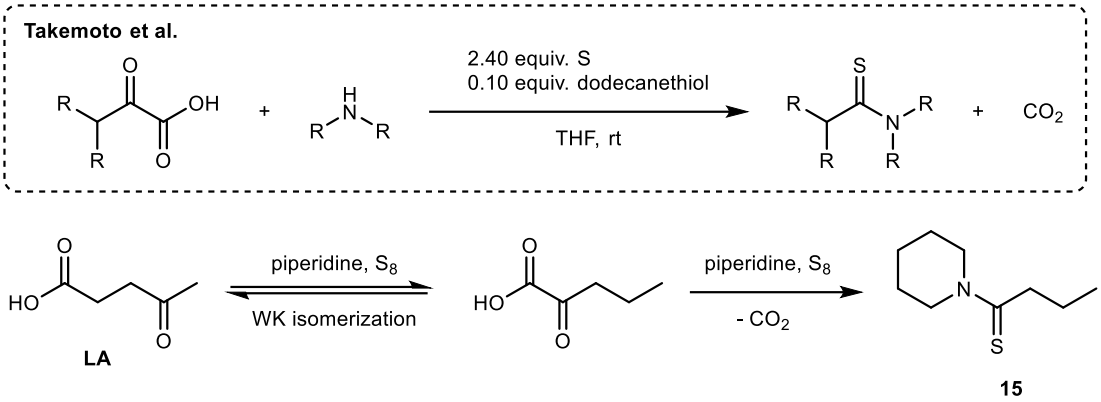

Scheme 74: Decaboxylative thioamidation of ketoacids, reported by Takemoto et al. (top) and illustration of its occurrence as a possible side reaction of the WK reaction of LA (bottom).[497]

The hypothesized side reactions were confirmed by high-resolution-ESI-MS analysis, where the characteristic *m/z* signals of levulinamide **13**, monothioglutaramide 14**,** as well as thiobutyramide **15** were detected. However, the desired ω-carboxythioamide **12** was also detected in the mass spectra, indicating that the expected reaction also proceeds to some degree. In order to gain further general insight into the reaction and to investigate if side product formation could be suppressed, a screening of different reaction conditions was conducted. 1,3,5-Trimethoxybenzene (TMB) was used as an internal standard for quantification of conversion and side product formation *via* ^{1}H NMR. The conversion was calculated by comparing the integrals of the signals of TMB to the ketone-α-methyl signals of LA. It was decided to utilize the triplet at 0.93 ppm, corresponding to the terminal methyl group of thiobutyramide **15**, as a representative "side product" signal, which allows to calculate the degree of side product formation by considering the integral ratios to the internal standard signal (see section 6.3.4.1 for details). Notably, since the side product signal at 0.93 ppm only reflects the formation of the thiobutyramide **15**, the degree of side product formation will be higher in reality. The results of the screenings are listed in Table 11.

As apparent from the results, the changes in the reaction conditions did not result in meaningful suppression of the amount of side reactions, which generally ranged between 26% and 38%. Still, some general trends on the impact of certain reaction conditions were observable. The reaction rate was found to increase with increasing amount of sulfur, which is in line with literature reports.[215] The reaction using 4.00 equivalents of sulfur (Table 11, entry 3) resulted in 97% conversion already after 2 hours and further featured the lowest amount of measured side reaction. Variations in the amount of piperidine had almost no measurable impact on the reaction conditions, the reaction still proceeding effectively with 1.20 equiv. (Table 11, entries 4-5). This is an important observation for eventual polymerization attempts, where equimolar stoichiometry is essential for obtaining high molecular weights in step-growth polymerizations.

Table 11: Results of the screening of different reaction conditions for the WK reaction of LA with piperidine and sulfur, with quantification of conversion and side reactions.

Entry	T / °C	Piperidine / equiv.	Sulfur / equiv.	Additional conditions	t / h	Conversion / %	Side product / % [a]
1	100	3.00	2.00	-	2	88	n.d.
					16	Full	38.2
2	100	3.00	1.20	-	2	79	n.d.
					16	96	33.2
3	100	3.00	4.00	-	2	97	n.d.
					16	Full	25.8
4	100	1.20	2.00	-	2	86	n.d.
					16	Full	35.9
5	100	5.00	2.00	-	2	85	n.d.
					16	Full	33.9
6	100	3.00	2.00	Argon atm.	2	92	n.d.
					16	Full	26.6
7	100	3.00	2.00	1.00 equiv. DBU	2	82	n.d.
					16	Full	37.5
8	100	3.00	2.00	Anisole (1M)	2	80	n.d.
					16	98	28.4
9[b]	100	3.00	2.00	DMSO (1M)	2	n.d.	n.d.
					16	n.d.	n.d.
10	100	3.00	2.00	DMF (1M)	2	86	n.d.
					16	98	39.1
11	120	3.00	2.00	-	2	97	n.d.
					16	Full	31.8

a) Side product formation was only calculated for the final sample due to higher conversion allowing for more accuracy. Values after 2 hours were sometimes difficult to calculate due to poor resolution, but generally similar to the 16-hour values.

b) The reaction in DMSO resulted in highly unselective reactions, indicated by many additional, poorly resolved signals in the spectra.

The use of an inert atmosphere had no significant impact on the reaction (Table 11, entry 6). Furthermore, the addition of 1.00 equivalents of DBU, which is a frequently used auxiliary base in reactions involving elemental sulfur, did not meaningfully affect the reaction rate and side product formation (Table 11, entry 7).[149,266] The use of solvents, namely anisole or DMF slightly decreased the reaction rate, however the reaction still proceeded with similar side product ratios as observed under bulk conditions. Notably, the use of DMSO was not feasible, resulting in very complex spectra, which indicates the occurrence of additional side reactions

in this case (Table 11, entries 8-10). Finally, increasing the reaction temperature to 120 °C was found to accelerate the reaction, yielding 97% conversion already after 2 hours. However, the formation of side products was also observed in this case (Table 11, entry 11).

Despite the unsuccessful suppression of the side reactions, the workup of the reaction mixture was attempted in order to investigate whether easy product isolation could compensate for the low selectivity of the reaction. Initially, it was attempted to isolate the product *via* dilution of the reaction mixture with water and acidification to ensure protonation of the carboxylic acid function of **12** while simultaneously ensuring excess piperidine would remain in the aqueous phase. Extraction of the mixture with DCM allowed the separation of a crude product, which was still contaminated with side products. Further attempts at extracting the carboxylic acid product from the mixture with sodium hydroxide solution and re-extracting it into DCM after acidification were also unsuccessful in furnishing pure **12**, still leaving it contaminated (see Experimental Section, Supplementary Figure 204). An equivalent reaction batch was purified *via* column chromatography, leading to the successful isolation of pure **12**, however in a very low yield of 12%.

Simultaneously to the test reactions **T1-A** and **T1-B**, described in Scheme 72, a set of similar reactions was conducted using benzylamine instead of piperidine, under otherwise identical conditions (**T2-A** and **T2-B**, respectively). The resulting ^{1}H NMR spectra, obtained after 18 hours, are depicted in Scheme 75.

As is evident from the spectra, the reactions with benzylamine show even lower selectivity compared to the reaction with piperidine. Already in the t_0 sample (Scheme 75, top spectrum), there is indication of an immediate reaction, evidenced by the presence of two singlets in the spectral region of the α-methyl group of LA (at 2.06 ppm), with an additional signal emerging at 1.85 ppm. This can presumably be attributed to the rapid formation of an imine from the condensation of benzylamine with the keto function of LA. The spectrum of **T2-A** after 16 hours (Scheme 75, middle spectrum) lacks clearly resolved signals in the aliphatic region, which is indicative of a product mixture. Nonetheless, the emergence of a signal at 10.8 ppm, which is the expected region for the N-H protons of primary thioamides, potentially indicates the occurrence of a WK reaction.[497] Still, integration of the N-H signal in comparison to the aromatic region shows that the maximum amount of thioamide formation equals 33%. ESI-MS analysis of the crude mixture reveals the formation of *N*-benzylthiobutyramide *via* the decarboxylative side reaction described in Scheme 74. However, no other signals in the mass spectrum could be attributed to any known product, including the desired WK product **16**. The spectrum of **T2-B** further indicates substantial side reactions already in the absence of sulfur.

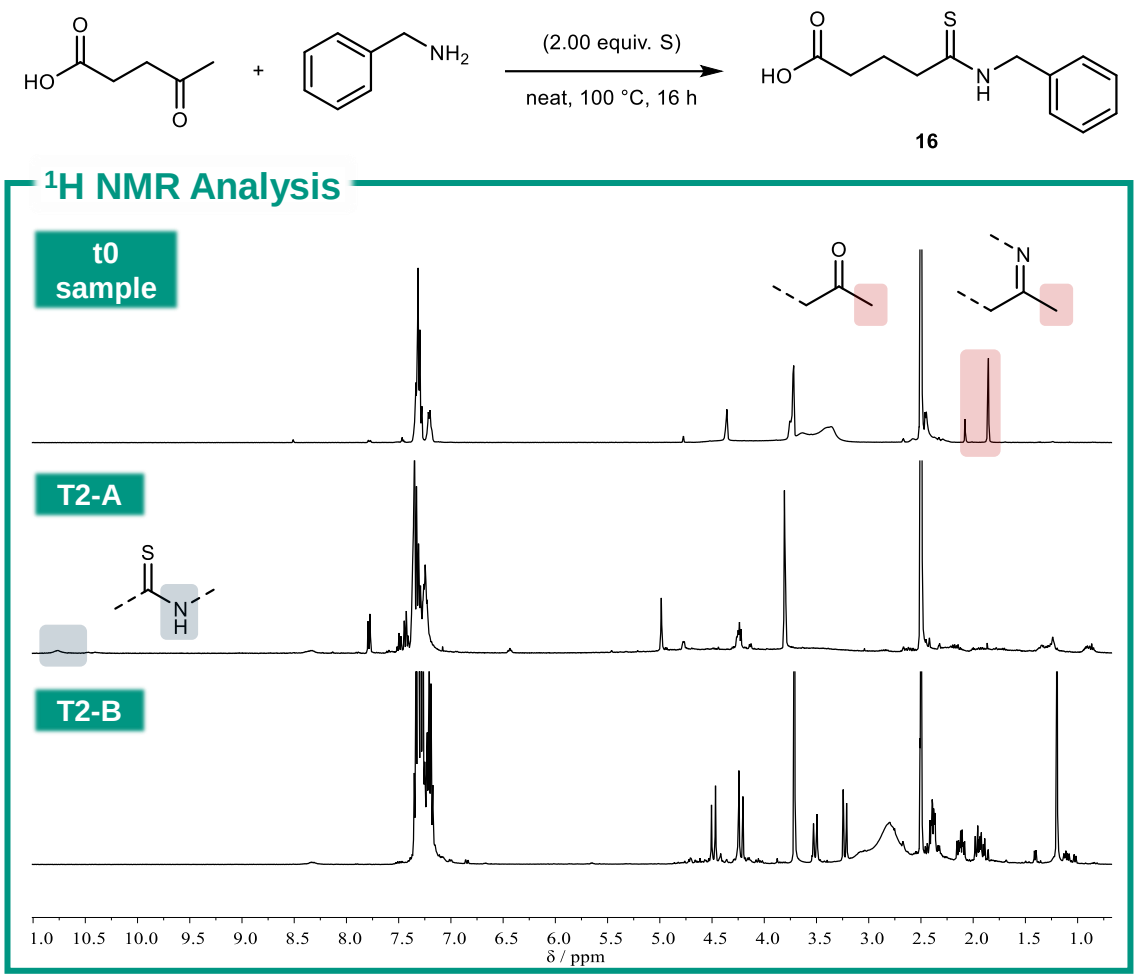

*Scheme 75: ^{1}H NMR screening (DMSO-d_6) of the reaction of LA with benzylamine, both in the presence (**T2-A**) and absence of sulfur (**T2-B**). Only the desired ω-carboxythioamide **16** is depicted in the reaction equation.*

Due to the increased prevalence of side reactions with benzylamine, it was decided to not further follow this approach, and instead use secondary amines in all subsequent studies conducted in the context of this work. The exact nature of the additional side reactions arising for benzylamine remains to be investigated. Generally, in literature, the use of secondary amines in WK reactions of ketones is much more common than the use of primary amines, which reportedly are less selective and generally result in lower yields.[149,213,215]

In summary, the WK reactions of free LA with benzylamine and piperidine were found to suffer from the occurrence of a substantial amounts of competitive side reactions, including decarboxylative thioamidation, as well as condensation of amine and carboxylic acid to yield a carboxamide. The use of the primary benzylamine resulted in even more unselective reactions, which were not further investigated in the context of this work. A screening of different reaction conditions for the WK reaction of LA and piperidine revealed that the occurrence of the side reactions presumably cannot be suppressed by altering the reaction conditions. This is generally in agreement with literature reports on the kinetics of the WK reaction, stating that the rates of

carbonyl isomerization and oxidation of the terminal isomer to the thioamide are very similar.[214] Hence, it is presumably not possible to inhibit the isomerization of the carbonyl function towards the carboxy function, which results in the occurrence of the decarboxylative side reaction.

The desired product **12** of the WK reaction of LA and piperidine was isolated *via* column chromatography in a yield of 11%. With the main focus on the synthesis of a α,ω-dicarboxylic acid as a monomer for further polycondensation, the use of a bifunctional amine would be required. Due to the low selectivity of the reaction, it can be expected that a synthesis of the desired α,ω-dicarboxylic acid is not feasible *via* direct WK reaction of LA, since the influence of statistics would result in even lower yields of difunctional products. Overall, it can hence be concluded that WK reactions of free LA are generally not viable, especially with focus on polymer synthesis.

4.4.2.2 WK reactions of Levulinamides

The second envisioned strategy to synthesize polythioamides from LA (compare Scheme 71) involves prefunctionalization of the carboxy function, for instance into amides or esters, and subsequently using the WK reaction as the polymerization method.

The insights gained in the previous chapter, namely the formation of a levulinamide from LA and piperidine under the WK conditions (reaction **T1-B**), have demonstrated that esters are presumably unviable for this approach, since they are more susceptible to nucleophilic attack on their carbonyl compounds than carboxylic acids. Yet, levulinamide **13** has shown potential as viable substrates for WK reactions, since the corresponding WK product **14** could be detected in the reaction mixture of **T1-A** *via* mass spectrometry.

In order to confirm the instability of esters under the reaction conditions and simultaneously establish a viable synthetic access to levulinamides, it was decided to synthesize methyl levulinate **17** and then investigate its reaction with piperidine at 100 °C. **17** was obtained in 93% yield by sulfuric acid-catalyzed esterification of LA with methanol (see section 6.3.4.2). Subsequently, **17** was mixed with 2.00 equivalents of piperidine and the reaction was monitored *via* ^{1}H NMR spectroscopy. As expected, the ester functionality is unstable in the presence of piperidine, with 83% conversion to the corresponding levulinamide **13** detected after 16 hours under elimination of methanol (Scheme 76). In order to investigate the potential of the reaction as a synthetic access to levulinamides, the reaction was continued at 100 °C. Full conversion of **17** to **13** was reached after a reaction time of 96 hours.

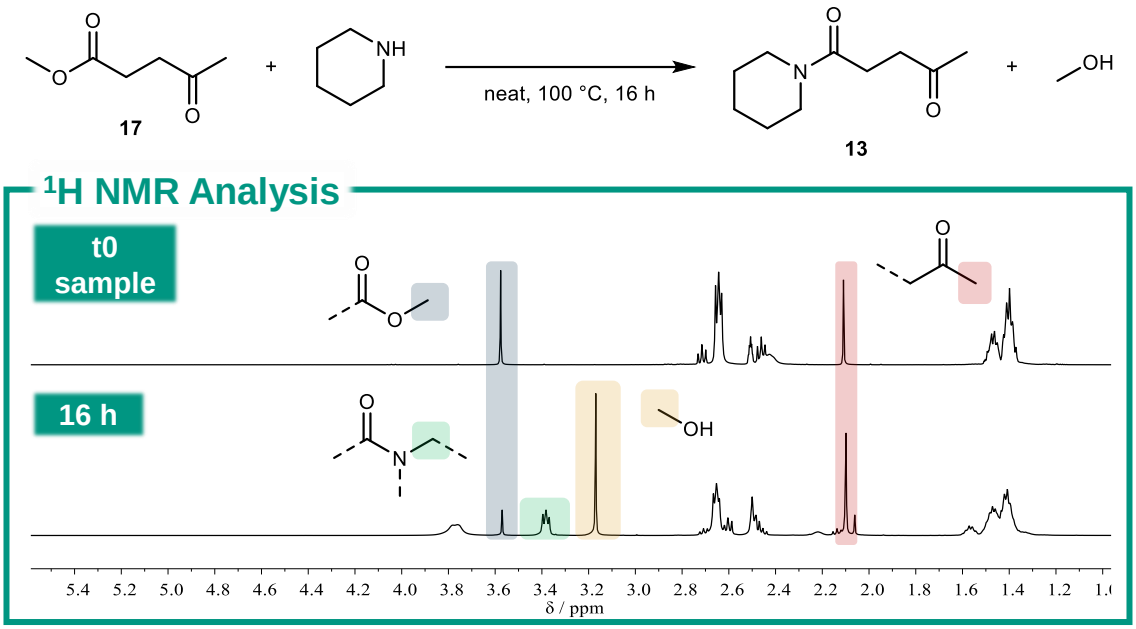

*Scheme 76: ^{1}H NMR screening ($CDCl_3$) of the reaction of methyl levulinate **17** with piperidine.*

It was attempted to isolate the product by separating excess piperidine *via* aqueous washing. However, this method was highly ineffective, since levulinamide **13** was found to exhibit substantial water solubility. Attempts to re-extract the product into diethyl ether resulted in a low yield of 33%. Due to the combination of long reaction time and non-straightforward product isolation, it was decided to pursue other methods for the synthesis of levulinamide **13**. It was found that levulinamides are also accessible by the reaction of amines with α-angelica lactone (AL), which is the enol lactone derivative of LA. AL is readily available by dehydration of LA *via* dry distillation under acidic conditions, and has thus also been described as a valuable renewable platform chemical.[498–500]

The reaction of AL with a slight excess of piperidine (1.01 equiv.) already proceeded very exothermically at room temperature. After stirring for 2 hours, the mixture was heated to 100 °C for 10 minutes to ensure complete conversion. The slight excess of piperidine was removed *in vacuo*, allowing the isolation of levulinamide **13** in a yield of 99 % (Scheme 77).

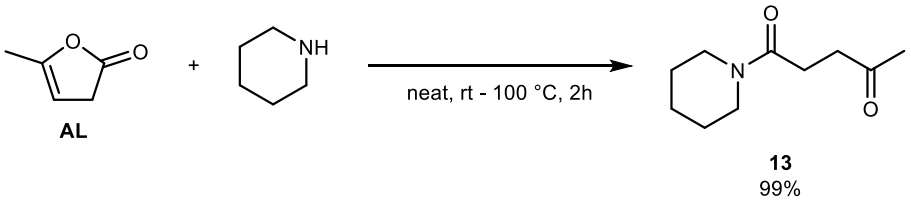

*Scheme 77: Synthesis of levulinamide **13** from AL and piperidine.*

After successful synthesis of levulinamide **13**, a set of test reactions was conducted to investigate its viability as a substrate for the WK reaction. A WK test reaction with 2.00 equiv. of piperidine and 2.00 equiv. of sulfur (**T3-A**), as well as a control experiment in the absence of sulfur (**T3-B**) were performed and monitored *via* ^{1}H NMR spectroscopy (Scheme 78).

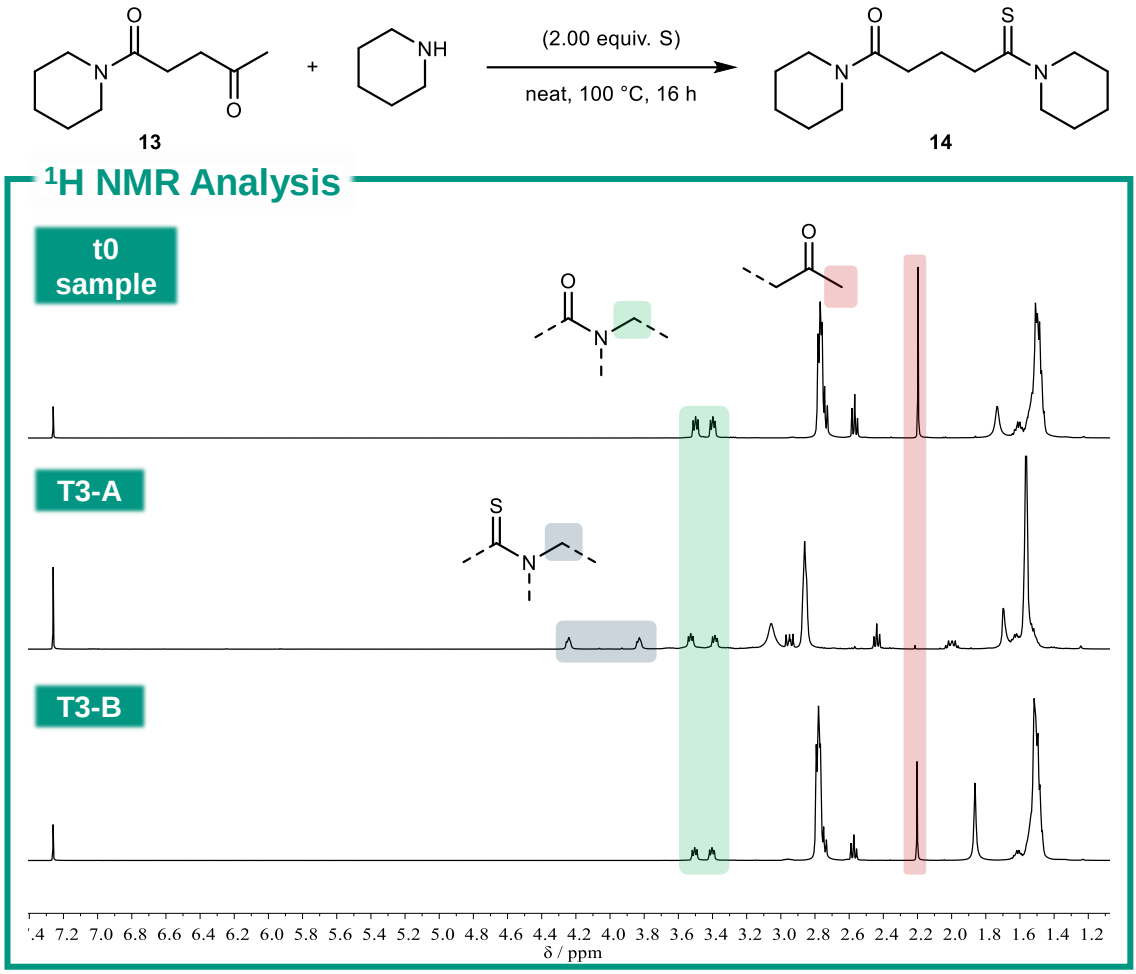

*Scheme 78: ^{1}H NMR screening ($CDCl_3$) of the reaction of levulinamide **14** with piperidine, both in the presence (**T3-A**) and absence of sulfur (**T3-B**).*

As is apparent from the ^{1}H NMR spectrum of reaction **T3-A** by the disappearance of the methyl ketone resonance at 2.20 ppm (marked in red in Scheme 78), the levulinamide **13** is almost entirely converted after a reaction time of 18 hours. Furthermore, the emergence of thioamide signals at 4.24 and 3.82 ppm (marked in blue in Scheme 78), as well as the absence of unidentifiable signals are indicative of a successful and selective WK reaction. This is further reinforced by the results of the control experiment **T3-B**, where levulinamide **13** was left completely unreacted in the absence of sulfur, indicating its stability under the reaction conditions. The product **14** was successfully isolated from the mixture of test reaction **T3-A** by extraction with diethyl ether and obtained in a yield of 76%.

Subsequently, a screening of different reaction conditions was conducted in order to gain more general insights into the WK reaction of **13** with piperidine. The conversion of **13** was quantified *via* ^{1}H NMR spectroscopy using TMB as an internal standard. The results are listed in Table 12.

*Table 12: Results of the screening of different reaction conditions for the WK reaction of levulinamide **13** with piperidine and sulfur, with quantification of conversion.*

Entry	T / °C	Piperidine / equiv.	Sulfur / equiv.	Additional conditions	t / h	Conversion / %
1	100	2.00	2.00	-	2	64
					18	99
2	100	2.00	1.20	-	2	49
					18	90
3	100	2.00	4.00	-	2	78
					18	Full
4	100	1.20	2.00	-	2	62
					18	97
5	100	4.00	2.00	-	2	80
					18	96
6	100	2.00	2.00	Argon atm.	2	66
					18	98
7[a)]	100	2.00	2.00	1.00 equiv. DBU	2	59
					18	94
8	400	2.00	2.00	1.00 equiv. NMPip	2	90
					18	Full
9	100	3.00	2.00	Anisole (1M)	2	43
					18	92
10[b)]	100	3.00	2.00	DMSO (1M)	2	n.d.
					18	n.d.
11[a)]	100	3.00	2.00	DMF (1M)	2	76
					18	Full
12	120	3.00	2.00	-	2	90
					18	Full

a) Substantial amounts unidentified side products were formed
b) No discernible product formation was observed.

Generally, the same trends were observed in this case as in the WK reaction of LA with piperidine described in the previous section. The rate of the reaction increased with increasing equivalents of elemental sulfur and is nearly unaffected by the amount of piperidine or by applying an inert atmosphere (Table 12, entries 2-6). The use of 1.00 equiv. of DBU as an auxiliary base did not result in a faster reaction and further resulted in the occurrence of

unidentified side reactions (Table 12, entry 7). In contrast, using 1.00 equiv. of *N*-methylpiperidine (NMPip), which has also been employed as a reagent in literature-described WK reactions, resulted in an acceleration of the reaction, with 90% conversion reached after 2 hours and full conversion after 18 hours (Table 12, entry 8).[218] The use of solvents did not have any beneficial impact. The use of anisole resulted in an overall slower, but still selective reaction, with 93% conversion after 16 hours (Table 12, entry 9). Using DMSO and DMF resulted in the occurrence of side reaction, with the former not exhibiting any discernible formation of the desired thioamide (Table 12, entries 10-11). Finally, an increase in temperature also resulted in an increase of the reaction rate, with 90% conversion already reached after 2 hours when conducting the reaction at a temperature of 120 °C (Table 12, entry 12).

Since the WK reaction proceeded efficiently with amides derived from piperidine, it was attempted to synthesize primary levulinamides and investigate their viability under WK conditions. Akin to the synthesis of **13**, primary levulinamides are accessible from AL and primary amines. However, it is reported that primary levulinamides or, by extension, primary γ-ketoamides are unstable towards thermodynamically driven cyclization under formation of 5-membered cyclic species. Illustrative examples are depicted in Scheme 79 (bottom).[498,500,501]

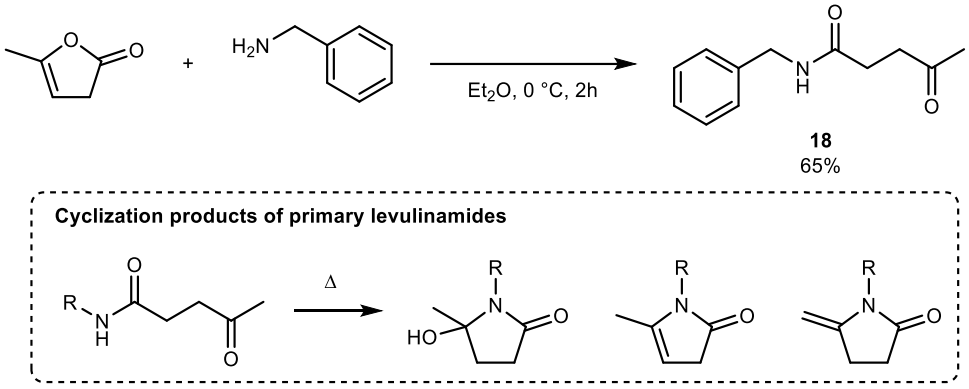

*Scheme 79: Synthesis of N-benzyllevulinamide **18** conducted in this work (top) and illustrative examples for literature-reported thermal cyclization products of primary levulinamides (bottom).[498,500,501]*

The synthesis of *N*-benzyllevulinamide **18** from benzylamine and AL was attempted. It was found that cooling of the reaction mixture was necessary in order to obtain a pure product. Without cooling, the exothermic reaction results in partial decomposition of the product, presumably under formation of pyrrolidone derivatives such as those depicted in Scheme 79. Still, it was possible to obtain pure **18** in a yield of 65% by conducting the reaction in diethyl ether at 0 °C (Scheme 79, top). The isolated *N*-benzyllevulinamide **18** was subsequently subjected to WK conditions at 120 °C (**T4-A**), while its thermal stability was investigated simultaneously at the same temperature in the absence of other reactants (**T4-B**). The reaction was monitored *via* ^{1}H NMR after 16 hours (Scheme 80).

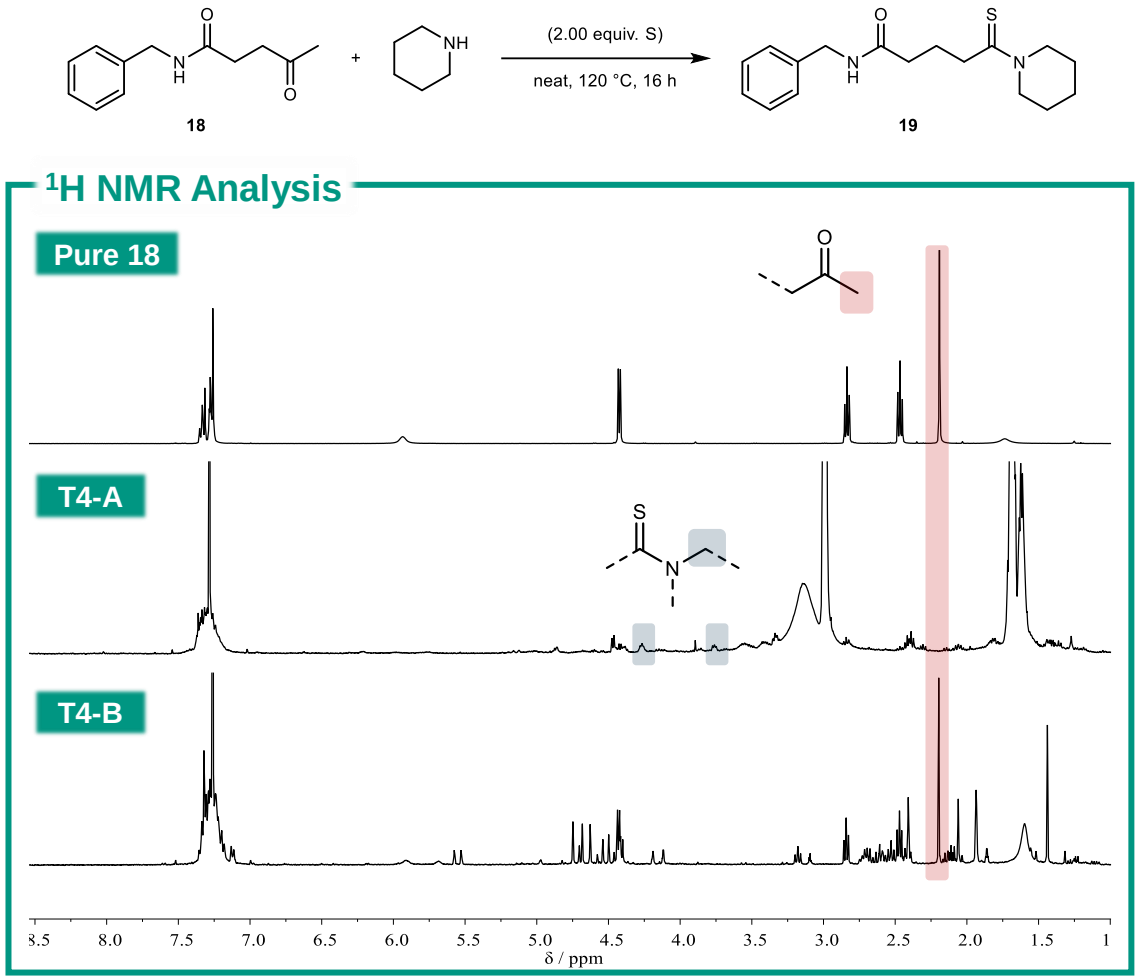

*Scheme 80: ^{1}H NMR screening ($CDCl_3$) of the reaction of N-benzyl levulinamide **18** with piperidine and sulfur (**T3-A**) and simple heating of the benzylamide to 120 °C for 16 hours (**T3-B**). Only the desired product **19** is depicted in the reaction equation.*

The spectrum of **T4-B** illustrates the thermal instability of **18** due to the emergence of numerous additional signals. In the spectrum of T1-A, weak thioamide signals are visible at 4.24 and 3.82 ppm (marked in blue in Scheme 80), indicating that the WK reaction proceeded to a certain degree. However, the presence of numerous other signals indicates a low selectivity for the WK reaction.

Overall, it can be expected that the thermally induced cyclization of primary levulinamides inhibits their viability as substrates for the WK reaction. However, it was found that the secondary levulinamide **13** undergoes efficient and selective WK reaction with piperidine. Notably, the viability of primary amines for the WK reaction of levulinamide **13** was not investigated in this work, and is thus potentially a subject for future studies.

4.4.3 Monomer and Polymer Synthesis

Having successfully demonstrated that the secondary levulinamide **13** reacts selectively in a WK reaction with piperidine, it was attempted to transfer these findings towards bifunctional substrates in order to synthesize WK-derived polymers. Accordingly, piperazine was selected as a bifunctional secondary amine for monomer synthesis and subsequent WK polymerization. Piperazine currently represents a cheaply available side product of the industrial synthesis of ethylenediamine.[502]

The synthesis of the bifunctional levulinamide *N*,*N*-bis(levulinoyl)piperazine **20** was conducted by mixing piperazine with a slight excess of AL at room temperature. The mixture quickly and exothermically solidified and was subsequently heated to 120 °C for 1 hour in order to ensure complete reaction. **20** was isolated by washing the solidified reaction mixture with cold ethanol and obtained in a yield of 73% (Scheme 81).

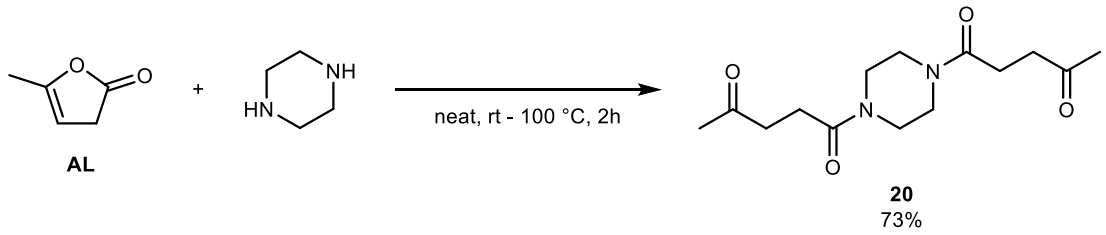

*Scheme 81: Synthesis of N,N-bis(levulionyl)piperazine **20**.*

After successful synthesis of monomer **20**, polymerization attempts were conducted using a combination of the optimized conditions obtained in the screening experiments described in Table 12, *i.e.*, the polymerization was carried out at 120 °C using 4.00 equivalents of atomic sulfur. It was decided to use 1.00 equiv. of piperazine, representing the ideal stoichiometric ratio between the reactants in order to achieve high molecular weight. It was opted to conduct one polymerization attempt under bulk conditions (**PTG-1-A**) and another attempt in the presence of 1.00 equiv. of NMPip (**PTG-1-B**), since it was demonstrated to be beneficial to the reaction rate and can potentially contribute to a more homogeneous polymerization mixture, since all starting materials are solids at room temperature (Scheme 82).

In both cases, the polymerization resulted in the formation of a dark solid after 16 hours. After cooling, the product was isolated by dissolving the crude mixture in a minimal amount of DMSO and subsequent precipitation into cold methanol. The polymers **PTG-1-A** and **PTG-1-B** were obtained as dark brown solids in yields of 40% and 94%, respectively, and identified as the desired polythioglutaramide **PTG**-1 *via* ^{1}H and ^{13}C NMR analysis (see section 6.3). ^{13}C NMR in particular clearly demonstrates the presence of both the carbonyl and thiocarbonyl moiety *via* two distinct signals at 170.5 and 202.1 ppm.

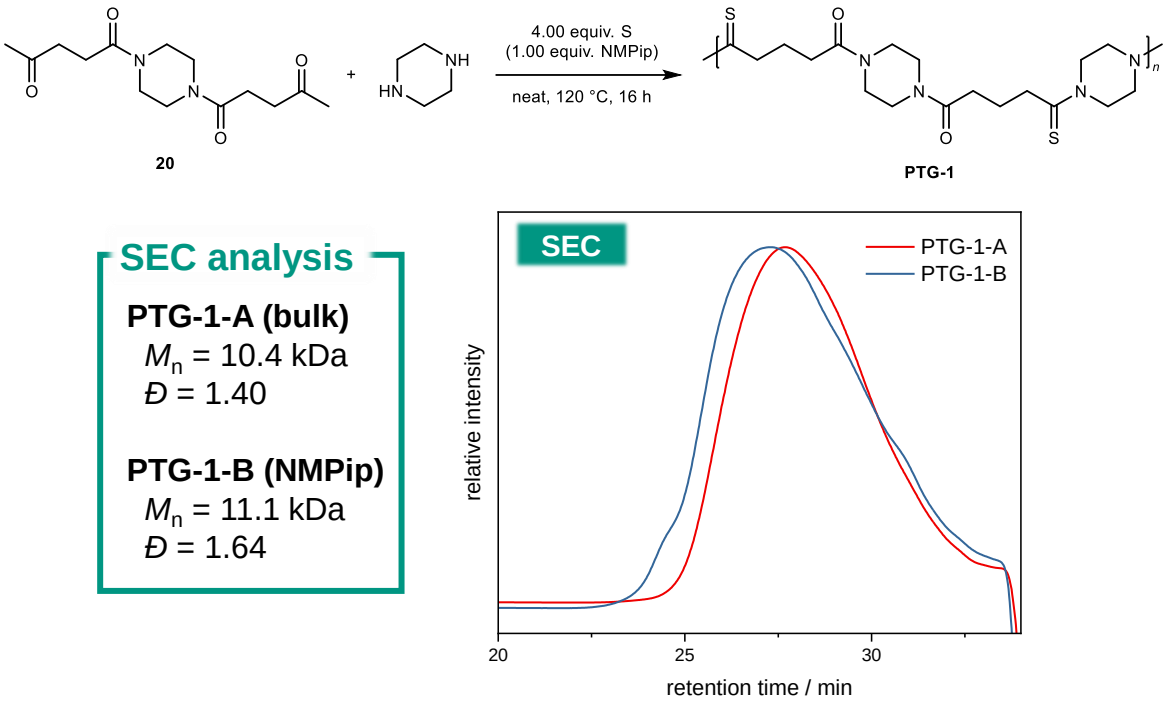

*Scheme 82: Polymerization of monomer **20** to polythioglutaramide **PTG-1**, both under bulk conditions (**PTG-1-A**) and in the presence of NMPip (**PTG-1-B**), along with SEC traces and the calculated number average molecular weights and dispersities.*

SEC analysis was conducted in *N*,*N*-dimethylacetamide (DMAc) + 0.003 wt% lithium bromide, revealing a slightly higher M_n of 11.1 kDa for **PTG-1-B** as compared to **PTG-1-A** (10.4 kDa), suggesting that the presence of NMPip contributes to a more efficient polymerization, since it increases the reaction rate and results in better mixing. The calculated dispersities were 1.64 for **PTG-1-B** and 1.40 for **PTG-1-A**. This is slightly below the expected value of 2.00, which is expected for step-growth polymerization. This can presumably be attributed to solubility issues, since it was found that the polymer **PTG** was generally poorly soluble, dissolving very slowly in DMAc for the preparation of the SEC samples and being completely insoluble in THF, anisole, acetonitrile, methanol, water, and chloroform. Furthermore, since the polymerization mixture solidified in both cases, it is conceivable that heterogeneity of the mixture could contribute to incomplete conversion, thus resulting in a lower than expected dispersity. Overall, it can be concluded that the polymerization in the presence of NMPip proceeded slightly more efficiently, allowing the isolation of the product in higher yield and with a higher molecular weight.

Thermal characterization of **PTG-1-B** was subsequently conducted *via* DSC and TGA (see section 6.3.4.2). TGA revealed a two-step degradation with an onset temperature of 276 °C. DSC revealed a thermal transition at 109 °C. Since this thermal transition is close to the melting point of elemental sulfur, it could also be related to the presence of residual sulfur in the isolated polymer. This could be further confirmed *via* elemental analysis, which was however no longer conducted in the context of this work. Yet, the absence of other thermal transitions in the range

of -60 to 170 °C, as well as the shape of the transition are arguments in favor of a glass transition of the polymer at that temperature.

4.4.4 Summary and Outlook

In conclusion, the applicability of the Willgerodt-Kindler reaction to a variety of derivatives of levulinic acid, a readily available platform chemical derived from biomass, was investigated. Benzylamine and piperidine were used as model amines for the investigations. It was found that the WK reaction is not feasible for free levulinic acid, resulting in numerous side reactions, including decarboxylative thioamidation. It was further observed that WK reactions with the secondary amine piperidine are significantly more selective than those using the primary benzylamine. A secondary levulinamide, which was easily accessible from the LA derivative α-angelica lactone and piperidine, was found to be suitable substrate for the WK reaction with piperidine, while a primary levulinamide derived from benzylamine was found to be insufficiently stable under the reaction conditions for a selective WK reaction. The optimization of the reaction conditions of the WK reaction of secondary levulinamide and piperidine allowed the transfer of the synthesis protocol to a bifunctional levulinamide, derived from piperazine. As a result, a model polythioglutaramide was successfully synthesized and characterized.
Future studies could be aimed at gaining more fundamental insights on the WK reaction of levulinamides. For instance, the feasibility of primary amines for the WK reaction of levulinamides has not yet been explored as part of this thesis. The polymerization scope could also be further elaborated by utilizing a broader scope of diamine comonomers. Furthermore, the synthesis of potential AB monomers could be an interesting approach in future investigations.

5 Conclusion and Outlook

In this work, several novel synthetic strategies involving the use of elemental sulfur and sulfur-containing compounds were established, both in the context of organic and polymer synthesis.

Firstly, a novel olefination reaction, involving the alkylidene-homocoupling of NTHs in the presence of elemental sulfur and potassium carbonate, was extended in scope. The homocoupling reaction was shown to proceed very selectively for aromatic substrates with a variety of different substituents, providing efficient synthetic access to various TAE derivatives in excellent yields. The method was shown to possess a complementary substrate scope to established methods such as the McMurry reaction, while exhibiting similar yields and not relying on complex reaction and workup setups as well as expensive, overly hazardous or metal-based additives. Mechanistic insights allowed the development of a variation of the olefination reaction that uses a thioketone as an additional stoichiometric reagent, thus allowing for an efficient alkylidene-cross coupling. The cross-coupling method was similarly demonstrated to be viable for the synthesis of TAEs comprising different alkylidene moieties. Furthermore, the cross-coupling method was shown to exhibit tolerance towards aliphatic substrates, greatly expanding the synthetic scope to a wider range of olefins. Thus, overall two methods for olefin synthesis *via* sulfur-mediated olefination of NTHs were established.

Secondly, the homocoupling olefination of NTHs was successfully transferred to bifunctional substrates, enabling the synthesis of PAV-DAs in good yields and molecular weights. In this context, further investigations upon the reaction conditions of the olefinations were undertaken, revealing that the reaction can also be performed at lower temperature under an inert atmosphere. Eight PAV-DA homopolymers and two copolymers were synthesized and characterized in terms of their thermal and optical properties. In this context, copolymerization was demonstrated to allow for efficient thermal and optical property adjustment. The newly established synthetic access to PAV-DAs was shown to be more feasible than literature-known procedures, producing PAV-DAs in similar or superior yields and molecular weights while simultaneously relying on cheap, bench-stable reactants.

Furthermore, a three-step strategy for the synthesis of polythiols from renewable vegetable oil feedstock was developed, involving initial $GaBr_3$-catalyzed deoxygenation of the triglyceride ester moieties with TMDS, followed by thiol-ene addition of HSAc and subsequent alcoholysis.

In this context, new insights on previously unreported homocoupling side reactions of the ester deoxygenation were gained, and a new method for the separation of the PDMS byproducts *via* alkaline hydrolysis was established. Three polythiols were synthesized in good overall yields and their viability as crosslinking agents for the synthesis of polymeric networks was exemplarily demonstrated by the successful synthesis of model materials, both *via* radical thiol-ene chemistry and *via* nucleophilic addition to isothiocyanates. Future studies could be aimed at further optimizing the polymerization conditions and investigating the comonomer scope.

Finally, the use of levulinic acid as a bio-based platform for the synthesis of polythioamides *via* the Willgerodt-Kindler reaction was investigated. It was found that free levulinic acid is not a suitable substrate for the WK reaction due to the prevalence of side reactions. However, levulinamides were identified as viable starting materials. A bifunctional levulinamide based on piperazine was thus synthesized and successfully polymerized using the WK reaction, successfully leading to a poly(monothioglutaramide). At this stage, an important proof-of-concept was demonstrated, and future studies can be aimed at further expanding the substrate scope of the polymerization and investigating potential applications of the materials.

In summary, the results obtained within this work represent advances on applications of elemental sulfur and sulfur-containing compounds in organic and polymer chemistry. The versatility of elemental sulfur both as a reagent and building block was highlighted. Novel, feasible synthetic accesses to a variety of compounds and materials with useful properties, namely TAEs, PAV-DAs, polythiols and polythioamides were established. Furthermore, the synthesis of polymeric materials from renewable resources and the application of sulfur chemistry under consideration of the principles of Green Chemistry represents a contribution towards more sustainable synthetic processes.

6 Experimental Section

6.1 Instrumentation

Nuclear Magnetic Resonance Spectroscopy (NMR)

^{1}H and ^{13}C-NMR spectra were recorded on a *BRUKER Avance DPX 400* NMR spectrometer at 400 MHz for ^{1}H and 101 MHz for ^{13}C-NMR, or a *BRUKER Avance DPX 500* spectrometer at 500 MHz for ^{1}H and 126 MHz for ^{13}C-NMR. Unless otherwise stated, all spectra were recorded at a temperature of 298 K. The chemical shift was reported in parts per million (ppm) and referenced to characteristic signals of the used deuterated solvents, *e.g.* chloroform-d_1 at 7.26 ppm for ^{1}H (77.16 ppm for ^{13}C), methylene chloride-d_2 at 5.32 ppm for ^{1}H (54.00 ppm) for ^{13}C, or DMSO-d_6 at 2.50 ppm for ^{1}H (39.52 ppm for ^{13}C). For centrosymmetrical signals, the centroid shift was given and for multiplets, the signal range was reported. The multiplets arising from spin-spin coupling were abbreviated as follows: s = singlet, d = doublet, t = triplet, q = quartet, p = quintet, sext. = sextet, m = multiplet, br = broad signal. Coupling constants J were reported in Hz. Furthermore, the 2D-NMR methods ^{1}H,^{1}H-correlated spectroscopy (COSY), ^{1}H,^{13}C-heteronuclear single quantum coherence spectroscopy (HSQC), ^{1}H,^{13}C-heteronuclear multiple bond correlation spectroscopy (HMBC) and ^{1}H,^{1}H-nuclear Overhauser enhancement spectroscopy (NOESY) were performed for signal assignment and structure elucidation.

Infrared Spectroscopy (IR)

IR measurements were performed on a *Bruker ALPHA attenuated total reflection (ATR)* IR spectrometer in a range from 4000 to 500 cm^{-1} at ambient temperature. Samples were placed directly onto the diamond without further sample preparation. Spectra were recorded in absorbance mode with 24 scans. Before measurement, the background was measured with 24 scans without sample. The bands were characterized according to their relative absorbance (A) intensity as follows: vs = very strong (90 – 100% A), s = strong (60 – 90% A), m = medium (30 – 60% A), w = weak (10 – 20% A), vw = very weak (>10% T). Broad signals were labelled with br.

High Resolution Mass Spectrometry (HRMS)

Fast Atom Bombardment (FAB) and electron impact ionization (EI) mass spectra were recorded using a *Finnigan MAT* mass spectrometer. A *Q Exactive* Orbitrap mass spectrometer (*Thermo*

Fisher Scientific) equipped with a *HESI II* probe was employed to record high resolution electrospray ionization (ESI) mass spectra. Calibration was carried out in the *m/z* range 74 – 1822 using premixed calibration standards (*Thermo Fisher Scientific*). The spectra were interpreted by indicating the *m/z* of the molecular peak $[M]^+$, protonated molecular peak $[M+H]^+$ or sodiated molecular peak $[M+Na]^+$ as well as characteristic fragments along with their relative intensities.

Ultraviolet-visible spectroscopy (UV/Vis)

Absorption spectroscopy was performed on an *Agilent Cary 3500 UV-Vis* multicell spectrometer with a Peltier Element. Spectra were recorded at a cell temperature of 20 °C in a range of 200 nm to 800 nm in 1 nm intervals using a scanning speed of 600 nm/min. Samples were measured using 1 cm *STARNA* quartz cuvettes in a concentration of 100 µM in tetrahydrofuran or chloroform.

Fluorescence Spectroscopy

Emission spectra were recorded on a *HORIBA FluoroMax Plus* spectrometer. Spectra were recorded at a cell temperature of 20°C in 1 nm intervals using an increment time of 200 ms and an integration time of 100 ms. Excitations wavelengths and slit sizes were adapted for each sample individually. Samples were prepared by injecting 10 µL of a 10 mM stock solution of the analyte in THF into 5 mL of water with 10 vol% THF under rapid stirring (corresponding to 20 µM of analyte in water with 10 vol% THF), or by injecting a chloroform stock solution into ethanol/chloroform, with the same concentrations and ratios.

Gas Chromatography / Mass Spectrometry (GC-MS)

GCMS measurements were performed on a *Varian 431 GC* instrument with a capillary column *FactorFour VS-5 ms* (30 m × 0.25 mm × 0.25 mm) coupled with a *Varian 210* electron impact (EI) ion trap mass spectrometer. Scans were performed from 40 to 650 *m/z* at a rate of 1.0 scans per second. The oven temperature program was initial temperature 95°C, ramp at 15°C min^{-1} to 220°C, hold for 4 min, ramp at 15°C min^{-1} to 300°C, hold for 2 min. The injector transfer line temperature was set to 250°C. Measurements were performed in split-split mode (split ratio 50:1) using He as carrier gas with a flow rate of 1.0 mL min^{-1}.

Thin Layer Chromatography (TLC)

TLC analyses were performed using aluminium plates coated with silica and a fluorescence indicator (*Merck, Silica Gel 60, F 254, layer thickness 0.25 mm*). The spots were visualized by

examining their fluorescence under UV light (λ = 365 nm) or their fluorescence quenching at a wavelength of 254 nm. If necessary, the TLC plates were stained with a potassium permanganate staining solution (1.50 g $KMnO_4$, 10.0 g K_2CO_3 and 0.50 g NaOH in 200 mL water) or vanillin solution (15 g vanillin, 2.5 mL concentrated sulfuric acid, 250 mL ethanol).

Column Chromatography

Column Chromatography was performed using *Silica Gel 60* (*Merck*, mesh size 40 – 63 µm) and quartz sand (*Bernd Kraft*) as column material and HPLC grade solvents as mobile phase.

Size Exclusion Chromatography

SEC measurements were performed on a *Shimadzu SEC* system equipped with a *Shimadzu* isocratic pump (*LC-20AD*), a *Shimadzu* refractive index detector (30 °C) (*RID-20A*), a *Shimadzu 164 autosampler* (*SIL-20A*) and a *Shimadzu* column oven (30 °C). The column system comprised an *SDV* 5 µm, 8×50 mm precolumn, an *SDV* 5 µm, 1,000 A, 8×300 mm column and a *SDV* 5 µm, 100,000 A, 8×300 mm column supplied by *PSS, Germany*. A mixture of THF stabilized with 250 ppm butylated hydroxytoluene (≥99.9%) and 2 vol% triethylamine (≥99.5%) supplied by *Sigma-Aldrich* was used at a flow rate of 1.00 mL/min. Calibration was carried out by injection of ten narrow PMMA standards ranging from 1,102 to 981,000 kDa.
Furthermore, a *PSS SECcurity2* GPC system based on *Agilent infinity 1260 II* hardware was used. The system is equipped with a refractive index detector *SECcurity² RI*, a column oven *"(Bio)SECcurity² column compartment TCC6500"*, a "*standard SECcurity²"* autosampler, isocratic pump *"SECcurity² isocratic pump"*. THF (flow rate 1 mL/min) at 30 °C was used as mobile phase. The analysis was performed using the following column system: Two columns *PSS SDV analytical* (3 µm, 300 × 8.0 mm2, 1000 Å) with a *PSS SDV analytical precolumn* (3 µm, 50 × 8.0 mm2). For the calibration, narrow linear poly(methyl methacrylate) standards (*Polymer Standards Service, PPS, Germany*) ranging from 102 to 62200 Da were used.
Furthermore, a *PL-SEC 50 Plus Integrated System* with a *PLgel 5* µm bead-size guard column (50 × 7.5 mm) followed by three *PLgel 5 µm Mixed C* columns (300 × 7.5 mm) and a differential RI detector was used. *N*,*N*-Dimethylacetamide (DMAc) enriched with 0.03 wt% lithium bromide was used as eluent at a temperature of 70 °C and a flow rate of 1.0 mL min^{-1}. The samples were prepared with a concentration of 2.0 mg mL^{-1} and 100 µL were injected into the system. A poly(methyl methacrylate) standard was used for extrapolation of the number average molar mass (M_n).

Thermogravimetric Analysis (TGA)

Thermogravimetric analysis was performed on a *TGA5500* from *TA instruments*. 5-15 mg of a sample were placed in an aluminum pan and heated at a rate of 10 K min−1 from ambient temperature to 600-1000 °C under nitrogen flow. The onset was evaluated using *Trios v5.0.044608* software.

Differential Scanning Calorimetry (DSC)

DSC experiments were performed on a *Mettler Toledo DSC 3* using a *Huber Intracooler TC100* and aluminum crucibles (40 and 100 µL). Measurements were performed under nitrogen flow (50 mL min^{-1}) in three consecutive heating / cooling cycles with a heating rate of 10 K min^{-1}. Each measurement was performed using 3-7 mg of substance for sample preparation. T_g values were determined as the onset of the transition in the second heating cycle.

Tensile Strength Measurements

Tensile strength measurements were performed using an *Inspect table 10kN* from *Hegewald & Peschke* equipped with a 1.5 kN load cell. Measurements were performed at an elongation rate of 10 mm min^{-1}.

Reactions under ultraviolet (UV) irradiation

Reactions under UV irradiation were performed using a *Vilber VL-315.BL* lamp with a power of 45 W and a wavelength of 365 nm. The samples / reaction vessels were placed underneath the lamp in an irradiation distance of 6 cm.

6.2 Materials

Unless otherwise stated, all chemicals were used as received. High Oleic Sunflower Oil (HOSO) was purchased at local supermarkets in Karlsruhe, Germany. The product is also available online (https://biozentrale.de/products/brat-backol-750-ml).

Substance	Supplier	Purity
4,4'-Dimethoxybenzophenone	Acros Organics	97%
1,3,5-Trimethoxybenzene (TMB)	Sigma-Aldrich	>99%
1,5,7-Triazabicyclo[4.4.0]dec-5-ene (TBD)	Sigma-Aldrich	98%
1,7-Octadiene	VWR	For synthesis
1,8-Diazabicyclo[5.4.0]undec-7-ene (DBU)	TCI	>98%
1-Methylpiperidine	Sigma-Aldrich	99%
2,5-Thiophenedicarboxylic acid	ChemPur	98%
2-Adamantanone	Acros Organics	98%
2-Methyltetrahydrofuran	Acros Organics	Anhydrous
3-Pentanone	Sigma-Aldrich	>99%
4,4'-Biphenyldicarboxylic acid	ChemPur	98%
4,4'-Dimethoxybenzophenone	Acros Organics	97%
4-Bromobenzophenone	Alfa Aesar	98%
4-Bromobenzoyl chloride	TCI	98%
4-Hydroxybenzophenone	Acros Organics	>98%
4-Methoxybenzaldehyde	abcr	98%
4-Nitrobenzophenone[a)]	Sigma-Aldrich	99%,
9-Fluorenone	Acros Organics	99%
Acetic acid	Fluka	Puriss, p.a.
Acetone	Fisher	99%
Acetonitrile	Fisher Scientific	>99.9%, HPLC grade
Acetyl Chloride	Sigma-Aldrich	99%, for synthesis
Aluminium chloride	Acros Organics	98.5%, anhydrous
Aniline	Sigma-Aldrich	99%
Anisole	Sigma-Aldrich	99%
Benzene	TCI	<99.5%
Benzophenone	Sigma-Aldrich	99%

Benzylamine	Sigma-Aldrich	99%
Bromobenzene	Acros Organics	99%
Caesium carbonate[b)]	Sigma-Aldrich	99%
Celite®	Acros Organics	Acid-washed
Chloroform	VWR	HPLC grade
Chloroform-d	Eurisotop	>99.9 atom-% D
Cyclohexane	VWR	HPLC grade
Dichloromethane (DCM)	VWR	HPLC grade
Diethyl ether	Oqema	Pharmaceutical grade
Dimethoxyphenylacetophenone (DMPA)	Fisher Scientific	99%
Dimethyl carbonate (DMC)	Sigma-Aldrich	>99%
Dimethyl sulfoxide (DMSO)	Acros Organics	>99.7%, extra dry
Dimethylsulfoxide-d_6 (DMSO-d_6)	Eurisotop	>99.9 atom-% D
Di-*n*-butyltin oxide	Sigma-Aldrich	98%
Diphenyl ether	Fisher Scientific	<99%
Diphenyl sulfide	ChemPur	98%
Diphenylmethane	Sigma-Aldrich	For synthesis
Ethanol, absolute	VWR	HPLC grade
Ethyl acetate	VWR	HPLC grade
Ethyl formate	ACROS	>98%
Ethylene glycol	Riedel-de Haën	>99.5%
Formic acid	Fluka	98%
Gallium bromide	Fisher Scientific	99.998%, ultra dry
Glycerol	Sigma-Aldrich	99%
Hydrazine hydrate	Sigma-Aldrich	99%
Hydrochloric acid, 37%	Fisher Scientific	For analysis
Hydroquinone	Sigma-Aldrich	puriss.
Isophthaloyl chloride	Fisher Scientific	98%
Lawesson's reagent	Acros Organics	99%
Levulinic acid	Sigma-Aldrich	99%
Manganese dioxide, activated	Fluka	90%, technical
Methanol	VWR	HPLC grade
Methyl Iodide	Acros Organics	98%, for synthesis
Methylene chloride-d_2	Eurisotop	> 99.8 %

N,*N*-Dimethyacetamide (DMAc)	VWR	HPLC grade
N,*N*-Dimethylformamide (DMF)	VWR	HPLC grade
n-Hexane	VWR	HPLC grade
Nitric acid, 65%	Fisher Scientific	For analysis
N-Methyl-2-pyrrolidone (NMP)	Thermo Fisher	99%, extra pure
n-Propanol	Fisher Scientific	For analysis
o-Nosyl chloride	TCI	97%
Oxalyl chloride	Sigma-Aldrich	98%
Phosphoric acid	Fisher Scientific	For analysis
Piperazine	Sigma-Aldrich	99%
Piperidne	Sigma-Aldrich	99%
p-Nosyl chloride	Sigma-Aldrich	97%
Potassium carbonate, anhydrous[b)]	Fluka	99%
Potassium hydroxide	Bernd Kraft	p.a.
Potassium permanganate	Supelco	krist,, EMPLURA®
p-Toluenesulfonic acid monohydrate	Acros Organics	>99%, extra pure
p-Toluenesulfonyl chloride	Sigma Aldrich	98%
p-Toluenesulfonyl hydrazide	Sigma-Aldrich	97%
Putrescine	Fisher Scientific	98%
Pyridine	Fisher Scientific	99.90%
Sodium bicarbonate	Fisher Scientific	>99%
Sodium Carbonate	Fisher Scientific	99%
Sodium hydride, dispersion in mineral oil	Sigma Aldrich	60%
Sodium hydroxide	Bernd Kraft	p.a.
Sodium *p*-toluenesulfinate (NaTs)	Sigma-Aldrich	95%
Sodium sulfate, anhydrous	Thermo	Extra pure, 99%
Sodium sulfate	Thermo	98%
Sulfur	BASF	technical
Sulfuric acid	Fisher Scientific	For analysis
Sunflower Seed Oil from Helianthus annuus	Sigma Aldrich	Tested according to Ph. Eur.
Terephthaloyl chloride	TCI	>99%
tert-Butylbenzene	Fisher Scientific	99%
Tetrabutylammonium hydrogensulfate	Fisher Scientific	99%

Tetrahydrofuran (THF)[c)]	Sigma-Aldrich	>99.8%, with 2.5 ppm BHT as stabilizer
Tetramethyldisiloxane (TMDS)	Sigma-Aldrich	97%
Thioacetic acid[c)]	Sigma-Aldrich	96%
Thioxanthene-9-one	Sigma-Aldrich	98%
Toluene	VWR	HPLC grade
Triethylamine	Fluorochem	anhydrous
Triglyme	Sigma-Aldrich	99%
Trisyl Chloride	Sigma-Aldrich	97%
Undecenoic Acid	Fisher Scientific	99%
γ-Butyrolactone (GBL)	Sigma-Aldrich	>99%

a) purified by column chromatography before use (cyclohexane / ethyl acetate 10:1)
b) vacuum-oven-dried before use
c) distilled before use

6.3 Procedures

6.3.1 Sulfur-mediated Olefination – Chapter 4.1

6.3.1.1 Synthesis of Carbonyl Compounds

Disclaimer

4f and **4j** were synthesized by the author during his master thesis. Their characterization is thus not included here.

4,4'-Dibromobenzophenone (4c)

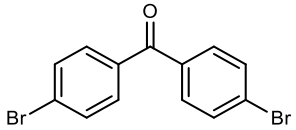

In a Schlenk flask under argon atmosphere, 2.00 g of aluminium chloride (15.0 mmol, 1.20 equiv.) were dispersed in 10 mL of bromobenzene and a solution of 2.74 g *p*-bromobenzoyl chloride (12.5 mmol, 1.00 equiv.) in 10 mL of bromobenzene was added dropwise. The mixture was stirred for 60 hours at 65 °C. Subsequently, the reaction mixture was poured onto 50 g of ice and 50 mL of DCM along with 200 mL of concentrated hydrochloric acid were added. The aqueous phase was extracted three times with 50 mL each of DCM and the combined extracts were washed once each with 1 M NaOH and water. The extracts were dried over sodium sulfate and the solvent was removed under reduced pressure. The product was obtained as a slightly yellow, crystalline solid in a yield of 82% (3.48 g, 10.2 mmol). Procedure adapted and modified from literature.[433]

^{1}H NMR (400 MHz, DMSO-d_6) δ/ppm = 7.82 – 7.74 (m, 4H), 7.71 – 7.63 (m, 4H).

^{13}C NMR (101 MHz, DMSO-d_6) δ/ppm = 193.99, 135.65, 131.72, 131.60, 126.93.

IR (ATR platinum diamond): $\tilde{\nu}/cm^{-1}$ = 1643 (vs), 1580 (vs), 1563 (m), 1479 (w), 1395 (m), 1378 (w), 1368 (w), 1312 (w), 1302 (m), 1284 (s), 1273 (s), 1174 (w), 1144 (w), 1111 (w), 1105 (w), 1070 (s), 1010 (s), 967 (w), 924 (s), 854 (vs), 825 (s), 749 (vs), 695 (w), 675 (w), 662 (s), 623 (w), 485 (m), 477 (s), 436 (m).

ESI-HRMS m/z: $[M+H]^+$ calculated for $C_{13}H_8O^{79}Br^{81}Br$ = 340.8994, found 340.8990.

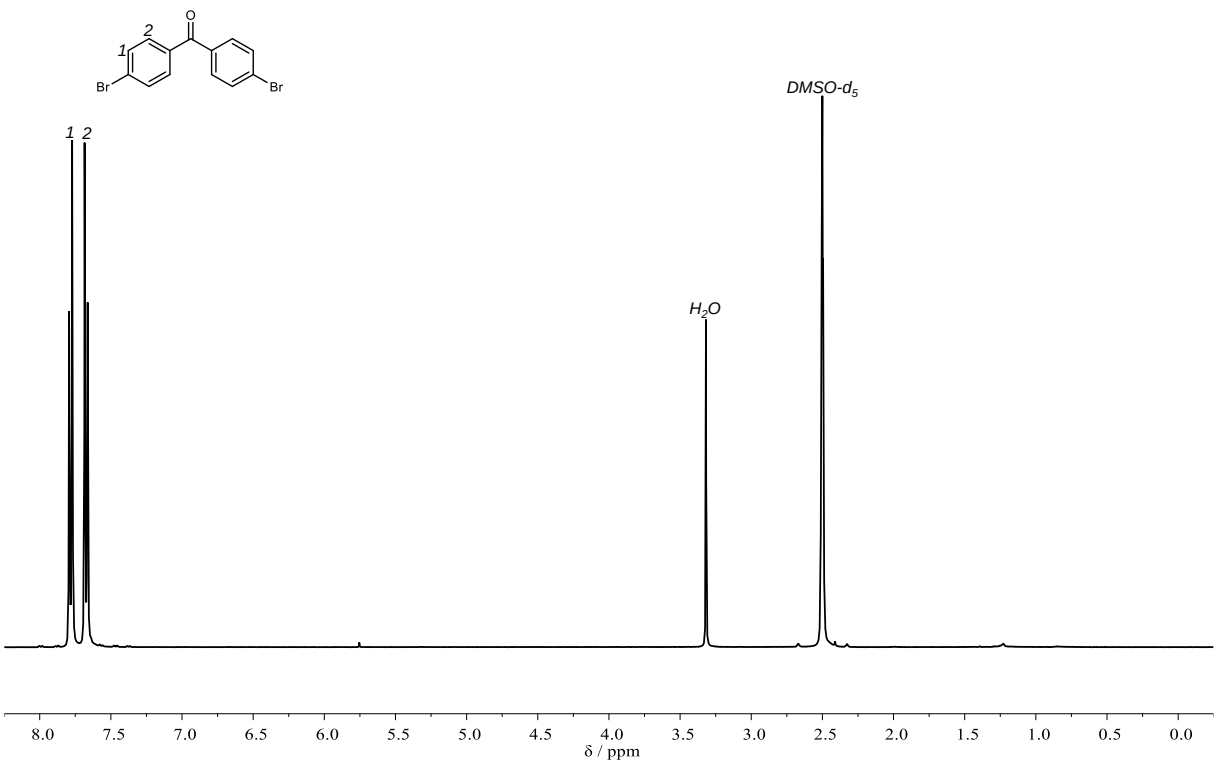

*Supplementary Figure 1:[1]H NMR spectrum of **4c** in DMSO-d_6.*

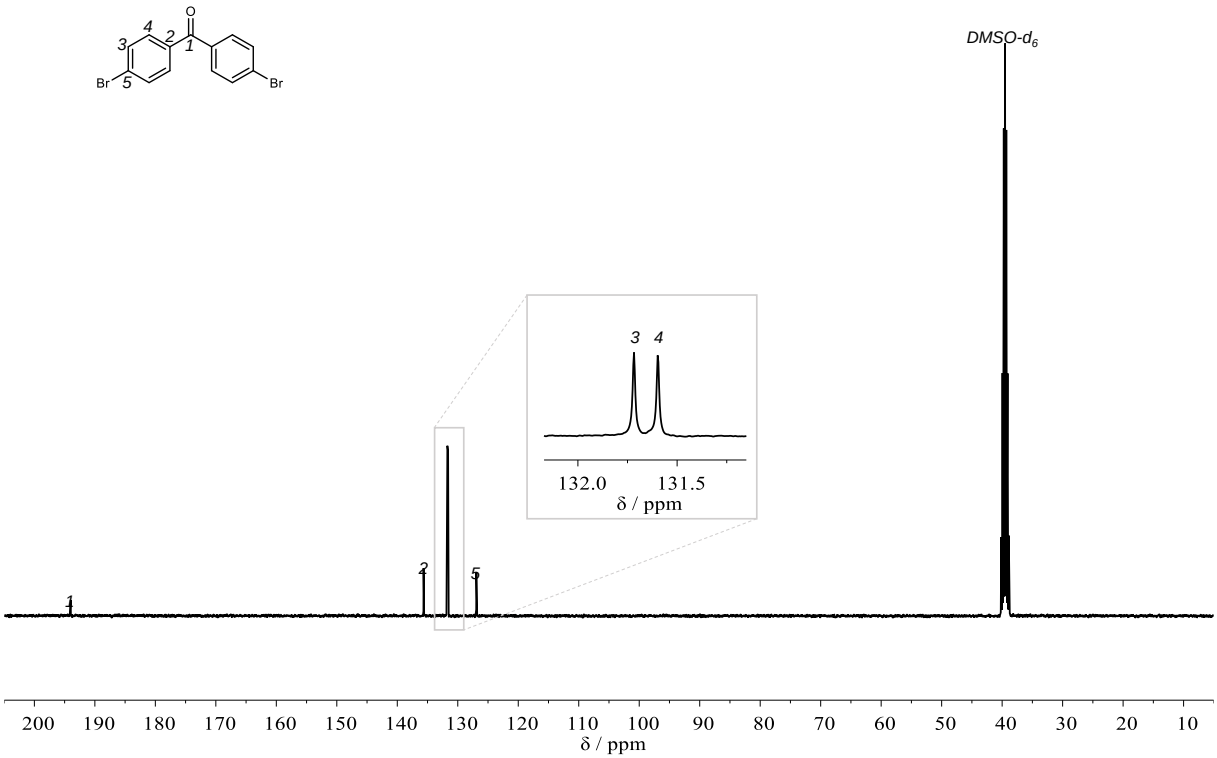

*Supplementary Figure 2:[13]C NMR spectrum of **4c** in DMSO-d_6.*

4,4'-Dinitrodiphenylmethane

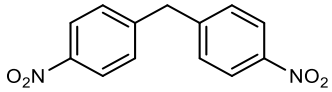

In a 1000 mL round bottom flask, 115 mL of 65% nitric acid were added dropwise to 105 mL of sulfuric acid. Afterwards, a solution of 30.0 g diphenylmethane (178 mmol, 1.00 equiv.) in 70 mL of acetic acid was added dropwise while maintaining a temperature lower than 10 °C. After complete addition, the mixture was stirred in an ice bath for 2 hours. Subsequently, the crude mixture was poured onto 500 g of ice, the precipitate was filtered and washed three times each with water and ethanol. The crude product was recrystallized from 350 mL of toluene to yield 4,4'-dinitrodiphenylmethane as a slightly yellow, crystalline solid in a yield of 30% (13.7 g, 53.1 mmol). Procedure adapted from literature.[433]

^{1}H NMR (400 MHz, $CDCl_3$) δ/ppm = 8.15 – 8.02 (m, 4H), 7.31 – 7.24 (m, 4H), 4.12 (s, 2H).

^{13}C NMR (101 MHz, $CDCl_3$) δ/ppm = 146.96, 146.68, 129.78, 124.10, 41.38.

IR (ATR platinum diamond): $\tilde{\nu}/cm^{-1}$ = 3106 (vw), 3079 (vw), 2941 (vw), 2836 (vw), 2448 (vw), 1927 (vw), 1798 (vw), 1604 (w), 1592 (w), 1506 (vs), 1446 (w), 1337 (vs), 1318 (vs), 1290 (m), 1174 (w), 1107 (s), 1014 (w), 973 (vw), 882 (w), 858 (m), 841 (w), 817 (w), 802 (m), 743 (s), 706 (s), 685 (w), 640 (w), 634 (w), 527 (w), 508 (m), 469 (w).

ESI-HRMS m/z: $[M+H]^+$ calculated for $C_{13}H_{10}N_2O_4$ = 259.0714, found 259.0712.

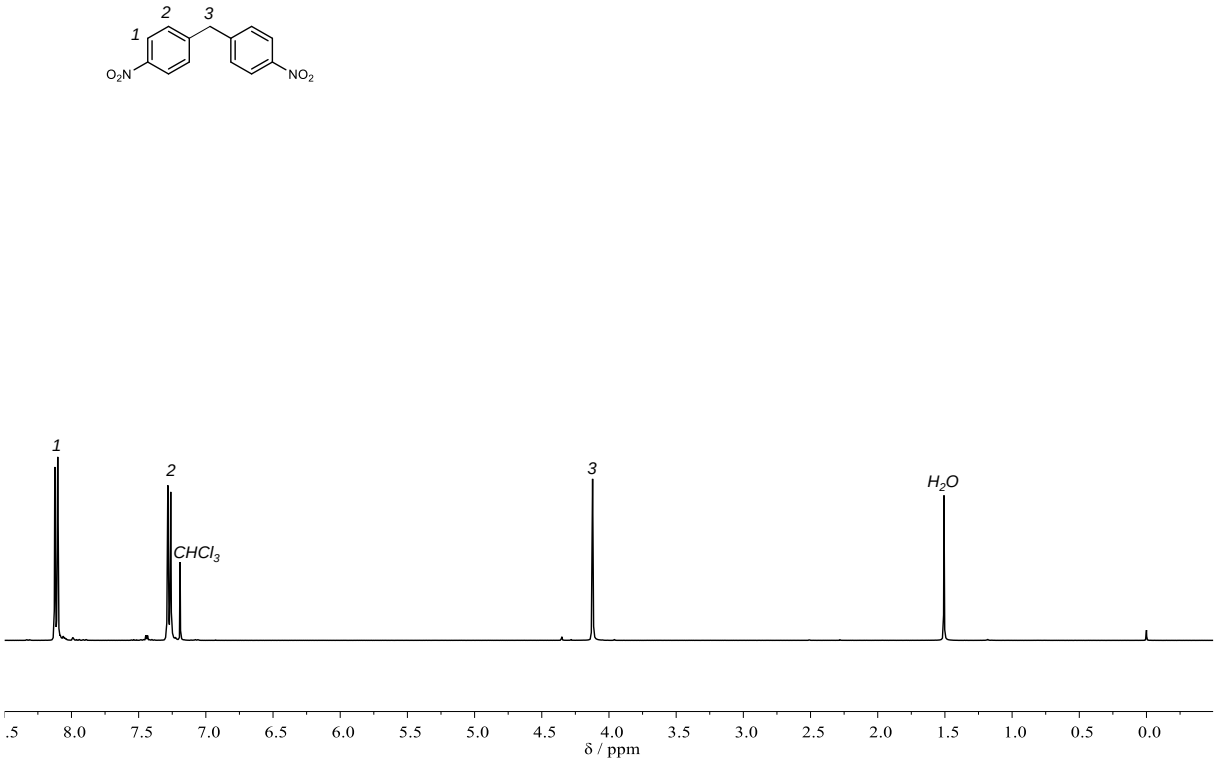

Supplementary Figure 3:[1]H NMR spectrum of 4,4'-dinitrodiphenylmethane in $CDCl_3$.

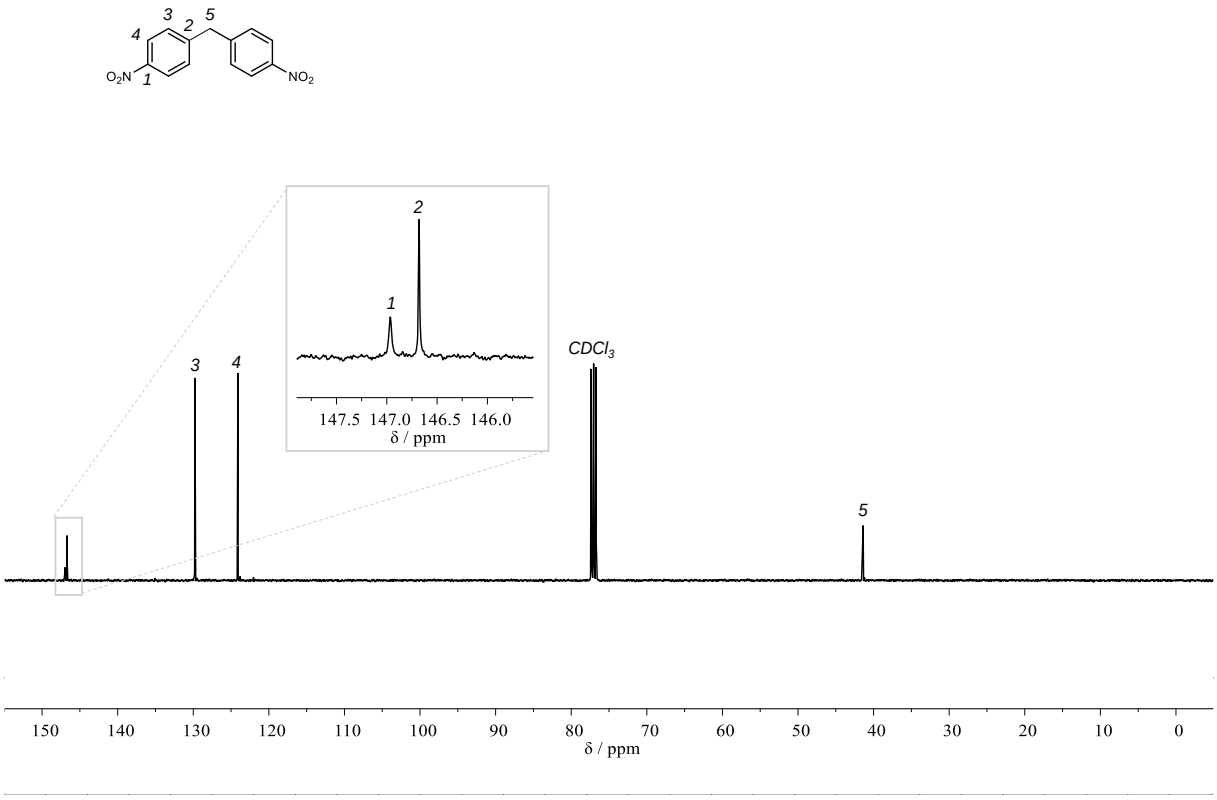

Supplementary Figure 4:[13]C NMR spectrum of 4,4'-dinitrodiphenylmethane in $CDCl_3$.

4,4'-Dinitrobenzophenone (4d)

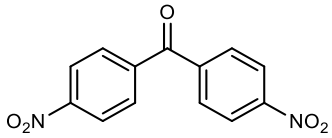

In a 500 mL Erlenmeyer flask, 2.58 g of 4,4'-dinitrodiphenylmethane (10.0 mmol, 1.00 equiv.) were dissolved in 50 mL of DCM. Afterwards, a solution of 2.37 g potassium permanganate (15.0 mmol, 1.50 equiv.), 340 mg of tetrabutylammonium bisulfate (1.00 mmol, 0.10 equiv.) and 281 mg of potassium hydroxide (5.00 mmol, 0.50 equiv.) in 50 mL of water was added. The mixture was stirred vigorously at room temperature for 5 hours. Subsequently, 5 mL of acetic acid were added and concentrated sodium sulfite solution was added until the disappearance of the brown manganese dioxide color. The organic phase was separated, dried over sodium sulfate and the solvent was removed under reduced pressure. The product was isolated as a white solid in a yield of 22% (596 mg, 2.19 mmol). The procedure was adapted from literature.[434]

^{1}H NMR (400 MHz, DMSO-d_6) δ/ppm = 8.44 – 8.36 (m, 4H), 8.07 – 7.97 (m, 4H).

^{13}C NMR (101 MHz, DMSO-d_6) δ/ppm = 193.89, 150.33, 141.73, 131.57, 124.28.

IR (ATR platinum diamond): $\tilde{\nu}/cm^{-1}$ = 3106 (vw), 3083 (vw), 2853 (vw), 1656 (m), 1600 (m), 1514 (vs), 1407 (w), 1343 (vs), 1312 (s), 1298 (s), 1271 (vs), 1172 (w), 1144 (w), 1107 (w), 1010 (w), 979 (w), 934 (s), 870 (m), 862 (m), 845 (vs), 788 (w), 738 (w), 708 (vs), 695 (vs), 654 (m), 621 (w), 494 (w), 432 (w).

EI-HRMS m/z: $[M]^+$ calculated for $C_{13}H_8N_2O_5$ = 272.0428, found 272.0426.

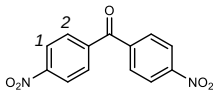

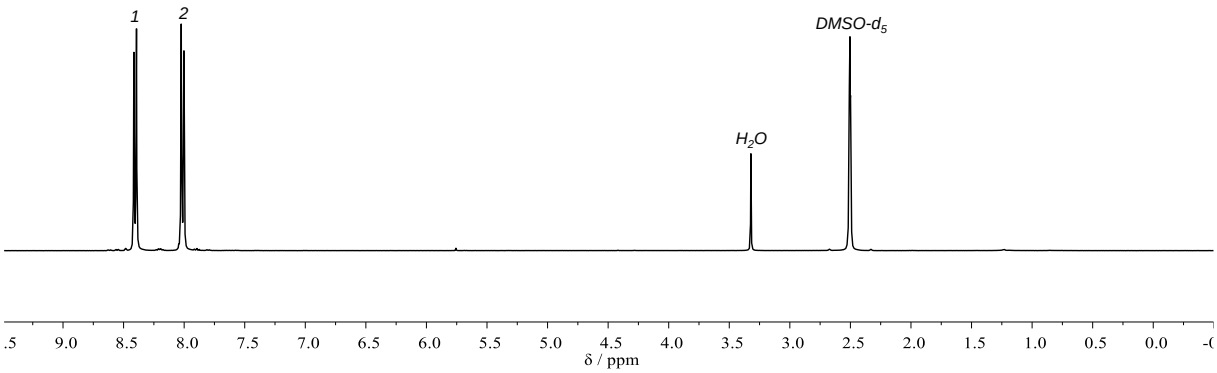

*Supplementary Figure 5:[1]H NMR spectrum of **4d** in DMSO-d6.*

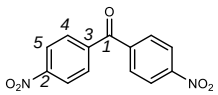

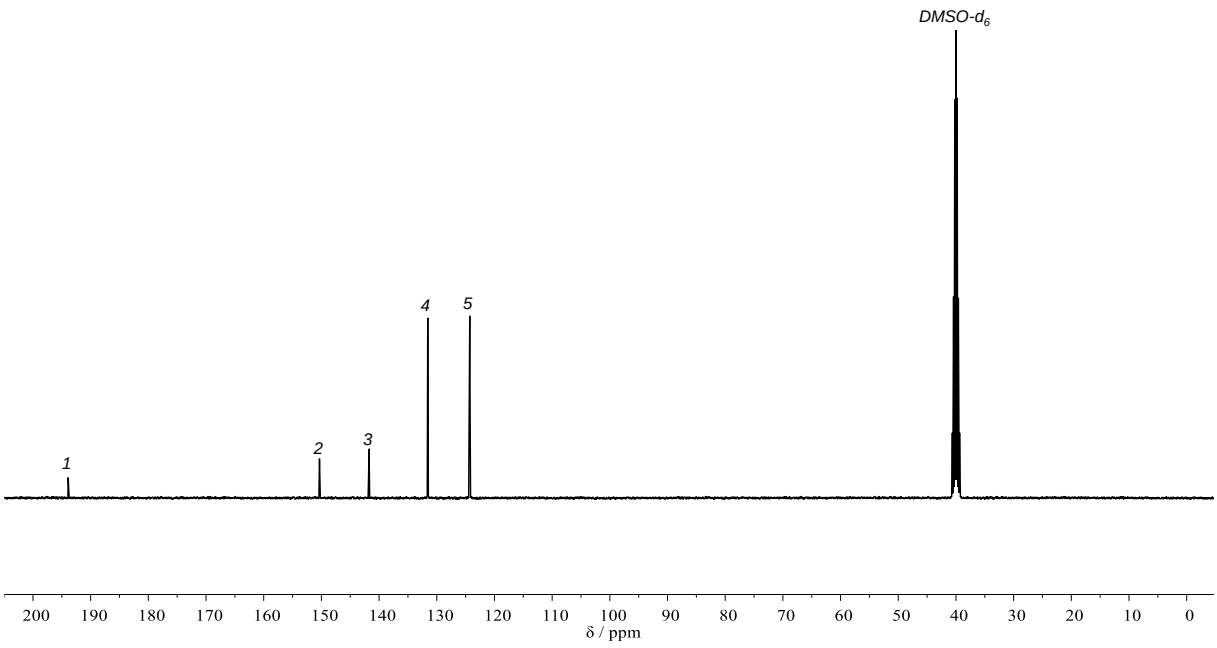

*Supplementary Figure 6:[13]C NMR spectrum of **4d** in DMSO-d6.*

6.3.1.2 Synthesis of N-tosylhydrazones

Disclaimer

1e, **1f**, **1g**, **1i**, **1j** and **1k** were synthesized by the author during his master thesis. Their characterization is thus not included here.

1c was synthesized by Maya Ludwig under supervision of the author.

1h was synthesized by Silas Leidenheimer under supervision of the author.

General procedures for the synthesis of N-tosylhydrazones from carbonyl compounds

Procedure A:

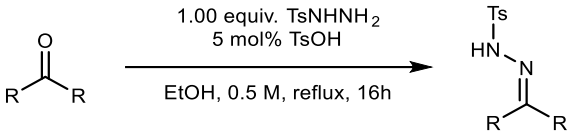

931 mg tosyl hydrazide (5.00 mmol, 1.00 eq.) were suspended in 10 mL of ethanol and 5.00 mmol (1.00 eq.) of the carbonyl component along with 47.5 mg of p-toluenesulfonic acid monohydrate (0.25 mmol, 0.05 eq.) were added. The mixture was refluxed overnight. Afterwards, the mixture was cooled down to -20 °C, the precipitate was filtered off and washed with cold ethanol. The filtered solid was dried *in vacuo*.

Procedure B:

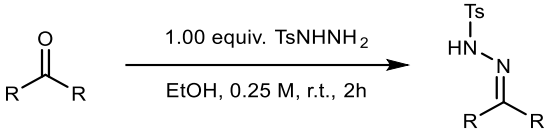

931 mg tosyl hydrazide (5.00 mmol, 1.00 eq.) were suspended in 10 mL of ethanol and 5.00 mmol (1.00 eq.) of the carbonyl component were dissolved in 10 mL of ethanol. The mixture was stirred at room temperature for 2 hours. Afterwards, the solvent was removed *in vacuo*.

4,4'-Dimethoxybenzophenone NTH (1a)

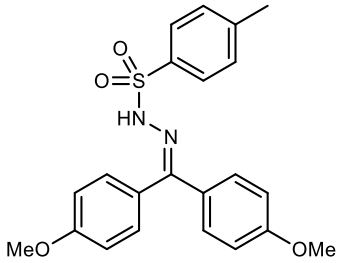

Prepared from 4,4'-dimethoxybenzophenone according to general procedure A. Obtained as a white, crystalline solid in a yield of 81% (1.66 g, 4.04 mmol).

^{1}H NMR (400 MHz, DMSO-d_6) δ/ppm = 10.19 (s, 1H), 7.83 – 7.76 (m, 2H), 7.45 – 7.39 (m, 2H), 7.23 – 7.11 (m, 4H), 7.10 – 7.02 (m, 2H), 6.93 – 6.85 (m, 2H), 3.83 (s, 3H), 3.74 (s, 3H), 2.39 (s, 3H).

^{13}C NMR (101 MHz, DMSO-d_6) δ/ppm = 160.46, 159.84, 154.47, 143.18, 136.13, 130.48, 130.00, 129.35, 128.91, 127.77, 124.77, 114.10, 113.69, 55.23, 21.05.

IR (ATR platinum diamond): $\tilde{\nu}/cm^{-1}$ = 3201 (w), 3065 (vw), 3028 (vw), 2956 (vw), 2925 (vw), 2832 (vw), 1606 (s), 1578 (w), 1510 (s), 1460 (w), 1440 (w), 1419 (w), 1386 (m), 1341 (m), 1310 (s), 1300 (m), 1249 (vs), 1187 (w), 1174 (s), 1158 (vs), 1113 (w), 1092 (w), 1053 (m), 1031 (vs), 1012 (m), 983 (s), 954 (w), 887 (m), 831 (vs), 810 (s), 782 (w), 734 (w), 706 (m), 689 (m), 664 (vs), 597 (w), 578 (w), 545 (vs), 518 (m), 498 (m), 481 (w), 444 (w).

ESI-HRMS m/z: $[M+H]^+$ calculated for $C_{22}H_{22}N_2O_4S$ = 411.1373, found 411.1370.

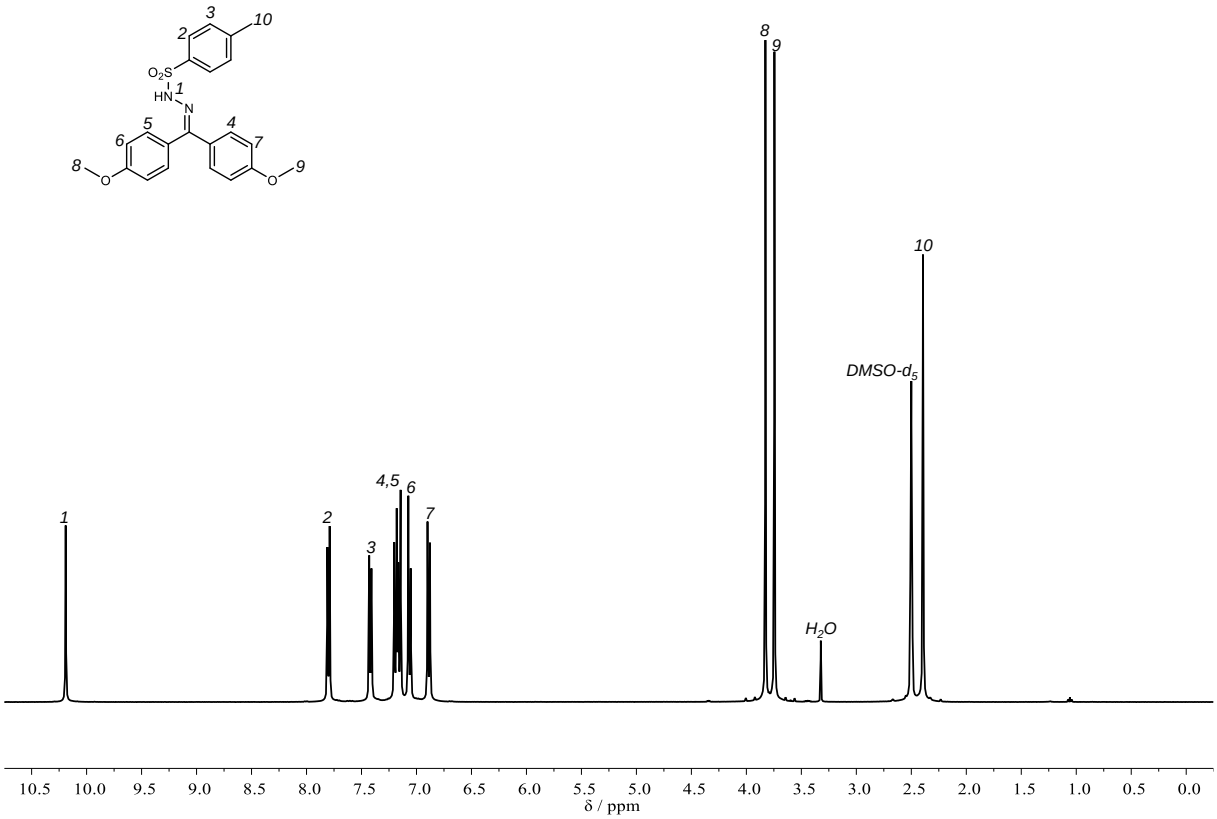

*Supplementary Figure 7:[1]H NMR spectrum of **1a** in DMSO-d6.*

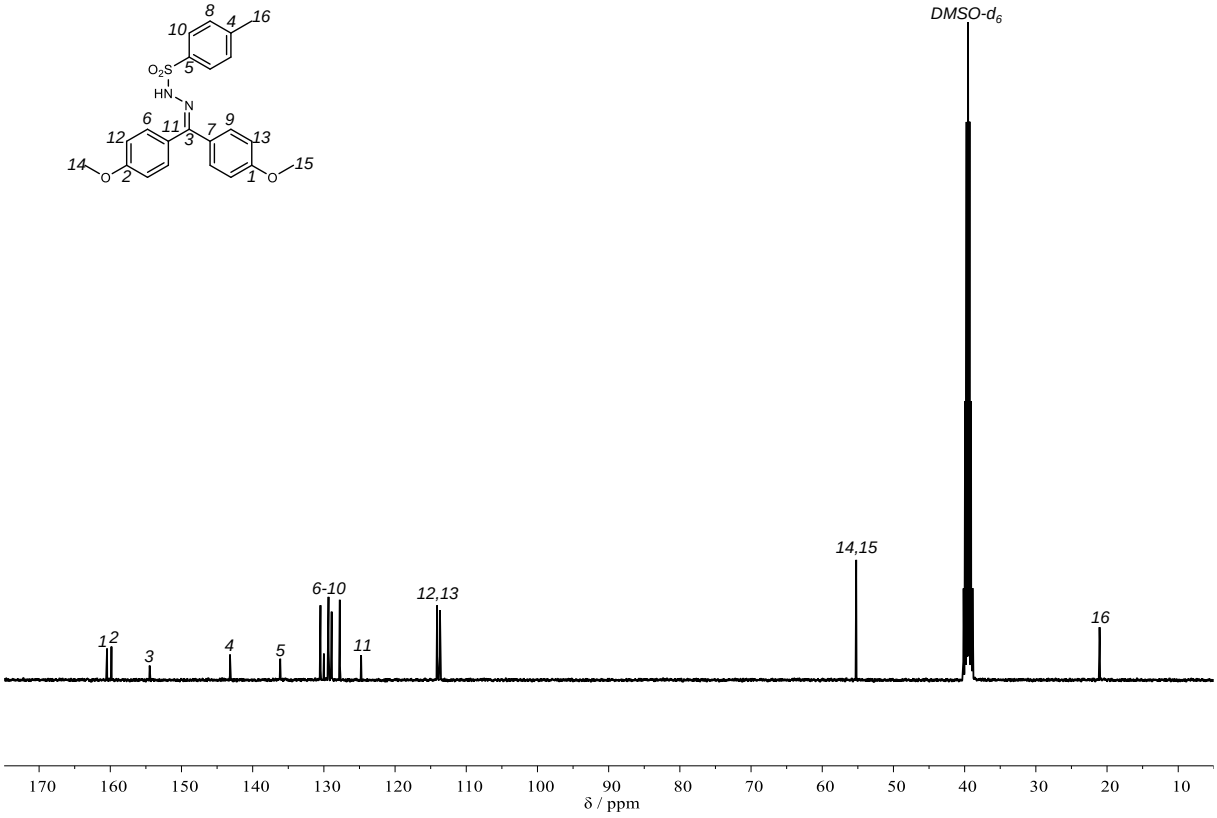

*Supplementary Figure 8:[13]C NMR spectrum of **1a** in DMSO-d6.*

Benzophenone NTH (1b)

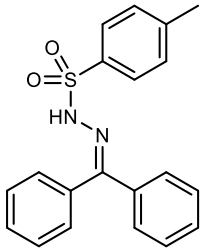

Prepared from benzophenone according to general procedure A. Obtained as a white, crystalline solid in a yield of 81% (1,43 g, 4.07 mmol).

^{1}H NMR (400 MHz, DMSO-d_6) δ/ppm = 10.43 (s, 1H), 7.85 – 7.78 (m, 2H), 7.58 – 7.47 (m, 3H), 7.47 – 7.40 (m, 2H), 7.42 – 7.29 (m, 3H), 7.29 – 7.17 (m, 4H), 2.40 (s, 3H).

^{13}C NMR (101 MHz, DMSO-d_6) δ/ppm = 154.54, 143.34, 137.16, 136.07, 132.56, 129.69, 129.43, 129.37, 128.81, 128.35, 127.75, 127.22, 21.05.

IR (ATR platinum diamond): $\tilde{\nu}/cm^{-1}$ = 3211 (w), 3061 (vw), 3028 (vw), 1594 (vw), 1571 (vw), 1446 (w), 1374 (m), 1347 (s), 1318 (m), 1302 (w), 1187 (w), 1168 (vs), 1094 (w), 1053 (m), 1026 (w), 1002 (w), 977 (m), 915 (w), 872 (m), 812 (m), 771 (vs), 732 (w), 697 (vs), 664 (vs), 640 (m), 609 (w), 553 (vs), 541 (vs), 508 (s), 455 (m).

ESI-HRMS m/z: $[M+H]^+$ calculated for $C_{20}H_{18}N_2O_2S$ = 351.1162, found 351.1157.

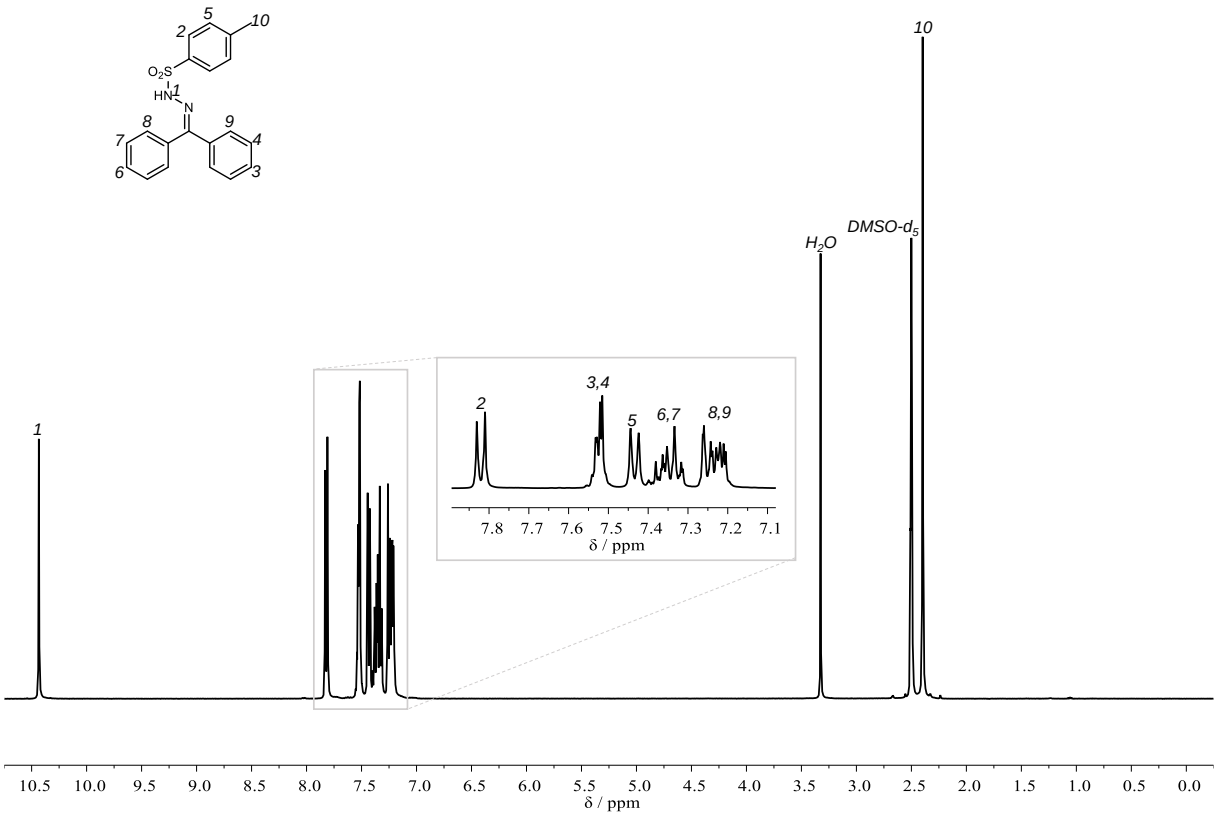

*Supplementary Figure 9:[1]H NMR spectrum of **1b** in DMSO-d_6.*

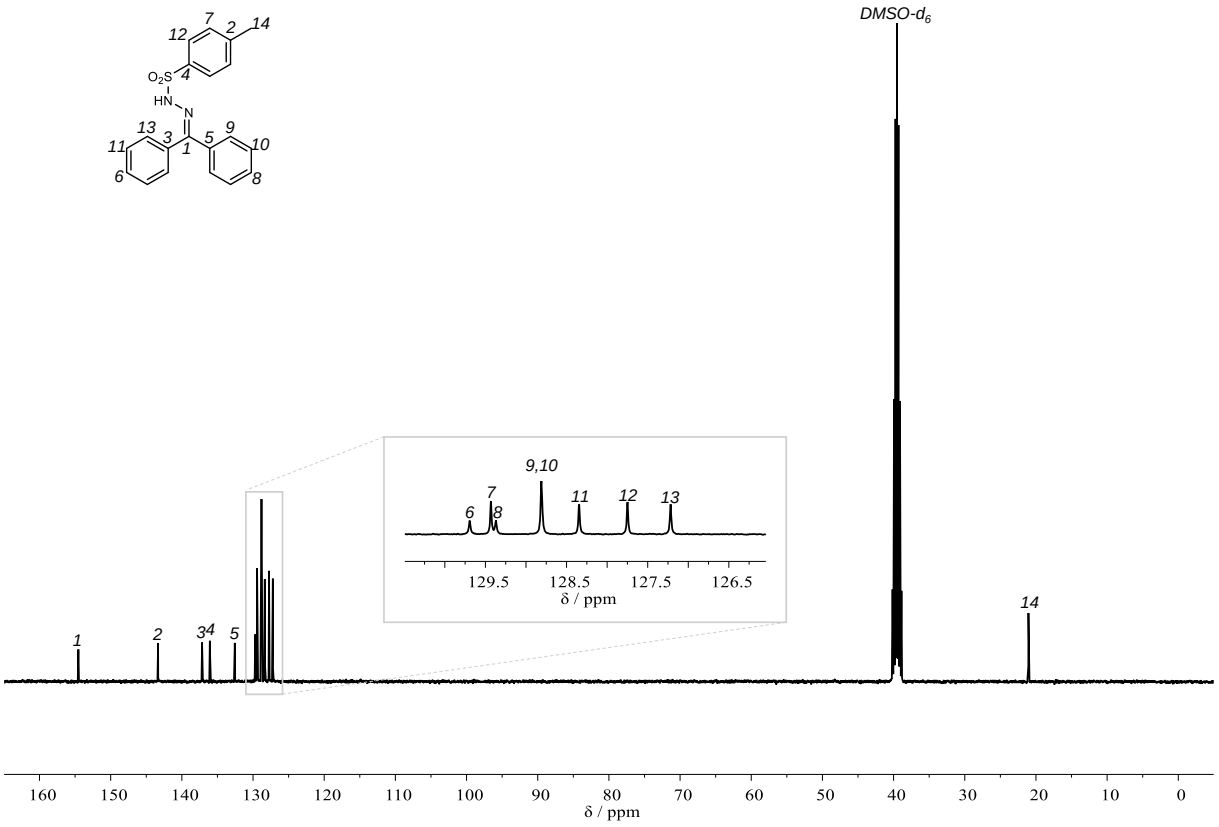

*Supplementary Figure 10:[13]C NMR spectrum of **1b** in DMSO-d_6.*

4,4'-dibromobenzophenone NTH (1c)

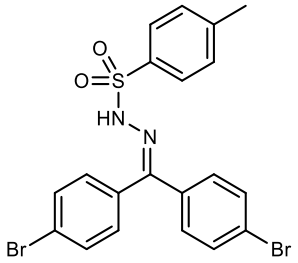

Prepared from **4c** according to general procedure A in a smaller scale scale of 2 mmol. Obtained as a light orange, crystalline solid in a yield of 82% (836 mg, 1.62 mmol).

^{1}H NMR (400 MHz, DMSO-d_6) δ/ppm = 10.68 (s, 1H), 7.82 – 7.76 (m, 2H), 7.76 – 7.69 (m, 2H), 7.59 – 7.51 (m, 2H), 7.46 – 7.39 (m, 2H), 7.23 – 7.12 (m, 4H), 2.39 (s, 3H).

^{13}C NMR (101 MHz, DMSO-d_6) δ/ppm = 152.29, 143.95, 136.49, 136.39, 132.48, 131.95, 131.66, 131.56, 130.03, 129.49, 128.05, 123.79, 123.58, 21.54.

IR (ATR platinum diamond): $\tilde{\nu}/cm^{-1}$ = 3184 (w), 3059 (vw), 1596 (w), 1485 (w), 1405 (m), 1395 (w), 1347 (s), 1316 (m), 1294 (w), 1189 (w), 1168 (vs), 1098 (w), 1068 (s), 1057 (s), 1008 (s), 987 (m), 948 (w), 884 (m), 835 (m), 825 (m), 812 (s), 755 (vw), 716 (w), 706 (w), 681 (s), 664 (m), 638 (m), 617 (w), 603 (w), 551 (vs), 510 (w), 492 (m), 465 (w).

ESI-HRMS m/z: $[M+H]^+$ calculated for $C_{20}H_{16}N_2O_2S^{79}Br^{81}Br$ = 508.9352, found 508.9349.

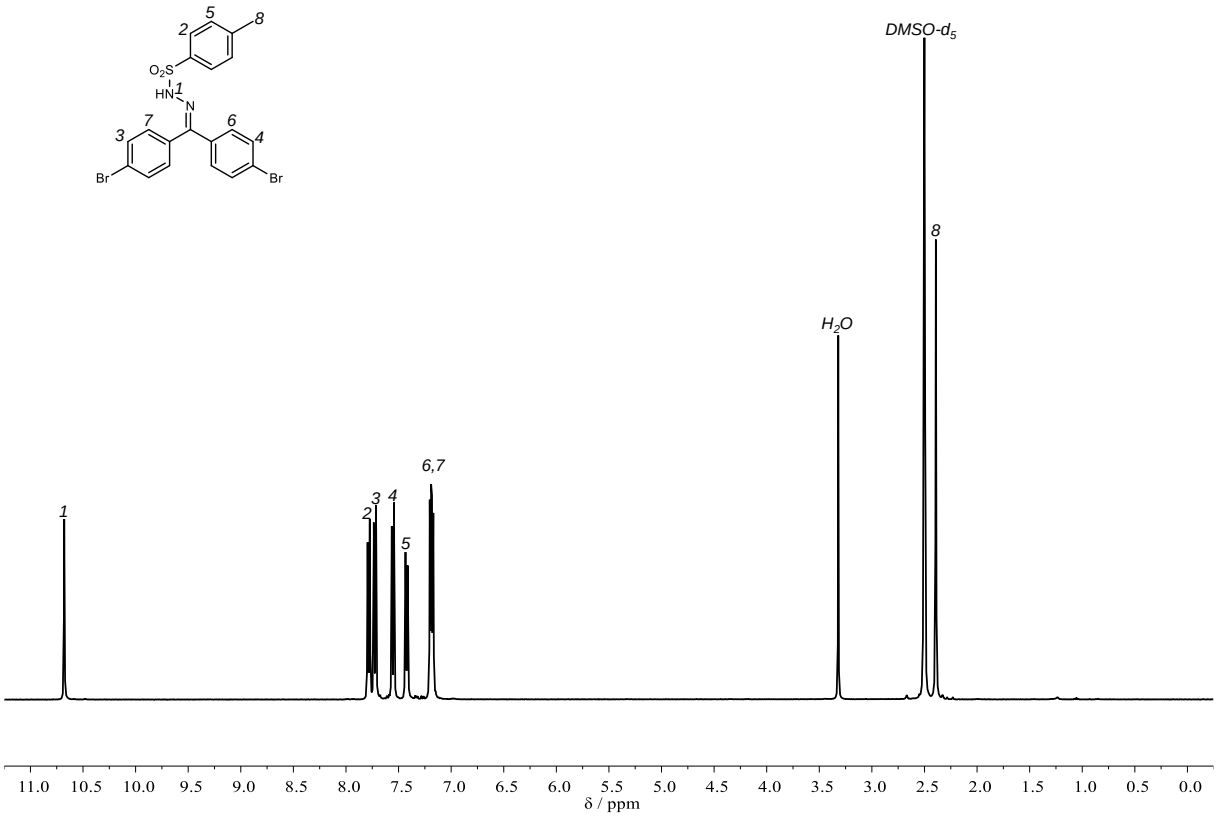

*Supplementary Figure 11:[1]H NMR spectrum of **1c** in DMSO-d6.*

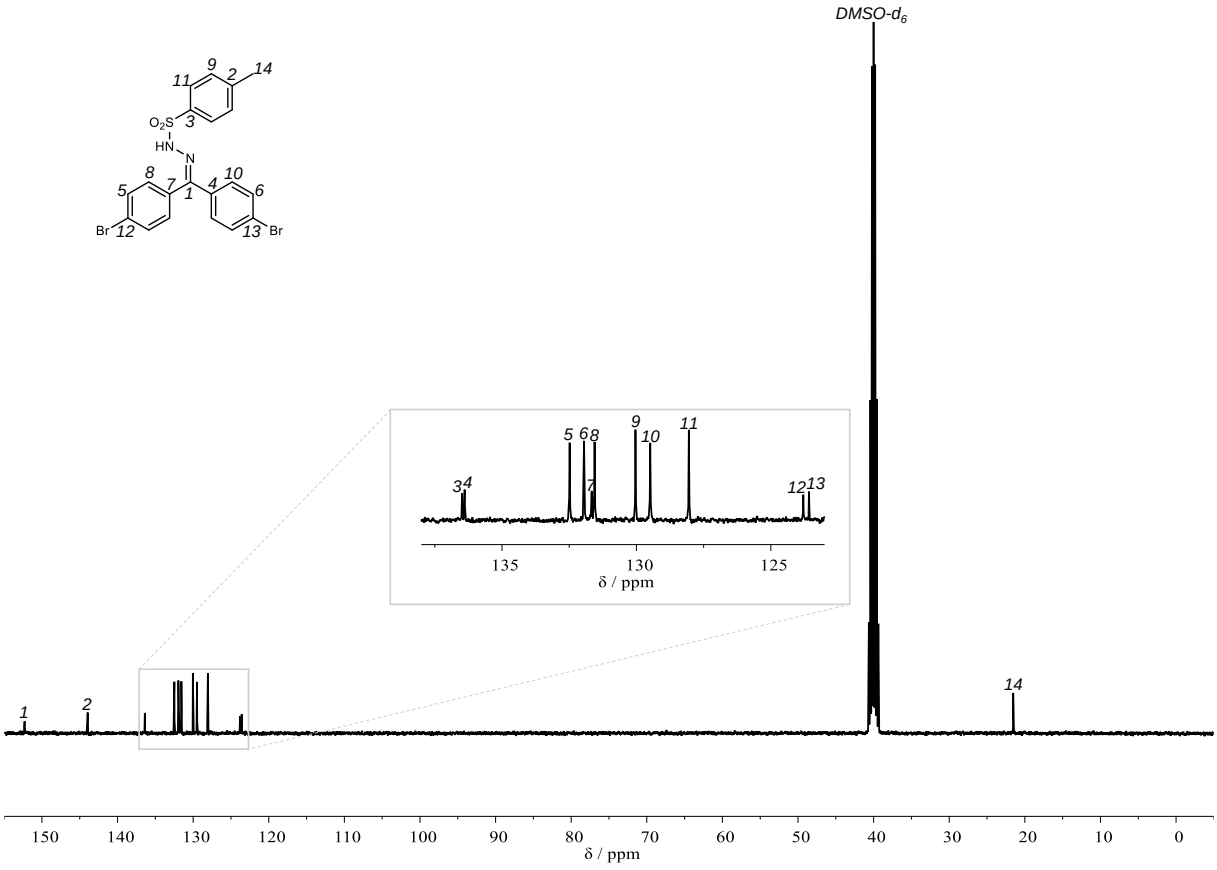

*Supplementary Figure 12:[13]C NMR spectrum of **1c** in DMSO-d6.*

4,4'-dinitrobenzophenone NTH (1d)

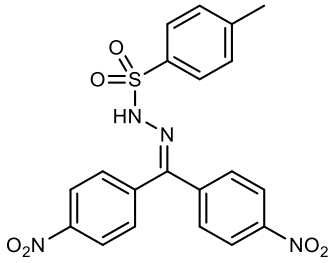

Prepared from **4d** according to general procedure A in a smaller scale of 2 mmol. The crude product was washed with hot ethanol. Obtained as an orange, crystalline solid in a yield of 75% (658 mg, 1.49 mmol).

^{1}H NMR (400 MHz, DMSO-d_6) δ/ppm = 11.09 (s, 1H), 8.46 – 8.33 (m, 2H), 8.30 – 8.16 (m, 2H), 7.81 (d, *J* = 8.2 Hz, 2H), 7.69 – 7.50 (m, 4H), 7.48 – 7.43 (m, 2H), 2.40 (s, 3H).

^{13}C NMR (101 MHz, DMSO-d_6) δ/ppm = 149.33, 148.28, 147.87, 143.80, 142.05, 138.28, 135.83, 130.78, 129.76, 128.04, 127.52, 124.34, 123.82, 21.08.

IR (ATR platinum diamond): $\tilde{\nu}/cm^{-1}$ = 3190 (w), 1596 (w), 1567 (w), 1512 (vs), 1489 (w), 1403 (w), 1345 (vs), 1312 (s), 1286 (w), 1187 (w), 1166 (vs), 1105 (w), 1092 (w), 1057 (m), 1016 (w), 983 (m), 961 (w), 882 (w), 860 (s), 843 (s), 810 (m), 767 (w), 757 (w), 745 (w), 693 (m), 679 (s), 642 (w), 619 (m), 605 (w), 547 (vs), 520 (w), 490 (w), 426 (w).

FAB-HRMS m/z: $[M+H]^+$ calculated for $C_{20}H_{16}N_4O_6S$ = 441.0863, found 441.0863.

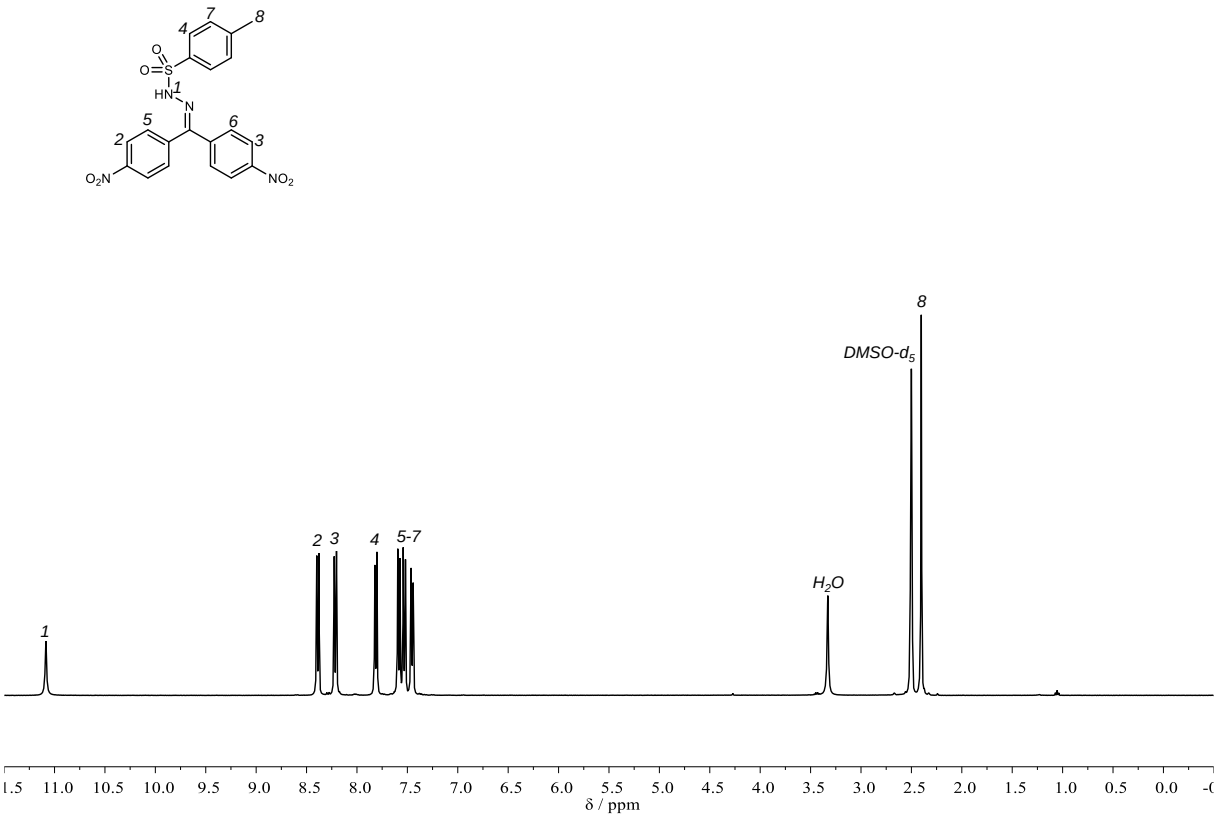

*Supplementary Figure 13:[1]H NMR spectrum of **1d** in DMSO-d6.*

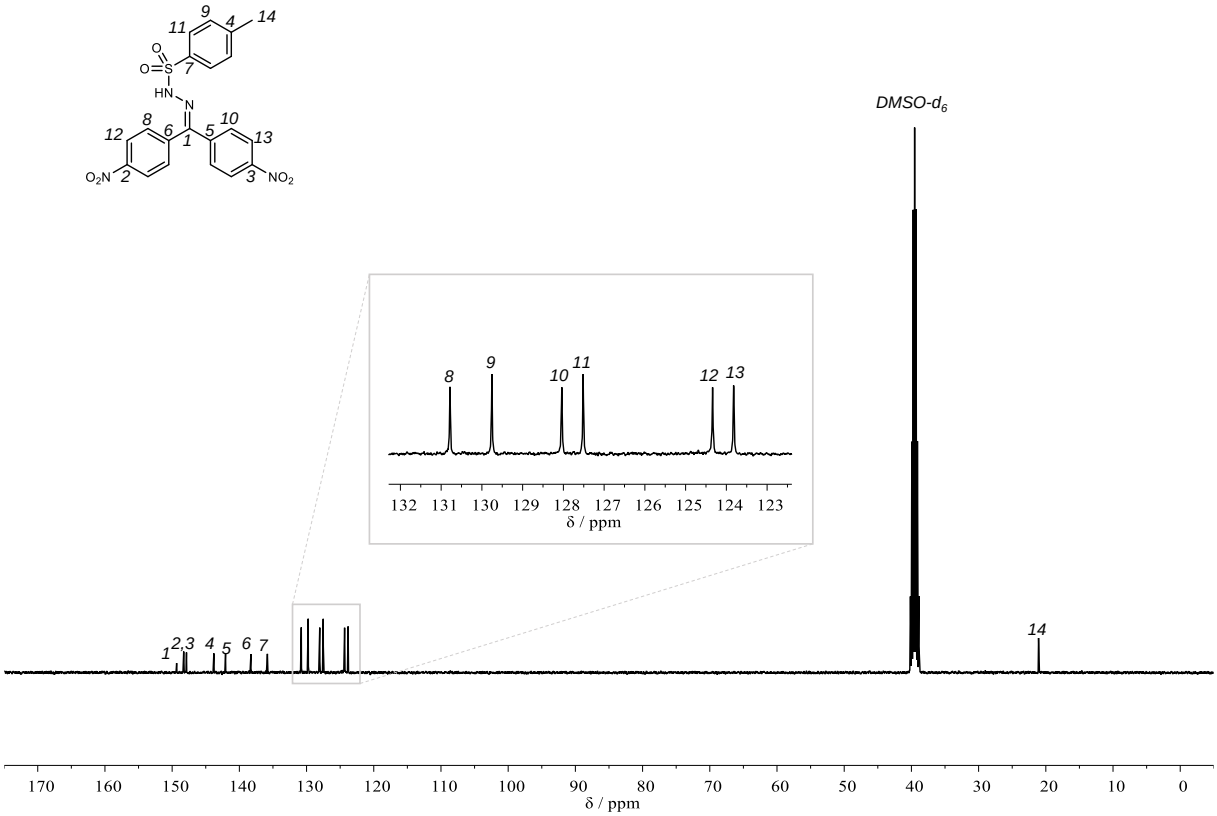

*Supplementary Figure 14:[13]C NMR spectrum of **1d** in DMSO-d6.*

4-Nitrobenzophenone NTH (1h)

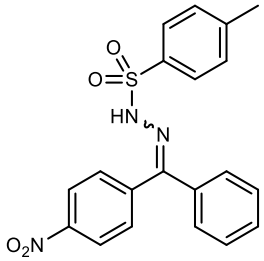

Prepared from 4-nitrobenzophenone according to general procedure A. Obtained as a slightly yellow solid in a yield of 75% (1.49 g, 3.77 mmol). The isolated product consisted only of the *(Z)*-stereoisomer.

^{1}H NMR (400 MHz, DMSO-d_6) δ/ppm = 10.67 (s, 1H), 8.39 – 8.34 (m, 2H), 7.83 – 7.78 (m, 2H), 7.55 – 7.50 (m, 2H), 7.46 – 7.42 (m, 2H), 7.42 – 7.33 (m, 3H), 7.29 – 7.24 (m, 2H), 2.40 (s, 3H).

^{13}C NMR (101 MHz, DMSO-d_6) δ/ppm = 152.04, 148.00, 143.55, 139.28, 136.15, 135.97, 130.67, 130.02, 129.60, 128.56, 127.58, 127.04, 124.08, 21.06.

IR (ATR platinum diamond): $\tilde{\nu}/cm^{-1}$ = 3168 (w), 3063 (vw), 2915 (vw), 1596 (w), 1520 (s), 1448 (w), 1401 (w), 1347 (s), 1321 (m), 1308 (m), 1292 (w), 1185 (w), 1160 (vs), 1119 (w), 1107 (w), 1090 (w), 1049 (w), 1014 (w), 975 (w), 884 (m), 854 (s), 847 (s), 817 (w), 771 (m), 765 (m), 738 (w), 695 (vs), 671 (vs), 627 (m), 617 (w), 547 (vs), 500 (m), 479 (w), 428 (vw).

ESI-HRMS m/z: $[M+H]^+$ calculated for $C_{20}H_{17}N_3O_4S$ = 396.1008, found 396.1013.

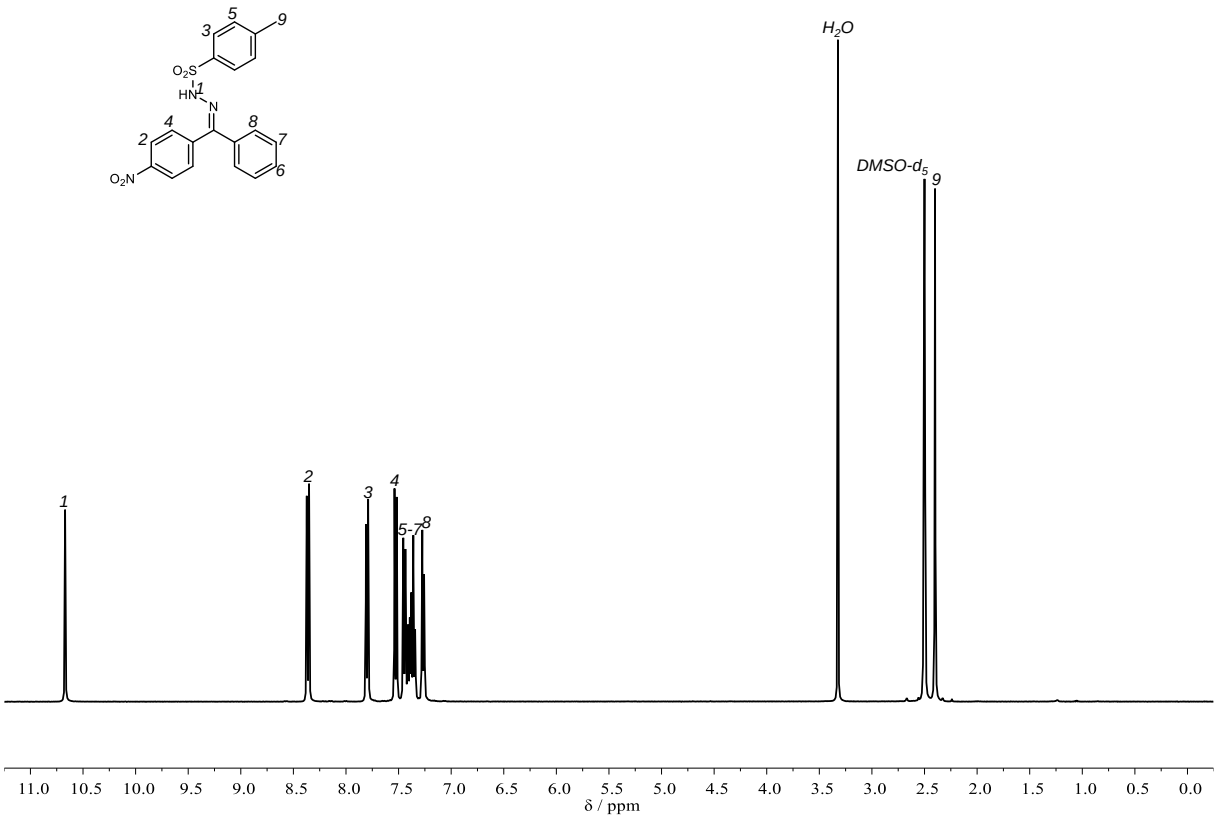

*Supplementary Figure 15:[1]H NMR spectrum of **1h** in DMSO-d_6.*

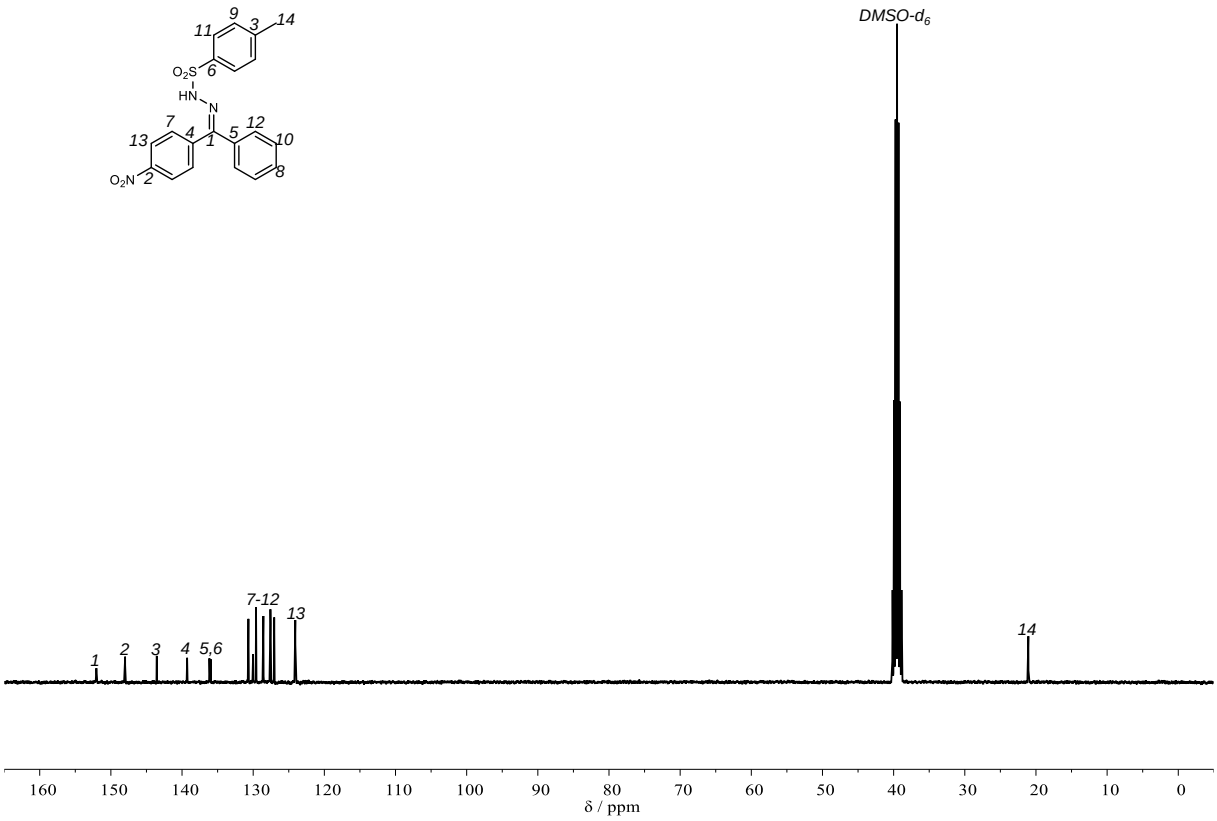

*Supplementary Figure 16:[13]C NMR spectrum of **1h** in DMSO-d_6.*

3-Pentanone NTH (1l)

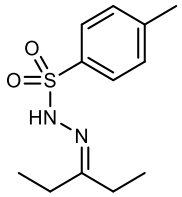

Prepared from 3-pentanone according to general procedure B. Obtained as a white solid in quantitative yield (1.27 g, 5.00 mmol).

^{1}H NMR (400 MHz, DMSO-d_6) δ/ppm = 9.96 (s, 1H), 7.78 – 7.64 (m, 2H), 7.44 – 7.30 (m, 2H), 2.37 (s, 3H), 2.19 (q, *J* = 7.6 Hz, 2H), 2.12 (q, *J* = 7.3 Hz, 2H), 0.93 (t, *J* = 7.6 Hz, 3H), 0.87 (t, *J* = 7.3 Hz, 3H).

^{13}C NMR (101 MHz, DMSO-d_6) δ/ppm =163.61, 142.94, 136.27, 129.20, 127.54, 28.33, 22.62, 20.99, 10.29, 9.44.

IR (ATR platinum diamond): $\tilde{\nu}/cm^{-1}$ = 3217 (w), 2980 (w), 2941 (vw), 2904 (vw), 2884 (vw), 1637 (vw), 1596 (w), 1495 (vw), 1465 (w), 1390 (w), 1376 (w), 1362 (w), 1335 (vs), 1308 (w), 1292 (w), 1189 (w), 1162 (vs), 1090 (m), 1020 (w), 993 (w), 950 (w), 909 (m), 812 (m), 767 (w), 706 (m), 679 (vs), 629 (w), 582 (vs), 555 (vs), 537 (s), 487 (w), 455 (w).

ESI-HRMS m/z: $[M]^+$ calculated for $C_{12}H_{18}N_2O_2S$ = 255.1084, found 255.1805.

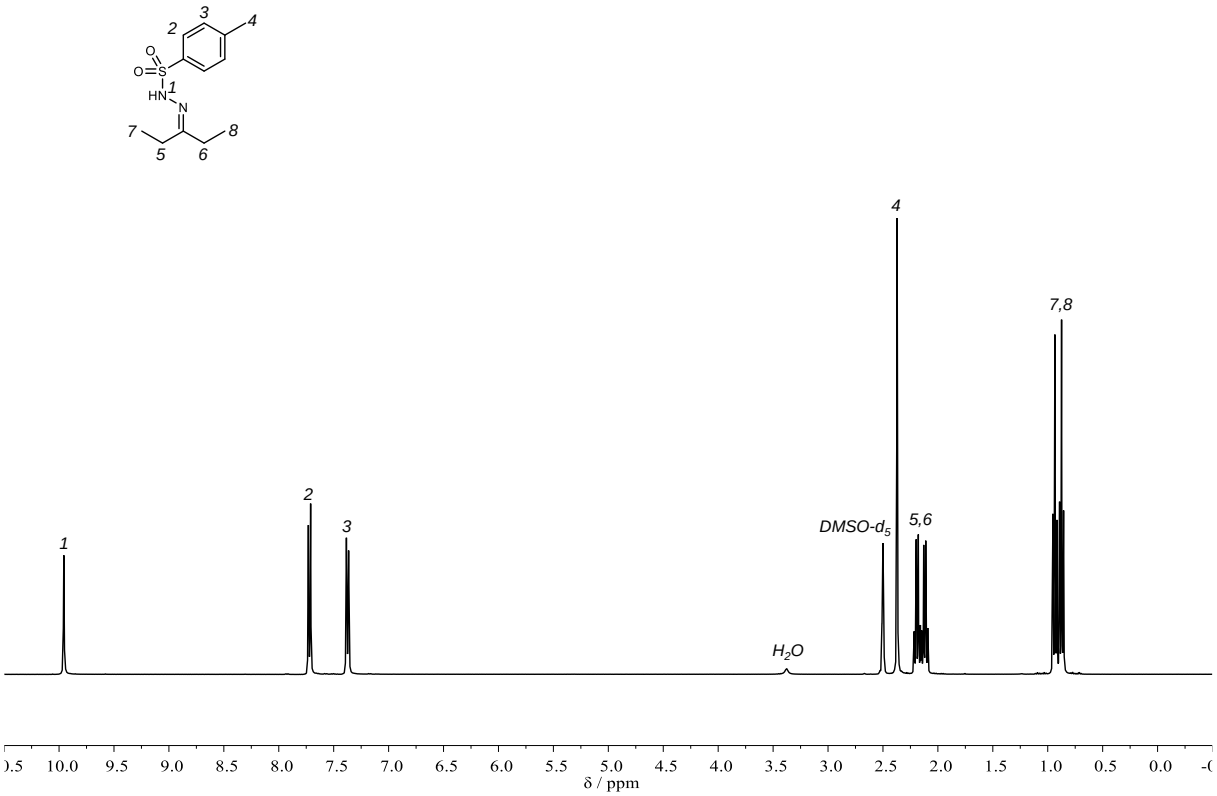

*Supplementary Figure 17:[1]H NMR spectrum of **1l** in DMSO-d6.*

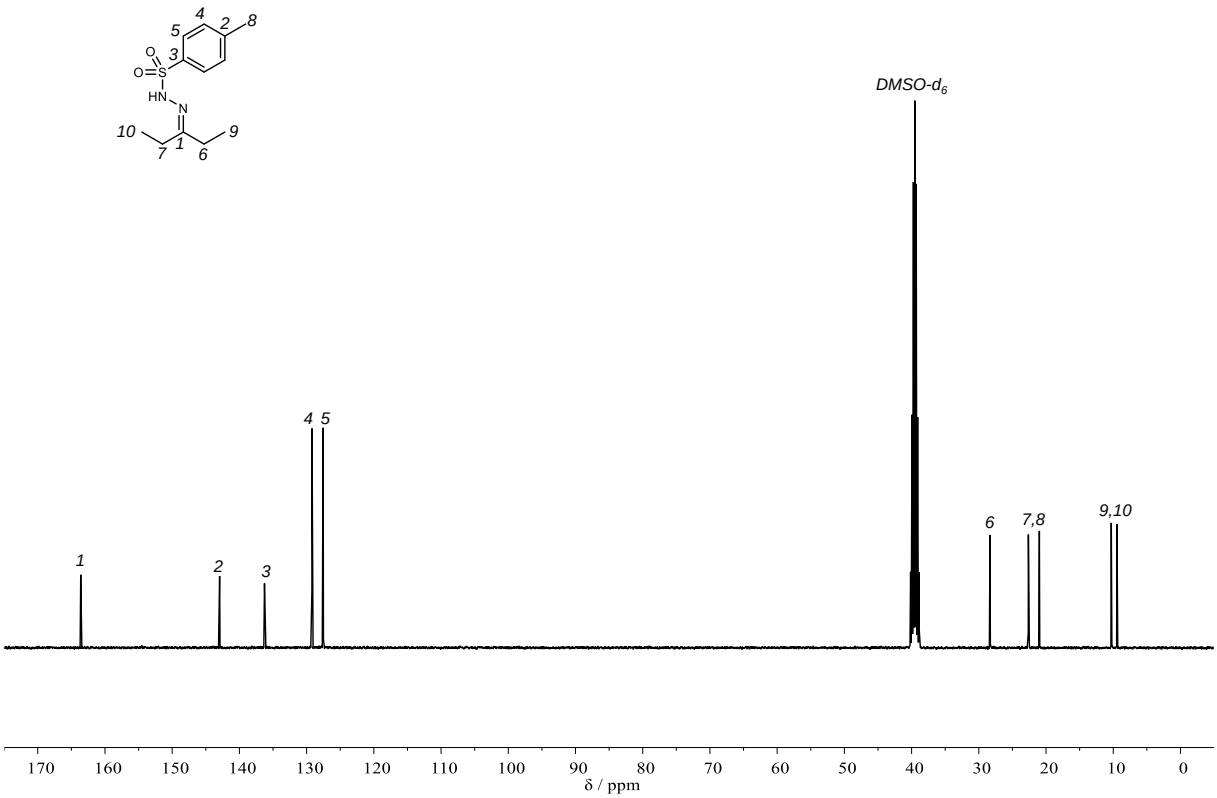

*Supplementary Figure 18:[13]C NMR spectrum of **1l** in DMSO-d6.*

6.3.1.3 Synthesis of homocoupled olefins

Disclaimer

2f and **2g** were synthesized by the author during his master thesis. Their characterization is thus not included here.

2b and **2c** were synthesized by Maya Ludwig under supervision of the author.

2e and **2h** was synthesized by Silas Leidenheimer under supervision of the author.

General procedure for alkylidene-homocouplings of N-tosylhydrazones:

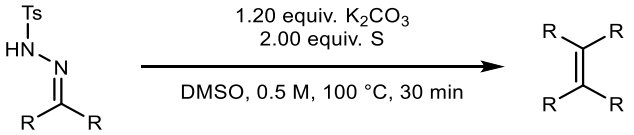

1.00 mmol of the NTH was dispersed in 2.00 mL of dry DMSO and 64.1 mg of elemental sulfur (2.00 mmol S, 2.00 equiv. S) was added. The mixture was heated to 100 °C and 166 mg of anhydrous potassium carbonate (1.20 mmol, 1.20 equiv.) were added. The mixture was stirred at 100 °C for 30 minutes. Afterwards, the crude mixture was transferred directly onto a column (packed in pure cyclohexane) and the product was isolated *via* column chromatography.

1,1,2,2-Tetrakis(4-methoxyphenyl)ethylene (2a)

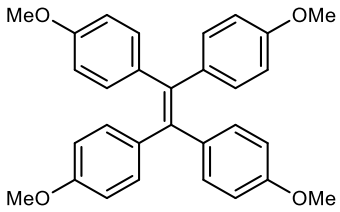

Prepared from **1a** according to the general procedure. The product was isolated *via* column chromatography (cyclohexane/ethyl acetate 30:1) as a colorless solid in a yield of 99% (225 mg, 0.497 mmol)

Upscaled synthesis:

Prepared from **1a** according to the general procedure in a larger scale of 10 mmol NTH. The product was isolated *via* column chromatography (cyclohexane/ethyl acetate 30:1) as a colorless solid in a yield of 95% (1.08 g, 2.38 mmol).

One-Pot synthesis:

485 mg 4,4'-dimethoxybenzophenone (2.00 mmol, 1.00 equiv.) were dispersed in 4 mL of ethanol and 373 mg *p*-toluenesulfonyl hydrazide (2.00 mmol, 1.00 equiv.) along with 19.0 mg *p*-toluenesulfonic acid monohydrate (0.10 mmol, 0.05 equiv.) were added. The mixture was refluxed for 12 hours. The solvent was removed *in vacuo* and the residue was dispersed in 4 mL of dry DMSO. 128 mg of elemental sulfur (4.00 mmol S, 2.00 equiv. S) were added and the mixture was heated to 100°C. 346 mg of potassium carbonate (2.50 mmol, 1.25 equiv.) were added and the mixture was stirred at 100°C for 30 minutes. The crude mixture was transferred to a column (packed in cyclohexane) and the product was isolated *via* column chromatography (cyclohexane/ethyl acetate 30:1). **2a** was obtained as a colorless solid in a yield of 85% (385 mg, 0.851 mmol).

^{1}H NMR (400 MHz, DMSO-d_6) δ/ppm = 6.89 – 6.80 (m, 8H), 6.73 – 6.65 (m, 8H), 3.68 (s, 12H).

^{13}C NMR (101 MHz, DMSO-d_6) δ/ppm = 157.43, 137.98, 136.24, 131.97, 113.19, 54.88.

IR (ATR platinum diamond): $\tilde{\nu}/cm^{-1}$ = 3052 (vw), 3003 (vw), 2952 (vw), 2896 (vw), 2830 (vw), 1604 (m), 1571 (w), 1506 (vs), 1454 (m), 1440 (m), 1411 (w), 1296 (s), 1271 (w), 1240 (vs), 1183 (w), 1168 (vs), 1105 (m), 1033 (vs), 1012 (m), 977 (w), 862 (w), 827 (vs), 808 (vs), 765 (m), 745 (w), 588 (vs), 568 (w), 525 (m).

ESI-HRMS m/z: $[M]^+$ calculated for $C_{30}H_{28}O_4$ = 452.1982, found 452.1980.

Fluorescence: λ_{em}(max) = 490 nm with λ_{ex} = 327 nm

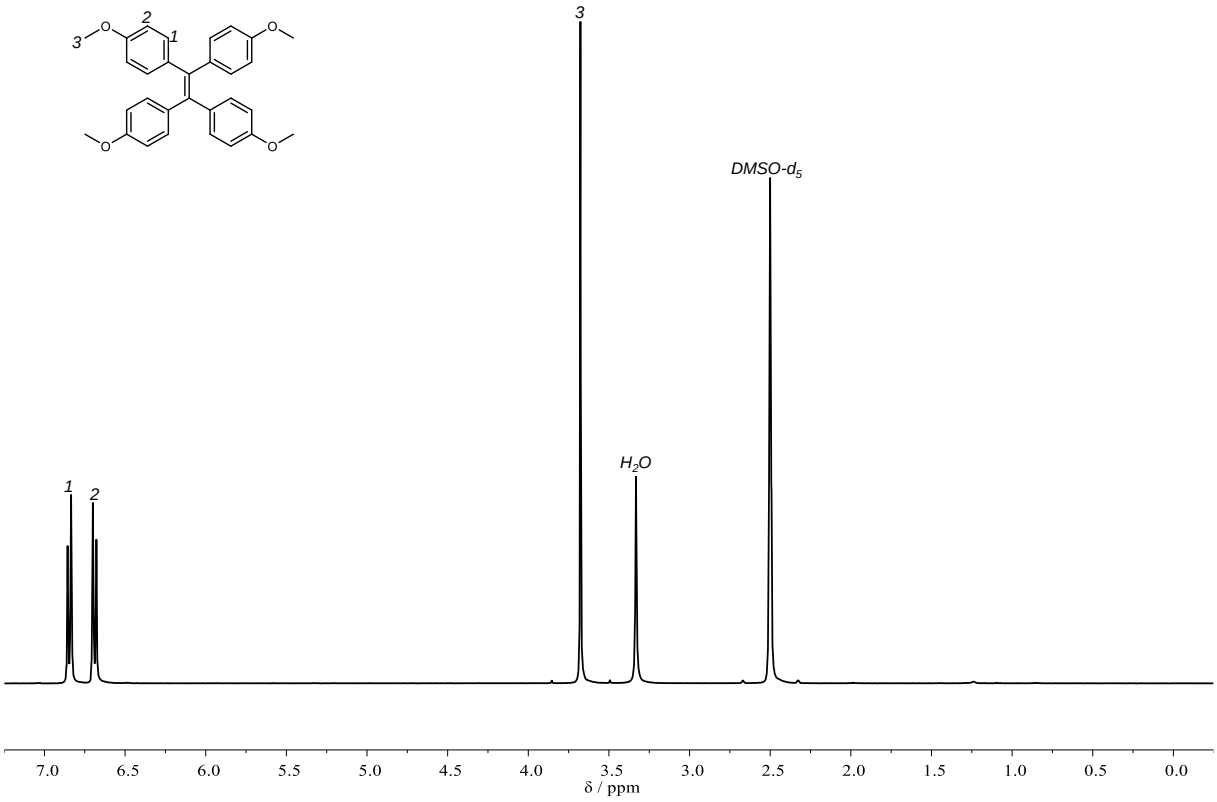

*Supplementary Figure 19:[1]H NMR spectrum of **2a** in DMSO-d6.*

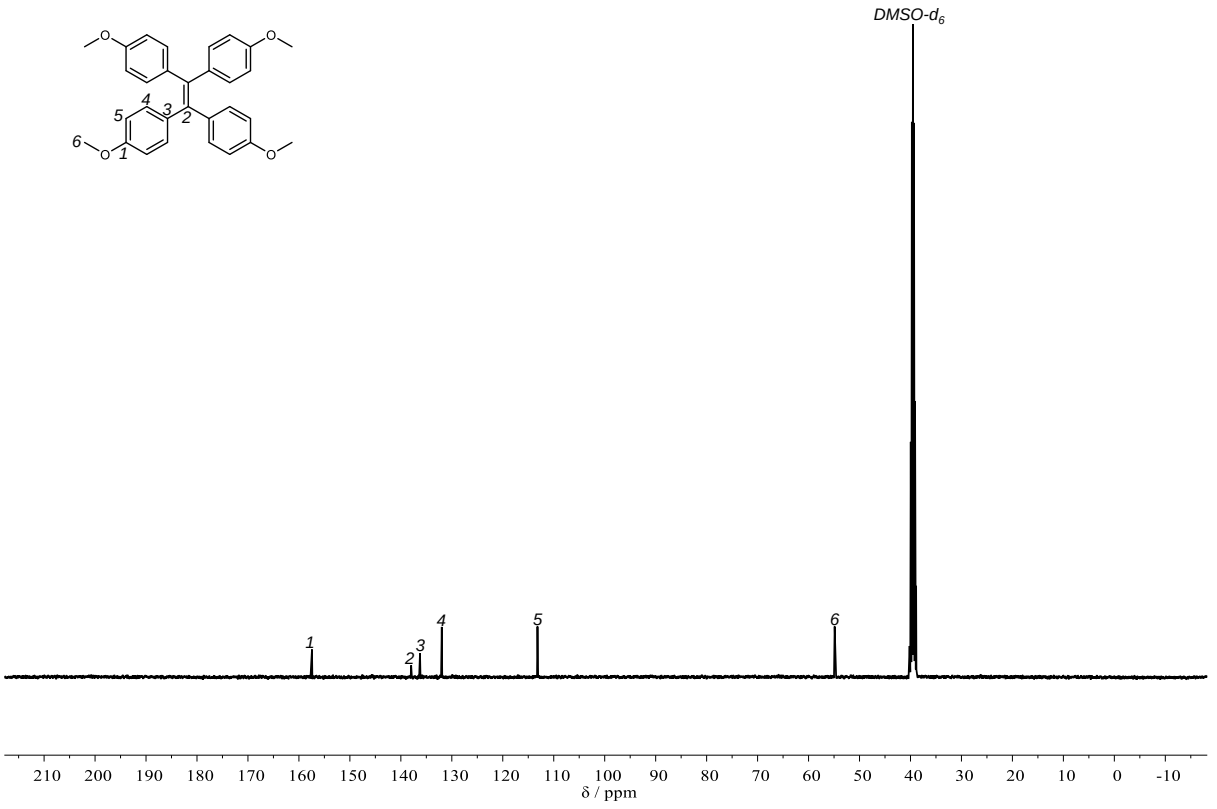

*Supplementary Figure 20: [13]C NMR spectrum of **2a** in DMSO-d6.*

Tetraphenylethylene (2b)

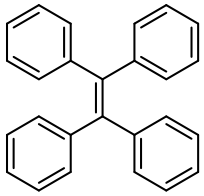

Prepared from **1b** according to the general procedure. The product was isolated *via* column chromatography (cyclohexane/ethyl acetate 50:1) as a colorless solid in a yield of 99% (164 mg, 0.493 mmol).

^{1}H NMR (400 MHz, DMSO-d_6) δ/ppm = 7.18 – 7.05 (m, 12H), 7.00 – 6.93 (m, 8H).

^{13}C NMR (101 MHz, DMSO-d_6) δ/ppm = 143.14, 140.55, 130.60, 127.81, 126.52.

IR (ATR platinum diamond): $\tilde{\nu}/cm^{-1}$ = 3075 (vw), 3050 (vw), 3022 (vw), 2923 (vw), 2855 (vw), 1594 (w), 1574 (vw), 1489 (w), 1442 (m), 1275 (vw), 1181 (vw), 1154 (w), 1074 (w), 1026 (w), 1000 (w), 981 (w), 919 (vw), 913 (w), 909 (w), 778 (w), 761 (m), 745 (s), 693 (vs), 625 (s), 613 (m), 568 (m), 471 (w), 465 (w), 440 (vw).

EI-HRMS m/z: $[M]^+$ calculated for $C_{26}H_{20}$ = 332.1560, found 332.1557.

Fluorescence: λ_{em}(max) = 469 nm with λ_{ex} = 309 nm

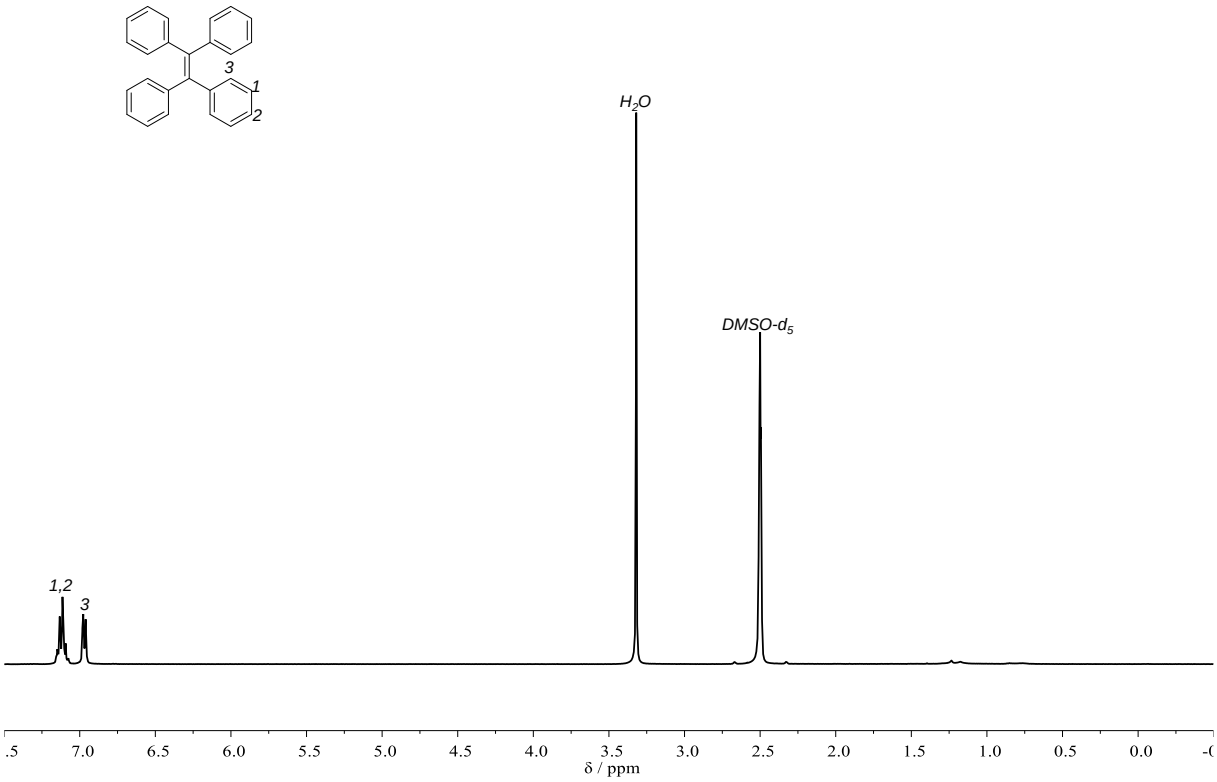

*Supplementary Figure 21: ^{1}H NMR spectrum of **2b** in DMSO-d_6.*

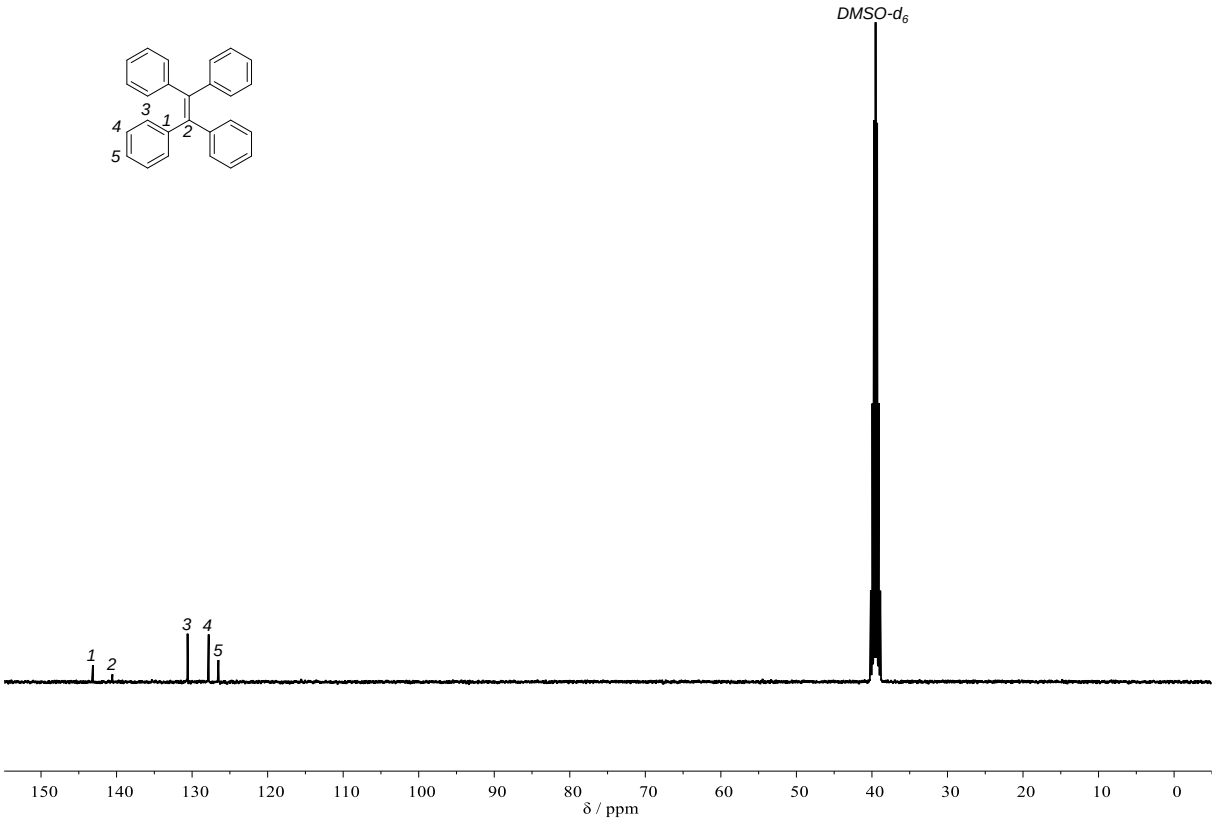

*Supplementary Figure 22: ^{13}C NMR spectrum of **2b** in DMSO-d_6.*

1,1,2,2-Tetrakis(4-bromophenyl)ethylene (2c)

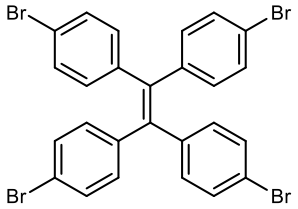

Prepared from **1c** according to the general procedure. The product was isolated *via* column chromatography (cyclohexane/ethyl acetate 50:1) as a colorless solid in a yield of 95% (307 mg, 0.474 mmol).

^{1}H NMR (400 MHz, DMSO-d_6) δ/ppm = 7.43 – 7.35 (m, 8H), 6.96 – 6.87 (m, 8H).

^{13}C NMR (101 MHz, DMSO-d_6) δ/ppm = 141.44, 139.32, 132.73, 131.13, 120.42.

IR (ATR platinum diamond): $\tilde{\nu}/cm^{-1}$ = 1582 (w), 1483 (vs), 1393 (m), 1103 (w), 1070 (s), 1008 (vs), 973 (w), 963 (w), 862 (w), 817 (s), 792 (vs), 736 (s), 716 (w), 685 (w), 652 (w), 631 (w), 623 (w), 566 (w), 502 (s), 490 (s), 477 (m).

ESI-HRMS m/z: $[M]^+$ calculated for $C_{26}H_{16}{}^{79}Br_2{}^{81}Br_2$ = 647.7939, found 647.7936.

Fluorescence: λ_{em}(max) = 476 nm with λ_{ex} = 321 nm

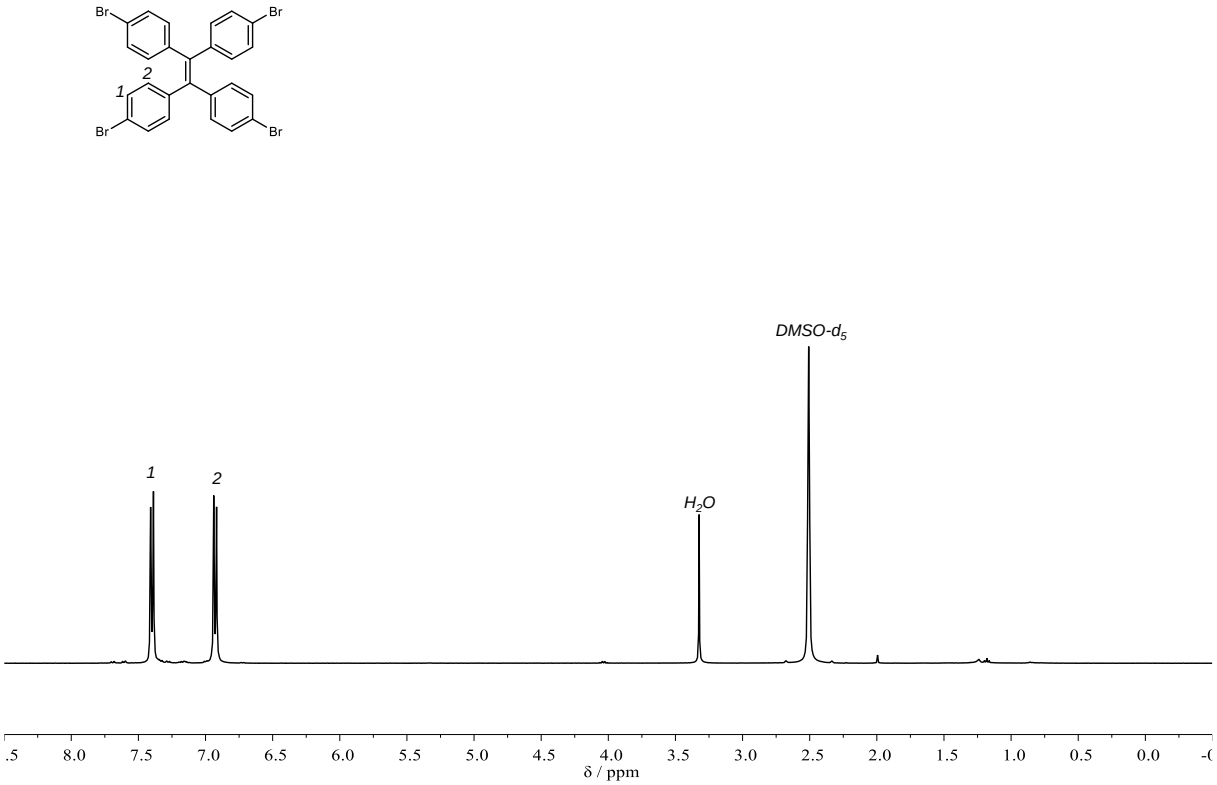

*Supplementary Figure 23: [1]H NMR spectrum of **2c** in DMSO-d6.*

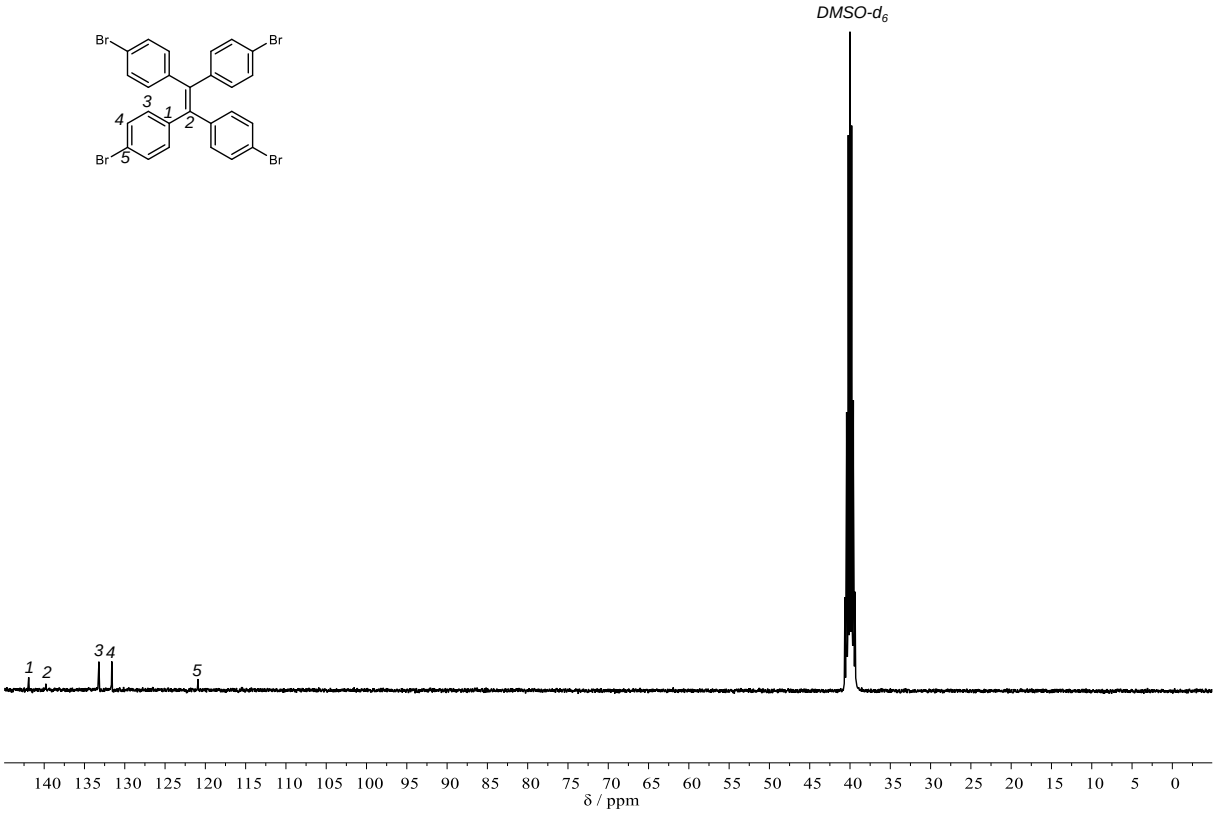

*Supplementary Figure 24: [13]C NMR spectrum of **2d** in DMSO-d6.*

1,1,2,2-Tetrakis(4-nitrophenyl)ethylene (2d)

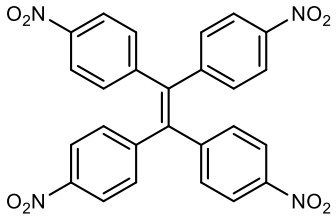

Prepared from **1d** according to the general procedure. The product was isolated *via* column chromatography (cyclohexane/ethyl acetate 10:1) as an orange solid in a yield of 83% (212 mg, 414 mmol).

^{1}H NMR (400 MHz, DMSO-d_6) δ/ppm = 8.36 – 7.98 (m, 8H), 7.54 – 7.26 (m, 8H).

^{13}C NMR (101 MHz, DMSO-d_6) δ/ppm = 148.08, 147.06, 141.29, 132.53, 124.06.

IR (ATR platinum diamond): $\tilde{\nu}/cm^{-1}$ = 3106 (vw), 2933 (vw), 2849 (vw), 1594 (w), 1512 (vs), 1407 (vw), 1341 (vs), 1281 (w), 1273 (w), 1179 (w), 1107 (w), 1014 (w), 880 (w), 854 (w), 847 (w), 835 (s), 810 (m), 747 (s), 720 (w), 703 (s), 689 (w), 650 (w), 504 (w), 487 (w), 471 (w).

FAB-HRMS m/z: $[M+H]^+$ calculated for $C_{26}H_{16}N_4O_8$ = 513.1040, found 513.1041.

Fluorescence: λ_{em}(max) = 509 nm with λ_{ex} = 325 nm.

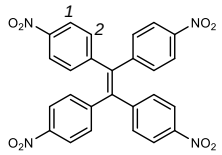

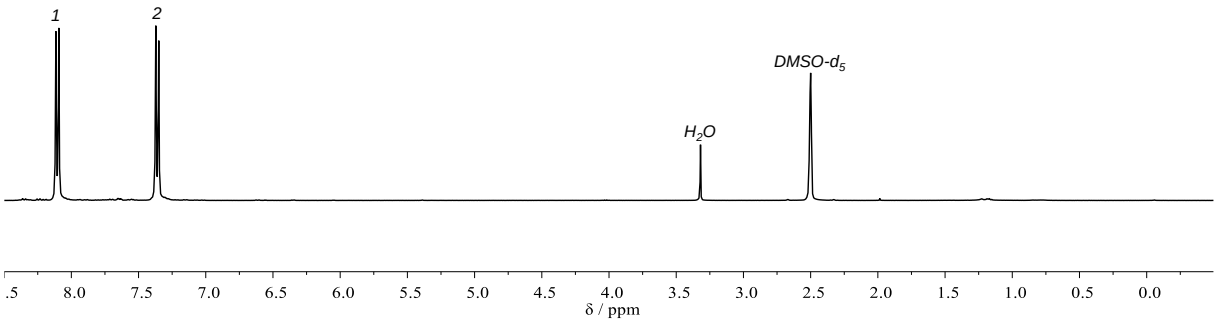

*Supplementary Figure 25: [1]H NMR spectrum of **2d** in DMSO-d_6.*

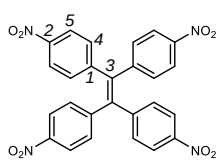

*Supplementary Figure 26: [13]C NMR spectrum of **2d** in DMSO-d_6.*

9,9'-Bifluorenylidene (2e)

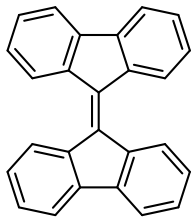

Prepared from **1e** according to the general procedure. The product was isolated *via* column chromatography (cyclohexane/ethyl acetate 50:1) as a red solid in a yield of 91% (149 mg, 0.417 mmol).

^{1}H NMR (400 MHz, DMSO-d_6) δ/ppm = 8.33 – 8.26 (m, 4H), 7.94 – 7.87 (m, 4H), 7.45 – 7.34 (m, 4H), 7.34 – 7.25 (m, 4H).

^{13}C NMR (101 MHz, DMSO-d_6) δ/ppm = 140.72, 140.21, 137.18, 129.71, 127.31, 126.21, 120.48.

IR (ATR platinum diamond): $\tilde{\nu}/cm^{-1}$ = 3077 (vw), 3052 (vw), 3030 (vw), 3013 (vw), 1604 (w), 1571 (vw), 1475 (w), 1440 (m), 1347 (w), 1310 (w), 1304 (w), 1279 (w), 1230 (w), 1205 (w), 1150 (w), 1100 (w), 1035 (w), 938 (w), 874 (w), 786 (w), 761 (s), 743 (m), 718 (vs), 638 (w), 617 (w), 586 (w), 422 (w).

EI-HRMS m/z: $[M]^+$ calculated for $C_{26}H_{16}$ = 328.1247, found 328.1245.

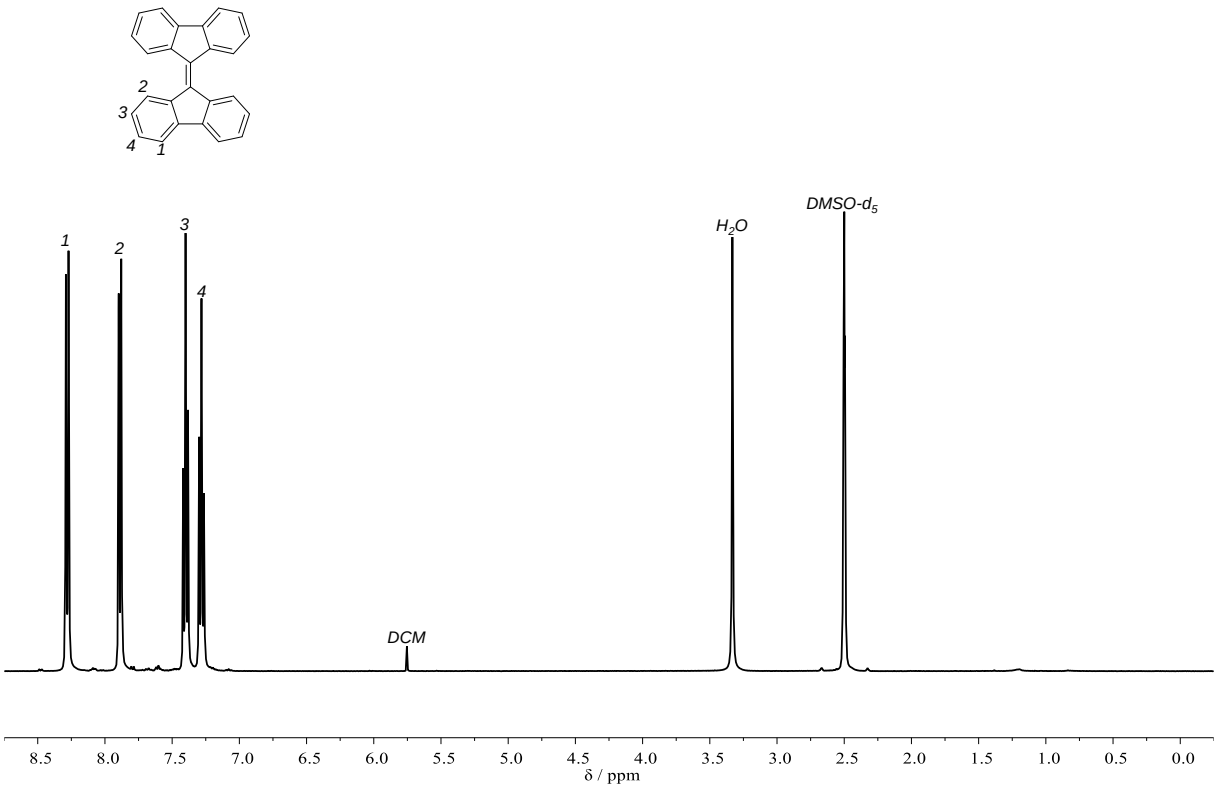

*Supplementary Figure 27: ^{1}H NMR spectrum of **2e** in DMSO-d_6.*

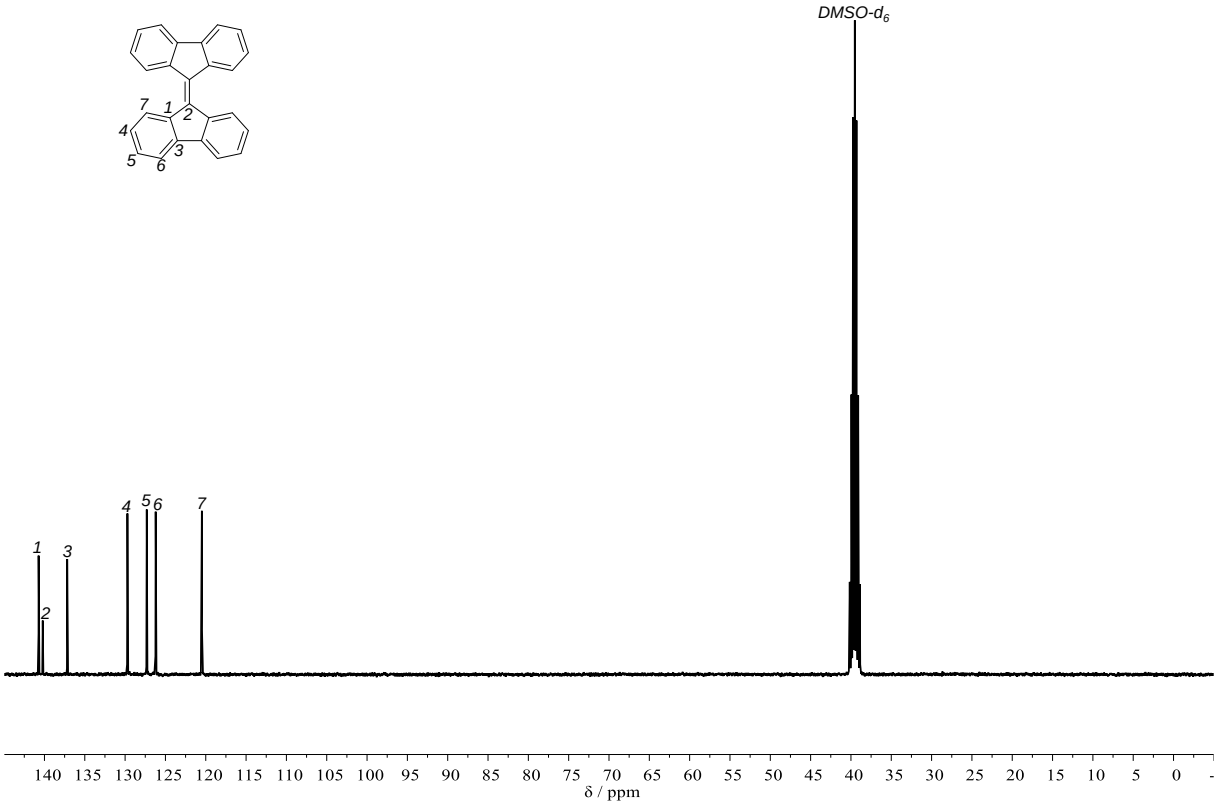

*Supplementary Figure 28: ^{13}C NMR spectrum of **2e** in DMSO-d_6.*

1,2-bis(4-nitrophenyl)-1,2-diphenylethylene (2h)

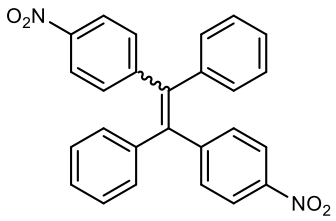

Prepared from **1h** according to the general procedure. The product was isolated *via* column chromatography (cyclohexane/ethyl acetate 40:1) as a yellow solid in a yield of 99% (210 mg, 0.498 mmol). According to ^{1}H-NMR, the isolated products consists of a 55:45 mixture of the *(E)*- and *(Z)*-isomers. Separation of the isomers was not attempted. With the employed methods, assignment of the signals to respective isomers was not possible.

^{1}H NMR (400 MHz, DMSO-d_6) δ/ppm = 8.09 – 8.00 (m, 4H), 7.32 – 7.23 (m, 4H), 7.27 – 7.13 (m, 6H), 7.07 – 6.96 (m, 4H).

^{13}C NMR (101 MHz, DMSO-d_6) δ/ppm 149.65, 149.41, 146.06, 145.92, 141.51, 141.25, 141.03, 140.96, 131.97, 131.86, 130.68, 130.57, 128.40, 128.18, 127.69, 127.47, 123.36, 123.14.

IR (ATR platinum diamond): $\tilde{\nu}/cm^{-1}$ = 3079 (vw), 3059 (vw), 3017 (vw), 2927 (vw), 2847 (vw), 1590 (m), 1512 (vs), 1491 (m), 1444 (w), 1407 (vw), 1337 (vs), 1269 (w), 1246 (w), 1179 (w), 1156 (vw), 1107 (w), 1074 (w), 1028 (w), 1014 (w), 977 (vw), 917 (vw), 870 (w), 856 (w), 843 (m), 821 (w), 771 (w), 749 (s), 697 (vs), 640 (w), 619 (vw), 594 (w), 570 (vw), 490 (w).

EI-HRMS m/z: $[M]^+$ calculated for $C_{26}H_{18}N_2O_4$ = 422.1261, found 422.1262.

Fluorescence: λ_{em}(max) = 534 nm with λ_{ex} = 456 nm

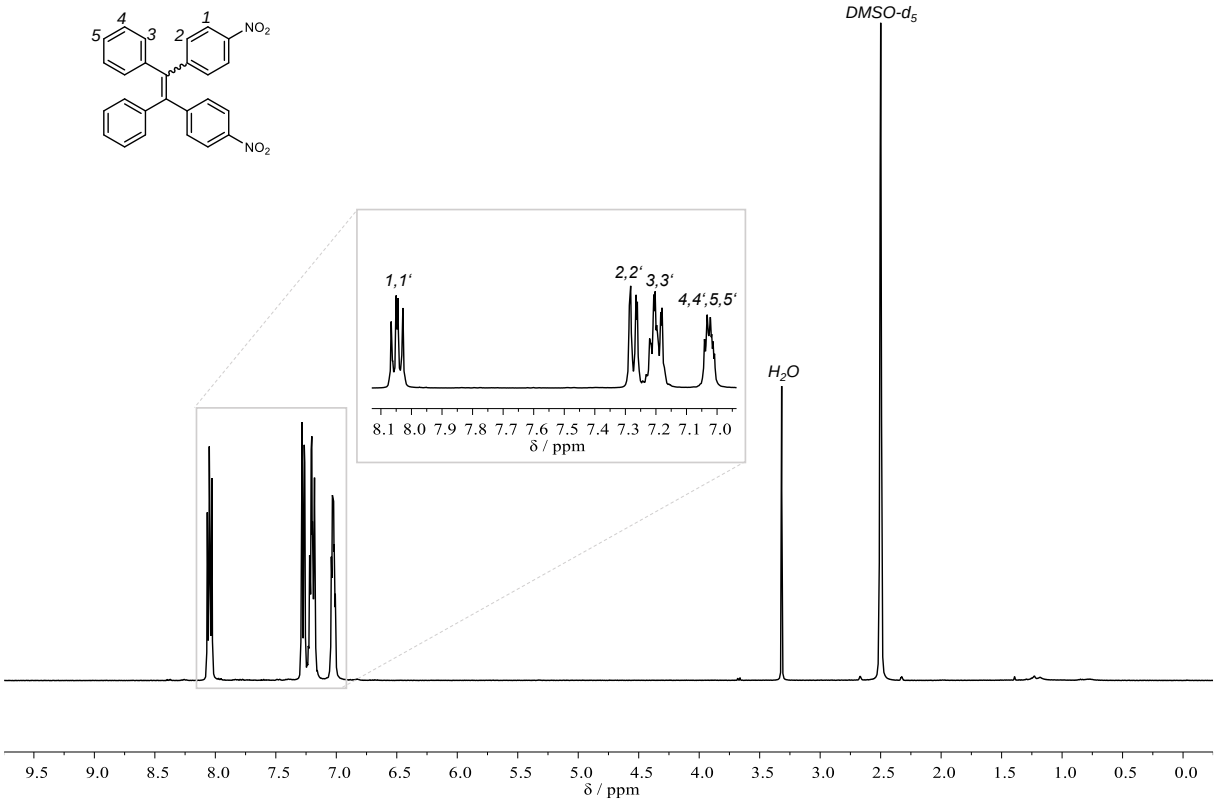

*Supplementary Figure 29: [1]H NMR spectrum of **2h** in DMSO-d6.*

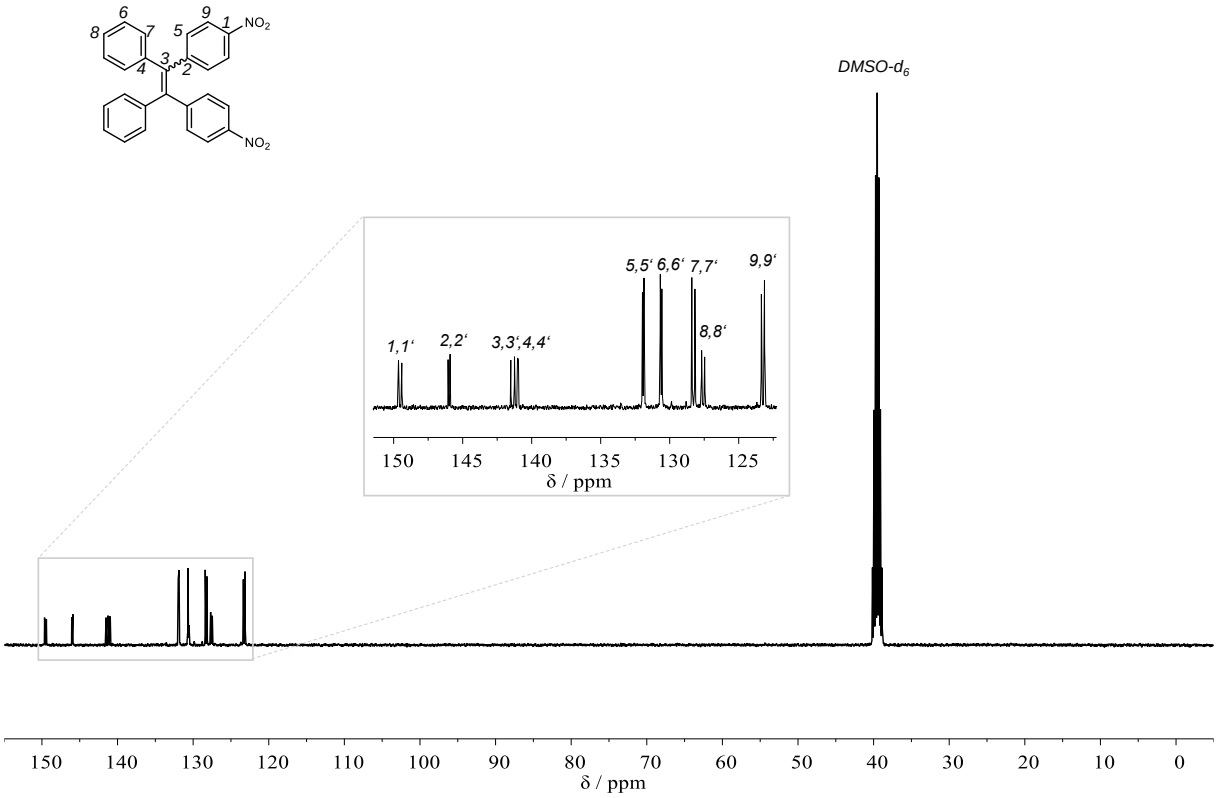

*Supplementary Figure 30: [13]C NMR spectrum of **2h** in DMSO-d6.*

6.3.1.4 Synthesis of thioketones

4,4-Dimethoxythiobenzophenone (3a)

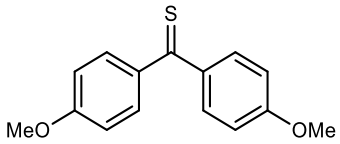

In a flame-dried Schlenk flask under argon atmosphere, 1.00 g (4.13 mmol, 1.00 equiv.) of 4,4'-dimethoxybenzophenone were dispersed in 40 mL of dry toluene and Lawesson's reagent (1.34 g, 3.30 mmol, 0.80 equiv.) was added. The mixture was refluxed for 16 hours under light exclusion. Afterwards, the crude reaction mixture was transferred onto a short filter column (cyclohexane with 3 vol% NEt_3) and all blue fractions were collected. After removal of the solvent under reduced pressure, the crude product was purified *via* another subsequent column chromatography (cyclohexane/ethyl acetate 30:1 with 1 vol% NEt_3). The product was isolated as a blue solid in a yield of 70% (860 mg, 3.33 mmol).

^{1}H NMR (400 MHz, DMSO-d_6) δ/ppm = 7.70 – 7.62 (m, 2H), 7.06 – 6.98 (m, 2H), 3.86 (s, 3H).

^{13}C NMR (101 MHz, DMSO-d_6) δ/ppm = 233.15, 163.57, 140.47, 132.44, 114.02, 56.15.

IR (ATR platinum diamond): $\tilde{\nu}/cm^{-1}$ = 3007 (vw), 2968 (vw), 2929 (vw), 2834 (w), 1588 (s), 1567 (m), 1502 (m), 1454 (m), 1440 (m), 1417 (w), 1300 (s), 1249 (vs), 1216 (s), 1162 (vs), 1117 (s), 1113 (s), 1045 (s), 1020 (vs), 963 (m), 897 (w), 833 (vs), 804 (s), 775 (w), 738 (w), 644 (w), 617 (vs), 543 (s), 508 (m).

ESI-HRMS m/z: $[M+H]^+$ calculated for $C_{15}H_{15}O_2S$ = 259.0787, found 259.0784

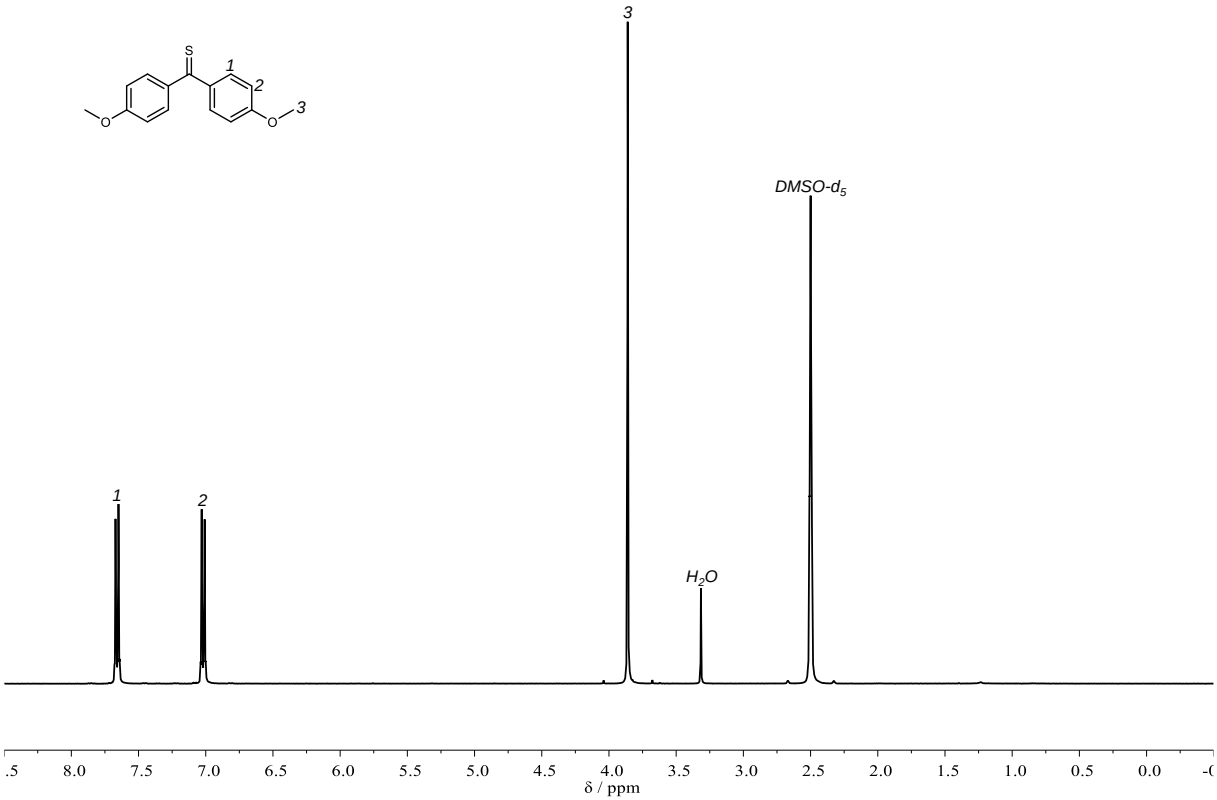

*Supplementary Figure 31: [1]H NMR spectrum of **3a** in DMSO-d6.*

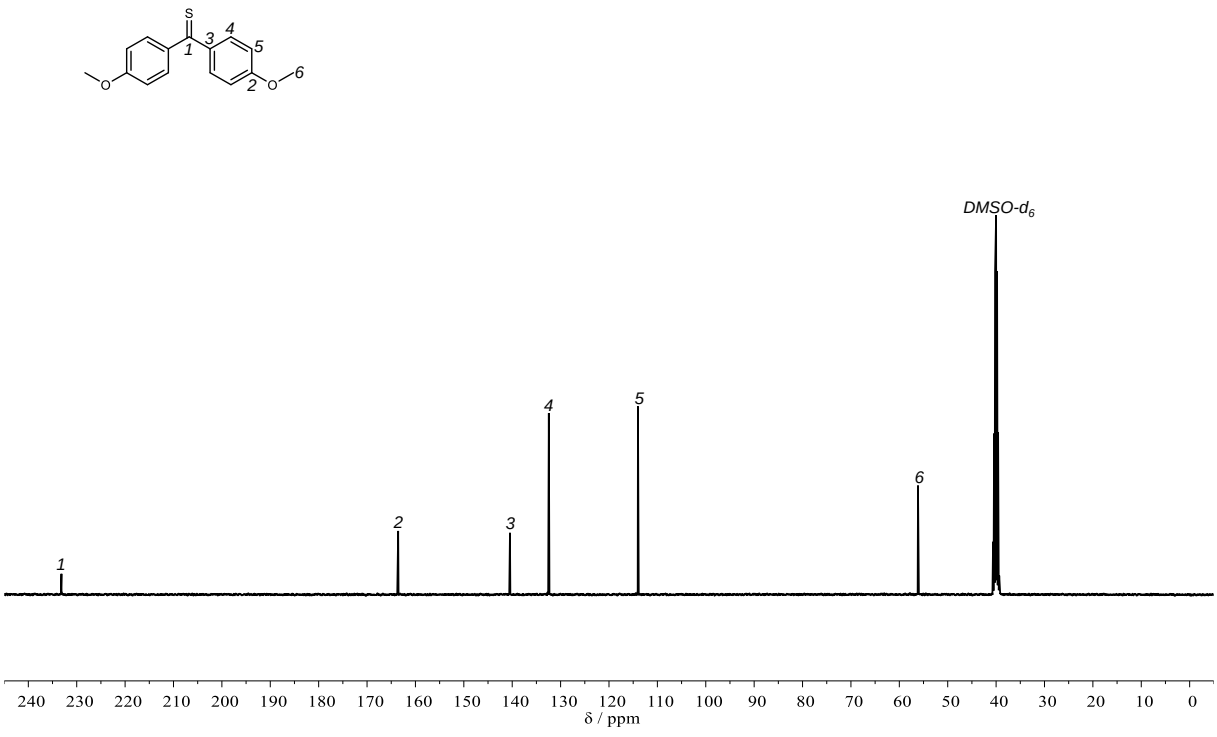

*Supplementary Figure 32: [13]C NMR spectrum of **3a** in DMSO-d6.*

Thioxanthene-9-thione (3b)

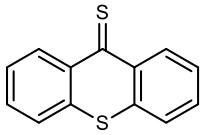

In a flame-dried Schlenk flask under argon atmosphere, 1.06 g (5.00 mmol, 1.00 equiv.) of thioxanthene-9-one were dispersed in 50 mL of dry toluene and Lawesson's reagent (1.62 g, 4.00 mmol, 0.80 equiv.) was added. The mixture was refluxed for 16 hours under light exclusion. Afterwards, the crude reaction mixture was transferred onto a short filter column (cyclohexane with 3 vol% NEt_3) and all dark green fractions were collected. The product was obtained as a dark green solid in a yield 94% (1.07 g, 4.70 mmol).

^{1}H NMR (400 MHz, DMSO-d_6) δ/ppm = 8.91 (dd, J = 8.4, 1.4 Hz, 1H), 7.90 (dd, J = 8.0, 1.4 Hz, 1H), 7.81 (ddd, J = 8.2, 7.0, 1.4 Hz, 1H), 7.59 (ddd, J = 8.4, 7.0, 1.4 Hz, 1H).

^{13}C NMR (101 MHz, DMSO-d_6) δ/ppm = 210.34, 136.94, 133.16, 133.11, 132.06, 128.10, 127.11.

IR (ATR platinum diamond): $\tilde{\nu}/cm^{-1}$ = 3048 (vw), 1586 (w), 1555 (w), 1456 (w), 1444 (w), 1417 (m), 1314 (w), 1284 (w), 1261 (m), 1187 (s), 1156 (m), 1113 (w), 1096 (m), 1072 (w), 1033 (w), 1006 (s), 959 (w), 952 (w), 897 (w), 854 (w), 769 (vs), 747 (w), 720 (vs), 660 (w), 621 (m), 607 (m), 529 (w), 475 (w) cm^{-1}.

ESI-HRMS m/z: $[M+H]^+$ calculated for $C_{13}H_8S_2$ = 229.0141, found 229.0141.

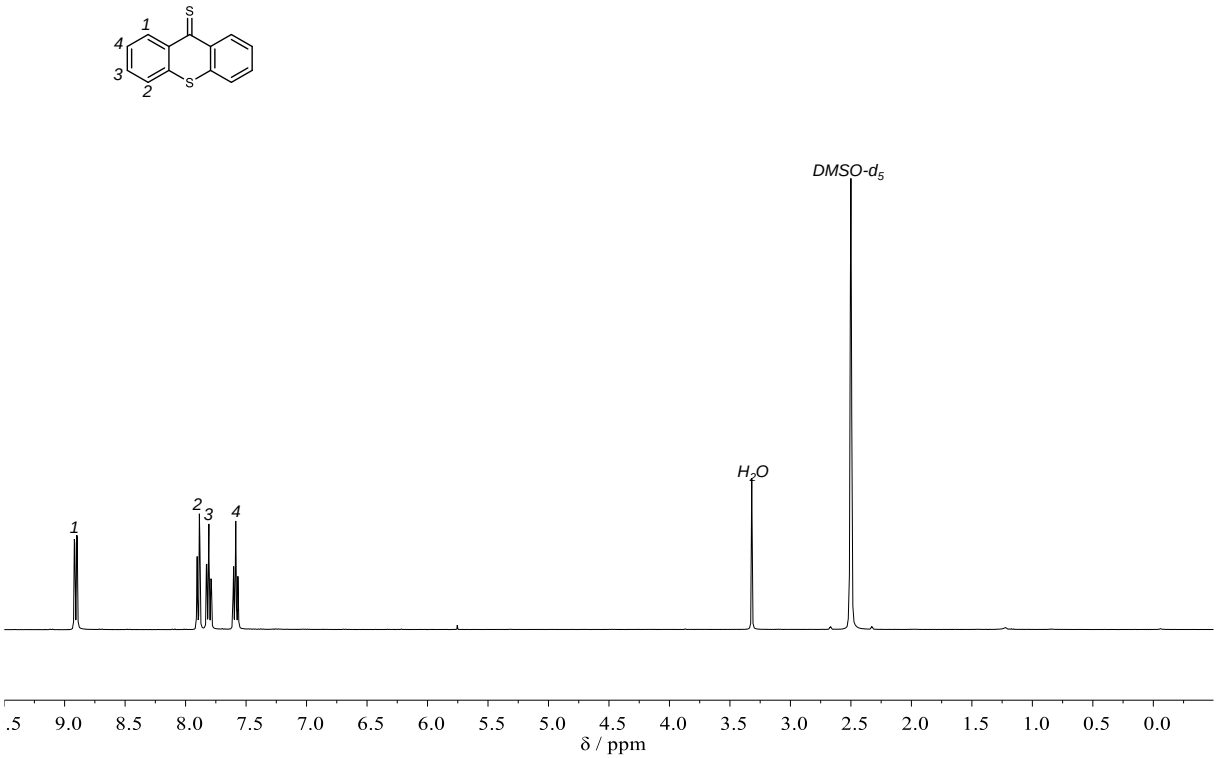

*Supplementary Figure 33: [1]H NMR spectrum of **3b** in DMSO-d6.*

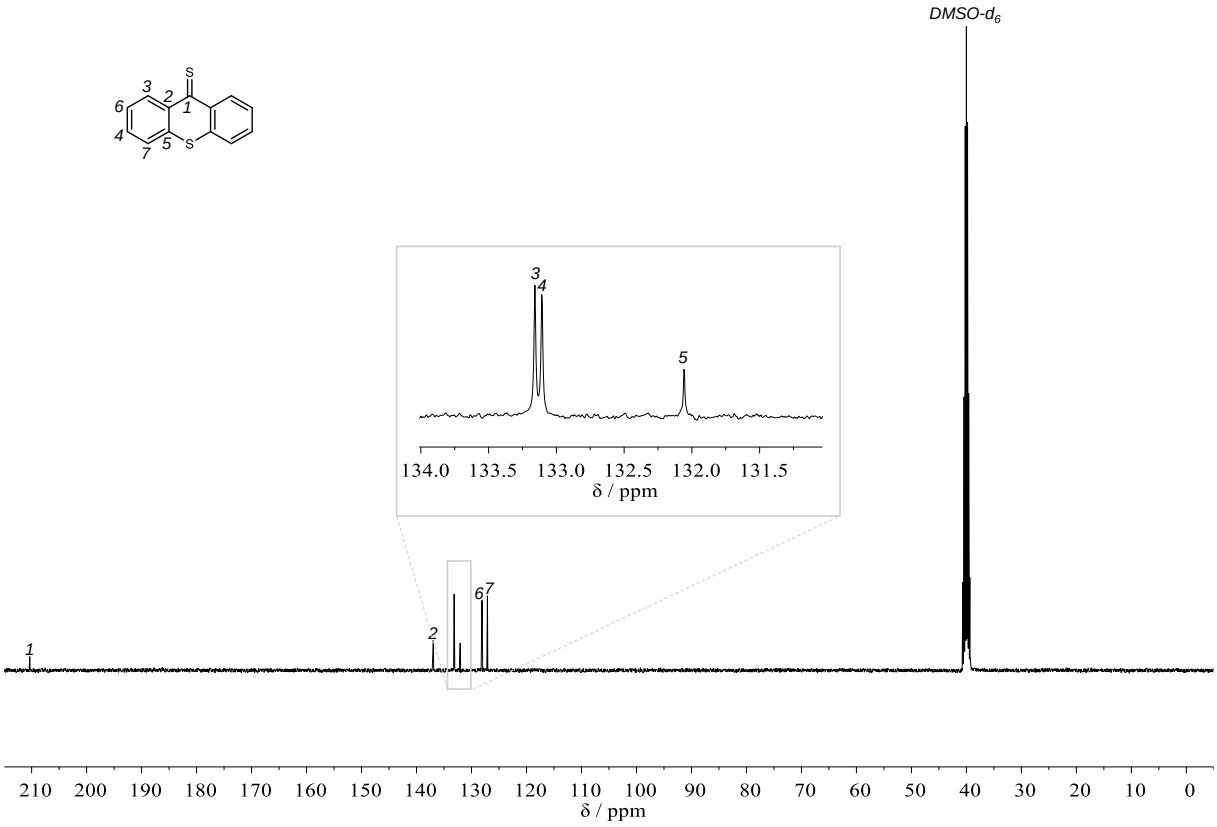

*Supplementary Figure 34: [13]C NMR spectrum of **3b** in DMSO-d6.*

4,4'-dibromothiobenzophenone (3c)

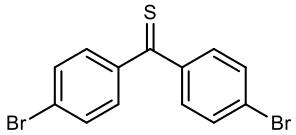

In a flame-dried Schlenk flask under argon atmosphere, 1.06 g (5.00 mmol, 1.00 equiv.) of 4,4'-dibromobenzophenone (**4c**) were dispersed in 50 mL of dry toluene and Lawesson's reagent (1.62 g, 4.00 mmol, 0.80 equiv.) was added. The mixture was refluxed for 16 hours under light exclusion. Afterwards, the crude reaction mixture was transferred onto a short filter column (cyclohexane with 3 vol% NEt_3) and all blue fractions were collected. The product was obtained as a blue solid in a yield of 83% (1.48 g, 4.15 mmol). Impurities in the ^{1}H-NMR spectra are due to contamination with ketone **4c** present caused by partial decomposition of the product before the measurements.

^{1}H NMR (400 MHz, DMSO-d_6) δ/ppm = 7.76 – 7.66 (m, 4H), 7.64 – 7.53 (m, 4H).

^{13}C NMR (101 MHz, DMSO-d_6) δ/ppm = 235.07, 145.16, 131.46, 131.06, 127.05.

IR (ATR platinum diamond): $\tilde{\nu}/cm^{-1}$ = 3057 (w), 2917 (w), 2849 (w), 1643 (vs), 1574 (vs), 1481 (s), 1417 (w), 1393 (s), 1316 (w), 1302 (m), 1286 (s), 1273 (s), 1263 (vs), 1207 (s), 1174 (s), 1146 (w), 1123 (w), 1105 (w), 1070 (vs), 1051 (s), 1004 (vs), 967 (m), 924 (s), 889 (m), 854 (m), 825 (vs), 749 (vs), 722 (s), 695 (w), 662 (m), 629 (w), 611 (m), 520 (w), 477 (w), 469 (s), 455 (w), 436 (w).

ESI-HRMS m/z: $[M+H]^+$ calculated for $C_{13}H_8S^{79}Br^{81}Br$ = 356.8766, found 356.8762.

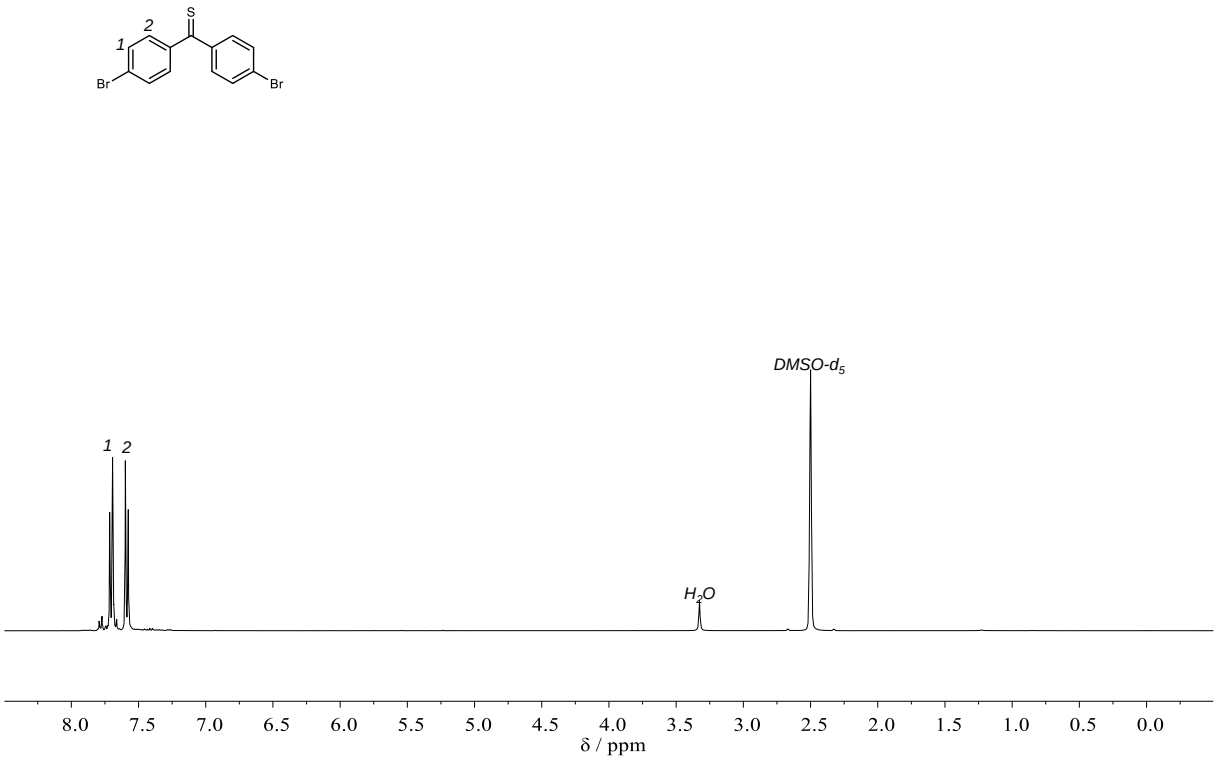

*Supplementary Figure 35: ^{1}H NMR spectrum of **3c** in DMSO-d_6.*

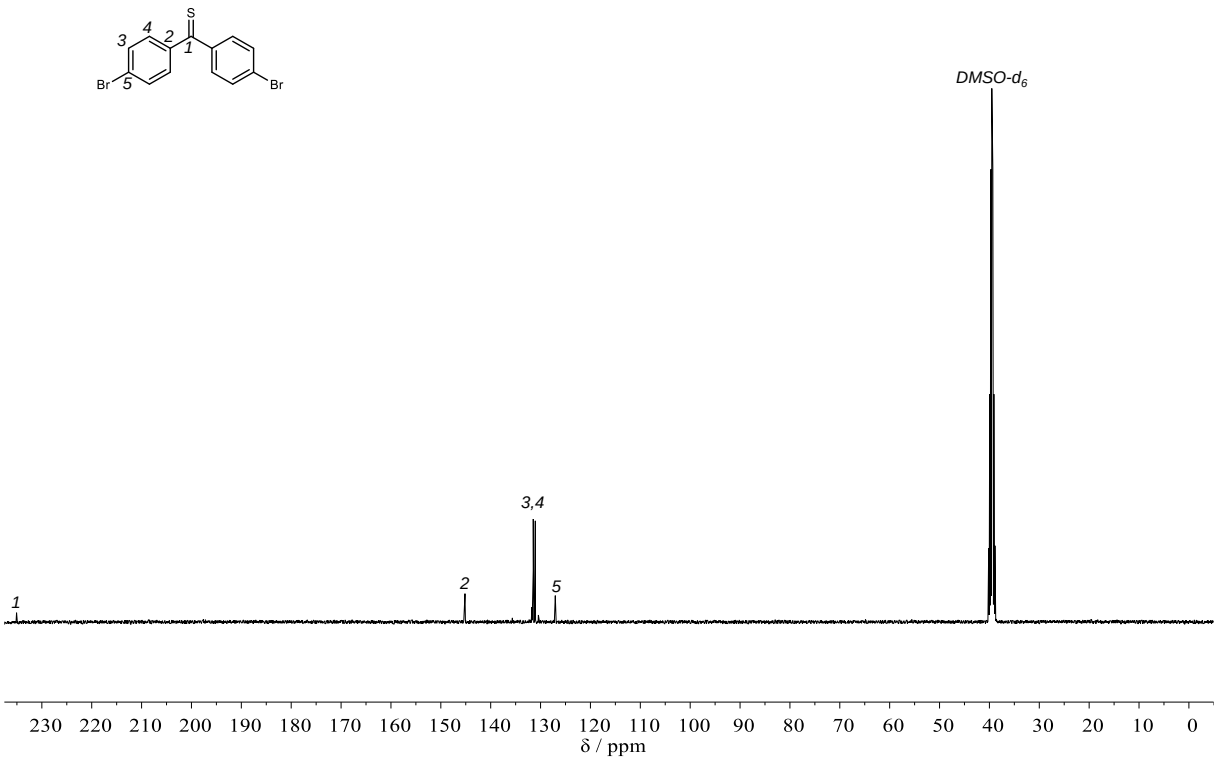

*Supplementary Figure 36: ^{13}C NMR spectrum of **3c** in DMSO-d_6.*

6.3.1.5 Synthesis of cross-coupled olefins

Disclaimer

5d was synthesized by the author during his master thesis. Its characterization is thus not included here.

5b (from **3c** and **1a**) and **5h** were synthesized by Silas Leidenheimer under supervision of the author.

General procedure for the alkylidene cross-coupling of N-tosylhydrazones and thioketones:

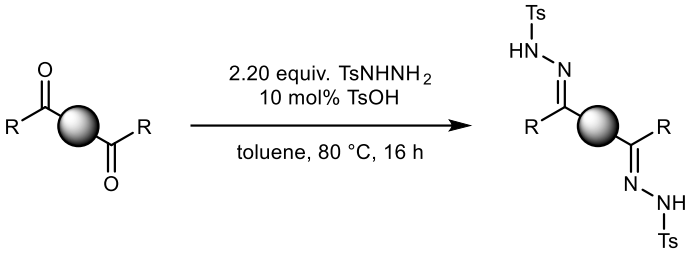

0.50 mmol (1.00 equiv.) of the N-tosylhydrazone were dissolved in 2 mL of dry DMSO and 0.51 mmol of the thioketone (1.02 equiv.) were added. The mixture was heated to 100 °C and 82.92 mg (0.60 mmol, 1.20 equiv.) of potassium carbonate were added. After stirring at 100 °C for 30 minutes, 32.1 mg (1 mmol S, 2.00 equiv.) of elemental sulfur were added and stirring at 100°C was continued for another 30 minutes. Afterwards, the crude mixture was transferred directly onto a column (packed in pure cyclohexane) and the product was isolated *via* column chromatography.

1,1-Bis(4-methoxyphenyl)-2,2-diphenylethylene (5a)

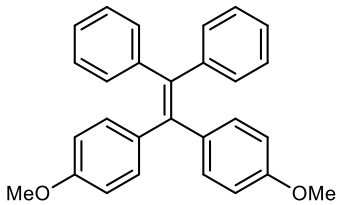

Prepared from NTH **1b** and thioketone **3a** according to general procedure. The product was isolated *via* column chromatography (cyclohexane/ethyl acetate 40:1). Obtained as a white solid in a yield of 85% (167 mg, 0.426 mmol).

^{1}H NMR (400 MHz, DMSO-d_6) δ/ppm = 7.18 – 7.09 (m, 4H), 7.13 – 7.04 (m, 2H), 6.99 – 6.91 (m, 4H), 6.90 – 6.81 (m, 4H), 6.72 – 6.64 (m, 4H), 3.67 (s, 6H).

^{13}C NMR (101 MHz, DMSO-d_6) δ/ppm = 157.69, 143.79, 139.81, 138.75, 135.62, 131.98, 130.69, 127.82, 126.21, 113.16, 54.90.

IR (ATR platinum diamond): $\tilde{\nu}/cm^{-1}$ = 3005 (w), 2964 (w), 2931 (vw), 2836 (w), 1604 (m), 1574 (w), 1506 (vs), 1462 (m), 1442 (m), 1413 (w), 1296 (m), 1240 (vs), 1174 (vs), 1158 (m), 1129 (w), 1113 (w), 1074 (w), 1026 (vs), 835 (s), 825 (s), 806 (m), 767 (s), 753 (s), 736 (m), 695 (vs), 660 (w), 640 (vw), 615 (vw), 592 (vs), 572 (w), 545 (s), 518 (w), 467 (w).

ESI-HRMS m/z: $[M]^+$ calculated for $C_{28}H_{24}O_2$ = 392.1771, found 392.1769.

Fluorescence: λ_{em}(max) = 480 nm with λ_{ex} = 321 nm

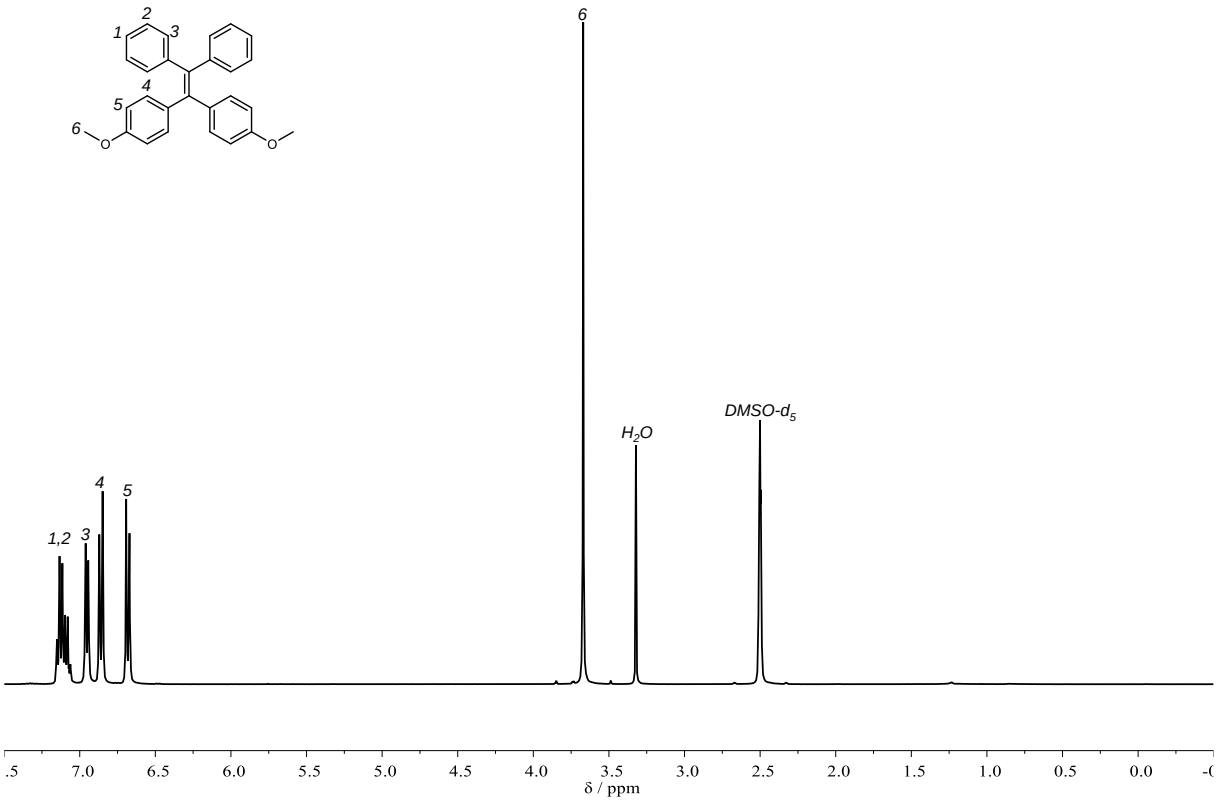

*Supplementary Figure 37: [1]H NMR spectrum of **5a** in DMSO-d6.*

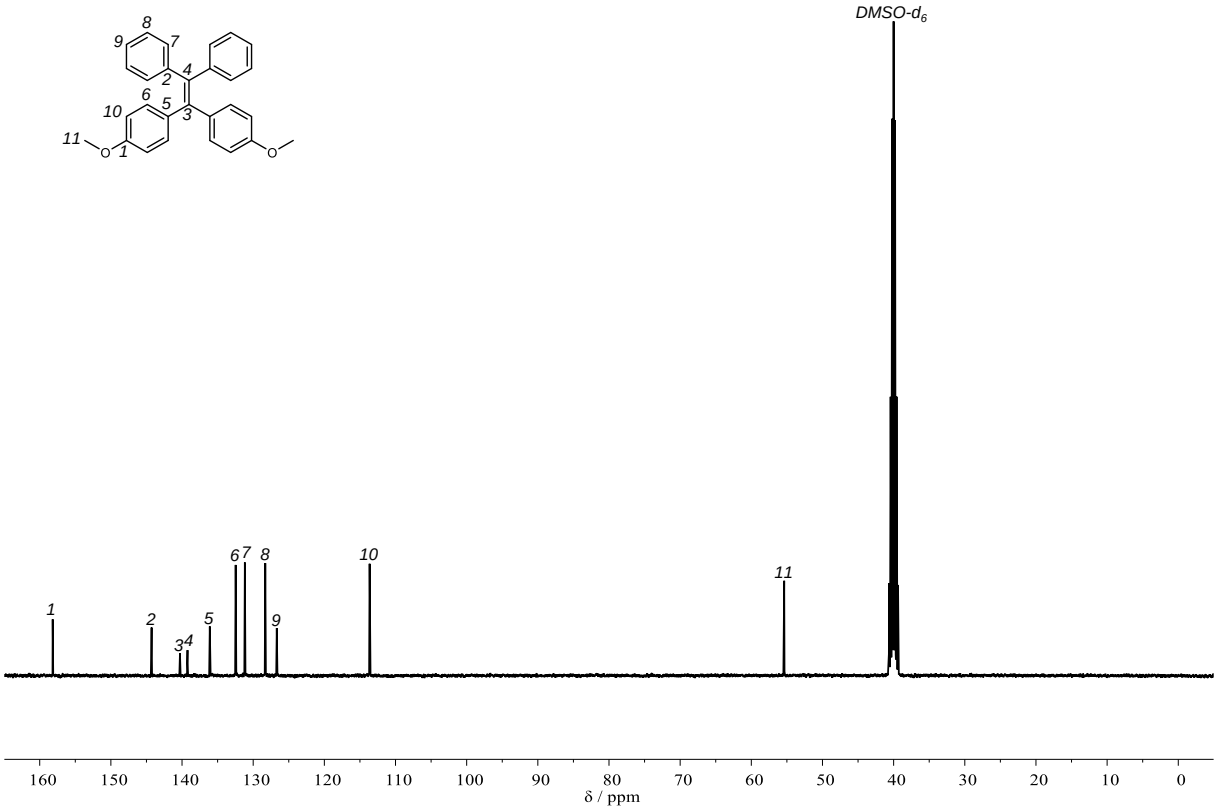

*Supplementary Figure 38: [13]C NMR spectrum of **5a** in DMSO-d6.*

1,1-Bis(4-bromophenyl)-2,2-bis(4-methoxyphenyl)ethylene (5b)

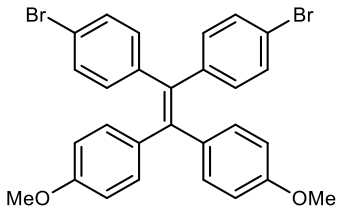

Method A: Prepared from NTH **1c** and thioketone **3a** according to general procedure. The product was isolated *via* column chromatography (cyclohexane/ethyl acetate 30:1). Obtained as a slightly yellow solid in a yield of 85% (233 mg, 0.423 mmol).

Method B: Prepared from NTH **1a** and thioketone **3c** according to general procedure in a smaller scale of 0.4 mmol. The product isolated *via* column chromatography (cyclohexane/ethyl acetate 30:1). Obtained as a slightly yellow solid in a yield of 83% (182 mg, 0.331 mmol).

^{1}H NMR (400 MHz, DMSO-d_6) δ/ppm = 7.41 – 7.32 (m, 4H), 6.95 – 6.83 (m, 8H), 6.80 – 6.62 (m, 4H), 3.69 (s, 6H).

^{13}C NMR (101 MHz, DMSO-d_6) δ/ppm = 158.02, 142.66, 141.23, 136.18, 135.03, 132.89, 132.00, 130.94, 119.58, 113.38, 54.95.

IR (ATR platinum diamond): $\tilde{\nu}/cm^{-1}$ = 3007 (vw), 2956 (vw), 2931 (vw), 2836 (vw), 1905 (vw), 1604 (m), 1586 (w), 1508 (vs), 1481 (m), 1458 (w), 1440 (w), 1388 (w), 1294 (w), 1281 (w), 1242 (vs), 1177 (s), 1127 (w), 1103 (w), 1068 (m), 1026 (vs), 1008 (vs), 975 (w), 862 (w), 829 (vs), 808 (vs), 780 (s), 740 (w), 726 (w), 666 (w), 592 (m), 570 (w), 559 (m), 508 (w), 483 (s), 465 (w).

ESI-HRMS m/z: $[M]^+$ calculated for $C_{28}H_{22}O_2{}^{79}Br^{81}Br$ = 549.9966, found 549.9963

Fluorescence: λ_{em}(max) = 493 nm with λ_{ex} = 332 nm

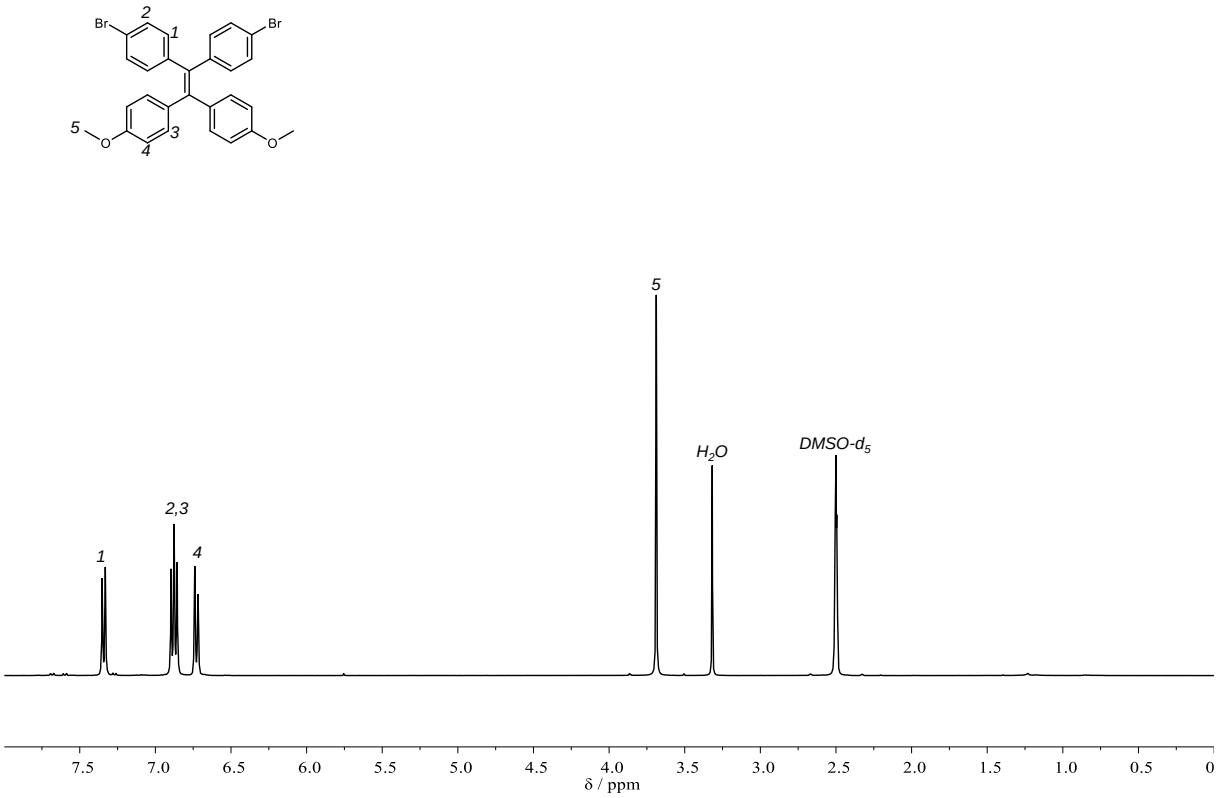

*Supplementary Figure 39: [1]H NMR spectrum of **5b** in DMSO-d6.*

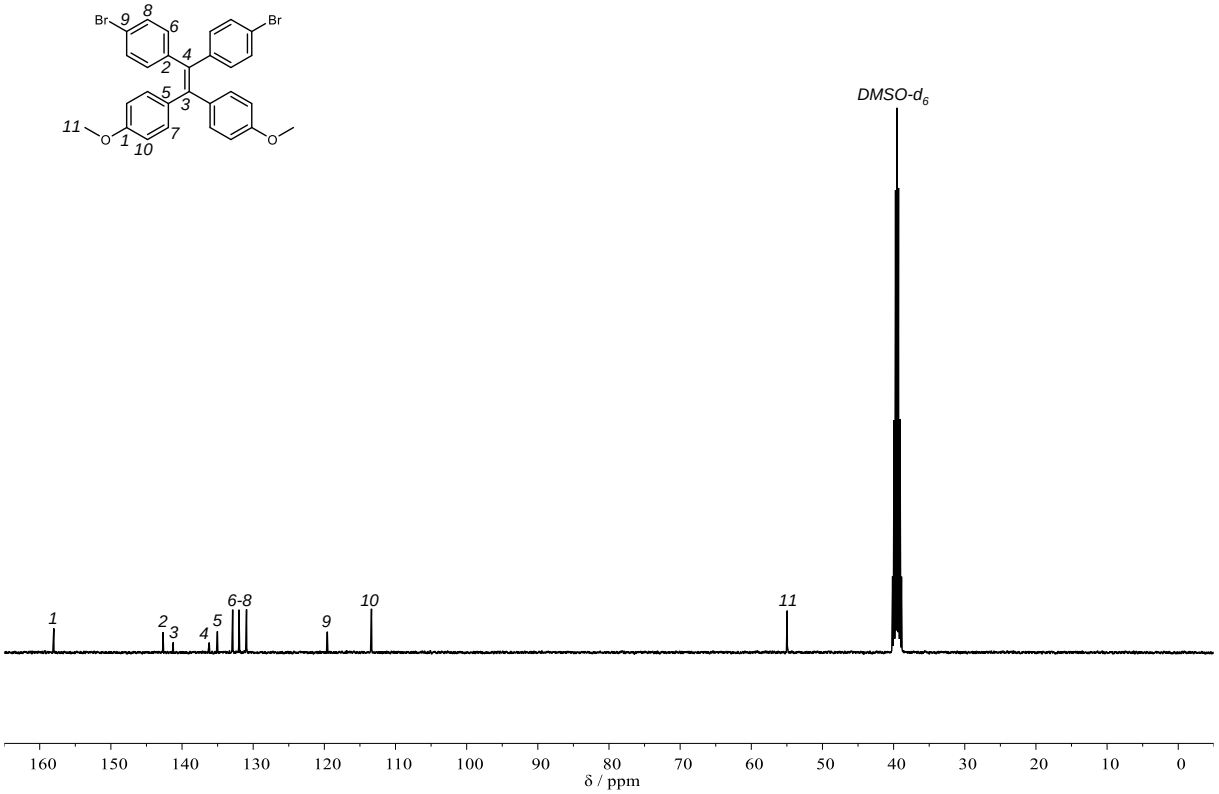

*Supplementary Figure 40: [13]C NMR spectrum of **5b** in DMSO-d6.*

1,1-Bis(4-methoxyphenyl)-2,2-bis(4-nitrophenyl)ethylene (5c)

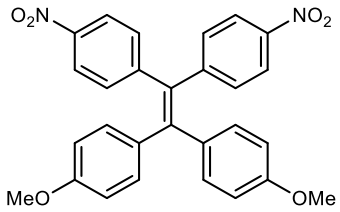

Prepared from NTH **1d** and thioketone **3a** according to general procedure. The product was isolated *via* column chromatography (cyclohexane/ethyl acetate 20:1). Obtained as an orange solid in a yield of 79% (190 mg, 0.394 mmol).

^{1}H NMR (400 MHz, DMSO-d_6) δ/ppm = 8.11 – 8.00 (m, 4H), 7.29 – 7.17 (m, 4H), 6.98 – 6.88 (m, 4H), 6.81 – 6.72 (m, 4H), 3.69 (s, 6H).

^{13}C NMR (101 MHz, DMSO-d_6) δ/ppm = 159.19, 150.77, 146.09, 145.67, 135.30, 134.56, 132.83, 132.68, 123.85, 114.05, 55.51.

IR (ATR platinum diamond): $\tilde{\nu}/cm^{-1}$ = 3073 (vw), 2958 (vw), 2933 (vw), 2836 (w), 1590 (m), 1506 (vs), 1462 (w), 1440 (w), 1337 (vs), 1292 (m), 1244 (vs), 1172 (vs), 1131 (w), 1107 (s), 1028 (s), 1014 (m), 977 (w), 961 (w), 874 (w), 856 (w), 841 (s), 833 (s), 815 (s), 784 (w), 753 (m), 736 (w), 703 (m), 689 (w), 668 (w), 594 (w), 570 (w), 559 (w), 514 (w).

ESI-HRMS m/z: $[M+H]^+$ calculated for $C_{28}H_{22}N_2O_6$ = 483.1551, found 483.1543.

Fluorescence: λ_{em}(max) = 581 nm with λ_{ex} = 383 nm.

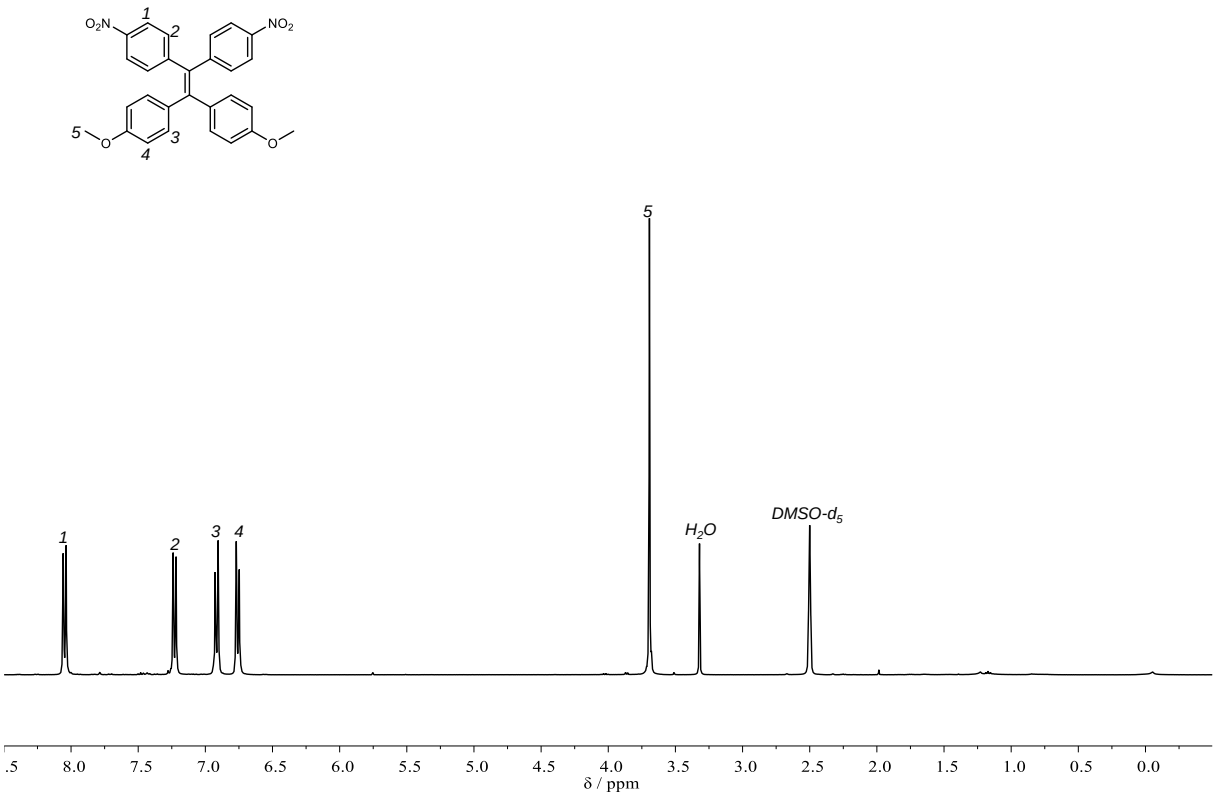

*Supplementary Figure 41: ^{1}H NMR spectrum of **5c** in DMSO-d_6.*

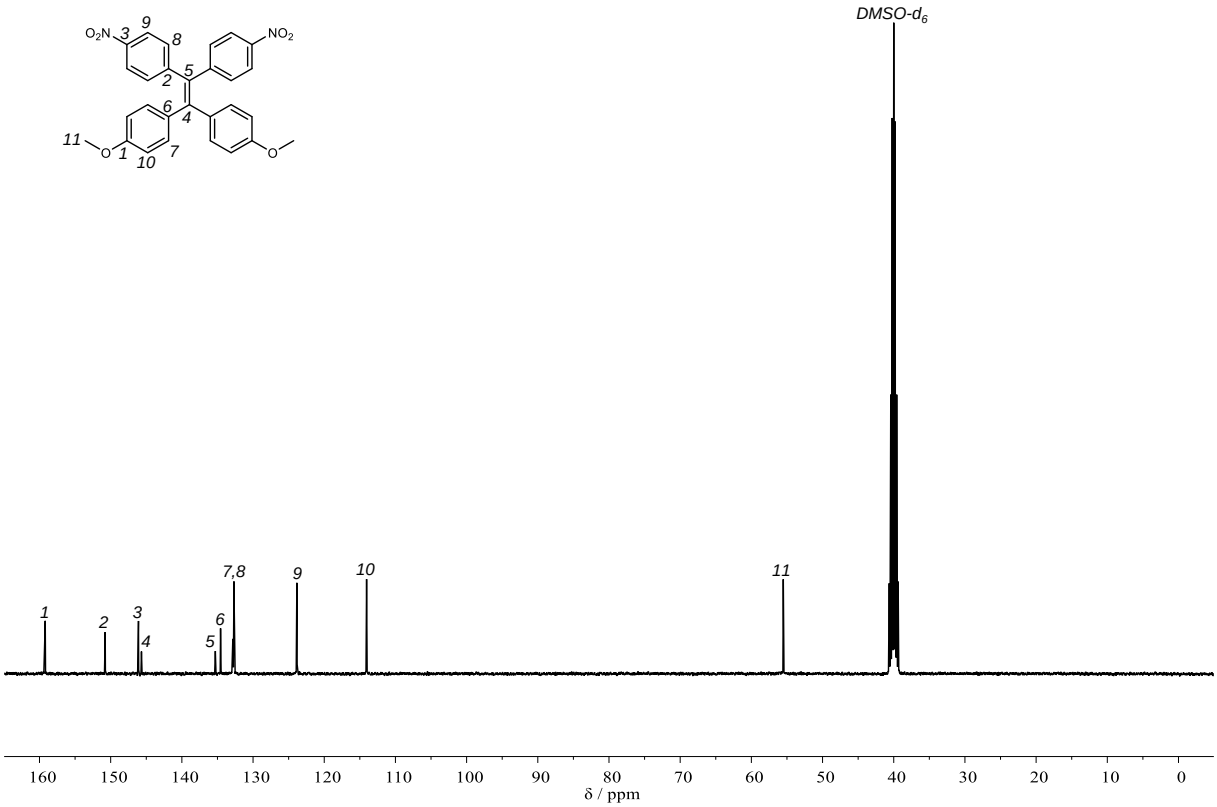

*Supplementary Figure 42: ^{13}C NMR spectrum of **5c** in DMSO-d_6.*

1,1,2-Tris(4-methoxyphenyl)propylene (5e)

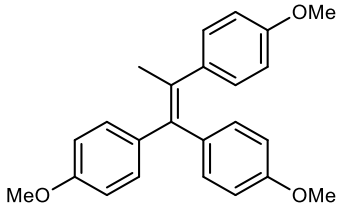

Prepared from NTH **1j** and thioketone **3a** according to general procedure on a smaller scale using 0.25 mmol NTH. The product was isolated *via* column chromatography (cyclohexane/ethyl acetate 30:1). Obtained as a colorless solid in a yield of 93% (84.2 mg, 0.234 mmol).

^{1}H NMR (400 MHz, DMSO-d_6) δ/ppm = 7.14 – 7.01 (m, 4H), 6.95 – 6.87 (m, 2H), 6.80 – 6.70 (m, 4H), 6.66 – 6.58 (m, 2H), 3.76 (s, 3H), 3.68 (s, 3H), 3.64 (s, 3H), 2.02 (s, 3H).

^{13}C NMR (101 MHz, DMSO-d_6) δ/ppm = 157.75, 157.37, 157.08, 137.27, 135.92, 135.81, 135.63, 133.25, 131.48, 130.78, 130.15, 113.53, 113.29, 112.97, 54.99, 54.88, 54.80, 23.20.

IR (ATR platinum diamond): $\tilde{\nu}/cm^{-1}$ = 3005 (vw), 2954 (w), 2929 (w), 2906 (w), 2853 (vw), 2834 (w), 1604 (m), 1571 (w), 1506 (vs), 1462 (m), 1442 (m), 1409 (vw), 1292 (m), 1273 (w), 1236 (vs), 1170 (vs), 1146 (w), 1107 (w), 1078 (w), 1028 (vs), 1002 (m), 954 (vw), 911 (w), 829 (vs), 808 (vs), 782 (w), 749 (w), 734 (w), 716 (w), 574 (s), 545 (w), 522 (w), 494 (w), 477 (w).

ESI-HRMS m/z: $[M]^+$ calculated for $C_{24}H_{24}O_3$ = 360.1720, found 360.1714.

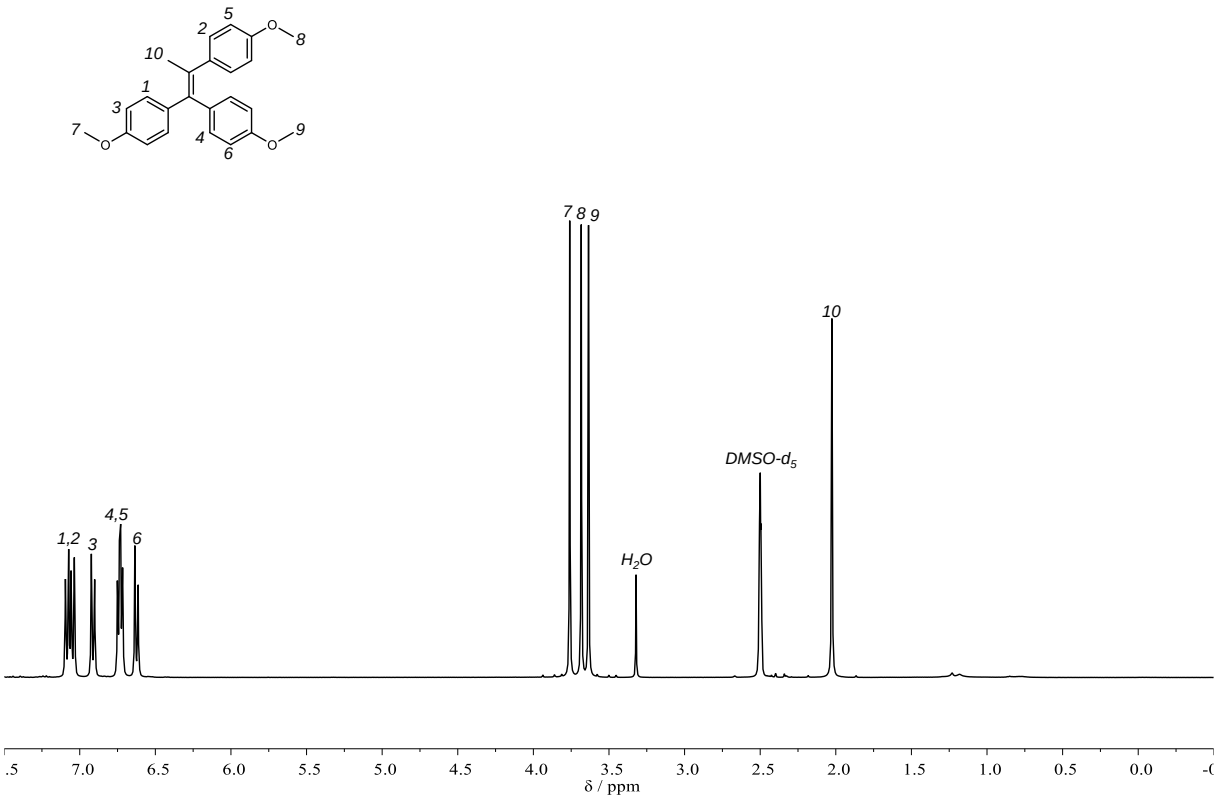

*Supplementary Figure 43: ^{1}H NMR spectrum of **5e** in DMSO-d_6.*

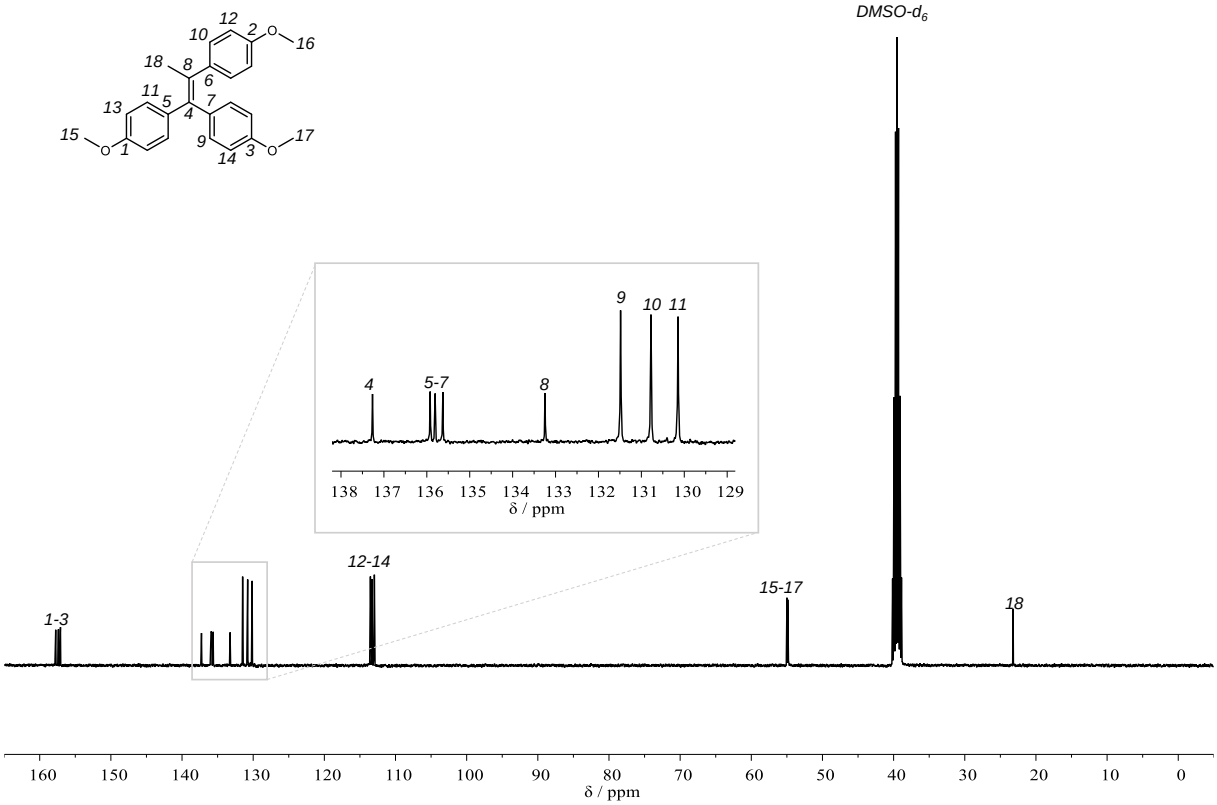

*Supplementary Figure 44: ^{13}C NMR spectrum of **5e** in DMSO-d_6.*

3-(4,4'-Dimethoxybenzhydrylidene)pentane (5f)

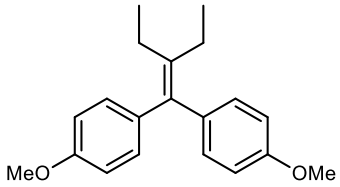

Prepared from NTH **1l** and thioketone **3a** according to general procedure. The product was isolated *via* column chromatography (cyclohexane/ethyl acetate 30:1). Obtained as a colorless solid in a yield of 79% (117 mg, 0.395 mmol).

^{1}H NMR (400 MHz, DMSO-d_6) δ/ppm = 7.04 – 6.96 (m, 4H), 6.90 – 6.80 (m, 4H), 3.72 (s, 6H), 2.06 (q, J = 7.4 Hz, 4H), 0.97 (t, J = 7.4 Hz, 6H).

^{13}C NMR (101 MHz, DMSO-d_6) δ/ppm = 157.94, 140.99, 136.53, 136.04, 130.29, 113.93, 55.41, 24.43, 13.72.

IR (ATR platinum diamond): $\tilde{\nu}/cm^{-1}$ = 3026 (vw), 3013 (vw), 2964 (w), 2931 (w), 2869 (w), 2841 (w), 1604 (m), 1574 (w), 1506 (vs), 1467 (m), 1454 (m), 1444 (m), 1378 (w), 1329 (w), 1302 (w), 1273 (m), 1261 (m), 1234 (vs), 1174 (vs), 1152 (w), 1107 (w), 1092 (w), 1031 (vs), 897 (w), 833 (vs), 825 (vs), 812 (vs), 792 (w), 780 (w), 730 (w), 634 (w), 621 (w), 578 (s), 570 (s), 551 (m), 522 (m).

ESI-HRMS m/z: $[M+H]^+$ calculated for $C_{20}H_{24}O_2$ = 297.1850, found 297.1847.

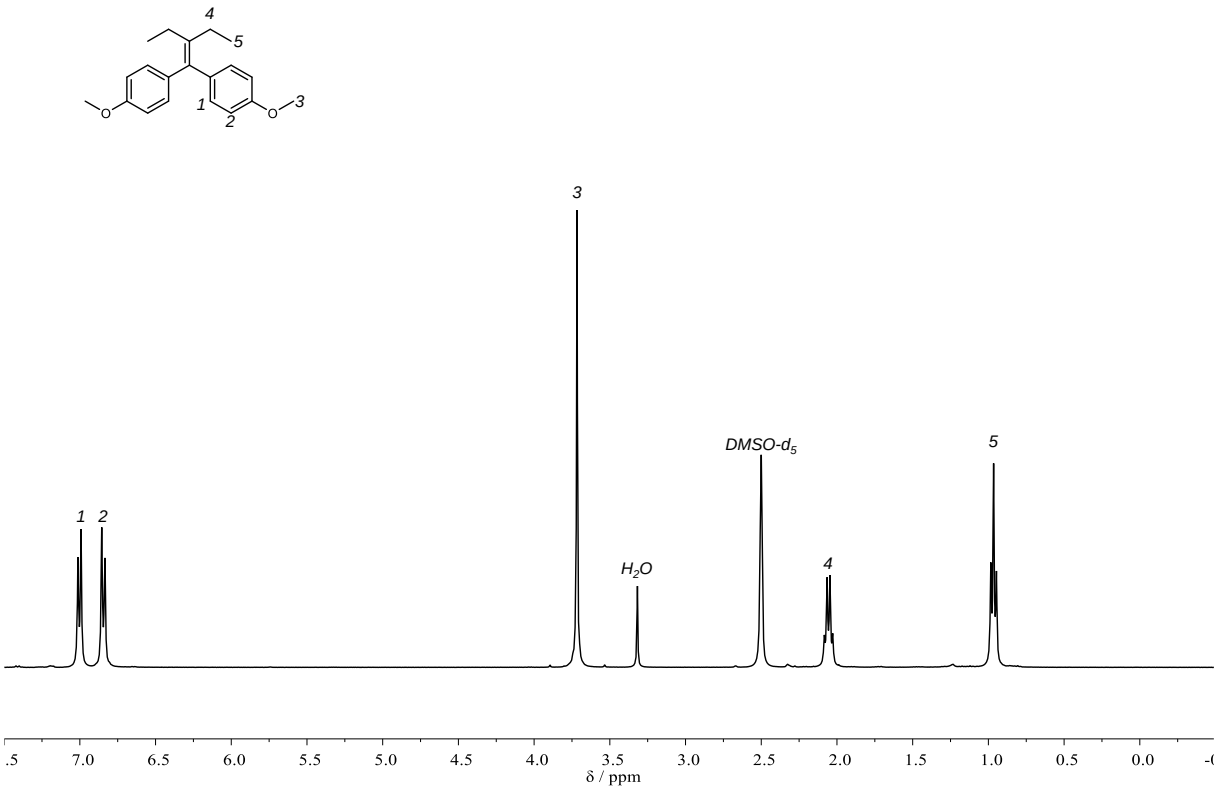

*Supplementary Figure 45: [1]H NMR spectrum of **5f** in DMSO-d6.*

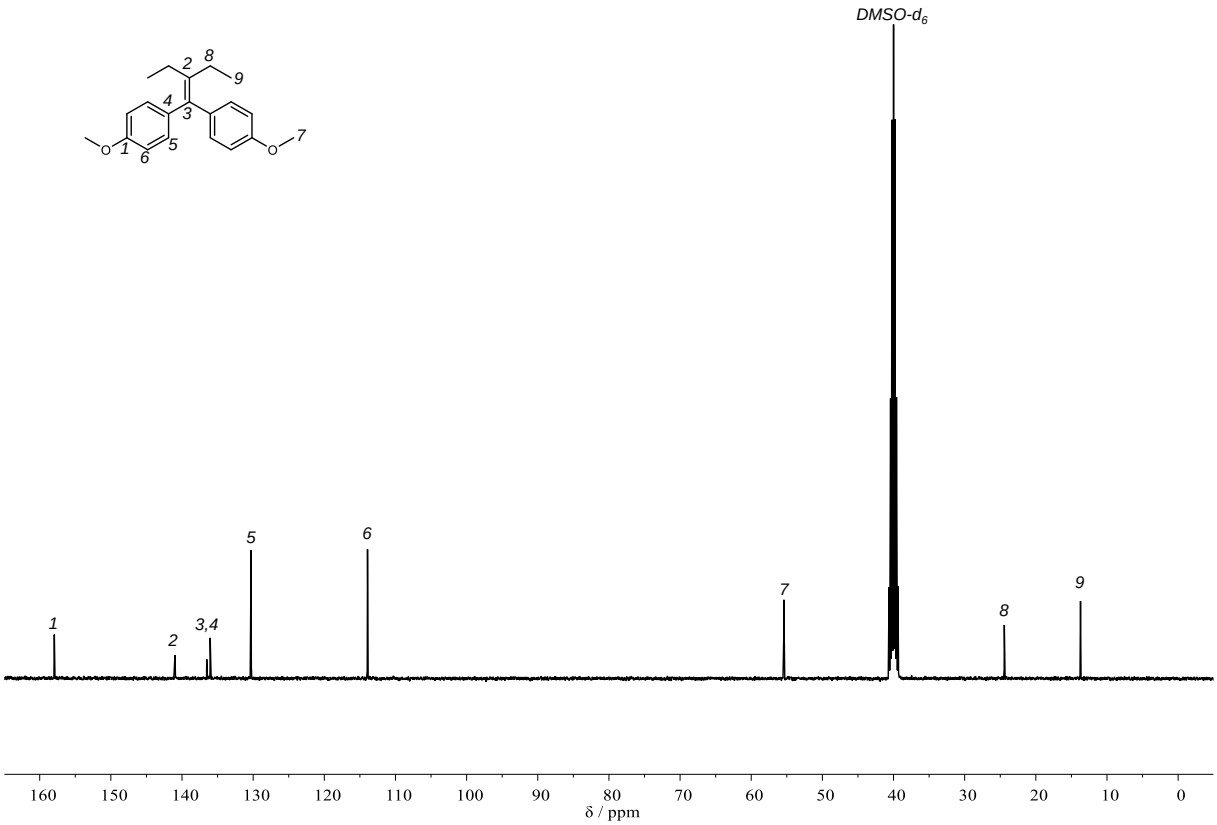

*Supplementary Figure 46: [13]C NMR spectrum of **5f** in DMSO-d6.*

9-(4,4'-Dimethoxybenzhydrylidene)thioxanthene (5g)

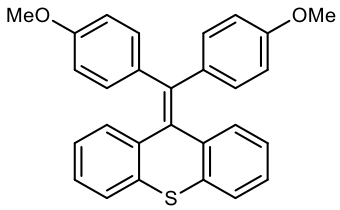

Prepared from NTH **1a** and thioketone **3b** according to general procedure. The product was isolated *via* column chromatography (cyclohexane/ethyl acetate 30:1). Obtained as a colorless solid in a yield of 95% (200 mg, 0.474 mmol).

^{1}H NMR (400 MHz, DMSO-d_6) δ/ppm = 7.54 – 7.47 (m, 2H), 7.16 – 7.04 (m, 8H), 7.01 – 6.94 (m, 2H), 6.80 – 6.72 (m, 4H), 3.67 (s, 6H).

^{13}C NMR (101 MHz, DMSO-d_6) δ/ppm = 158.25, 142.26, 137.13, 134.60, 134.48, 134.27, 130.84, 129.88, 127.00, 126.92, 126.35, 113.95, 55.43.

IR (ATR platinum diamond): $\tilde{\nu}/cm^{-1}$ = 3055 (vw), 2999 (vw), 2950 (vw), 2927 (w), 2902 (vw), 2834 (w), 1602 (m), 1571 (w), 1506 (vs), 1456 (m), 1436 (m), 1286 (m), 1267 (w), 1240 (vs), 1172 (vs), 1144 (w), 1109 (w), 1065 (w), 1031 (vs), 973 (w), 940 (w), 852 (vw), 821 (s), 769 (vs), 743 (vs), 736 (vs), 699 (w), 654 (w), 592 (m), 580 (m), 547 (m), 525 (w), 450 (w).

ESI-HRMS m/z: $[M]^+$ calculated for $C_{28}H_{22}O_2S$ = 422.1336, found 422.1332.

Fluorescence: λ_{em}(max) = 448 nm with λ_{ex} = 328 nm

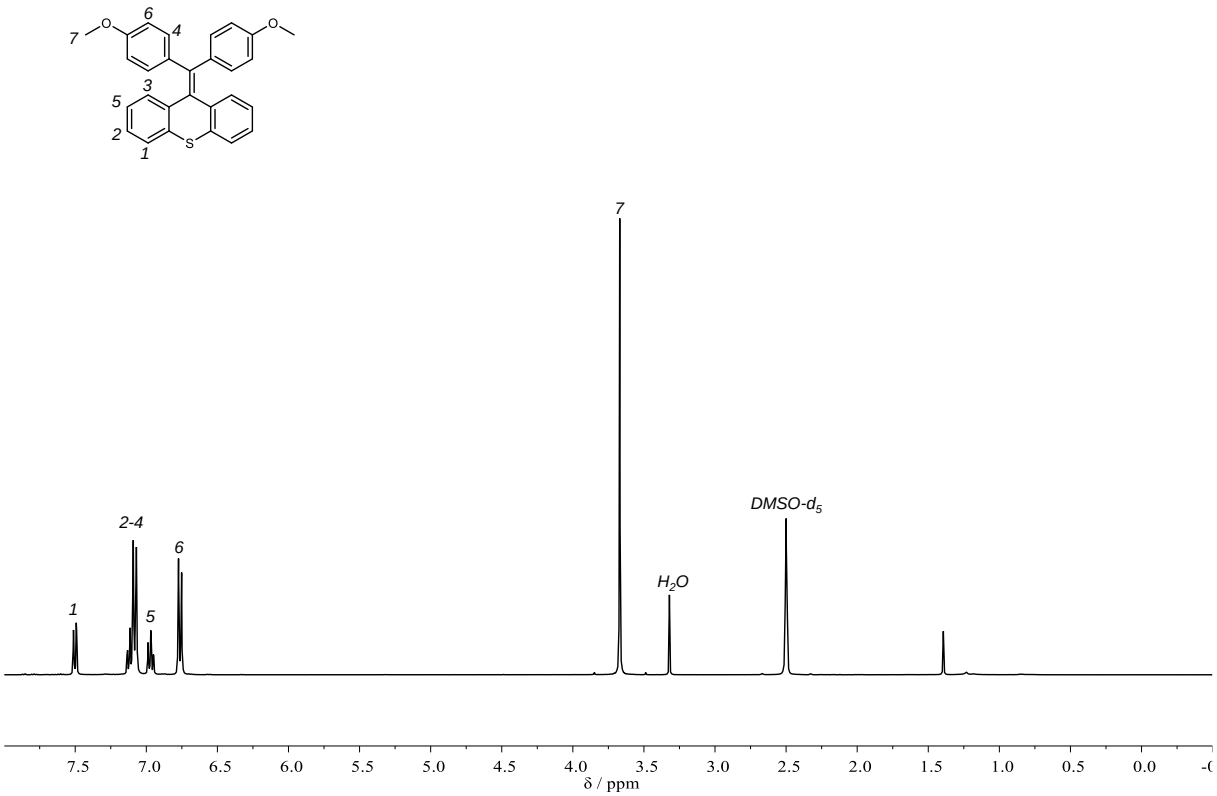

*Supplementary Figure 47: ^{1}H NMR spectrum of **5g** in DMSO-d_6.*

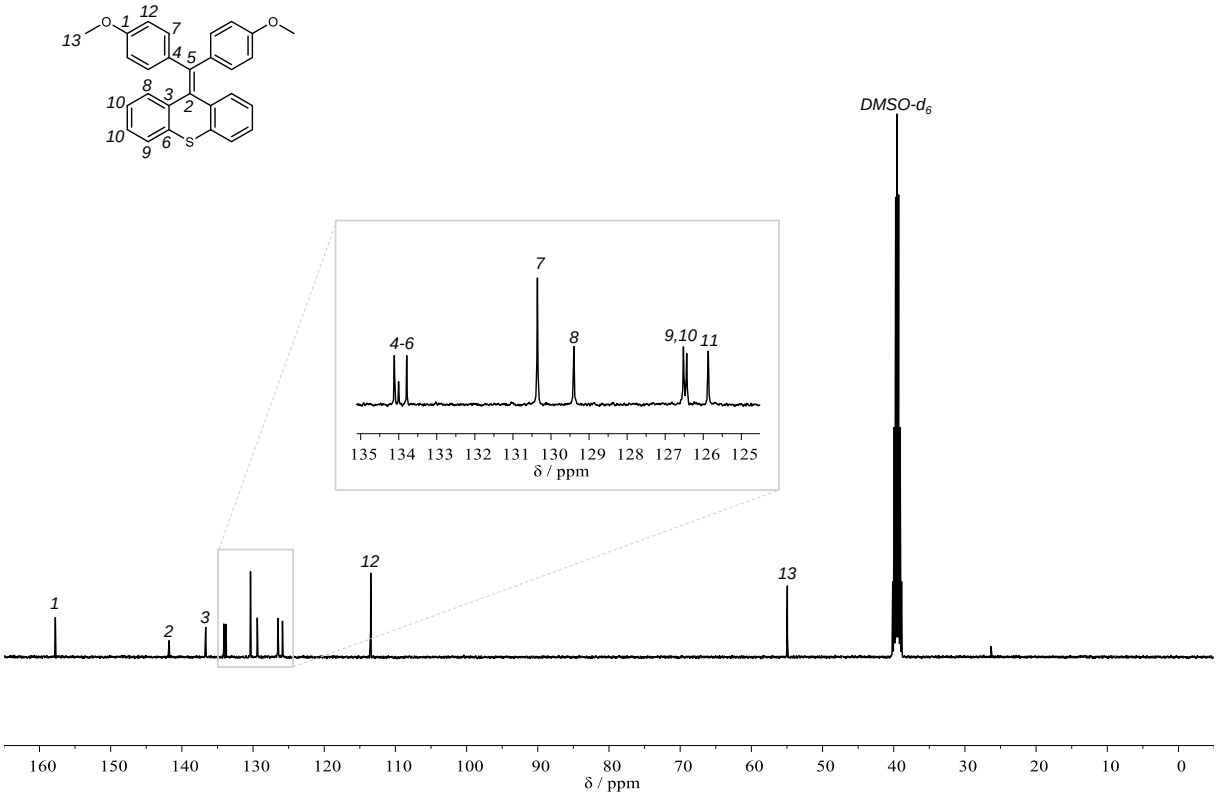

*Supplementary Figure 48: ^{13}C NMR spectrum of **5g** in DMSO-d_6.*

9-Benzhydrylidenethioxanthene (5h)

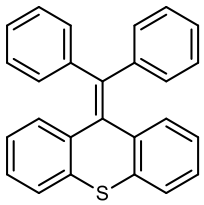

Prepared from NTH **1b** and thioketone **3b** according to general procedure. The product was isolated *via* column chromatography (cyclohexane/ethyl acetate 30:1). Obtained as a colorless solid in a yield of 99% (179 mg, 0.494 mmol).

^{1}H NMR (400 MHz, DMSO-d_6) δ/ppm = 7.54 – 7.50 (m, 2H), 7.25 – 7.18 (m, 8H), 7.17 – 7.09 (m, 4H), 7.08 – 7.04 (m, 2H), 6.96 – 6.90 (m, 2H).

^{13}C NMR (101 MHz, DMSO-d_6) δ/ppm = 142.96, 142.10, 136.59, 134.84, 134.19, 129.84, 129.56, 128.64, 127.17, 127.10, 126.97, 126.31.

IR (ATR platinum diamond): $\tilde{\nu}/cm^{-1}$ = 3044 (vw), 3020 (vw), 2962 (vw), 2921 (w), 2855 (vw), 1738 (w), 1594 (w), 1574 (w), 1555 (w), 1489 (w), 1454 (w), 1438 (s), 1316 (w), 1263 (w), 1240 (w), 1212 (w), 1162 (w), 1156 (w), 1117 (w), 1078 (w), 1065 (w), 1026 (m), 1002 (w), 981 (w), 973 (w), 944 (w), 919 (w), 903 (w), 868 (w), 761 (vs), 755 (vs), 745 (vs), 701 (vs), 631 (m), 613 (s), 580 (m), 539 (m), 518 (w), 485 (w), 475 (w), 448 (w), 409 (w).

ESI-HRMS m/z: $[M]^+$ calculated for $C_{26}H_{18}S$ = 362.1124, found 362.1121.

Fluorescence: λ_{em}(max) = 421 nm with λ_{ex} = 322 nm.

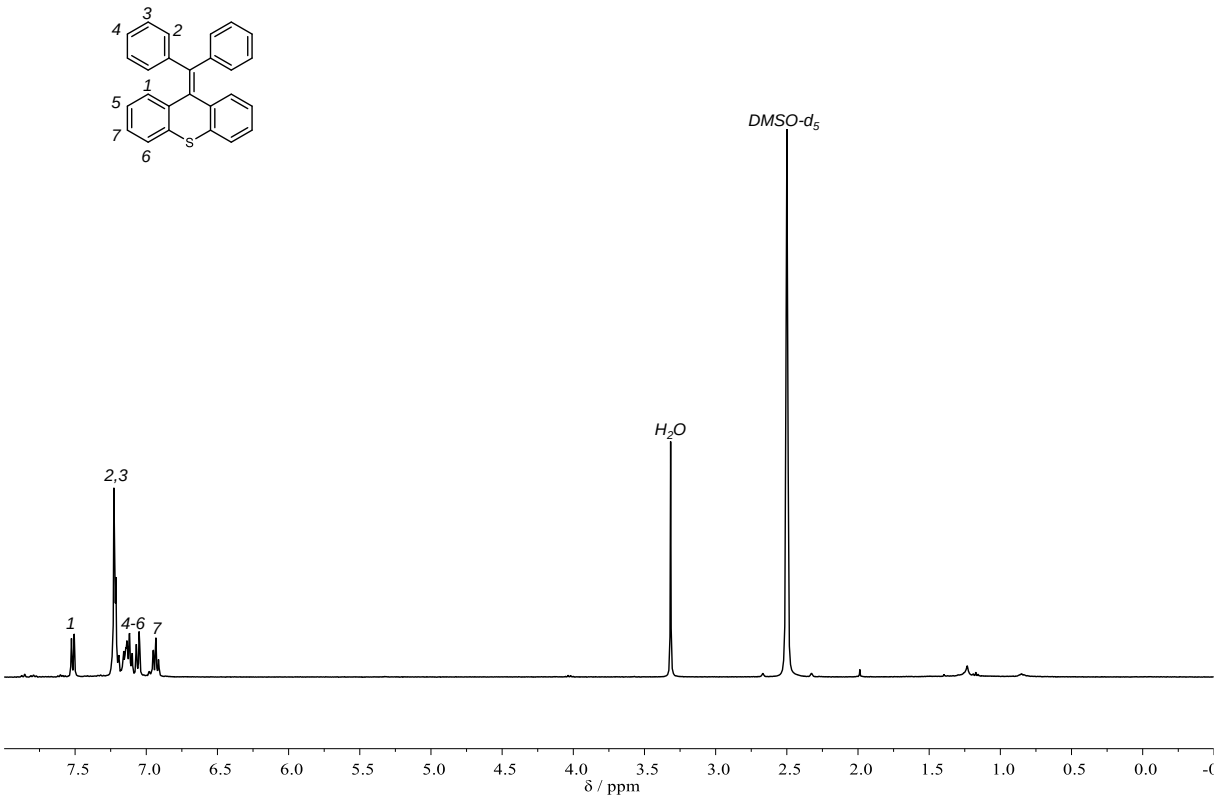

*Supplementary Figure 49: [1]H NMR spectrum of **5h** in DMSO-d6.*

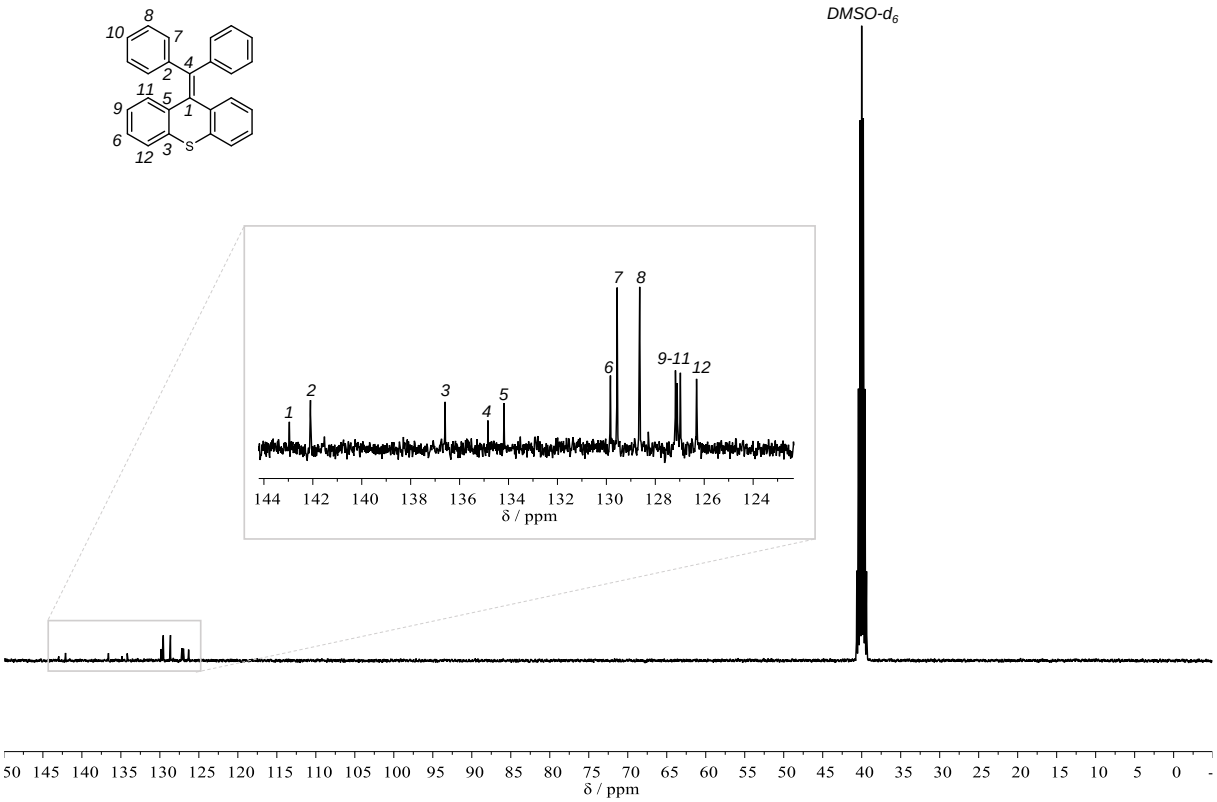

*Supplementary Figure 50: [13]C NMR spectrum of **5h** in DMSO-d6.*

1,1-bis(4-bromophenyl)-2,2-diphenylethylene (5i)

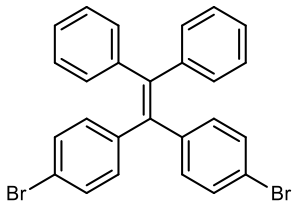

Prepared from NTH **1b** and thioketone **3c** according to general procedure. The product was isolated *via* column chromatography (cyclohexane/ethyl acetate 30:1). Obtained as a colorless solid in a yield of 99% (220 mg, 0.494 mmol).

^{1}H NMR (400 MHz, DMSO-d_6) δ/ppm = 7.38 – 7.29 (m, 4H), 7.22 – 7.10 (m, 6H), 7.02 – 6.95 (m, 4H), 6.94 – 6.88 (m, 4H).

^{13}C NMR (101 MHz, DMSO-d_6) δ/ppm =143.05, 142.45, 142.37, 138.56, 133.26, 131.40, 131.01, 128.50, 127.44, 120.45.

IR (ATR platinum diamond): $\tilde{\nu}/cm^{-1}$ = 3052 (vw), 3026 (vw), 2923 (vw), 2853 (vw), 1660 (vw), 1586 (w), 1487 (m), 1442 (w), 1390 (w), 1275 (vw), 1179 (vw), 1105 (w), 1070 (m), 1028 (vw), 1010 (s), 971 (w), 924 (vw), 864 (vw), 831 (s), 810 (w), 767 (m), 757 (s), 726 (w), 697 (vs), 673 (w), 638 (w), 623 (w), 617 (w), 570 (w), 485 (m), 455 (w).

EI-HRMS m/z: $[M]^+$ calculated for $C_{26}H_{18}{}^{79}Br^{81}Br$ = 489.9749, found 489.9751.

Fluorescence: λ_{em}(max) = 476 nm with λ_{ex} = 313 nm.

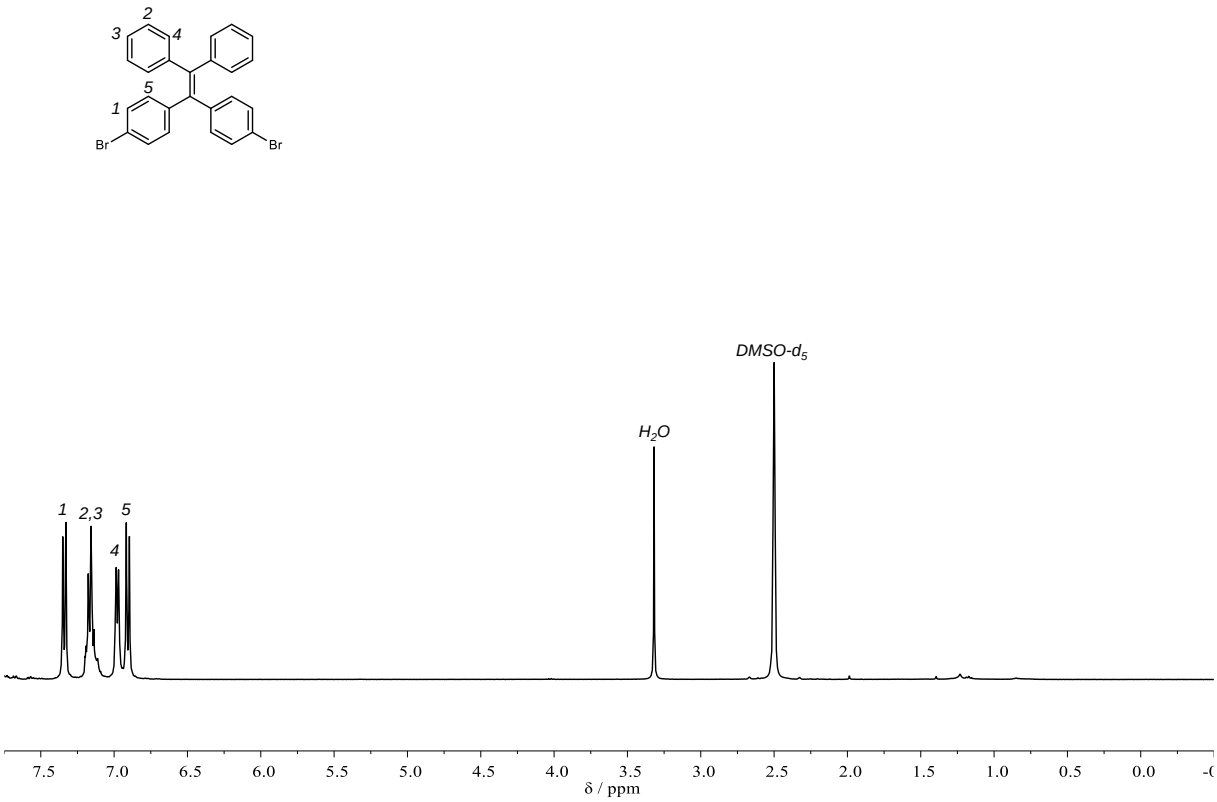

*Supplementary Figure 51: [1]H NMR spectrum of **5i** in DMSO-d6.*

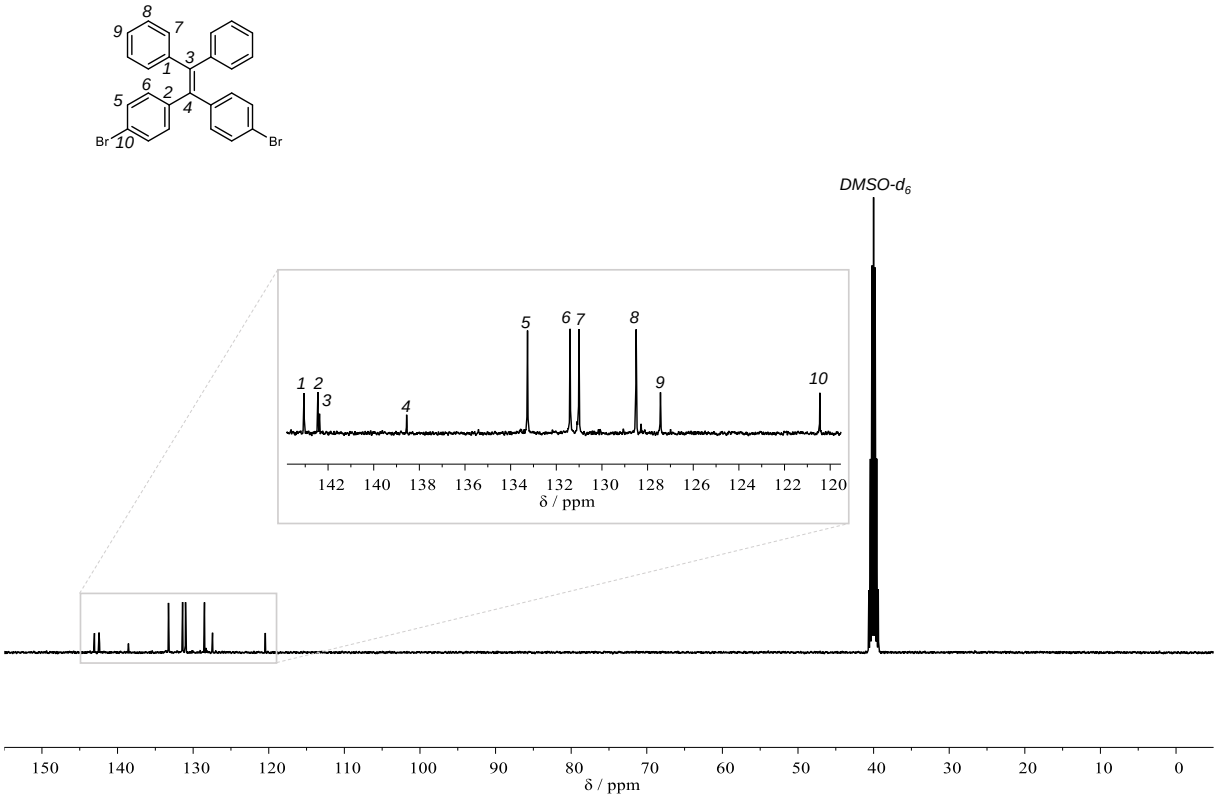

*Supplementary Figure 52: [13]C NMR spectrum of **5i** in DMSO-d6.*

6.3.2 Sulfur-mediated Polyolefination – Chapter 4.2

6.3.2.1 Synthesis of diketones

Disclaimer

The procedures for diketone synthesis were adapted from Carreira *et al*.[445]

6c-6f were synthesized by Sophia Abou el Mirate under supervision of the author.

6h was synthesized by Philipp Mehr under supervision of the author.

4,4'-dimethoxyterephthalophenone (6a)

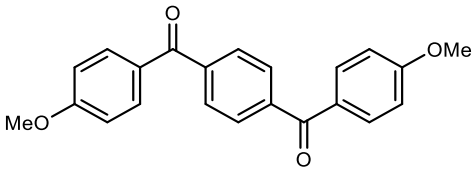

In a Schlenk flask under argon atmosphere, terephthaloyl chloride (5.00 g, 24.6 mmol, 1.00 equiv.) was suspended in anisole (53.3 g, 53.8 mL, 493 mmol, 20.0 equiv.). The mixture was placed in an ice bath and aluminium chloride (7.88 g, 59.1 mmol, 2.40 equiv.) was added in small portions. The mixture was stirred at room temperature for 16 hours. The crude mixture was subsequently poured onto ice. The precipitate was filtered, washed twice with 10% NaOH, once with water, once more with EtOH and dried *in vacuo*. **6a** was obtained as a light pink solid in a yield of 77% (6.58 g, 19.0 mmol).

^{1}H NMR (500 MHz, Chloroform-*d*): δ/ppm = 7.82 – 7.78 (m, 4H), 7.76 (s, 4H), 6.95 – 6.89 (m, 4H), 3.84 (s, 6H).

^{13}C NMR (126 MHz, Chloroform-*d*): δ/ppm = 195.02, 163.76, 141.21, 132.81, 129.81, 129.51, 113.91, 55.71.

IR (ATR platinum diamond): $\tilde{\nu}/cm^{-1}$ = 3069 (vw), 3061 (vw), 2976 (vw), 2950 (vw), 2925 (vw), 2843 (vw), 1639 (s), 1594 (s), 1510 (m), 1493 (w), 1469 (w), 1458 (w), 1440 (w), 1421 (vw), 1397 (w), 1341 (w), 1318 (s), 1302 (m), 1277 (m), 1261 (vs), 1195 (m), 1177 (s), 1154 (s), 1113 (m), 1082 (vw), 1016 (s), 977 (vw), 969 (w), 928 (s), 860 (m), 845 (s), 839 (m), 821 (w), 796 (m), 749 (s), 691 (s), 638 (w), 627 (m), 578 (m), 522 (w), 514 (w), 434 (m), 416 (w), 405 (w).

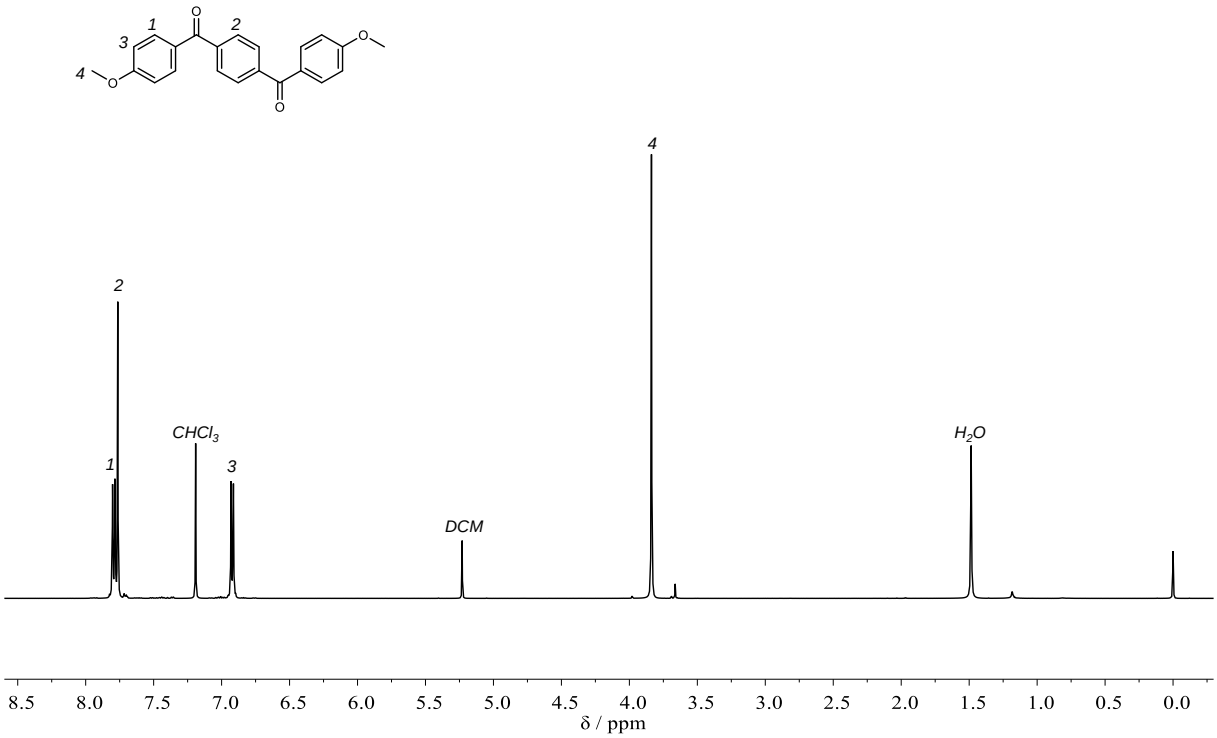

*Supplementary Figure 53: ^{1}H NMR spectrum of **6a** in $CDCl_3$.*

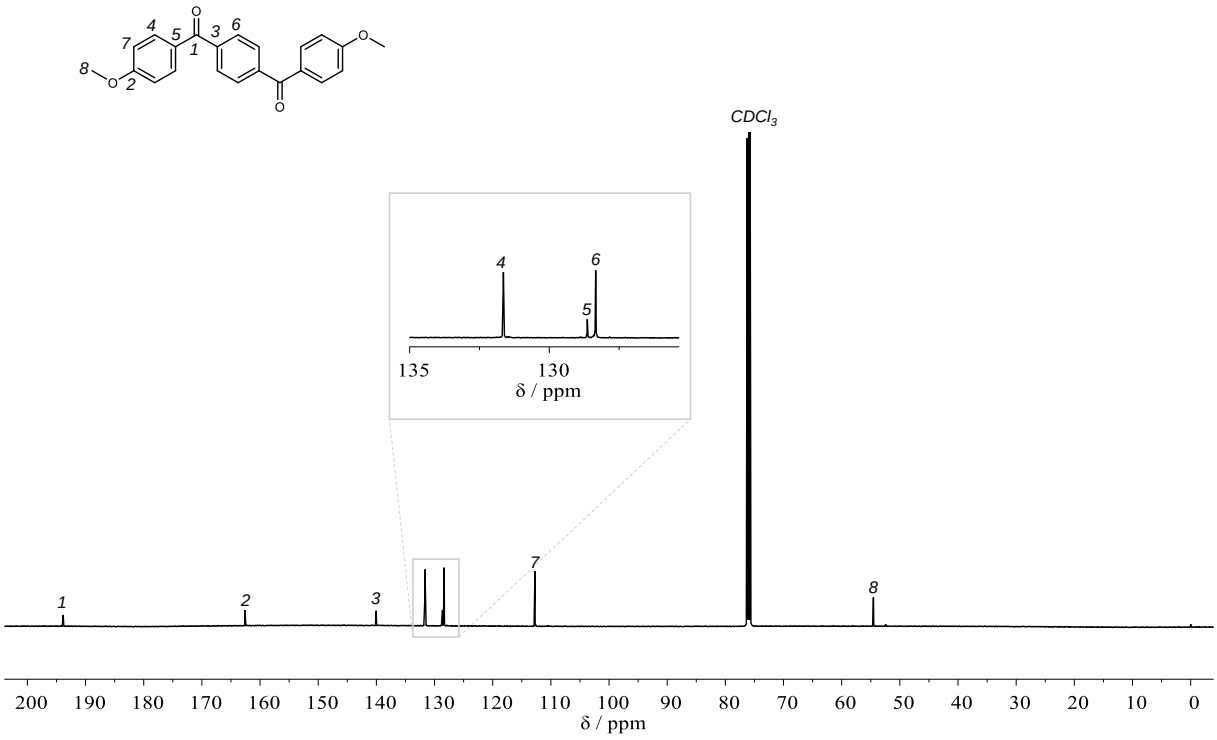

*Supplementary Figure 54 ^{13}C NMR spectrum of **6a** in $CDCl_3$.*

Terephthalophenone (6b)

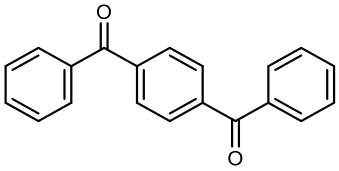

In a Schlenk flask under argon atmosphere, terephthaloyl chloride (2.00 g, 9,85 mmol, 1.00 equiv.) was suspended in benzene (17.5 mL, 15.4 g, 197 mmol, 20.0 equiv.). The mixture was placed in a water bath and aluminium chloride (2.89 g, 21.7 mmol, 2.20 equiv.) was added in small portions. The mixture was stirred at room temperature for 16 hours. The crude mixture was subsequently poured onto ice. The precipitate was filtered, washed twice with 10% NaOH, once with water, once more with EtOH and dried *in vacuo*. **6b** was obtained as a white solid in a yield of 73% (2.06 g, 7.21 mmol).

^{1}H NMR (500 MHz, Chloroform-*d*): δ/ppm = 7.89 (s, 4H), 7.86 – 7.82 (m, 4H), 7.65 – 7.60 (m, 2H), 7.51 (t, *J* = 7.8 Hz, 4H).

^{13}C NMR (126 MHz, Chloroform-*d*): δ/ppm = 196.14, 140.78, 137.08, 133.09, 130.25, 129.86, 128.61.

IR (ATR platinum diamond): $\tilde{\nu}/cm^{-1}$ = 1654 (s), 1594 (m), 1576 (w), 1539 (w), 1500 (w), 1446 (w), 1401 (w), 1382 (w), 1310 (m), 1288 (w), 1263 (m), 1203 (w), 1181 (m), 1156 (m), 1109 (w), 1086 (w), 1074 (w), 1022 (w), 998 (w), 977 (w), 969 (w), 938 (m), 922 (m), 856 (m), 847 (m), 782 (m), 732 (w), 706 (s), 691 (vs), 675 (s), 619 (w), 584 (m), 522 (w), 465 (m), 450 (m), 418 (w).

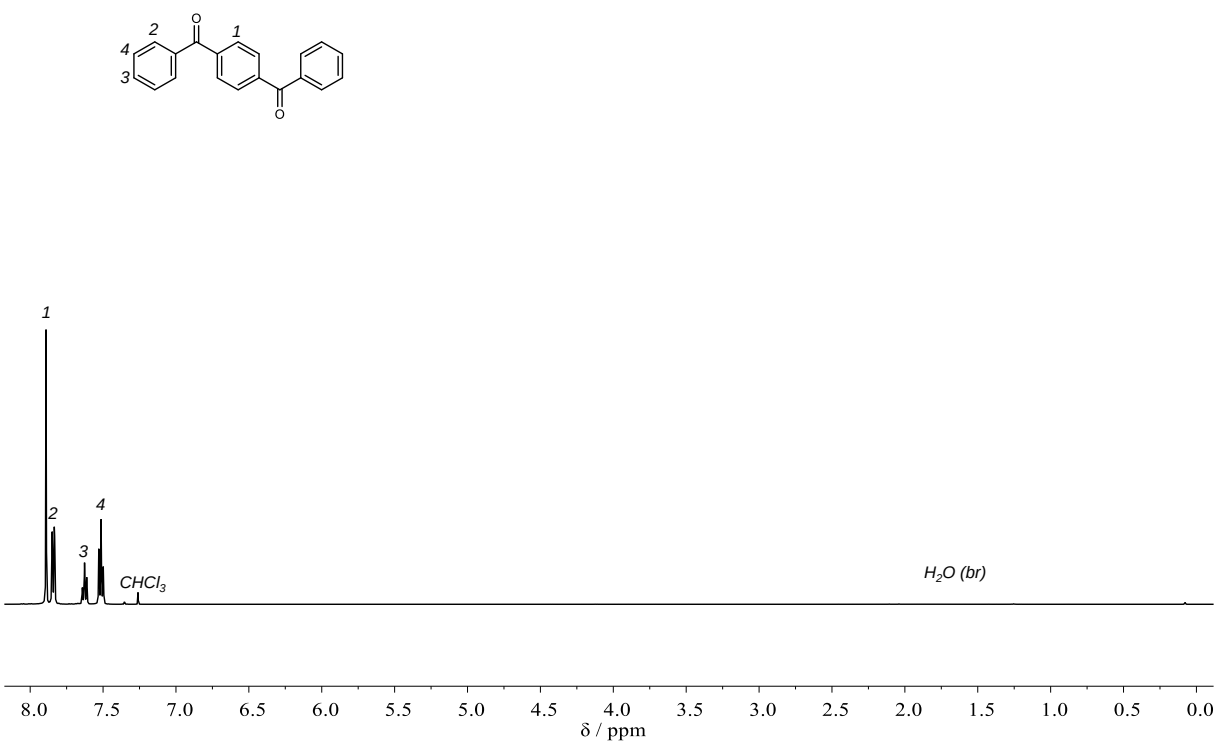

*Supplementary Figure 55 ^{1}H NMR spectrum of **6b** in $CDCl_3$.*

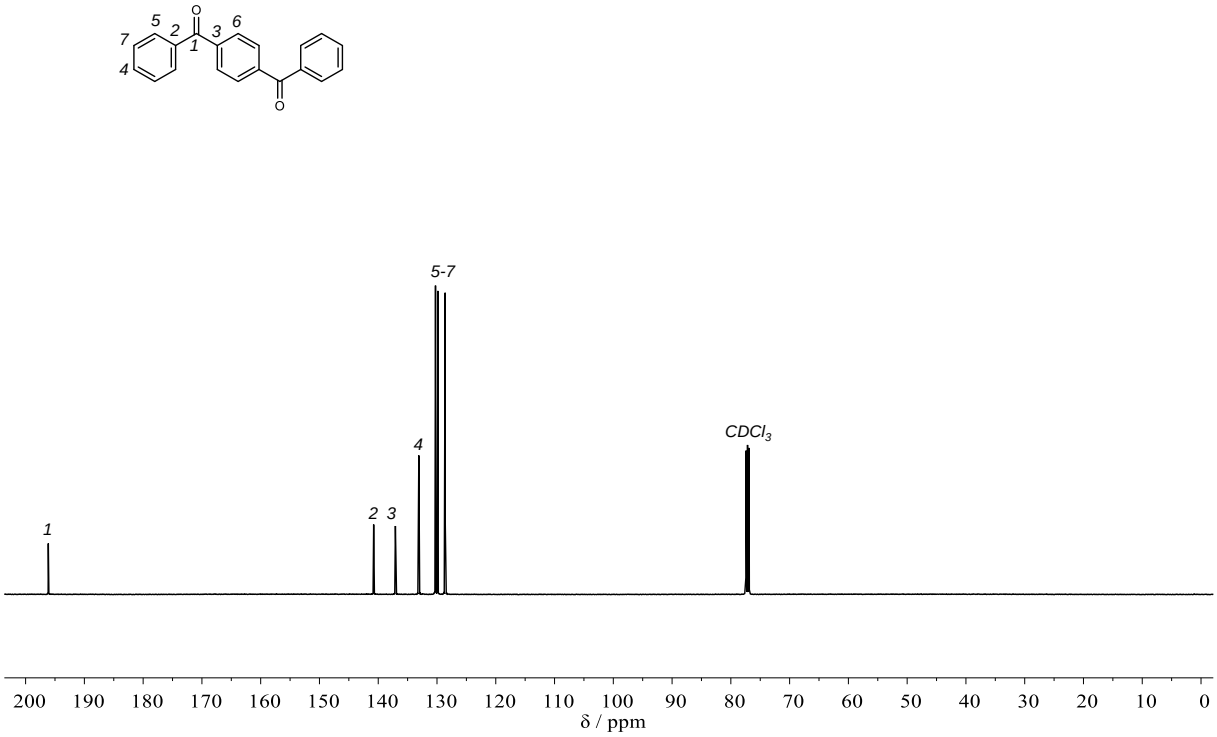

*Supplementary Figure 56 ^{13}C NMR spectrum of **6b** in $CDCl_3$.*

4,4'-Diphenoxyterephthalophenone (6c)

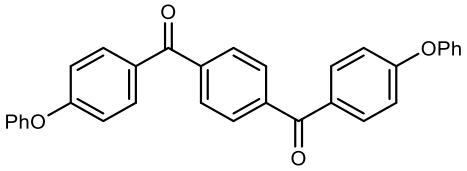

In a Schlenk flask under argon atmosphere, terephthaloyl chloride (2.00 g, 9.85 mmol, 1.00 equiv.) was suspended in diphenyl ether (15.7 mmol, 16.8 g, 98.5 mmol, 10.0 equiv.). The mixture was placed in an ice bath and aluminium chloride (2.89 g, 21.7 mmol, 2.20 equiv.) was added in small portions. The mixture was stirred at room temperature for 16 hours. The crude mixture was subsequently poured onto ice. The precipitate was filtered, washed twice with 10% NaOH, once with water, once more with EtOH and dried *in vacuo*. **6c** was obtained as a white solid in a yield of 65% (3.03 g, 6.44 mmol).

^{1}H NMR (400 MHz, Chloroform-*d*): δ/ppm = 7.85 (d, *J* = 8.0 Hz, 8H), 7.48 – 7.35 (m, 4H), 7.25 – 7.19 (m, 2H), 7.14 – 7.08 (m, 4H), 7.08 – 7.02 (m, 4H).

^{13}C NMR (101 MHz, Chloroform-*d*): δ/ppm = 194.88, 162.28, 155.48, 141.02, 132.72, 131.39, 130.26, 129.62, 124.93, 120.44, 117.34.

IR (ATR platinum diamond): $\tilde{\nu}/cm^{-1}$ = 3065 (vw), 3038 (vw), 1643 (s), 1586 (s), 1487 (m), 1454 (w), 1413 (w), 1401 (w), 1378 (w), 1304 (m), 1286 (m), 1251 (s), 1197 (m), 1152 (s), 1119 (m), 1109 (m), 1072 (m), 1016 (w), 1004 (w), 977 (w), 961 (w), 926 (m), 901 (m), 872 (m), 864 (m), 839 (s), 829 (m), 792 (m), 743 (vs), 687 (vs), 658 (m), 638 (w), 611 (w), 597 (w), 570 (w), 508 (m), 500 (m), 492 (m), 465 (w), 432 (w), 409 (vw).

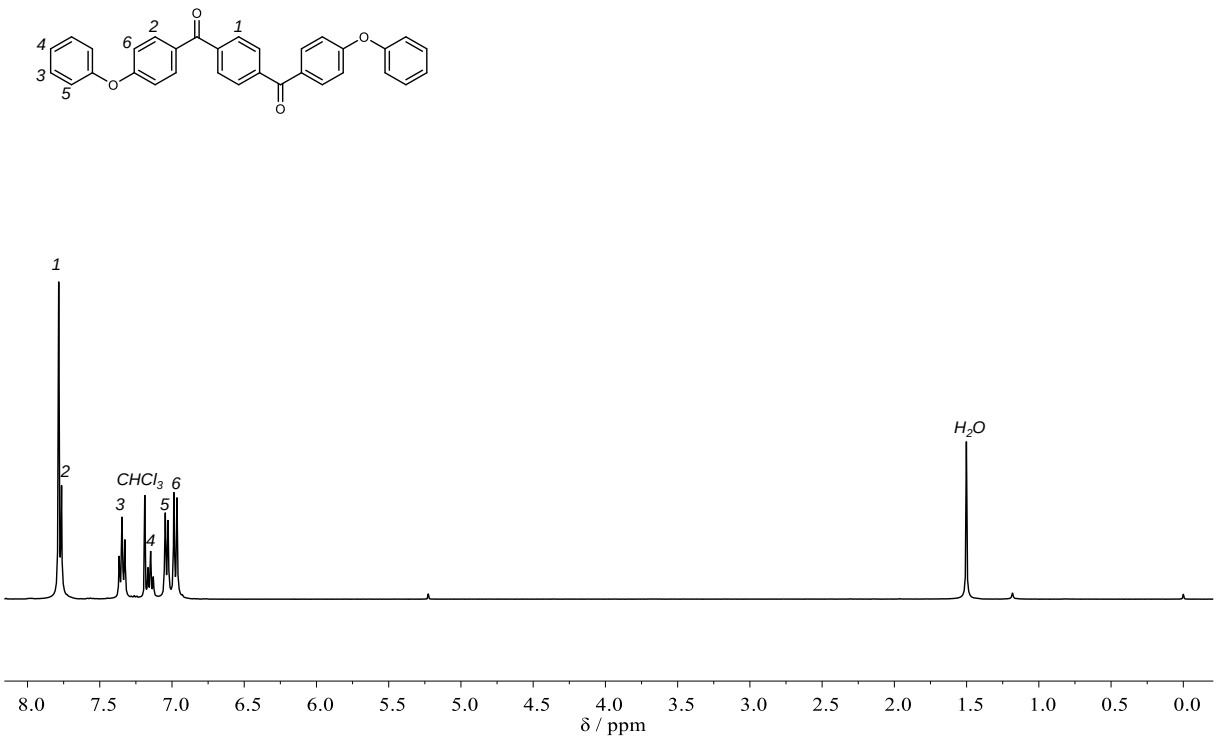

*Supplementary Figure 57 ^{1}H NMR spectrum of **6c** in $CDCl_3$.*

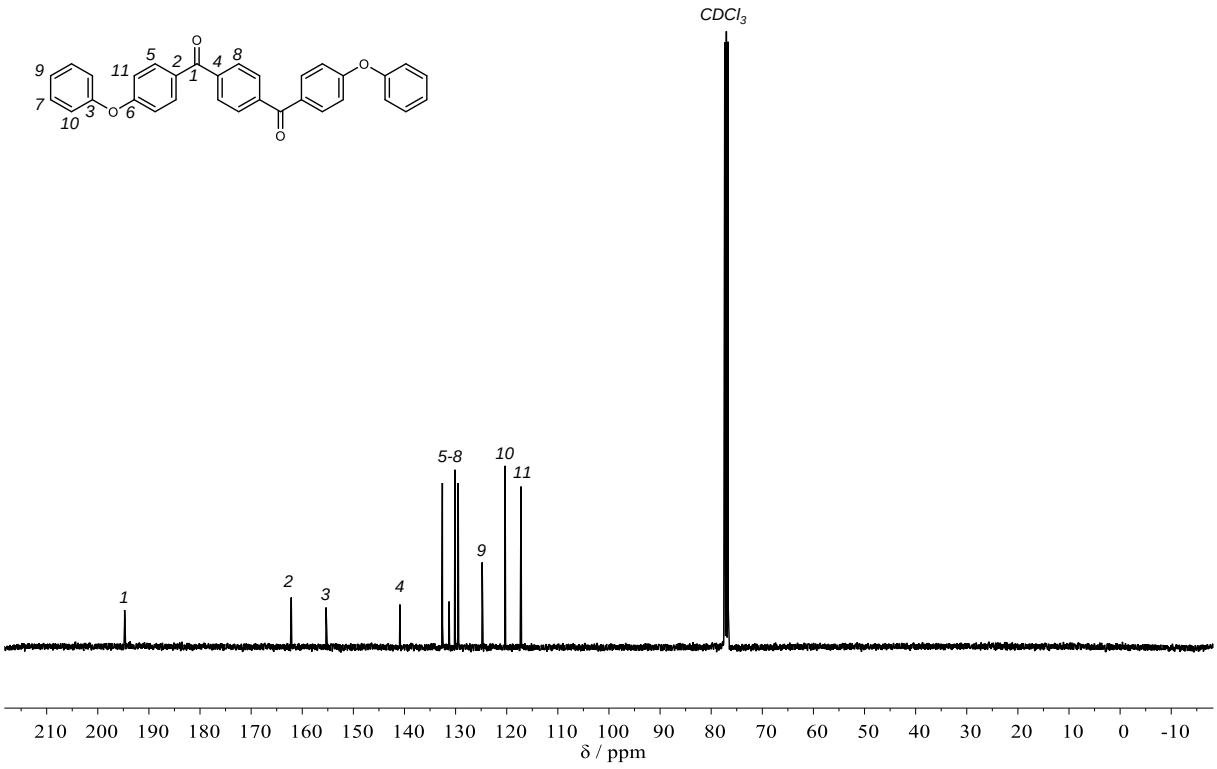

*Supplementary Figure 58 ^{13}C NMR spectrum of **6c** in $CDCl_3$.*

4,4'-Bis(phenylthio)terephthalophenone (6d)

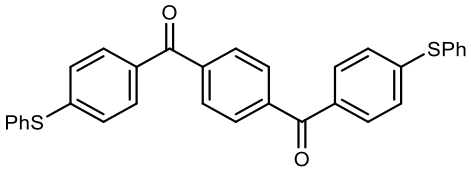

In a Schlenk flask under argon atmosphere, terephthaloyl chloride (1.00 g, 4.93 mmol, 1.00 equiv.) was suspended in diphenyl sulfide (8.34 mL, 9.78 g, 49.3 mmol, 10.0 equiv.). The mixture was placed in an ice bath and aluminium chloride 1.45 g (10.8 mmol, 2.20 g) was added in small portions. The mixture was stirred at room temperature for 16 hours. The crude mixture was subsequently poured onto ice. The precipitate was filtered, washed twice with 10% NaOH, once with water, once more with EtOH and dried *in vacuo*. **6d** was obtained as a white solid in a yield of 62% (1.52 g, 3.03 g).

^{1}H NMR (500 MHz, Chloroform-*d*): δ/ppm = 7.82 (s, 4H), 7.73 – 7.68 (m, 4H), 7.55 – 7.51 (m, 4H), 7.41 (m, 6H), 7.25 – 7.21 (m, 4H).

^{13}C NMR (126 MHz, Chloroform-*d*): δ/ppm = 195.13, 145.48, 140.82, 134.29, 134.13, 131.88, 130.93, 129.91, 129.68, 129.14, 127.27.

IR (ATR platinum diamond): $\tilde{\nu}/cm^{-1}$ = 3057 (vw), 1643 (s), 1586 (m), 1549 (w), 1497 (vw), 1485 (vw), 1475 (w), 1440 (w), 1399 (w), 1306 (m), 1273 (s), 1183 (w), 1156 (w), 1121 (vw), 1078 (m), 1022 (w), 1012 (w), 1000 (vw), 977 (vw), 963 (w), 924 (s), 860 (m), 841 (w), 827 (m), 749 (w), 734 (vs), 695 (w), 683 (vs), 631 (w), 617 (vw), 597 (vw), 516 (w), 498 (w), 483 (w), 422 (w), 411 (vw).

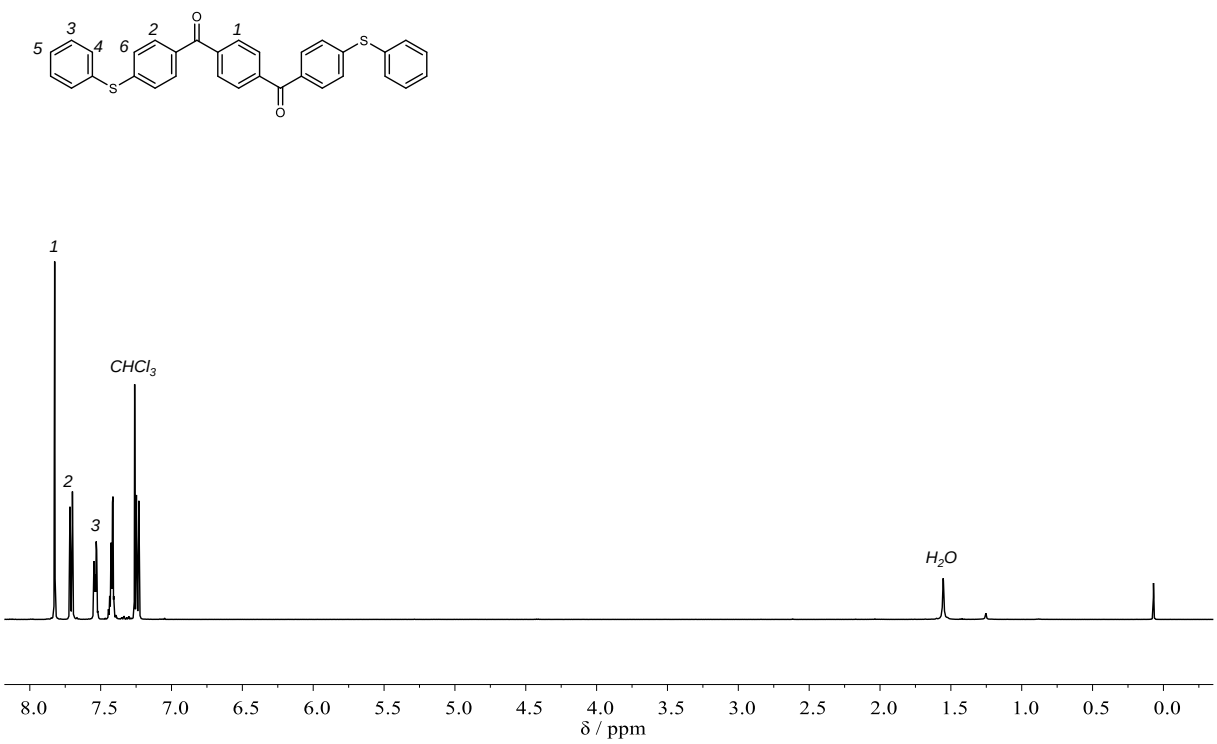

*Supplementary Figure 59 [1]H NMR spectrum of **6d** in $CDCl_3$.*

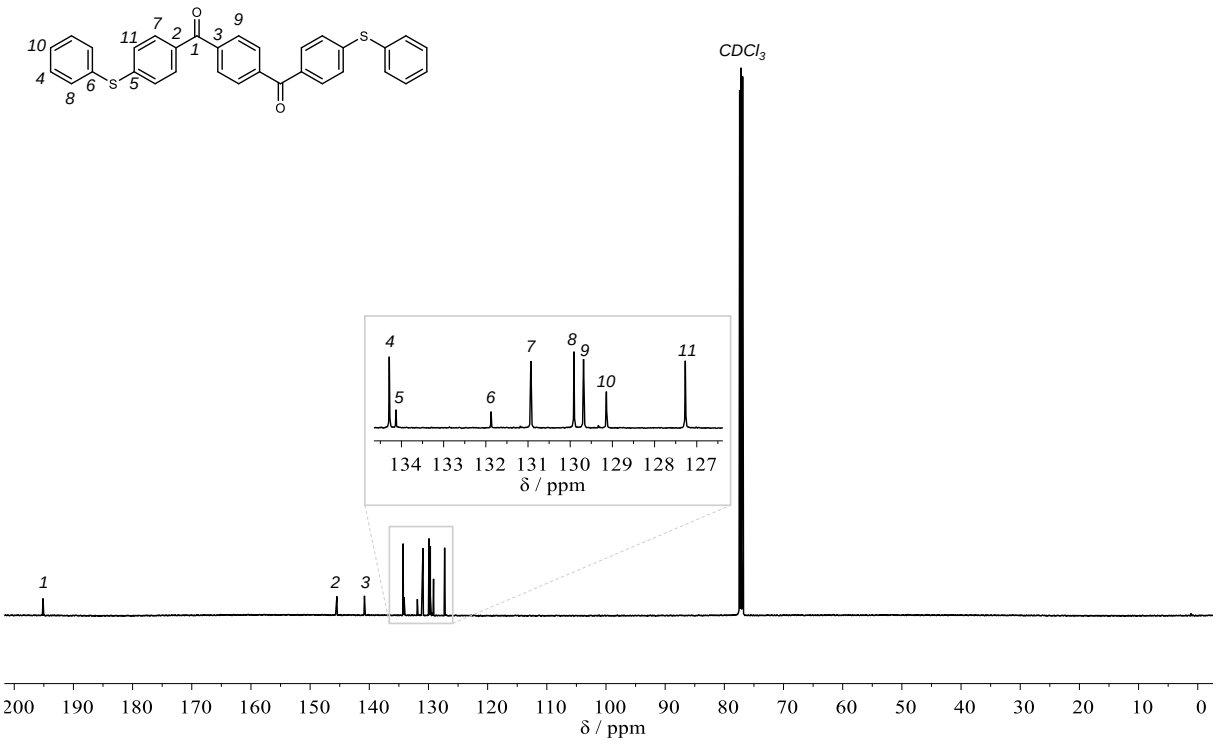

*Supplementary Figure 60 [13]C NMR spectrum of **6d** in $CDCl_3$.*

Isophthalophenone (6e)

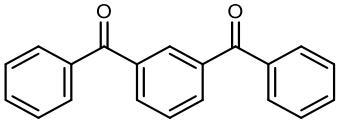

In a Schlenk flask under argon atmosphere, isophthaloyl chloride (2.00 g, 9.85 mmol, 1.00 equiv.) was suspended in benzene (17.5 mL, 15.4 g, 197 mmol, 20.0 equiv.). The mixture was placed in a water bath and aluminium chloride (2.89 g, 21.7 mmol, 2.20 equiv.) was added in small portions. The mixture was stirred at room temperature for 16 hours. The crude mixture was subsequently poured onto ice. The precipitate was filtered, washed twice with 10% NaOH, once with water, once more with EtOH and dried *in vacuo*. **6e** was obtained as a white solid in a yield of 83% (2.35 g, 8.20 mmol).

^{1}H NMR (400 MHz, Chloroform-*d*): δ/ppm = 8.21 – 8.17 (m, 1H), 8.03 (dd, *J* = 7.7, 1.8 Hz, 2H), 7.86 – 7.78 (m, 4H), 7.67 – 7.57 (m, 3H), 7.54 – 7.45 (m, 4H).

^{13}C NMR (101 MHz, Chloroform-*d*): δ/ppm = 195.94, 137.93, 137.11, 133.61, 133.01, 131.34, 130.21, 128.65, 128.61.

IR (ATR platinum diamond): $\tilde{\nu}/cm^{-1}$ = 3063 (vw), 3052 (vw), 3036 (vw), 3024 (vw), 2923 (vw), 1654 (s), 1594 (m), 1576 (m), 1514 (vw), 1467 (vw), 1444 (m), 1397 (vw), 1318 (w), 1310 (w), 1286 (m), 1265 (m), 1247 (m), 1166 (m), 1115 (m), 1076 (w), 1002 (m), 991 (m), 973 (w), 946 (w), 930 (w), 909 (w), 850 (vw), 821 (w), 798 (w), 778 (m), 757 (w), 689 (vs), 648 (m), 638 (m), 617 (w), 592 (w), 555 (w), 510 (vw), 446 (w), 438 (w), 420 (vw), 405 (vw).

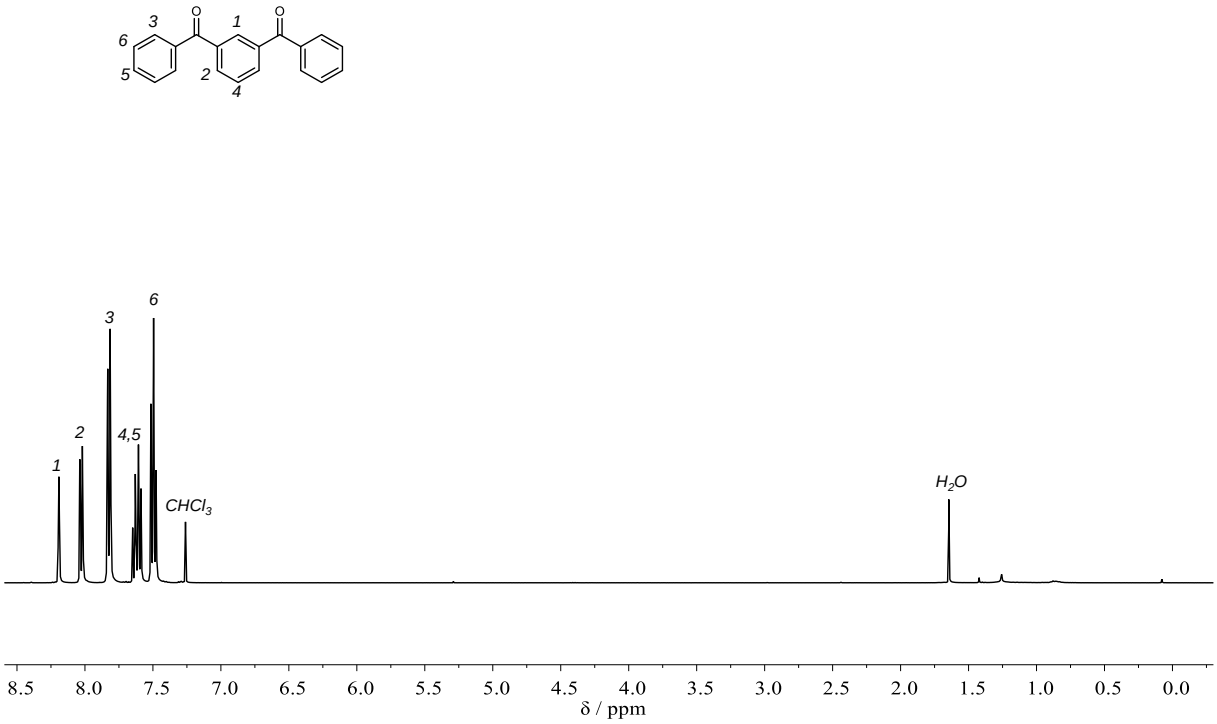

*Supplementary Figure 61 ^{1}H NMR spectrum of **6e** in $CDCl_3$.*

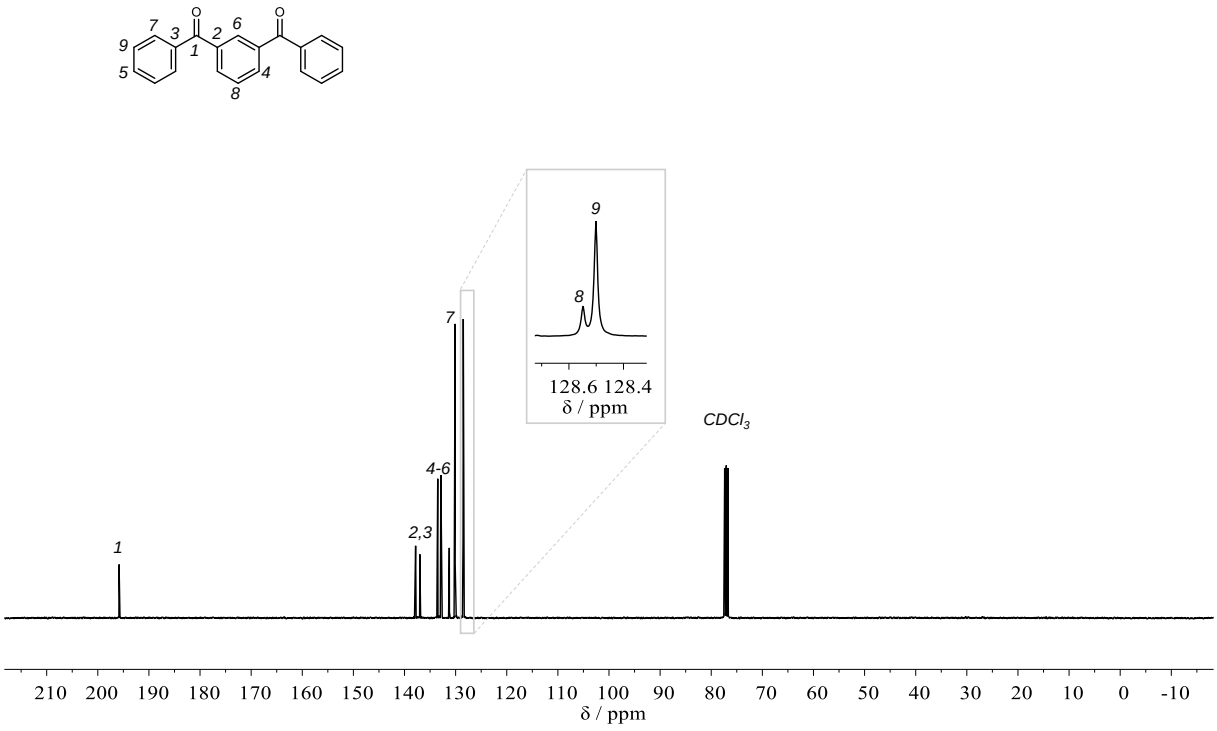

*Supplementary Figure 62 ^{13}C NMR spectrum of **6e** in $CDCl_3$.*

4,4'-Bis(benzoyl)biphenyl (6f)

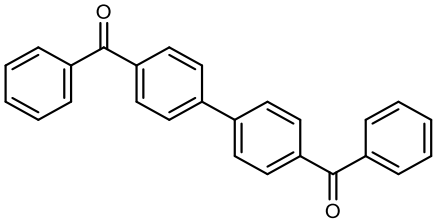

In a Schlenk flask under argon atmosphere, 4,4'-biphenyldicarboxylic acid (2.42 g, 9.99 mmol, 1.00 equiv.) was dissolved in 8 mL of dichloromethane and oxalyl chloride (2.23 mL, 3.30 mg, 26.0 mmol, 2.60 equiv.) was added. The mixture was stirred at room temperature for 30 minutes and then refluxed for 2 hours. Afterwards, the solvent was removed *in vacuo*. The residue was subsequently dissolved in benzene (17.9 mL, 15.6 g, 200 mmol, 20.0 equiv.). The mixture was placed in a water bath and aluminium chloride (2.93 g, 22.0 mmol, 2.20 equiv) was added in small portions. The mixture was stirred at room temperature for 16 hours. The crude mixture was subsequently poured onto ice. The precipitate was filtered, washed twice with 10% NaOH, once with water, once more with EtOH and dried *in vacuo*. **6f** was obtained as a white solid in a yield of 82% (2.96 mmol, 81.6 mmol).

^{1}H NMR (500 MHz, Chloroform-*d*): δ/ppm = 7.97 – 7.89 (m, 4H), 7.88 – 7.82 (m, 4H), 7.80 – 7.73 (m, 4H), 7.65 – 7.58 (m, 2H), 7.55 – 7.48 (m, 4H).

^{13}C NMR (126 MHz, Chloroform-*d*): δ/ppm = 196.32, 144.00, 137.68, 137.18, 132.68, 130.93, 130.16, 128.51, 127.32.

IR (ATR platinum diamond): $\tilde{\nu}/cm^{-1}$ = 3050 (vw), 3036 (vw), 1643 (s), 1602 (m), 1596 (m), 1578 (w), 1549 (w), 1491 (vw), 1444 (w), 1411 (vw), 1395 (w), 1380 (vw), 1368 (vw), 1331 (w), 1316 (w), 1306 (w), 1284 (m), 1179 (w), 1152 (w), 1111 (vw), 1074 (w), 1026 (w), 1000 (w), 987 (vw), 971 (w), 938 (m), 919 (m), 841 (m), 788 (m), 734 (m), 714 (m), 691 (vs), 644 (w), 636 (m), 617 (w), 566 (vw), 450 (w).

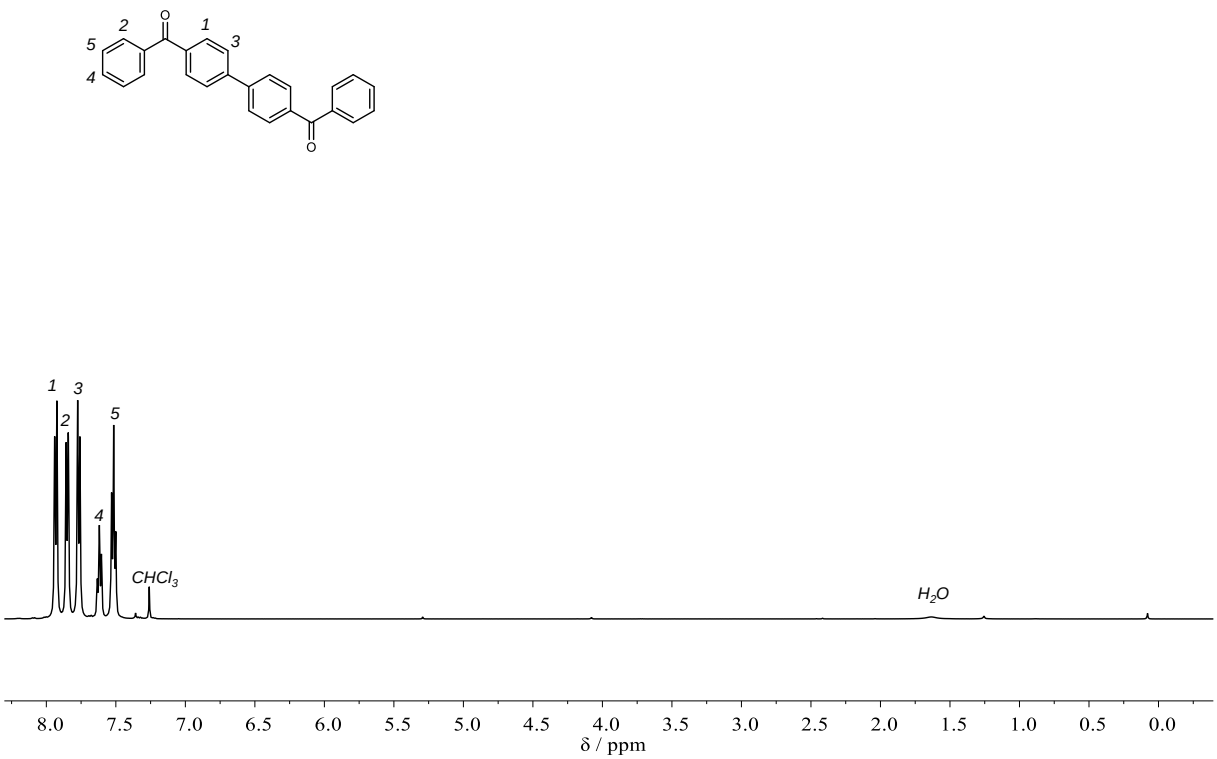

*Supplementary Figure 63 ^{1}H NMR spectrum of **6f** in $CDCl_3$.*

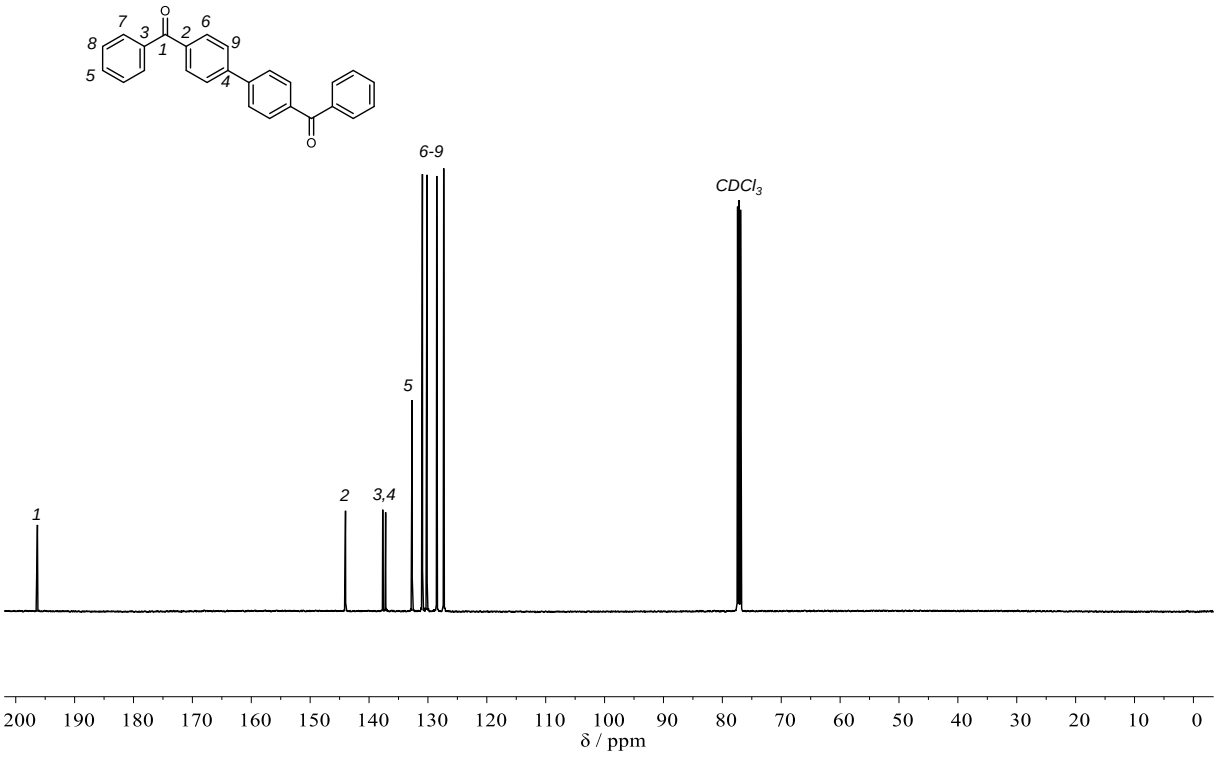

*Supplementary Figure 64 ^{13}C NMR spectrum of **6f** in $CDCl_3$.*

2,5-Bis(benzoyl)thiophene (6g)

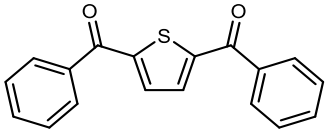

In a Schlenk flask under argon atmosphere, 2,5-thiophenedicarboxylic acid (2.00 g, 11.6 mmol, 1.00 equiv.) was dissolved in 20 mL dichloromethane and oxalyl chloride (2.59 mL, 3.83 g, 30.2 mmol, 2.60 equiv.) was added. The mixture was stirred at room temperature for 30 minutes and subsequently refluxed for 2 hours. Afterwards, the solvent was removed *in vacuo*. The residue was subsequently dissolved in in benzene (20.8 mL, 18.2 g., 232 mmol, 20.0 equiv.). The mixture was placed in a water bath and aluminium chloride (3.41 g, 25.6 mmol, 2.20 equiv.) was added in small portions. The mixture was stirred at room temperature for 16 hours. The crude mixture was subsequently poured onto ice. The precipitate was filtered, washed twice with 10% NaOH, once with water, once more with EtOH and dried *in vacuo*. **6g** was obtained as a white solid in a yield of 74% (2.50 g, 8.57 mmol).

^{1}H NMR (400 MHz, Chloroform-*d*): δ/ppm = 7.94 – 7.88 (m, 4H), 7.68 (s, 2H), 7.66 – 7.60 (m, 2H), 7.56 – 7.49 (m, 4H).

^{13}C NMR (101 MHz, Chloroform-*d*): δ/ppm = 195.83, 137.83, 137.00, 133.50, 132.90, 131.23, 130.10, 128.55, 128.50.

IR (ATR platinum diamond): $\tilde{\nu}/cm^{-1}$ = 3116 (vw), 3057 (vw), 1631 (s), 1596 (m), 1576 (m), 1512 (m), 1444 (m), 1405 (vw), 1345 (w), 1316 (m), 1286 (m), 1275 (m), 1253 (m), 1216 (m), 1203 (w), 1177 (w), 1127 (m), 1076 (m), 1059 (w), 1049 (w), 1022 (w), 1000 (w), 979 (vw), 969 (vw), 936 (vw), 928 (vw), 911 (w), 880 (m), 868 (w), 858 (w), 843 (w), 831 (w), 788 (w), 749 (vw), 716 (m), 701 (vs), 691 (s), 673 (s), 654 (m), 615 (w), 588 (w), 555 (w), 535 (w), 465 (w).

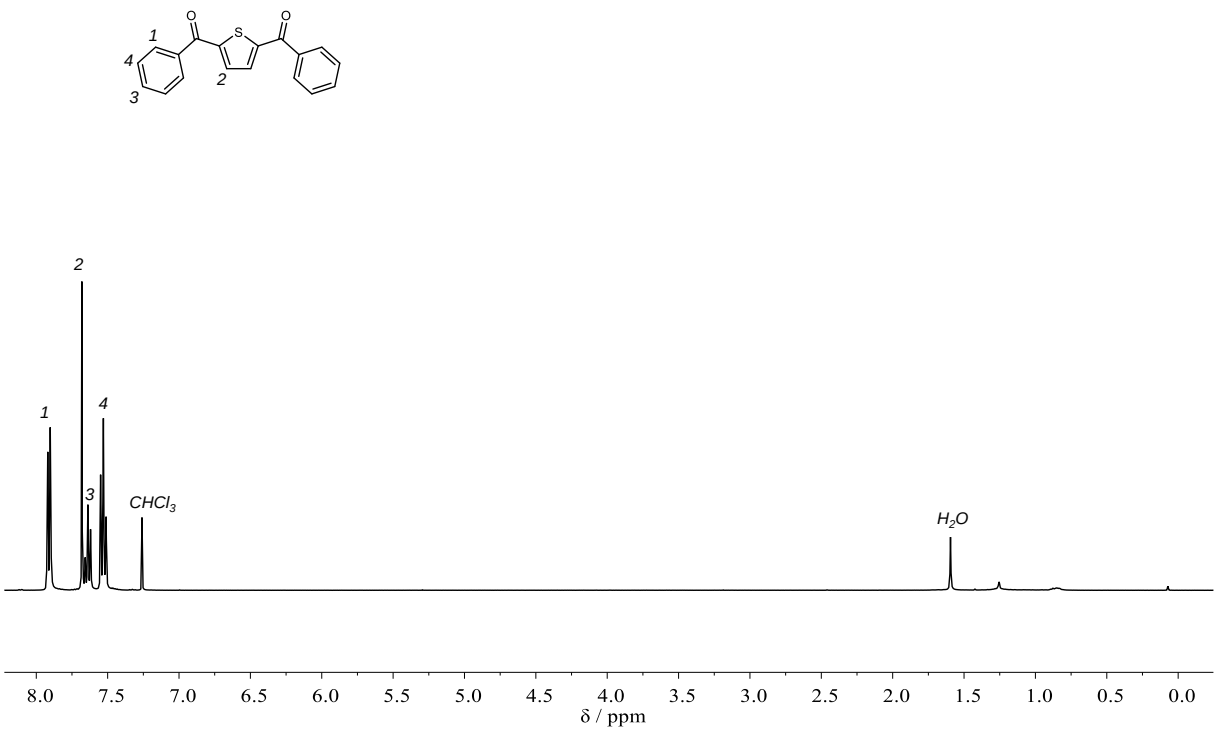

*Supplementary Figure 65 ^{1}H NMR spectrum of **6g** in $CDCl_3$.*

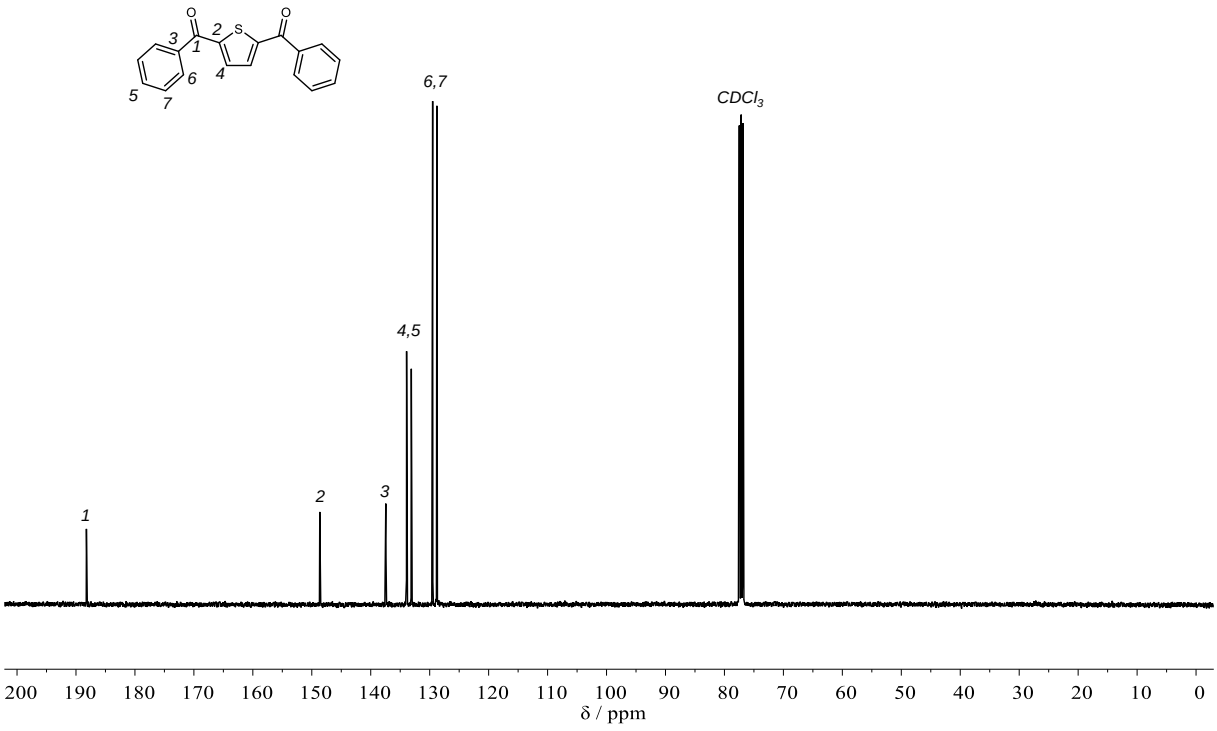

*Supplementary Figure 66 ^{13}C NMR spectrum of **6g** in $CDCl_3$.*

Bis(*tert*-butyl)terephthalophenone (6h)

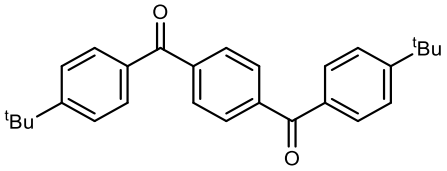

In a Schlenk flask under argon atmosphere, terephthaloyl chloride (2.00 g, 9.85 mmol, 1.00 equiv.) was suspended in *tert*-butylbenzene (30.4 mL, 26.4 g, 197 mmol, 20.0 equiv.). The mixture was placed in a water bath and aluminium chloride (2.89 g, 21.7 mmol, 2.20 equiv.) was added in small portions. The mixture was stirred at room temperature for 16 hours. The crude mixture was subsequently poured onto ice. The precipitate was filtered, washed twice with 10% NaOH, once with water, once more with EtOH and dried *in vacuo*. **6h** was obtained as a white solid in a yield of 34% (1.45 g, 3.65 mmol).

^{1}H NMR (500 MHz, Chloroform-*d*): δ/ppm = 7.81 (s, 4H), 7.76 – 7.68 (m, 4H), 7.50 – 7.40 (m, 4H), 1.30 (s, 18H).

^{13}C NMR (126 MHz, Chloroform-*d*): δ/ppm = 195.92, 156.96, 140.99, 134.40, 130.36, 129.73, 125.59, 35.34, 31.26.

IR (ATR platinum diamond): $\tilde{\nu}/cm^{-1}$ = 2960 (w), 2902 (w), 2865 (vw), 1643 (vs), 1604 (s), 1559 (w), 1497 (w), 1469 (vw), 1460 (vw), 1405 (w), 1360 (w), 1314 (m), 1298 (m), 1277 (s), 1195 (w), 1158 (w), 1127 (vw), 1105 (m), 1024 (w), 1016 (w), 979 (vw), 971 (w), 928 (vs), 862 (m), 837 (s), 761 (m), 734 (w), 695 (s), 640 (vw), 613 (vw), 564 (w), 543 (m), 473 (vw), 455 (vw), 442 (m), 416 (vw).

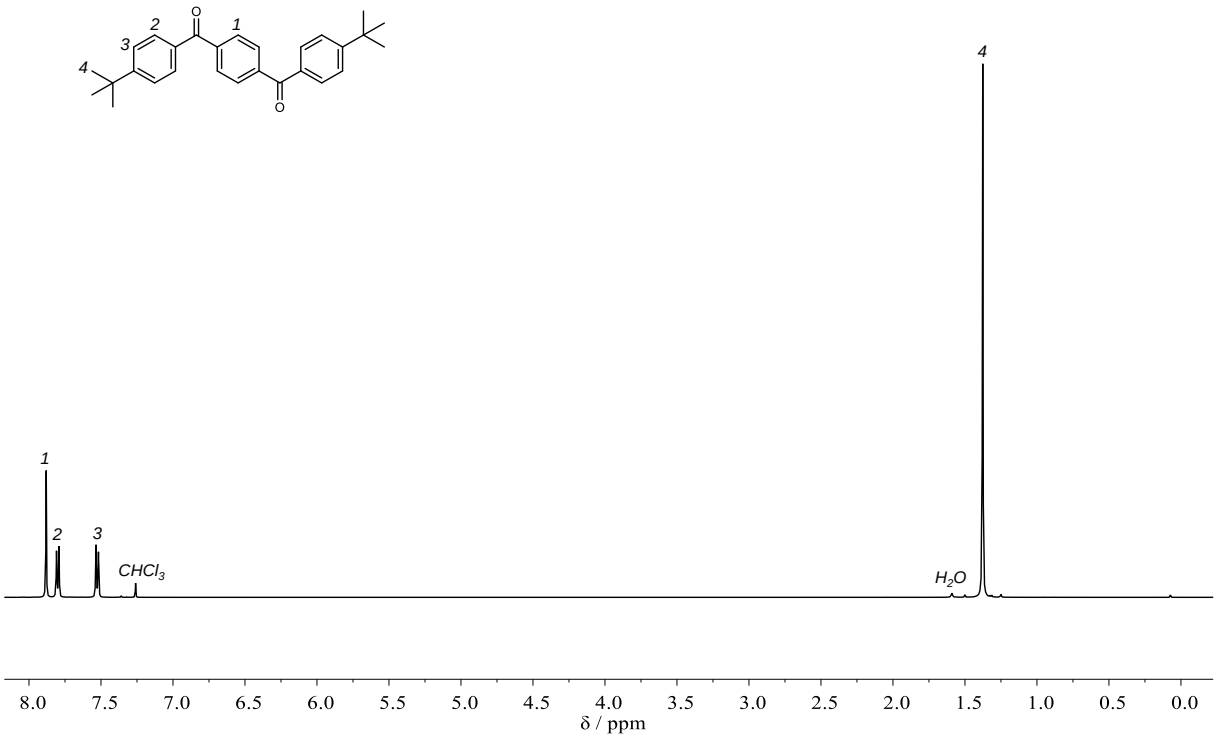

*Supplementary Figure 67 ^{1}H NMR spectrum of **6h** in $CDCl_3$.*

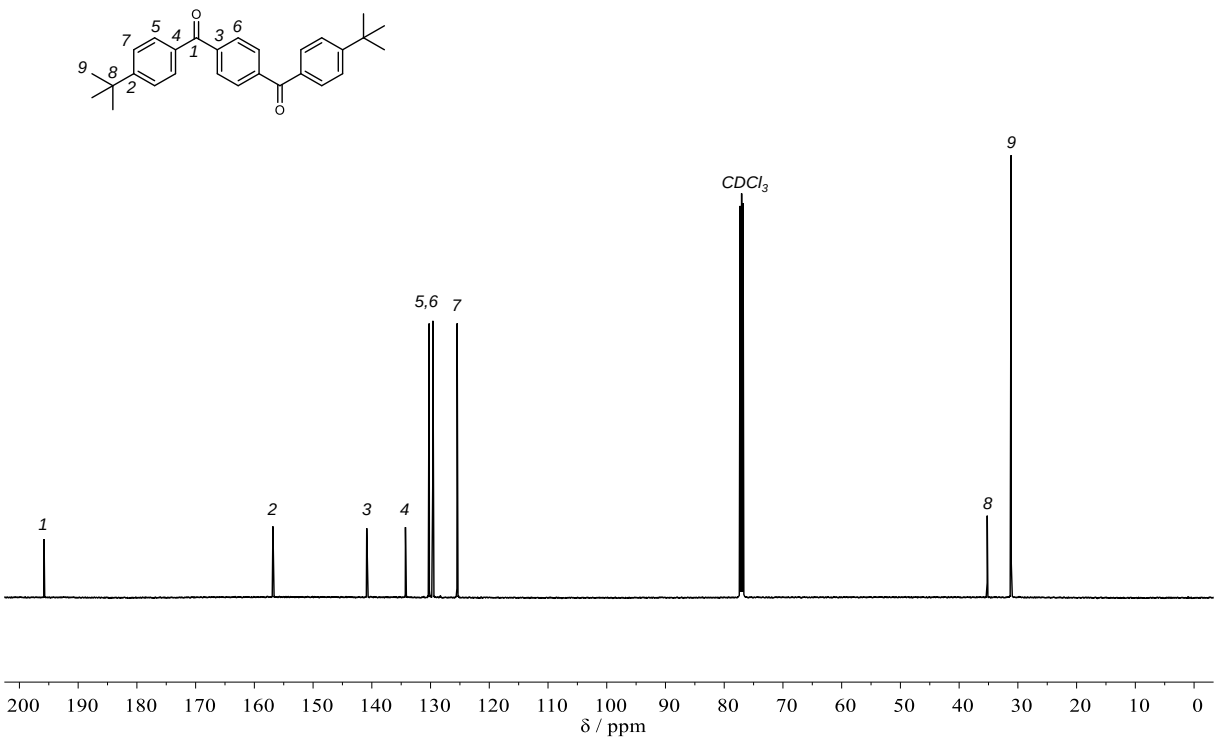

*Supplementary Figure 68 ^{13}C NMR spectrum of **6h** in $CDCl_3$.*

6.3.2.2 Synthesis of bis(N-tosylhydrazones)

Disclaimer

7a was synthesized by Florian J. O. Niedermaier under supervision of the author.

7c-7g was synthesized by Sophia Abou el Mirate under supervision of the author.

7h was synthesized by Philipp Mehr under supervision of the author.

General procedure for the synthesis of bifunctional N-tosylhydrazones:

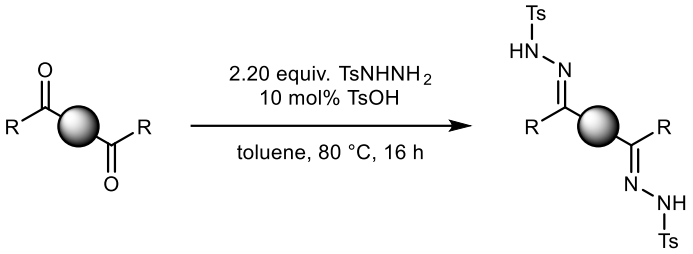

In a glass pressure vial, the respective diketone was suspended in toluene (c = 0.25 M) and tosyl hydrazide (2.20 equiv.) along with *p*-toluenesulfonic acid monohydrate (0.10 equiv.) was added. The vial was sealed and stirred at 80 °C for 16 hours. Afterwards, the mixture was cooled to room temperature, the precipitate was filtered, washed with cold ethanol and dried under vacuum. If necessary, the product was further purified *via* column chromatography.

4,4'-Dimethoxyterephthalophenone bisNTH (7a)

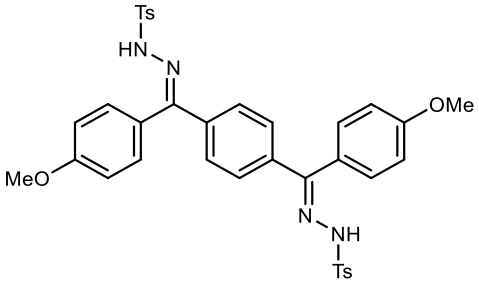

Synthesized from **6a** according to general procedure in a scale of 2.25 g (6.48 mmol). Obtained as a slightly yellow solid in a yield of 78% (3.45 g, 5.05 mmol).

^{1}H NMR (500 MHz, DMSO-d_6): δ/ppm = 10.46 (s, 2H), 7.83 – 7.74 (m, 4H), 7.50 – 7.37 (m, 4H), 7.23 (s, 4H), 7.20 – 7.11 (m, 4H), 7.09 – 7.02 (m, 4H), 3.83 (s, 6H), 2.39 (s, 6H).

^{13}C NMR (126 MHz, DMSO-d_6): δ/ppm = 159.96, 153.55, 143.31, 138.50, 135.97, 130.49, 129.43, 127.75, 127.32, 124.27, 114.22, 55.25, 21.05.

IR (ATR platinum diamond): $\tilde{\nu}/cm^{-1}$ = 3178 (w), 1604 (m), 1571 (w), 1512 (w), 1493 (vw), 1440 (vw), 1421 (vw), 1372 (w), 1337 (m), 1316 (w), 1304 (w), 1298 (w), 1281 (w), 1255 (m), 1193 (w), 1185 (w), 1175 (m), 1160 (vs), 1123 (w), 1090 (w), 1045 (w), 1026 (m), 991 (vw), 959 (w), 946 (w), 878 (w), 858 (m), 839 (m), 810 (w), 792 (w), 738 (w), 710 (s), 689 (m), 662 (m), 625 (w), 578 (m), 557 (vs), 545 (s), 525 (m), 500 (vw), 490 (w), 483 (w), 469 (vw).

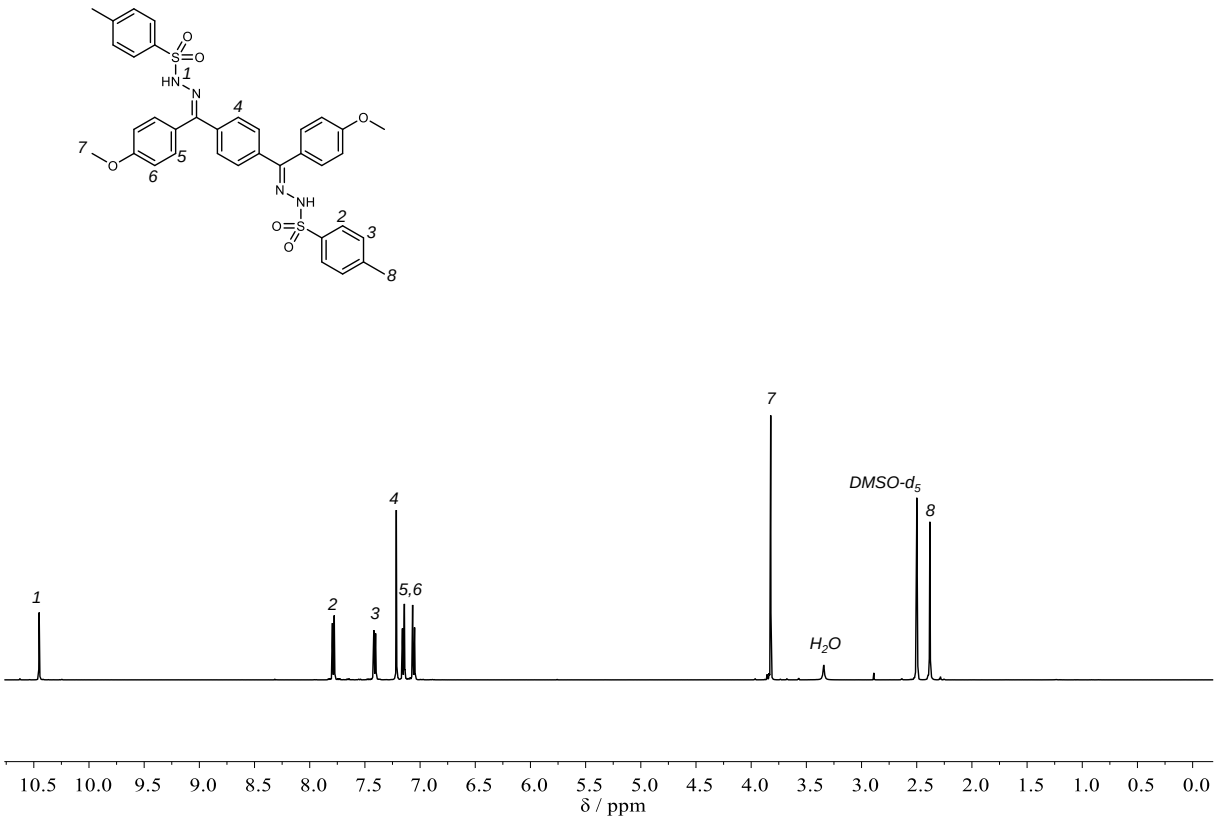

*Supplementary Figure 69 ^{1}H NMR spectrum of **7a** in DMSO-d_6.*

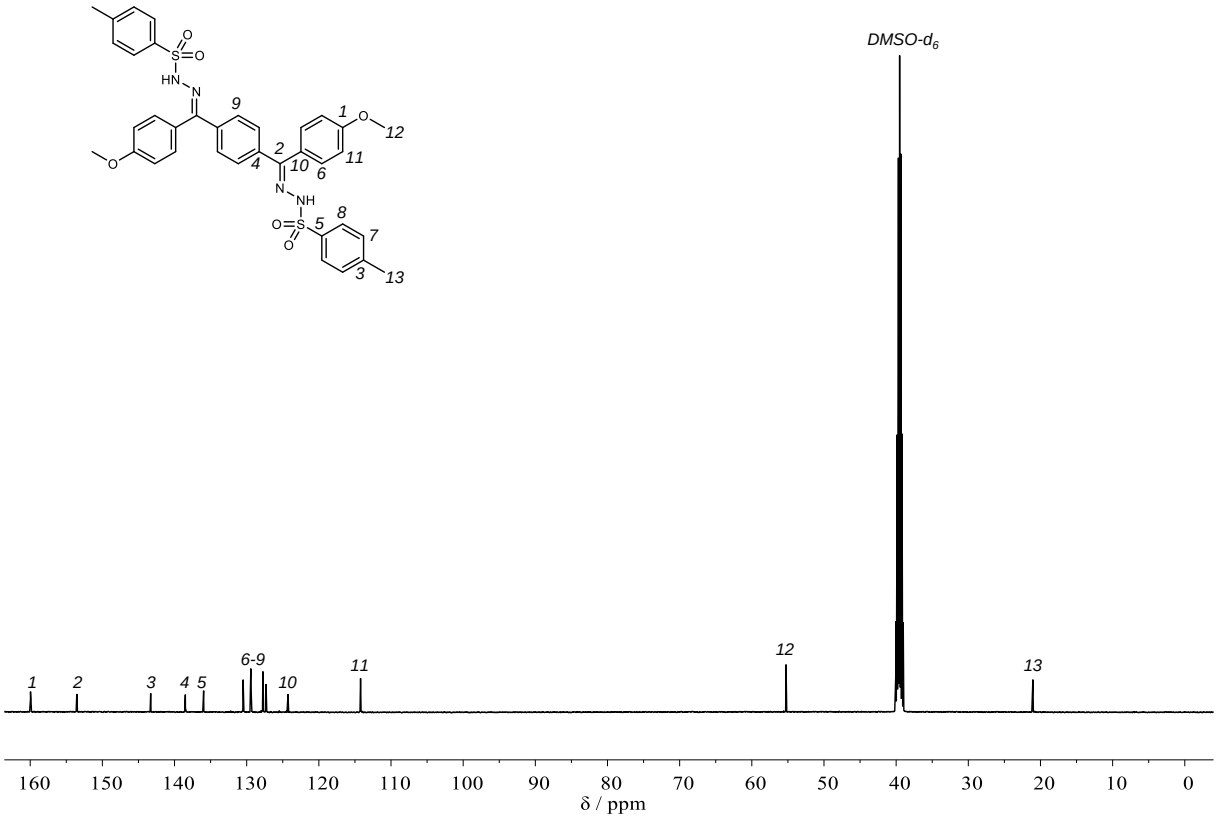

*Supplementary Figure 70 ^{13}C NMR spectrum of **7a** in DMSO-d_6.*

Attempted Synthesis of 7a in ethanol

The synthesis of **7a** was initially attempted akin to a slightly adapted general procedure for monofunctional NTHs described in section 6.3.1.2. Accordingly, **6a** (693 mg, 2.00 mmol, 1.00 equiv.), *p*-toluenesulfonyl hydrazide (894 mg, 4.80 mmol, 2.40 equiv.) and *p*-toluenesulfonic acid monohydrate (38.0 mg, 200 µmol, 0.10 equiv.) were dissolved in 5 mL of EtOH and the mixture was refluxed for 16 hours. After cooling, the precipitate was filtered, washed with cold EtOH and analyzed *via* ^{1}H NMR. The spectrum indicated that 50% of 6a were converted to **7a**, while the remaining **6a** remained unreacted. Repeating the reaction under the same conditions, but instead refluxing for 72 hours resulted in 78% conversion of **6a** to **7a**. Conversions were calculated using the respective integral ratios of the methoxy signals associated with **6a** (marked in green in Supplementary Figure 71) and **7a** (marked in yellow in Supplementary Figure 71).

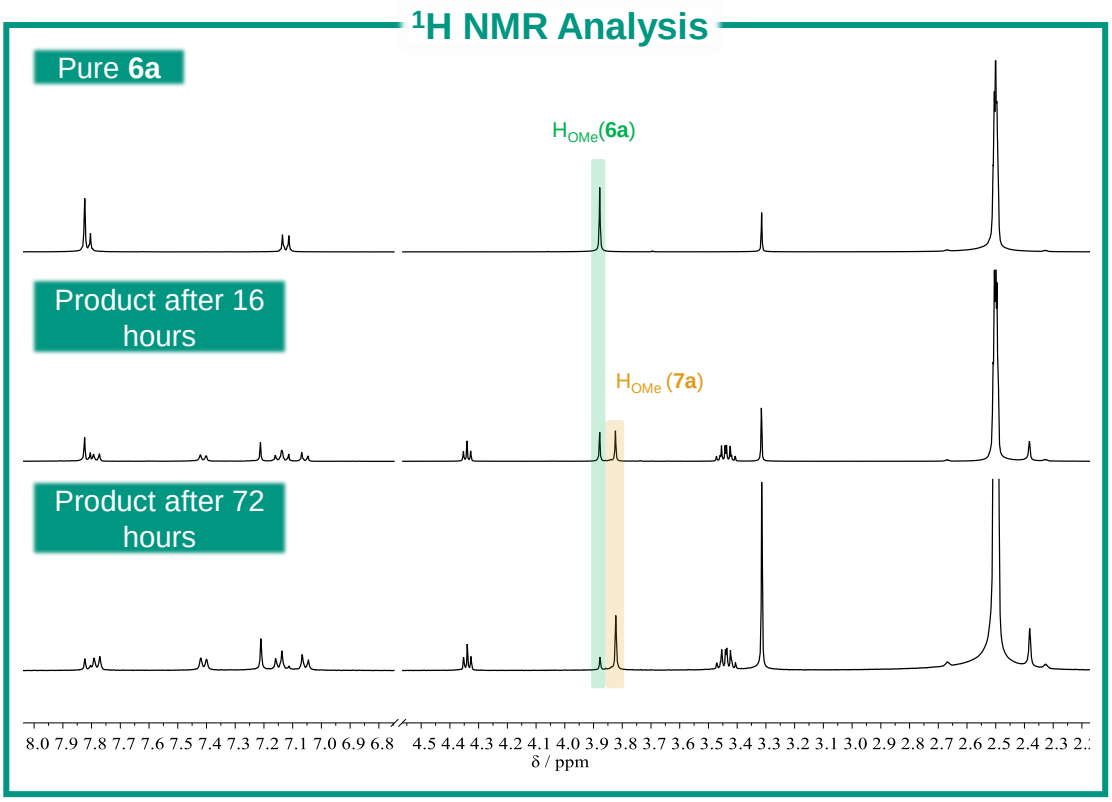

*Supplementary Figure 71: Comparison of the ^{1}H NMR spectra of pure **6a** (top) and the isolated products of the attempted synthesis of **7a** in ethanol after 16 hours (middle) and 72 hours (bottom).*

Terephthalophenone bisNTH (7b)

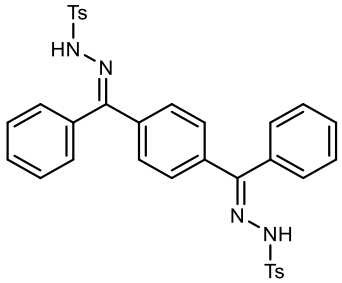

Synthesized from **6b** according to general procedure in a scale of 1.68 g (5.87 mmol). Obtained as a white solid in a yield of 89% (3.42 g, 5.21 mmol).

^{1}H NMR (400 MHz, DMSO-d_6): δ 10.50 (s, 2H), 7.88 – 7.71 (m, 4H), 7.59 – 7.47 (m, 6H), 7.47 – 7.36 (m, 4H), 7.22 (s, 4H), 7.21 – 7.17 (m, 4H), 2.38 (s, 6H).

^{13}C NMR (101 MHz, DMSO-d_6): δ/ppm = 153.66, 143.35, 138.15, 135.95, 132.25, 129.46, 128.85, 128.79, 127.75, 127.19, 21.05.

IR (ATR platinum diamond): $\tilde{\nu}/cm^{-1}$ = 3277 (vw), 3180 (w), 1596 (vw), 1491 (vw), 1444 (vw), 1397 (w), 1378 (m), 1345 (w), 1312 (w), 1183 (m), 1164 (vs), 1117 (vw), 1094 (vw), 1059 (m), 1028 (w), 1020 (w), 998 (vw), 973 (m), 928 (w), 872 (m), 845 (m), 808 (m), 775 (s), 718 (m), 703 (m), 669 (m), 662 (m), 603 (m), 557 (vs), 545 (s), 522 (w), 508 (w), 477 (w), 453 (w).

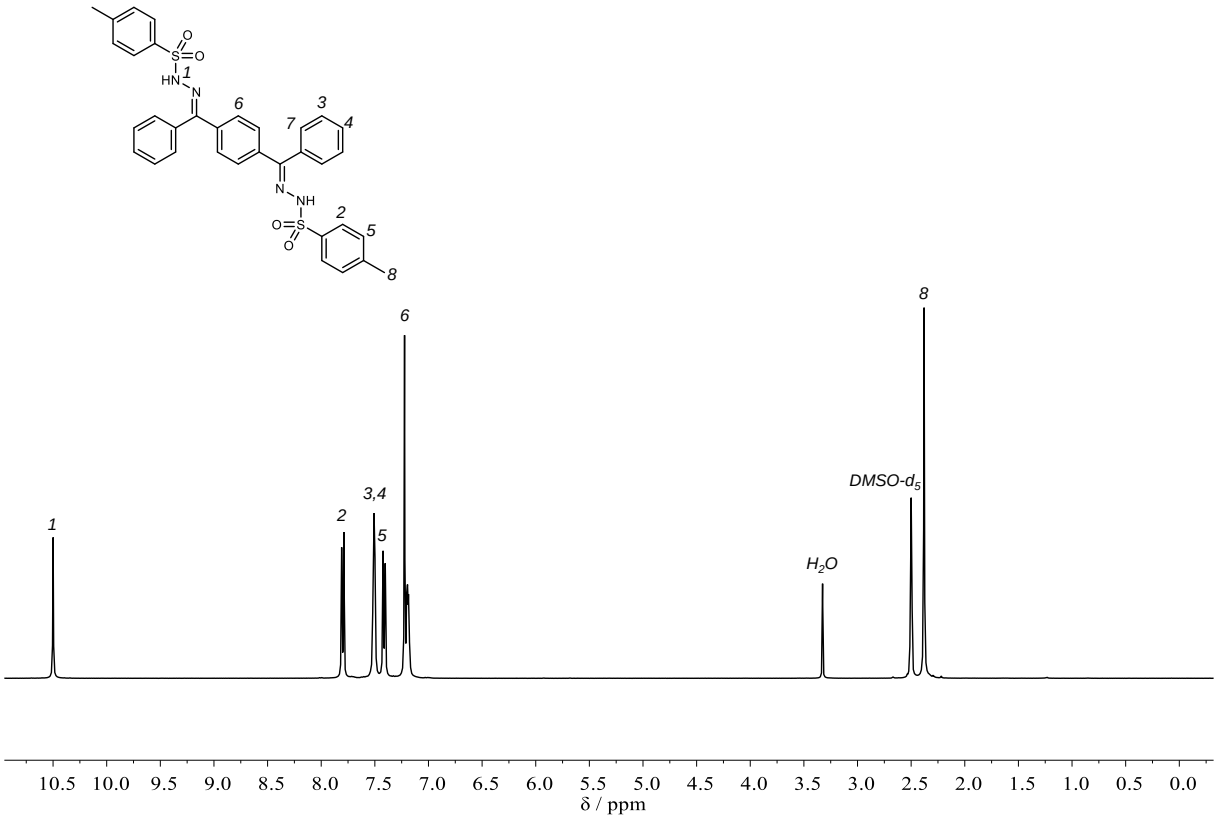

*Supplementary Figure 72: [1]H NMR spectrum of **7b** in DMSO-d6.*

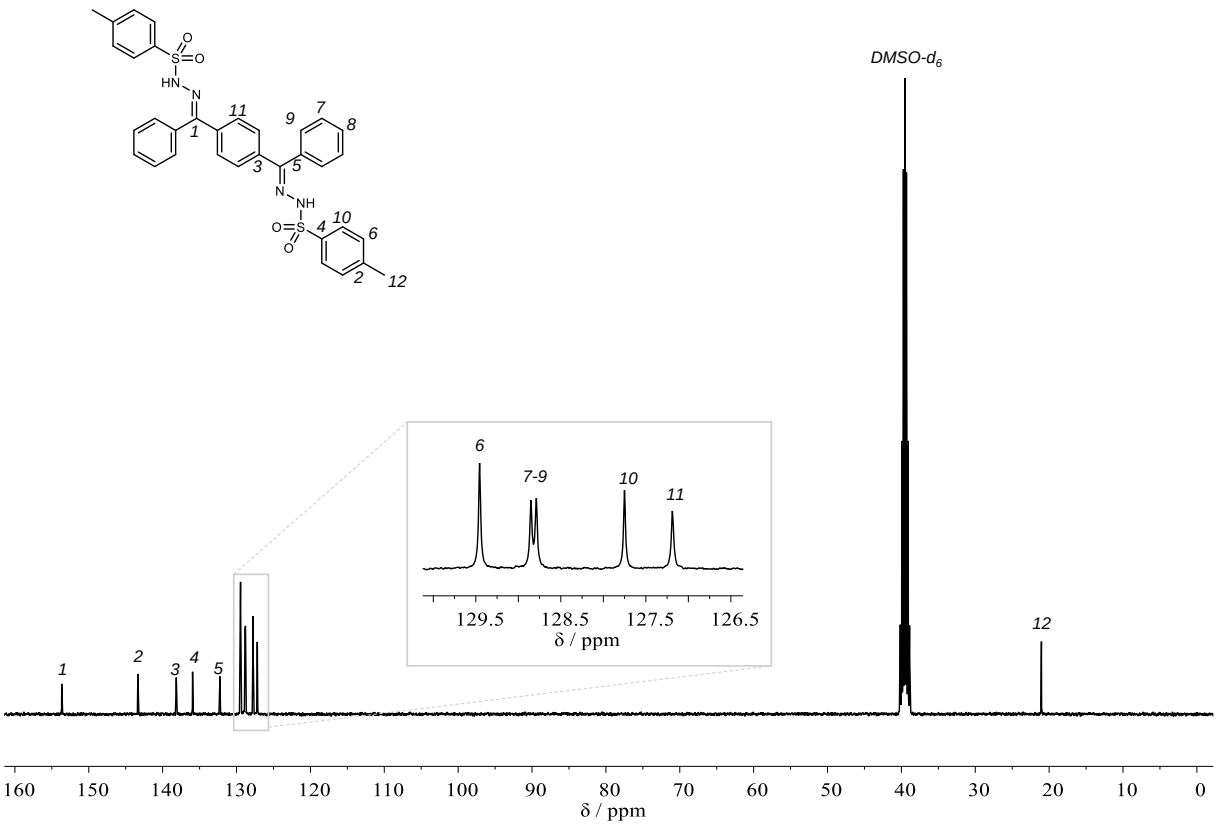

*Supplementary Figure 73: [13]C NMR spectrum of **7b** in DMSO-d6.*

4,4'-Diphenoxyterephthalophenone bisNTH (7c)

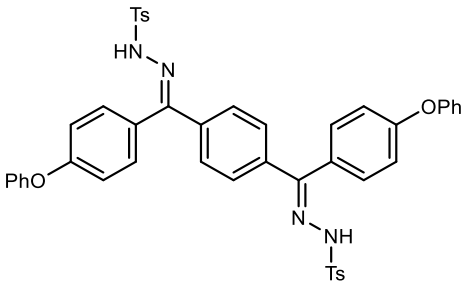

Synthesized from **6c** according to general procedure in a scale of 2.35 g (5.00 mmol). Obtained as a white solid in a yield of 89% (3.58 g, 4.43 mmol).

^{1}H NMR (500 MHz, DMSO-d_6): δ/ppm = 10.56 (s, 2H), 7.88 – 7.76 (m, 4H), 7.52 – 7.38 (m, 8H), 7.27 (s, 4H), 7.26 – 7.20 (m, 6H), 7.16 – 7.08 (m, 8H), 2.40 (s, 6H).

^{13}C NMR (126 MHz, DMSO-d_6): δ/ppm = 157.76, 155.79, 152.95, 143.38, 138.26, 135.99, 130.90, 130.23, 129.50, 127.71, 127.28, 126.86, 124.16, 119.36, 118.26, 21.06.

IR (ATR platinum diamond): $\tilde{\nu}/cm^{-1}$ = 3223 (w), 1588 (m), 1500 (w), 1487 (s), 1456 (vw), 1405 (w), 1370 (m), 1349 (s), 1308 (w), 1290 (w), 1230 (vs), 1187 (m), 1166 (vs), 1119 (vw), 1098 (w), 1063 (m), 1014 (w), 977 (m), 963 (vw), 950 (w), 878 (m), 868 (s), 854 (m), 812 (m), 788 (vw), 749 (m), 708 (m), 699 (w), 687 (m), 660 (s), 617 (w), 601 (w), 580 (w), 553 (s), 541 (vs), 508 (w), 496 (m), 479 (m).

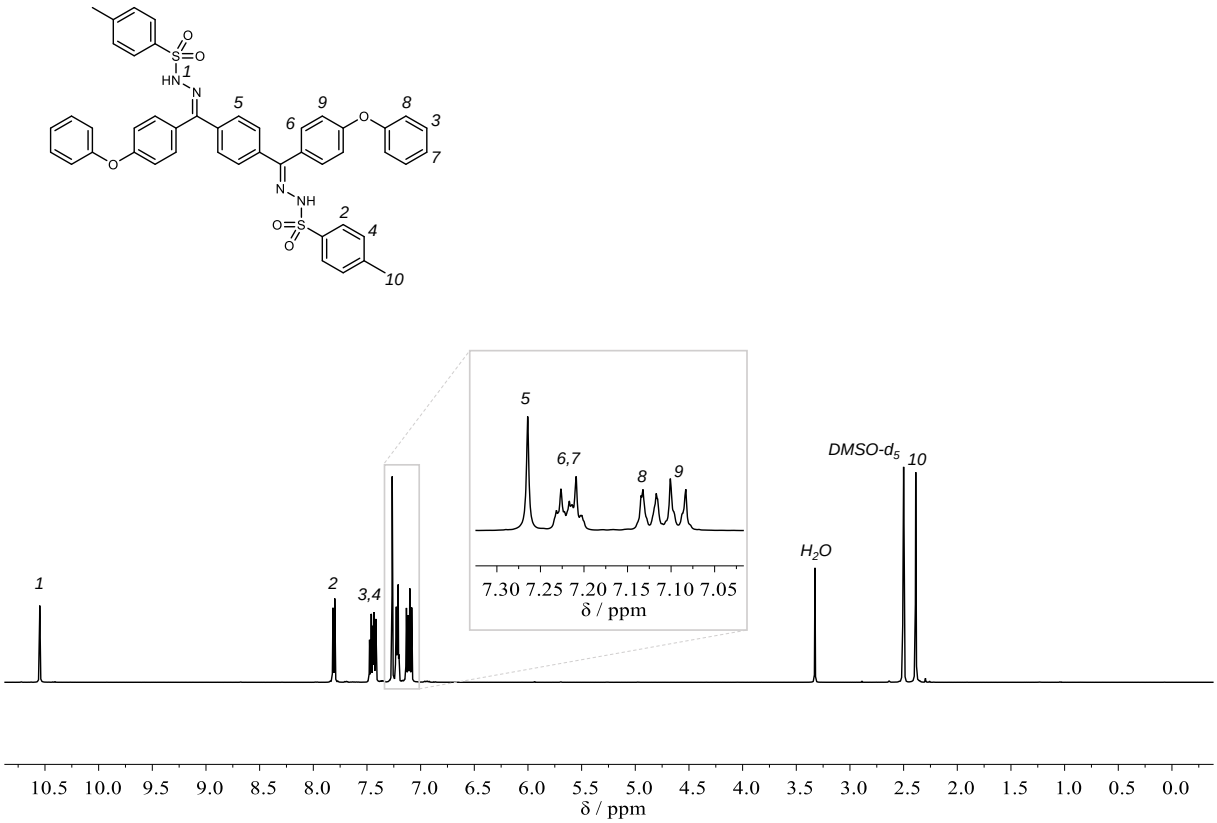

*Supplementary Figure 74: [1]H NMR spectrum of **7c** in DMSO-d6.*

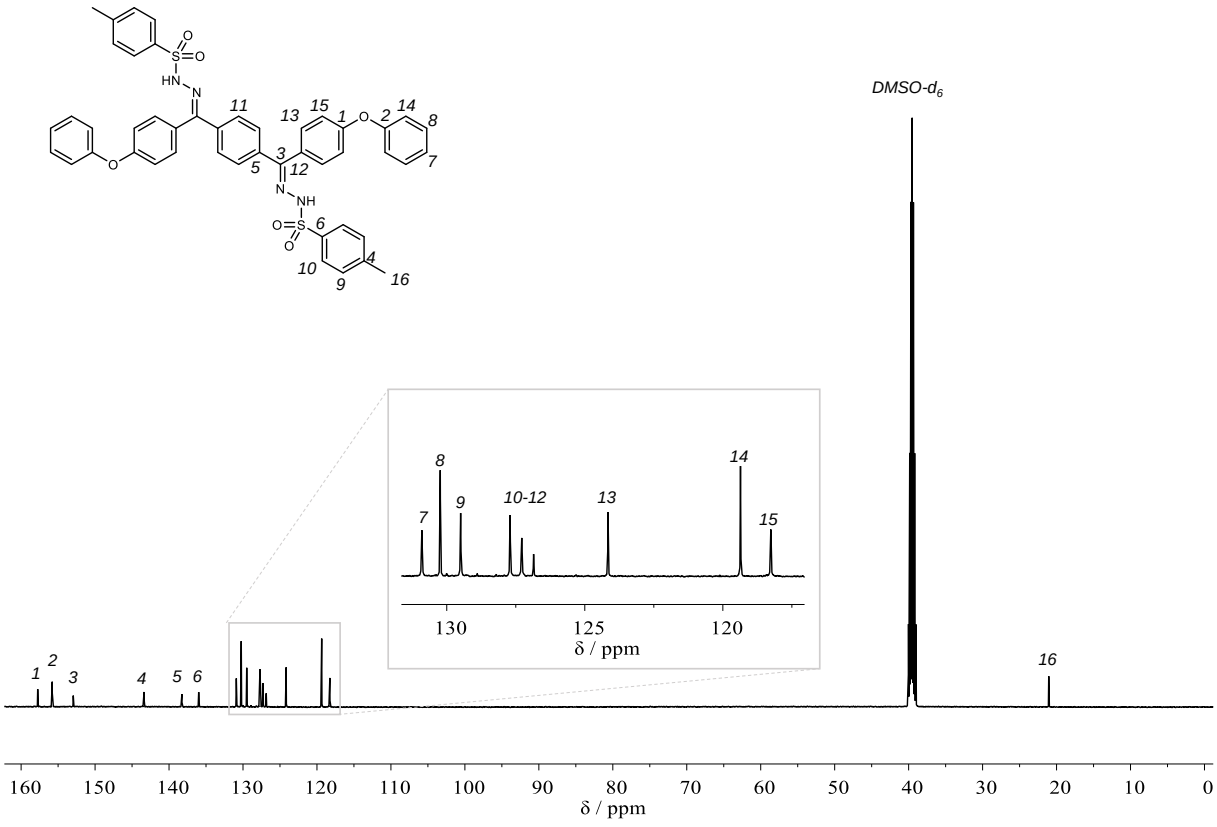

*Supplementary Figure 75: [13]C NMR spectrum of **7c** in DMSO-d6.*

4,4'-Bis(phenylthio)terephthalophenone bisNTH (7d)

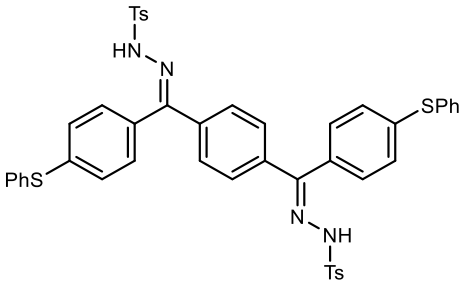

Synthesized from **6d** according to general procedure in a scale of 1.01 g (2.00 mmol). Obtained as an off-white solid in a yield of 80% (1.35 g, 1.60 mmol).

^{1}H NMR (500 MHz, Chloroform-*d*): δ/ppm 7.85 – 7.80 (m, 4H), 7.60 – 7.58 (m, 2H), 7.57 – 7.53 (m, 4H), 7.46 – 7.39 (m, 7H), 7.35 – 7.30 (m, 8H), 7.28 – 7.23 (m, 7H), 6.99 – 6.92 (m, 4H), 2.42 (s, 6H).

^{13}C NMR (126 MHz, Chloroform-*d*): δ/ppm = 152.81, 144.47, 141.62, 137.74, 135.45, 134.19, 132.12, 129.91, 129.86, 129.04, 128.99, 128.06, 127.85, 127.53, 21.79.

IR (ATR platinum diamond): $\tilde{\nu}/cm^{-1}$ = 3203 (w), 1600 (w), 1489 (w), 1475 (w), 1442 (vw), 1407 (w), 1382 (m), 1345 (m), 1316 (m), 1306 (w), 1290 (w), 1185 (w), 1164 (vs), 1117 (vw), 1109 (vw), 1094 (w), 1082 (w), 1057 (m), 1016 (w), 1000 (vw), 981 (m), 946 (vw), 878 (m), 852 (m), 833 (w), 823 (m), 810 (m), 759 (m), 718 (w), 706 (w), 695 (w), 683 (w), 664 (s), 642 (w), 621 (vw), 555 (vs), 535 (m), 512 (w), 494 (w), 440 (w), 422 (vw).

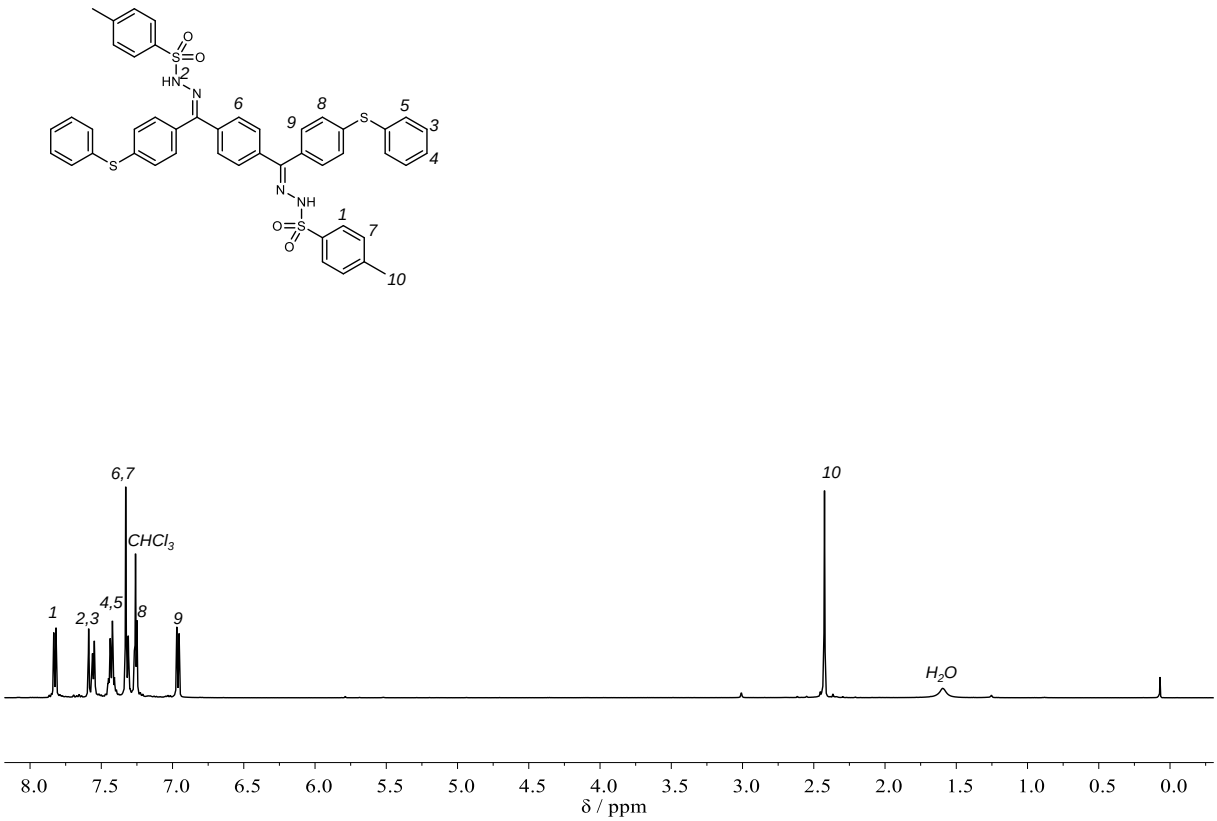

*Supplementary Figure 76: ^{1}H NMR spectrum of **7d** in $CDCl_3$*

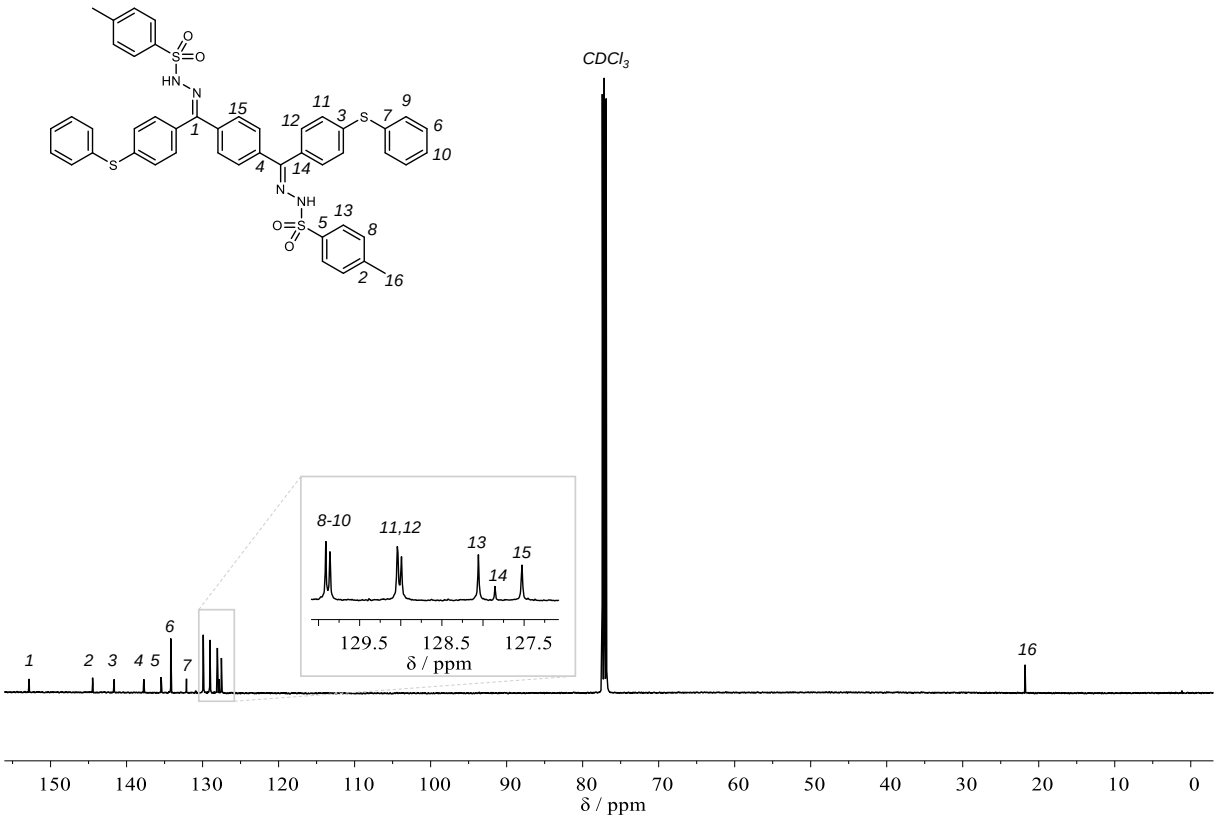

*Supplementary Figure 77: ^{13}C NMR spectrum of **7d** in $CDCl_3$.*

Isophthalophenone bisNTH (7e)

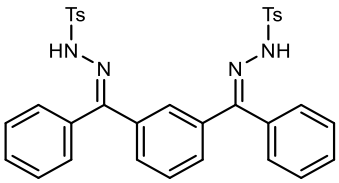

Synthesized from **6e** according to general procedure in a scale of 1.43 g (5.00 mmol,). Obtained as a white solid in a yield of (1.03 g, 1.66 mmol). Further purified by column chromatography (cyclohexane / ethyl acetate 5:1).

^{1}H NMR (400 MHz, DMSO-d_6): δ/ppm = 10.23 (s, 2H), 7.80 (t, 1H), 7.76 – 7.70 (m, 4H), 7.45 (dd, *J* = 7.7, 1.7 Hz, 2H), 7.37 (t, *J* = 2.0 Hz, 10H), 7.27 (d, *J* = 8.1 Hz, 4H), 6.32 (t, *J* = 1.7 Hz, 1H), 2.27 (s, 6H).

^{13}C NMR (101 MHz, DMSO-d_6): δ/ppm = 152.58, 143.52, 136.21, 135.99, 133.57, 130.59, 129.83, 129.76, 129.68, 128.52, 127.89, 127.27, 126.96, 20.94.

IR (ATR platinum diamond): $\tilde{\nu}/cm^{-1}$ = 3176 (w), 1596 (vw), 1446 (w), 1403 (m), 1347 (m), 1333 (w), 1323 (m), 1308 (w), 1290 (w), 1187 (w), 1166 (s), 1144 (m), 1121 (vw), 1094 (w), 1055 (m), 1028 (w), 1018 (w), 1000 (w), 989 (m), 940 (vw), 924 (w), 899 (w), 878 (vw), 821 (m), 812 (m), 792 (w), 771 (w), 730 (vw), 701 (s), 687 (m), 673 (s), 644 (w), 625 (w), 601 (m), 572 (w), 543 (vs), 500 (w), 483 (m), 428 (w).

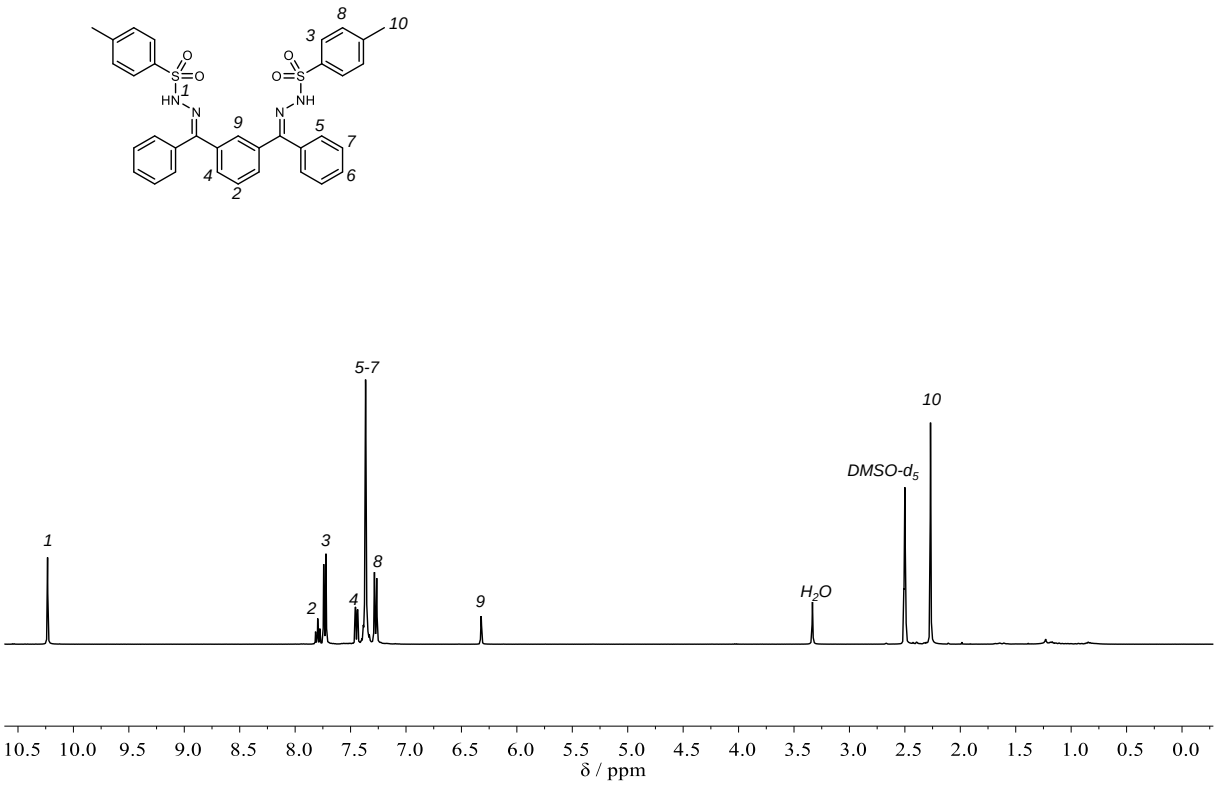

*Supplementary Figure 78: [1]H NMR spectrum of **7e** in DMSO-d6.*

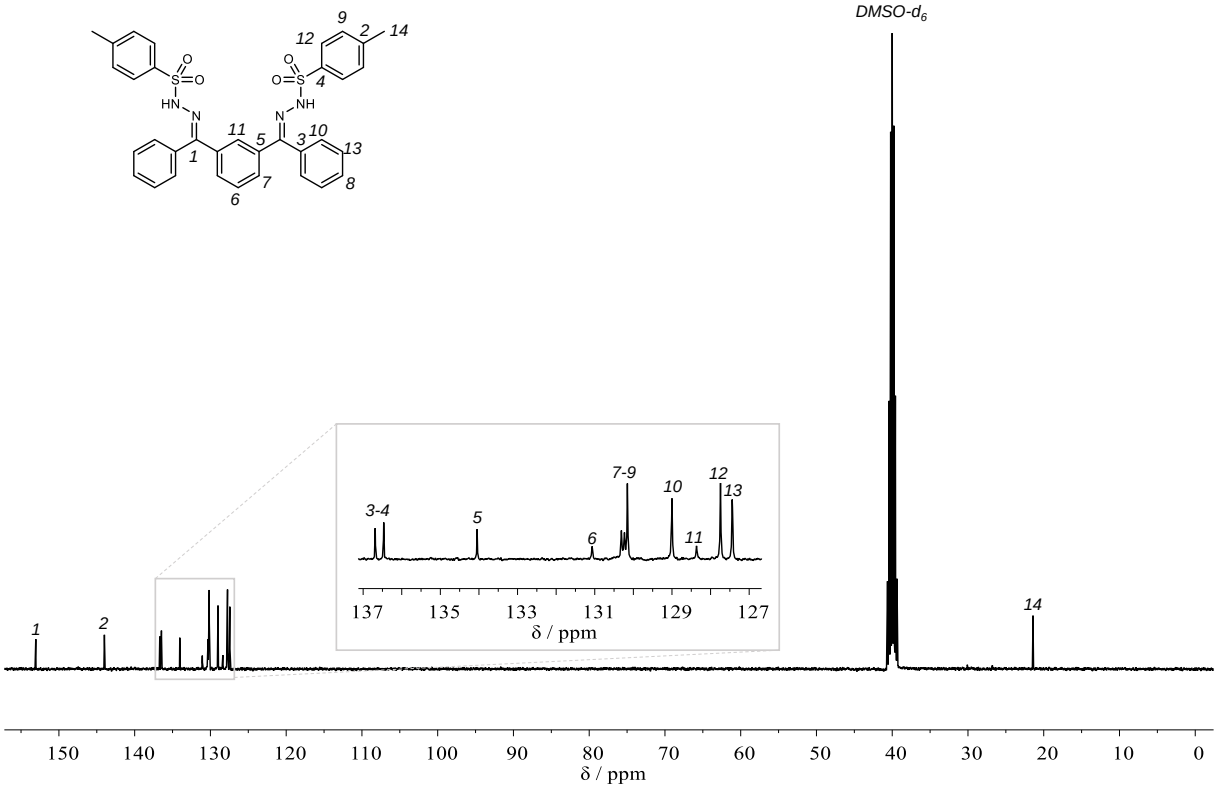

*Supplementary Figure 79: [13]C NMR spectrum of **7e** in DMSO-d6.*

4,4'-Bis(benzoyl)biphenyl bisNTH (7f)

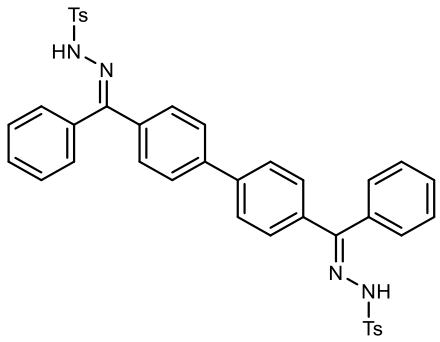

Synthesized from **6f** according to general procedure in a scale 362 mg (1.00 mmol). Obtained as a white solid in a yield of 65% (452 mg, 0.65 mmol).

^{1}H NMR (500 MHz, DMSO-d_6): δ/ppm = 10.61 (s, 2H), 7.94 – 7.89 (m, 4H), 7.87 – 7.82 (m, 4H), 7.48 – 7.44 (m, 4H), 7.43 – 7.34 (m, 10H), 7.32 – 7.28 (m, 4H), 2.41 (s, 6H).

^{13}C NMR (126 MHz, DMSO-d_6): δ/ppm = 154.19, 143.40, 140.36, 137.16, 136.04, 132.07, 129.78, 129.76, 129.46, 128.42, 127.80, 127.33, 127.11, 21.08.

IR (ATR platinum diamond): $\tilde{\nu}/cm^{-1}$ = 3199 (vw), 1609 (vw), 1598 (w), 1493 (w), 1444 (w), 1401 (w), 1337 (m), 1318 (m), 1304 (w), 1185 (vw), 1160 (vs), 1121 (vw), 1092 (w), 1076 (vw), 1055 (w), 1018 (w), 1004 (vw), 981 (w), 967 (vw), 950 (vw), 876 (m), 823 (m), 806 (w), 778 (m), 747 (vw), 722 (w), 697 (s), 675 (m), 619 (w), 551 (vs), 498 (w), 477 (w).

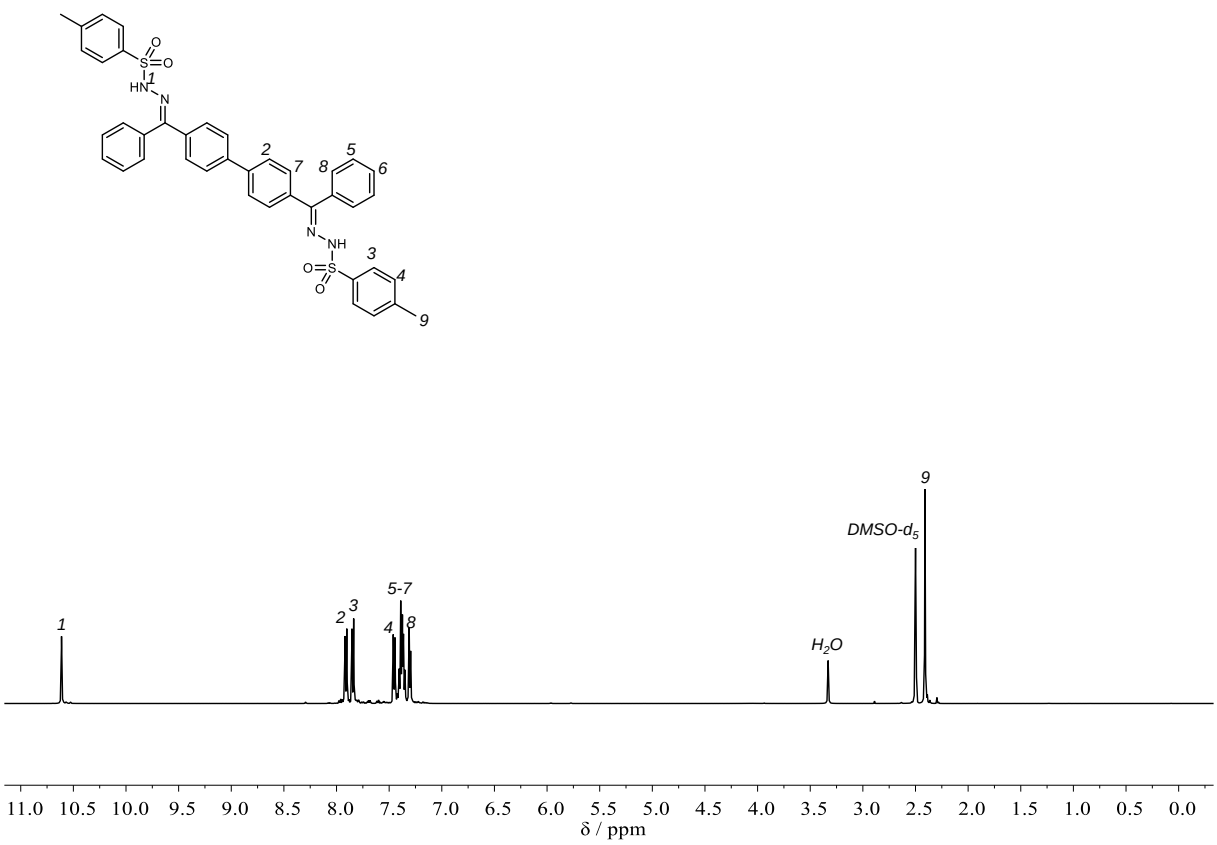

*Supplementary Figure 80: [1]H NMR spectrum of **7f** in DMSO-d6.*

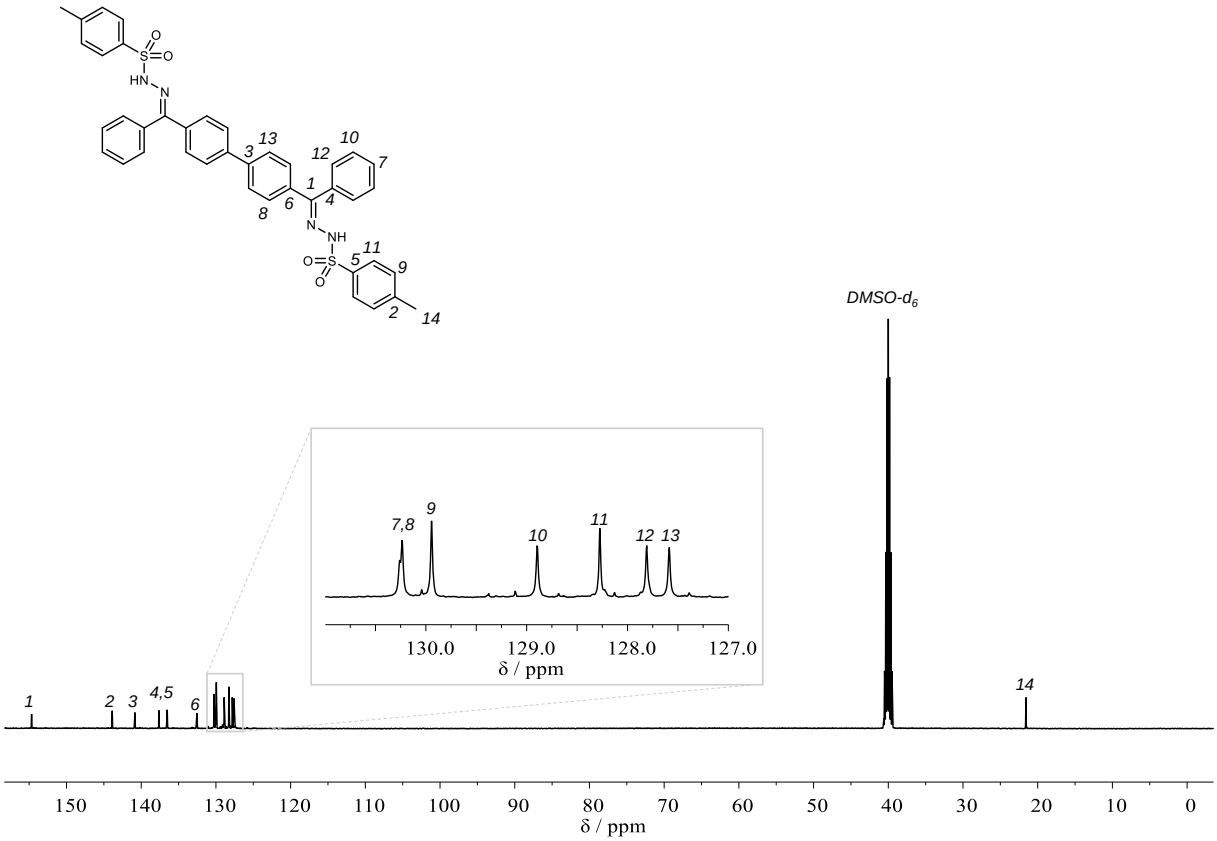

*Supplementary Figure 81: [13]C NMR spectrum of **7f** in DMSO-d6.*

2,5-Bis(benzoyl)thiophene bisNTH (7g)

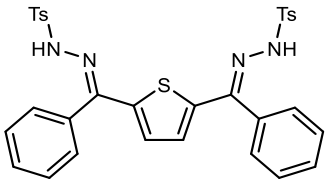

Synthesized from **6g** according to general procedure in a scale of 1.17 g (4.00 mmol). Obtained as an off-white solid in a yield of 93% (2.35 g, 3.73 mmol).

^{1}H NMR (500 MHz, DMSO-d_6): δ/ppm = 10.63 (s, 2H), 7.91 – 7.76 (m, 4H), 7.57 – 7.46 (m, 6H), 7.46 – 7.36 (m, 4H), 7.33 – 7.21 (m, 4H), 6.50 (s, 2H), 2.42 (s, 6H).

^{13}C NMR (126 MHz, DMSO-d_6): δ/ppm = 150.01, 144.13, 143.47, 135.91, 131.22, 129.82, 129.37, 129.34, 128.82, 128.60, 127.82, 21.11.

IR (ATR platinum diamond): $\tilde{\nu}/cm^{-1}$ = 3176 (w), 1596 (w), 1491 (vw), 1444 (w), 1386 (m), 1353 (w), 1343 (m), 1323 (m), 1290 (w), 1187 (w), 1168 (s), 1158 (s), 1121 (vw), 1094 (w), 1068 (m), 1049 (m), 1031 (w), 1018 (w), 1000 (vw), 950 (w), 938 (w), 915 (m), 843 (m), 810 (m), 773 (m), 716 (w), 695 (m), 664 (s), 588 (m), 572 (w), 541 (vs), 518 (m), 494 (w), 469 (w).

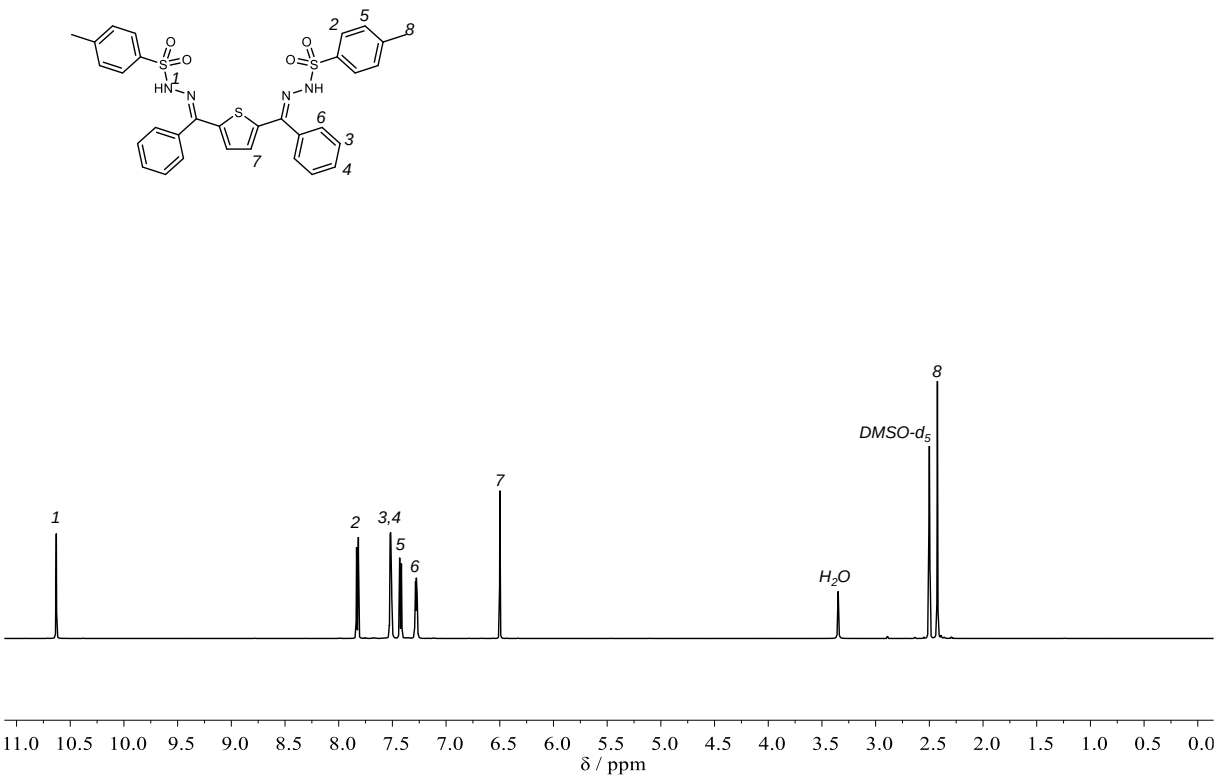

*Supplementary Figure 82: [1]H NMR spectrum of **7g** in DMSO-d6.*

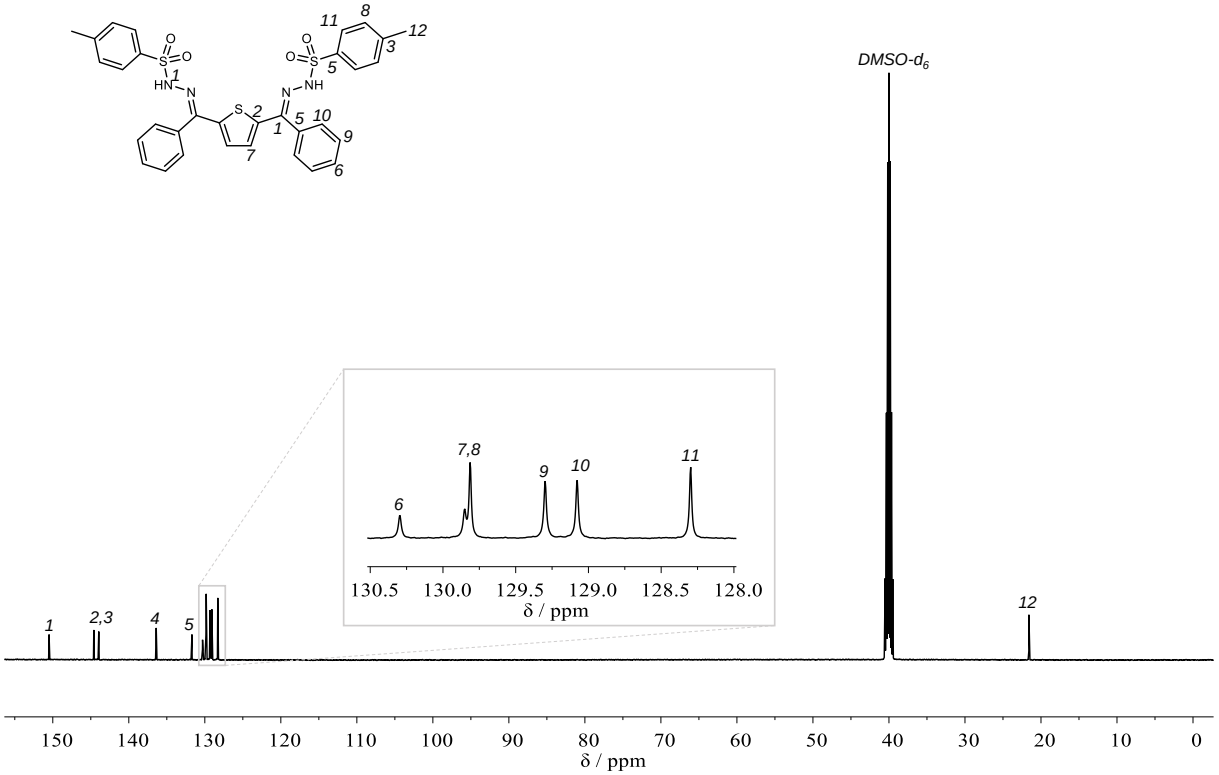

*Supplementary Figure 83: [13]C NMR spectrum of **7g** in DMSO-d6.*

4,4'-Bis(tert-butyl)terephthalophenone bisNTH (7h)

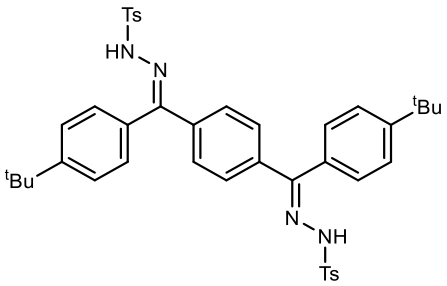

Synthesized from **6h** according to general procedure on a scale of 1.20 g (3.00 mmol). Obtained as a white solid in a yield of 53% (1.17 mg, 1.60 mmol).

^{1}H NMR (500 MHz, Chloroform-*d*): δ/ppm = 7.86 – 7.81 (m, 4H), 7.64 (s, 2H), 7.52 – 7.47 (m, 4H), 7.36 (s, 4H), 7.35 – 7.31 (m, 4H), 7.04 – 6.97 (m, 4H), 2.43 (s, 6H), 1.36 (s, 18H).

^{13}C NMR (126 MHz, Chloroform-*d*): δ/ppm = 153.77, 153.58, 144.35, 137.88, 135.60, 129.84, 128.11, 128.05, 127.80, 127.51, 126.88, 35.09, 31.33, 21.79.

IR (ATR platinum diamond): $\tilde{\nu}/cm^{-1}$ = 3186 (w), 2966 (vw), 1611 (vw), 1598 (vw), 1497 (vw), 1460 (vw), 1380 (m), 1345 (m), 1310 (w), 1296 (w), 1265 (vw), 1214 (vw), 1189 (w), 1170 (s), 1115 (vw), 1105 (vw), 1094 (w), 1059 (w), 1020 (w), 975 (m), 944 (vw), 876 (w), 854 (w), 841 (w), 831 (w), 812 (w), 761 (m), 753 (m), 728 (w), 706 (w), 679 (m), 652 (w), 636 (w), 617 (w), 570 (s), 553 (vs), 529 (m), 496 (w), 479 (vw), 438 (vw).

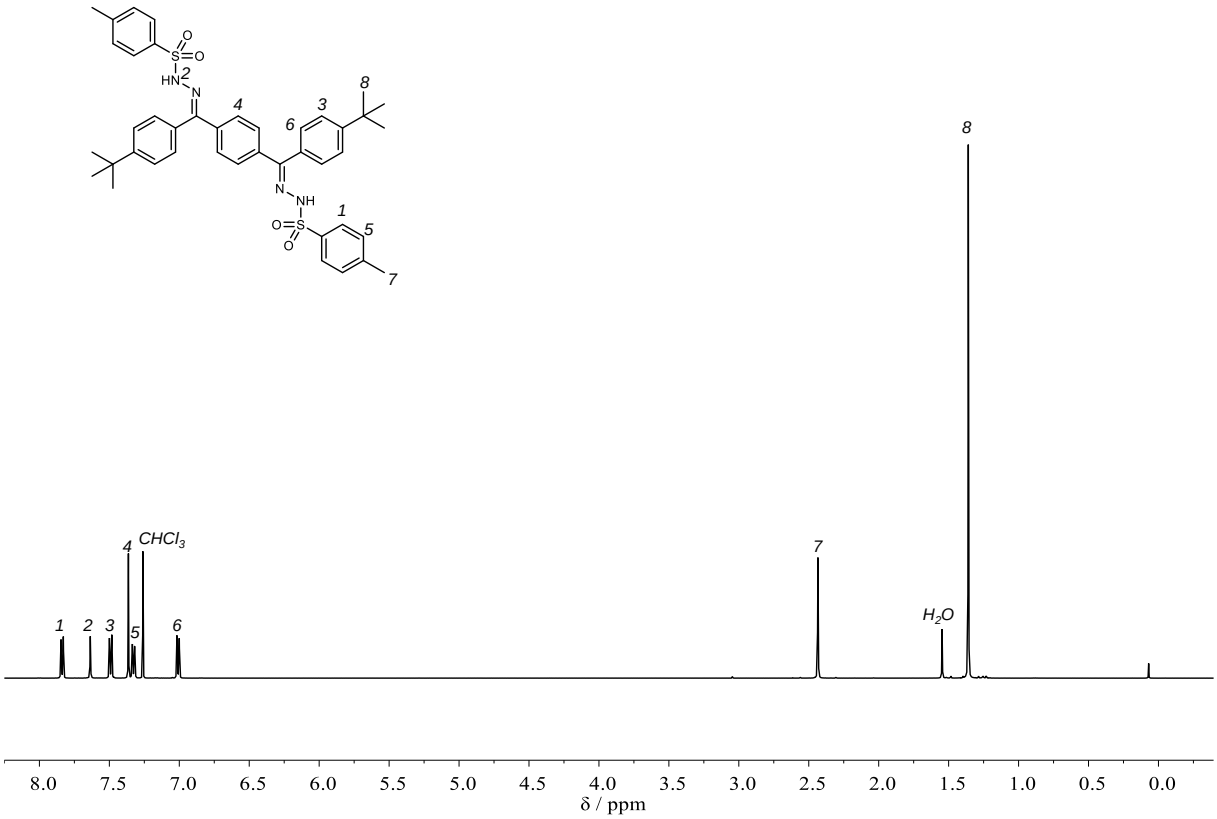

*Supplementary Figure 84: ^{1}H NMR spectrum of **7h** in $CDCl_3$.*

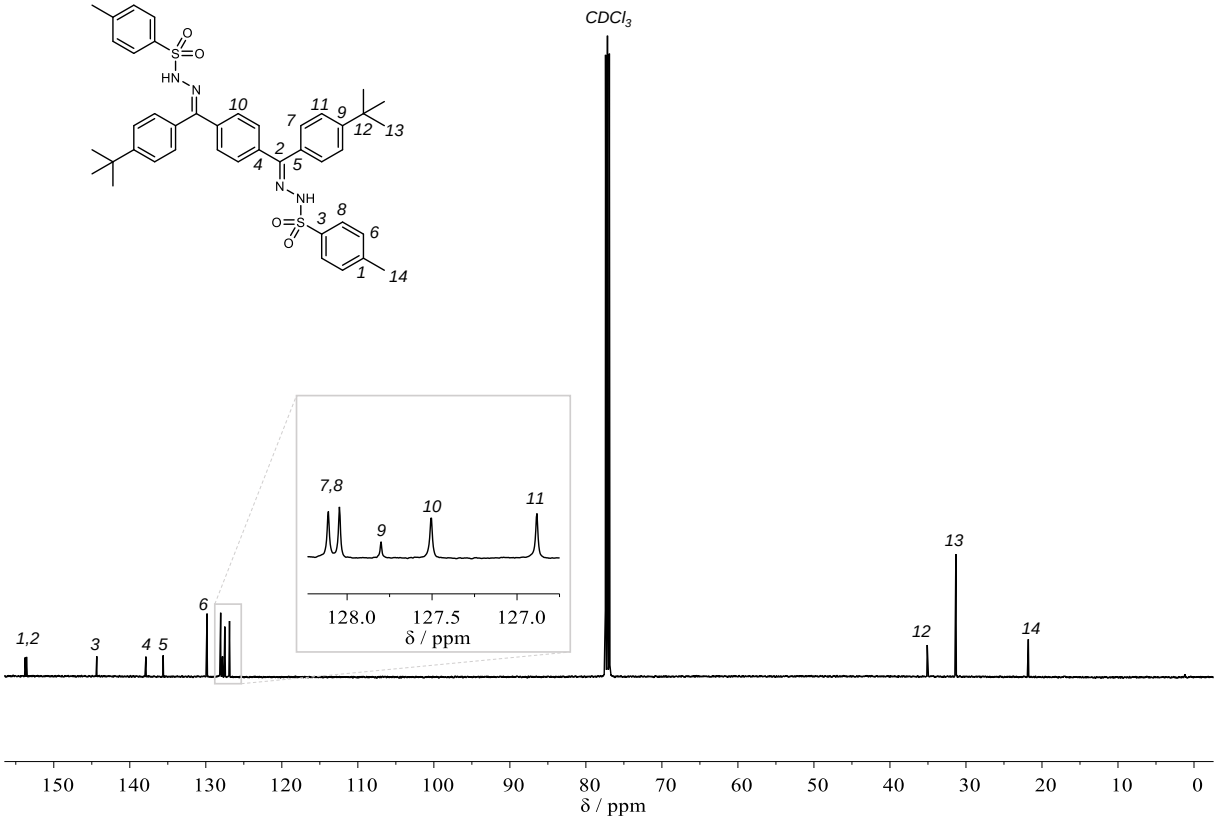

*Supplementary Figure 85: ^{13}C NMR spectrum of **7h** in $CDCl_3$.*

6.3.2.3 Other sulfonylhydrazides

Disclaimer

***p*-Nosyl hydrazide** and **8a** were synthesized by Florian J. O. Niedermaier under supervision of the author.

_p_-Nosyl hydrazide

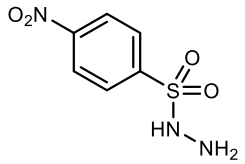

Hydrazine hydrate (2.50 mL, 4.43 g, 125 mmol, 2.50 equiv.) was dissolved in 8 mL of tetrahydrofuran (THF) and cooled to 0 °C. *p*-Nosyl chloride (2.50 g, 50 mmol, 1.00 equiv.) was added in small portions. After complete addition, the mixture was stirred for 2 hours at 0 °C. Afterwards, 40 mL of water were added, the precipitate was filtered, washed with water and dried *in vacuo*. The product was obtained as a white solid in a yield of 86% (3.74 g, 17.2 mmol). The procedure was adapted from Serrano *et al*.[503]

^{1}H NMR (400 MHz, DMSO-d_6): δ/ppm = 8.76 (s, 1H), 8.46 – 8.38 (m, 1H), 8.09 – 8.01 (m, 1H), 4.32 (s, 1H).

^{13}C NMR (101 MHz, DMSO-d_6): δ/ppm = 149.71, 144.20, 129.26, 124.24.

IR (ATR platinum diamond): *ṽ/cm-1* = 3258 (m), 3102 (w), 3013 (w), 2972 (w), 2960 (w), 2943 (w), 2913 (w), 2900 (w), 2837 (w), 1604 (m), 1565 (w), 1526 (s), 1504 (s), 1467 (w), 1442 (w), 1419 (w), 1401 (w), 1384 (s), 1343 (s), 1308 (s), 1288 (m), 1244 (vs), 1177 (vs), 1160 (s), 1115 (m), 1107 (m), 1090 (m), 1047 (m), 1028 (s), 1010 (m), 977 (s), 959 (m), 938 (w), 880 (m), 854 (s), 831 (s), 815 (s), 784 (m), 734 (s), 683 (s), 613 (s), 594 (s), 576 (m), 551 (s), 527 (s), 494 (m), 459 (s), 438 (m).

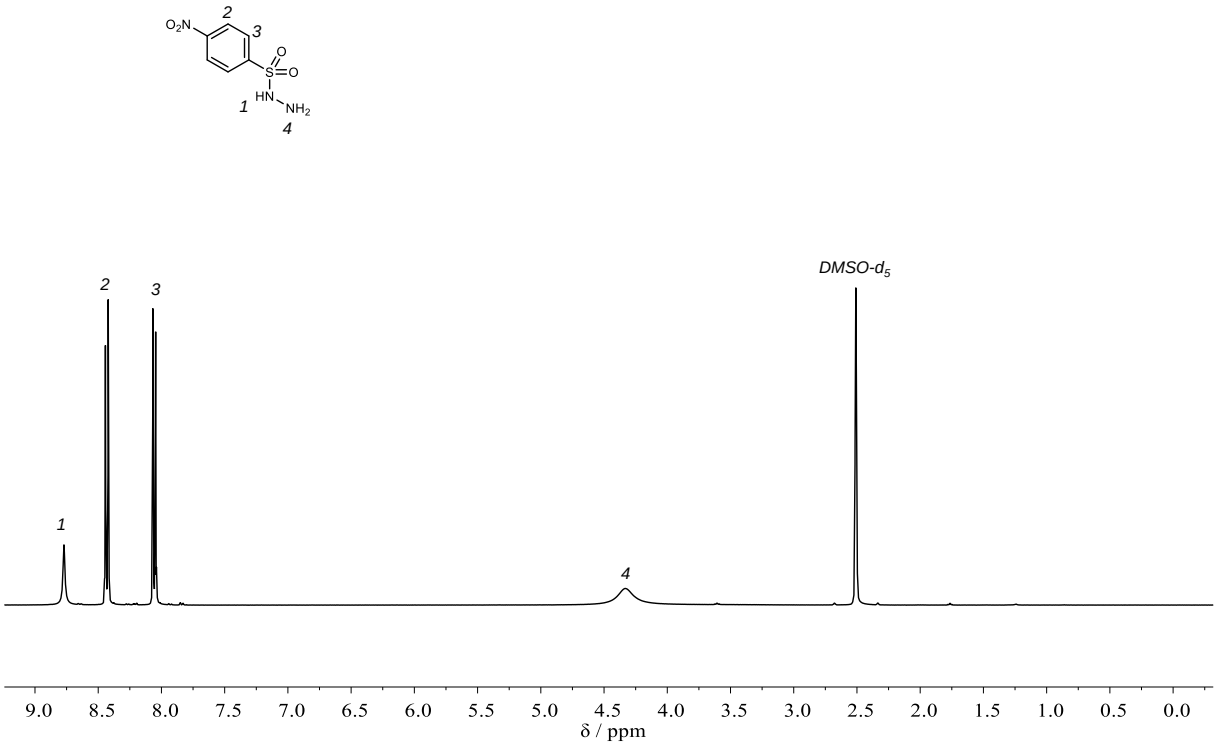

Supplementary Figure 86: ^{1}H NMR spectrum of p-nosyl hydrazide in DMSO-d_6.

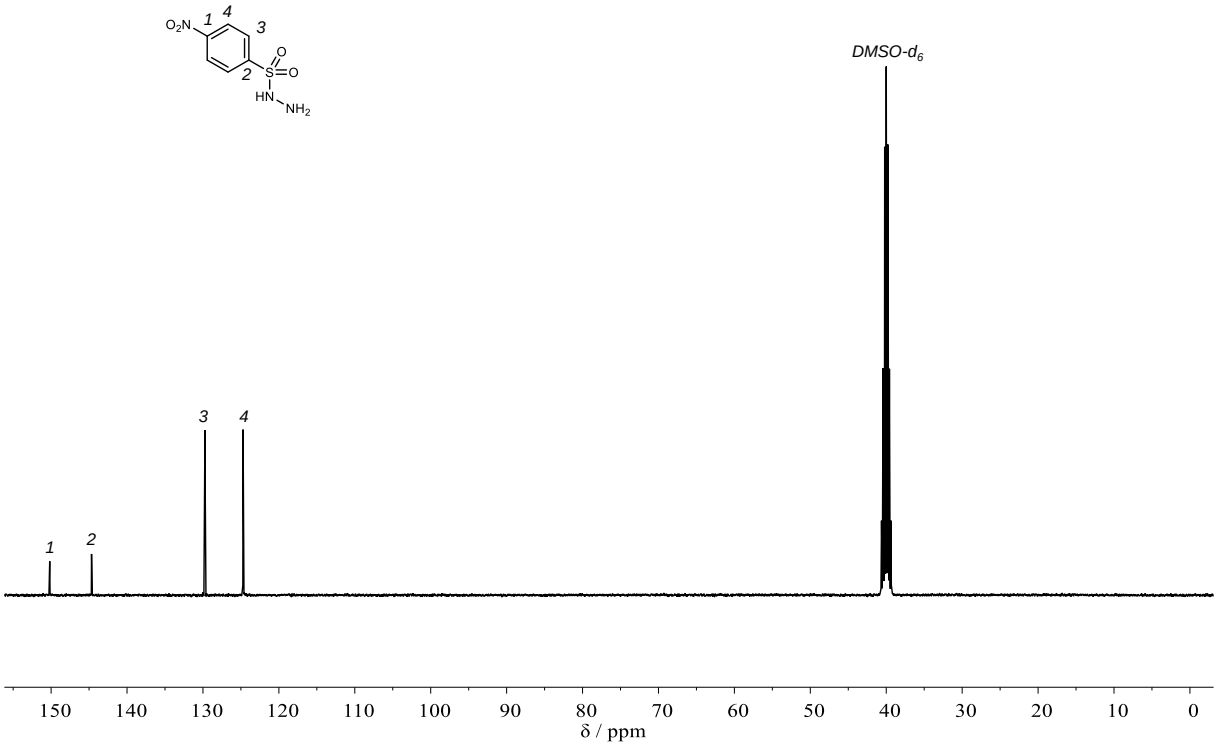

Supplementary Figure 87: ^{13}C NMR spectrum of p-nosyl hydrazide in DMSO-d_6.

4,4'-dimethoxybenzophenone *p*-nosylhydrazone (8a)

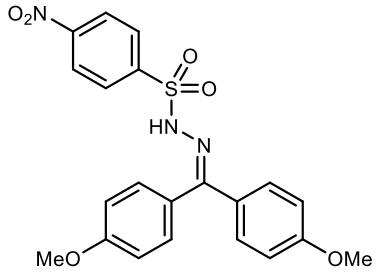

4,4'-Dimethoxybenzophenone (1.21 g, 5.00 mmol, 1.00 equiv.) and *p*-nosyl hydrazide (1.30 g, 6.00 mmol, 1.20 equiv.) were dissolved in 5 mL EtOH and *p*-toluenesulfonic acid monohydrate (47.6 mg, 0.25 mmol, 0.10 equiv.) was added. The mixture was refluxed overnight. The precipitate was filtered and washed with cold EtOH. The product was obtained as a yellow in a yield of 92% (2.02, 4.61 mmol).

^{1}H NMR (500 MHz, DMSO-d_6): δ/ppm = 10.64 (s, 1H), 8.49 – 8.43 (m, 2H), 8.20 – 8.14 (m, 2H), 7.24 – 7.15 (m, 4H), 7.11 – 7.04 (m, 2H), 6.93 – 6.86 (m, 2H), 3.83 (s, 3H), 3.75 (s, 3H).

^{13}C NMR (126 MHz, DMSO-d_6): δ/ppm = 160.66, 159.98, 156.01, 149.92, 144.29, 130.56, 129.69, 129.36, 129.17, 124.66, 124.29, 114.11, 113.75, 55.27, 55.25.

IR (ATR platinum diamond): *ṽ/cm-1* = 3258 (m), 3102 (w), 3061 (vw), 3013 (w), 2972 (w), 2960 (w), 2943 (w), 2913 (w), 2900 (w), 2837 (w), 1604 (m), 1565 (w), 1526 (s), 1504 (s), 1467 (w), 1442 (w), 1419 (w), 1401 (w), 1384 (s), 1343 (s), 1308 (s), 1288 (m), 1244 (vs), 1177 (vs), 1160 (s), 1115 (m), 1107 (m), 1090 (m), 1047 (m), 1028 (s), 1010 (m), 977 (s), 959 (m), 938 (w), 880 (m), 854 (s), 831 (s), 815 (s), 784 (m), 734 (s), 683 (s), 613 (s), 594 (s), 576 (m), 551 (s), 527 (s), 494 (m), 459 (s), 438 (m).

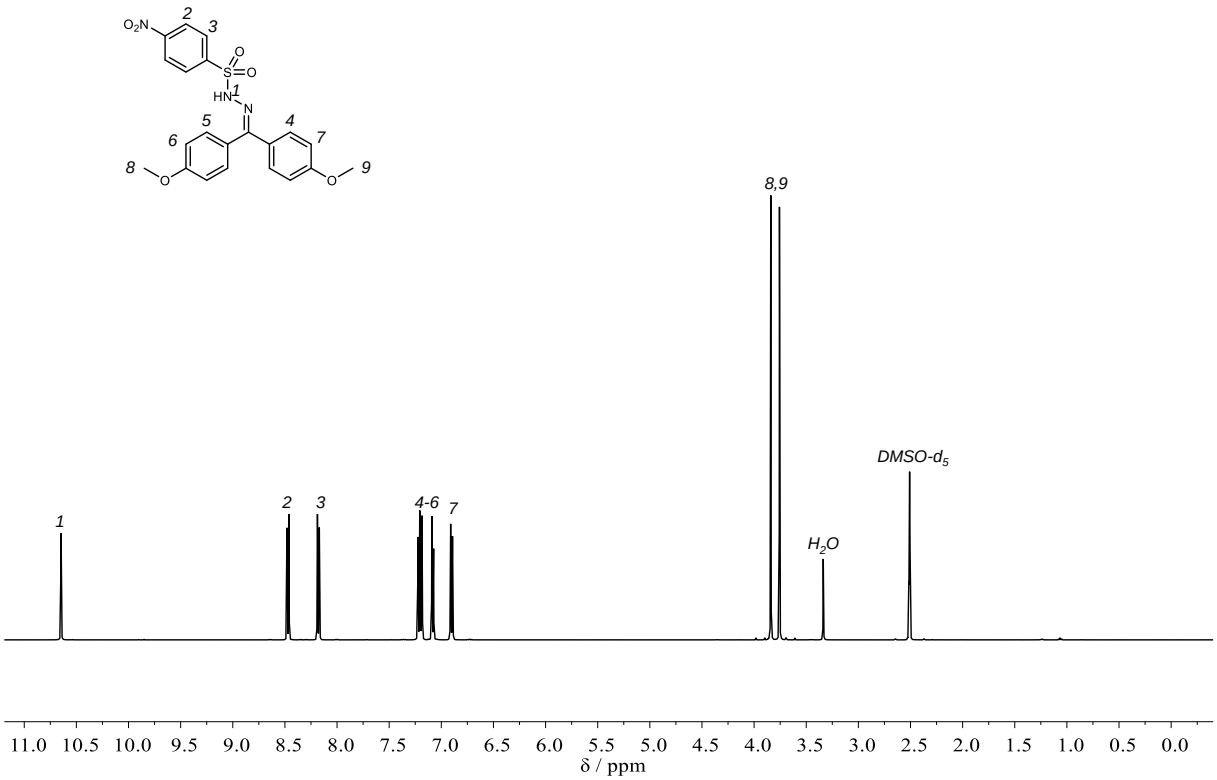

*Supplementary Figure 88: [1]H NMR spectrum of **8a** in DMSO-d6.*

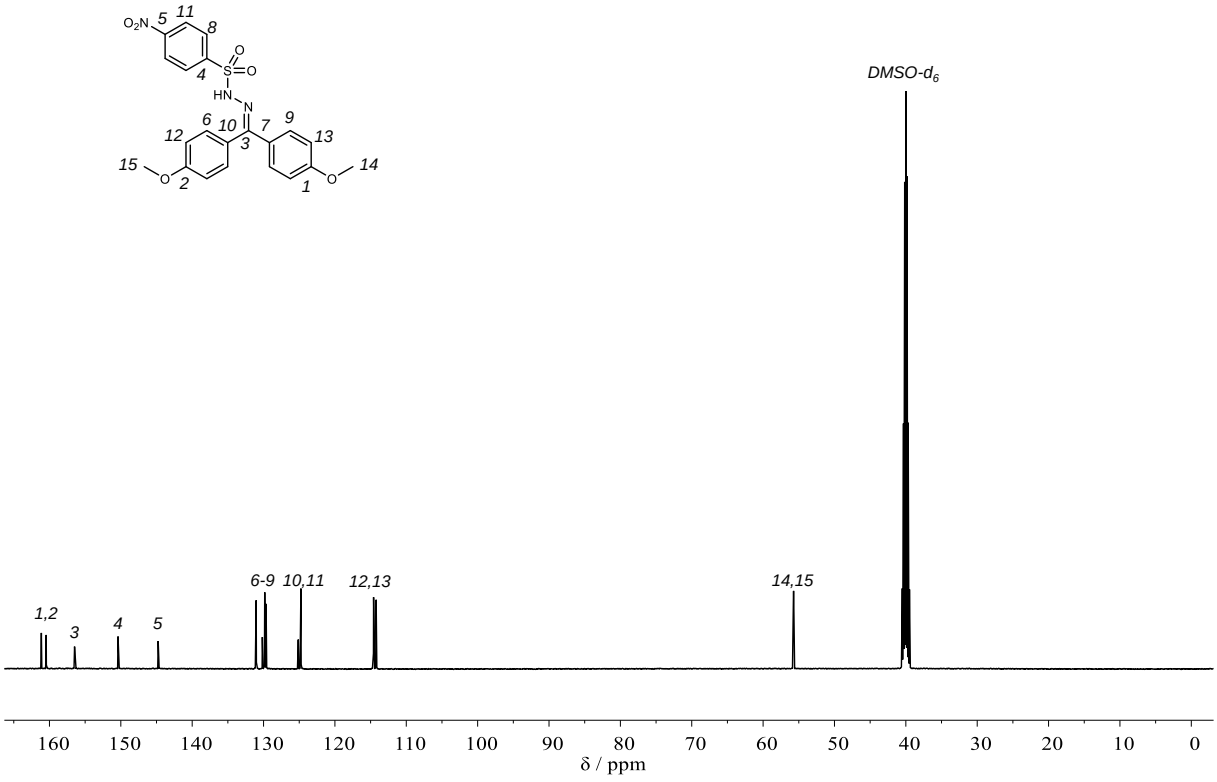

*Supplementary Figure 89: [13]C NMR spectrum of **8a** in DMSO-d6.*

Attempted synthesis of 4,4'-dimethoxyterephthalophenone bis-(p-nosylhydrazone) (7a')

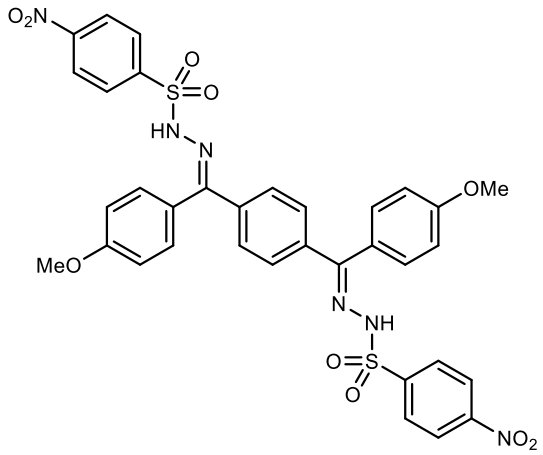

In a glass pressure vial, diketone **6a** (866 mg, 2.50 mmol, 1.00 equiv.) was suspended in 10 mL of ethanol and *p*-nosyl hydrazide (1.63 g, 7.50 mmol, 3.00 equiv.) along with *p*-toluenesulfonic acid monohydrate (47.6 mg, 0.250 mmol, 0.10 equiv.) was added. The vial was closed and stirred at 80 °C for 8 hours. Afterwards, the mixture was cooled to room temperature, the precipitate was filtered, washed with cold ethanol and dried under vacuum. The ^{1}H-NMR of the isolated product indicated that only 38% of **6a** were converted into the desired product **7a'**.

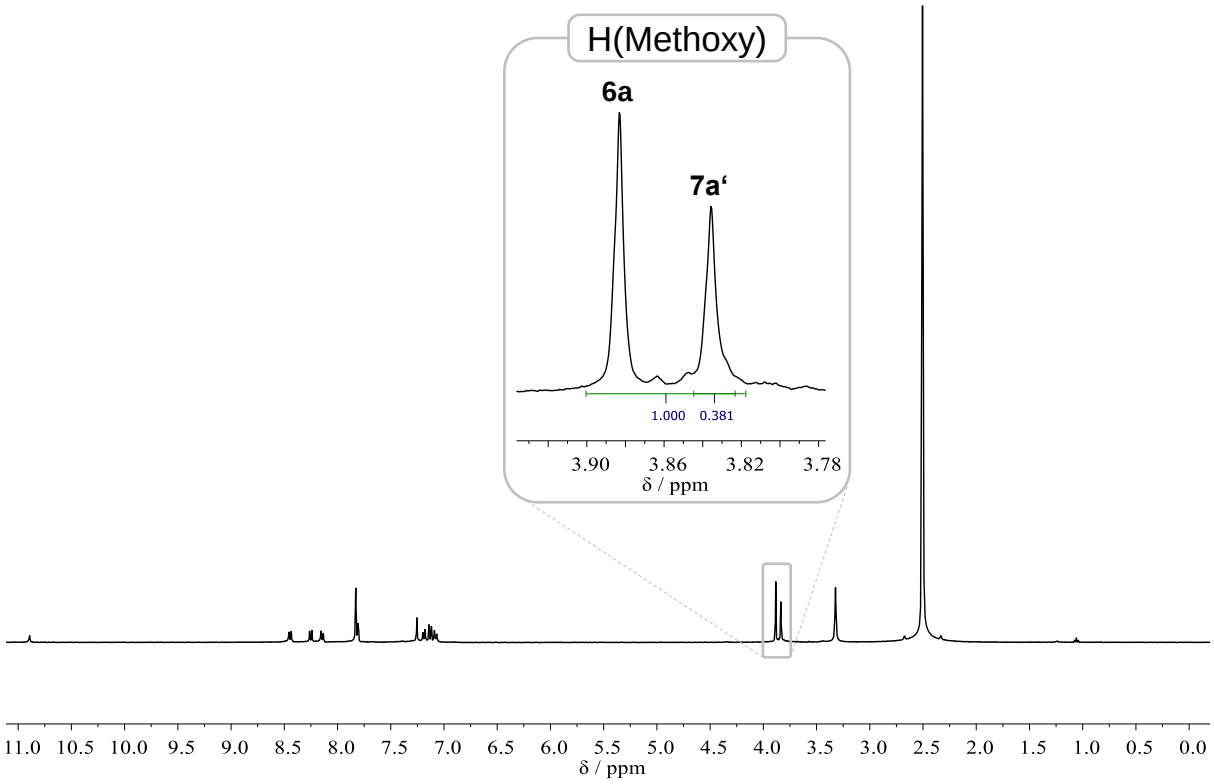

*Supplementary Figure 90: ^{1}H NMR spectrum of the isolated product of the synthesis attempt of **7a'** from **6a.** The highlighted signals in the methoxy region indicate only 38% conversion of **6a**.*

o-Nosyl hydrazide

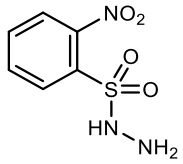

In a Schlenk flask under argon atmosphere, *o*-nosyl chloride (2.22 g, 10.0 mmol, 1.00 equiv.) was dissolved in 20 mL of THF and the solution was cooled to -30 °C (bromobenzene / dry ice bath). Afterwards, hydrazine hydrate (1.23 mL, 1.25 g, 25.0 mmol, 2.50 equiv.) was added dropwise over a period of 10 minutes. The mixture was stirred at -30 °C for 1 hour. Afterwards, 20 mL of ethyl acetate were added and the organic phase was extracted 5 times with 15 mL of 10% NaCl solution. The organic phase was dried over sodium sulfate and precipitated into 120 mL of *n*-hexane. The precipitate was filtered, washed with n-hexane and dried under vacuum. The product was obtained as an off-white solid in a yield of 58% (1.26 g, 5.80 mmol). The procedure was adapter from Myers *et al*.[448]

^{1}H NMR (400 MHz, DMSO-d_6): δ/ppm = 8.88 (s, 1H), 8.07 – 7.92 (m, 2H), 7.86 (dt, *J* = 5.4, 3.7 Hz, 2H), 4.47 (s, 2H).

Note: Due to the thermal instability of the compound in solution, the unassigned signals correspond to the decomposition products (presumably the corresponding sulfinic acid). No ^{13}C NMR spectra were recorded for this reason.

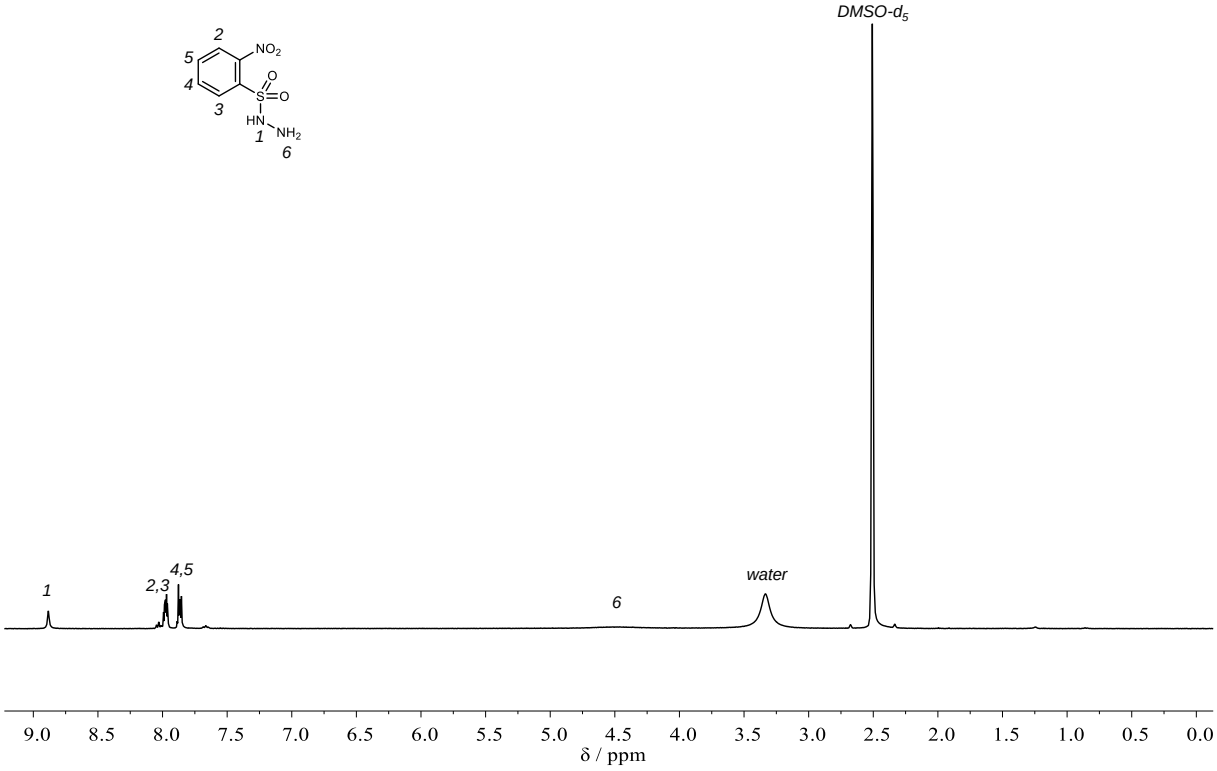

Supplementary Figure 91: ^{1}H NMR spectrum of o-nosyl hydrazide in DMSO-d_6.

Attempted synthesis of 4,4'-dimethoxybenzophenone *o*-nosylhydrazone (8b)

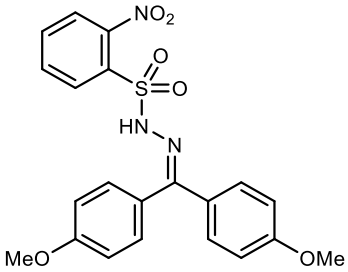

4,4'-Dimethoxybenzophenone (1.21 g, 5.00 mmol, 1.00 equiv.) and *o*-nosyl hydrazide (1.30 g, 6.00 mmol, 1.20 equiv.) were dissolved in 5 mL EtOH and *p*-toluenesulfonic acid monohydrate (47.6 mg, 0.25 mmol, 0.10 equiv.) was added. The mixture was refluxed overnight. The reaction resulted in the formation of an insoluble, black mass and was not further investigated.

Trisyl hydrazide

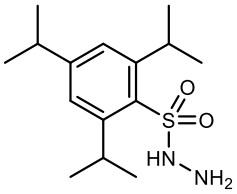

In a Schlenk flask under argon atmosphere, trisyl chloride (3.03 g, 10.0 mmol, 1.00 equiv.) was dissolved in 20 mL of THF and the solution was cooled to -30 °C (bromobenzene / dry ice bath). Afterwards, hydrazine hydrate (1.23 mL, 1.25 g, 25.0 mmol, 2.50 equiv.) was added dropwise over a period of 10 minutes. The mixture was stirred at -30 °C for 1 hour. Afterwards, 20 mL of ethyl acetate were added and the organic phase was extracted 5 times with 15 mL of 10% NaCl solution. The organic phase was dried over sodium sulfate and precipitated in 120 mL of *n*-hexane. The precipitate was filtered, washed with n-hexane and dried under vacuum. The product was obtained as an off-white solid in a yield of 89% (2.66 g, 8.90 mmol). The procedure was adapter from Myers *et al*.[448]

^{1}H NMR (400 MHz, DMSO-d_6): δ/ppm = 8.20 (s, 1H), 7.21 (s, 2H), 4.19 (hept, J = 6.8 Hz, 2H), 2.91 (hept, J = 6.9 Hz, 1H), 1.28 – 1.13 (m, 19H).

Note: Due to the thermal instability of the compound in solution, the unassigned signals correspond to the decomposition products (presumably the corresponding sulfinic acid). No ^{13}C NMR spectra were recorded for this reason.

Furthermore, the NH_2 signal is not visible in the ^{1}H NMR spectrum, presumably due to high water content.

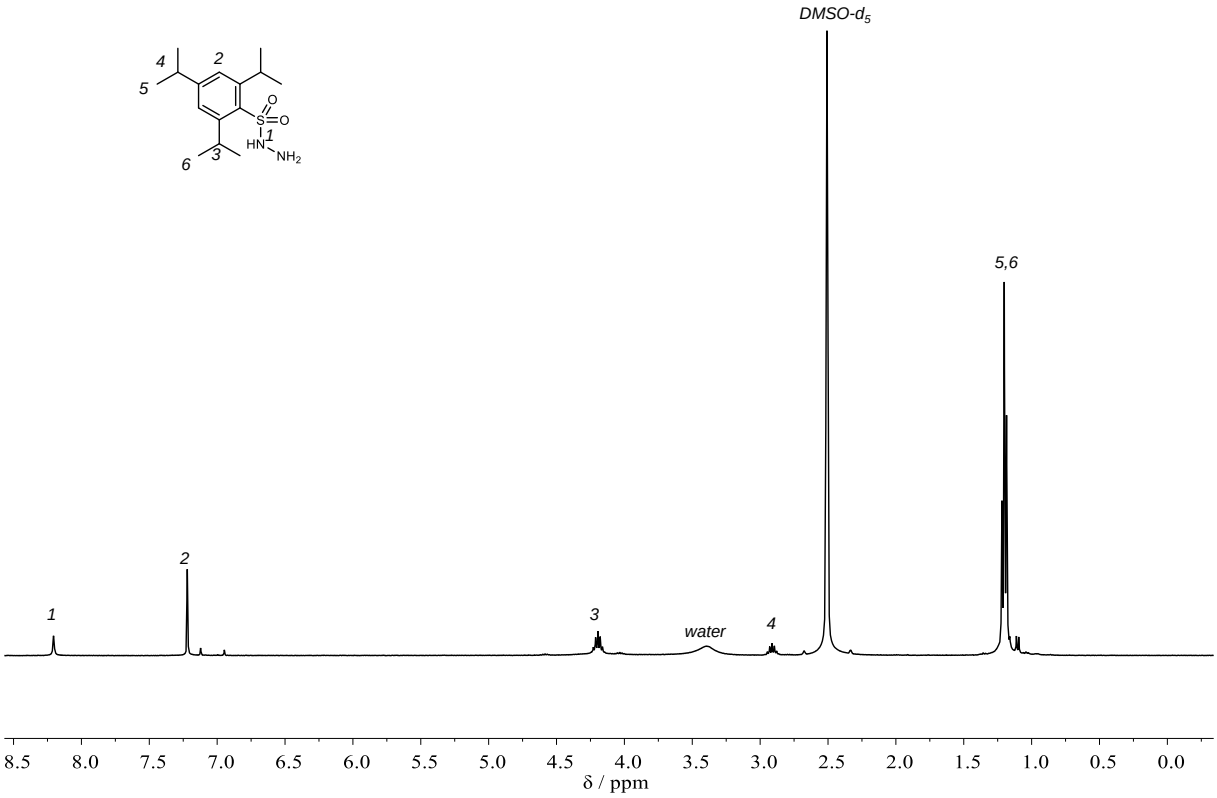

Supplementary Figure 92: ^{1}H NMR spectrum of trisyl hydrazide in DMSO-d_6.

Attempted synthesis of 4,4'-dimethoxybenzophenone trisylhydrazone (8c)

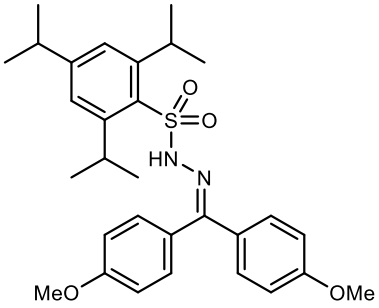

4,4'-Dimethoxybenzophenone (606 mg, 2.50 mmol, 1.00 equiv.) and trisyl hydrazide (895 mg, 3.00 mmol, 1.20 equiv.) were dissolved in 5 mL of toluene and *p*-toluenesulfonic acid monohydrate (47.6 mg, 0.25 mmol, 0.10 equiv.) was added. The mixture was stirred at 80 °C overnight. After cooling, the precipitate was filtered and washed with EtOH. ^{1}H NMR analysis revealed that the reactant 4,4'-dimethoxybenzophenone was recovered.

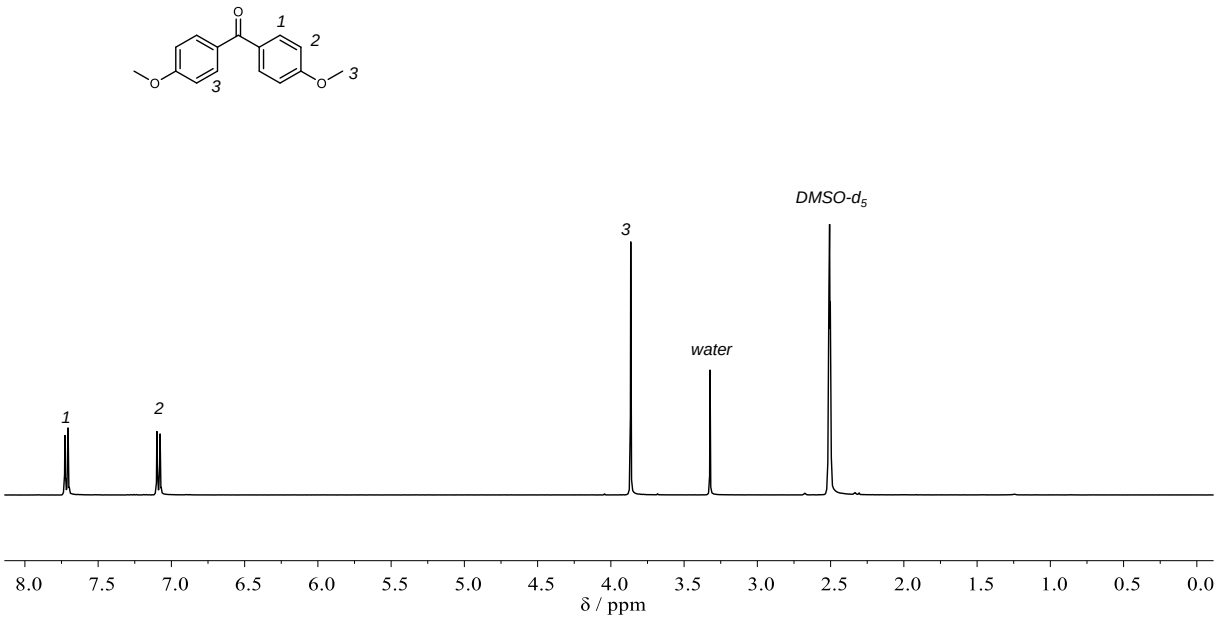

*Supplementary Figure 93: ^{1}H NMR spectrum of the isolated product of the attempted synthesis of **8c**. All signals correspond to recovered starting material.*

6.3.2.4 Monofunctional Homocoupling Screenings

Disclaimer

Screenings were conducted by Florian J. O. Niedermaier under supervision of the author.

The temperature screening reactions for the homocoupling of monofunctional NTH **1a** and *p*-nosylhydrazone **8a** described in chapter 4.2.3.2 were conducted according to the following procedure.

The sulfonylhydrazone (**1a** or **8a**, 0.250 mmol, 1.00 equiv.) was added to a crimp vial and potassium carbonate (41.5 mg, 0.300 mmol, 1.20 equiv.) and elemental sulfur (16.0 mg, 0.500 mmol S, 2.00 equiv. S) were added. If the screening reaction was conducted under inert atmosphere, all glassware was flame-dried before use and the reagents and starting materials were previously dried in a vacuum oven. The vial was closed and, if the reaction was conducted under inert atmosphere, flushed with argon. Afterwards, 0.50 mL of solvent were added using a syringe. The reaction was then heated to the desired temperature. NMR samples were taken after the desired time by retrieving approximately 20-50 µL of the crude mixture from the reaction vessel with a syringe and dissolving the sample in DMSO-d_6. The sulfonylhydrazone conversion was calculated by measuring the integrals of the spectral methoxy region (I_{OMe}, 3.60 ppm to 3.90 ppm) and one of the methoxy integrals of the sulfonylhydrazones ($I_{\mathrm{Hydrazone}}$) according to Equation 7.

$$\text{Conversion (\%)} = \left(1 - \frac{2 \cdot I_{Hydrazone}}{I_{Methoxy}}\right) \cdot 100\% \qquad (7)$$

Notably, the methoxy signals of the sulfonylhydrazone are shifted comparted to the isolated compounds due to the influence of potassium carbonate. They were recognized by their characteristic appearance, exhibiting of two singlets of equal intensity, and integrated manually. The integration is shown for an exemplary sample in Supplementary Figure 94. All results of the conducted screenings are listed in the Results and Discussion section 4.2.3.2 in Table 3.

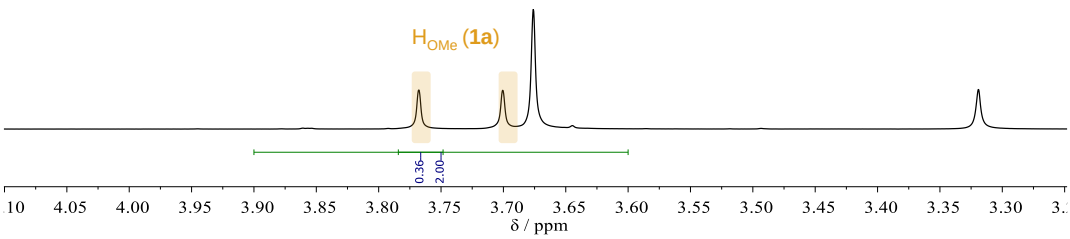

Supplementary Figure 94: Integration for the conversion calculation for a representative sample (Table 3, entry 5, 2h). Using equation 7. 64% conversion are obtained.

6.3.2.5 Synthesis of Polymers

Disclaimer

P2-P8 were synthesized by Sophia Abou El Mirate under supervision of the author.

General procedure for the polymerization of bifunctional NTHs:

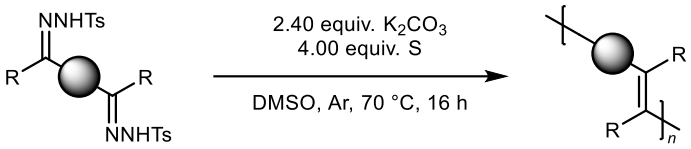

All reagents were dried *in vacuo* before use. All glassware was flame-dried before use.
In a Schlenk flask under argon atmosphere, the respective bis(NTH) **7x** (0.5 mmol, 1.00 equiv.) was suspended in 1 mL DMSO (c = 0.25 M) and potassium carbonate (2.40 equiv.) and elemental sulfur (4.00 equiv. S) were added. The mixture was heated to 70 °C and stirred for 16 hours.
Afterwards, the mixture was cooled to room temperature and diluted with 10 mL of chloroform. After stirring for an additional 5 minutes, the mixture was filtered over celite. The organic phase was washed twice with 50 mL each of 10% sodium sulfite solution and thrice with water. After drying over sodium sulfate, the organic phase was concentrated under reduced pressure (V ~ 1mL) and subsequently precipitated into cold MeOH. The precipitated polymer was filtered, washed with MeOH and dried *in vacuo*.

Polymerization Screenings

The screenings of different polymerization conditions described in sections 4.2.3.1 and 4.2.3.3 were conducted according to the herein described general procedure with slight modifications. The screening reactions used a reduced scale of 0.125 mmol **7a**, and crimp vials were used as the reaction vessels. The desired reaction temperature was adjusted accordingly, and the reactions were conducted for as long as was necessary to achieve full conversion of NTH **1a** at the respective temperature in the screenings described in Table 3 (30 min for T ≥ 90 °C, 3 h for T = 80 °C, 16 h for T = 70 °C). Afterwards, the polymers were isolated according to general procedure and analyzed *via* SEC. Only in the case of the first screening reaction (Table 4, entry 1), DCM was used as the workup solvent instead of chloroform and the organic phase was not washed with either water or sodium sulfite solution.
The full results are listed in section 4.2.3.3 in Table 4.

Poly-(1,4-phenylene-1,2-bis(methoxyphenyl)vinylene) (P1)

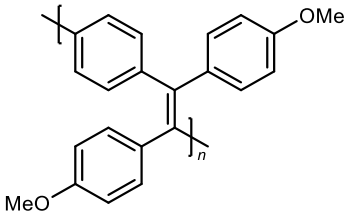

Synthesized from **7a** according to general procedure. Obtained as a yellow solid in a yield of 76% (119 mg, 0.379 mmol).

^{1}H NMR (500 MHz, Chloroform-*d*): δ/ppm = 6.99 – 6.45 (m, 12H), 3.84 – 3.52 (m, 6H).

^{13}C NMR (126 MHz, Chloroform-*d*): δ/ppm = 159.13 – 157.01 (m), 143.29 – 141.35 (m), 140.41 – 138.80 (m), 137.43 – 135.39 (m), 133.70 – 132.41 (m), 131.90 – 129.96 (m), 114.13 – 111.58 (m), 55.80 – 53.79 (m).

IR (ATR platinum diamond): $\tilde{\nu}/cm^{-1}$ = 3030 (vw), 2997 (vw), 2950 (vw), 2931 (vw), 2904 (vw), 2832 (vw), 1604 (m), 1574 (w), 1508 (s), 1462 (w), 1440 (w), 1411 (vw), 1401 (vw), 1288 (m), 1242 (vs), 1172 (s), 1140 (vw), 1109 (w), 1033 (m), 975 (vw), 956 (vw), 930 (vw), 860 (vw), 829 (m), 804 (m), 780 (w), 765 (w), 751 (w), 718 (vw), 658 (vw), 625 (vw), 588 (w), 568 (w), 522 (w), 475 (vw).

Elemental Analysis: %**C**, calculated 84.05%, found 81.33%; %**H**, calculated 5.77%, found 5.61%; %**S**, calculated 0.00%, found 0.00 %.

SEC (THF): M_n = 16.2 kDa, M_w = 34.2 kDa, $Đ$ = 2.11.

TGA: $T_{d,5\%}$ = 457 °C , Residue = 63.3 %.

DSC: T_g = 227 °C.

Fluorescence: $\lambda_{em,max}$ = 530 nm with λ_{ex} = 373 nm.

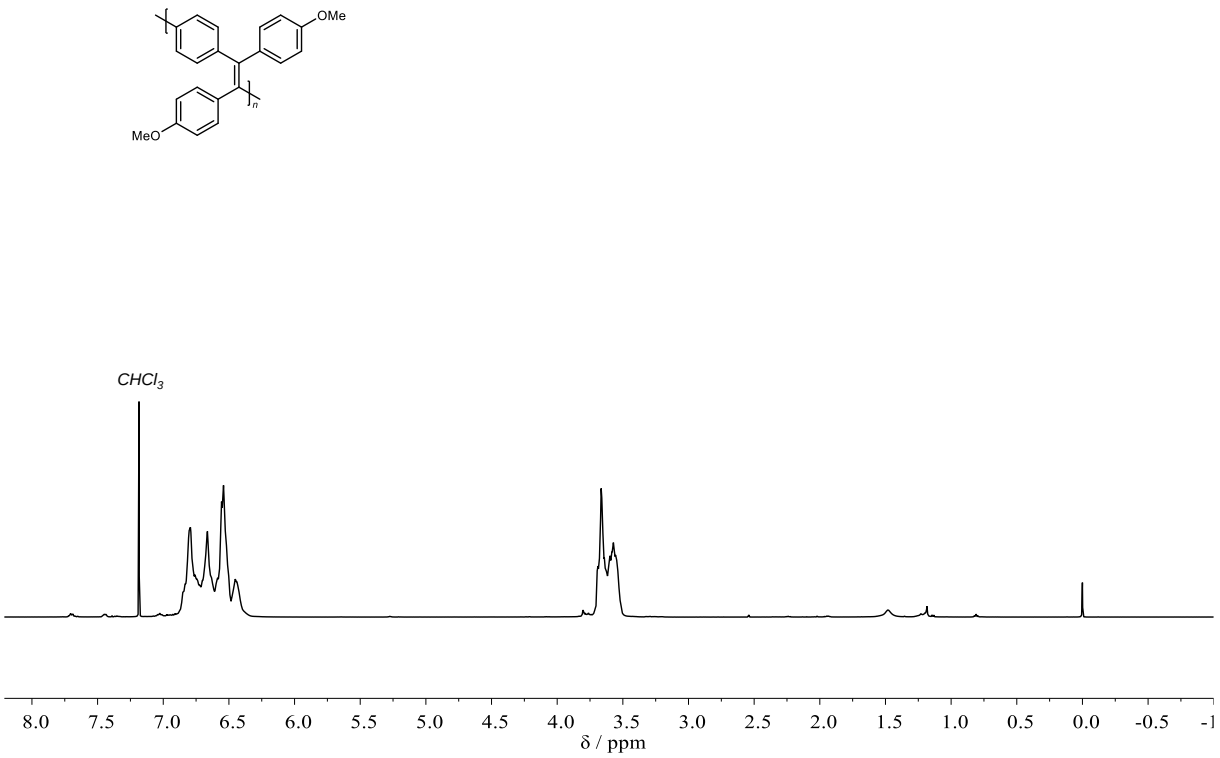

*Supplementary Figure 95: ^{1}H NMR spectrum of **P1** in $CDCl_3$.*

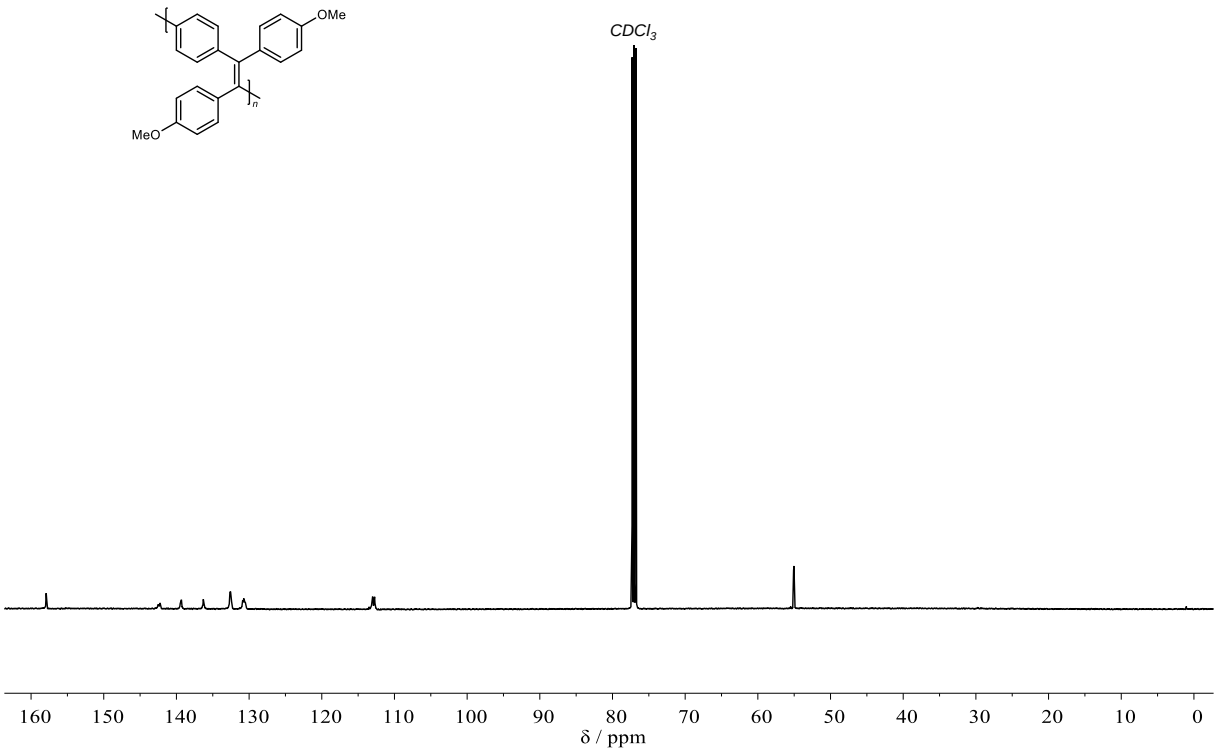

*Supplementary Figure 96: ^{13}C NMR spectrum of **P1** in $CDCl_3$.*

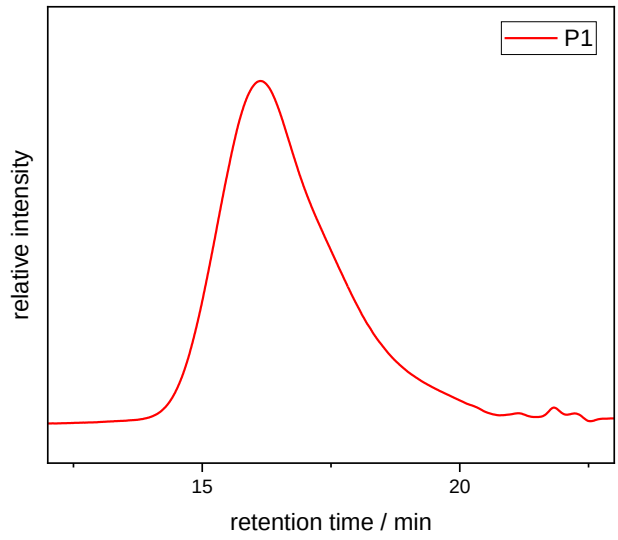

*Supplementary Figure 97: SEC trace of **P1** (measured in THF).*

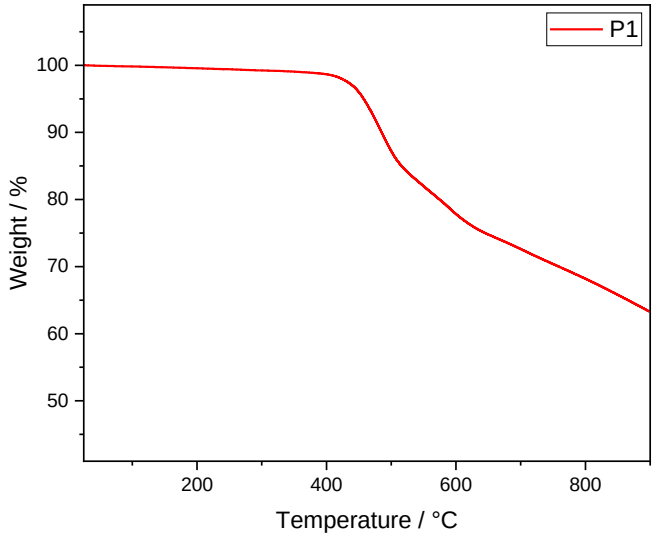

*Supplementary Figure 98: TGA curve of **P1**.*

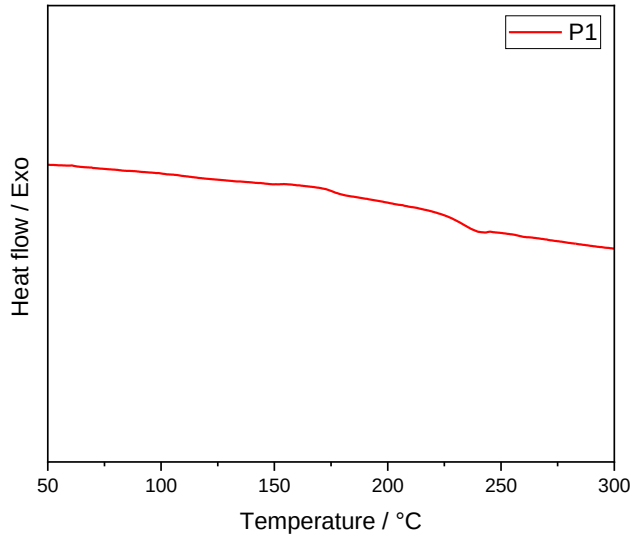

*Supplementary Figure 99: DSC curve of **P1**.*

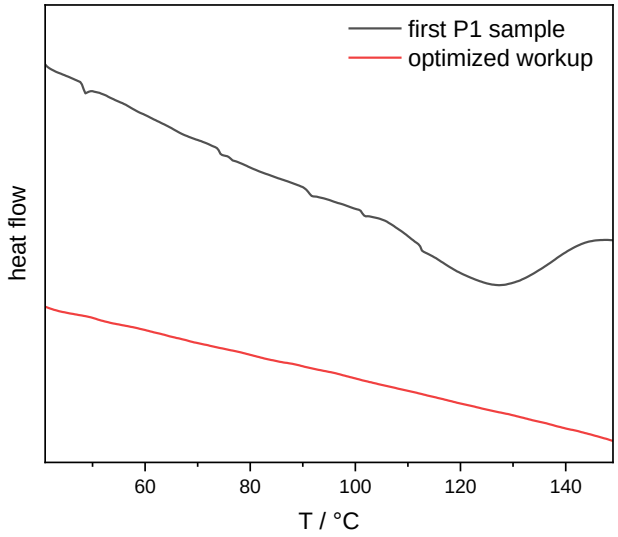

*Supplementary Figure 100: DSC curve of the first obtained sample of **P1** (Table 4, entry 1, black curve) and a **P1** sample obtained after workup optimization (Table 4, entry 2, red curve). The endothermic peak at ~120 °C for the pre-optimized **P1** sample indicates the presence of residual sulfur in the polymer.*

Poly-(1,4-phenylene-1,2-diphenylvinylene) (P2)

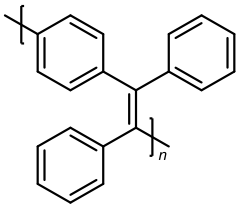

Synthesized from **7b** according to general procedure. Obtained as a yellow solid in a yield of 60% (76.3 mg, 0.300 mmol)

^{1}H NMR (500 MHz, Chloroform-*d*): δ/ppm = 7.18 – 6.47 (m, 14H).

^{13}C NMR (126 MHz, Chloroform-*d*): δ/ppm = 144.02 – 143.29 (m), 142.60 – 141.62 (m), 141.19 – 140.29 (m), 131.86 – 131.17 (m), 131.13 – 130.26 (m), 128.09 – 127.29 (m), 127.04 – 126.06 (m).

IR (ATR platinum diamond): $\tilde{\nu}/cm^{-1}$ = 3075 (vw), 3022 (vw), 1596 (vw), 1576 (vw), 1504 (w), 1491 (w), 1442 (w), 1401 (vw), 1275 (vw), 1179 (vw), 1154 (w), 1129 (w), 1111 (w), 1074 (vw), 1028 (w), 1018 (w), 975 (m), 913 (vw), 864 (vw), 852 (vw), 802 (w), 761 (w), 736 (w), 695 (vs), 631 (w), 576 (vw), 492 (w).

SEC (THF): M_n = 26.9 kDa, M_w = 50.1 kDa, $Đ$ = 1.86.

TGA: $T_{d,5\%}$ = 541 °C , Residue = 66.4 %.

DSC: T_g = 256 °C.

Fluorescence: $\lambda_{em,max}$ = 516 nm with λ_{ex} = 357 nm.

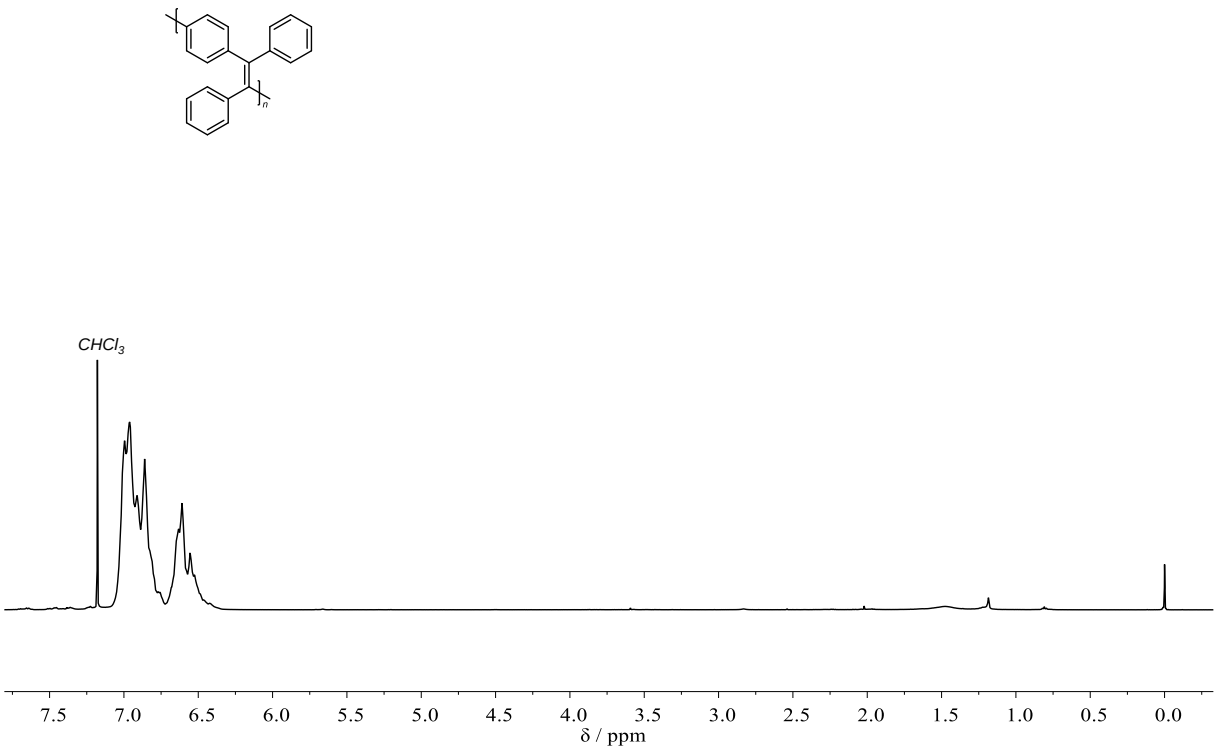

*Supplementary Figure 101: ^{1}H NMR spectrum of **P2** in $CDCl_3$.*

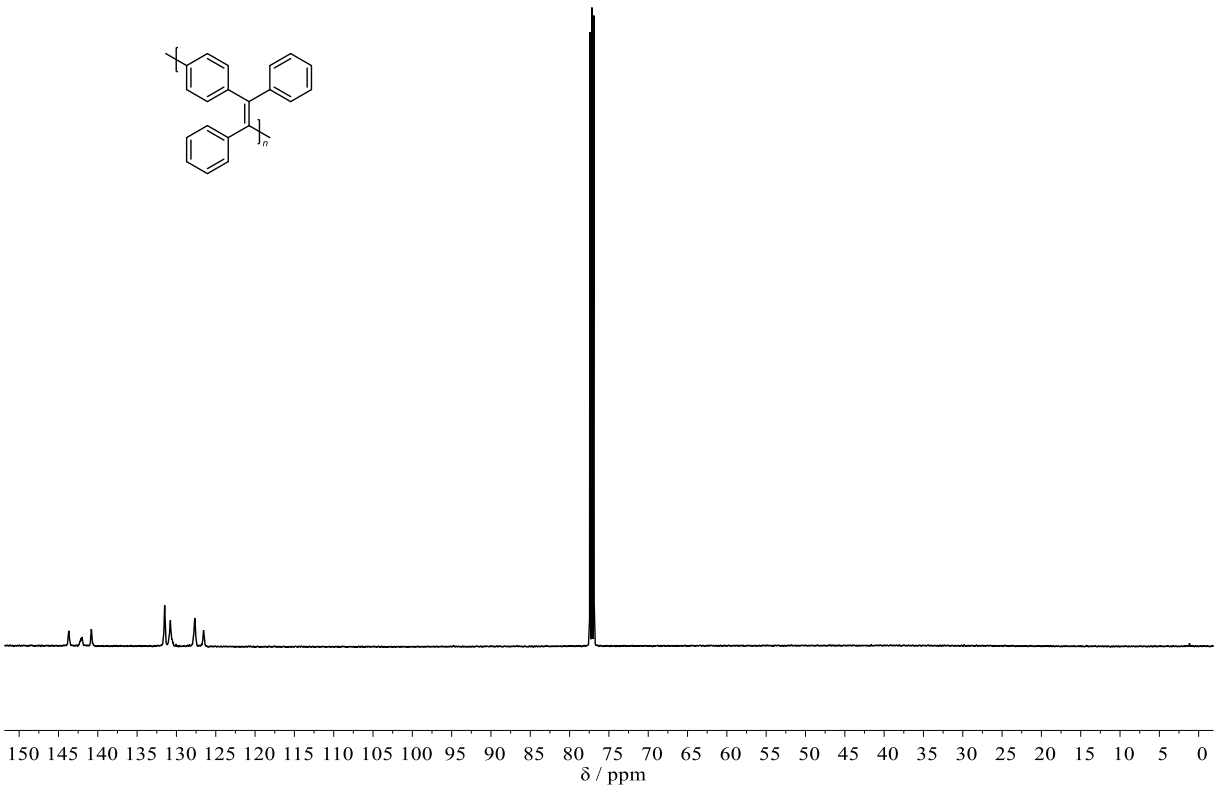

*Supplementary Figure 102: ^{13}C NMR spectrum of **P2** in $CDCl_3$.*

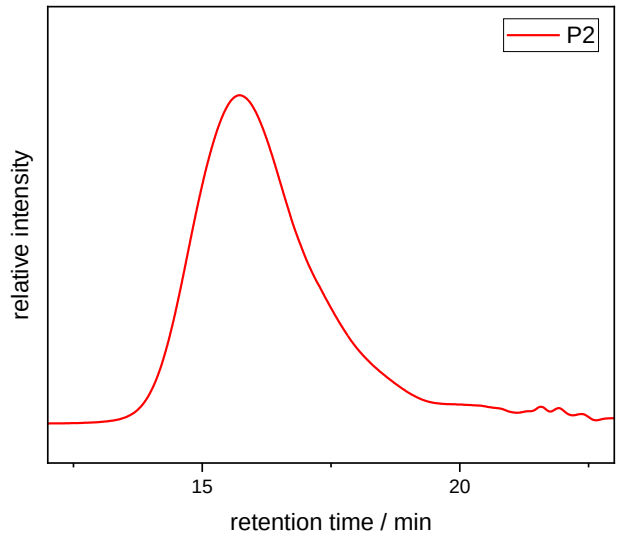

*Supplementary Figure 103: SEC trace of **P2** (measured in THF).*

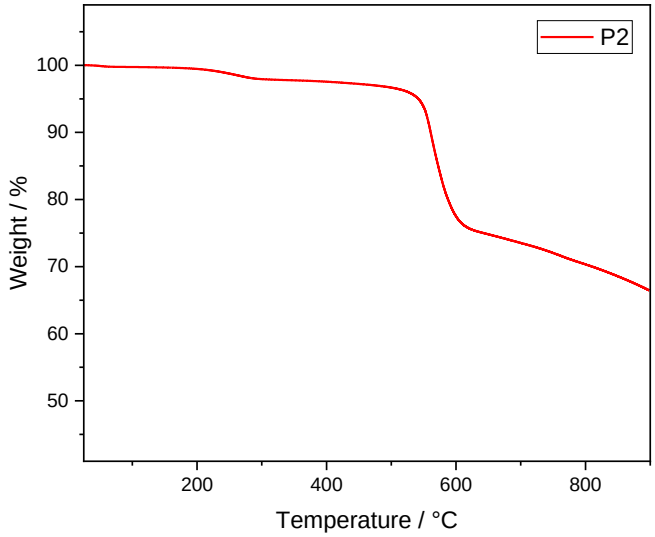

*Supplementary Figure 104: TGA curve of **P2**.*

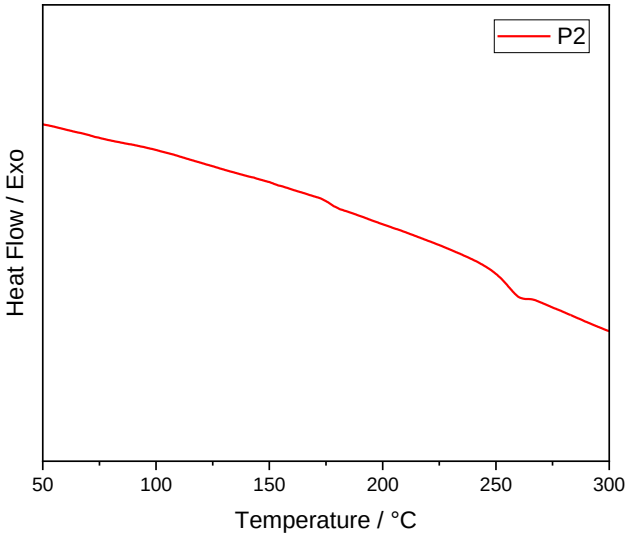

*Supplementary Figure 105: DSC curve of **P2**.*

Poly-(1,4-phenylene-1,2-bis(4-phenoxyphenyl)vinylene) (P3)

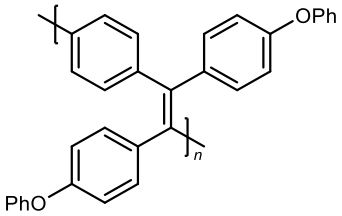

Synthesized from **7c** according to general procedure. Obtained as a yellow solid in a yield of 76% (167 mg, 0.380 mmol).

^{1}H NMR (500 MHz, Chloroform-*d*): δ/ppm = 7.37 – 6.49 (m, 22H).

^{13}C NMR (126 MHz, Chloroform-*d*): δ/ppm = 157.42 – 156.70 (m), 156.13 – 155.40 (m), 142.58 – 141.92 (m), 140.34 – 139.76 (m), 138.90 – 138.14 (m), 133.25 – 132.59 (m), 131.29 – 130.42 (m), 130.20 – 129.47 (m), 123.69 – 122.91 (m), 119.47 – 118.62 (m), 118.52 – 117.50 (m).

IR (ATR platinum diamond): $\tilde{\nu}/cm^{-1}$ = 3063 (vw), 3055 (vw), 3030 (vw), 1586 (m), 1502 (m), 1485 (vs), 1456 (w), 1405 (vw), 1331 (vw), 1277 (w), 1228 (vs), 1201 (m), 1164 (m), 1107 (w), 1072 (w), 1014 (m), 977 (w), 961 (vw), 907 (vw), 862 (m), 835 (m), 800 (w), 747 (s), 689 (s), 669 (w), 625 (w), 607 (vw), 590 (w), 574 (vw), 539 (vw), 496 (w), 416 (vw), 409 (vw).

SEC (THF): M_n = 14.7 kDa, M_w = 28.1 kDa, $Đ$ = 1.90.

TGA: $T_{d,5\%}$ = 516 °C , Residue = 68.6 %.

DSC: T_g = 155 °C.

Fluorescence: $\lambda_{em,max}$ = 518 nm with λ_{ex} = 370 nm.

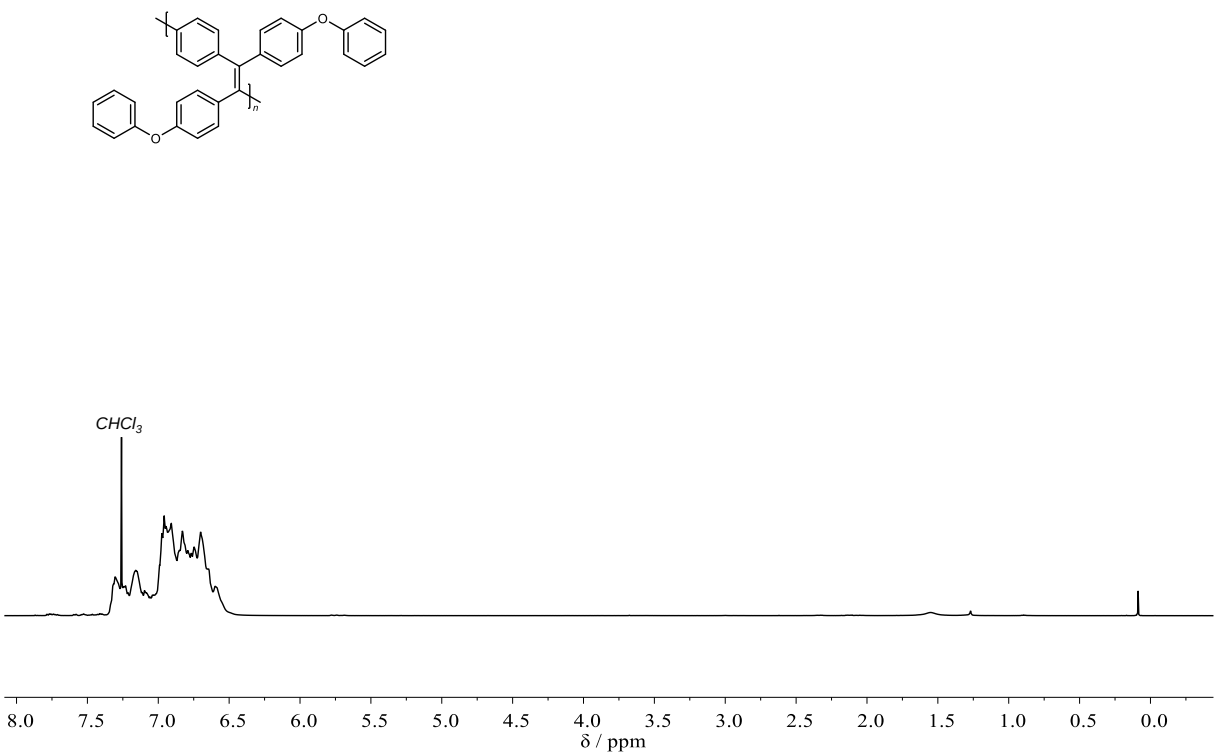

*Supplementary Figure 106: ^{1}H NMR spectrum of **P3** in $CDCl_3$.*

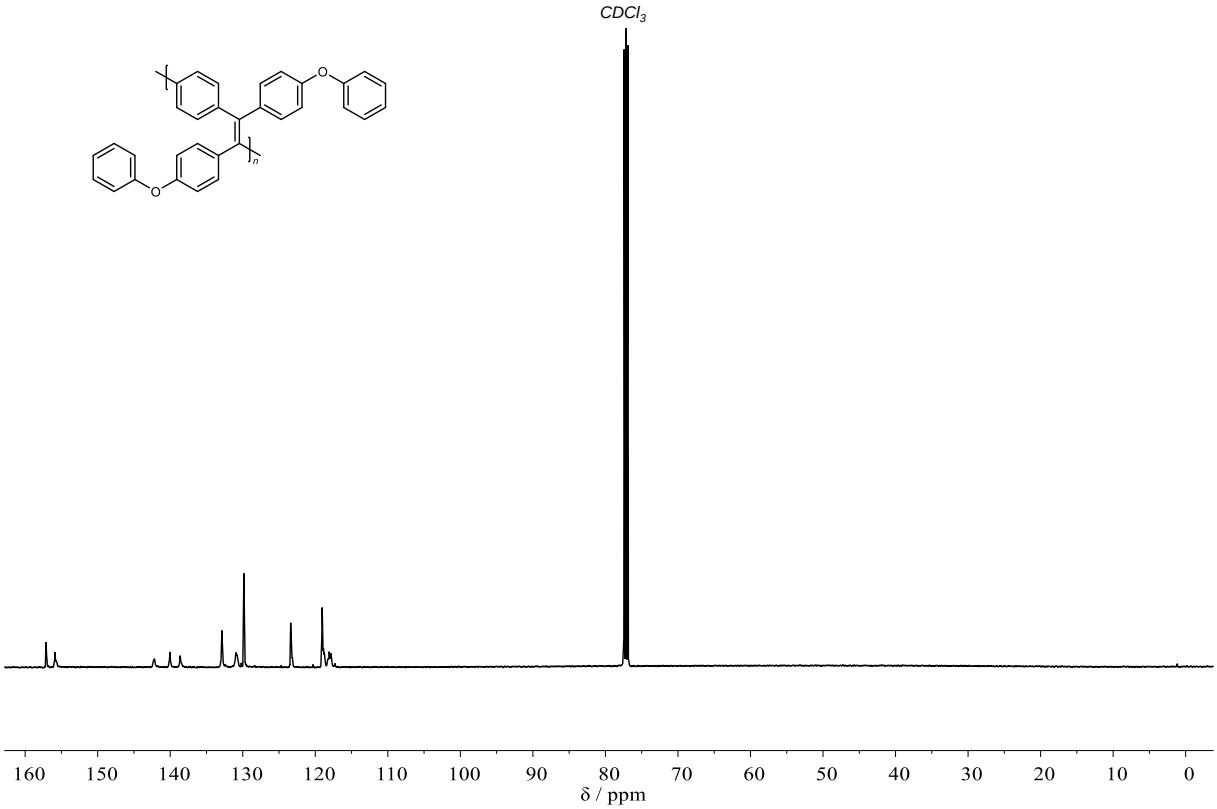

*Supplementary Figure 107: ^{13}C NMR spectrum of **P3** in $CDCl_3$.*

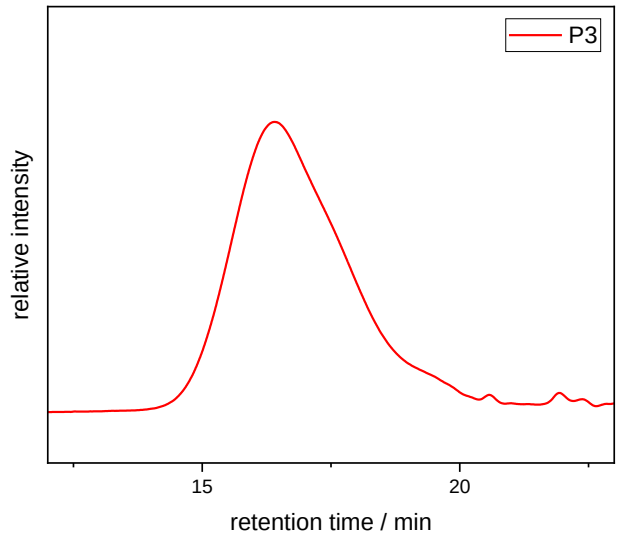

*Supplementary Figure 108: SEC trace of **P3** (measured in THF).*

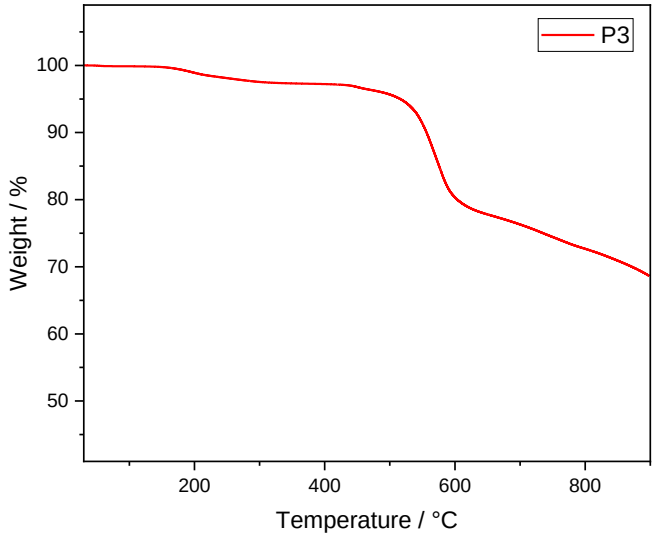

*Supplementary Figure 109: TGA curve of **P3**.*

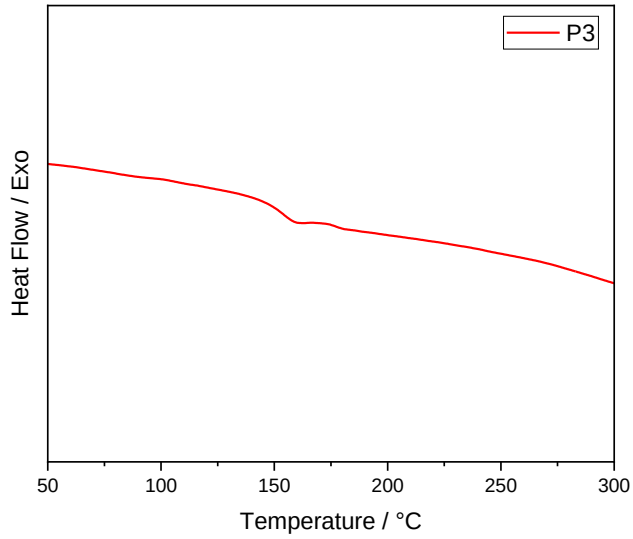

*Supplementary Figure 110: DSC curve of **P3**.*

Poly-(1,4-phenylene-1,2-bis(4-phenylthiophenyl)vinylene) (P4)

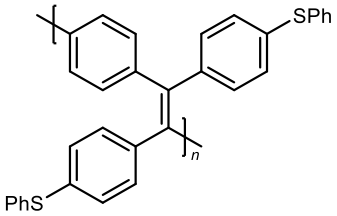

Synthesized from **7d** according to general procedure. Obtained as a yellow solid in a yield of 88% (207 mg, 0.440 mmol).

^{1}H NMR (500 MHz, Chloroform-*d*): δ/ppm = 7.37 – 6.45 (m, 22H).

^{13}C NMR (126 MHz, Chloroform-*d*): δ/ppm = 142.47 – 141.67 (m), 140.89 – 140.35 (m), 136.00 – 135.34 (m), 134.58 – 133.82 (m), 132.65 – 131.99 (m), 131.79 – 129.76 (m), 129.65 – 129.04 (m), 127.45 – 126.79 (m).

IR (ATR platinum diamond): $\tilde{\nu}/cm^{-1}$ = 3055 (vw), 3048 (vw), 3020 (vw), 1580 (m), 1551 (vw), 1500 (w), 1487 (m), 1475 (s), 1438 (m), 1395 (w), 1302 (vw), 1269 (w), 1179 (vw), 1135 (w), 1109 (w), 1080 (m), 1014 (m), 1000 (m), 975 (w), 926 (vw), 870 (w), 858 (w), 825 (m), 790 (m), 734 (vs), 687 (vs), 627 (w), 578 (w), 568 (w), 525 (w), 514 (w), 467 (m), 438 (vw), 432 (vw), 424 (vw).

SEC (THF): M_n = 12.5 kDa, M_w = 27.8 kDa, $Đ$ = 2.23.

TGA: $T_{d,5\%}$ = 471 °C , Residue = 64.4 %.

DSC: T_g = 161 °C.

Fluorescence: $\lambda_{em,max}$ = 531 nm with λ_{ex} = 370 nm.

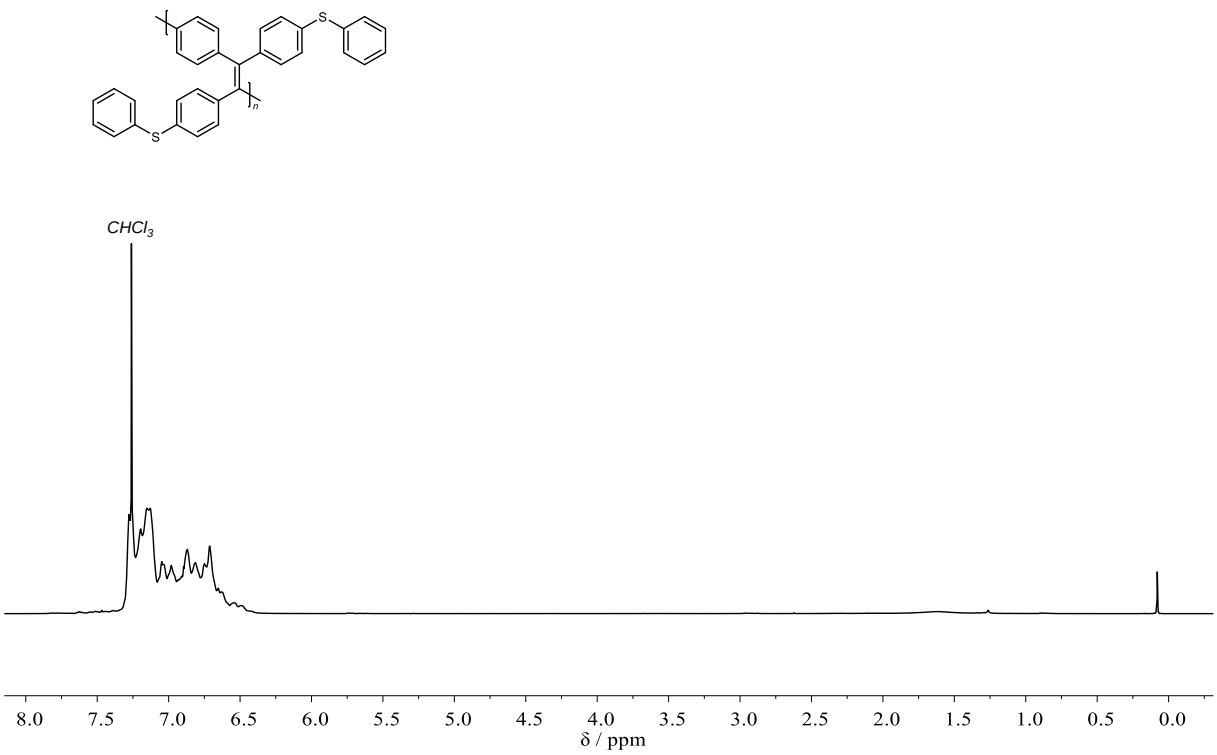

*Supplementary Figure 111: ^{1}H NMR spectrum of **P4** in $CDCl_3$.*

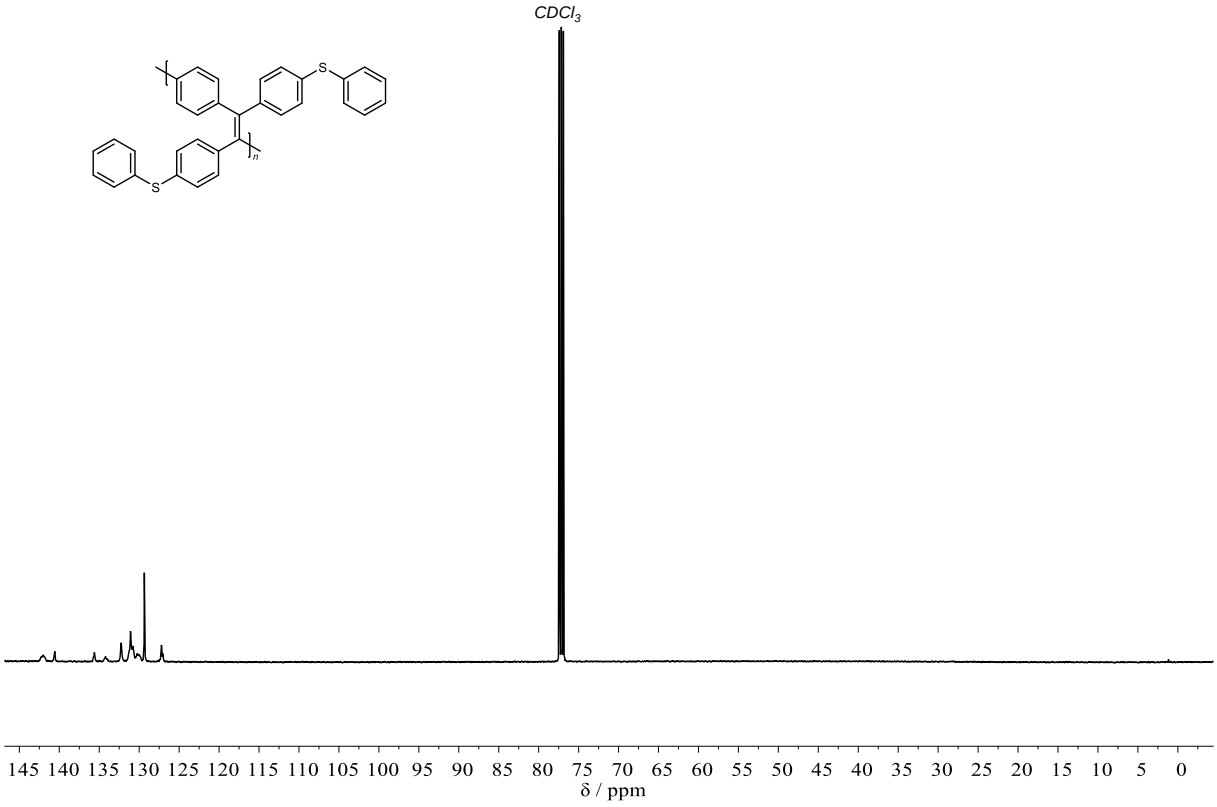

*Supplementary Figure 112: ^{13}C NMR spectrum of **P4** in $CDCl_3$.*

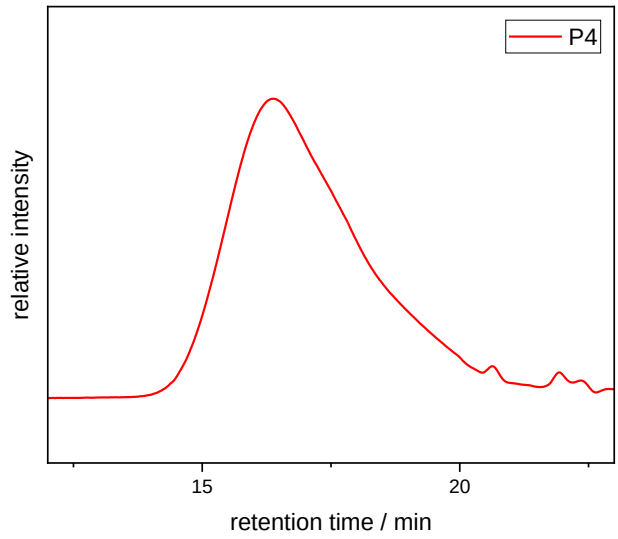

*Supplementary Figure 113: SEC trace of **P4** (measured in THF).*

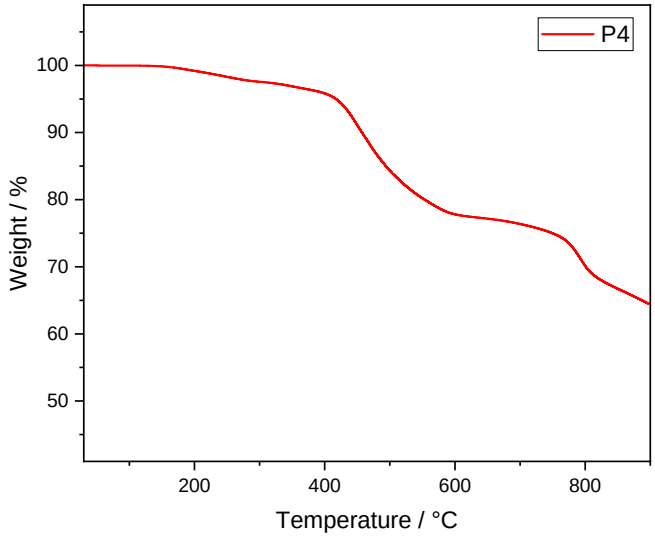

*Supplementary Figure 114: TGA curve of **P4**.*

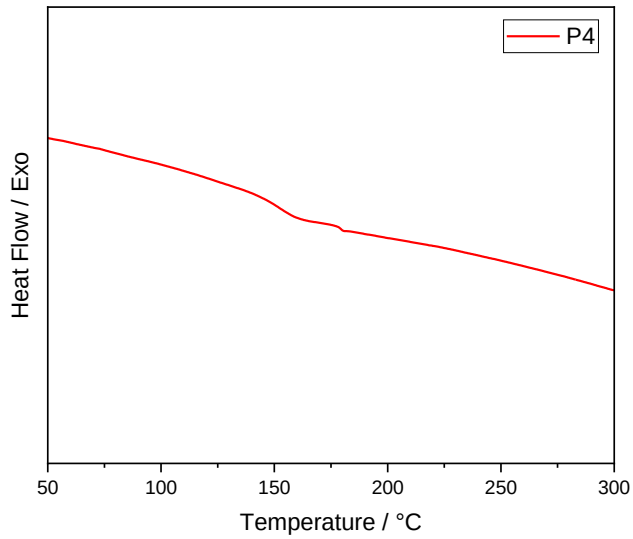

*Supplementary Figure 115: DSC curve of **P4**.*

Poly-(1,3-phenylene-1,2-diphenylvinylene) (P5)

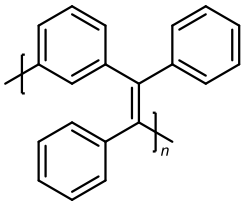

Synthesized from **7e** according to general procedure. Obtained as an off-white solid in a yield of 47% (60.2 mg, 0.237 mmol).

^{1}H NMR (500 MHz, Chloroform-*d*): δ/ppm = 7.12 – 6.53 (m, 14H).

^{13}C NMR (126 MHz, Chloroform-*d*): δ/ppm = 143.82 – 142.61 (m), 141.15 – 140.43 (m), 134.28 – 133.48 (m), 131.39 – 130.74 (m), 129.82 – 128.81 (m), 127.92 – 126.91 (m), 126.52 – 125.86 (m).

IR (ATR platinum diamond): $\tilde{\nu}/cm^{-1}$ = 3077 (vw), 3052 (vw), 3020 (vw), 1596 (w), 1576 (vw), 1491 (w), 1442 (w), 1179 (vw), 1156 (vw), 1086 (vw), 1074 (w), 1031 (vw), 1000 (vw), 911 (vw), 788 (w), 761 (w), 695 (vs), 671 (w), 640 (vw), 619 (w), 564 (w), 487 (vw), 463 (vw), 453 (vw), 440 (vw), 434 (vw).

SEC (THF): M_n = 10.3 kDa, M_w = 20.7 kDa, $Đ$ = 2.01.

TGA: $T_{d,5\%}$ = 538 °C , Residue = 46.3 %.

DSC: T_g = 194 °C.

Fluorescence: $\lambda_{em,max}$ = 473 nm with λ_{ex} = 312 nm.

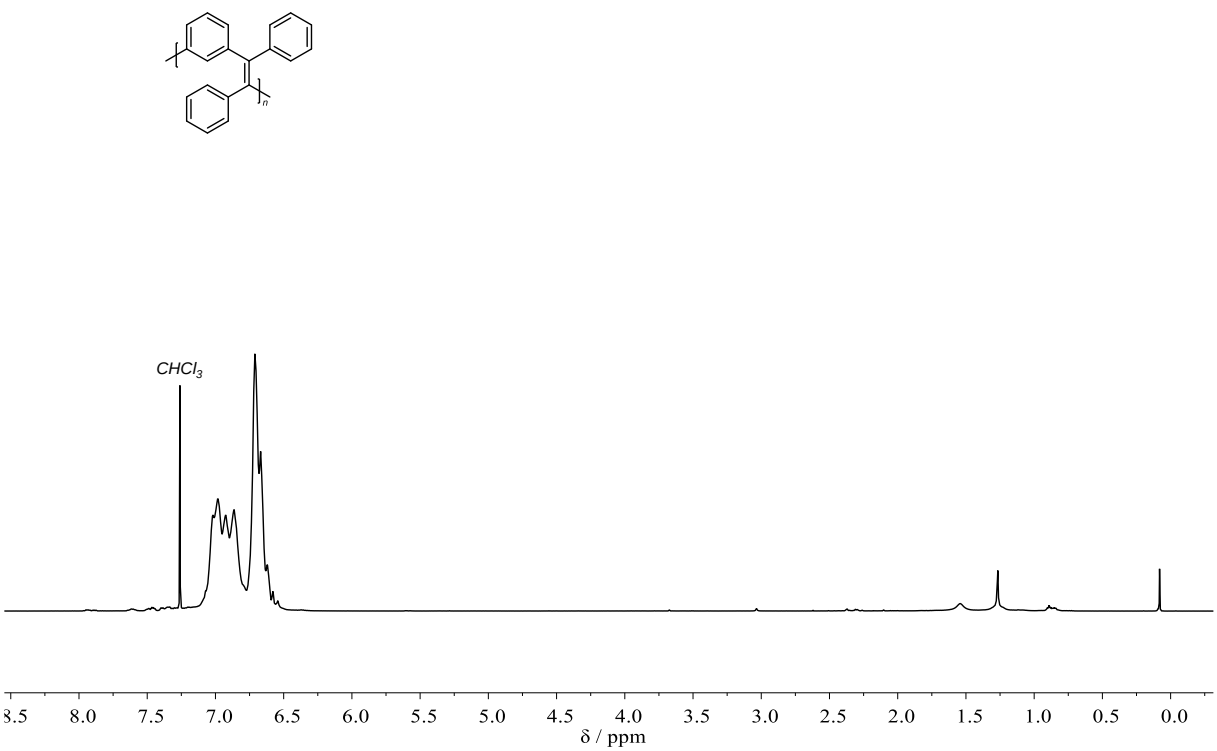

*Supplementary Figure 116: ^{1}H NMR spectrum of **P5** in $CDCl_3$.*

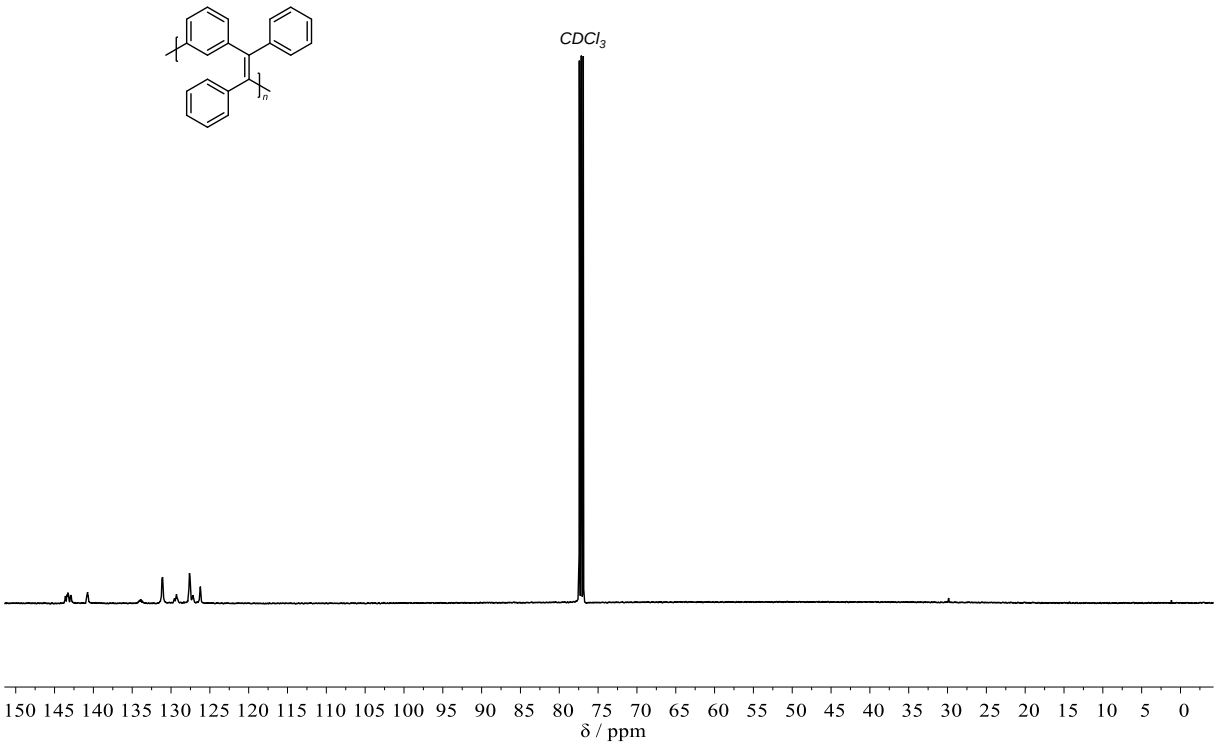

*Supplementary Figure 117: ^{13}C NMR spectrum of **P5** in $CDCl_3$.*

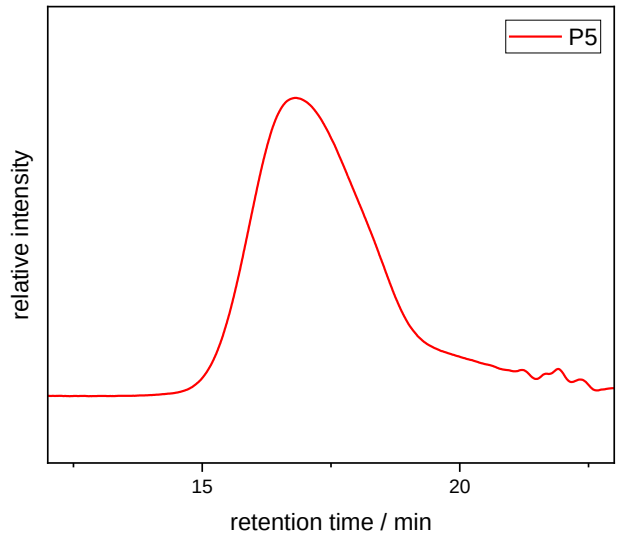

*Supplementary Figure 118: SEC trace of **P5** (measured in THF).*

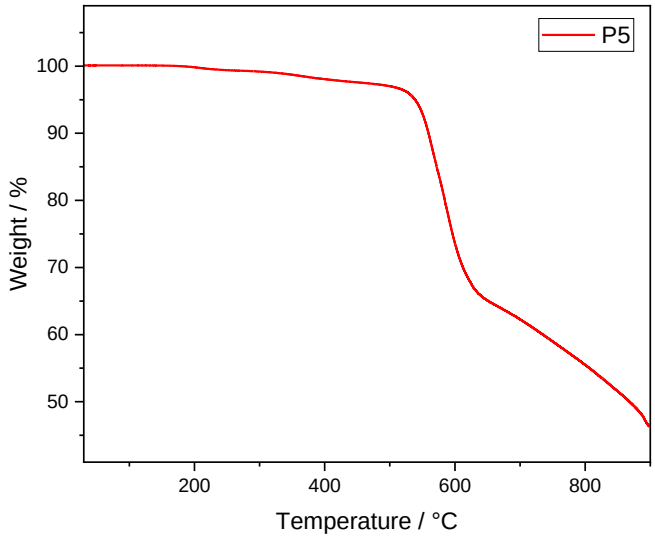

*Supplementary Figure 119: TGA curve of **P5**.*

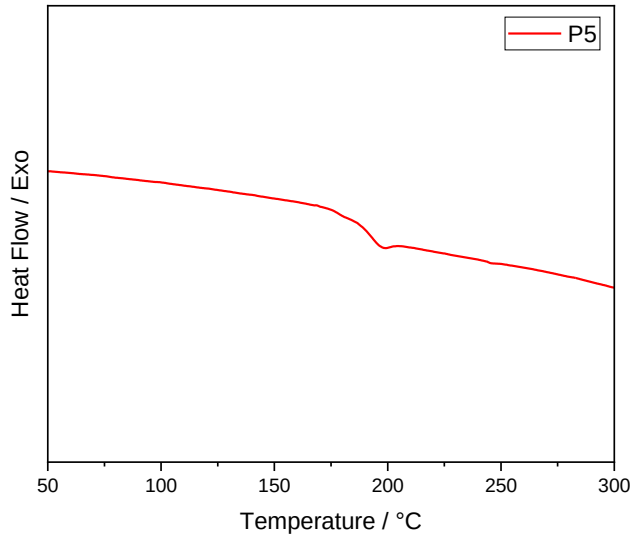

*Supplementary Figure 120: DSC curve of **P5**.*

Poly-(4,4'-biphenylene-1,2-diphenylvinylene) (P6)

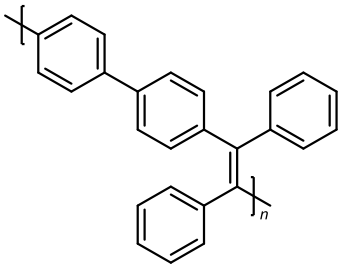

Synthesized from **7f** according to general procedure. Obtained as a yellow solid in a yield of 74% (122 mg, 0.368 mmol).

^{1}H NMR (500 MHz, Chloroform-*d*): δ/ppm 7.35 – 7.23 (m, 4H), 7.18 – 6.95 (m, 14H).

^{13}C NMR (126 MHz, Chloroform-*d*): δ/ppm = 144.12 – 143.59 (m), 143.10 – 142.60 (m), 140.88 – 140.51 (m), 138.62 – 138.05 (m), 132.05 – 131.84 (m), 128.12 – 127.65 (m), 126.98 – 126.49 (m), 126.33 – 125.72 (m).

IR (ATR platinum diamond): $\tilde{\nu}/cm^{-1}$ = 3075 (vw), 3048 (vw), 3024 (w), 1660 (vw), 1574 (vw), 1491 (m), 1442 (w), 1413 (vw), 1393 (w), 1312 (vw), 1275 (w), 1177 (vw), 1119 (w), 1074 (w), 1018 (w), 1002 (m), 975 (w), 938 (vw), 915 (w), 839 (w), 806 (m), 763 (m), 747 (m), 695 (vs), 664 (m), 625 (w), 619 (w), 603 (w), 574 (m), 547 (w), 539 (w), 490 (w), 481 (w), 473 (w), 463 (w).

SEC (THF): M_n = 9.30 kDa, M_w = 15.0 kDa, $Đ$ = 1.61.

TGA: $T_{d,5\%}$ = 535 °C , Residue = 76.6 %.

DSC: T_g = 263 °C.

Fluorescence: $\lambda_{em,max}$ = 513 nm with λ_{ex} = 362 nm.

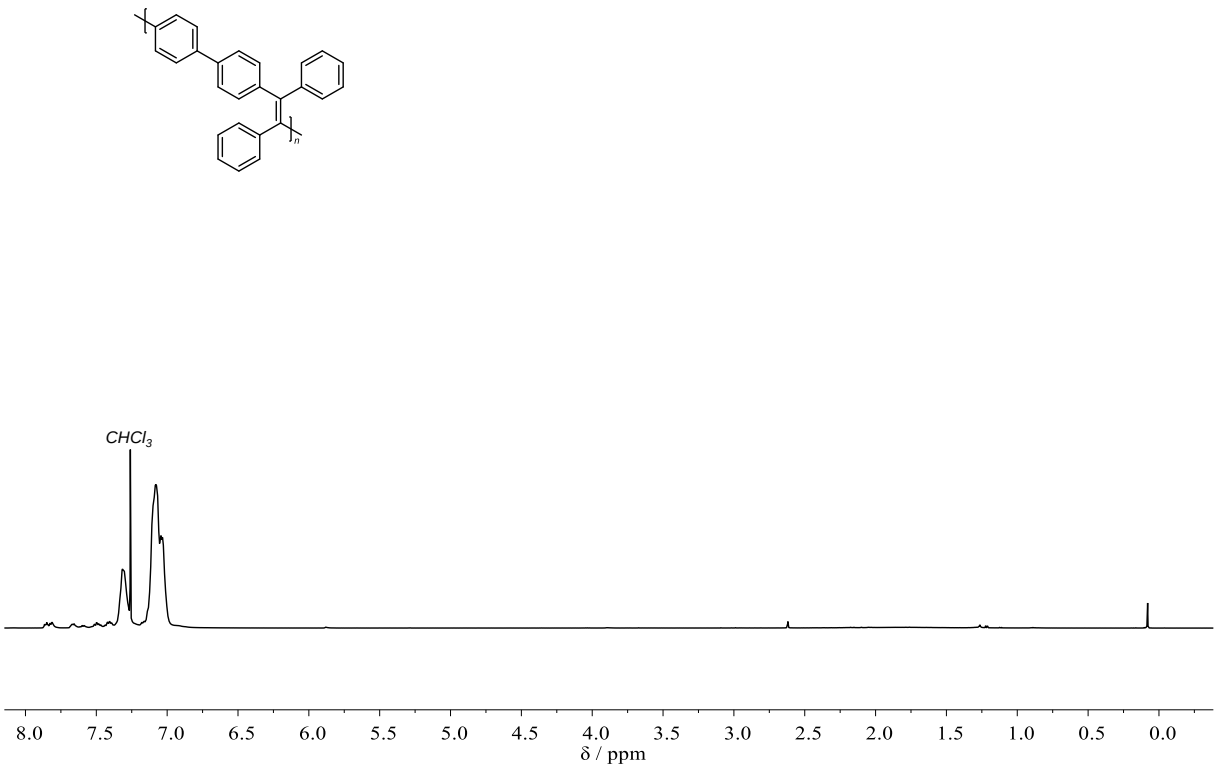

*Supplementary Figure 121: ^{1}H NMR spectrum of **P6** in $CDCl_3$.*

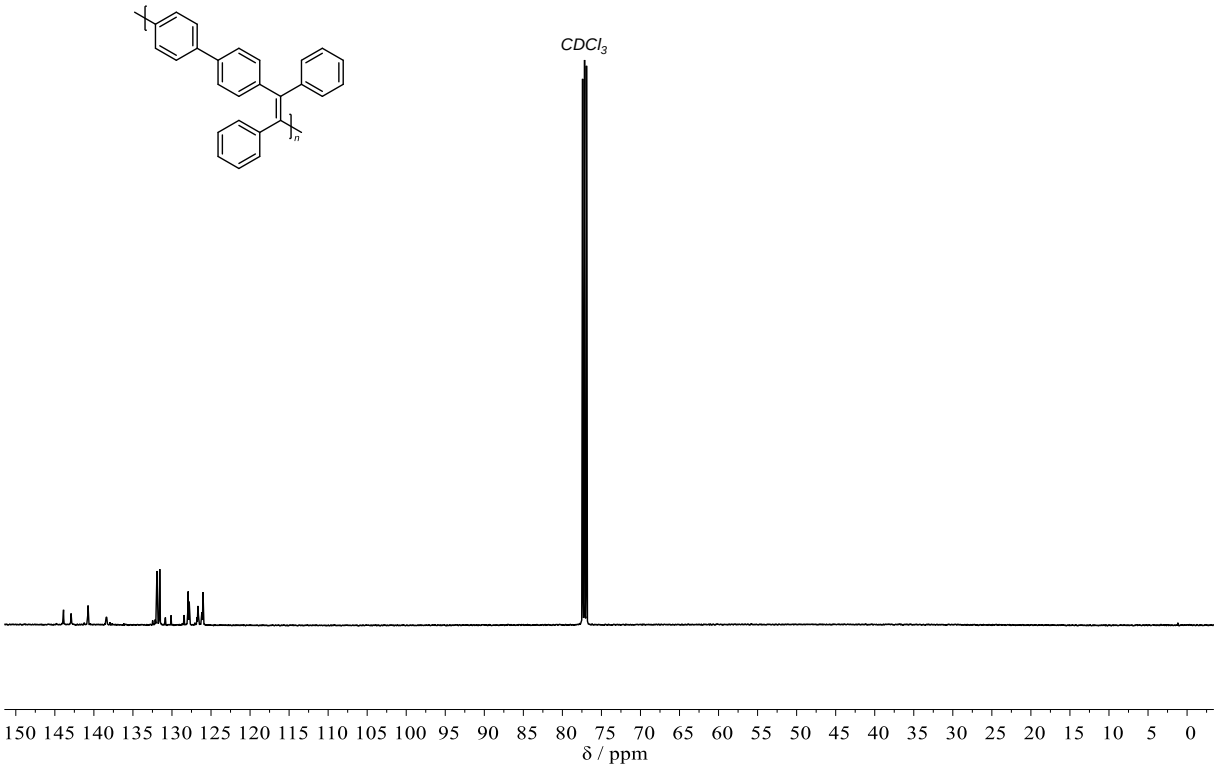

*Supplementary Figure 122: ^{13}C NMR spectrum of **P6** in $CDCl_3$.*

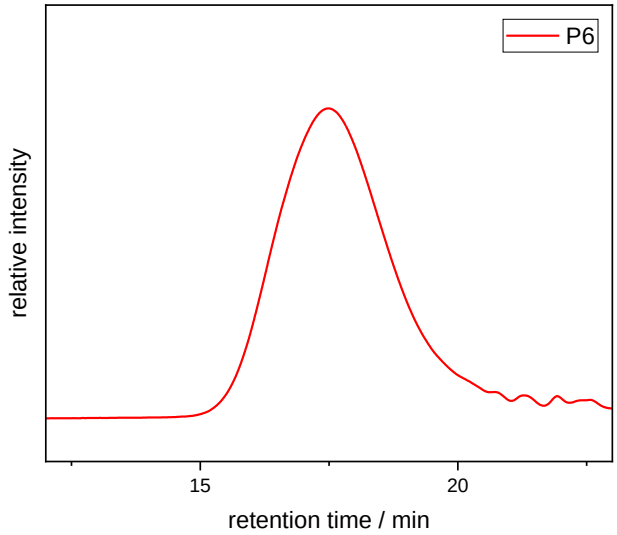

*Supplementary Figure 123: SEC trace of **P6** (measured in THF).*

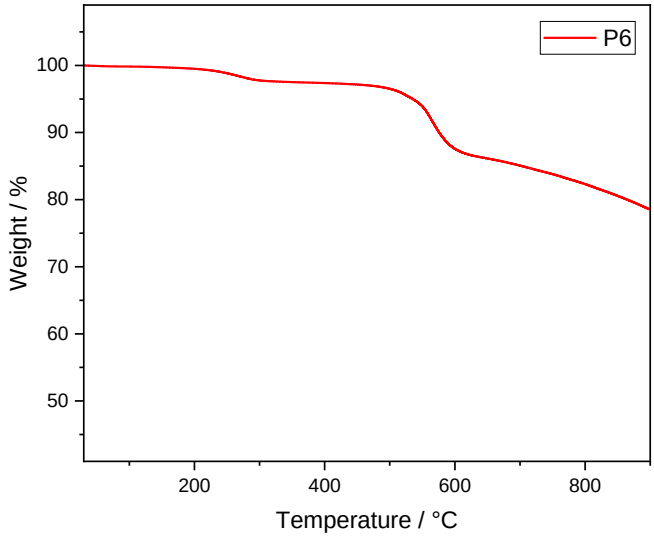

*Supplementary Figure 124: TGA curve of **P6**.*

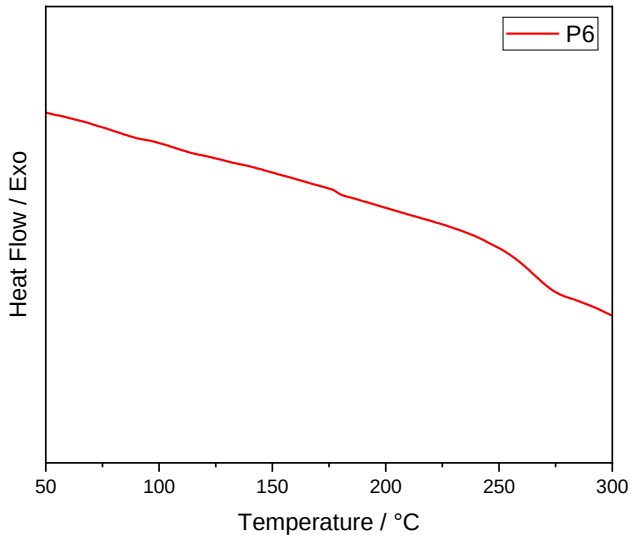

*Supplementary Figure 125: DSC curve of **P6**.*

Poly-(2,5-thienylene-1,2-diphenylvinylene) (P7)

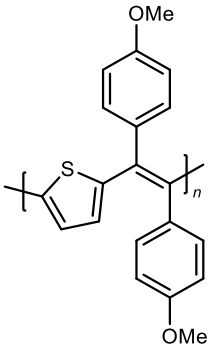

Synthesized from **7g** according to general procedure. Obtained as a dark red solid in a yield of 24% (30.6 mg, 0.118 mmol).

^{1}H NMR (500 MHz, Chloroform-*d*): δ/ppm = 7.54 – 6.68 (m, 12H).

^{13}C NMR (126 MHz, Chloroform-*d*): δ/ppm = 147.20 – 146.80 (m), 142.66 – 141.38 (m), 131.50 – 130.53 (m), 129.85 – 126.53 (m).

IR (ATR platinum diamond): $\tilde{\nu}/cm^{-1}$ = 3055 (vw), 1598 (vw), 1489 (w), 1442 (w), 1275 (vw), 1261 (vw), 1220 (vw), 1177 (vw), 1156 (vw), 1107 (vw), 1072 (w), 1028 (w), 915 (vw), 841 (vw), 804 (w), 759 (w), 736 (w), 726 (m), 693 (vs), 640 (w), 617 (vw), 584 (vw), 496 (vw), 453 (vw), 444 (vw), 438 (vw).

SEC (THF): M_n = 1.67 kDa, M_w = 8.28 kDa, $Đ$ = 4.97.

TGA: $T_{d,5\%}$ = 430 °C , Residue = 71.1 °C.

DSC: No glass transition could be detected.

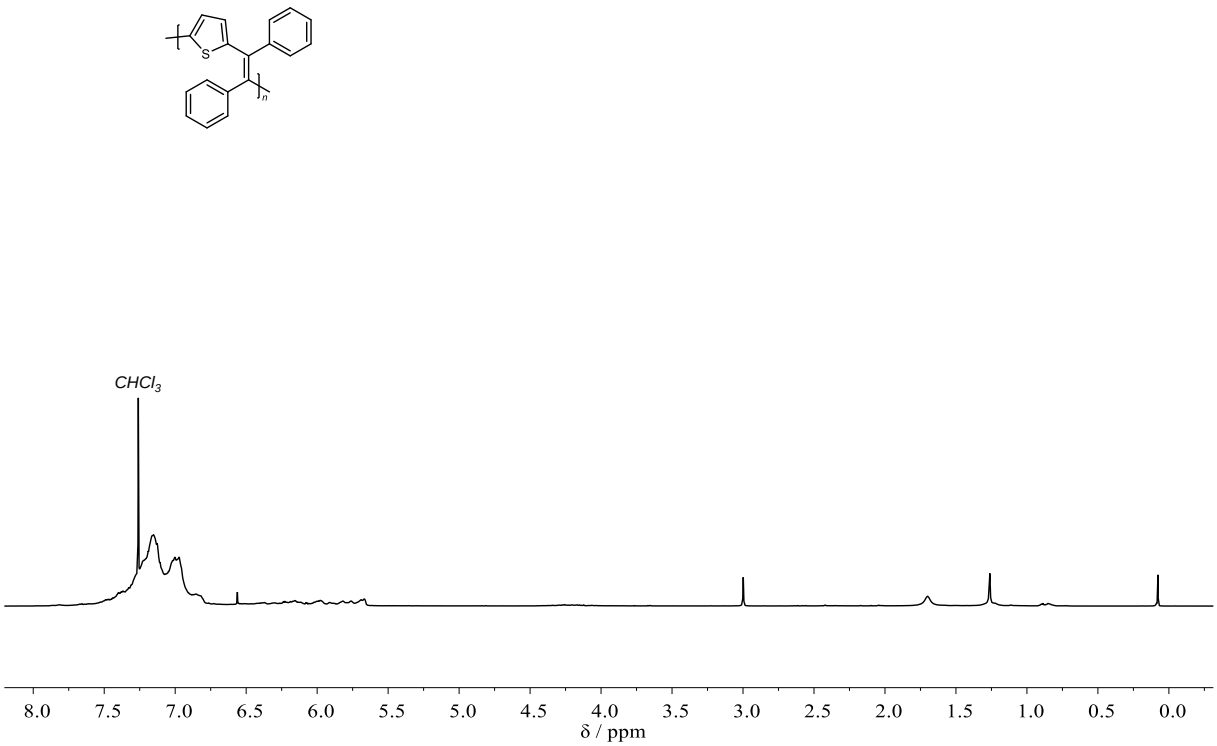

*Supplementary Figure 126: ^{1}H NMR spectrum of **P7** in $CDCl_3$.*

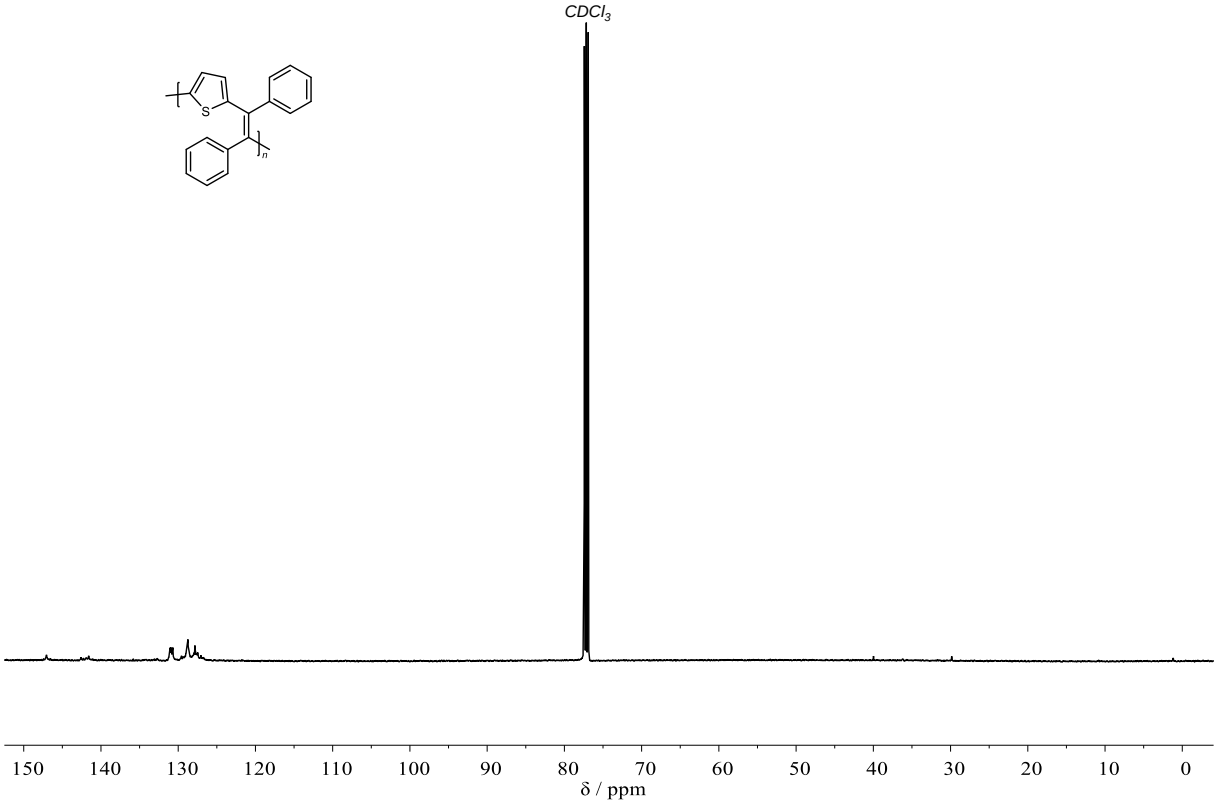

*Supplementary Figure 127: ^{13}C NMR spectrum of **P7** in $CDCl_3$.*

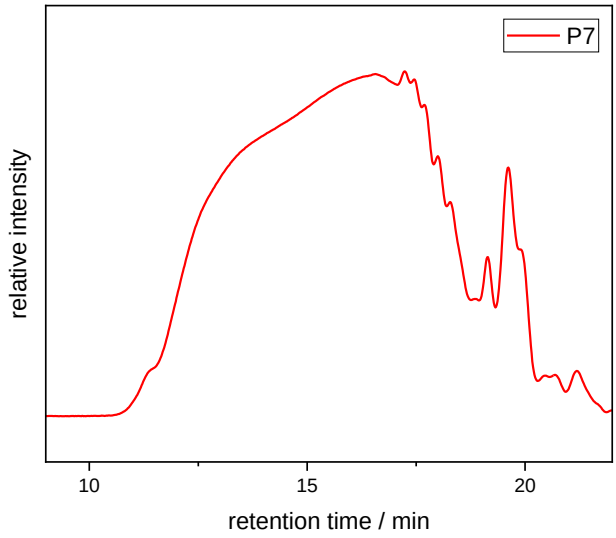

*Supplementary Figure 128: SEC trace of **P7** (measured in THF).*

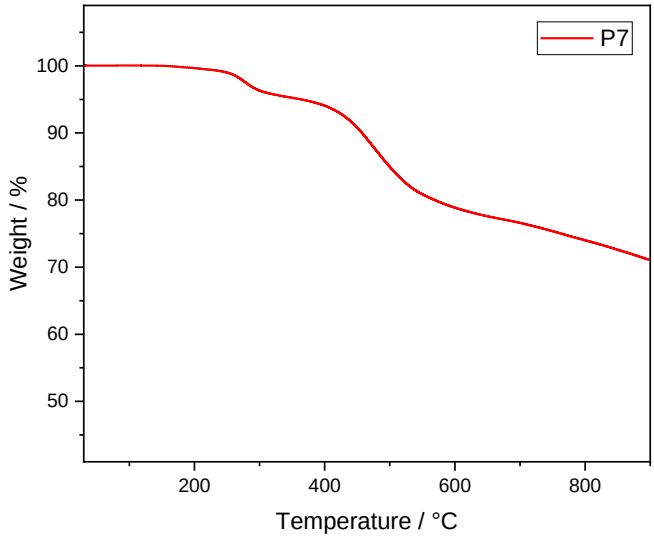

*Supplementary Figure 129: TGA curve of **P7**.*

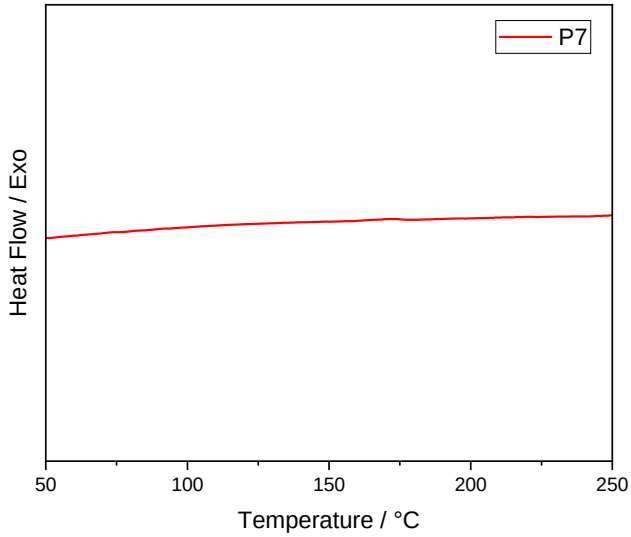

*Supplementary Figure 130: DSC curve of **P7**.*

Poly-(1,4-phenylene-1,2-bis(4-tert-butylphenyl)vinylene) (P8)

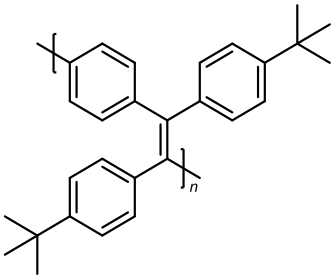

Synthesized from **7h** according to general procedure. Obtained as a yellow solid in a yield of 73% (134 mg, 0.366 mmol).

^{1}H NMR (500 MHz, Chloroform-*d*): δ/ppm = 7.18 – 6.54 (m, 12H), 1.40 – 1.01 (m, 18H).

^{13}C NMR (126 MHz, Chloroform-*d*): δ/ppm = 149.48 – 148.40 (m), 142.81 – 141.95 (m), 141.50 – 140.15 (m), 132.05 – 129.72 (m), 125.03 – 123.61 (m), 35.47 – 33.79 (m), 33.04 – 30.79 (m).

IR (ATR platinum diamond): $\tilde{\nu}/cm^{-1}$ = 3028 (w), 2958 (s), 2902 (m), 2867 (m), 1506 (m), 1475 (w), 1460 (m), 1395 (m), 1362 (m), 1269 (m), 1201 (w), 1164 (w), 1107 (m), 1018 (m), 977 (w), 860 (w), 829 (vs), 792 (s), 755 (w), 685 (m), 666 (m), 627 (w), 574 (s), 543 (m), 504 (w), 494 (w).

SEC (THF): M_n = 14.9 kDa, M_w = 33.5 kDa, $Đ$ = 2.19.

TGA: $T_{d,5\%}$ = 514 °C , Residue = 68.1 %.

DSC: T_g = 175 °C.

Fluorescence: $\lambda_{em,max}$ = 514 nm with λ_{ex} = 360 nm.

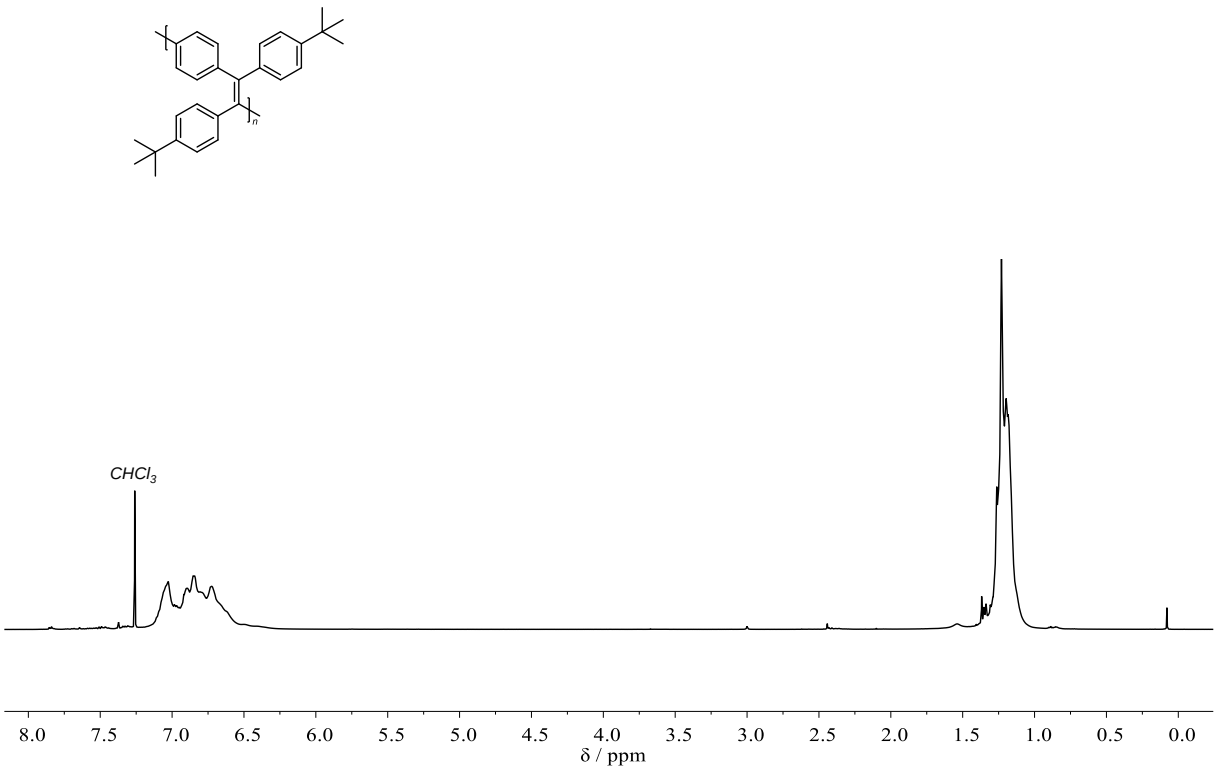

*Supplementary Figure 131: ^{1}H NMR spectrum of **P8** in $CDCl_3$.*

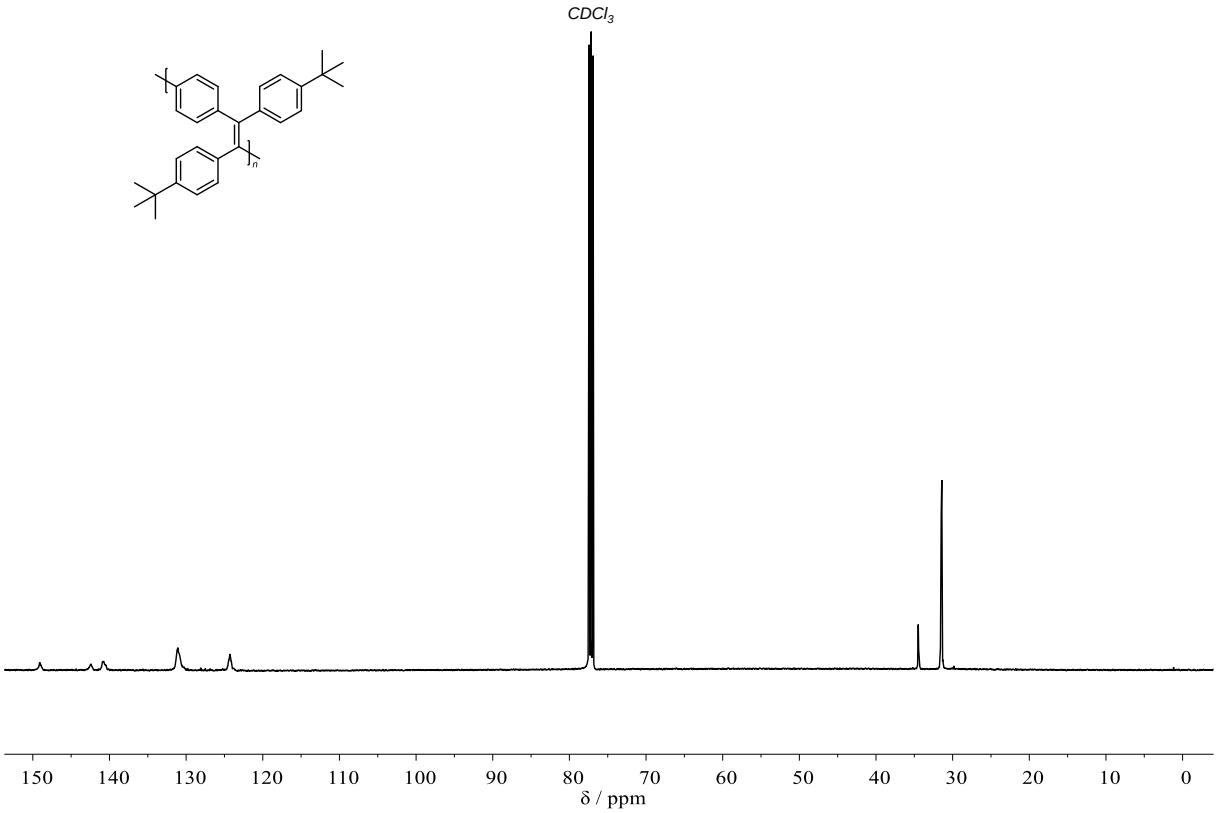

*Supplementary Figure 132: ^{13}C NMR spectrum of **P8** in $CDCl_3$.*

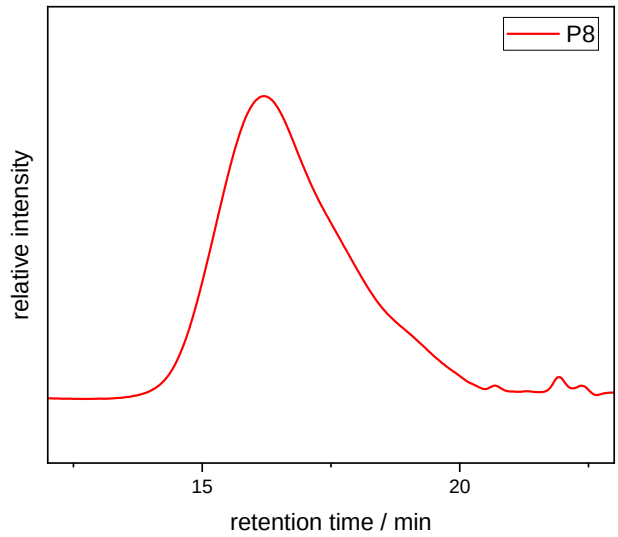

*Supplementary Figure 133: SEC trace of **P8** (measured in THF).*

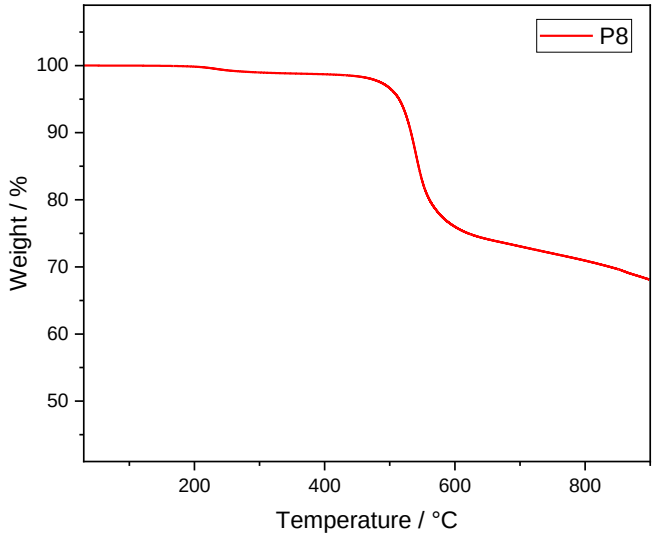

*Supplementary Figure 134: TGA curve of **P8**.*

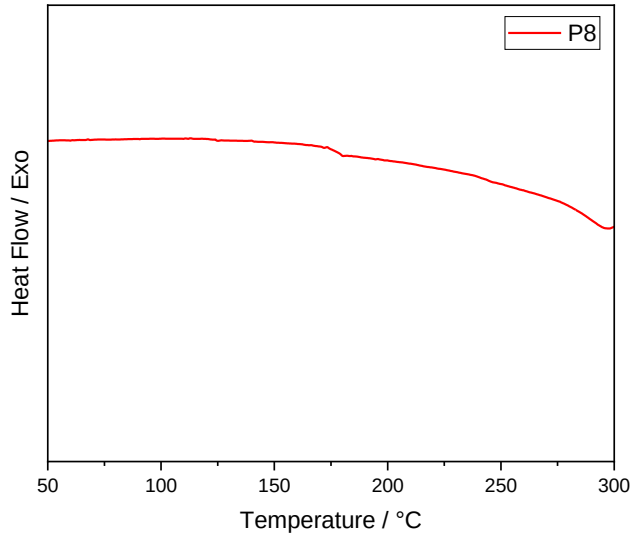

*Supplementary Figure 135: DSC curve of **P8**.*

Copolymer from 7a and 7b (CP1)

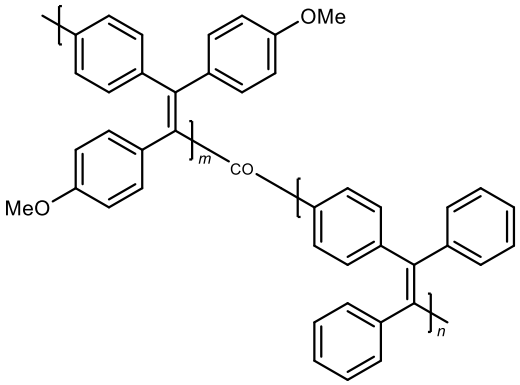

Synthesized from **7a** and **7b** in a 1:1 ratio according to general procedure. Obtained as a yellow solid in a yield of 64% (90.7 mg, 0.159 mmol).

^{1}H NMR (500 MHz, Chloroform-*d*): δ/ppm = 7.16 – 6.41 (m, 26H), 3.82 – 3.50 (m, 6H).

^{13}C NMR (126 MHz, Chloroform-*d*): δ/ppm = 158.59 – 157.46 (m), 144.53 – 143.28 (m), 142.74 – 141.49 (m), 136.73 – 135.82 (m), 133.63 – 132.03 (m), 132.01 – 131.28 (m), 131.14 – 130.31 (m), 128.12 – 127.19 (m), 126.73 – 126.11 (m), 113.46 – 112.49 (m), 55.31 – 55.02 (m).

IR (ATR platinum diamond): $\tilde{\nu}/cm^{-1}$ = 3052 (vw), 3024 (vw), 2995 (vw), 2933 (vw), 2902 (vw), 2832 (vw), 1604 (m), 1574 (w), 1506 (s), 1462 (w), 1442 (m), 1401 (w), 1288 (m), 1242 (vs), 1172 (s), 1137 (w), 1109 (m), 1074 (w), 1033 (m), 975 (w), 930 (vw), 913 (vw), 858 (w), 829 (m), 802 (m), 784 (w), 761 (m), 747 (m), 697 (s), 671 (w), 629 (w), 617 (w), 572 (w), 551 (w), 543 (w), 525 (w), 516 (w), 479 (w), 469 (w), 455 (vw), 440 (vw).

SEC (THF): M_n = 19.2 kDa, M_w = 39.0 kDa, $Đ$ = 2.03.

TGA: $T_{d,5\%}$ = 487 °C , Residue = 79.4 %.

DSC: T_g = 241 °C.

Fluorescence: $\lambda_{em,max}$ = 523 nm with λ_{ex} = 366 nm.

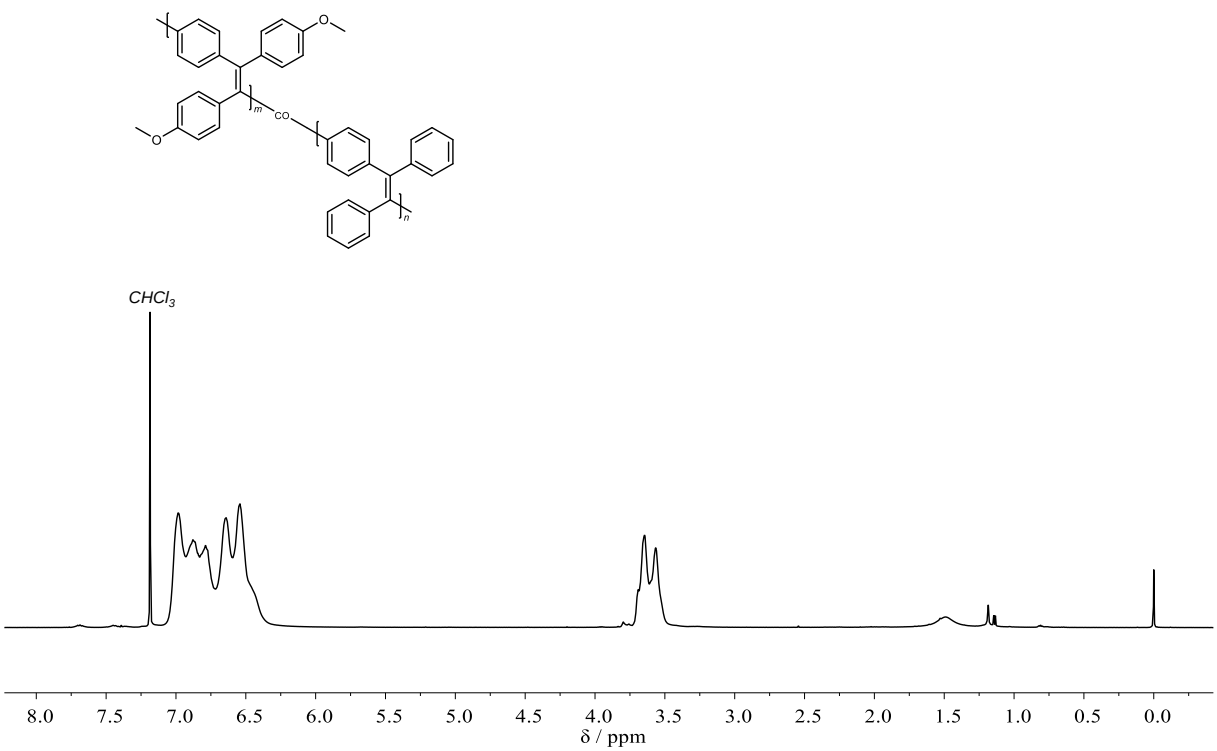

*Supplementary Figure 136: ^{1}H NMR spectrum of **CP1** in $CDCl_3$.*

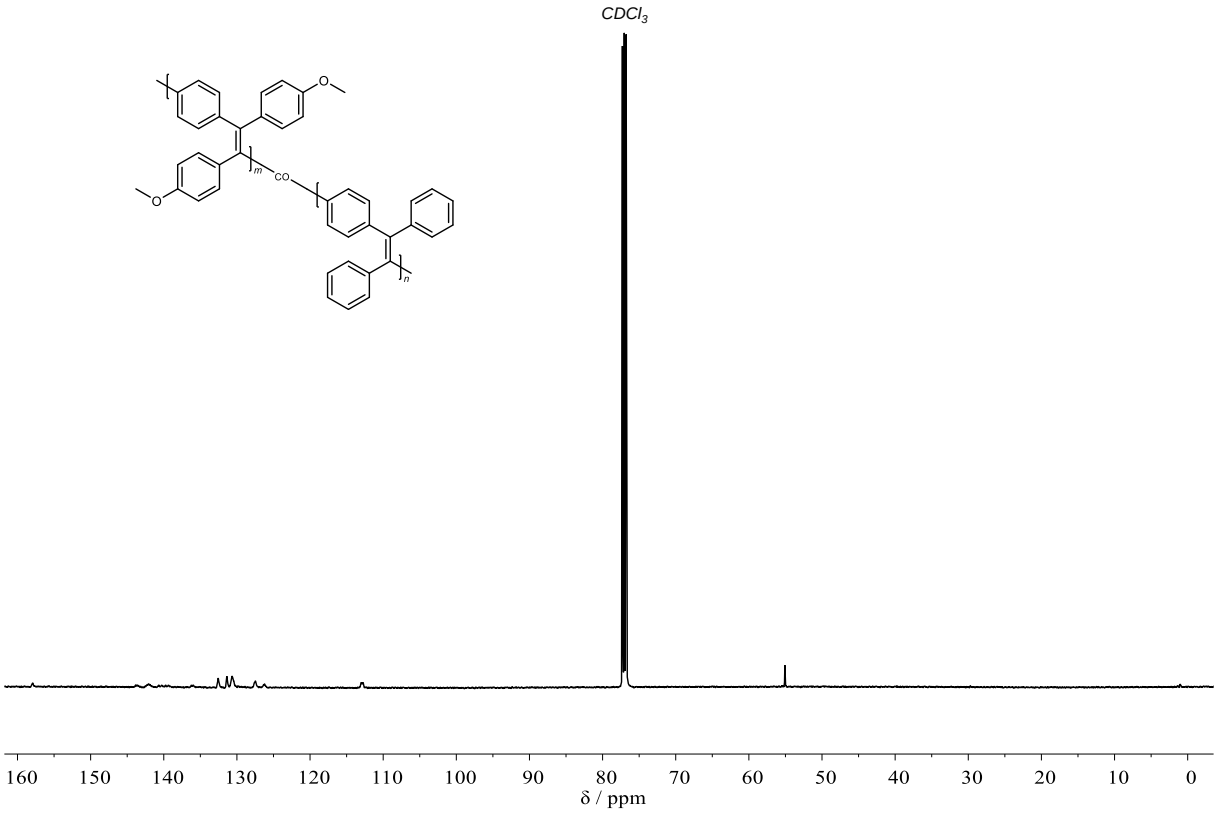

*Supplementary Figure 137: ^{13}C NMR spectrum of **CP1** in $CDCl_3$.*

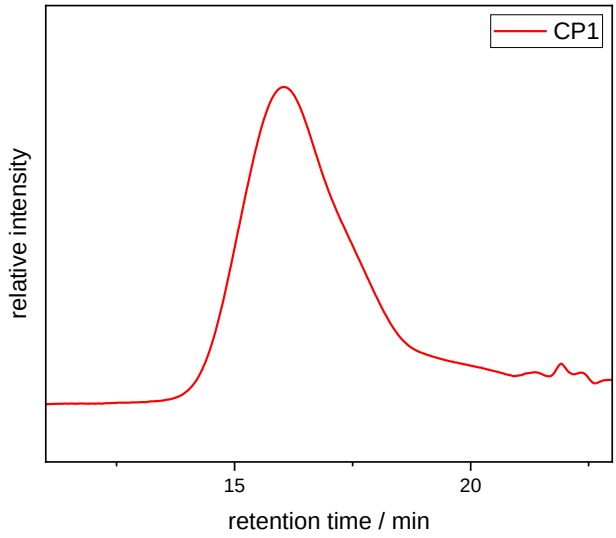

*Supplementary Figure 138: SEC trace of **CP1** (measured in THF).*

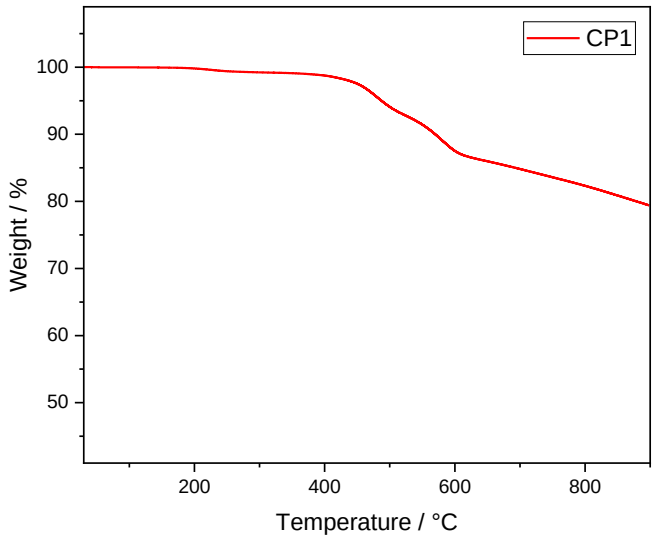

*Supplementary Figure 139: TGA curve of **CP1**.*

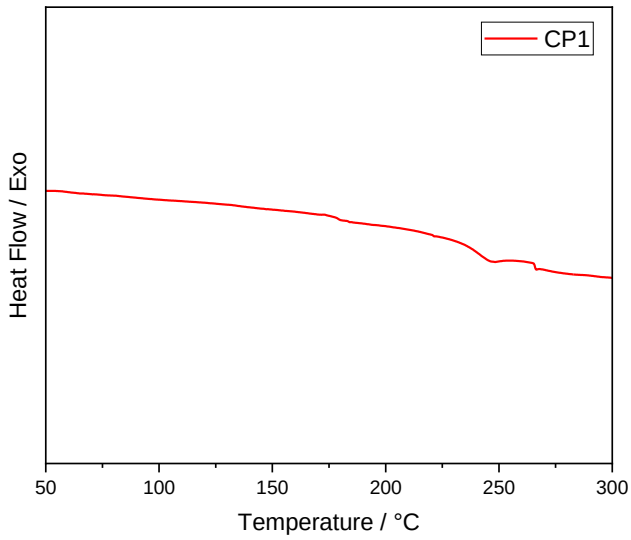

*Supplementary Figure 140: DSC curve of **CP1**.*

Copolymer from 7b and 7e (CP2)

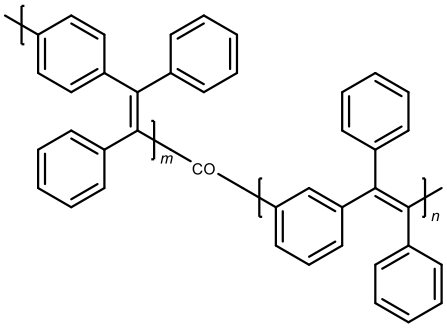

Synthesized from **7b** and **7e** in a 1:1 ratio according to general procedure. Obtained as a light yellow solid in a yield of 63% (80.0 mg, 0.157 mmol) .

^{1}H NMR (500 MHz, Chloroform-*d*): δ/ppm = 7.17 – 6.49 (m, 28H).

^{13}C NMR (126 MHz, Chloroform-*d*): δ/ppm = 144.42 – 143.25 (m), 142.54 – 141.82 (m), 141.48 – 140.55 (m), 132.33 – 130.35 (m), 130.16 – 129.29 (m), 128.55 – 127.26 (m), 127.13 – 126.05 (m).

IR (ATR platinum diamond): $\tilde{\nu}/cm^{-1}$ = 3052 (vw), 3020 (vw), 1596 (vw), 1504 (vw), 1491 (w), 1442 (w), 1154 (vw), 1137 (w), 1111 (vw), 1074 (w), 1031 (vw), 1020 (vw), 1008 (w), 998 (w), 913 (vw), 854 (vw), 843 (vw), 790 (vw), 759 (w), 695 (vs), 673 (w), 629 (w), 619 (w), 603 (vw), 566 (w), 539 (vw), 485 (vw), 473 (vw).

SEC (THF): M_n = 15.1 kDa, M_w = 30.1 kDa, $Đ$ = 1.99.

TGA: $T_{d,5\%}$ = 558 °C , Residue = 80.9 %.

DSC: T_g = 214 °C.

Fluorescence: $\lambda_{em,max}$ = 505 nm with λ_{ex} = 360 nm.

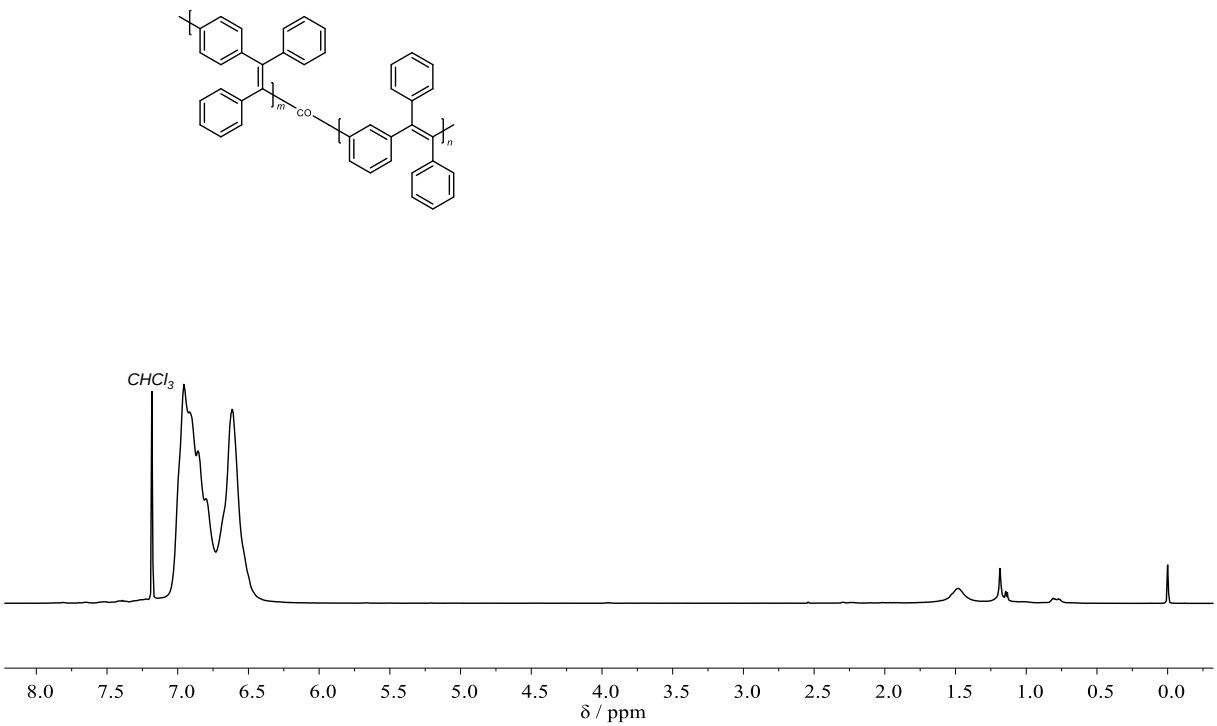

*Supplementary Figure 141: ^{1}H NMR spectrum of **CP2** in $CDCl_3$.*

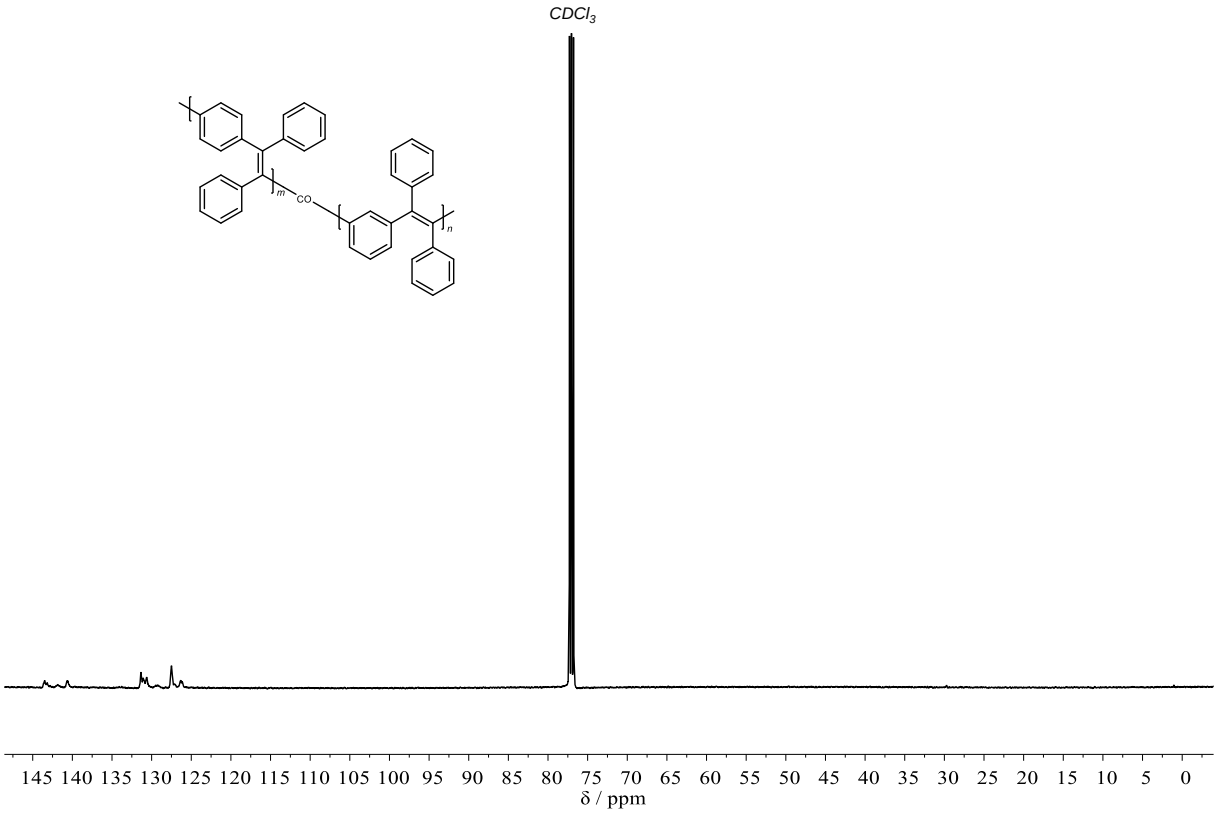

*Supplementary Figure 142: ^{13}C NMR spectrum of **CP2** in $CDCl_3$.*

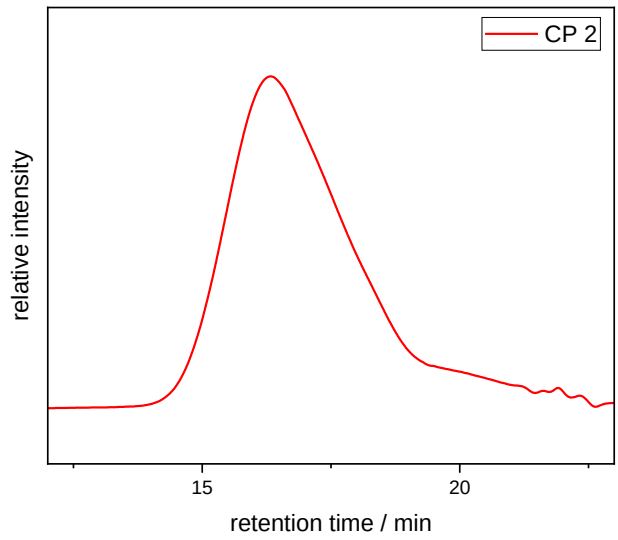

*Supplementary Figure 143: SEC trace of **CP2** (measured in THF).*

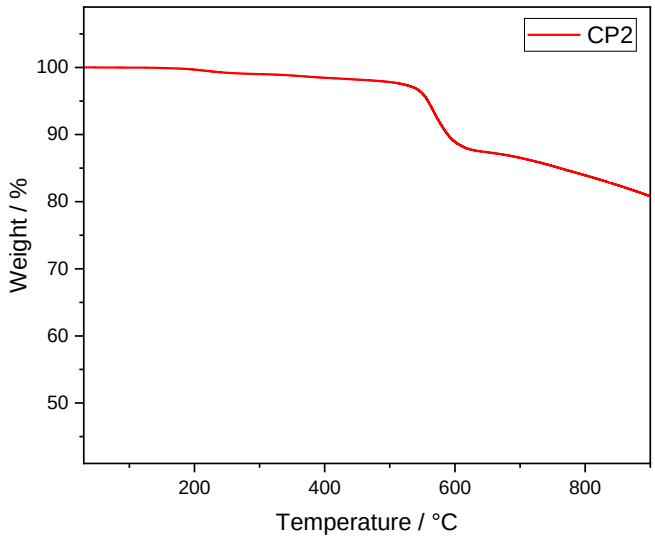

*Supplementary Figure 144: TGA curve of **CP2**.*

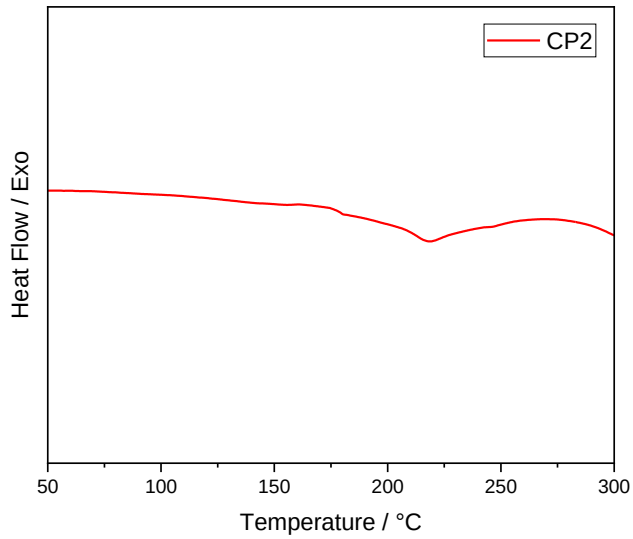

*Supplementary Figure 145: DSC curve of **CP2**.*

6.3.3 Vegetable Oil-based Polythiols – Chapter 4.3

6.3.3.1 Substrate Synthesis and Characterization

Characterization of Vegetable Oils

The fatty acid composition of the used High Oleic Sunflower Oil (**HOSO**) and High Linoleic Sunflower Oil (**HLSO**) was determined *via* ^{1}H NMR spectroscopy according to the method of Herrera *et al.*[476] For this, 200 µL of the oil were mixed with 400 µL of $CDCl_3$ and 10.0 µL of dimethylsulfoxide-d_6. The mixture was vortexed for 1 minute and transferred into an NMR tube. A ^{1}H NMR spectrum was recorded at 25 °C (64 scans, 5 s relaxation delay) and the relevant signals were evaluated. The spectra are depicted in Supplementary Figure 146 (HOSO) and (HLSO). The calculated fatty acid contents are listed in Table 13.

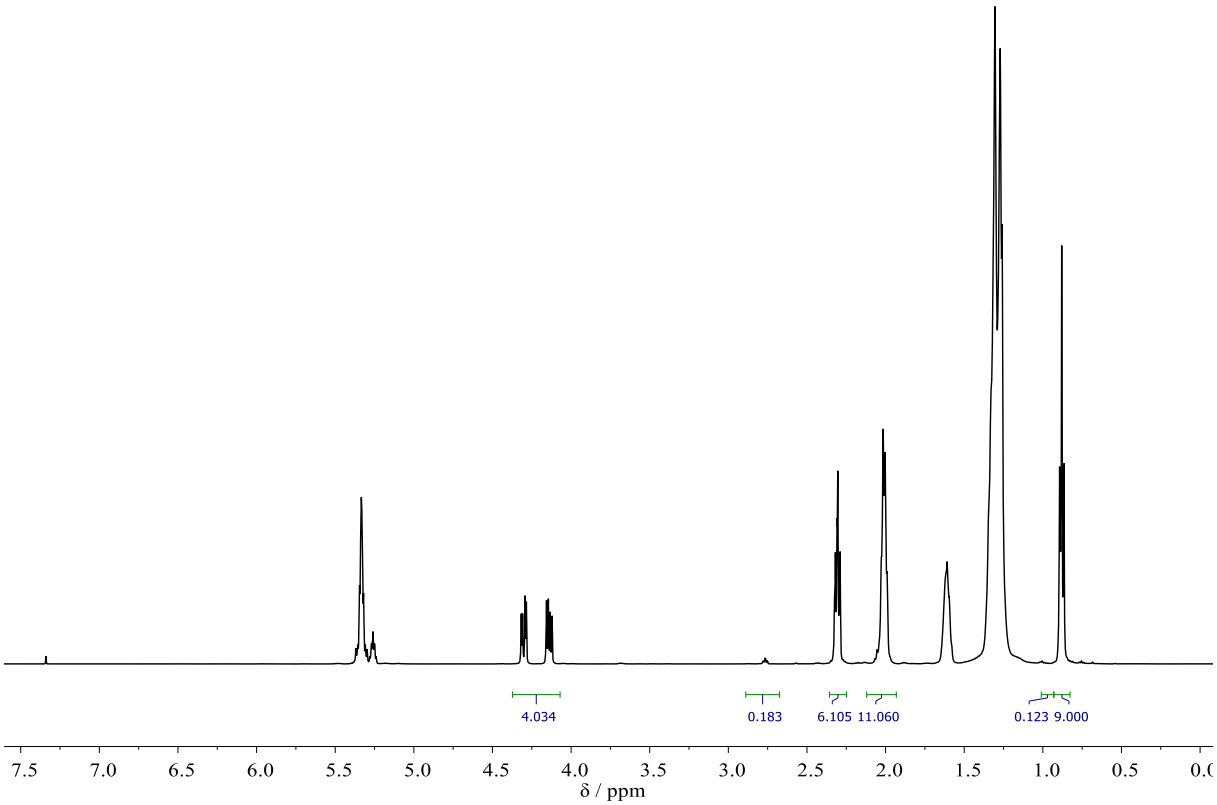

*Supplementary Figure 146: ^{1}H NMR spectrum of **HOSO** used for the quantification of its fatty acid composition.*

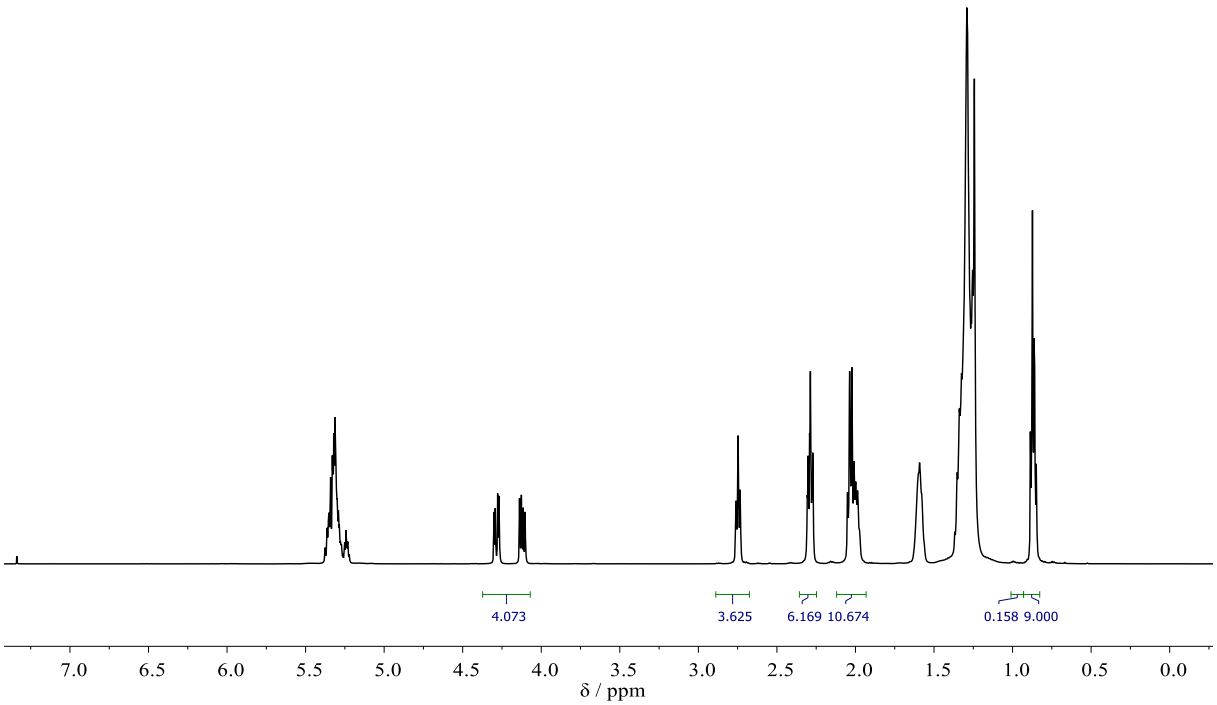

*Supplementary Figure 147: ^{1}H NMR spectrum of **HLSO** used for the quantification of its fatty acid composition.*

*Table 13: Calculated fatty acid contents of **HOSO** and **HLSO**.*

Entry	Oil	SFA content / %	MUFA content / %	PUFA content / %
1	HOSO	8.6	89.7	1.7
2	HLSO	12.6	29.8	57.6

For the calculation of representative molecular weights, the molecular weights of palmitic acid, oleic acid and linoleic acid were used to represent the SFA, MUFA and PUFA content, respectively. The following molecular weights were obtained for subsequent stoichiometry calculations:

M(**HOSO**) = 869 g mol^{-1}
M(**HLSO**) = 859 g mol^{-1}

Synthesis of glyceryl triundecenoate (GTU)

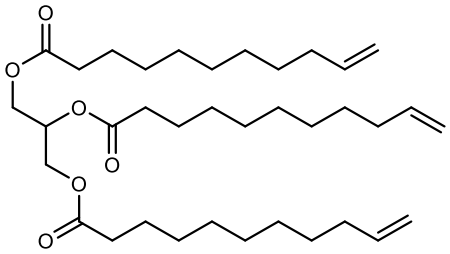

1.84 g Glycerol (20.0 mmol, 1.00 equiv.), 49.8 mg of dibutyltin oxide (0.20 mmol, 0.01 equiv.), 22.0 mg of hydroquinone (0.20 mmol, 0.01 equiv.) and 29.5 g of 10-undecenoic acid (160 mmol, 8.00 equiv.) were added to a Schlenk flask and the flask was purged with argon. The mixture was stirred for 24 hours at 160 °C under continuous argon flow. Afterwards, the mixture was cooled to room temperature and added dropwise to 500 mL of a 10% aqueous sodium carbonate solution. The aqueous phase was extracted twice with 200 mL each of ethyl acetate. The combined extracts were washed once with 200 mL 10% sodium carbonate solution and twice with 200 mL of water. The washed extract was then dried over sodium sulfate and solvent was removed *in vacuo*. The product glyceryl triundecenoate (**GTU**) was obtained as a yellow oil in 91% yield (10.8 g, 18.2 mmol). The synthesis was adapted from Rios *et al*.[480]

^{1}H NMR (500 MHz, Chloroform-*d*) δ/ppm 5.80 (ddt, *J* = 16.9, 10.2, 6.6 Hz, 3H), 5.26 (tt, *J* = 6.0, 4.3 Hz, 1H), 5.04 – 4.88 (m, 6H), 4.29 (dd, *J* = 11.9, 4.3 Hz, 2H), 4.14 (dd, *J* = 11.9, 6.0 Hz, 2H), 2.37 – 2.26 (m, 6H), 2.08 – 1.98 (m, 6H), 1.65 – 1.56 (m, 7H), 1.47 – 1.18 (m, 30H).

^{13}C NMR (126 MHz, Chloroform-*d*) δ 173.42, 139.29, 139.26, 114.32, 114.30, 69.00, 62.24, 34.34, 34.17, 33.92, 29.45, 29.43, 29.36, 29.34, 29.22, 29.20, 29.19, 29.03, 25.02, 24.98.

IR (ATR platinum diamond) $\tilde{\nu}/cm^{-1}$ = 3077 (vw), 2925 (m), 2855 (m), 1740 (vs), 1641 (w), 1462 (w), 1442 (w), 1417 (w), 1372 (w), 1362 (w), 1356 (w), 1234 (w), 1158 (s), 1115 (m), 1098 (m), 1026 (w), 993 (w), 907 (m), 724 (w), 636 (vw), 553 (vw), 461 (vw), 455 (vw).

ESI-HRMS: $[M+Na]^+$ calculated for $C_{36}H_{62}O_6$ = 613.4439, found 613.4436.

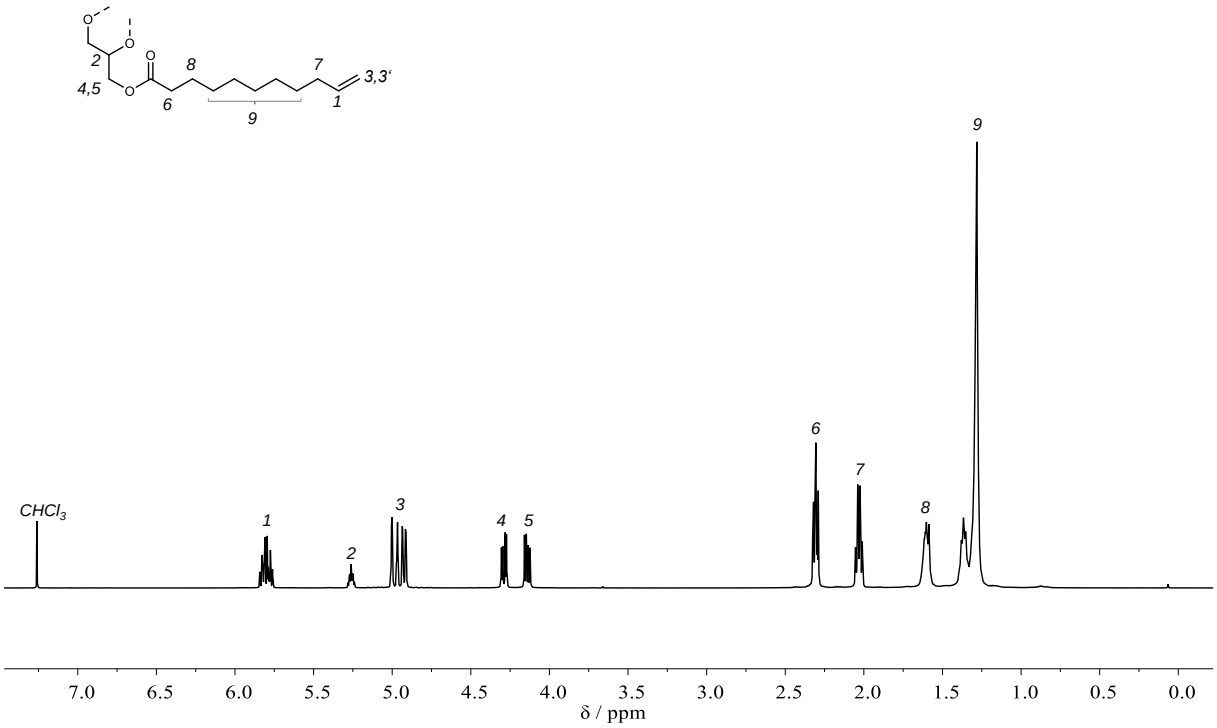

*Supplementary Figure 148: ^{1}H NMR spectrum of **GTU** in $CDCl_3$.*

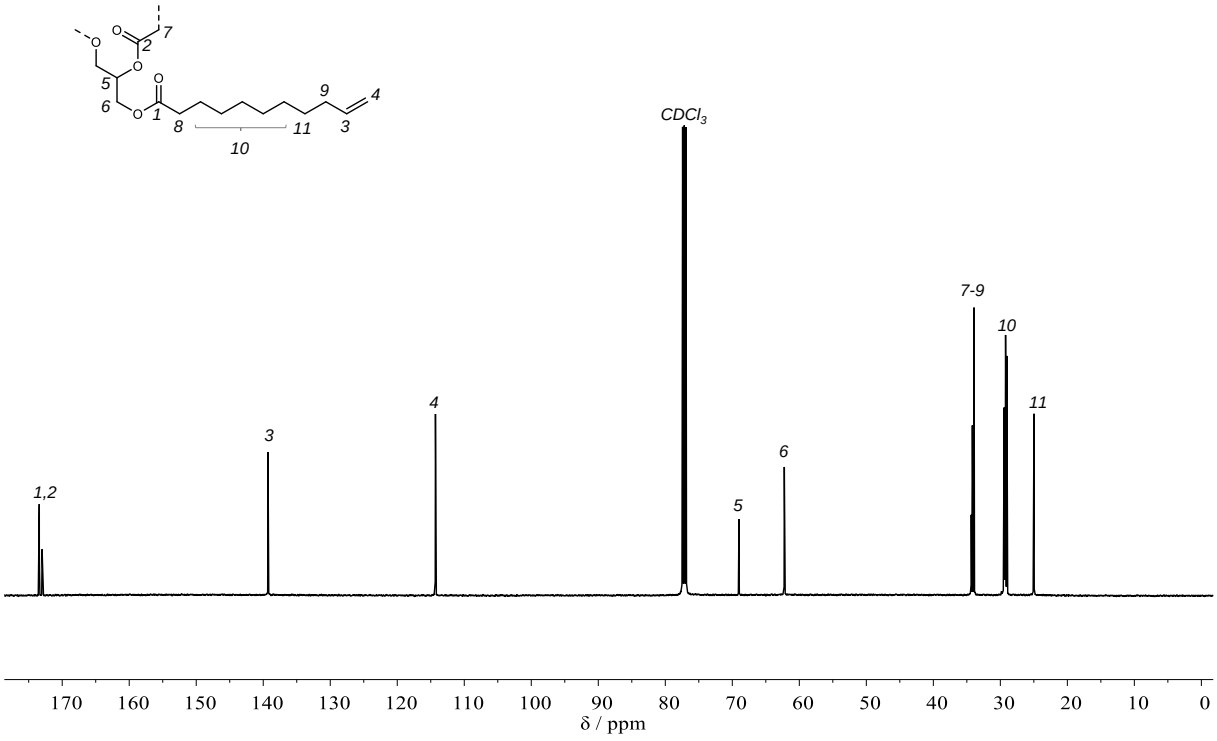

*Supplementary Figure 149: ^{13}C NMR spectrum of **GTU** in $CDCl_3$..*

6.3.3.2 Ester Deoxygenation

General procedure for the deoxygenative reduction of triglycerides:

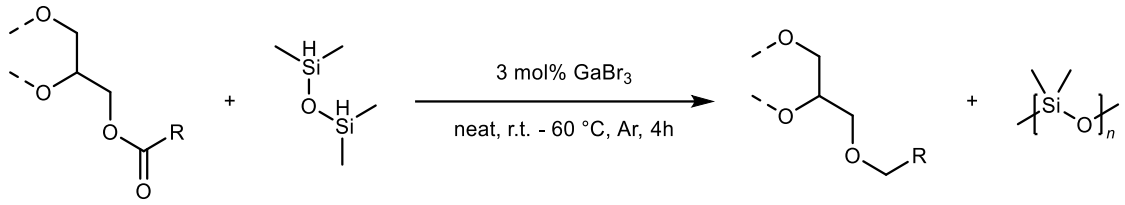

All reagents and glassware were dried before use. In a crimp vial under argon atmosphere, the triglyceride (21.5 mmol, 1.00 equiv.) was added to 200 mg of gallium bromide (0.646 mmol, 0.03 equiv.) and stirred for 5 minutes. The mixture was placed inside an ice bath and 12.6 mL of tetramethyldisiloxane (TMDS) (9.55 g, 71.1 mmol, 3.30 equiv.) were added dropwise with a syringe pump over the course of 2 hours while stirring. After complete addition of TMDS, the mixture was removed from the ice bath and stirred at room temperature for 3 hours, then heated to 60 °C for 1 additional hour. Afterwards, the reaction was quenched by addition of 5 mL of 10% sodium carbonate solution and stirring for 1 hour at room temperature. The aqueous phase was separated and unreacted TMDS was removed under reduced pressure.
In order to remove the polymeric silicone byproducts, 250 mL of 2.5 M sodium hydroxide solution (corresponds to ~30 equiv. NaOH) and 25 mL of ethanol were added to the crude product. The mixture was heated to 100 °C overnight under vigorous stirring. Afterwards, the aqueous phase was separated and the process was repeated once more with the same amount of fresh NaOH solution and EtOH. The aqueous phase was separated, the product was washed once with water, diluted with EtOAc, dried over sodium sulfate and the solvent was removed *in vacuo*. The final triether products were obtained as colorless liquids.

Note: Using 4.50 equiv. of TMDS results in complete reaction after 4 hours of stirring at room after complete addition of TMDS without the need for heating. However, all reactions described in this section were carried out using the above-described general procedure.

For **9a** and **11a**, representative molecular weights were derived from the calculated molecular weights of **HOSO** and **HLSO**, respectively (see section 6.3.3.1).

M(**9a**) = 827 g mol^{-1}
M(**11a**) = 817 g mol^{-1}

Reduction of HOSO to triether 9a

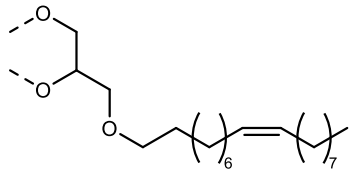

Synthesized according to general procedure (18.7 g **HOSO**, 21.5 mmol). The product **9a** was obtained as a colorless liquid in 76% yield (13.6 g, 16.4 mmol).

^{1}H NMR (400 MHz, Chloroform-*d*) δ/ppm = 5.34 (t, *J* = 5.0 Hz, 5.54H), 3.67 – 3.35 (m, 11H), 2.01 (q, *J* = 6.4 Hz, 11H), 1.56 (p, *J* = 6.5 Hz, 6H), 1.29 (dt, *J* = 13.2, 6.9 Hz, 67H), 0.88 (t, *J* = 6.7 Hz, 9H).

^{13}C NMR (126 MHz, Methylene Chloride-d_2) δ/ppm = 130.40 (m), 78.51, 72.05, 71.32, 70.84, 32.51, 30.37, 30.32, 30.29, 30.25, 30.16 – 30.05 (m), 29.98 – 29.84 (m), 27.75, 26.94 – 26.60 (m), 23.28, 14.47.

IR (ATR platinum diamond) $\tilde{\nu}$/cm^{-1} = 3005 (vw), 2921 (vs), 2853 (s), 1465 (w), 1403 (vw), 1376 (vw), 1351 (vw), 1327 (vw), 1304 (vw), 1261 (vw), 1232 (vw), 1117 (m), 971 (vw), 917 (vw), 911 (vw), 903 (vw), 889 (vw), 878 (vw), 856 (vw), 812 (vw), 763 (vw), 722 (w), 599 (vw), 588 (vw).

ESI-HRMS: $[M+H]^+$ calculated for $C_{57}H_{110}O_3$ = 843.8528, found 843.8540

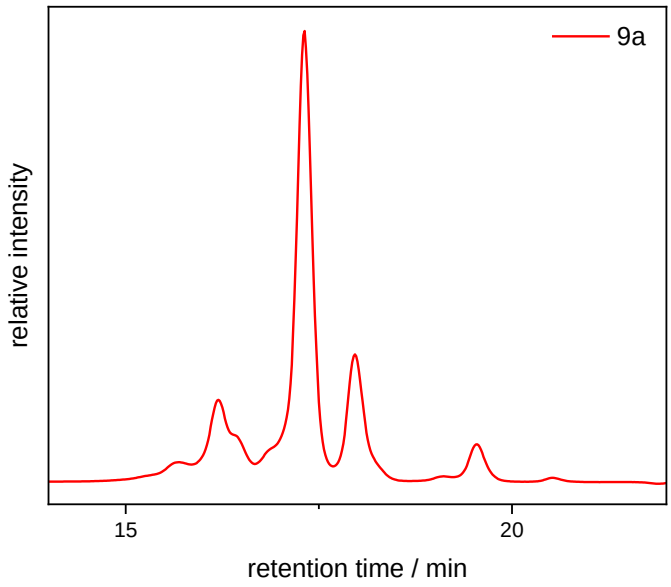

*Supplementary Figure 150: SEC trace of **9a**, measured in THF*

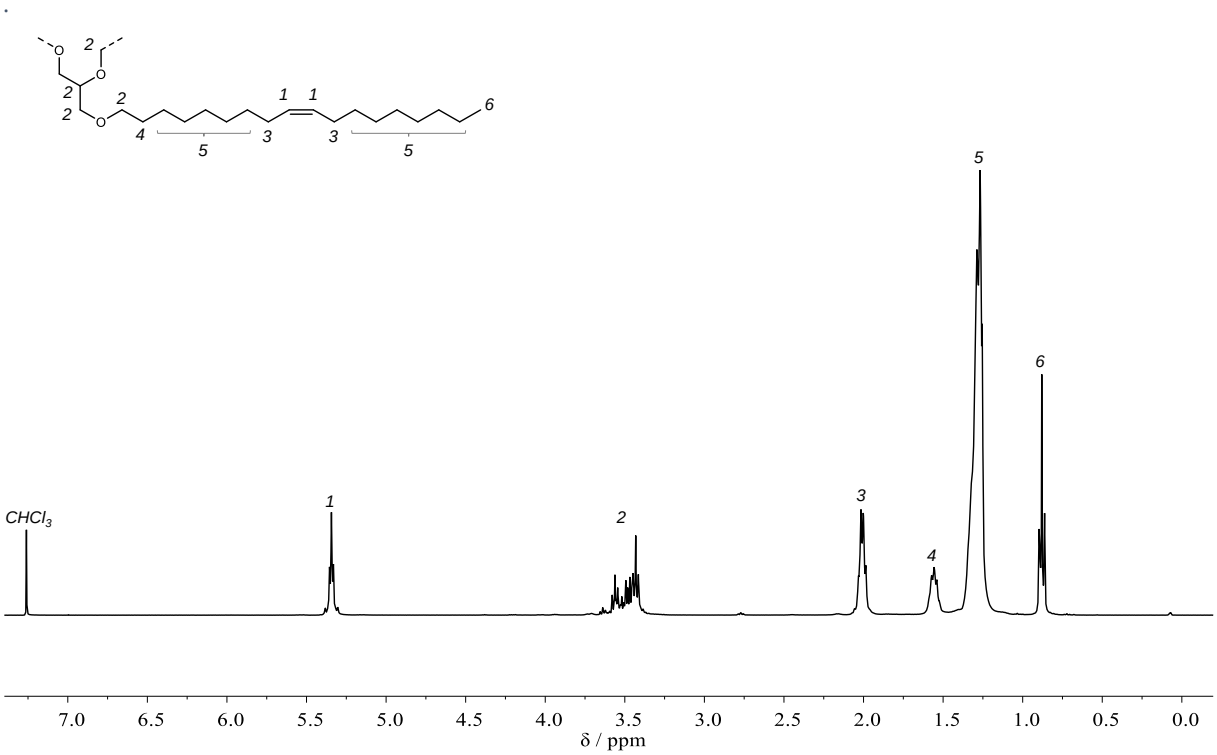

*Supplementary Figure 151: ^{1}H NMR spectrum of **9a** in $CDCl_3$.*

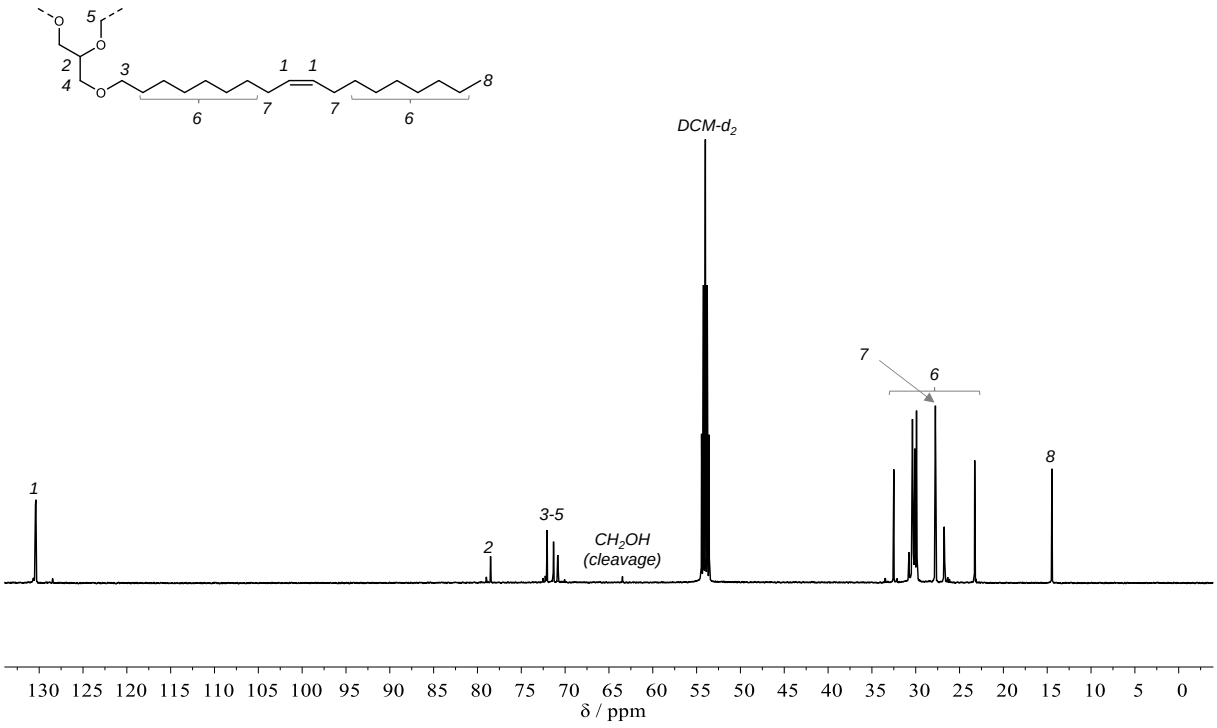

*Supplementary Figure 152: ^{13}C NMR spectrum of **9a** in CD_2Cl_2.*

Reduction of GTU to triether 10a

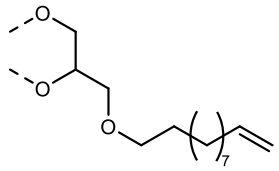

Synthesized according to general procedure (13.0 g GTU, 22.0 mmol). The product **10a** was obtained as a colorless liquid in 64% yield (7.74 g, 14.1 mmol).

^{1}H NMR (500 MHz, Chloroform-*d*) δ/ppm = 5.81 (ddt, *J* = 16.9, 10.2, 6.7 Hz, 3H), 5.05 – 4.87 (m, 6H), 3.65 – 3.38 (m, 11H), 2.03 (q, *J* = 6.9 Hz, 6H), 1.63 – 1.49 (m, 6H), 1.46 – 1.18 (m, 30H).

^{13}C NMR (126 MHz, Methylene Chloride-d_2) δ/ppm = 139.90, 114.35, 78.49, 72.03, 71.30, 70.83, 34.38, 30.75, 30.30, 30.19 – 30.13 (m), 29.72, 29.54, 27.90 – 26.42 (m).

IR (ATR platinum diamond) $\tilde{\nu}$/cm^{-1} = 3077 (vw), 3065 (vw), 2995 (vw), 2974 (vw), 2923 (vs), 2853 (s), 2802 (vw), 2767 (vw), 2756 (vw), 2742 (vw), 2730 (vw), 1641 (w), 1465 (w), 1440 (w), 1415 (vw), 1370 (vw), 1351 (vw), 1327 (vw), 1304 (vw), 1259 (vw), 1232 (vw), 1224 (vw), 1115 (s), 991 (m), 907 (s), 722 (w), 636 (vw), 553 (vw).

ESI-HRMS: $[M+Na]^+$ calculated for $C_{36}H_{68}O_3$ = 571.5061, found 571.5059

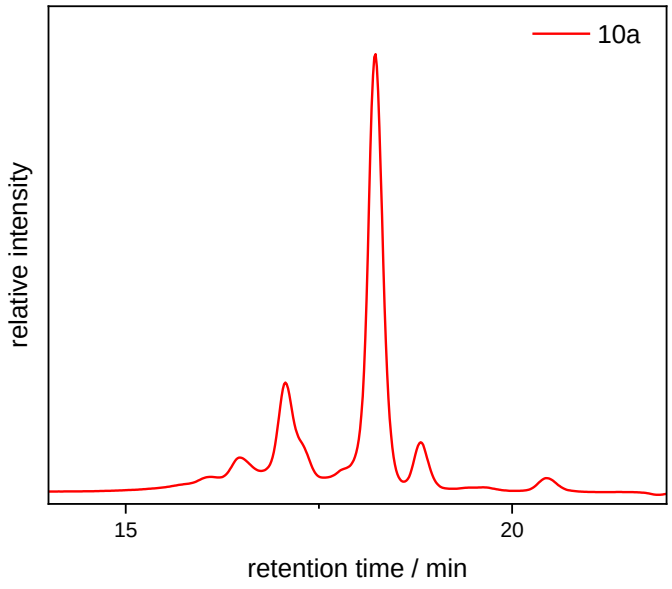

*Supplementary Figure 153: SEC trace of **10a**, measured in THF*

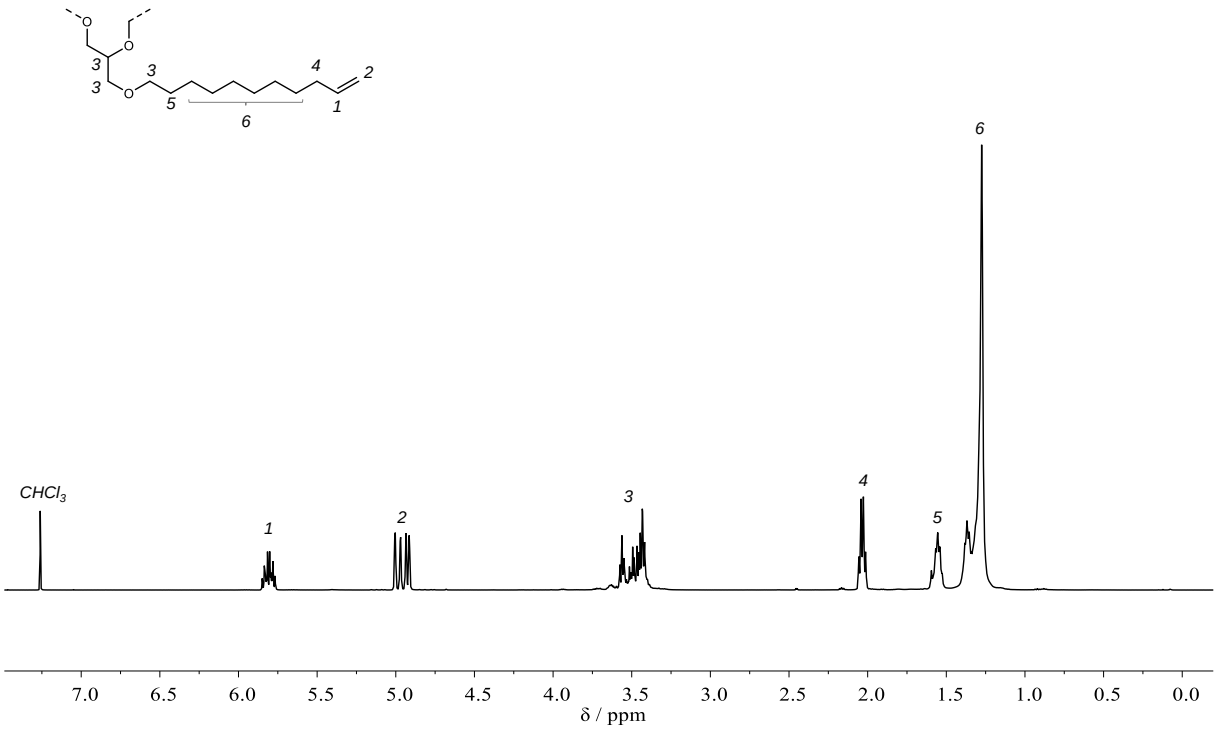

*Supplementary Figure 154: ^{1}H NMR spectrum of **10a** in $CDCl_3$.*

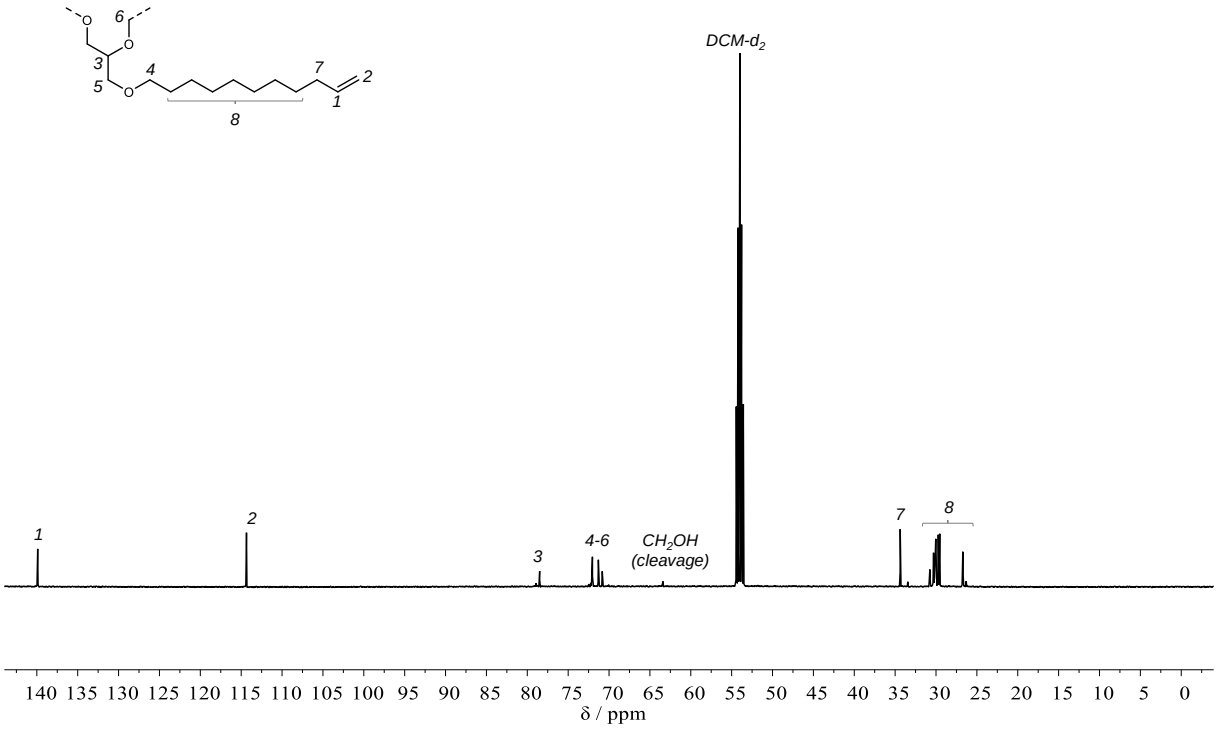

*Supplementary Figure 155: ^{13}C NMR spectrum of **10a** in CD_2Cl_2.*

Reduction of HLSO to triether 11a

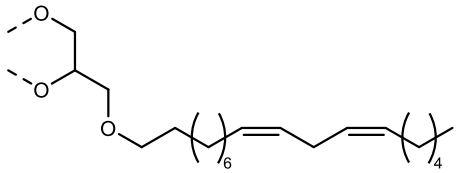

Synthesized according to general procedure in half scale (9.19 g HLSO, 10.7 mmol). The product **11a** was obtained as a colorless liquid in 83% yield (7.30 g, 8.94 mmol).

^{1}H NMR (500 MHz, Chloroform-*d*) δ/ppm = 5.35 (dtt, *J* = 17.5, 10.8, 5.0 Hz, 8.51H), 3.63 – 3.35 (m, 11H), 2.77 (t, *J* = 6.8 Hz, 3H), 2.03 (dq, *J* = 18.6, 6.7 Hz, 10H), 1.62 – 1.51 (m, 6H), 1.42 – 1.21 (m, 57H), 0.95 – 0.83 (m, 9H).

^{13}C NMR (126 MHz, Methylene Chloride-d_2) δ/ppm = 130.85 – 130.62 (m), 130.55 – 130.16 (m), 128.46, 78.49, 72.04, 71.31, 70.83, 32.50 (d, *J* = 2.3 Hz), 32.11, 30.76, 30.36, 30.33 – 30.22 (m), 30.16 – 30.01 (m), 29.99 – 29.82 (m), 27.89 – 27.40 (m), 26.98 – 26.52 (m), 26.15, 23.45 – 22.97 (m), 14.61 – 14.16 (m).

IR (ATR platinum diamond) $\tilde{\nu}$/cm^{-1} = 3009 (w), 2923 (vs), 2853 (s), 1465 (w), 1399 (vw), 1376 (w), 1351 (w), 1327 (vw), 1304 (vw), 1269 (vw), 1115 (m), 985 (w), 971 (w), 913 (vw), 884 (vw), 872 (vw), 862 (vw), 722 (w), 603 (vw), 592 (vw), 584 (vw), 576 (vw).

ESI-HRMS: $[M+Na]^+$ calculated for $C_{57}H_{106}O_3$ = 861.8035, found 861.8025.

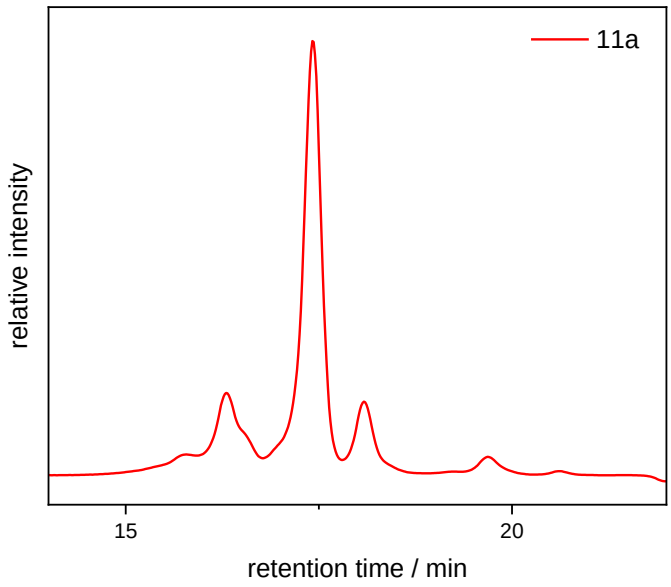

*Supplementary Figure 156: SEC trace of **11a**, measured in THF*

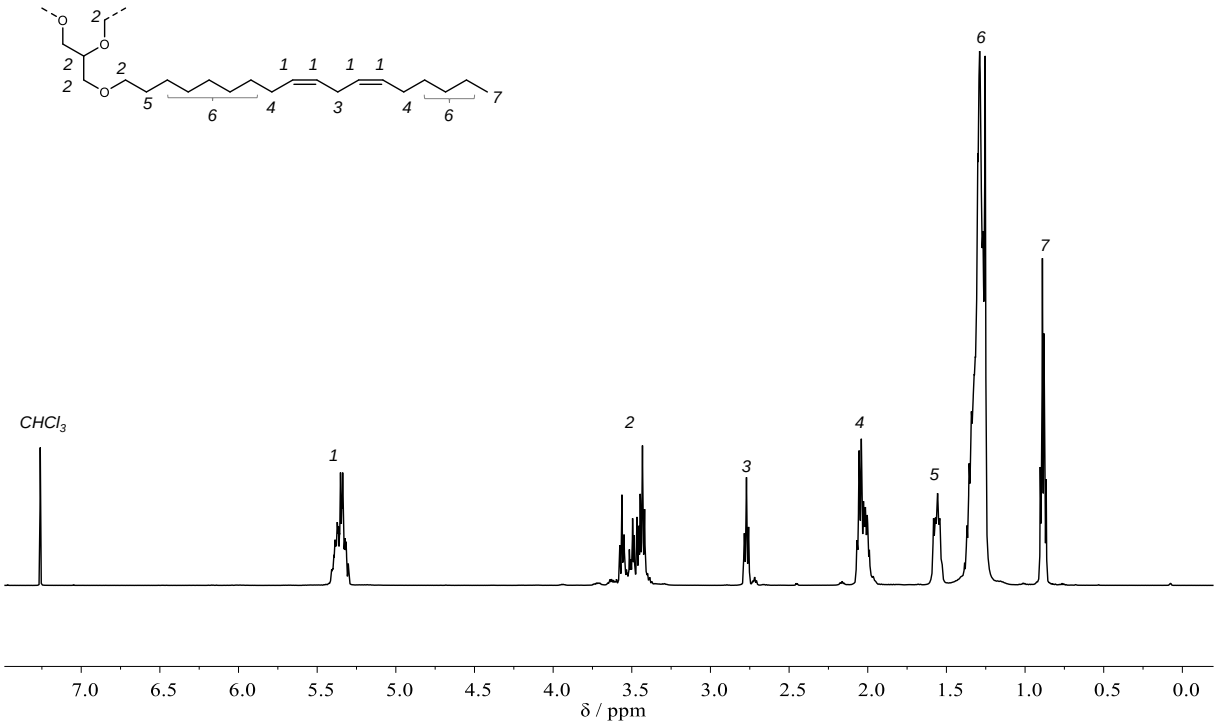

*Supplementary Figure 157: ^{1}H NMR spectrum of **11a** in $CDCl_3$.*

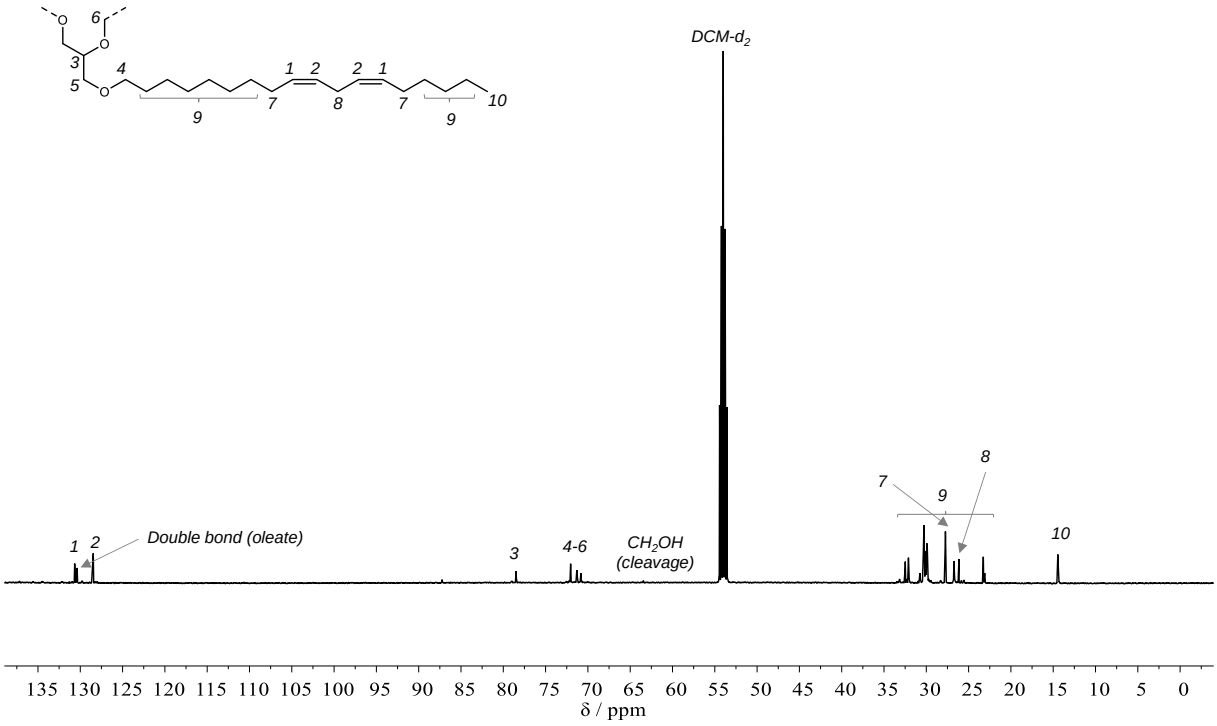

*Supplementary Figure 158: ^{13}C NMR spectrum of **11a** in CD_2Cl_2.*

6.3.3.3 Silicone Removal Investigations

Calculation of Silicone Removal Efficiency

Silicone Removal Efficiency (SRE) is used in section 4.3.3 to compare the silicone contents of different samples of **HOSO**-derived triether **9a** and is calculated from the ^{1}H NMR spectrum of the respective sample according to Equation 6:

$$SRE = \left(1 - \frac{I\ (Si - CH_3)}{4\ \cdot I\ (fatty\ CH_3)}\right) \cdot 100\% \qquad (6)$$

I(Si-CH_3) is obtained from the integral of the resonance associated with the silicone species (0.3 to -0.1 ppm), while I(fatty CH_3) represents the integral of the termial methyl groups of the fatty acid chains of **1a** (0.95 to 0.82 ppm). The calculation operated unter the assumption that only a stoichiometric amount of TMDS reacts to non-volatile silicone products under reduction of the ester moieties, and the excess TMDS can be removed under reduced pressure after the reaction. Hence, the ideal ratio of I(Si-CH_3)/I(fatty CH_3) is equal to 4, thus representing an SRE of 0%.

Attempted silicone removal from crude 9a via acetone washing

All reagents and glassware were dried before use. In a crimp vial under argon atmosphere, **HOSO** (18.7 g, 21.5 mmol, 1.00 equiv.) was added to 200 mg of gallium bromide (0.646 mmol, 0.03 equiv.) and stirred for 5 minutes. The mixture was placed inside an ice bath and 12.6 mL of tetramethyldisiloxane (TMDS) (9.55 g, 71.1 mmol, 3.30 equiv.) were added dropwise with a syringe pump over the course of 2 hours while stirring. After complete addition of TMDS, the mixture was removed from the ice bath and stirred at room temperature for 3 hours, then heated to 60 °C for 1 additional hour. Afterwards, the reaction was quenched by addition of 5 mL of 10% sodium carbonate solution and stirring for 1 hour at room temperature. The aqueous phase was separated and unreacted TMDS was removed under reduced pressure. Afterwards, the crude product was transferred to a separatory funnel and washed with 20 mL of acetone. After phase separation (after ~1 hour), the lower phase was separated and washed 3 more times with 20 mL each of acetone. ^{1}H NMR spectra were recorded after each washing step (see Figure 5 in section 4.3.3.1). After the fourth acetone washing, 7.11 g of crude product with an SRE of 83% were obtained.

Silicone removal screenings via aqueous hydrolysis

All reagents and glassware were dried before use. In a crimp vial under argon atmosphere, HOSO (1.90 g, 2.18 mmol, 1.00 equiv.) was added to 20.0 mg of gallium bromide (64.6 µmol, 0.03 equiv.) and stirred for 5 minutes. The mixture was placed inside an ice bath and 1.26 mL of tetramethyldisiloxane (TMDS) (955 mg, 7.11 mmol, 3.26 equiv.) were added dropwise with a syringe pump over the course of 2 hours while stirring. After complete addition of TMDS, the mixture was removed from the ice bath and stirred at room temperature for 3 hours, then heated to 60 °C for 1 additional hour. Afterwards, the reaction was quenched by addition of 0.5 mL of 10% sodium carbonate solution and stirring for 1 hour at room temperature. The aqueous phase was separated and unreacted TMDS was removed under reduced pressure.
Afterwards, the crude reaction mixture was transferred to a 100 mL flask and the desired amount of aqueous sodium hydroxide (c = 2.5 M or 5 M) solution was added, followed by the desired volume of EtOH (corresponding to volume of NaOH solution). The mixture was heated to 100 °C for the desired time under vigorous stirring. Afterwards, the lower, aqueous phase was removed and the product was washed once with water. Afterwards, SRE was determined *via* ^{1}H NMR. The screening results are listed in Table 7 in section 4.3.3.1

Attempted silicone removal via column chromatography

Disclaimer

This reaction was performed by Ramon Häusl under co-supervision of the author.

All reagents and glassware were dried before use. In a crimp vial under argon atmosphere, HOSO (1.77 g, 2.06 mmol, 1.00 equiv.) was added to 20.0 mg of gallium bromide (64.6 µmol, 0.03 equiv.) and stirred for 5 minutes. The mixture was placed inside a water bath and 1.60 mL of tetramethyldisiloxane (TMDS) (955 mg, 9.06 mmol, 4.40 equiv.) were added dropwise with a syringe pump over the course of 2 hours while stirring. After complete addition of TMDS, the mixture was removed from the ice bath and stirred at room temperature for 4 hours. Afterwards, the crude mixture was purified *via* column chromatography (cyclohexane/ethyl acetate 20:1). 1.31 g of **9a** were isolated with an SRE of 67% (Supplementary Figure 159).

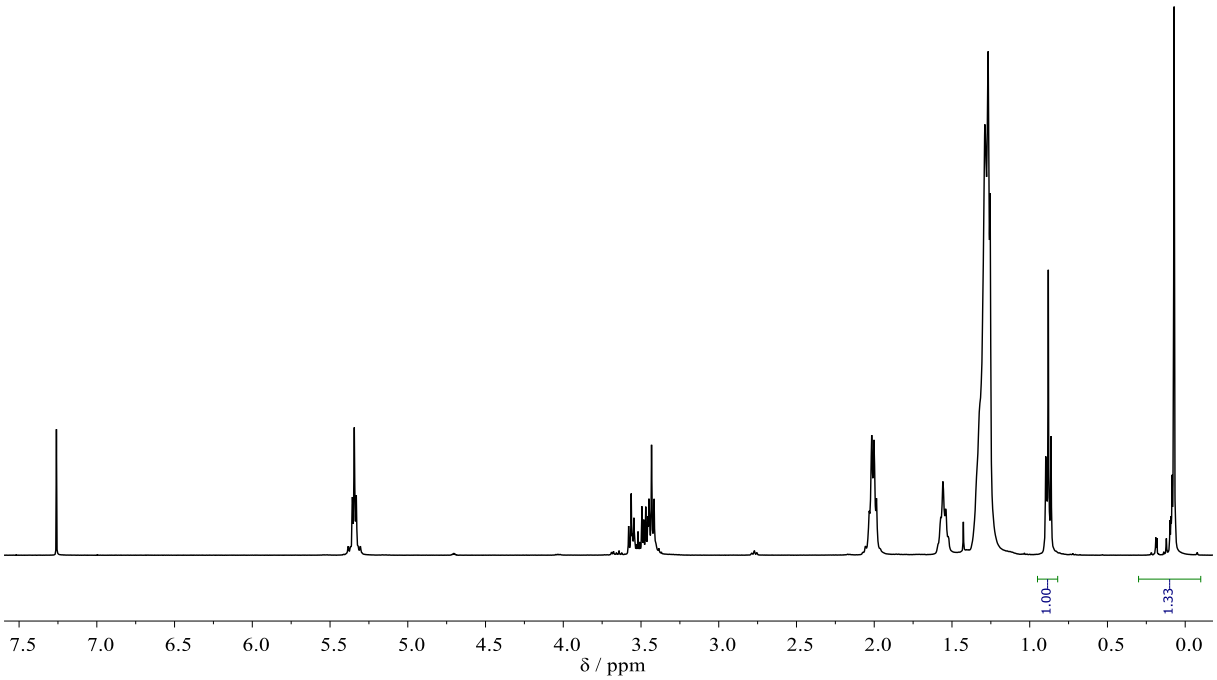

*Supplementary Figure 159: ^{1}H NMR of the fraction of **9a** isolated via column chromatography.*

6.3.3.4 Acetylthiolation

General procedure for thioester synthesis:

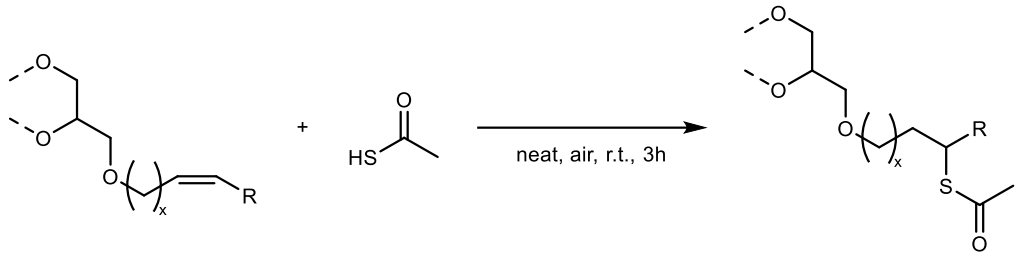

Thioacetic acid was purified by vacuum distillation before use. The respective triether (1.00 equiv.) was mixed with thioacetic acid (761 mg/mmol triether, 707 µL/mmol triether, 10.0 equiv.) and the mixture was stirred under air atmosphere at room temperature for 3 hours. Afterwards, excess thioacetic acid was recovered under reduced pressure and the product was further dried under vacuum.

For **9b** and **11b**, representative molecular weights were derived from the calculated molecular weights of **9a** and **11a**, respectively, taking into account their respective double bond functionality and assuming full double bond conversion (see section 6.3.3.2).

M(**1b**) = 1038 g mol^{-1}
M(**3b**) = 1140 g mol^{-1}

Synthesis of thioester 9b from triether 9a

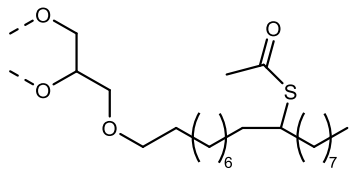

Synthesized from **9a** according to general procedure in 16.4 mmol scale (13.6 g **9a**). The product **9b** was obtained as a colorless liquid in quantitative yield (17.2 g, 16.5 mmol). The slightly overstoichiometric yield is due to inaccurate molecular weight determination.

^{1}H NMR (500 MHz, Chloroform-*d*) δ/ppm = 3.73 – 3.30 (m, 14H), 2.31 (s, 8.51H), 1.63 – 1.45 (m, 17H), 1.42 – 1.18 (m, 74H), 0.87 (t, *J* = 6.9 Hz, 9H).

^{13}C NMR (126 MHz, Methylene Chloride-d_2) δ/ppm = 196.26 (d, *J* = 4.8 Hz), 78.49, 72.04, 71.31, 70.83, 45.21, 35.38, 32.87 – 32.13 (m), 31.15, 30.57 – 29.50 (m), 27.34, 26.98 – 26.47 (m), 23.26 (d, *J* = 1.9 Hz), 14.46.

IR (ATR platinum diamond) $\tilde{\nu}$/cm^{-1} = 2923 (s), 2853 (s), 1691 (vs), 1462 (w), 1374 (w), 1368 (w), 1351 (w), 1327 (vw), 1304 (vw), 1261 (vw), 1111 (s), 950 (m), 804 (vw), 722 (w), 631 (s).

ESI-HRMS: $[M+Na]^+$ calculated for $C_{53}H_{122}O_6S_3$ = 1093.8296, found 1093.8284.

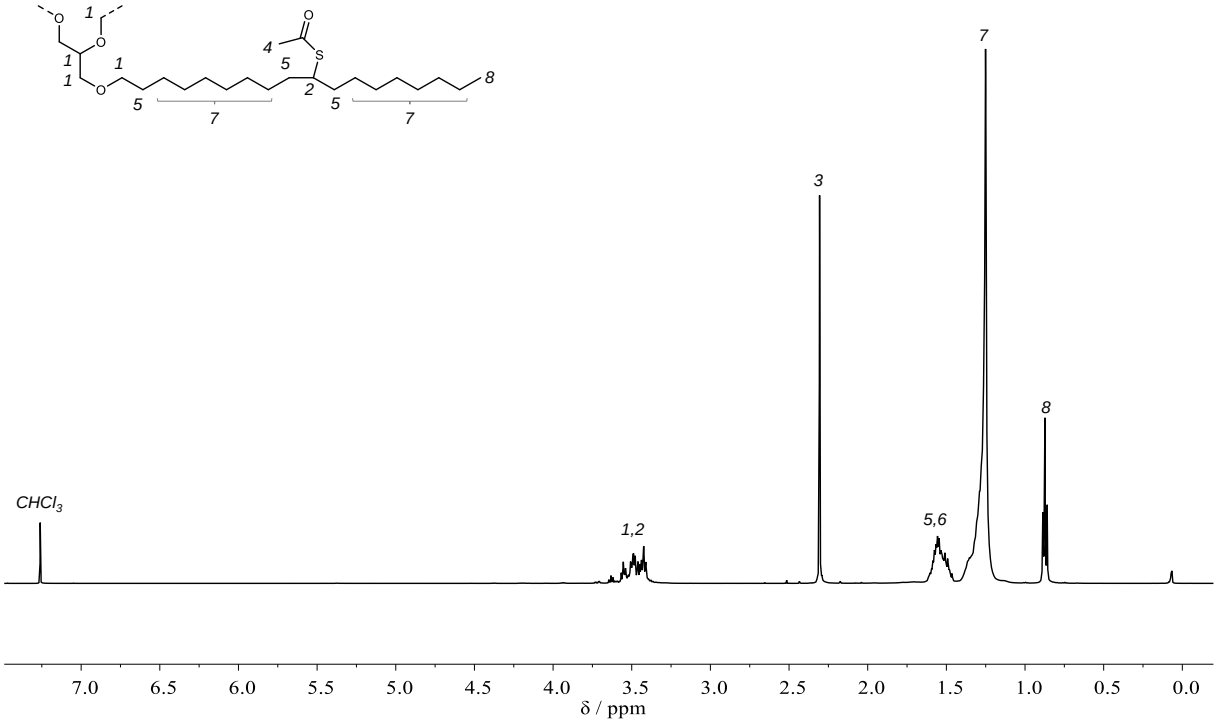

*Supplementary Figure 160: ^{1}H NMR spectrum of **9b** in $CDCl_3$.*

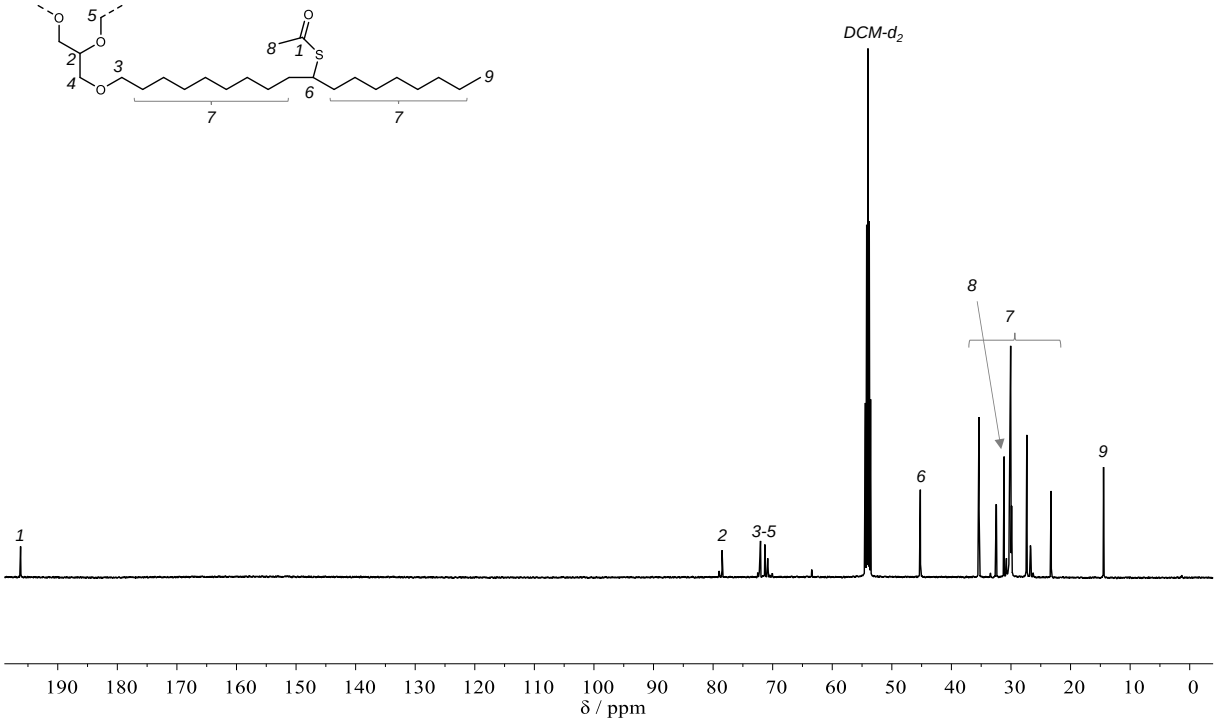

*Supplementary Figure 161: ^{13}C NMR spectrum of **9b** in CD_2Cl_2.*

Synthesis of thioester 10b from triether 10a

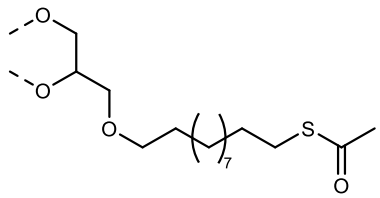

Synthesized from **10a** on 14.0 mmol scale (7.70 g **10a**). The product **10b** was obtained as a colorless liquid in quantitative yield (10.7 g, 14.0 mmol).

^{1}H NMR (400 MHz, Chloroform-*d*) δ/ppm = 3.60 – 3.38 (m, 11H), 2.86 (t, *J* = 7.3 Hz, 6H), 2.32 (s, 9H), 1.55 (m, 12H), 1.25 (s, 42H).

^{13}C NMR (126 MHz, Methylene Chloride-d_2) δ/ppm = 197.57 – 194.76 (m), 78.48, 72.03, 71.29, 70.82, 30.99, 30.75, 30.30, 30.25 – 29.95 (m), 29.80 – 29.59 (m), 29.54 – 29.20 (m), 26.92 – 26.46 (m).

IR (ATR platinum diamond) $\tilde{\nu}$/cm^{-1} = 2923 (s), 2853 (m), 1740 (vw), 1691 (vs), 1462 (w), 1436 (w), 1413 (vw), 1353 (w), 1304 (vw), 1279 (vw), 1240 (vw), 1129 (s), 1107 (s), 1004 (w), 952 (m), 722 (vw), 673 (vw), 625 (s).

ESI-HRMS: $[M+Na]^+$ calculated for $C_{42}H_{80}O_6S_3$ = 799.5010, found 799.5003.

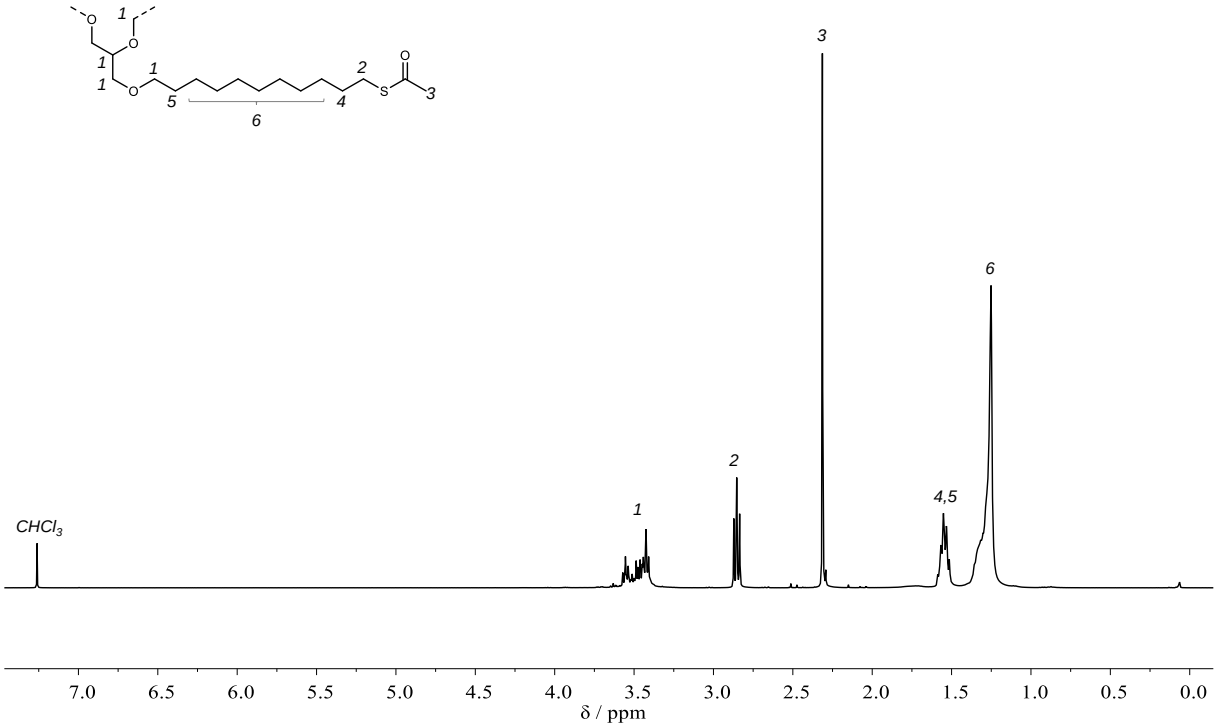

*Supplementary Figure 162: ^{1}H NMR spectrum of **10b** in $CDCl_3$.*

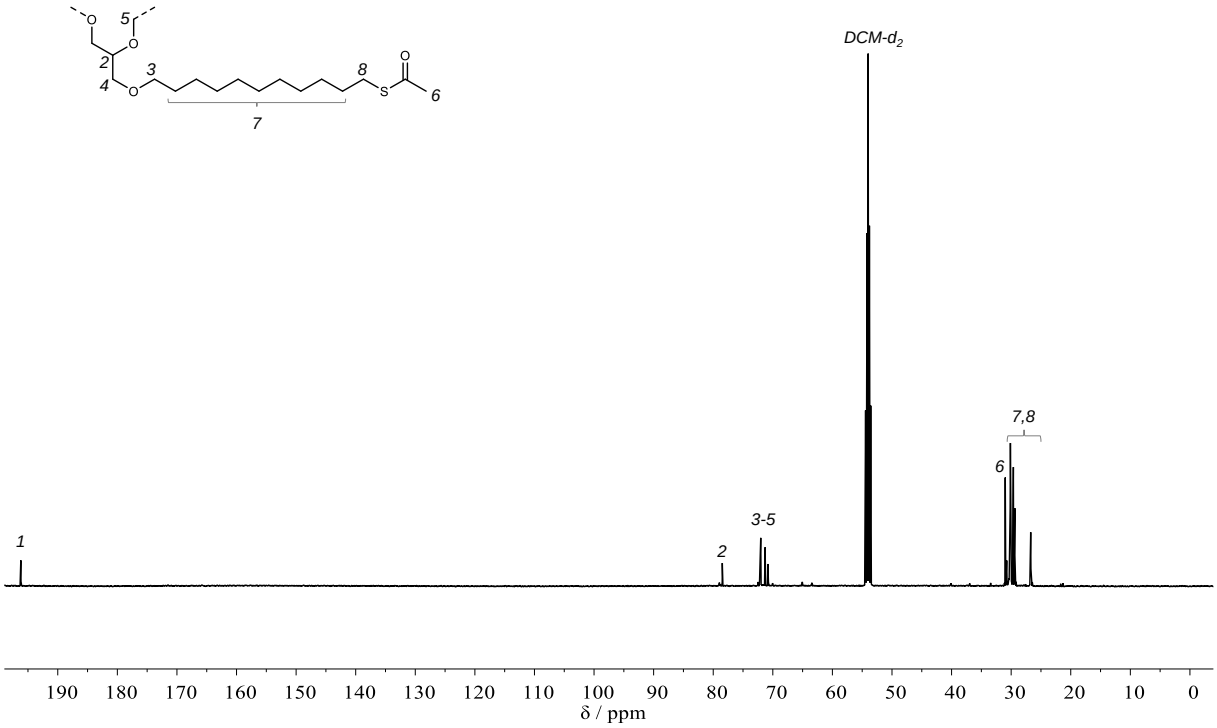

*Supplementary Figure 163: ^{13}C NMR spectrum of **10b** in CD_2Cl_2.*

Synthesis of thioester 11b from triether 11a

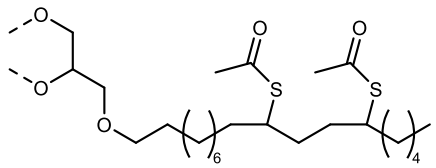

Synthesized from **11a** according to general procedure in 8.94 mmol scale (7.30 g **11a**). The mixture was stirred for 72 hours at room temperature, including 22 hours of irradiation at 365 nm. The product **11b** was obtained as a colorless liquid in a yield of 92% (9.41 g, 8.25 mmol).

^{1}H NMR (400 MHz, Chloroform-*d*) δ/ppm = 3.59 – 3.36 (m, 15H), 2.38 – 2.25 (m, 11.8H), 1.71 – 1.45 (m, 18H), 1.26 (d, *J* = 6.7 Hz, 65H), 0.87 (t, *J* = 6.7 Hz, 9H).

^{13}C NMR (126 MHz, Methylene Chloride-d_2) δ/ppm = 195.87 – 194.95 (m), 77.91, 71.47, 70.73, 70.26, 45.07 – 43.93 (m), 42.82 – 41.96 (m), 35.25 – 34.28 (m), 32.34 – 31.22 (m), 30.58, 30.19, 30.08 – 28.85 (m), 27.08 – 26.71 (m), 26.63 – 26.40 (m), 26.35 – 25.97 (m), 23.17 – 22.12 (m), 14.27 – 13.67 (m).

IR (ATR platinum diamond) $\tilde{\nu}$/cm^{-1} = 2923 (s), 2853 (m), 1742 (vw), 1689 (vs), 1458 (w), 1351 (w), 1327 (vw), 1304 (vw), 1236 (vw), 1111 (s), 950 (m), 722 (w), 631 (s).

ESI-HRMS: $[M+Na]^+$ calculated for $C_{67}H_{126}O_8S_5$ =1241.7949, found 1241.7938.

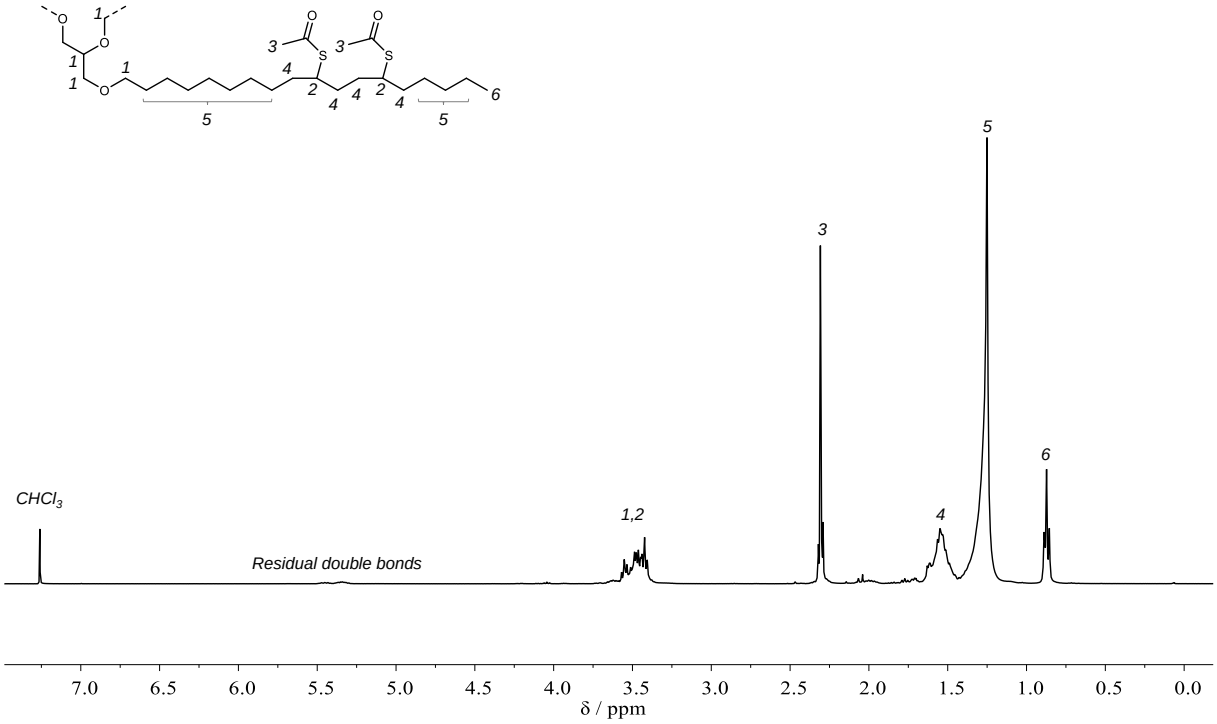

*Supplementary Figure 164: ^{1}H NMR spectrum of **11b** in $CDCl_3$.*

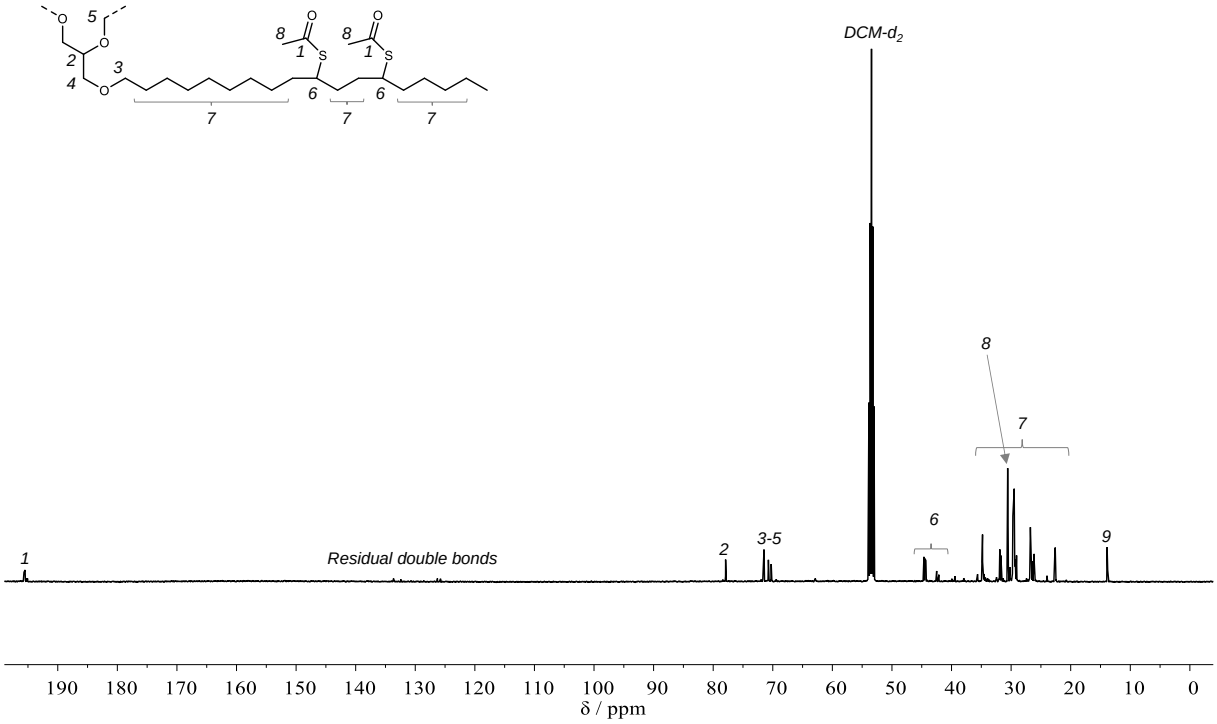

*Supplementary Figure 165: ^{13}C NMR spectrum of **11b** in CD_2Cl_2.*

Initial attempt to synthesize thioester 9b with undistilled HSAc under UV irradiation

Disclaimer

This reaction was performed by Mathilde Bourcier under co-supervision of the author.

In a crimp vial under air atmosphere, 16.1 g **9a** (19.4 mmol, 1.00 equiv.) were mixed with 12.9 mL (13.8 g, 181 mmol,.9.30 equiv.) of thioacetic acid. The vial was closed and the mixture was stirred at room temperature under UV irradiation. The conversion was monitored by recording ^{1}H NMR spectra after a certain time and comparing the integral of the carbon-carbon double bonds (5.41 to 5.26 ppm) to that of 9a prior to the reaction (Supplementary Figure 166, top spectrum). The NMR analysis indicated 59% conversion after 22 hours (Supplementary Figure 166, 2nd spectrum from top) and 73% conversion after 72 hours of irradiation (Supplementary Figure 166, 2nd spectrum from bottom). Afterwards, HSAc was removed from the mixture *in vacuo* and 12.9 mL of fresh HSAc were added. After an additional 72 h of irradiation, NMR analysis indicates 84% conversion (Supplementary Figure 166, bottom spectrum).

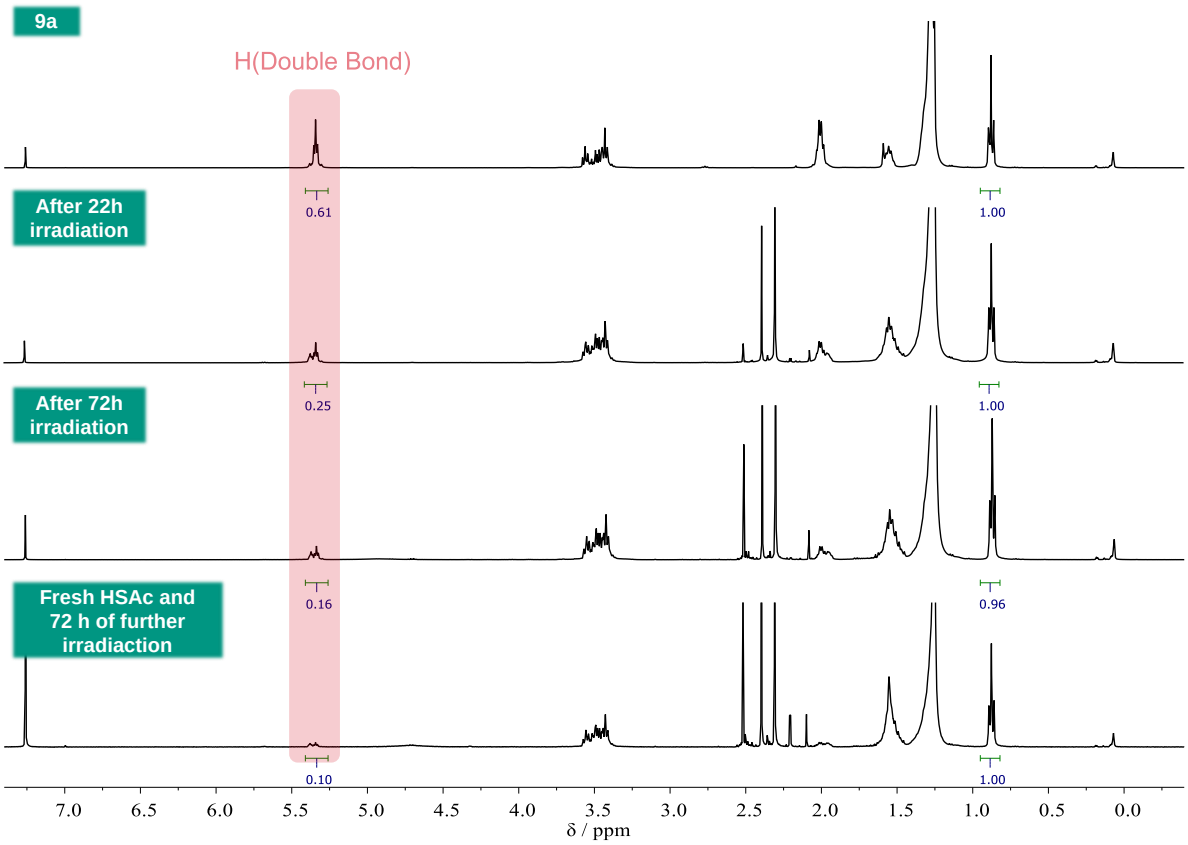

*Supplementary Figure 166: ^{1}H NMR spectra recorded during the initial attempt at synthesizing thioester **9b** from **9a**.*

Distillation of HSAc

The distillation of HSAc prior to its usage was found to have significant impact on the success of the acetylthiolation reaction. Distillation was conducted at ambient temperature under reduced pressure. The receiving flask was cooled with liquid nitrogen. ^{1}H NMR analysis of HSAc before and after the distillation was conducted, indicating the disappearance of contamination signals (Supplementary Figure 167). However, as stated in section 4.3.4, no further investigations on the nature of the contaminants or their impact on radical reactions were conducted as part of this work.

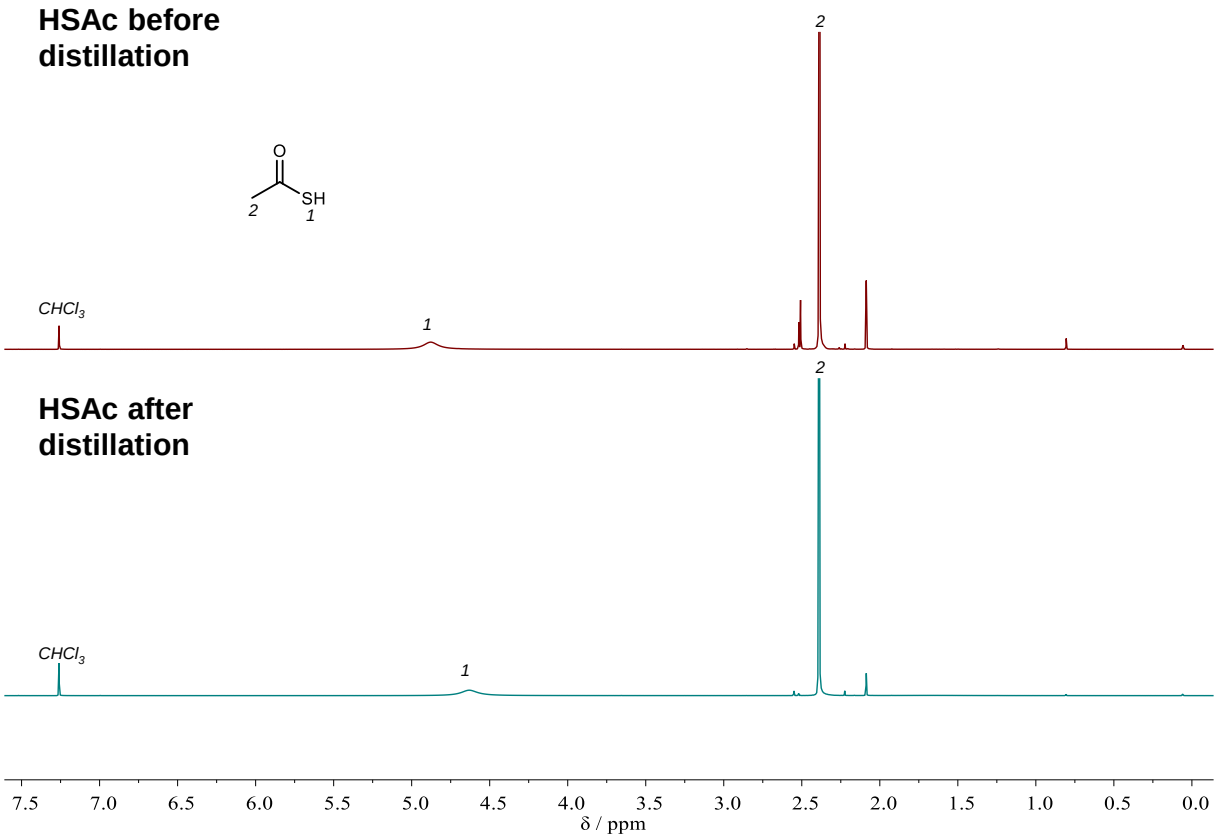

Supplementary Figure 167: Comparison of the ^{1}H NMR spectra of HSAc before (top) and after purification via distillation (bottom).

6.3.3.5 Alcoholysis

General procedure for alcoholysis of thioesters:

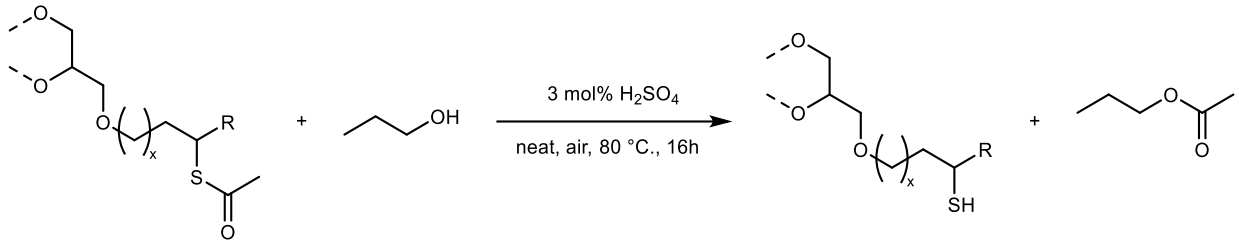

The thioester (1.00 equiv.) was mixed with *n*-propanol (601 mg/mmol thioester, 751 µL/mmol thioester, 10.0 equiv.) and sulfuric acid (2.94 mg/mmol thioester, 1.60 µL/mmol thioester, 0.03 equiv.) was added. The mixture was stirred at 80 °C for 16 hours. Afterwards, excess *n*-propanol and propyl acetate were removed *in vacuo*. The product was washed once with saturated sodium bicarbonate solution and once with water. Afterwards, the crude product was diluted with EtOAc, dried over sodium sulfate and then dried under reduced pressure. Thiol products were subsequently stored under argon atmosphere.

For **9c** and **11c**, representative molecular weights were derived from the calculated molecular weights of **9b** and **11b**, respectively, taking into account their respective thioester functionality (see section 3.3). Notably, M(**11b**) = 1115 g/mol was used, considering its incomplete conversion in the previous step.

M(**9c**) = 923 g mol^{-1}
M(**11c**) = 973 g mol^{-1}

Screening reactions for optimization of transesterification of 9b

In a crimp vial, 500 mg of **9b** (0.481 mmol, 1.00 equiv.) were mixed with 361 µL of *n*-propanol (289 mg, 4.81 mmol, 10.00 equiv.) and the respective catalyst was added. The vial was closed and the mixture was stirred at 80 °C for 16 h. Afterwards, ^{1}H NMR spectra were recorded and the conversion was determined with Equation 8. I(Thioester) for 9b and the sample were obtained by integration between 2.33 and 2.28 ppm. I(Methyl) for 9b and the sample were obtained by integration between 0.91 and 0.83 ppm. The screening results are listed in Table 8 in section 4.3.5.

$$Conversion\ [\%] = \left(\frac{I(Thioester\ 9b)}{I(Methyl)} - \frac{I(Thioester\ sample)}{I(Methyl\ sample)}\right) \cdot 100\% \qquad (8)$$

The formation of thiol **9c** was indicated by the emergence of a sextet at 2.76 ppm. When TBD and DBU were used as the catalysts of the transesterification, a small amount of disulfide formation was discernible by the emergence of an additional quintet at 2.59 ppm. An illustrative example is provided in Supplementary Figure 168.

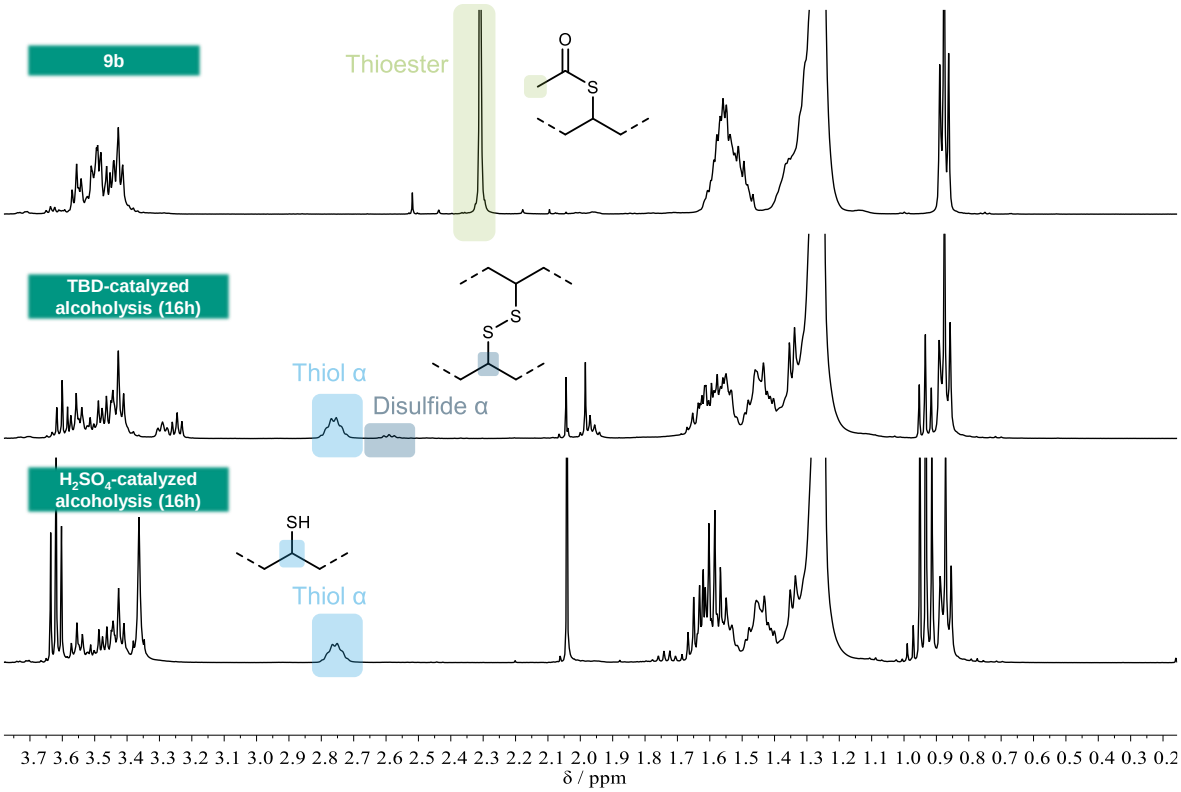

*Supplementary Figure 168: Comparison of ^{1}H NMR spectra of thioester **9b** (top) and the crude transesterification reactions catalyzed by TBD (middle) and sulfuric acid (bottom), illustrating the formation of disulfide side product in the TBD-catalyzed reaction.*

Synthesis of thiol 9c from thioester 9b

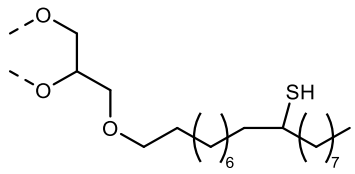

Synthesized from **9b** according to general procedure in 16.6 mmol scale (17.2 g **9b**). The product **9c** was obtained as a viscous, yellowish liquid in a yield of 94% (14.3 g, 15.5 mmol).

^{1}H NMR (400 MHz, Chloroform-*d*) δ/ppm = 3.67 – 3.37 (m, 11H), 2.76 (sext., *J* = 7.4, 3.7 Hz, 2.64H), 1.68 – 1.39 (m, 18H), 1.39 – 1.21 (m, 80H), 0.88 (t, *J* = 6.7 Hz, 9H).

^{13}C NMR (126 MHz, Methylene Chloride-d_2) δ/ppm = 78.50, 72.04, 71.32, 70.83, 41.70, 39.60, 33.17 – 31.79 (m), 30.76, 30.80 – 29.36 (m), 27.67, 27.20 – 26.36 (m), 23.26, 14.46.

IR (ATR platinum diamond) $\tilde{\nu}$/cm^{-1} = 2921 (vs), 2853 (s), 1465 (w), 1376 (vw), 1353 (vw), 1302 (vw), 1257 (vw), 1242 (vw), 1115 (m), 973 (vw), 722 (w).

ESI-HRMS: $[M+Na]^+$ calculated for $C_{57}H_{116}O_3S_3$ = 967.7979, found 967.7968.

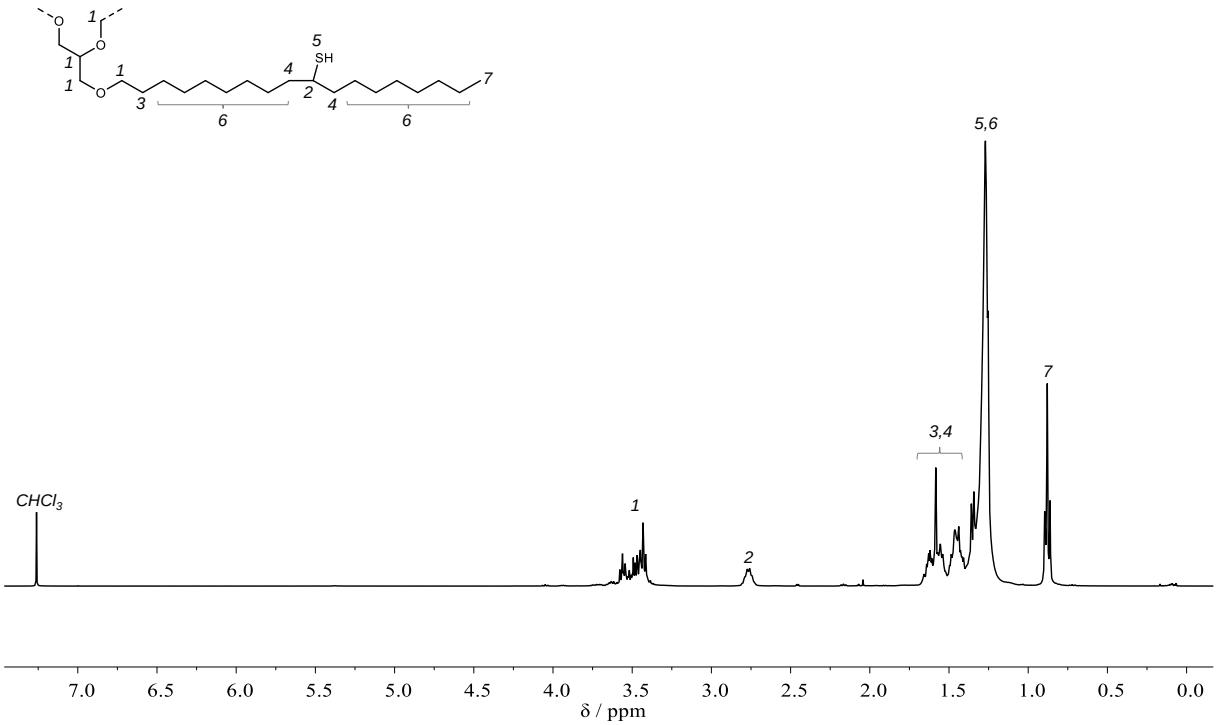

*Supplementary Figure 169: ^{1}H NMR spectrum of **9c** in $CDCl_3$.*

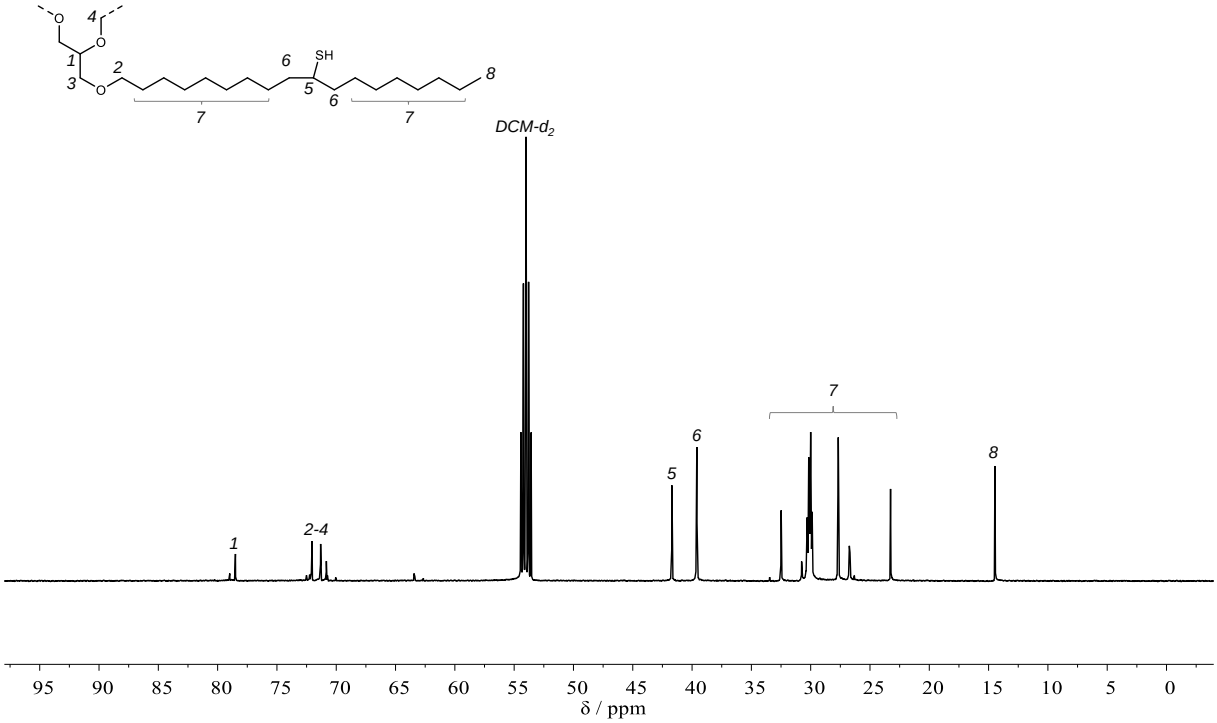

*Supplementary Figure 170: ^{13}C NMR spectrum of **9c** in CD_2Cl_2.*

SEC analysis was conducted to confirm that no side reactions that result in further degradation of the glyceryl backbone occur during acetylthiolation and transesterification of **9a**. Supplementary Figure 171 depicts an overlay of the SEC traces of **9a**, **9b**, and **9c**, illustrating that the ratio of the signals remains mostly visually equal throughout the synthesis steps, confirming the stability of the glyceryl backbone towards the conditions of acetylthiolation and transesterification.

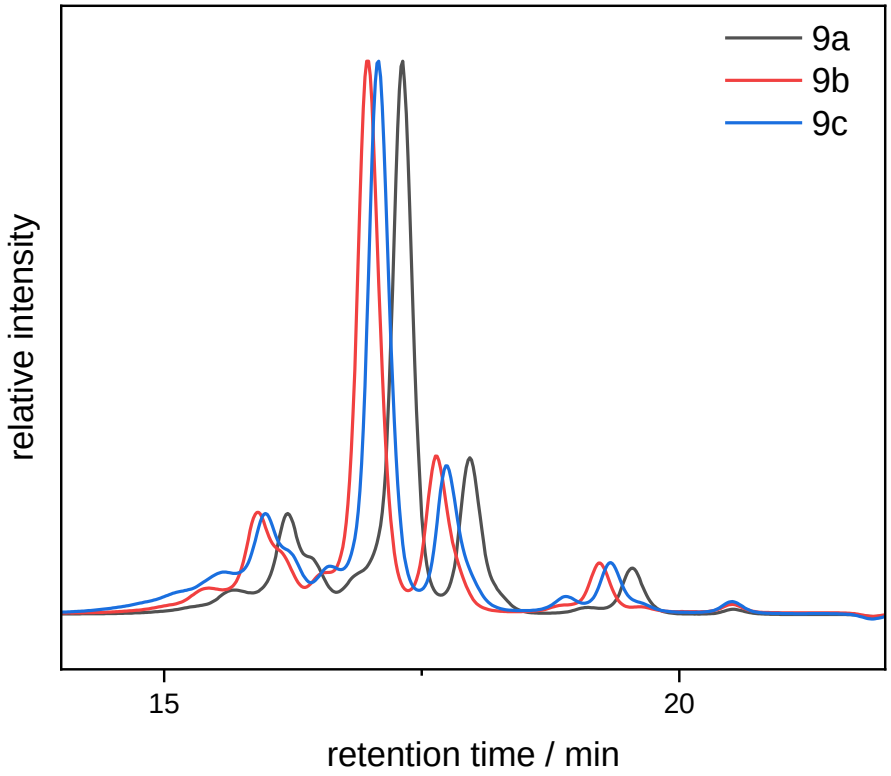

*Supplementary Figure 171: Overlay of the SEC traces of **9a**, **9b** and **9c**.*

Synthesis of thiol 10c from thioester 10b

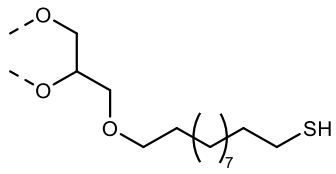

Synthesized from **10b** according to general procedure in 13.6 mmol scale (10.6 g **10b**). The product **10c** was obtained as a viscous, yellowish liquid in a yield of 91% (8.07 g, 12.4 mmol).

^{1}H NMR (500 MHz, Chloroform-*d*) δ/ppm = 3.61 – 3.38 (m, 11H), 2.51 (q, *J* = 7.5 Hz, 6H), 1.67 – 1.50 (m, 12H), 1.43 – 1.20 (m, 48H).

^{13}C NMR (126 MHz, Methylene Chloride-d_2) δ/ppm = 78.49, 72.03, 71.30, 70.82, 34.72, 30.76, 30.43 – 29.98 (m), 29.66, 28.96, 26.85 – 26.59 (m), 25.12.

IR (ATR platinum diamond) $\tilde{\nu}$/cm^{-1} = 2921 (vs), 2851 (s), 1462 (w), 1395 (vw), 1368 (w), 1351 (vw), 1325 (vw), 1302 (w), 1281 (w), 1261 (vw), 1242 (vw), 1195 (vw), 1113 (s), 913 (vw), 880 (vw), 860 (vw), 852 (vw), 722 (w).

ESI-HRMS: $[M+Na]^+$ calculated for $C_{42}H_{80}O_6S_3$ = 673.4693, found 673.4689.

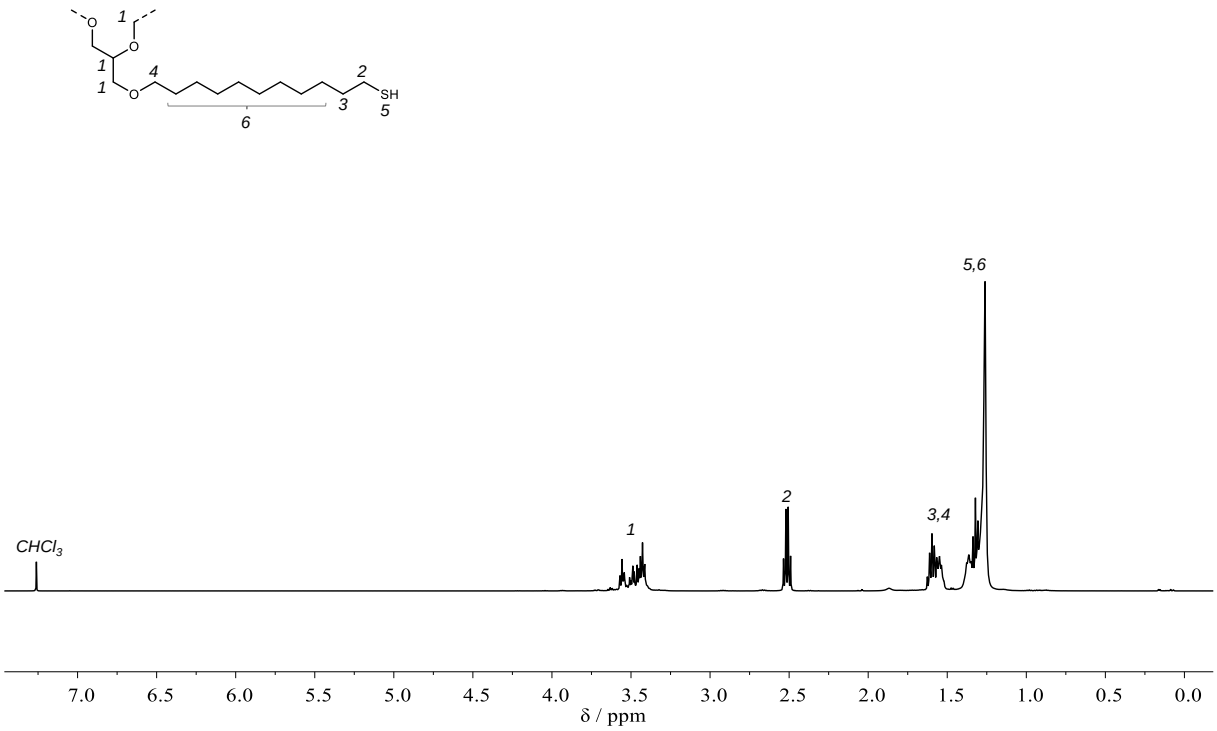

*Supplementary Figure 172: ^{1}H NMR spectrum of **10c** in $CDCl_3$.*

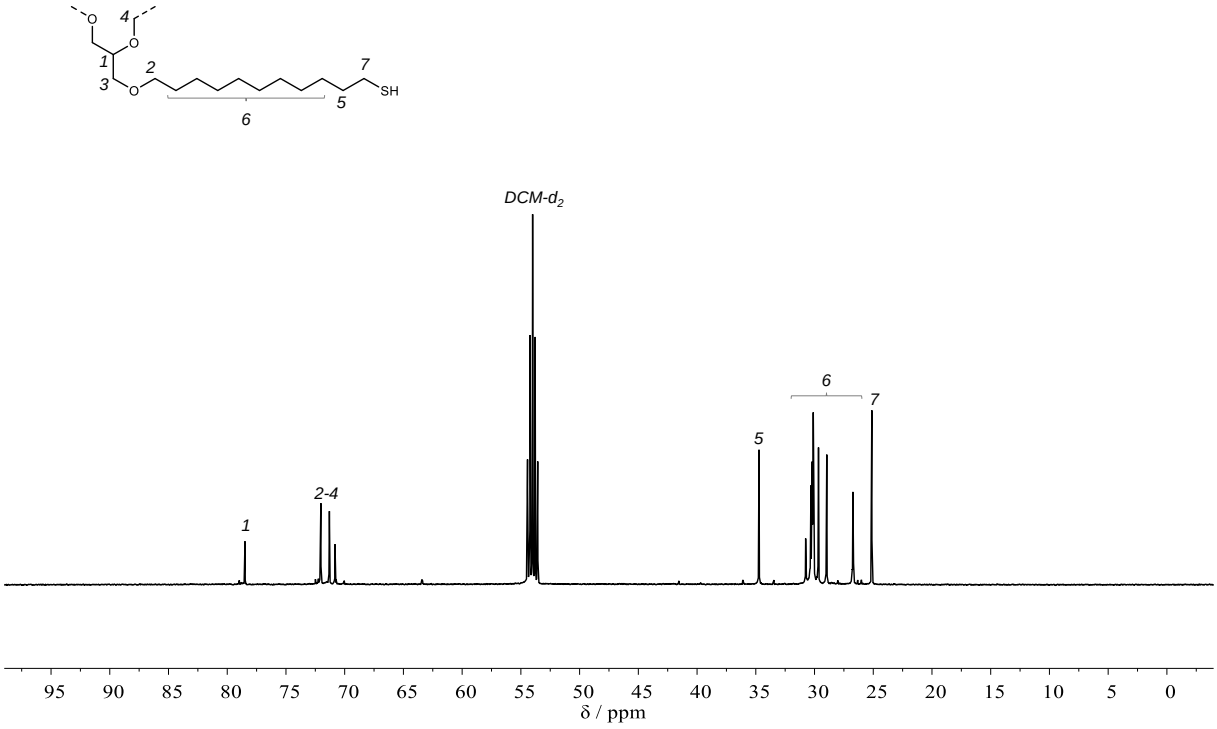

*Supplementary Figure 173: ^{13}C NMR spectrum of **10c** in CD_2Cl_2.*

Synthesis of thiol 11c from thioester 11b

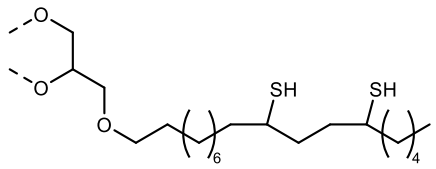

Synthesized from **11b** according to general procedure in 5.36 mmol scale (5.97 g **11b**). The product **11c** was obtained as a viscous, yellowish liquid in a yield of 95% (4.97 g, 5.11 mmol).

^{1}H NMR (400 MHz, Chloroform-*d*) δ/ppm = 3.69 – 3.37 (m, 11H), 3.17 – 2.68 (m, 3.70H), 1.71 – 1.41 (m, 16H), 1.40 – 1.20 (m, 59H), 0.95 – 0.83 (m, 9H).

^{13}C NMR (126 MHz, Methylene Chloride-d_2) δ/ppm = 78.49, 72.03, 71.30, 70.82, 41.83 – 41.38 (m), 39.84 (d, *J* = 2.7 Hz), 39.57 (d, *J* = 5.0 Hz), 37.11, 36.76, 32.69 – 32.42 (m), 32.34, 32.27 – 31.99 (m), 30.75, 30.50 – 29.84 (m), 29.69 – 29.51 (m), 27.88 – 27.51 (m), 27.44 – 27.27 (m), 26.83 – 26.40 (m), 23.34 – 23.01 (m), 14.69 – 14.24 (m).

IR (ATR platinum diamond) $\tilde{\nu}$/cm^{-1} = 2923 (vs), 2853 (s), 1462 (w), 1376 (w), 1370 (w), 1353 (vw), 1304 (w), 1261 (vw), 1242 (w), 1187 (vw), 1115 (m), 987 (vw), 969 (vw), 891 (vw), 868 (vw), 850 (vw), 722 (w).

ESI-HRMS: $[M+Na]^+$ calculated for $C_{57}H_{116}O_3S_5$ = 1031.7421, found 1031.7424.

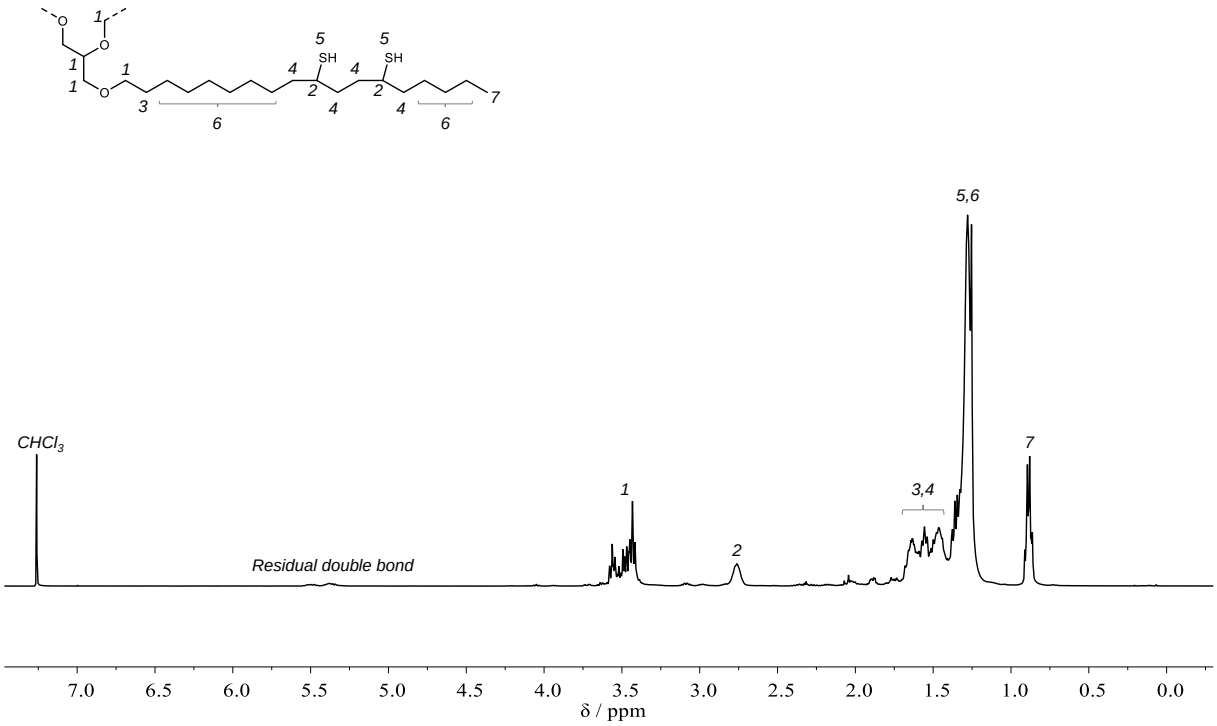

*Supplementary Figure 174: ^{1}H NMR spectrum of **11c** in $CDCl_3$.*

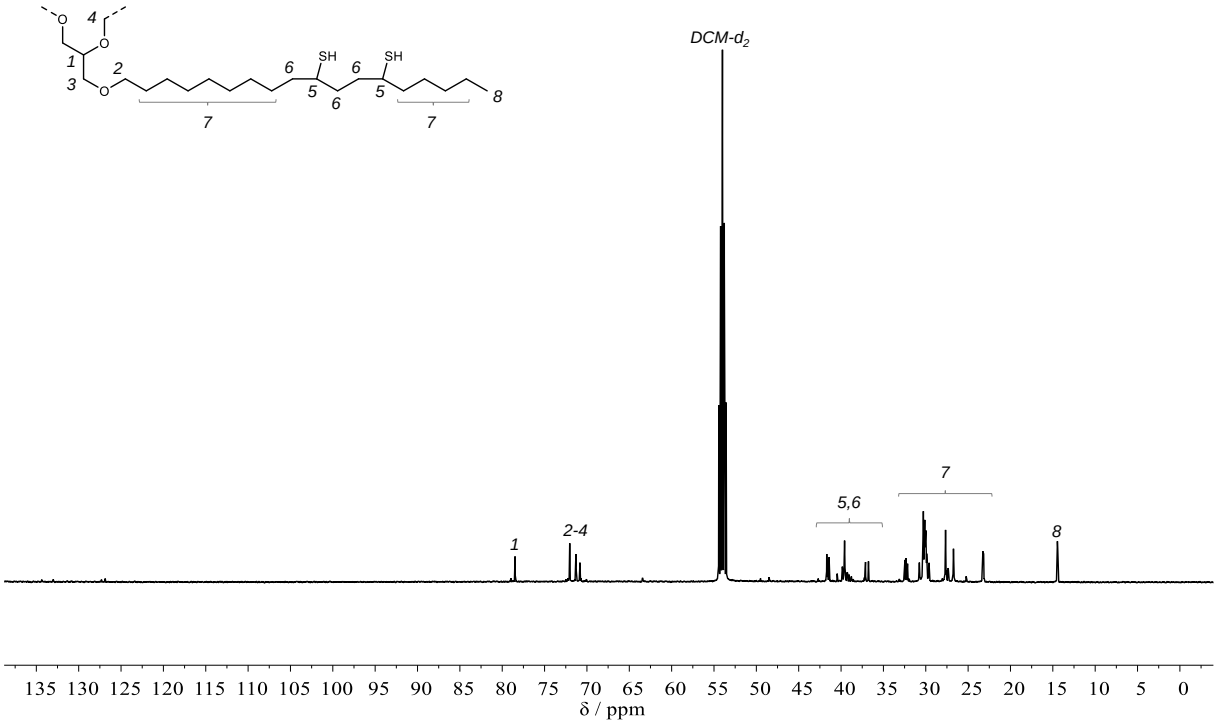

*Supplementary Figure 175: ^{13}C NMR spectrum of **11c** in CD_2Cl_2.*

6.3.3.6 Miscellaneous Syntheses

Synthesis of 1,4-diisocyanobutane (4IC)

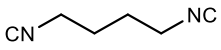

4IC was synthesized according to the procedure of Meier *et al*.[492] Putrescine (2.20 g, 25.0 mmol, 1.00 equiv.) was dissolved in ethyl formate (20.1 mL, 18,5 g, 250 mmol, 10.0 equiv.) and the mixture was refluxed overnight. Afterwards, the solvent was removed under reduced pressure. The residue was dissolved in 50 mL of DCM and pyridine (12.1 mL, 11.9 g, 150 mmol, 6.00 equiv.) was added. The mixture was placed inside a water bath and *p*-toluenesulfonyl chloride was added in small portions while stirring. After complete addition, the mixture was stirred at room temperature for 2 hours. Afterwards, 50 mL of saturated sodium carbonate solution were added and the mixture was stirred for another 30 minutes at room temperature. 100 mL each of water and DCM were added and the phases were separated. The aqueous phase was extracted 3 more times with 50 mL each of DCM. The combined extracts were washed three times with water and dried over sodium sulfate. The solvent was removed *in vacuo* and the crude product was purified *via* flash column chromatography (cyclohexane/ethyl acetate 10:1). The product was obtained as a yellow liquid in 55% yield (1.49 g, 13.7 mmol).

^{1}H NMR (400 MHz, Chloroform-*d*) δ/ppm 3.53 – 3.41 (m, 4H), 1.91 – 1.80 (m, 4H).

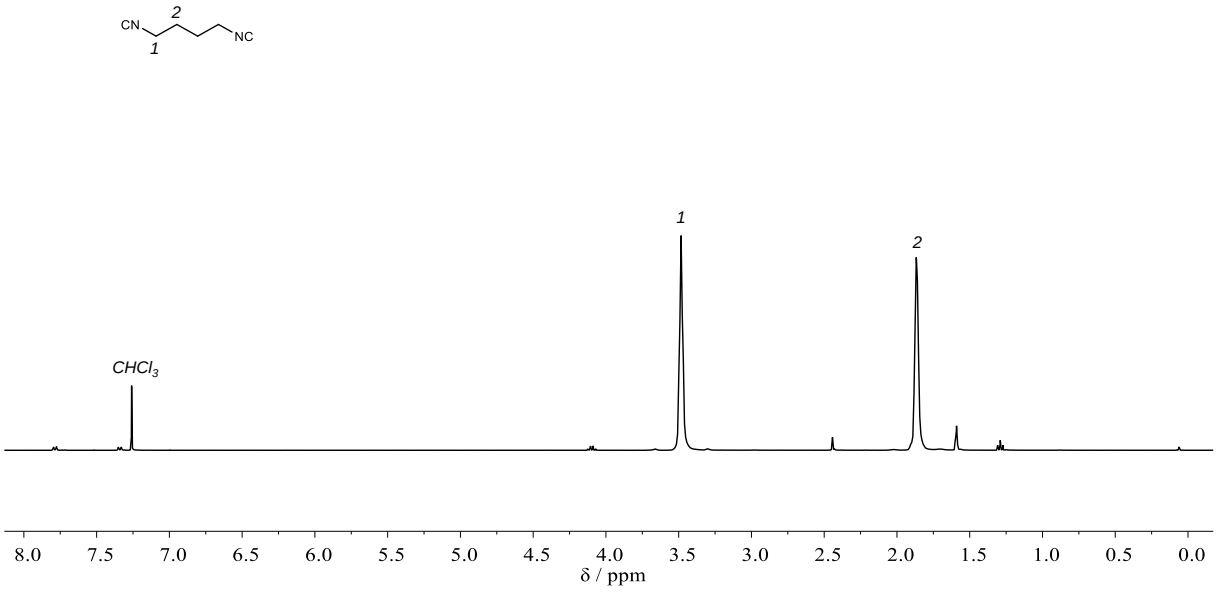

*Supplementary Figure 176: ^{1}H NMR spectrum of **4IC** in $CDCl_3$.*

Synthesis of 1,4-diisothiocyanatobutane (4ITC)

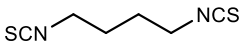

4ITC was synthesized according to a modified procedure of Meier *et al.*[266] **4IC** (1.45 g, 13.4 mmol, 1.00 equiv.) was dissolved in 27 mL of acetone and sulfur (963 mg, 3.75 mmol, 0.28 equiv.) and 1,8-diazabicycloundec-7-ene (400 µL, 408 mg, 2.68 mmol, 0.20 equiv.) were added. The mixture was refluxed for 4 hours. Afterwards, the solvent was removed under reduced pressure and the crude product was purified *via* column chromatography (cyclohexane / ethyl acetate 10:1). The product was obtained as an orange liquid in 65% yield (1.51 g, 8.77 mmol).

^{1}H NMR (400 MHz, Chloroform-*d*) δ/ppm = 3.66 – 3.54 (m, 4H), 1.91 – 1.76 (m, 4H).

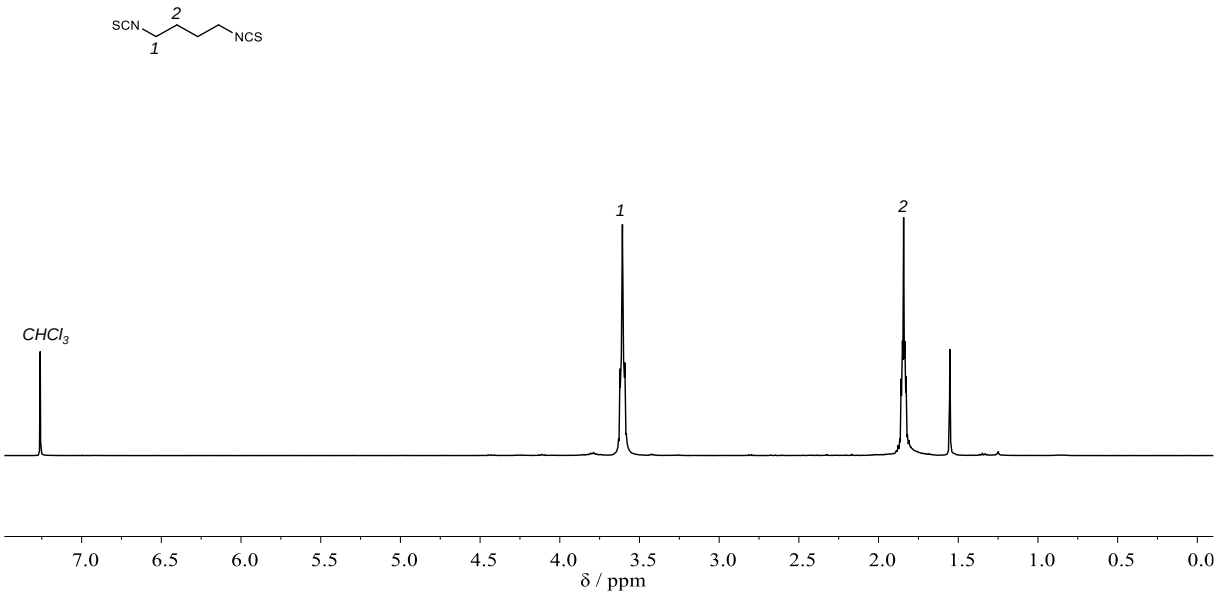

*Supplementary Figure 177: ^{1}H NMR spectrum of **4ITC** in $CDCl_3$.*

6.3.3.7 Synthesis of Polymer Networks

Determination of Thiol functionality

Thiol functionality was determined *via* quantitative ^{1}H NMR. Approx. 30 mg of thiol were mixed with approx. 500 µL of a stock solution of 1,3,5-trimethoxybenzene in $CDCl_3$ (0.0406 mmol TMB / g $CDCl_3$) and the weight of added stock solution was noted. Afterwards, an ^{1}H NMR spectrum was recorded (298 K, 128 scans, 2 s delay) and the integrals of the aromatic protons of TMB (6.13 to 6.03 ppm) and the thiol α-protons were evaluated. The integration ranges for thiol α-protons were selected as follows: 2.83 to 2.70 ppm for **9a**, 2.56 to 2.45 ppm for **10a**, 2.86 to 2.70 ppm for **11a**. The integral of the aromatic protons of TMB was normalized to 1 and thiol content was calculated with Equation 9. The results are listed in Table 14.

$$Thiol\ Ct.\left[\frac{mmol}{g}\right] = \frac{I(Thiol\ \alpha) \cdot m(TMB\ sln.) \cdot 0.0406\ \cdot 1000 \cdot f}{m(Thiol) \cdot f} \qquad (9)$$

f accounts for the proton ratio of the evaluated signals (3 for **9a** and **11a**, 1.5 for **10a**). The factor 1000 accounts for unit conversion.

Table 14: Quantification of thiol functionality via quantitative ^{1}H NMR.

Thiol	m(Thiol) / mg	m(TMB sln.)/mg	I(Thiol-α)	Thiol content / mmol g^{-1}
9c	30.9	673.7	1.127	**2.99**
10c	28.3	674.1	3.027	**4.46**
11c	35.1	650.9	1.555	**3.51**

Polymer Synthesis and Characterization

Synthetic Procedure A: Synthesis of polymer networks via thiol-ene reaction

The polythiol and the polyene component (octadiene or GTU) were mixed in equal stoichiometry (with respect to functional groups) and 1 mol% of DMPA was added. The mixture was vortexed until DMPA had completely dissolved. Afterwards, the mixture was cast into a mold and irradiated for 16 hours at a wavelength of 365 nm.

Synthetic Procedure B: Synthesis of dithiourethane polymer networks

The polythiol and the diisothiocyanate component (**4ITC**) were mixed in equal stoichiometry (with respect to functional groups) and 5 mol% of triethylamine were added. The mixture was vortexed and cast into a mold. The polymer was cured at 50 °C for 16 hours.

A list of all synthesized polymer networks is provided in Table 15.

Table 15: List of all synthesized polymer networks.

Entry	Thiol	Comonomer	Procedure	Material	Description
1	**9c**	**OD**	**A**	**9c**+OD	Sticky, light brown solid
2	**10c**	**OD**	**A**	**10c**+OD	Light brown solid
3	**9c**	**GTU**	**A**	**9c**+GTU	Light brown solid
4	**10c**	**GTU**	**A**	**10c**+GTU	Light brown solid
5	**11c**	**GTU**	**A**	**11c**+GTU	Light brown liquid
6	**9c**	**4ITC**	**B**	**9c**+4ITC	Yellow Solid
7	**10c**	**4ITC**	**B**	**10c**+4ITC	Yellow Solid
8	**11c**	**4ITC**	**B**	**11c**+4ITC	Yellow Solid

Gel fraction (THF):

Gel fraction (GF) was determined by submerging ~100 mg of material in 10 mL of THF for 24 hours. Afterwards, the remaining solids were filtered, dried under air for 24 hours and the weight of the residue was determined. Gel fractions of all materials are listed in Table 16. A gel fraction of >99% signifies no measurable weight loss.

Table 16: Gel fractions of all synthesized polymer networks.

Entry	Material	GF / %
1	**9c**+OD	61
2	**10c**+OD	>99
3	**9c**+GTU	98
4	**10c**+GTU	>99
5	**11c**+GTU	0
6	**9c**+4ITC	89
7	**10c**+4ITC	>99
8	**11c**+4ITC	>99

Infrared Spectroscopy (IR)

All materials were characterized using IR spectroscopy. The IR spectra are depicted in Supplementary Figure 178 to Supplementary Figure 185.

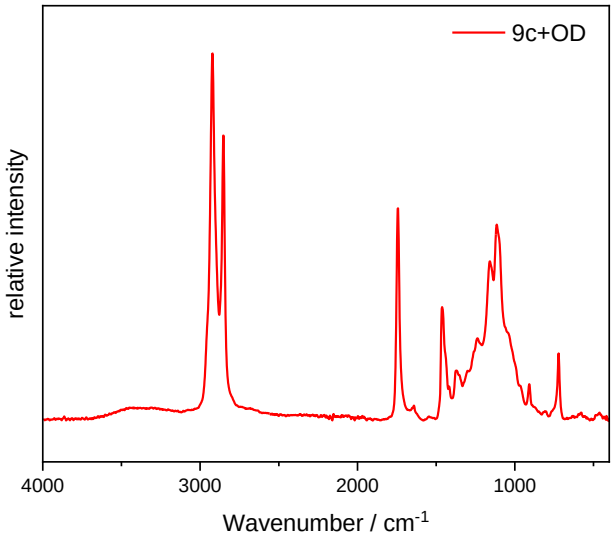

*Supplementary Figure 178: IR spectrum of material **9c+OD**.*

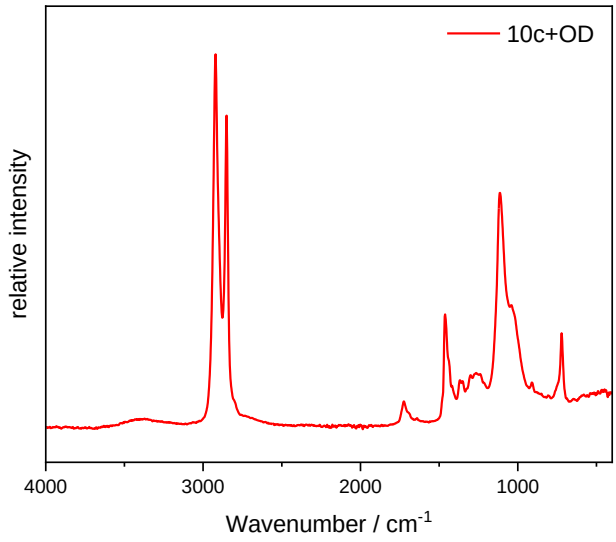

*Supplementary Figure 179: IR spectrum of material **10c+OD**.*

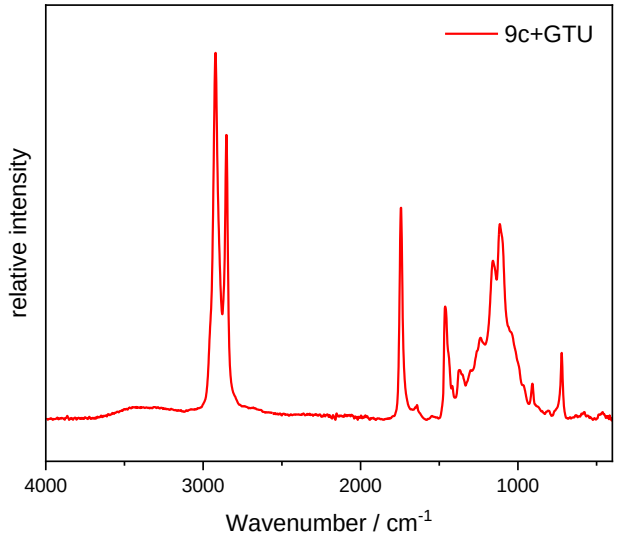

*Supplementary Figure 180: IR spectrum of material **9c+GTU**.*

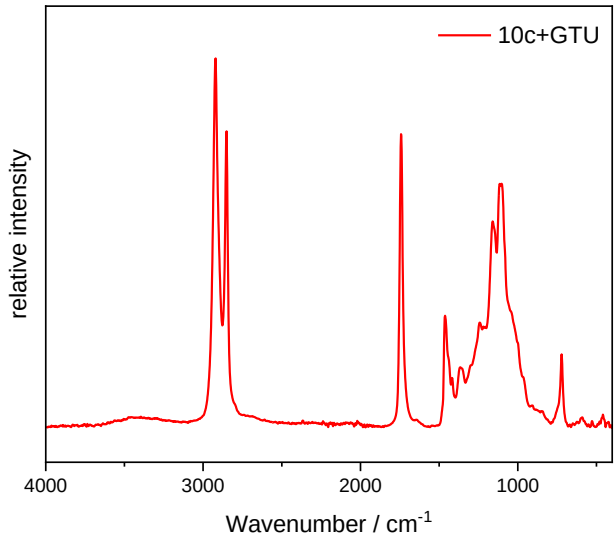

*Supplementary Figure 181: IR spectrum of material **10c+GTU**.*

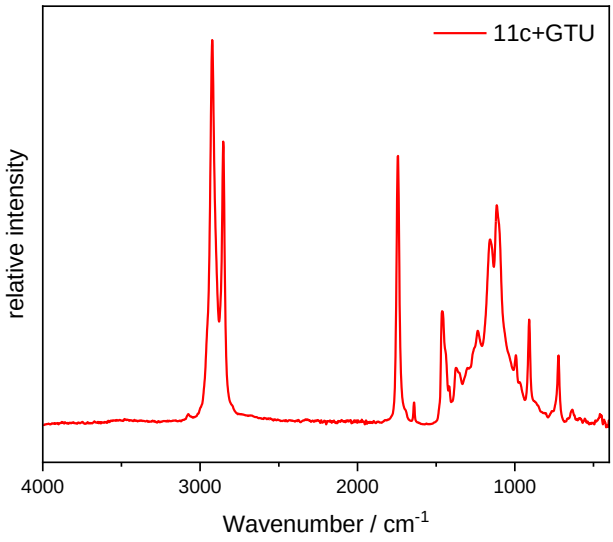

*Supplementary Figure 182: IR spectrum of material **11c+OD**.*

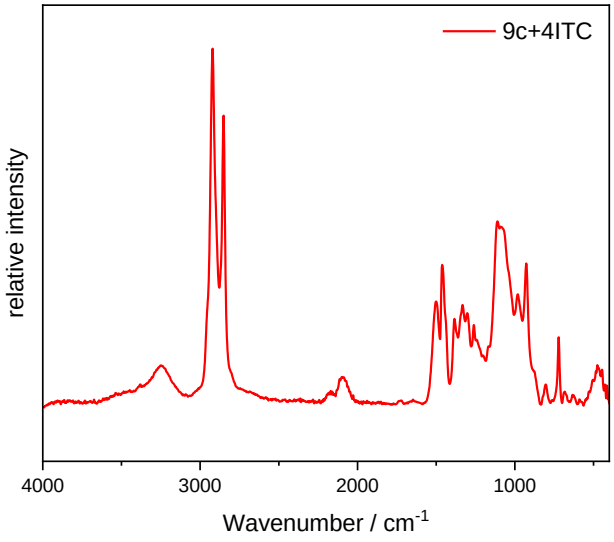

*Supplementary Figure 183: IR spectrum of material **9c+4ITC**.*

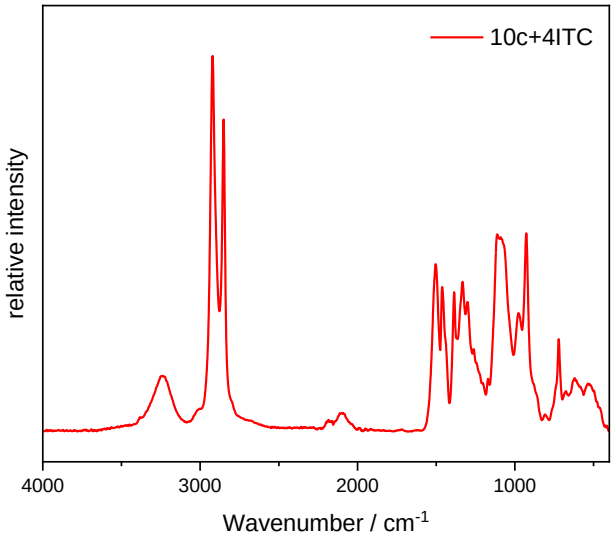

*Supplementary Figure 184: IR spectrum of material **10c+4ITC**.*

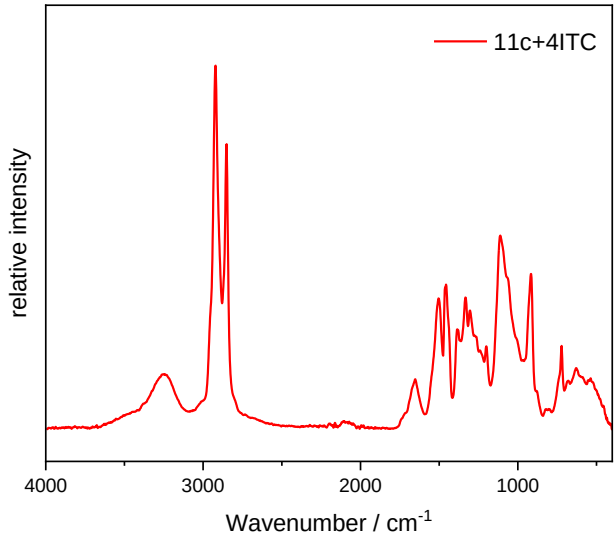

*Supplementary Figure 185: IR spectrum of material **11c+4ITC**.*

Differential Scanning Calorimetry (DSC)

All materials with a GF > 89% were characterized using DSC. The observed glass transition temperatures are listed in Table 17. The DSC traces are depicted in Supplementary Figure 186 - Supplementary Figure 191.

Table 17: Glass transition temperatures determined via DSC.

Entry	Material	T_g / °C
1	**10c**+OD	-9
2	**9c**+GTU	-36
3	**10c**+GTU	-8
4	**9c**+4ITC	-28
5	**10c**+4ITC	-11
6	**11c**+4ITC	1

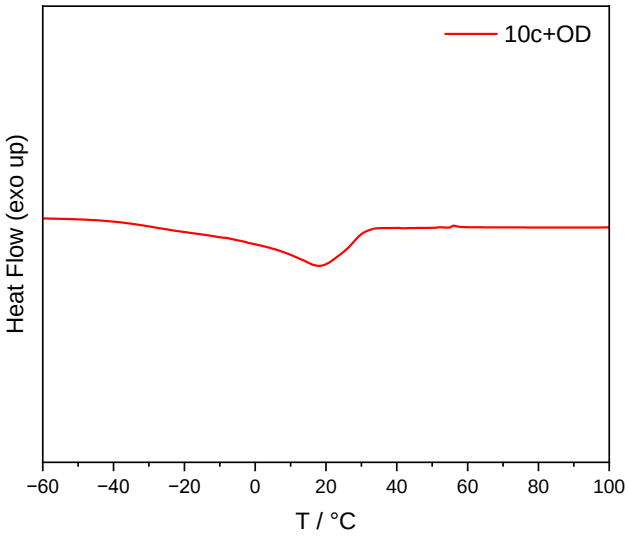

*Supplementary Figure 186: DSC trace of material **10c+OD**.*

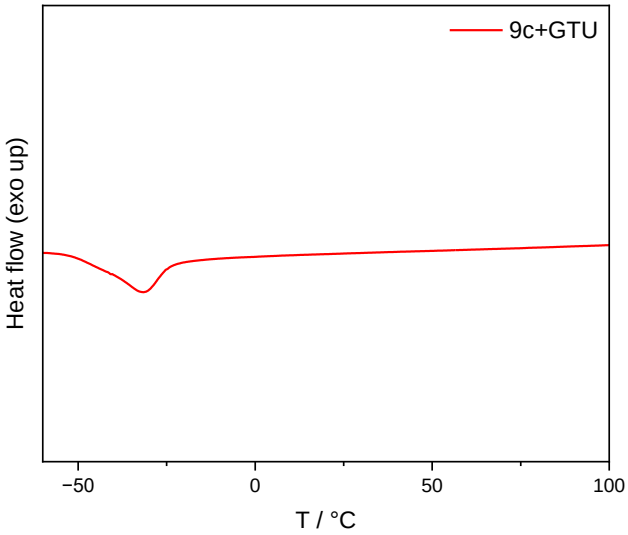

*Supplementary Figure 187: DSC trace of material **9c+GTU**.*

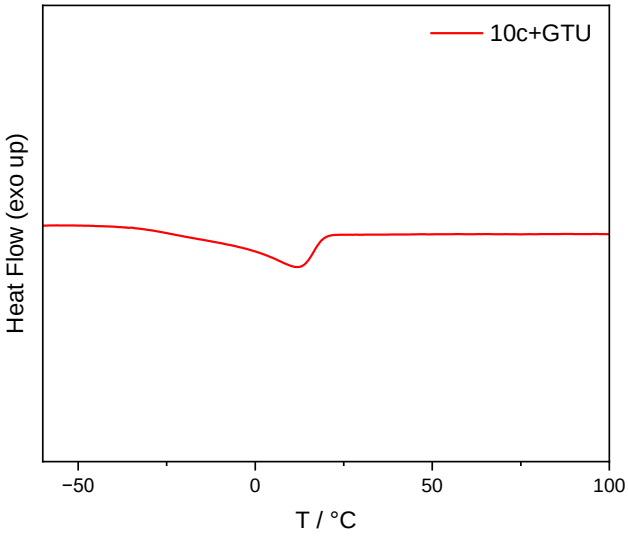

*Supplementary Figure 188: DSC trace of material **10c+GTU**.*

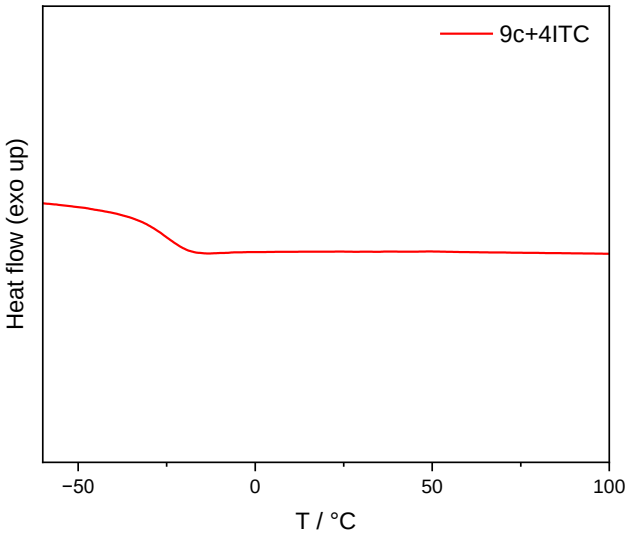

*Supplementary Figure 189: DSC trace of material **9c+4ITC**.*

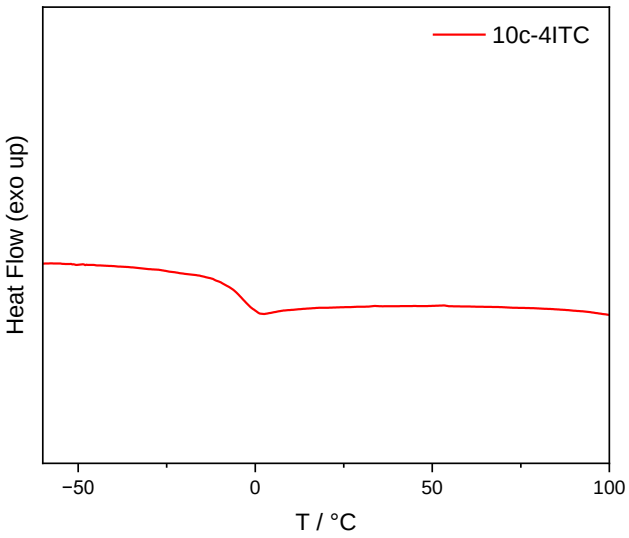

*Supplementary Figure 190: DSC trace of material **10c+4ITC**.*

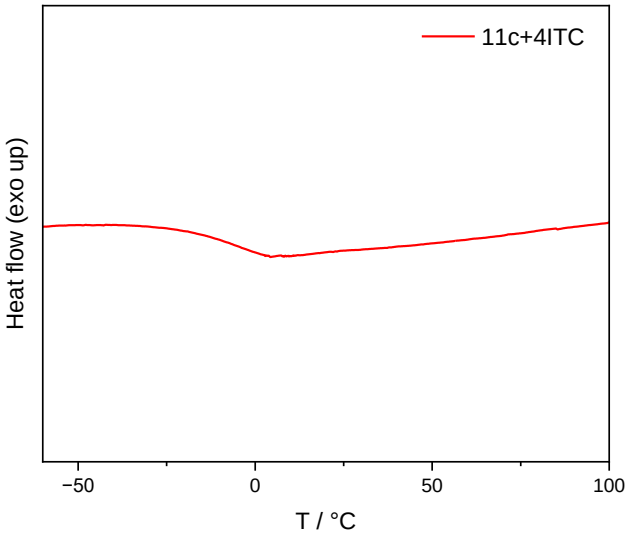

*Supplementary Figure 191: DSC trace of material **11c+4ITC**.*

Thermogravimetric analysis (TGA)

All materials with a GF > 89% were characterized using TGA. The observed decomposition temperatures ($T_{d.5\%}$) and residual weight percentages are listed in Table 7. The TGA traces are depicted in Supplementary Figure 192 - Supplementary Figure 197.

Table 18: Results of TGA analysis of all synthesized materials.

Entry	Material	$T_{d,5\%}$ / °C	Residue / %
1	**10c**+OD	356	1.8
2	**9c**+GTU	345	0.9
3	**10**+GTU	359	0.3
4	**9c**+4ITC	224	0.3
5	**10c**+4ITC	214	0.6
6	**44c**+4ITC	232	0.6

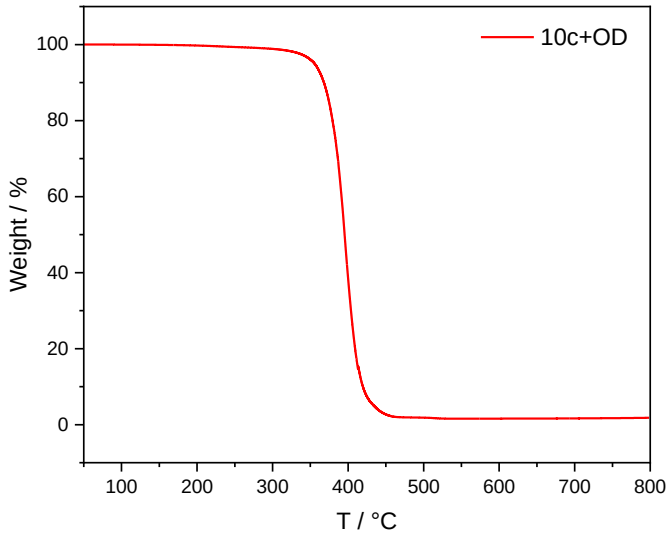

*Supplementary Figure 192: TGA curve of material **10c+OD**.*

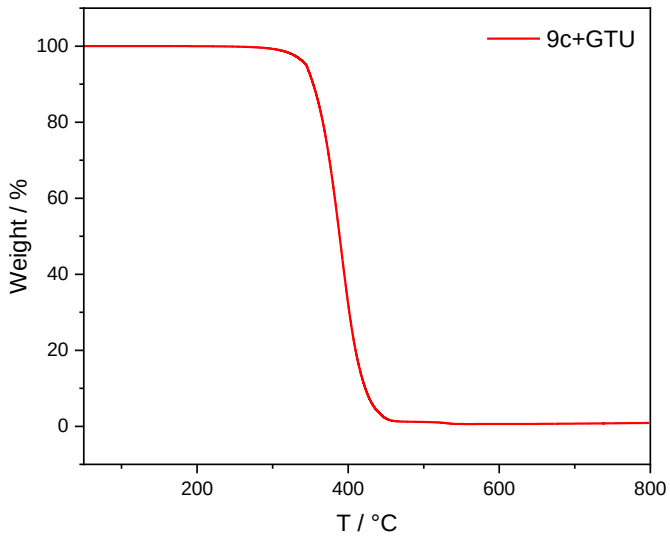

*Supplementary Figure 193: TGA curve of material **9c+GTU**.*

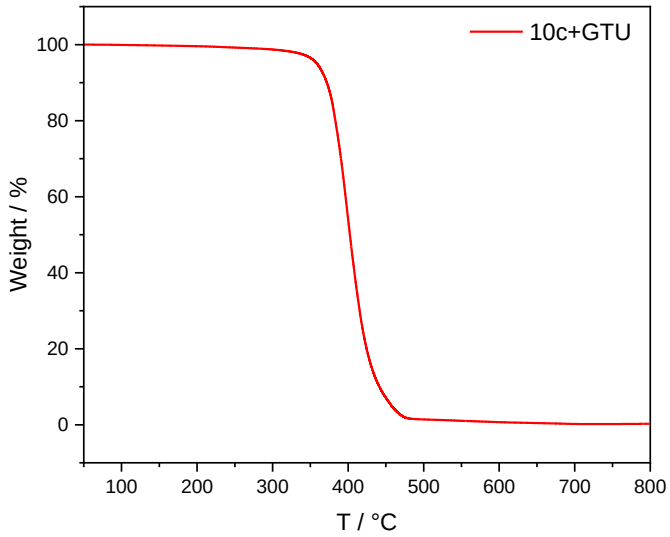

*Supplementary Figure 194: TGA curve of material **10c+GTU**.*

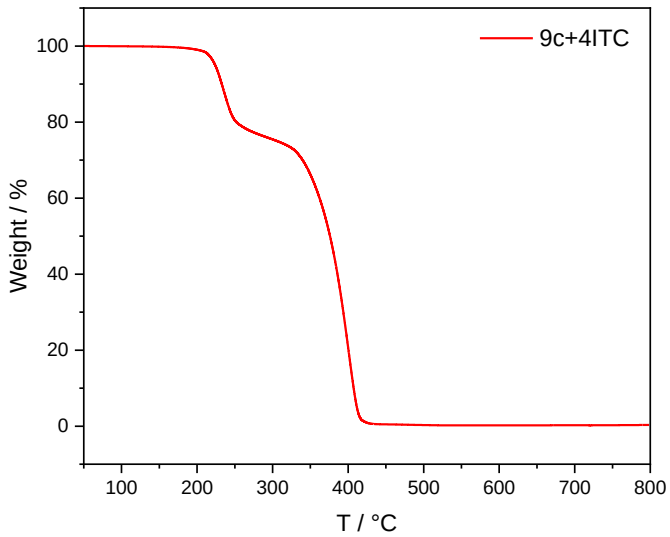

*Supplementary Figure 195: TGA curve of material **9c+4ITC**.*

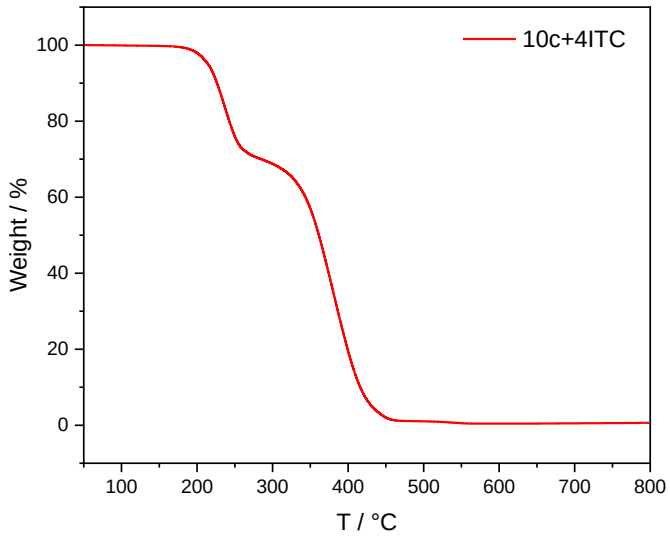

*Supplementary Figure 196: TGA curve of material **10c+4ITC**.*

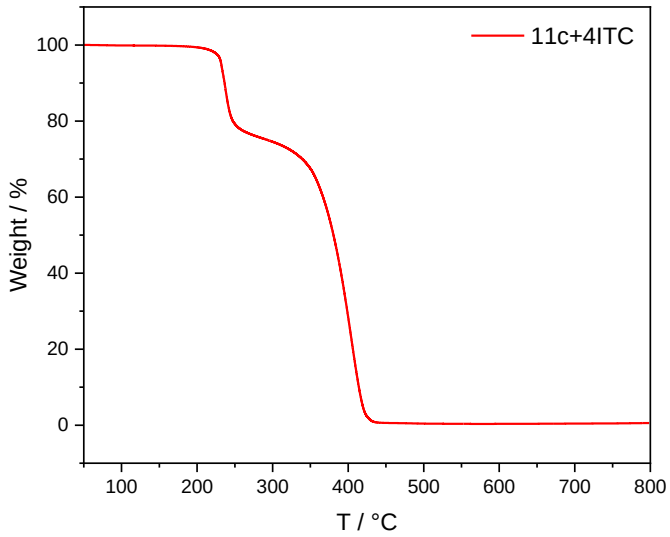

*Supplementary Figure 197: TGA curve of material **11c+4ITC**.*

Tensile Strength Measurements

Tensile strength measurements were performed for materials **9c+GTU**, **10+GTU**, **10c+4ITC** and **11c+4ITC**. For materials **10c+OD** and **9c+4ITC,** no suitable samples for measurements could be obtained. The measured Young's moduli, maximum stress and elongations at break are listed in Table 19. The stress-strain graphs are depicted in Supplementary Figure 198 - Supplementary Figure 201.

Table 19: Tensile strength measurements of all syntheized materials.

Entry	Material	E / MPa	σ_{max} / MPa	ε_{max} / %
1	**9c**+GTU	2.39±0.52	0.44±0.10	21.7±1.55
2	**10c**+GTU	9.41±0.98	1.36±0.23	18.7±1.00
3	**10c**+4ITC	7.51±0.59	1.84±0.22	35.8±2.39
4	**11c**+4ITC	7.04±0.39	1.83±0.15	31.6±0.17

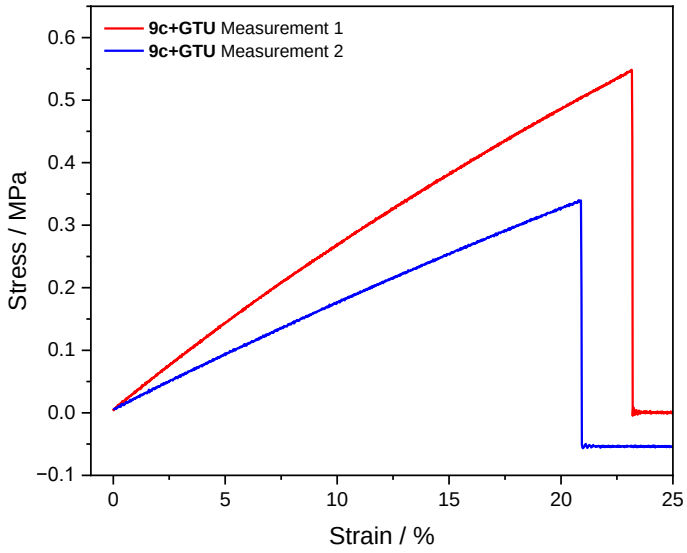

*Supplementary Figure 198: Stress-strain curves of material **9c+GTU**.*

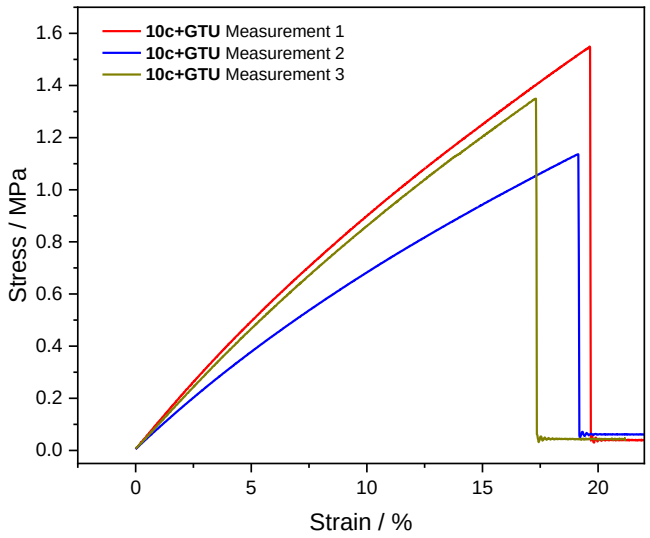

*Supplementary Figure 199: Stress-strain curves of material **10c+GTU**.*

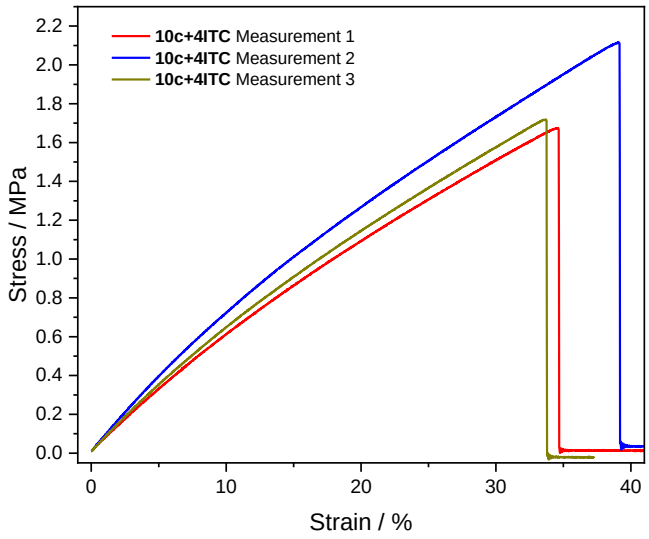

*Supplementary Figure 200: Stress-strain curves of material **10c+4ITC**.*

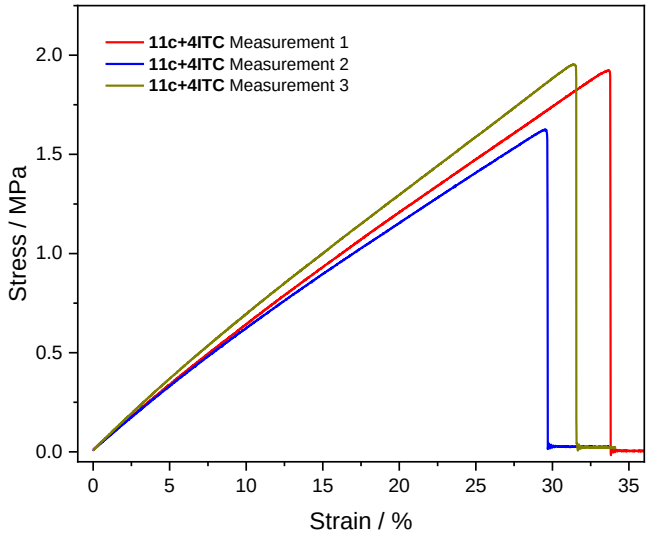

*Supplementary Figure 201: Stress-strain curves of material **11c+4ITC**.*

6.3.4 Bio-based Polythioamides – Chapter 4.4

6.3.4.1 Screening reactions of LA derivatives

Disclaimer

17 was synthesized by Sophia Abou el Mirate under supervision of the author.

The remaining syntheses were conducted by Maximilian L. Schmitt under co-supervision of the author.

General procedure for screening reactions using LA derivatives without internal standard:

The screening reactions described in chapter 4.4.2 (Scheme 72, Scheme 75, Scheme 76, Scheme 78, Scheme 80) were conducted according to the following procedure. In a crimp vial, 500 mg of LA derivative (**LA**, **13**, **17** or **18**, 1.00 equiv.) was mixed with amine (piperidine or benzylamine, 3.00 equiv for **LA**, 2.00 equiv for **13**, **17** and **18**) and elemental sulfur (2.00 equiv. S) was added (no sulfur was added in control experiments). The vial was closed and the mixture was stirred at 100 °C for 16 hours. Afterwards, a small amount of the crude reaction mixture was retrieved with a syringe and dissolved in 500 µL of the desired NMR solvent (DMSO-d_6 for **LA**, $CDCl_3$ for **13**, **17** or **18**).

General procedure for screening reactions using LA derivatives with internal standard:

The screening reactions described in chapter 4.4.2 that used TMB as the internal standard (Table 11, Table 12) were conducted according to the following procedure. In a crimp vial 500 mg of the LA derivative (**LA** or **13**) were mixed with the desired amount of piperidine, and, if necessary for the test reaction, the appropriate solvent or reagents. Afterwards, ~20 mg of TMB were added. After complete dissolution of TMB, a small amount of the mixture was retrieved for a t_0 NMR sample. Subsequently, the desired amount of sulfur was added, the vial was closed and heated to the desired temperature. A small amount of crude mixture for NMR analysis was retrieved after 2 hours and 16 hours.

Conversions were quantified by evaluating the integrals I(TMB) at 6.08 ppm. I(Acetyl) at 2.07 ppm for **LA** and at 2.21 for **13**. For assessment of side product formation (in the case of **LA**), I(side product) between 0.95 and 0.85 ppm was used. Notably, exact integration ranges cannot be given due to slightly irreproducible signal shifts and overlapping signals, hence integration was conducted manually. In the case of overlapping signals, the Line Fitting Tool

of the utilized version of MestReNova (Version 12.0.0) was used for integral determination *via* peal deconvolution.

Reactant conversions were determined using Equation 10. Side product formation was determined using Equation 11.

$$Conversion\ [\%] = \left(1 - \frac{I(Acetyl, sample)}{I(TMB, sample)} \cdot \frac{I(TMB, t0)}{I(Acetyl, t0)}\right) \cdot 100\% \qquad (10)$$

$$Side\ Products\ [\%] = \frac{I(side\ product) \cdot I(TMB, t0)}{I(Acetyl, t0) \cdot I(TMB, sample)} \cdot 100\% \qquad (11)$$

6.3.4.2 Synthetic Procedures

5-(1-piperidyl)-5-thioxopentanoic acid (12)

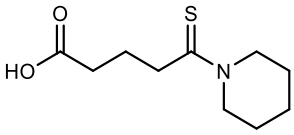

In a glass vial, levulinic acid (500 mg, 4.31 mmol. 1.00 equiv,) was mixed with piperidine (1.28 mL, 1.10 g, 12.92 mmol, 3.00 equiv.) and elemental sulfur (276 mg, 8.62 mmol S, 2.00 equiv. S) was added. The vial was sealed and the mixture was stirred at 100 °C for 16 hours. The product was isolated *via* column chromatography (*n*-hexane/ethyl acetate 1:1 with 5 vol% formic acid). **12** was obtained as an orange solid in a yield of 12% (113 mg, 0.523 mmol).

In a previous attempt under the same conditions, isolation of **12** was attempted as follows: The crude reaction mixture was diluted with 20 mL water and acidified with 1M HCl (pH < 4). The mixture was extracted twice with 20 mL each of DCM. The organic phase was dried and the solvent was removed *in vacuo*. Afterwards, the residue was dissolved in 20 mL of 1M NaOH and washed twice with DCM. The aqueous phase was acidified again with HCl and extracted twice with DCM. After drying over sodium sulfate and solvent removal under reduced pressure, an orange solid was obtained. The presence of methyl signals at 0.9 ppm in the ^{1}H NMR spectrum indicates contamination with the side product **15** (Supplementary Figure 204).

^{1}H NMR (400 MHz, DMSO-d_6) δ/ppm = 12.22 (s, 2H), 4.20 – 4.12 (m, 2H), 3.78 – 3.71 (m, 2H), 2.83 – 2.74 (m, 2H), 2.32 (t, J = 7.2 Hz, 2H), 1.86 – 1.73 (m, 2H), 1.69 – 1.50 (m, 6H).

^{13}C NMR (101 MHz, DMSO-d_6) δ/ppm = 200.33, 174.64, 51.05, 50.69, 42.53, 33.21, 27.10, 25.62, 24.23, 23.96.

IR (ATR platinum diamond) $\tilde{\nu}$/cm^{-1} = 3030 (w), 2993 (w), 2939 (m), 2925 (m), 2894 (m), 2871 (m), 2853 (m), 2758 (w), 2682 (w), 2674 (w), 2645 (w), 2604 (w), 2561 (w), 2536 (w), 2466 (w), 1693 (vs), 1635 (w), 1483 (s), 1462 (m), 1452 (m), 1434 (s), 1417 (m), 1403 (m), 1349 (m), 1343 (m), 1302 (w), 1275 (s), 1255 (s), 1238 (vs), 1203 (vs), 1164 (m), 1148 (m), 1129 (m), 1094 (w), 1065 (m), 1047 (m), 1024 (w), 1002 (s), 938 (s), 901 (m), 872 (m), 852 (m), 817 (w), 775 (w), 749 (w), 695 (m), 652 (w), 453 (w), 420 (m).

ESI-HRMS m/z: $[M-H]^-$ calculated for $C_{10}H_{16}NO_2S$ = 214.0907, found 214.0899.

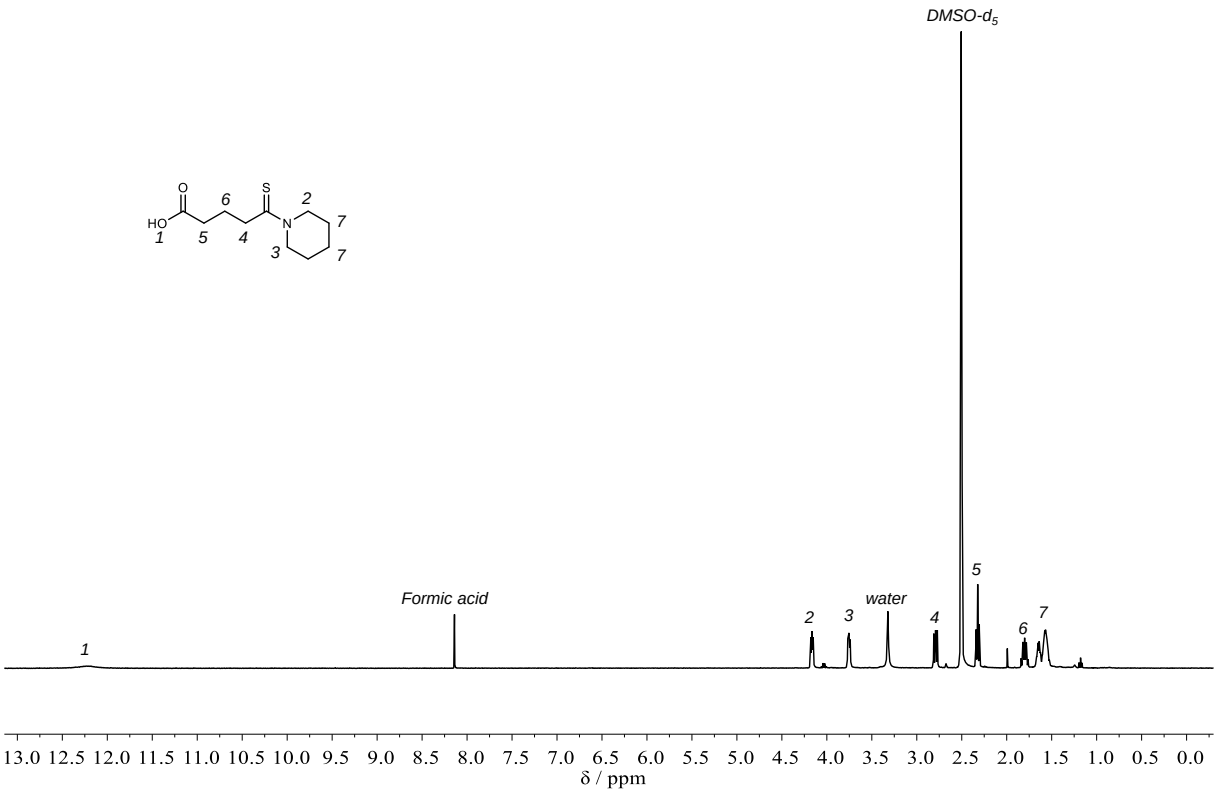

*Supplementary Figure 202: ^{1}H NMR spectrum of **12** in DMSO-d_6.*

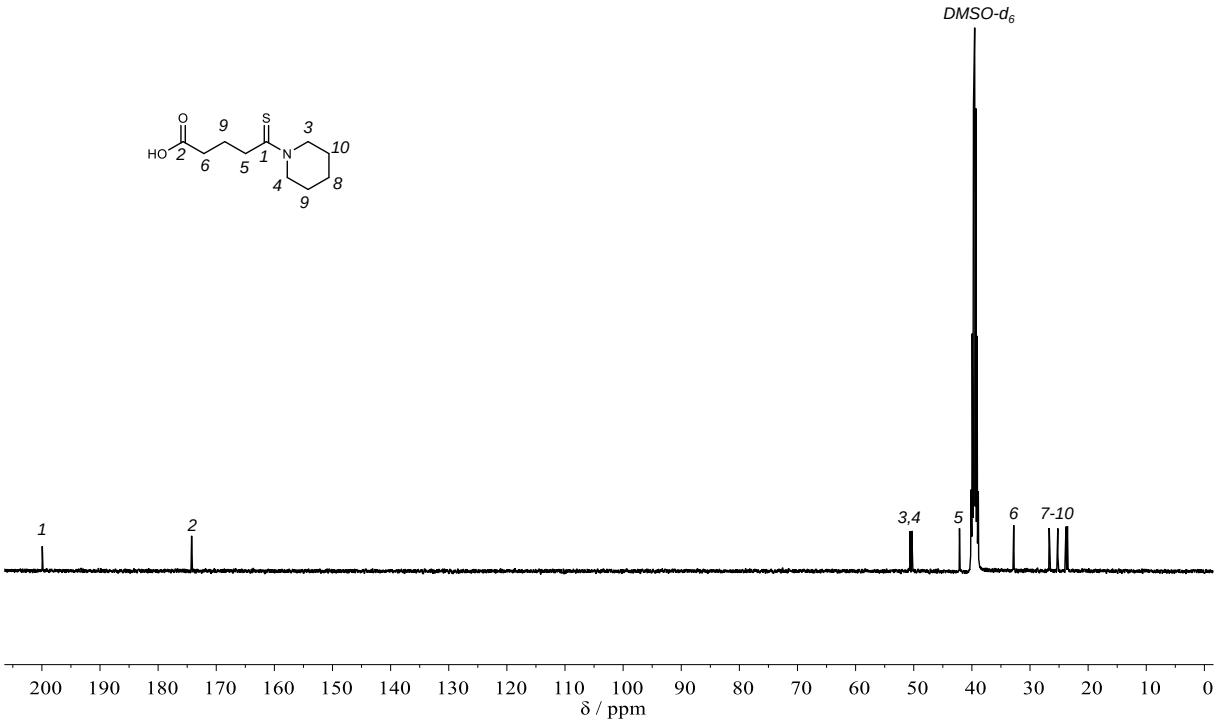

*Supplementary Figure 203: ^{13}C NMR spectrum of **12** in DMSO-d_6.*

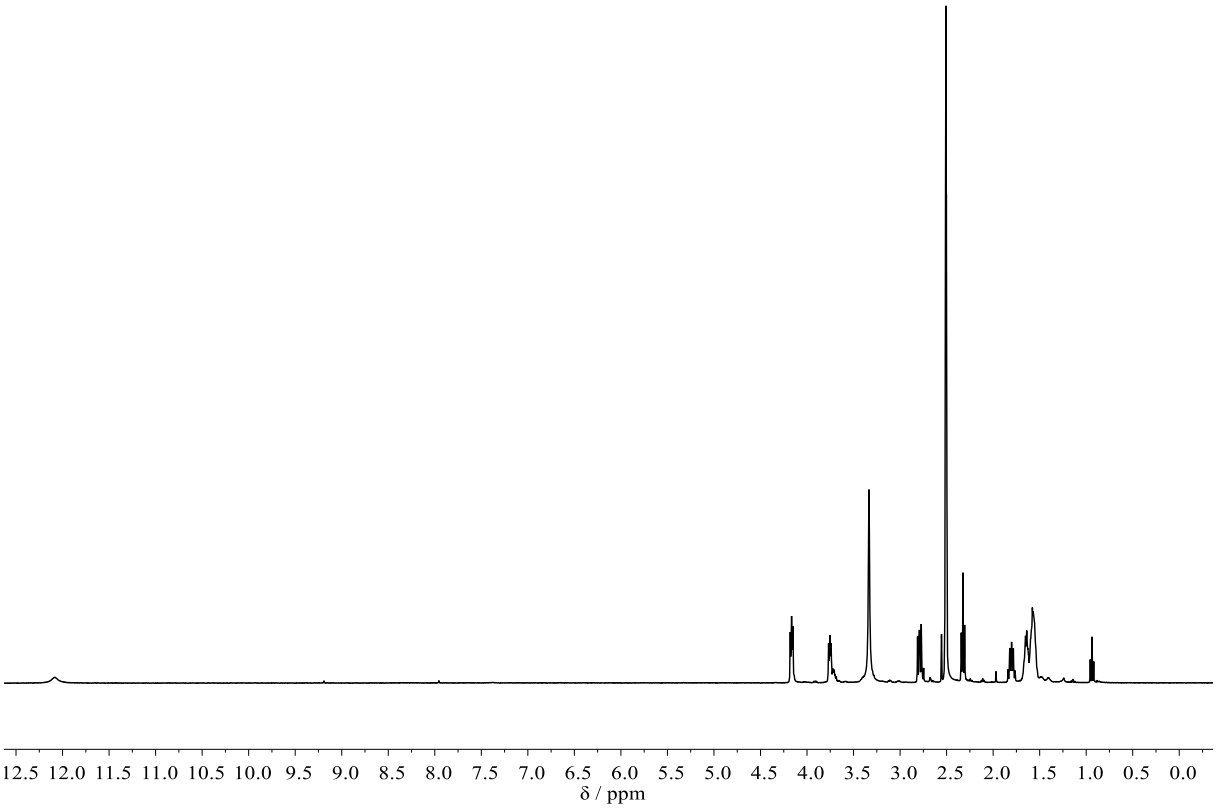

*Supplementary Figure 204: ^{1}H NMR spectrum of **12** in DMSO-d_6, obtained via extraction. The triplet at 0.95 ppm indicated contamination with side product **15**.*

Methyl levulinate (17)

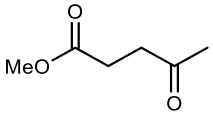

Levulinic acid (10.0 g, 86.1 mmol, 1.00 equiv.) was dissolved in methanol (34.5 mL, 27.6 g, 861 mmol, 10.0 equiv.) and sulfuric acid (459 µL, 845 mg, 8.61 mmol, 0.10 equiv.) was added. The mixture was stirred at 65 °C for 16 hours. Afterwards, the crude mixture was concentrated under reduced pressure and added to 50 mL of saturated $NaHCO_3$ solution. The aqueous phase was extracted 3 times with 50 mL each of EtOAc. The organic phase was dried over sodium sulfate and the solvent was removed *in vacuo*. **17** was obtained as a colorless liquid in a yield of 93% (10.4 g, 79.8 mmol).

^{1}H NMR (400 MHz, Chloroform-*d*) δ/ppm = 3.66 (s, 3H), 2.74 (t, *J* = 6.5 Hz, 2H), 2.57 (t, *J* = 6.5 Hz, 3H), 2.18 (s, 3H).

^{13}C NMR (101 MHz, Chloroform-*d*) δ/ppm = 206.64, 173.21, 51.78, 37.93, 29.84, 27.72.

IR (ATR platinum diamond) $\tilde{\nu}$/cm^{-1}= 3001 (vw), 2956 (vw), 2921 (vw), 1734 (s), 1715 (vs), 1438 (w), 1409 (w), 1360 (m), 1314 (w), 1263 (w), 1209 (m), 1179 (m), 1156 (vs), 1070 (w), 1031 (w), 1000 (w), 969 (w), 895 (vw), 847 (vw), 810 (vw), 765 (vw), 660 (vw), 615 (vw), 572 (w), 533 (vw), 475 (w), 434 (vw), 424 (vw).

ESI-HRMS m/z: $[M+Na]^+$ calculated for $C_6H_{10}NaO_3$ = 153.0528, found 153.0521.

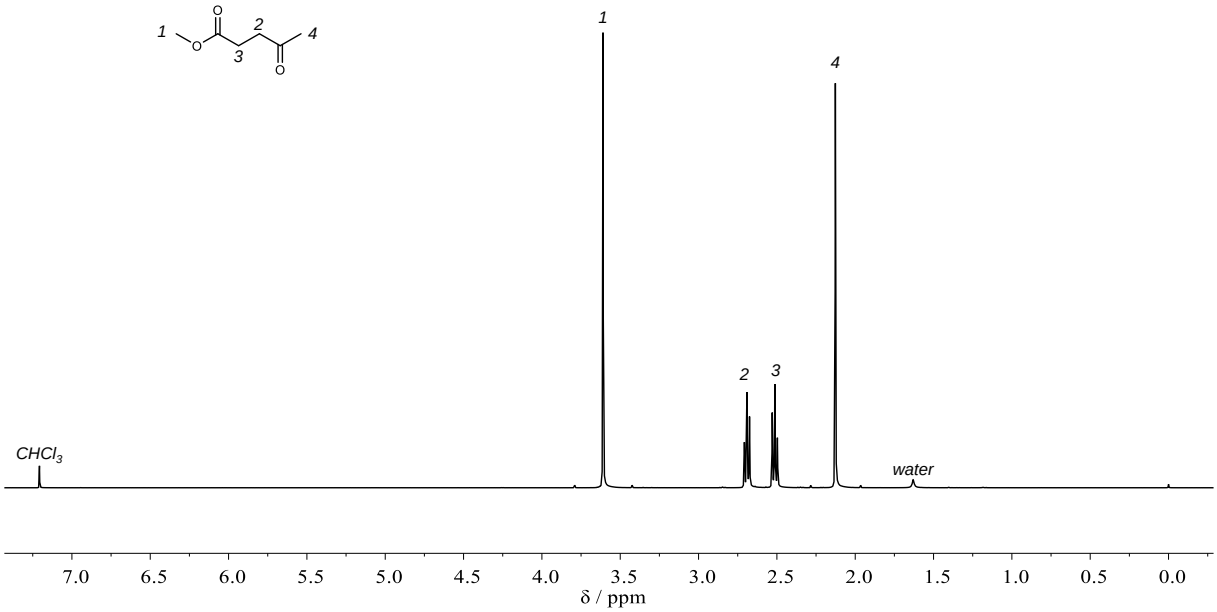

*Supplementary Figure 205: ^{1}H NMR spectrum of **17** in $CDCl_3$.*

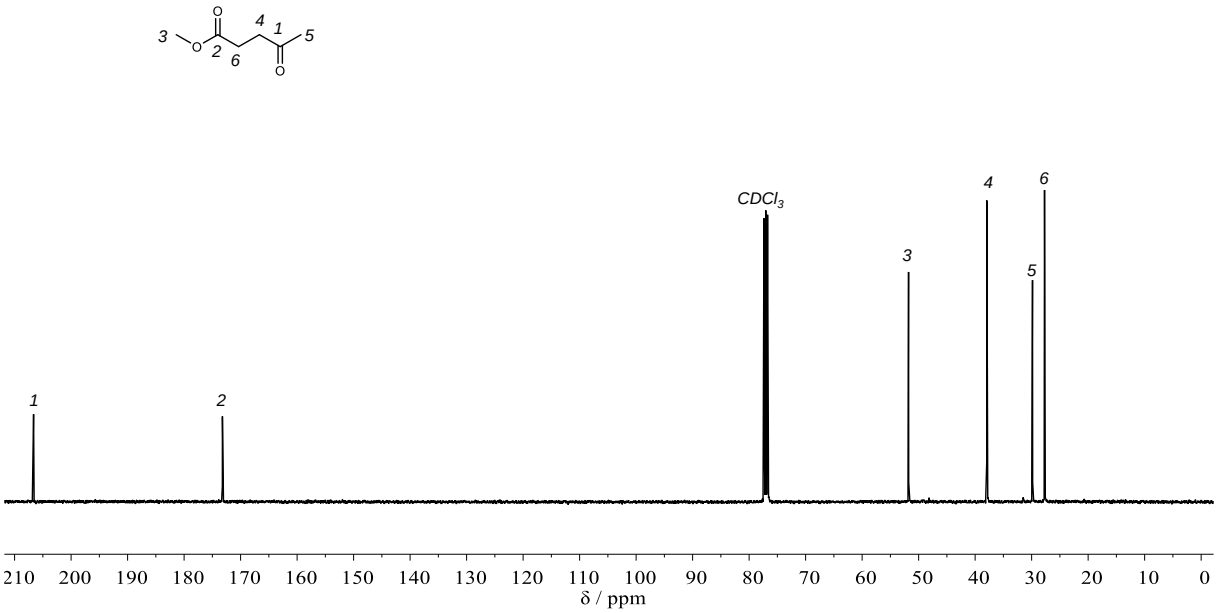

*Supplementary Figure 206: ^{13}C NMR spectrum of **17** in $CDCl_3$.*

***N*-levulinoylpiperidine (13)**

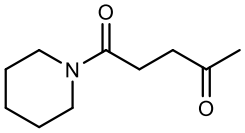

Method A: 10.0 g **13** (76.8 mmol, 1.00 equiv.) were mixed with piperidine (22.8 mL, 19.6 g, 231 mmol, 3.00 equiv.) and the mixture was stirred for 84 hours at 80 °C. Afterwards, the mixture was cooled and diluted with 100 mL of water. The aqueous phase was acidified (pH = 4) and extracted 5 times with 100 mL each of Et_2O. The organic phase was dried over sodium sulfate and the solvent was removed *in vacuo*. **13** was obtained as a yellowish liquid in a yield of 33% (4.63 g, 25.3 mmol).

Method B: α-Angelica lactone (4.58 mL, 5.00 g, 51.0 mmol, 1.00 equiv.) was mixed with piperidine (5.10 mL, 4.38 g, 51.5 mmol, 1.01 equiv.) and the mixture was stirred at room temperature for 2 hours, then heated to 100 °C for 10 minutes. Afterwards, the mixture was dried under reduced pressure. **13** was obtained as a yellowish liquid in a yield of 99% (9.26 g, 50.5 mmol).

^{1}H NMR (400 MHz, Chloroform-*d*) δ/ppm = 3.47 (d, *J* = 38.8 Hz, 4H), 2.76 (t, *J* = 6.4 Hz, 4H), 2.59 (t, *J* = 6.4 Hz, 4H), 2.22 (s, 3H), 1.70 – 1.42 (m, 6H).

^{13}C NMR (101 MHz, Chloroform-*d*) δ/ppm = 208.14, 169.67, 46.36, 42.81, 38.06, 30.16, 27.01, 26.26, 25.46, 24.46.

IR (ATR platinum diamond) $\tilde{\nu}/cm^{-1}$ = 3501 (w), 3486 (w), 3472 (w), 3419 (vw), 3345 (vw), 3336 (vw), 3318 (vw), 3297 (vw), 3289 (vw), 3283 (vw), 3271 (vw), 3260 (vw), 3001 (vw), 2933 (w), 2857 (w), 1757 (vw), 1711 (m), 1621 (vs), 1442 (s), 1366 (m), 1279 (w), 1251 (m), 1220 (m), 1164 (m), 1137 (m), 1125 (w), 1063 (vw), 1014 (m), 987 (vw), 954 (vw), 942 (vw), 895 (vw), 854 (w), 767 (vw), 627 (vw), 564 (w), 537 (w), 494 (w), 471 (vw), 440 (vw), 415 (vw).

ESI-HRMS m/z: $[M+H]^+$ calculated for $C_{10}H_{18}NO_2$ = 184.1338, found 184.1327.

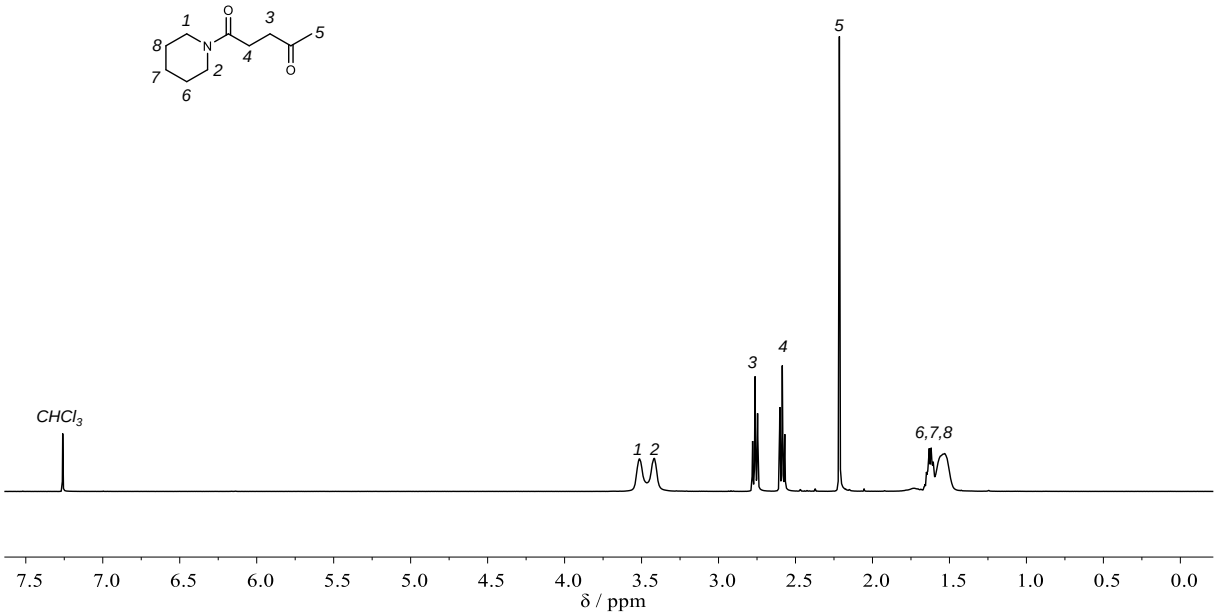

*Supplementary Figure 207: ^{1}H NMR spectrum of **13** in $CDCl_3$.*

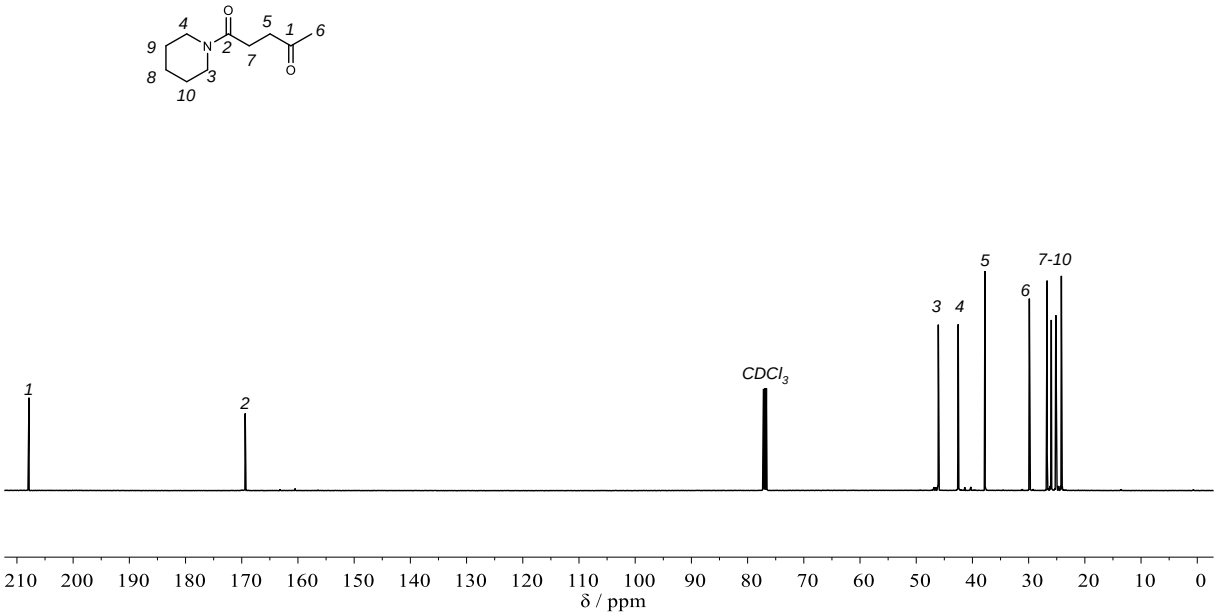

*Supplementary Figure 208: ^{13}C NMR spectrum of **13** in $CDCl_3$.*

Monothioglutarpiperide (14)

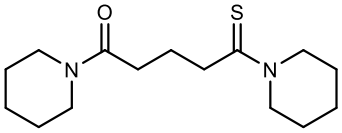

500 mg **13** (2.73 mmol, 1.00 equiv.) and 540 µL piperidine (465 mg, 5.46 mmol, 2.00 equiv.) were mixed in a glass vial and elemental sulfur (350 mg, 10.9 mmol S, 4.00 equiv. S) was added. The mixture was stirred at 100 °C for 18 hours. Afterwards, the crude mixture was diluted with 5 mL of water and acidified with 1M HCl (pH < 4). The aqueous phase was extracted 3 times with 20 mL each of Et_2O. The organic phase was dried over sodium sulfate and the solvent was removed *in vacuo*. **14** was obtained as an orange solid in a yield of 74% (573 mg, 2.03 mmol).

^{1}H NMR (400 MHz, Chloroform-*d*) δ/ppm = 4.29 – 4.19 (m, 2H), 3.88 – 3.77 (m, 2H), 3.58 – 3.49 (m, 2H), 3.44 – 3.33 (m, 2H), 3.01 – 2.88 (m, 2H), 2.44 (t, *J* = 6.7 Hz, 2H), 2.08 – 1.92 (m, 2H), 1.77 – 1.44 (m, 12H).

^{13}C NMR (101 MHz, Chloroform-*d*) δ/ppm = 201.50, 170.61, 51.69, 51.21, 46.63, 44.23, 42.85, 32.37, 27.20, 26.57, 25.73, 25.56, 24.67, 24.28, 24.25.

IR (ATR platinum diamond) $\tilde{\nu}/cm^{-1}$= 3009 (vw), 2987 (vw), 2933 (m), 2855 (m), 2666 (vw), 1718 (vw), 1635 (vs), 1495 (s), 1483 (m), 1465 (m), 1438 (vs), 1364 (w), 1351 (w), 1323 (vw), 1284 (m), 1255 (s), 1240 (s), 1207 (s), 1175 (w), 1162 (w), 1137 (m), 1121 (m), 1092 (w), 1068 (w), 1053 (w), 1026 (w), 996 (s), 952 (w), 907 (vw), 893 (w), 852 (m), 819 (m), 771 (vw), 753 (vw), 710 (vw), 636 (vw), 611 (w), 584 (vw), 570 (vw), 535 (vw), 487 (w), 461 (vw), 440 (vw), 411 (w).

ESI-HRMS m/z: $[M+H]^+$ calculated for $C_{15}H_{27}N_2OS$= 283.1844, found 283.1828.

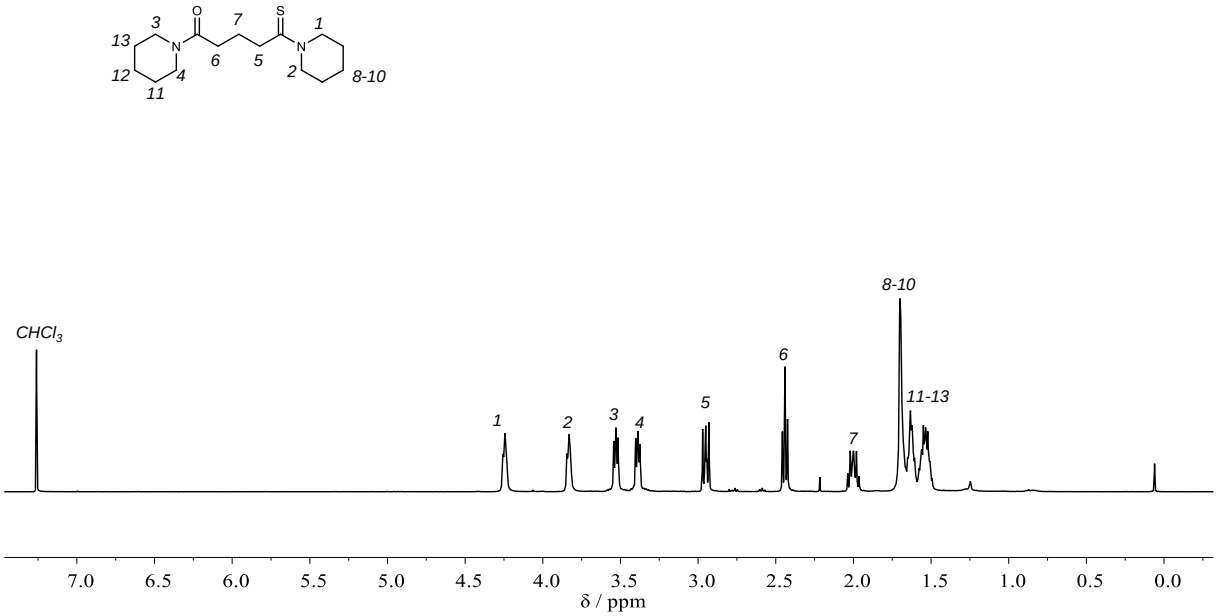

*Supplementary Figure 209: ^{1}H NMR spectrum of **14** in $CDCl_3$.*

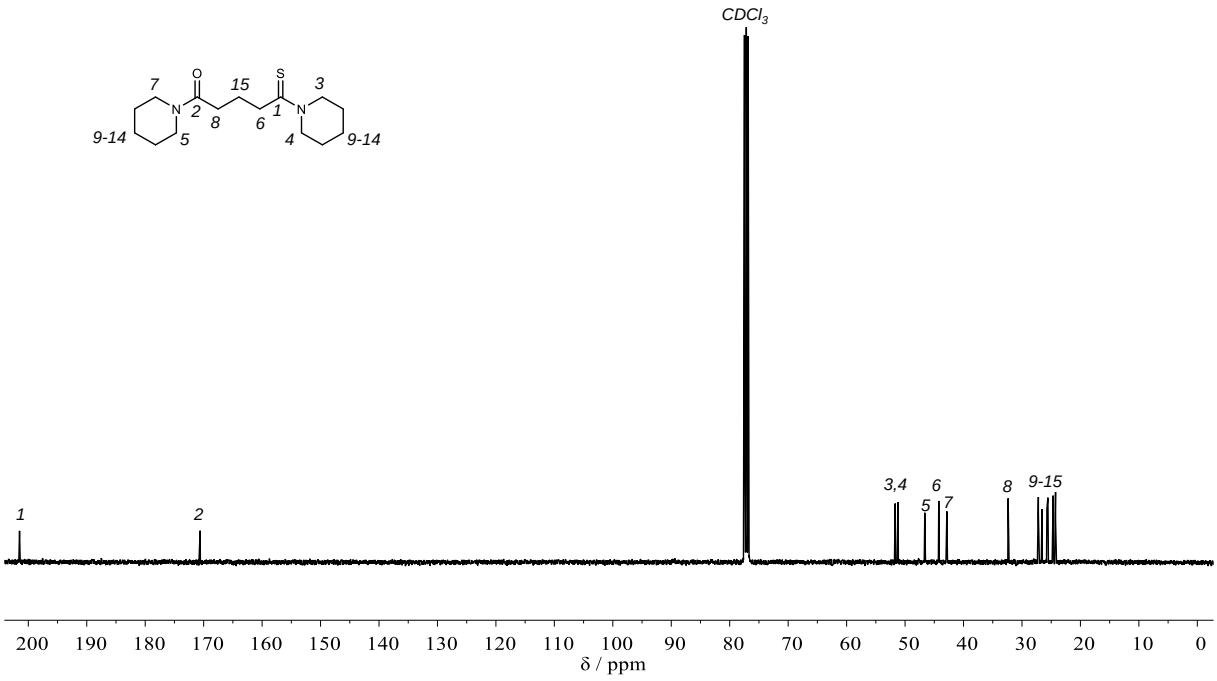

*Supplementary Figure 210: ^{13}C NMR spectrum of **14** in $CDCl_3$.*

***N*-Benzyllevulinamide (18)**

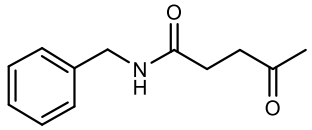

α-Angelica lactone (455 µL, 500 mg, 5.10 mmol, 1.00 equiv.) was dissolved in 4 mL of Et_2O and the solution was placed in an ice bath. Afterwards, a solution of benzylamine (611 µL, 601 mg, 5.61 mmol, 1.10 equiv.) was added dropwise and the mixture was stirred at 0 °C for 30 minutes. The precipitate was filtered, washed with Et_2O and dried under reduced pressure. **18** was obtained as a white solid in a yield of 99% (9.26 g, 50.5 mmol). The product partially decomposed during storage at room temperature. Hence, the recorded ^{13}C NMR spectrum is contaminated.

In an earlier synthesis attempt of **18**, α-angelica lactone (455 µL, 500 mg, 5.10 mmol, 1.00 equiv.) was mixed with benzylamine (611 µL, 601 mg, 5.61 mmol, 1.10 equiv.) and the mixture was heated to 100 °C for 2 hours. ^1H NMR of the resulting product (Supplementary Figure 213) mixture indicated decomposition of the product, as described in chapter 4.4.2.2.

^{1}H NMR (400 MHz, Chloroform-*d*) δ/ppm = 7.41 – 7.21 (m, 5H), 5.91 (d, *J* = 15.6 Hz, 1H), 4.45 (d, *J* = 5.7 Hz, 2H), 2.87 (t, *J* = 6.4 Hz, 2H), 2.49 (t, *J* = 6.5 Hz, 2H), 2.22 (s, 3H).

^{13}C NMR (101 MHz, Chloroform-*d*) δ/ppm = 207.94, 171.88, 138.34, 128.82, 127.84, 127.59, 43.79, 38.68, 30.05, 30.03.

IR (ATR platinum diamond) $\tilde{\nu}/cm^{-1}$ = 3499 (vw), 3452 (vw), 3392 (vw), 3373 (vw), 3308 (m), 3141 (vw), 3127 (vw), 3106 (vw), 3085 (vw), 3063 (w), 3048 (vw), 3034 (w), 2972 (vw), 2929 (w), 2913 (w), 2882 (vw), 2874 (vw), 2839 (vw), 2810 (vw), 1757 (vw), 1699 (m), 1637 (s), 1586 (w), 1549 (m), 1493 (m), 1454 (m), 1436 (m), 1409 (m), 1388 (m), 1370 (m), 1353 (m), 1302 (w), 1257 (m), 1234 (m), 1195 (m), 1162 (s), 1103 (w), 1082 (w), 1045 (w), 1026 (m), 1002 (w), 987 (w), 942 (w), 926 (w), 901 (w), 884 (vw), 827 (vw), 817 (vw), 800 (vw), 788 (vw), 755 (m), 730 (s), 712 (s), 697 (vs), 623 (w), 590 (m), 555 (m), 514 (m), 455 (m), 409 (w).

ESI-HRMS m/z: $[M+Na]^+$ calculated for $C_{12}H_{15}NNaO_2$ = 228.1000, found 228.0998.

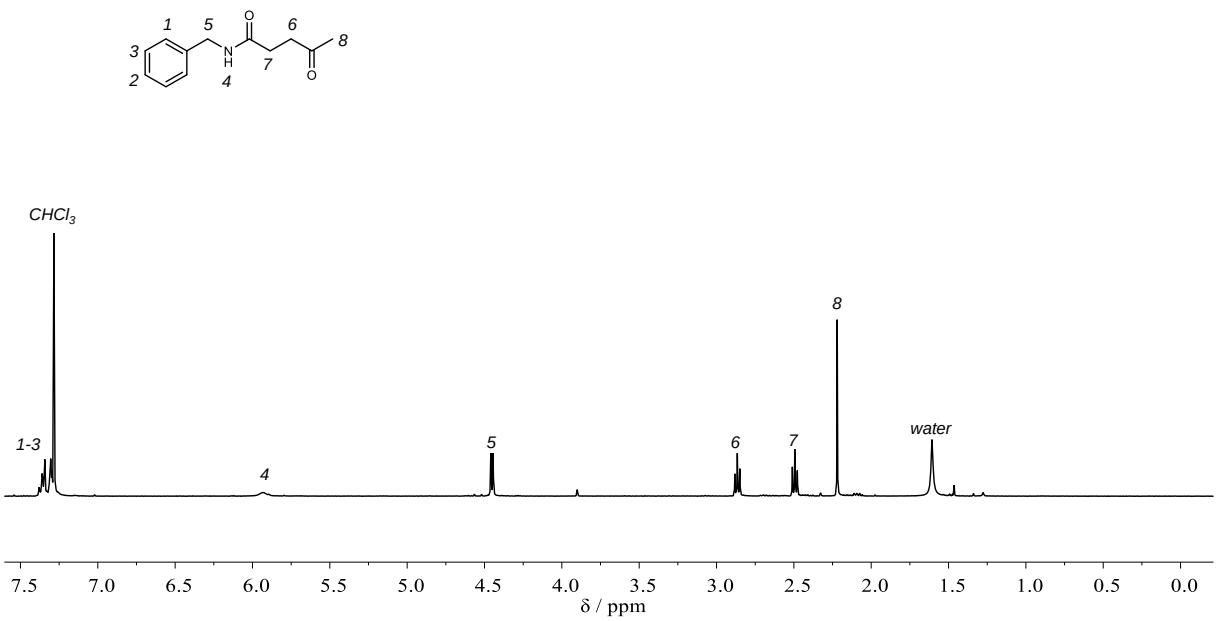

*Supplementary Figure 211: ^{1}H NMR spectrum of **18** in $CDCl_3$.*

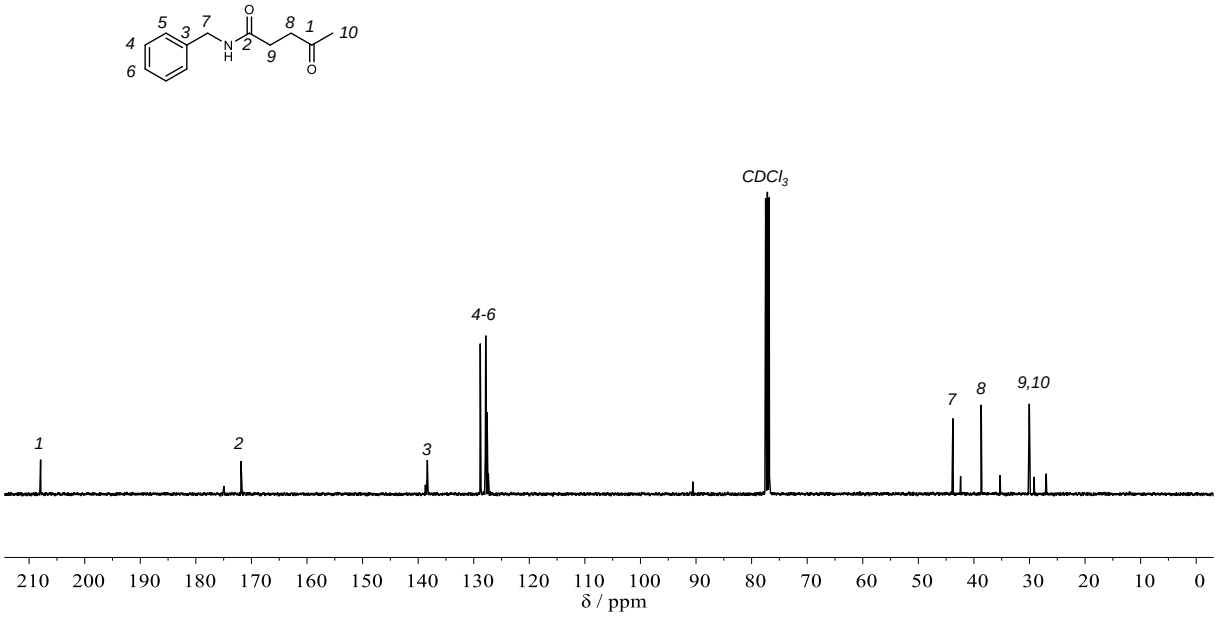

*Supplementary Figure 212: ^{13}C NMR spectrum of **18** in $CDCl_3$.Only the signals corresponding to 18 are assigned. The additionally visible signals represent thermal decomposition products.*

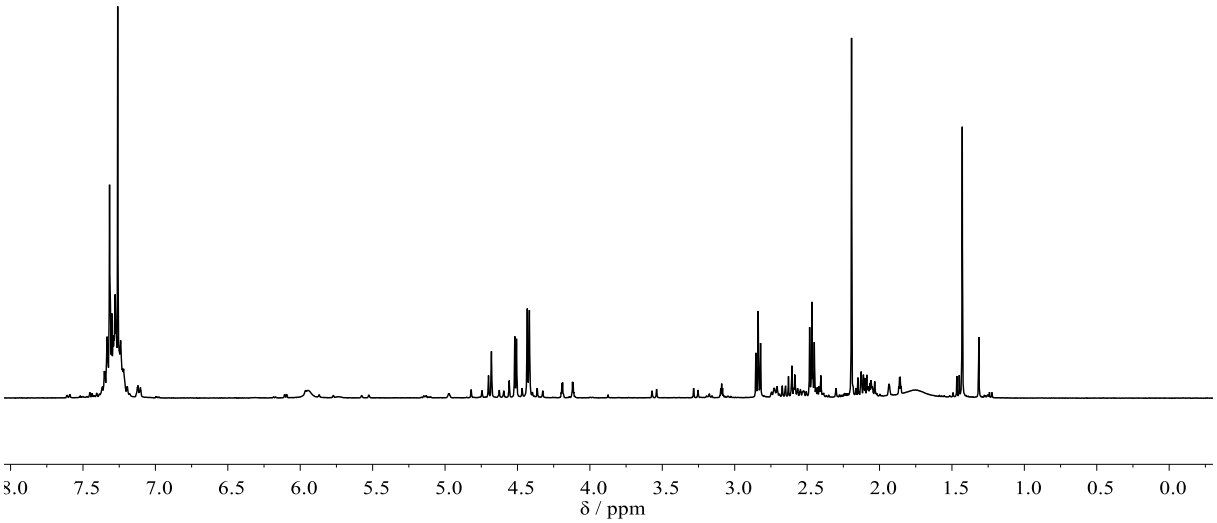

*Supplementary Figure 213: ^{13}C NMR spectrum of **18** synthesized at 100 °C in $CDCl_3$, indicating thermal decomposition of **18**.*

1,4-Bis(levulinoyl)piperazine (20)

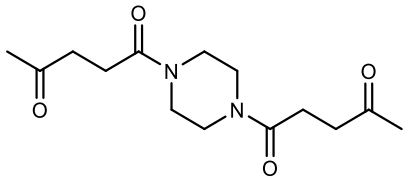

Piperazine (834 mg, 9.68 mmol, 1.00 equiv.) was added to α-angelica lactone (2.00 g, 1.82 mL 20.4 mmol, 2.10 equiv.) and the mixture was stirred at 120 °C for 1 hour. Afterwards, the mixture was cooled to -18 °C, the resulting solid was transferred to a filter, washed with cold EtOH and dried under reduced pressure. **20** was obtained as a white solid in a yield of 73% (2.09 g, 7.42 mmol).

^{1}H NMR (400 MHz, Chloroform-*d*) δ/ppm = 3.71 – 3.45 (m, 8H), 2.92 – 2.73 (m, 4H), 2.59 (t, *J* = 6.3 Hz, 4H), 2.21 (s, 6H).

^{13}C NMR (101 MHz, Chloroform-*d*) δ/ppm = 207.78, 170.47 (d, *J* = 17.7 Hz), 45.27 (d, *J* = 18.7 Hz), 41.66 (d, *J* = 6.6 Hz), 38.11 (d, *J* = 10.7 Hz), 30.25, 27.01.

IR (ATR platinum diamond) $\tilde{\nu}/cm^{-1}$ = 3013 (vw), 2941 (vw), 2919 (w), 2906 (w), 2869 (vw), 1707 (s), 1635 (vs), 1524 (vw), 1512 (vw), 1493 (vw), 1462 (m), 1434 (s), 1401 (m), 1378 (m), 1366 (m), 1347 (m), 1279 (m), 1242 (m), 1216 (s), 1166 (s), 1070 (w), 1053 (w), 1028 (m), 1014 (s), 987 (m), 938 (w), 926 (w), 866 (vw), 850 (vw), 831 (vw), 825 (vw), 771 (w), 722 (vw), 646 (vw), 615 (w), 551 (m), 525 (m), 500 (vw), 475 (m), 463 (w).

ESI-HRMS m/z: $[M+Na]^+$ calculated for $C_{14}H_{22}N_2NaO_4$ = 305.1477, found 305.1480.

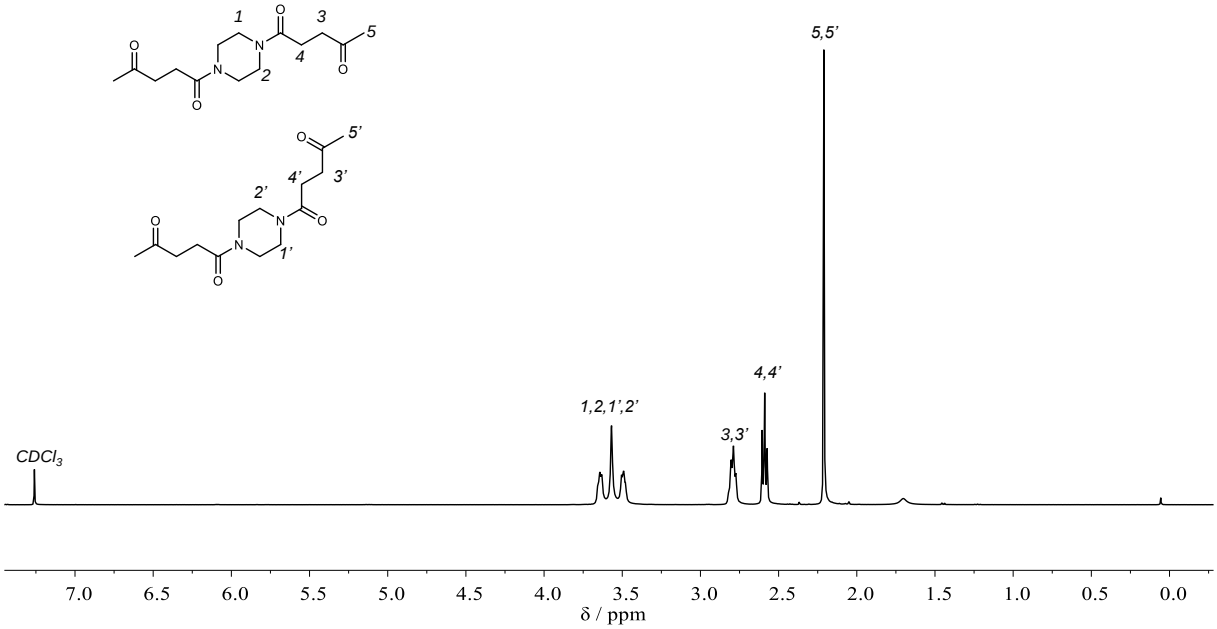

*Supplementary Figure 214: ^{1}H NMR spectrum of **20** in $CDCl_3$.*

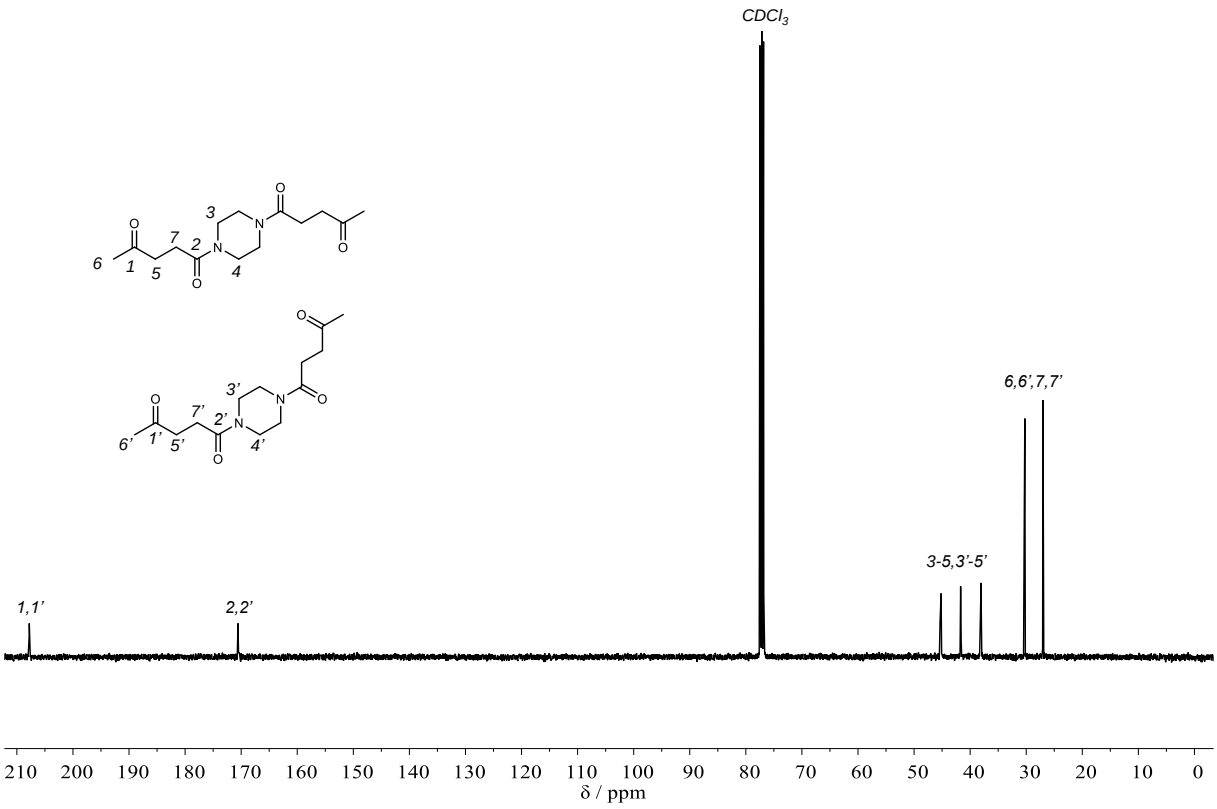

*Supplementary Figure 215: ^{13}C NMR spectrum of **20** in $CDCl_3$.*

WK polymerization of 20 with sulfur and piperazine (PTG-1)

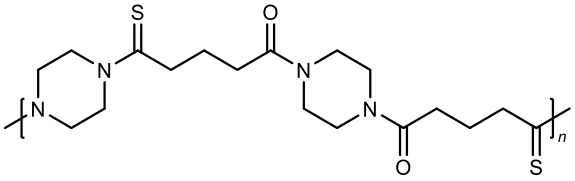

In a glass vial, **20** (500 mg, 1.77 mmol, 1.00 equiv.), piperazine (153 mg, 1.77 mmol, 1.00 equiv.) and elemental sulfur (227 mg, 7.08 mmol S, 4.00 equiv. S) were mixed and *N*-methylpiperidine (214 µL, 176 mg, 1.77 mmol, 1.00 equiv.) was added. The vial was sealed and the mixture was heated to 120 °C for 16 hours. Afterwards, the crude mixture was dissolved in 25 mL of DMSO and precipitated into cold MeOH. The precipitate was filtered, washed with MeOH and dried under reduced pressure. **PTG-**1 was obtained as a dark brown solid in a yield of 94% (713 mg, 1.67 mmol). SEC analysis (DMAc/LiBr) revealed a number average molecular weight of 11.1 kDa ($Đ$ = 1.64). A polymerization conducted without *N*-methylpiperidine under otherwise equal conditions yielded **PTG-1** in 40% yield (304 mg, 713 µmol) with a number average molecular weight of 10.4 kDa ($Đ$ = 1.40).

^{1}H NMR (500 MHz, DMSO-d_6) δ/ppm = 4.43 – 3.76 (m, 4H), 3.67 – 3.34 (m, 4H), 2.88 – 2.75 (m, 2H), 2.51 – 2.39 (m, 4H), 1.95 – 1.79 (m, 2H).

^{13}C NMR (126 MHz, DMSO-d_6) δ/ppm = 202.56 – 201.80 (m), 170.91 – 170.32 (m), 49.48 – 40.64 (m), 31.76 – 30.87 (m), 24.31 – 23.50 (m).

IR (ATR platinum diamond) $\tilde{\nu}$/cm^{-1} = 3478 (m), 3468 (m), 3447 (m), 3427 (m), 3417 (m), 3404 (m), 3396 (m), 3382 (m), 3371 (m), 3355 (m), 3347 (m), 3336 (m), 2958 (m), 2919 (m), 2904 (m), 2894 (m), 2874 (m), 2867 (m), 2859 (m), 1615 (s), 1557 (m), 1462 (s), 1456 (s), 1423 (vs), 1360 (m), 1281 (s), 1203 (s), 1150 (s), 1098 (s), 1043 (m), 987 (vs), 878 (m), 831 (m), 806 (m), 792 (m), 765 (m), 751 (m), 728 (m), 710 (m), 658 (m), 650 (m), 634 (m), 613 (m), 599 (m), 592 (m), 576 (s), 562 (s), 541 (s), 531 (s), 508 (s), 500 (s), 481 (s), 475 (s), 467 (s), 461 (s), 440 (s), 432 (s), 413 (s), 401 (s).

SEC (DMAc/LiBr): M_n = 11.4 kDa, M_w = 18.7 kDa, $Đ$ = 1.64.

TGA: $T_{d,10\%}$ = 276 °C , Residue = 0.1 %.

DSC: T_g = 109 °C.

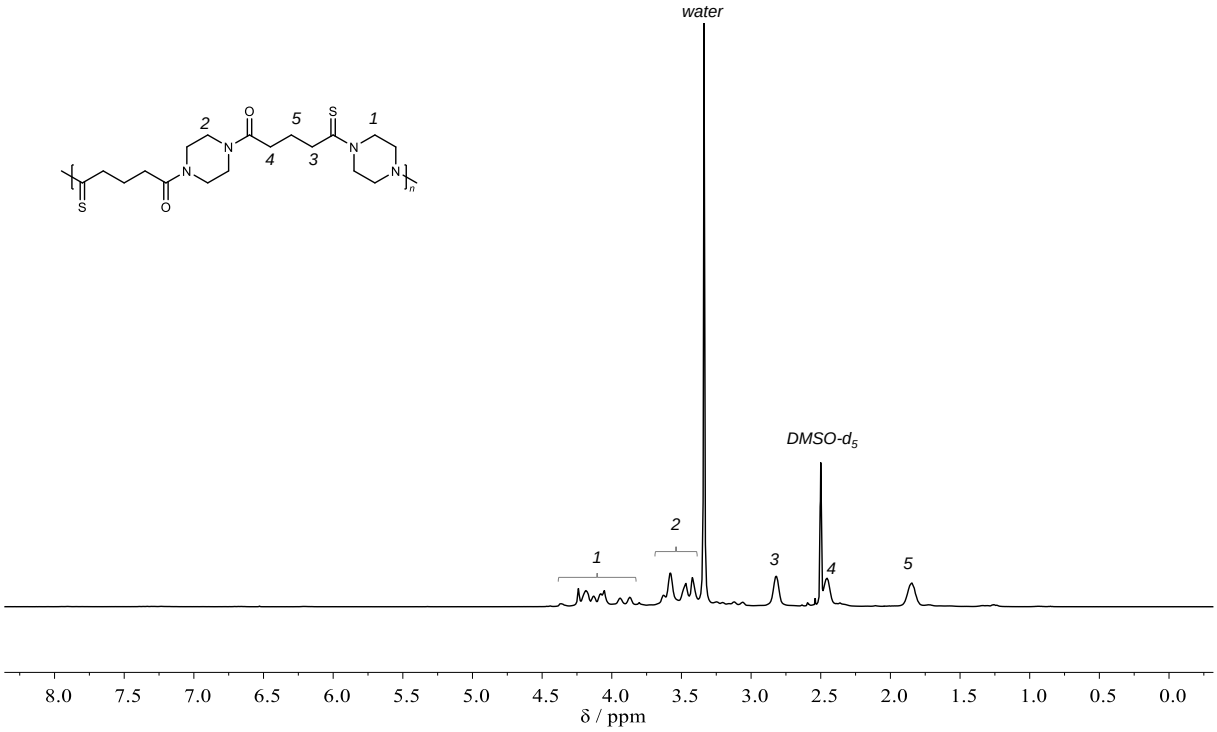

*Supplementary Figure 216: [1]H NMR spectrum of **PTG-1** in DMSO-d6.*

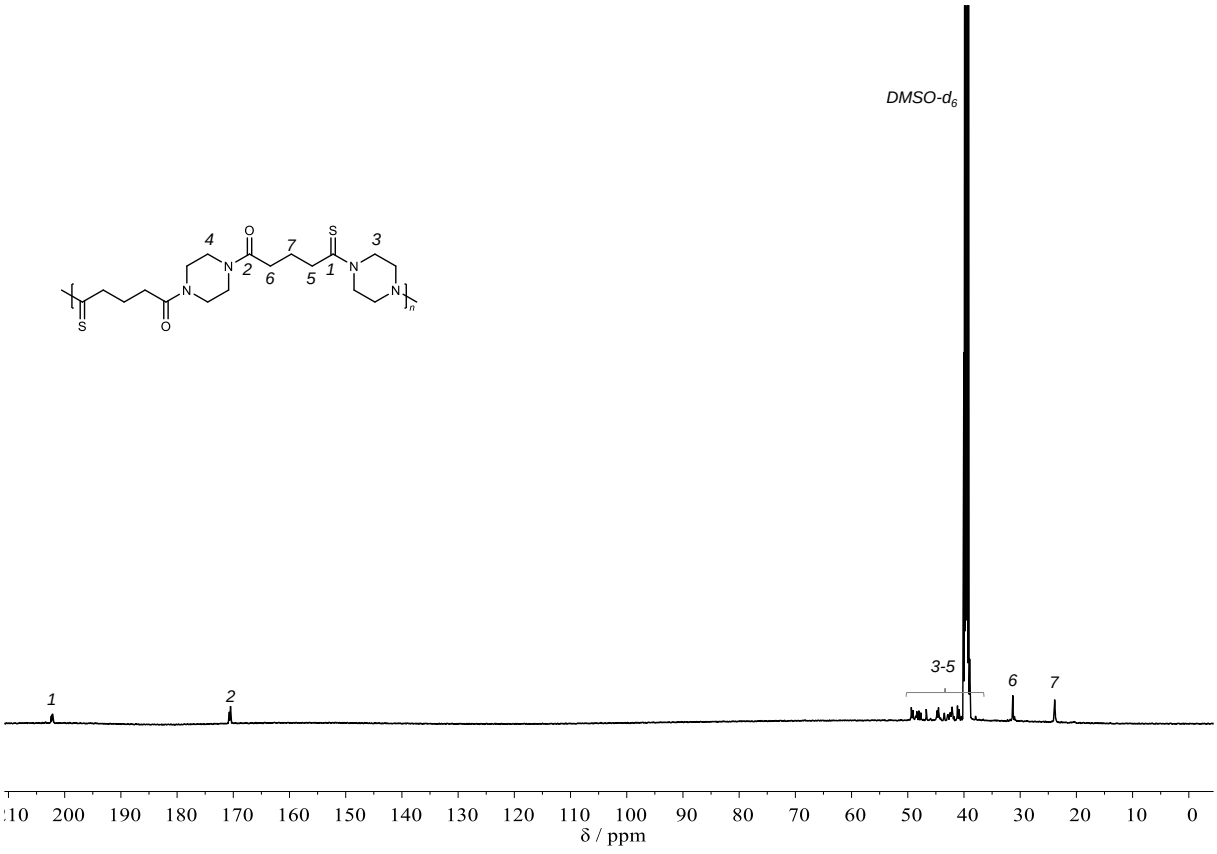

*Supplementary Figure 217: [13]C NMR spectrum of **PTG-1** in DMSO-d6.*

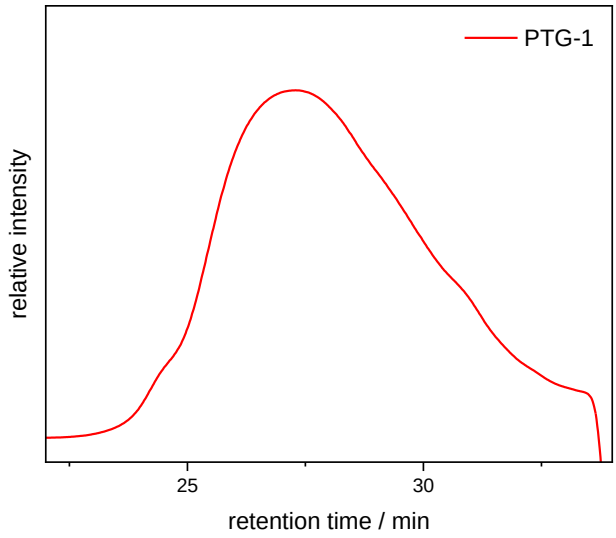

*Supplementary Figure 218: SEC trace of **PTG-1** (measured in DMAc/LiBr).*

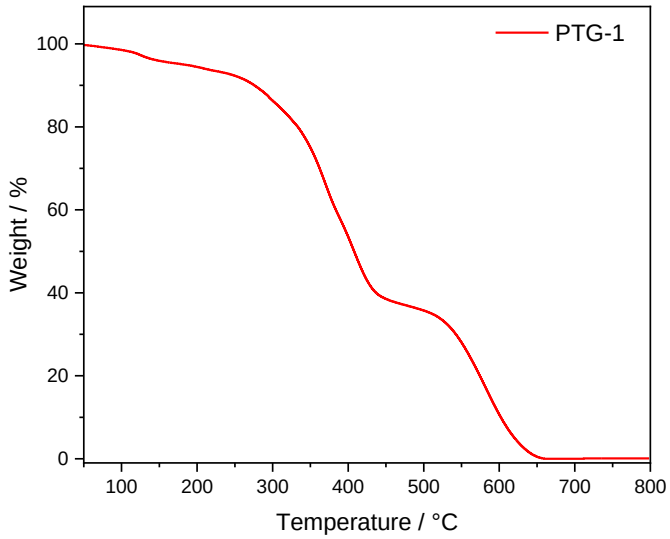

*Supplementary Figure 219: TGA curve of **PTG-1**.*

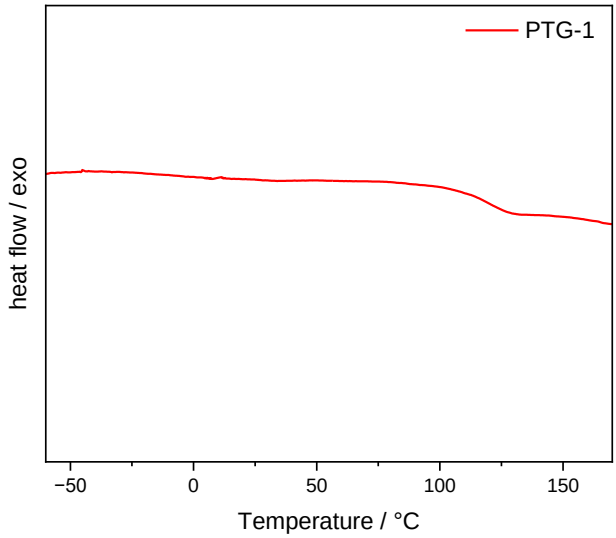

*Supplementary Figure 220: DSC curve of **PTG-1**.*

7 Appendix

7.1 List of Abbreviations

ACQ	Aggregation-caused quenching
AE	Atom economy
AIE	Aggregation-induced emission
AL	α-Angelica lactone
CAN	Covalent adaptable network
CDI	Carbonyldiimidazole
cEF	Complete E-factor
DBN	1,5-Diazabicyclo[4.3.0]non-5-ene
DBPO	Dibenzoyl peroxide
DBU	1,8-Diazabicyclo[5.4.0]-undec-7-ene
DCM	Dichloromethane
DFT	Density functional theory
DIB	1,3-Diisopropenyl benzene
DME	1,2-Dimethoxyethane
DMF	*N*,*N*-Dimethylformamide
DMPA	2,2-Dimethoxy-2-phenylacetophenone
DMPU	*N*,*N*-Dimethylpropyleneurea
DMSO	Dimethylsulfoxide
DSC	Differential scanning calorimetry
ECH	Epichlorohydrin
EPR	Electron paramagnetic resonance
ESI	Electrospray ionization
FAME	Fatty acid methyl ester
FDCA	Furan-2,5-dicarboxylic acid
GC-MS	Gas chromatography – mass spectrometry
GF	Gel fraction
GTU	Glyceryl tri(10-undecenoate)
GVL	γ-Valerolactone
GSK	GlaxoSmithKline
HLSO	High linoleic sunflower oil
HMF	5-Hydroxymethylfurfural
HMPA	Hexamethylphosphoramide

HOSO	High oleic sunflower oil
IR	Infrared (spectroscopy)
ITC	Isothiocyanate
IV	Inverse vulcanization
LA	Levulinic Acid
LCA	Life-cycle assessment
MCR	Multicomponent Reaction
MCP	Multicomponent Polymerization
MeTHF	2-Methyltetrahydrofuran
MPA	3-Mercaptopropionic acid
MS	Mass spectrometry
MSO	Mercaptanized soybean oil
MTBD	7-Methyl-1,5,7-triazabicyclo[4.4.0]dec-5-ene
MUFA	Monounsaturated fatty acid
NIPU	Non-isocyanate polyurethane
NMPip	*N*-Methylpiperidine
NMR	Nuclear magnetic resonance
NOESY	Nuclear Overhauser enhancement spectroscopy
NTH	*N*-Tosylhydrazone
OD	1,7-Octadiene
OLED	Organic light-emitting diode
PAV-DA	Polyarylene(1,2-diarylvinylene)
PEF	Polyethylenefuranoate
PEI	Process mass intensity
PET	Polyethyleneterephthalate
PETMP	Pentaerythritol tetramercaptopropionate
PMI	Process mass intensity
PPM	Post-polymerization modification
PTA	Polythioamide
PTC	Polythionocarbamate
PTU	Polythiourea
PUFA	Polyunsaturated fatty acid
PVC	Poly(vinyl chloride)
ROP	Ring-opening polymerization
SEC	Size exclusion chromatography

sEF	Simple E-factor
SFA	Saturated fatty acid
SRE	Silicone removal efficiency
TAE	Tetraarylethylene
TBD	1,5,7-Triazabicyclo[4.4.0]dec-5-ene
TES	Triethylsilane
TGA	Thermogravimetric analysis
THF	Tetrahydrofuran
TLC	Thin layer chromatography
TMB	1,3,5-Trimethoxybenzene
TMCC	Transition metal-catalyzed cross-coupling
TMDS	Tetramethyldisiloxane
TMPMP	Trimethylolpropane trimercaptopropionate
TPE	Tetraphenylethylene
UA	10-Undecenoic acid
UN	United Nations
UV/Vis	Ultraviolet/visible (spectroscopy)
WK	Willgerodt-Kindler (reaction)

7.2 List of Publications

1) R. Nickisch, **P. Conen**, S. M. Gabrielsen, M. A. R. Meier, A more sustainable Isothiocyanate synthesis by amine catalyzed sulfurization of isocyanides with elemental sulfur, *RSC Adv.* **2021**, *11*, 3134-3142, https://doi.org/10.1039/D0RA10436A.

2) R. Nickisch, **P. Conen**, M. A. R. Meier, Polythiosemicarbazones by Condensation of Dithiosemicarbazides and Dialdehydes, *Macromolecules* **2022**, *55*, 3267-3275, https://doi.org/10.1021/acs.macromol.2c00409.

3) **P. Conen**, R. Nickisch, M. A. R. Meier, Synthesis of highly substituted alkenes by sulfur-mediated olefination of N-tosylhydrazones, *Commun. Chem.* **2023**, *6*, 255, https://doi.org/10.1038/s42004-023-01058-2.

4) **P. Conen**, M. A. R. Meier, Reactivities and mechanisms in organic reactions involving activation of elemental sulfur under basic conditions, *Tetrahedron Chem* **2024**, *11*, 100086, https://doi.org/10.1016/j.tchem.2024.100086.

5) **P. Conen**, F. J. O. Niedermaier, S. Abou El Mirate, M. A. R. Meier, A Novel Synthesis Strategy for Poly(Arylene-Vinylene) Derivatives by Elemental Sulfur-Mediated Polyolefination, *Macromol. Rapid Commun.* **2025**, 2500166, https://doi.org/10.1002/marc.202500166.

6) L. J. Bartlewski, **P. Conen**, Q. Cai, M. Bürk, D. Armspach, M. A. R. Meier, A more sustainable two-step synthesis of alkylated β-cyclodextrin *via* acetylation and $GaBr_3$-catalyzed reduction, *RSC Sustainability* **2025**, *3*, 4126-4136, https://doi.org/10.1039/D5SU00590F.

7) **P. Conen**, F. C. M. Scheelje, R. Häusl, M. A. R. Meier, Synthesis of Novel Vegetable Oil-derived Polythiols and their Thermosets, *ACS Sustainable Chem. Eng.* **2025**, *13*, 19899-19908, https://doi.org/10.1021/acssuschemeng.5c10328.

7.3 List of Conference Contributions

1) Presentation: “Synthesis of highly substituted alkenes *via* sulfur-mediated olefination of *N*-tosylhydrazones” at the *ACS Fall 2023*, held in San Francisco, USA, **August 2023**.

2) Poster: “Synthesis of novel vegetable-oil based polythiol crosslinking agents” at the *EPF European Polymer Congress*, held in Groningen, Netherlands, **June 2025**.

8 References

[1] J. Huo, Z. Wang, C. Oberschelp, G. Guillén-Gosálbez, S. Hellweg, "Net-zero transition of the global chemical industry with CO_2 -feedstock by 2050: feasible yet challenging" *Green Chem.* **2023**, *25*, 415–430.

[2] P. Gabrielli, L. Rosa, M. Gazzani, R. Meys, A. Bardow, M. Mazzotti, G. Sansavini, "Net-zero emissions chemical industry in a world of limited resources" *One Earth* **2023**, *6*, 682–704.

[3] G. Lopez, D. Keiner, M. Fasihi, T. Koiranen, C. Breyer, "From fossil to green chemicals: sustainable pathways and new carbon feedstocks for the global chemical industry" *Energy Environ. Sci.* **2023**, *16*, 2879–2909.

[4] J. B. Zimmerman, P. T. Anastas, H. C. Erythropel, W. Leitner, "Designing for a green chemistry future" *Science* **2020**, *367*, 397–400.

[5] P. G. Levi, J. M. Cullen, "Mapping Global Flows of Chemicals: From Fossil Fuel Feedstocks to Chemical Products" *Environ. Sci. Technol.* **2018**, *52*, 1725–1734.

[6] E. T. C. Vogt, B. M. Weckhuysen, "The refinery of the future" *Nature* **2024**, *629*, 295–306.

[7] P. T. Anastas, J. C. Warner ,*Green chemistry: theory and practice*, Oxford University Press, Oxford, **1998**.

[8] P. Anastas, N. Eghbali, "Green Chemistry: Principles and Practice" *Chem. Soc. Rev.* **2010**, *39*, 301–312.

[9] T. Keijer, V. Bakker, J. C. Slootweg, "Circular chemistry to enable a circular economy" *Nat. Chem.* **2019**, *11*, 190–195.

[10] C. S. P. Vieira, D. Malafaia, D. R. Cunha, J. F. Leal, J. P. M. António, P. M. P. Gois, J. Garcia-Martinez, T. Noël, M. Poliakoff, "RESILIENCE by design: ten principles to guide chemistry in a volatile world" *Green Chem.* **2025**, *27*, 7742–7747.

[11] T.-L. Chen, H. Kim, S.-Y. Pan, P.-C. Tseng, Y.-P. Lin, P.-C. Chiang, "Implementation of green chemistry principles in circular economy system towards sustainable development goals: Challenges and perspectives" *Sci. Total Environ.* **2020**, *716*, 136998.

[12] J.-G. Wagenfeld, K. Al-Ali, S. Almheiri, A. F. Slavens, N. Calvet, "Sustainable applications utilizing sulfur, a by-product from oil and gas industry: A state-of-the-art review" *Waste Manage.* **2019**, *95*, 78–89.

[13] J. A. Ober, *Materials Flow of Sulfur*, U.S. Geological Survey, Reston, VA, **2002**.

[14] A. Ivanov, Y. Smirnov, V. Lisay, G. Borowski, “Issues of the Impact of Granulated Sulfur Transportation on the Environmental Components” *J. Ecol. Eng.* **2023**, *24*, 86–97.

[15] T. A. Rappold, K. S. Lackner, “Large scale disposal of waste sulfur: From sulfide fuels to sulfate sequestration” *Energy* **2010**, *35*, 1368–1380.

[16] T. B. Nguyen, “Recent Advances in Organic Reactions Involving Elemental Sulfur” *Adv. Synth. Catal.* **2017**, *359*, 1066–1130.

[17] W. J. Chung, J. J. Griebel, E. T. Kim, H. Yoon, A. G. Simmonds, H. J. Ji, P. T. Dirlam, R. S. Glass, J. J. Wie, N. A. Nguyen, B. W. Guralnick, J. Park, Á. Somogyi, P. Theato, M. E. Mackay, Y.-E. Sung, K. Char, J. Pyun, “The use of elemental sulfur as an alternative feedstock for polymeric materials” *Nat. Chem.* **2013**, *5*, 518–524.

[18] X. Zhang, P. Theato, Eds. , *Sulfur-containing polymers: from synthesis to functional materials*, Wiley, Hoboken, **2021**.

[19] C. E. Hoyle, C. N. Bowman, “Thiol–Ene Click Chemistry” *Angew. Chem. Int. Ed.* **2010**, *49*, 1540–1573.

[20] E. Paglia, “The Swedish initiative and the 1972 Stockholm Conference: the decisive role of science diplomacy in the emergence of global environmental governance” *Humanit. Soc. Sci. Commun.* **2021**, *8*, 2.

[21] D. H. Meadows, *Limits to Growth, a report for the club of Rome’s project on the predicament of mankind*, Universe Books, New York, **1974**.

[22], “Report of the World Commission on Environment and Development: Our Common Future,” can be found under https://sustainabledevelopment.un.org/content/documents/5987our-common-future.pdf (accessed 20 September 2025), **1987**.

[23], “The 17 Goals,” can be found under https://sdgs.un.org/goals(accessed 21 September 2025), **2015**.

[24], “The Paris Agreement,” can be found under https://unfccc.int/process-and-meetings/the-paris-agreement(accessed 21 September 2025), **2016**.

[25] C. Calculli, A. M. D’Uggento, A. Labarile, N. Ribecco, “Evaluating people’s awareness about climate changes and environmental issues: A case study” *J. Clean. Prod.* **2021**, *324*, 129244.

[26] S. A. Matlin, G. Mehta, H. Hopf, A. Krief, “The role of chemistry in inventing a sustainable future” *Nat. Chem.* **2015**, *7*, 941–943.

[27] W. W. Y. Lau, Y. Shiran, R. M. Bailey, E. Cook, M. R. Stuchtey, J. Koskella, C. A. Velis, L. Godfrey, J. Boucher, M. B. Murphy, R. C. Thompson, E. Jankowska, A.

Castillo Castillo, T. D. Pilditch, B. Dixon, L. Koerselman, E. Kosior, E. Favoino, J. Gutberlet, S. Baulch, M. E. Atreya, D. Fischer, K. K. He, M. M. Petit, U. R. Sumaila, E. Neil, M. V. Bernhofen, K. Lawrence, J. E. Palardy, "Evaluating scenarios toward zero plastic pollution" *Science* **2020**, *369*, 1455–1461.

[28] P. Stegmann, V. Daioglou, M. Londo, D. P. Van Vuuren, M. Junginger, "Plastic futures and their CO2 emissions" *Nature* **2022**, *612*, 272–276.

[29] L. Cabernard, S. Pfister, C. Oberschelp, S. Hellweg, "Growing environmental footprint of plastics driven by coal combustion" *Nat. Sustain.* **2021**, *5*, 139–148.

[30] J. Clark, R. Sheldon, C. Raston, M. Poliakoff, W. Leitner, "15 years of Green Chemistry" *Green Chem.* **2014**, *16*, 18–23.

[31] P. T. Anastas, J. B. Zimmerman, "Peer Reviewed: Design Through the 12 Principles of Green Engineering" *Environ. Sci. Technol.* **2003**, *37*, 94A-101A.

[32] F. Kurul, B. Doruk, S. N. Topkaya, "Principles of green chemistry: building a sustainable future" *Discov. Chem.* **2025**, *2*, 68.

[33] J. Martínez, J. F. Cortés, R. Miranda, "Green Chemistry Metrics, A Review" *Processes* **2022**, *10*, 1274.

[34] R. A. Sheldon, "Fundamentals of green chemistry: efficiency in reaction design" *Chem. Soc. Rev.* **2012**, *41*, 1437–1451.

[35] B. Trost, "The Atom Economy—A Search for Synthetic Efficiency" *Science* **1991**, *254*, 1471–1477.

[36] R. A. Sheldon, "Atom efficiency and catalysis in organic synthesis" *Pure Appl. Chem.* **2000**, *72*, 1233–1246.

[37] B. M. Trost, "On Inventing Reactions for Atom Economy" *Acc. Chem. Res.* **2002**, *35*, 695–705.

[38] R. A. Sheldon, "Organic synthesis - past, present and future" *Chem. Ind.* **1992**, *23*, 903–906.

[39] R. A. Sheldon, "The E factor at 30: a passion for pollution prevention" *Green Chem.* **2023**, *25*, 1704–1728.

[40] C. P. Huang, C. Dong, Z. Tang, "Advanced chemical oxidation: Its present role and potential future in hazardous waste treatment" *Waste Manag.* **1993**, *13*, 361–377.

[41] F. Roschangar, R. A. Sheldon, C. H. Senanayake, "Overcoming barriers to green chemistry in the pharmaceutical industry – the Green Aspiration Level^{TM} concept" *Green Chem.* **2015**, *17*, 752–768.

[42] D. J. C. Constable, A. D. Curzons, L. M. Freitas Dos Santos, G. R. Geen, J. Kitteringham, P. Smith, R. E. Hannah, M. A. McGuire, R. L. Webb, M. Yu, J. D. Hayler,

J. E. Richardson, “Green chemistry measures for process research and development” *Green Chem.* **2001**, *3*, 7–9.

[43] C. Jimenez-Gonzalez, C. S. Ponder, Q. B. Broxterman, J. B. Manley, “Using the Right Green Yardstick: Why Process Mass Intensity Is Used in the Pharmaceutical Industry To Drive More Sustainable Processes” *Org. Process Res. Dev.* **2011**, *15*, 912–917.

[44] R. A. Sheldon, “Consider the environmental quotient” *ChemTech* **1994**, *24*.

[45] M. Eissen, J. O. Metzger, “Environmental Performance Metrics for Daily Use in Synthetic Chemistry” *Chem. Eur. J.* **2002**, *8*, 3580.

[46] T. V. T. Phan, C. Gallardo, J. Mane, “GREEN MOTION: a new and easy to use green chemistry metric from laboratories to industry” *Green Chem.* **2015**, *17*, 2846–2852.

[47] B. Voss, S. I. Andersen, E. Taarning, C. H. Christensen, “C Factors Pinpoint Resource Utilization in Chemical Industrial Processes” *ChemSusChem* **2009**, *2*, 1152–1162.

[48] C. H. Christensen, J. Rass-Hansen, C. C. Marsden, E. Taarning, K. Egeblad, “The Renewable Chemicals Industry” *ChemSusChem* **2008**, *1*, 283–289.

[49] L. M. Tufvesson, P. Tufvesson, J. M. Woodley, P. Börjesson, “Life cycle assessment in green chemistry: overview of key parameters and methodological concerns” *Int. J. Life Cycle Assess.* **2013**, *18*, 431–444.

[50] D. Kralisch, D. Ott, D. Gericke, “Rules and benefits of Life Cycle Assessment in green chemical process and synthesis design: a tutorial review” *Green Chem.* **2015**, *17*, 123–145.

[51] C. Jiménez-González, A. D. Curzons, D. J. C. Constable, V. L. Cunningham, “Cradle-to-gate life cycle inventory and assessment of pharmaceutical compounds” *Int. J. Life Cycle Assess.* **2004**, *9*, 114–121.

[52] P. Saling, A. Kicherer, B. Dittrich-Krämer, R. Wittlinger, W. Zombik, I. Schmidt, W. Schrott, S. Schmidt, “Eco-efficiency analysis by basf: the method” *Int. J. Life Cycle Assess.* **2002**, *7*, 203–218.

[53] P. T. Anastas, M. M. Kirchhoff, T. C. Williamson, “Catalysis as a foundational pillar of green chemistry” *Appl. Catal. A Gen.* **2001**, *221*, 3–13.

[54] R. A. Sheldon, “E factors, green chemistry and catalysis: an odyssey” *Chem. Commun.* **2008**, 3352.

[55] J. S. Hertel, P. Bitterwolf, S. Kröll, A. Winterhalter, A. J. Weber, M. Grösche, L. B. Walkowsky, S. Heißler, M. Schwotzer, C. Wöll, T. Van De Kamp, M. Zuber, T. Baumbach, K. S. Rabe, C. M. Niemeyer, “Biocatalytic Foams from Microdroplet-Formulated Self-Assembling Enzymes” *Adv. Mater.* **2023**, *35*, 2303952.

[56] R. A. Sheldon, D. Brady, "Green Chemistry, Biocatalysis, and the Chemical Industry of the Future" *ChemSusChem* **2022**, *15*, e202102628.

[57] S. Wu, R. Snajdrova, J. C. Moore, K. Baldenius, U. T. Bornscheuer, "Biocatalysis: Enzymatic Synthesis for Industrial Applications" *Angew. Chem. Int. Ed.* **2021**, *60*, 88–119.

[58] R. C. Cioc, E. Ruijter, R. V. A. Orru, "Multicomponent reactions: advanced tools for sustainable organic synthesis" *Green Chem.* **2014**, *16*, 2958–2975.

[59] O. Kreye, T. Tóth, M. A. R. Meier, "Introducing Multicomponent Reactions to Polymer Science: Passerini Reactions of Renewable Monomers" *J. Am. Chem. Soc.* **2011**, *133*, 1790–1792.

[60] D. L. Priebbenow, C. Bolm, "Recent advances in the Willgerodt–Kindler reaction" *Chem. Soc. Rev.* **2013**, *42*, 7870.

[61], "The Nobel Prize in Chemistry 2022," can be found under https://www.nobelprize.org/prizes/chemistry/2022/summary/, **2022**.

[62] S. Bräse, C. Gil, K. Knepper, V. Zimmermann, "Organic Azides: An Exploding Diversity of a Unique Class of Compounds" *Angew. Chem. Int. Ed.* **2005**, *44*, 5188–5240.

[63] A. Loupy, "Solvent-free microwave organic synthesis as an efficient procedure for green chemistry" *C. R. Chim* **2004**, *7*, 103–112.

[64] T. Sehn, M. A. R. Meier, "Structure–Property Relationships of Short Chain (Mixed) Cellulose Esters Synthesized in a DMSO/TMG/CO_2 Switchable Solvent System" *Biomacromolecules* **2023**, *24*, 5255–5264.

[65] T. P. Yoon, M. A. Ischay, J. Du, "Visible light photocatalysis as a greener approach to photochemical synthesis" *Nat. Chem.* **2010**, *2*, 527–532.

[66] J. D. Williams, C. O. Kappe, "Recent advances toward sustainable flow photochemistry" *Curr. Opin. Green Sustain. Chem.* **2020**, *25*, 100351.

[67] Z. Amara, J. F. B. Bellamy, R. Horvath, S. J. Miller, A. Beeby, A. Burgard, K. Rossen, M. Poliakoff, M. W. George, "Applying green chemistry to the photochemical route to artemisinin" *Nat. Chem.* **2015**, *7*, 489–495.

[68] D. J. C. Constable, C. Jimenez-Gonzalez, R. K. Henderson, "Perspective on Solvent Use in the Pharmaceutical Industry" *Org. Process Res. Dev.* **2007**, *11*, 133–137.

[69] C. M. Alder, J. D. Hayler, R. K. Henderson, A. M. Redman, L. Shukla, L. E. Shuster, H. F. Sneddon, "Updating and further expanding GSK's solvent sustainability guide" *Green Chem.* **2016**, *18*, 3879–3890.

[70] P. Licence, J. Ke, M. Sokolova, S. K. Ross, M. Poliakoff, “Chemical reactions in supercritical carbon dioxide: from laboratory to commercial plantThis work was presented at the Green Solvents for Catalysis Meeting held in Bruchsal, Germany, 13–16th October 2002.” *Green Chem.* **2003**, *5*, 99–104.

[71] X. Kang, L. Mao, J. Shi, Y. Liu, B. Zhai, J. Xu, Y. Jiang, E. Lichtfouse, H. Jin, L. Guo, “Supercritical carbon dioxide systems for sustainable and efficient dissolution of solutes: a review” *Environ. Chem. Lett.* **2024**, *22*, 815–839.

[72] J. M. DeSimone, “Practical Approaches to Green Solvents” *Science* **2002**, *297*, 799–803.

[73] H. Röper, “Renewable Raw Materials in Europe - Industrial Utilisation of Starch and Sugar [1]” *Starch/Stärke* **2002**, *54*, 89–99.

[74] Y. Zhu, C. Romain, C. K. Williams, “Sustainable polymers from renewable resources” *Nature* **2016**, *540*, 354–362.

[75] J. J. Bozell, G. R. Petersen, “Technology development for the production of biobased products from biorefinery carbohydrates—the US Department of Energy’s ‘Top 10’ revisited” *Green Chem.* **2010**, *12*, 539.

[76] C.-H. Zhou, X. Xia, C.-X. Lin, D.-S. Tong, J. Beltramini, “Catalytic conversion of lignocellulosic biomass to fine chemicals and fuels” *Chem. Soc. Rev.* **2011**, *40*, 5588.

[77] J. Rao, Z. Lv, G. Chen, F. Peng, “Hemicellulose: Structure, chemical modification, and application” *Prog. Polym. Sci.* **2023**, *140*, 101675.

[78] S. C. Gondhalekar, P. J. Pawar, S. S. Dhumal, S. S. Thakre, “Mechanism of xanthation reaction in viscose process” *Cellulose* **2019**, *26*, 1595–1604.

[79] P. Rustemeyer, “1. History of CA and evolution of the markets” *Macromol. Symp.* **2004**, *208*, 1–6.

[80] R. C. Law, “5. Applications of cellulose acetate 5.1 Cellulose acetate in textile application” *Macromol. Symp.* **2004**, *208*, 255–266.

[81] J. Wolfs, R. Nickisch, L. Wanner, M. A. R. Meier, “Sustainable One-Pot Cellulose Dissolution and Derivatization via a Tandem Reaction in the DMSO/DBU/CO_2 Switchable Solvent System” *J. Am. Chem. Soc.* **2021**, *143*, 18693–18702.

[82] J. Wolfs, M. A. R. Meier, “A more sustainable synthesis approach for cellulose acetate using the DBU/CO_2 switchable solvent system” *Green Chem.* **2021**, *23*, 4410–4420.

[83] K. N. Onwukamike, S. Grelier, E. Grau, H. Cramail, M. A. R. Meier, “Critical Review on Sustainable Homogeneous Cellulose Modification: Why Renewability Is Not Enough” *ACS Sustainable Chem. Eng.* **2019**, *7*, 1826–1840.

[84] Md. D. Islam, F. J. Uddin, T. U. Rashid, M. Shahruzzaman, "Cellulose acetate-based membrane for wastewater treatment—A state-of-the-art review" *Mater. Adv.* **2023**, *4*, 4054–4102.

[85] H. C. Arca, L. I. Mosquera-Giraldo, V. Bi, D. Xu, L. S. Taylor, K. J. Edgar, "Pharmaceutical Applications of Cellulose Ethers and Cellulose Ether Esters" *Biomacromolecules* **2018**, *19*, 2351–2376.

[86] D. S. Bajwa, G. Pourhashem, A. H. Ullah, S. G. Bajwa, "A concise review of current lignin production, applications, products and their environmental impact" *Ind. Crops Prod.* **2019**, *139*, 111526.

[87] M. Fache, B. Boutevin, S. Caillol, "Vanillin Production from Lignin and Its Use as a Renewable Chemical" *ACS Sustainable Chem. Eng.* **2016**, *4*, 35–46.

[88] C. Libretti, L. Santos Correa, M. A. R. Meier, "From waste to resource: advancements in sustainable lignin modification" *Green Chem.* **2024**, *26*, 4358–4386.

[89] F. C. Destaso, C. Libretti, C. Le Coz, E. Grau, H. Cramail, M. A. R. Meier, "Optimized synthesis of a high oleic sunflower oil derived polyamine and its lignin-based NIPUs" *Green Chem.* **2025**, *27*, 1440–1450.

[90] S. M. Ioannidou, C. Pateraki, D. Ladakis, H. Papapostolou, M. Tsakona, A. Vlysidis, I. K. Kookos, A. Koutinas, "Sustainable production of bio-based chemicals and polymers via integrated biomass refining and bioprocessing in a circular bioeconomy context" *Bioresour. Technol.* **2020**, *307*, 123093.

[91] S. Wegelin, M. A. R. Meier, "Bio-based aromatics for chemicals and materials: Advances in renewable drop-in and functional alternatives" *Curr. Opin. Green Sustain. Chem.* **2024**, *47*, 100931.

[92] R. Ahorsu, F. Medina, M. Constantí, "Significance and Challenges of Biomass as a Suitable Feedstock for Bioenergy and Biochemical Production: A Review" *Energies* **2018**, *11*, 3366.

[93] Y. Lin, S. Tanaka, "Ethanol fermentation from biomass resources: current state and prospects" *Appl. Microbiol. Biotechnol.* **2006**, *69*, 627–642.

[94] S. Jain, S. Kumar, "A comprehensive review of bioethanol production from diverse feedstocks: Current advancements and economic perspectives" *Energy* **2024**, *296*, 131130.

[95] M. Balat, H. Balat, C. Öz, "Progress in bioethanol processing" *Prog. Energy Combust. Sci.* **2008**, *34*, 551–573.

[96] R. Chauhan, R. Sartape, N. Minocha, I. Goyal, M. R. Singh, "Advancements in Environmentally Sustainable Technologies for Ethylene Production" *Energy Fuels* **2023**, *37*, 12589–12622.

[97] R. T. Mathers, "How well can renewable resources mimic commodity monomers and polymers?" *J. Polym. Sci. A Polym. Chem.* **2012**, *50*, 1–15.

[98] A. Morschbacker, "Bio-Ethanol Based Ethylene" *Polym. Rev.* **2009**, *49*, 79–84.

[99] A. Adil, B. Prasad, L. Rao, "Methanol generation from bio-syngas: experimental analysis and modeling studies" *Environ. Dev. Sustain.* **2023**, *26*, 21503–21527.

[100] M. Wang, H. Zhou, F. Wang, "Photocatalytic Production of Syngas from Biomass" *Acc. Chem. Res.* **2023**, *56*, 1057–1069.

[101] N. Couto, A. Rouboa, V. Silva, E. Monteiro, K. Bouziane, "Influence of the Biomass Gasification Processes on the Final Composition of Syngas" *Energy Procedia* **2013**, *36*, 596–606.

[102] T. Werpy, G. Petersen, *Top Value Added Chemicals from Biomass: Volume I -- Results of Screening for Potential Candidates from Sugars and Synthesis Gas*, U.S. Department of Energy, Washington, DC, **2004**.

[103] M. Dashtban, A. Gilbert, P. Fatehi, "Recent advancements in the production of hydroxymethylfurfural" *RSC Adv.* **2014**, *4*, 2037–2050.

[104] Y. Román-Leshkov, J. N. Chheda, J. A. Dumesic, "Phase Modifiers Promote Efficient Production of Hydroxymethylfurfural from Fructose" *Science* **2006**, *312*, 1933–1937.

[105] E. De Jong, H. (Roy) A. Visser, A. S. Dias, C. Harvey, G.-J. M. Gruter, "The Road to Bring FDCA and PEF to the Market" *Polymers* **2022**, *14*, 943.

[106] S. K. Burgess, J. E. Leisen, B. E. Kraftschik, C. R. Mubarak, R. M. Kriegel, W. J. Koros, "Chain Mobility, Thermal, and Mechanical Properties of Poly(ethylene furanoate) Compared to Poly(ethylene terephthalate)" *Macromolecules* **2014**, *47*, 1383–1391.

[107] J.-G. Rosenboom, D. K. Hohl, P. Fleckenstein, G. Storti, M. Morbidelli, "Bottle-grade polyethylene furanoate from ring-opening polymerisation of cyclic oligomers" *Nat. Commun.* **2018**, *9*, 2701.

[108] D. W. Rackemann, W. O. Doherty, "The conversion of lignocellulosics to levulinic acid" *Biofuels Bioprod. Biorefin.* **2011**, *5*, 198–214.

[109] M. Sajid, U. Farooq, G. Bary, M. M. Azim, X. Zhao, "Sustainable production of levulinic acid and its derivatives for fuel additives and chemicals: progress, challenges, and prospects" *Green Chem.* **2021**, *23*, 9198–9238.

[110] W. Xu, X. Chen, H. Guo, H. Li, H. Zhang, L. Xiong, X. Chen, "Conversion of levulinic acid to valuable chemicals: a review" *J. Chem. Technol. Biotechnol.* **2021**, *96*, 3009–3024.

[111] M. R. Sahasrabudhe, "Crismer values and erucic acid contents of rapeseed oils" *J. Am. Oil Chem. Soc.* **1977**, *54*, 323–324.

[112] M. A. R. Meier, J. O. Metzger, U. S. Schubert, "Plant oil renewable resources as green alternatives in polymer science" *Chem. Soc. Rev.* **2007**, *36*, 1788.

[113] H. Mutlu, M. A. R. Meier, "Castor oil as a renewable resource for the chemical industry" *Eur. J. Lipid Sci. Technol.* **2010**, *112*, 10–30.

[114] Y. B. Che Man, T. Haryati, H. M. Ghazali, B. A. Asbi, "Composition and thermal profile of crude palm oil and its products" *J. Am. Oil Chem. Soc.* **1999**, *76*, 237–242.

[115] U. Biermann, U. Bornscheuer, M. A. R. Meier, J. O. Metzger, H. J. Schäfer, "Oils and Fats as Renewable Raw Materials in Chemistry" *Angew. Chem. Int. Ed.* **2011**, *50*, 3854–3871.

[116] U. Biermann, U. T. Bornscheuer, I. Feussner, M. A. R. Meier, J. O. Metzger, "Fatty Acids and their Derivatives as Renewable Platform Molecules for the Chemical Industry" *Angew. Chem. Int. Ed.* **2021**, *60*, 20144–20165.

[117] W. N. A. Wan Osman, M. H. Rosli, W. N. A. Mazli, S. Samsuri, "Comparative review of biodiesel production and purification" *Carbon Capture Sci. Technol.* **2024**, *13*, 100264.

[118] P. J. M. Lima, R. M. Da Silva, C. A. C. G. Neto, N. C. Gomes E Silva, J. E. D. S. Souza, Y. L. Nunes, J. C. Sousa Dos Santos, "An overview on the conversion of glycerol to value-added industrial products via chemical and biochemical routes" *Biotechnol. Appl. Biochem.* **2022**, *69*, 2794–2818.

[119] B. M. Bell, J. R. Briggs, R. M. Campbell, S. M. Chambers, P. D. Gaarenstroom, J. G. Hippler, B. D. Hook, K. Kearns, J. M. Kenney, W. J. Kruper, D. J. Schreck, C. N. Theriault, C. P. Wolfe, "Glycerin as a Renewable Feedstock for Epichlorohydrin Production. The GTE Process" *CLEAN - Soil Air Water* **2008**, *36*, 657–661.

[120] P. Munkajohnpong, C. Kesornpun, S. Buttranon, J. Jaroensuk, N. Weeranoppanant, P. Chaiyen, "Fatty alcohol production: an opportunity of bioprocess" *Biofuels Bioprod. Biorefin.* **2020**, *14*, 986–1009.

[121] P. Foley, A. Kermanshahi Pour, E. S. Beach, J. B. Zimmerman, "Derivation and synthesis of renewable surfactants" *Chem. Soc. Rev.* **2012**, *41*, 1499–1518.

[122] M. Lazzari, O. Chiantore, "Drying and oxidative degradation of linseed oil" *Polym. Degrad. Stab.* **1999**, *65*, 303–313.

[123] H. Wexler, "Polymerization of Drying Oils" *Chem. Rev.* **1964**, *64*, 591–611.

[124] A. Hofland, "Alkyd resins: From down and out to alive and kicking" *Prog. Org. Coat.* **2012**, *73*, 274–282.

[125] L. De Viguerie, G. Ducouret, F. Lequeux, T. Moutard-Martin, P. Walter, "Historical evolution of oil painting media: A rheological study" *C. R. Phys.* **2009**, *10*, 612–621.

[126] L. H. Dunlap, "Drying oils in floor coverings" *J. Am. Oil Chem. Soc.* **1959**, *36*, 590–596.

[127] K. Hübner, "Linoleum: Geburtstag für einen Klassiker" *Chem. Unserer Zeit* **2014**, *48*, 396–401.

[128] S. Kumar, S. K. Samal, S. Mohanty, S. K. Nayak, "Recent Development of Biobased Epoxy Resins: A Review" *Polym.-Plast. Technol. and Eng.* **2018**, *57*, 133–155.

[129] R. Mustapha, A. R. Rahmat, R. Abdul Majid, S. N. H. Mustapha, "Vegetable oil-based epoxy resins and their composites with bio-based hardener: a short review" *Polym.-Plast. Technol. Mater.* **2019**, *58*, 1311–1326.

[130] B. R. Moser, S. C. Cermak, K. M. Doll, J. A. Kenar, B. K. Sharma, "A review of fatty epoxide ring opening reactions: Chemistry, recent advances, and applications" *J. Am. Oil Chem. Soc.* **2022**, *99*, 801–842.

[131] S. Samanta, S. Selvakumar, J. Bahr, D. S. Wickramaratne, M. Sibi, B. J. Chisholm, "Synthesis and Characterization of Polyurethane Networks Derived from Soybean-Oil-Based Cyclic Carbonates and Bioderivable Diamines" *ACS Sustainable Chem. Eng.* **2016**, *4*, 6551–6561.

[132] L. Tao, K. Liu, T. Li, R. Xiao, "Preparation and properties of biobased polyamides based on 1,9-azelaic acid and different chain length diamines" *Polym. Bull.* **2020**, *77*, 1135–1156.

[133] X. Feng, J. Shang, Z. Gu, J. Gong, Y. Chen, Y. Liu, "Azelaic Acid: Mechanisms of Action and Clinical Applications" *Clin. Cosmet. Investig. Dermatol.*, **2024**, *17*, 2359–2371.

[134] R. S. Atapalkar, P. R. Athawale, D. Srinivasa Reddy, A. A. Kulkarni, "Scalable, sustainable and catalyst-free continuous flow ozonolysis of fatty acids" *Green Chem.* **2021**, *23*, 2391–2396.

[135] A. Köckritz, A. Martin, "Synthesis of azelaic acid from vegetable oil-based feedstocks" *Eur. J. Lipid Sci. Tech.* **2011**, *113*, 83–91.

[136] A. Behr, N. Tenhumberg, A. Wintzer, "Efficient ruthenium-catalysed oxidative cleavage of methyl oleate with hydrogen peroxide as oxidant" *RSC Adv.* **2013**, *3*, 172–180.

[137] L. Santos Correa, M. A. R. Meier, "Ruthenium Catalyzed Oxidative Cleavage of High Oleic Sunflower Oil: Considerations Regarding the Synthesis of a Fully Biobased Triacid" *Eur. J. Lipid Sci. Tech.* **2023**, *125*, 2200171.

[138] L. Santos Correa, S. Leidenheimer, M. A. R. Meier, "Sunflower oil-based thermosets *via* the Passerini three-component reaction" *Polym. Chem.* **2025**, *16*, 821–832.

[139] M. Van der Steen, C. V. Stevens, "Undecylenic Acid: A Valuable and Physiologically Active Renewable Building Block from Castor Oil" *ChemSusChem* **2009**, *2*, 692–713.

[140] M. Genas, "Rilsan (Polyamid 11), Synthese und Eigenschaften" *Angew. Chem.* **1962**, *74*, 535–540.

[141] J. Wolfs, I. Ribca, M. A. R. Meier, M. Johansson, "Polythionourethane Thermoset Synthesis via Activation of Elemental Sulfur in an Efficient Multicomponent Reaction Approach" *ACS Sustainable Chem. Eng.* **2023**, *11*, 3952–3962.

[142] S. Chikkali, S. Mecking, "Refining of Plant Oils to Chemicals by Olefin Metathesis" *Angew. Chem. Int. Ed.* **2012**, *51*, 5802–5808.

[143] M. Winkler, C. Romain, M. A. R. Meier, C. K. Williams, "Renewable polycarbonates and polyesters from 1,4-cyclohexadiene" *Green Chem.* **2015**, *17*, 300–306.

[144] H. Mutlu, R. Hofsäß, R. E. Montenegro, M. A. R. Meier, "Self-metathesis of fatty acid methyl esters: full conversion by choosing the appropriate plant oil" *RSC Adv.* **2013**, *3*, 4927.

[145] U. Biermann, J. O. Metzger, M. A. R. Meier, "Acyclic Triene Metathesis Oligo- and Polymerization of High Oleic Sun Flower Oil" *Macromol. Chem. Phys.* **2010**, *211*, 854–862.

[146] J. Spekreijse, J. P. M. Sanders, J. H. Bitter, E. L. Scott, "The Future of Ethenolysis in Biobased Chemistry" *ChemSusChem* **2017**, *10*, 470–482.

[147] F. C. M. Scheelje, F. C. Destaso, H. Cramail, M. A. R. Meier, "Nitrogen-Containing Polymers Derived from Terpenes: Possibilities and Limitations" *Macromol. Chem. Phys.* **2023**, *224*, 2200403.

[148] Marta. E. G. Mosquera, G. Jiménez, V. Tabernero, J. Vinueza-Vaca, C. García-Estrada, K. Kosalková, A. Sola-Landa, B. Monje, C. Acosta, R. Alonso, M. Á. Valera, "Terpenes and Terpenoids: Building Blocks to Produce Biopolymers" *Sustain. Chem.* **2021**, *2*, 467–492.

[149] P. Conen, M. A. R. Meier, "Reactivities and mechanisms in organic reactions involving activation of elemental sulfur under basic conditions" *Tetrahedron Chem* **2024**, *11*, 100086.

[150] A. N. Lin, R. J. Reimer, D. M. Carter, “Sulfur revisited” *J. Am. Acad. Dermatol.* **1988**, *18*, 553–558.

[151] G. Kutney, *Sulfur: History, Technology, Applications and Industry*, ChemTec Publishing, Toronto, **2023**.

[152] U. S. Geological Survey, *Mineral commodity summaries 2025*, **2025**.

[153] Q. Shi, J. Wu, “Review on Sulfur Compounds in Petroleum and Its Products: State-of-the-Art and Perspectives” *Energy Fuels* **2021**, *35*, 14445–14461.

[154] J. Yun, C. Zhu, Q. Wang, Q. Hu, G. Yang, “Catalytic conversions of atmospheric sulfur dioxide and formation of acid rain over mineral dusts: Molecular oxygen as the oxygen source” *Chemosphere* **2019**, *217*, 18–25.

[155] F. L. Plantenga, R. G. Leliveld, “Sulfur in fuels: more stringent sulfur specifications for fuels are driving innovation” *Appl. Catal. A Gen.* **2003**, *248*, 1–7.

[156] J. S. Eow, “Recovery of sulfur from sour acid gas: A review of the technology” *Environ. Prog.* **2002**, *21*, 143–162.

[157] H. Ghahraloud, M. Farsi, M. R. Rahimpour, “Modeling and optimization of an industrial Claus process: Thermal and catalytic section” *J. Taiwan Inst. Chem. Eng.* **2017**, *76*, 1–9.

[158] J. J. Griebel, R. S. Glass, K. Char, J. Pyun, “Polymerizations with elemental sulfur: A novel route to high sulfur content polymers for sustainability, energy and defense” *Prog. Polym. Sci.* **2016**, *58*, 90–125.

[159] W. Kang, N. Deng, J. Ju, Q. Li, D. Wu, X. Ma, L. Li, M. Naebe, B. Cheng, “A review of recent developments in rechargeable lithium–sulfur batteries” *Nanoscale* **2016**, *8*, 16541–16588.

[160] S. A. Carn, A. J. Krueger, N. A. Krotkov, M. A. Gray, “Fire at Iraqi sulfur plant emits SO_2 clouds detected by Earth Probe TOMS” *Geophys. Res. Lett.* **2004**, *31*, L19105.

[161] F. Crescenzi, A. Crisari, E. D’Angel, A. Nardella, “Control of Acidity Development on Solid Sulfur Due to Bacterial Action” *Environ. Sci. Technol.* **2006**, *40*, 6782–6786.

[162] F. Devillanova, Ed. , *Handbook of Chalcogen Chemistry: New Perspectives in Sulfur, Selenium and Tellurium*, Royal Society Of Chemistry, Cambridge, **2007**.

[163] S. Oae, Ed. , *Organic Chemistry of Sulfur*, Springer US, Boston, MA, **1977**.

[164] R. Steudel, Ed. , *Elemental Sulfur and Sulfur-Rich Compounds I*, Springer Berlin Heidelberg, Berlin, Heidelberg, **2003**.

[165] R. Steudel, Ed. , *Elemental Sulfur and Sulfur-Rich Compounds II*, Springer Berlin Heidelberg, Berlin, Heidelberg, **2003**.

[166] R. Steudel, "Properties of Sulfur-Sulfur Bonds" *Angew. Chem. Int. Ed. Engl.* **1975**, *14*, 655–664.

[167] R. Steudel, T. Chivers, "The role of polysulfide dianions and radical anions in the chemical, physical and biological sciences, including sulfur-based batteries" *Chem. Soc. Rev.* **2019**, *48*, 3279–3319.

[168] S. J. Rettig, J. Trotter, "Refinement of the structure of orthorhombic sulfur, α-S8" *Acta Crystallogr. C Cryst. Struct. Commun.* **1987**, *43*, 2260–2262.

[169] S. C. Greer, "Physical Chemistry of Equilibrium Polymerization" *J. Phys. Chem. B* **1998**, *102*, 5413–5422.

[170] B. Meyer, J. M. Austin, D. Jensen, "Solubility of sulfur in liquid sulfur dioxide, carbon disulfide, and carbon tetrachloride" *J. Chem. Eng. Data* **1971**, *16*, 364–366.

[171] Y. Ren, H. Shui, C. Peng, H. Liu, Y. Hu, "Solubility of elemental sulfur in pure organic solvents and organic solvent–ionic liquid mixtures from 293.15 to 353.15K" *Fluid Phase Equilib.* **2011**, *312*, 31–36.

[172] R. Wang, B. Shen, H. Sun, J. Zhao, "Measurement and Correlation of the Solubilities of Sulfur S_8 in 10 Solvents" *J. Chem. Eng. Data* **2018**, *63*, 553–558.

[173] R. Steudel, G. Holdt, "Solubilization of Elemental Sulfur in Water by Cationic and Anionic Surfactants" *Angew. Chem. Int. Ed. Engl.* **1988**, *27*, 1358–1359.

[174] A. Kamyshny, A. Goifman, J. Gun, D. Rizkov, O. Lev, "Equilibrium Distribution of Polysulfide Ions in Aqueous Solutions at 25 °C: A New Approach for the Study of Polysulfides' Equilibria" *Environ. Sci. Technol.* **2004**, *38*, 6633–6644.

[175] A. Amrani, A. Kamyshny, O. Lev, Z. Aizenshtat, "Sulfur Stable Isotope Distribution of Polysulfide Anions in an $(NH_4)_2S_n$ Aqueous Solution" *Inorg. Chem.* **2006**, *45*, 1427–1429.

[176] F. Seel in *Studies in Inorganic Chemistry*, Elsevier, **1984**, pp. 67–89.

[177] T. Chivers, I. Drummond, "Characterization of the trisulfur radical anion S3- in blue solutions of alkali polysulfides in hexamethylphosphoramide" *Inorg. Chem.* **1972**, *11*, 2525–2527.

[178] T. Chivers, "Ubiquitous trisulphur radical ion S3−·" *Nature* **1974**, *252*, 32–33.

[179] W. Giggenbach, "On the nature of the blue solutions of sulfur" *J. Inorg. Nucl. Chem.* **1968**, *30*, 3189–3201.

[180] W. Giggenbach, "Blue solutions of sulfur in water at elevated temperatures" *Inorg. Chem.* **1971**, *10*, 1306–1308.

[181] T. Chivers, P. J. W. Elder, "Ubiquitous trisulfur radical anion: fundamentals and applications in materials science, electrochemistry, analytical chemistry and geochemistry" *Chem. Soc. Rev.* **2013**, *42*, 5996.

[182] G. Bieker, J. Wellmann, M. Kolek, K. Jalkanen, M. Winter, P. Bieker, "Influence of cations in lithium and magnesium polysulphide solutions: dependence of the solvent chemistry" *Phys. Chem. Chem. Phys.* **2017**, *19*, 11152–11162.

[183] K. H. Wujcik, D. R. Wang, A. Raghunathan, M. Drake, T. A. Pascal, D. Prendergast, N. P. Balsara, "Lithium Polysulfide Radical Anions in Ether-Based Solvents" *J. Phys. Chem. C* **2016**, *120*, 18403–18410.

[184] R. Steudel, Y. Steudel, "Polysulfide Chemistry in Sodium–Sulfur Batteries and Related Systems— A Computational Study by G3X(MP2) and PCM Calculations" *Chem. Eur. J.* **2013**, *19*, 3162–3176.

[185] M. Hojo, D. T. Sawyer, "Hydroxide-induced reduction of elemental sulfur (S8) to trisulfur anion radical (S3˙-)" *Inorg. Chem.* **1989**, *28*, 1201–1202.

[186] R. P. Martin, W. H. Doub, J. L. Roberts, D. T. Sawyer, "Electrochemical reduction of sulfur in aprotic solvents" *Inorg. Chem.* **1973**, *12*, 1921–1925.

[187] F. Seel, H.-J. Güttler, G. Simon, A. Wieckowski, "Colored Sulfur Species in EPD-Solvents" *Pure Appl. Chem.* **1977**, *49*, 45–54.

[188] P. Song, W. Rao, T. Chivers, S.-Y. Wang, "Applications of trisulfide radical anion $S_3^{\cdot-}$ in organic synthesis" *Org. Chem. Front.* **2023**, *10*, 3378–3400.

[189] V. Pinon, E. Levillain, J. P. Lelieur, "ESR study of solutions of sulfur in liquid ammonia" *J. Phys. Chem.* **1991**, *95*, 6462–6465.

[190] T. Chivers, C. Lau, "Raman spectroscopic identification of the S4N- and S3- ions in blue solutions of sulfur in liquid ammonia" *Inorg. Chem.* **1982**, *21*, 453–455.

[191] P. Dubois, J. P. Lelieur, G. Lepoutre, "The solubilization process of sulfur in liquid ammonia and the equilibrium state of these solutions" *Inorg. Chem.* **1989**, *28*, 195–200.

[192] P. Dubois, J. P. Lelieur, G. Lepoutre, "Chemical species in solutions of sulfur in liquid ammonia" *Inorg. Chem.* **1987**, *26*, 1897–1902.

[193] A. Kerouanton, M. Herìem, A. Thiébault, "The Behavior of Sulfur in Liquid Ammonia" *Anal. Lett.* **1973**, *6*, 171–175.

[194] T. Chivers, W. G. Laidlaw, R. T. Oakley, M. Trsic, "Synthesis and crystal and molecular structure of [(Ph3P)2N+][S4N-] and the electronic structure of the planar acyclic anion, S4N-" *J. Am. Chem. Soc.* **1980**, *102*, 5773–5781.

[195] R. E. Davis in *Survey of Progress in Chemistry*, Elsevier, **1964**, pp. 189–238.

[196] R. Earl. Davis, H. F. Nakshbendi, “Sulfur in Amine Solvents” *J. Am. Chem. Soc.* **1962**, *84*, 2085–2090.

[197] W. G. Hodgson, S. A. Buckler, Grace. Peters, “Free Radicals in Amine Solutions of Elemental Sulfur” *J. Am. Chem. Soc.* **1963**, *85*, 543–546.

[198] F. P. Daly, C. W. Brown, “Raman spectra of sulfur dissolved in primary amines” *J. Phys. Chem.* **1973**, *77*, 1859–1861.

[199] F. P. Daly, C. W. Brown, “Raman spectra of rhombic sulfur dissolved in secondary amines” *J. Phys. Chem.* **1976**, *80*, 480–482.

[200] J. W. Thomson, K. Nagashima, P. M. Macdonald, G. A. Ozin, “From Sulfur−Amine Solutions to Metal Sulfide Nanocrystals: Peering into the Oleylamine−Sulfur Black Box” *J. Am. Chem. Soc.* **2011**, *133*, 5036–5041.

[201] K. C. Nicolaou, D. Giguère, S. Totokotsopoulos, Y. Sun, “A Practical Sulfenylation of 2,5-Diketopiperazines” *Angew. Chem. Int. Ed.* **2012**, *51*, 728–732.

[202] J. Chao, T. Yue, B. Ren, G. Gu, X. Lu, W. Ren, “Controlled Disassembly of Elemental Sulfur: An Approach to the Precise Synthesis of Polydisulfides” *Angew. Chem. Int. Ed.* **2022**, *61*, e202115950.

[203] P. D. Bartlett, G. Meguerian, “Reactions of Elemental Sulfur. I. The Uncatalyzed Reaction of Sulfur with Triarylphosphines” *J. Am. Chem. Soc.* **1956**, *78*, 3710–3715.

[204] P. D. Bartlett, R. E. Davis, “Reactions of Elemental Sulfur. II. The Reaction of Alkali Cyanides with Sulfur, and Some Single-Sulfur Transfer Reactions” *J. Am. Chem. Soc.* **1958**, *80*, 2513–2516.

[205] J. Sharma, P. A. Champagne, “Mechanisms of the Reaction of Elemental Sulfur and Polysulfides with Cyanide and Phosphines” *Chem. Eur. J.* **2023**, *29*, e202203906.

[206] F. H. McMillan, J. A. King, “Studies on the Willgerodt Reaction. VI. A Mechanism for the Primary Thiol Oxidation” *J. Am. Chem. Soc.* **1948**, *70*, 4143–4150.

[207] B. D. Vineyard, “Mercaptan—Sulfur Reaction. Alkyl Trisulfides” *J. Org. Chem.* **1966**, *31*, 601–602.

[208] B. D. Vineyard, “Versatility and the mechanism of the n-butyl-amine-catalyzed reaction of thiols with sulfur” *J. Org. Chem.* **1967**, *32*, 3833–3836.

[209] R. Sato, S. Saito, H. Chiba, T. Goto, M. Saito, “Synthesis of Cyclic Polysulfides. Reactions of Dithiols and Related Compounds with Elemental Sulfur in Liquid Ammonia” *Bull. Chem. Soc. Jpn.* **1988**, *61*, 1647–1651.

[210] R. Sato, “Heteroatom chemistry of cyclic benzopolychalcogenides: Synthesis and characterization” *Heteroatom Chem.* **2002**, *13*, 419–423.

[211] D. Aebisher, E. M. Brzostowska, N. Sawwan, R. Ovalle, A. Greer, "Implications for the Existence of a Heptasulfur Linkage in Natural *o* -Benzopolysulfanes" *J. Nat. Prod.* **2007**, *70*, 1492–1494.

[212] C. Willgerodt, "Ueber die Einwirkung von gelbem Schwefelammonium auf Ketone und Chinone" *Ber. Dtsch. Chem. Ges.* **1887**, *20*, 2467–2470.

[213] E. V. Brown, "The Willgerodt Reaction" *Synthesis* **1975**, *1975*, 358–375.

[214] M. Carmack, "The willgerodt-kindler reactions. 7. The mechanisms" *J. Heterocycl. Chem.* **1989**, *26*, 1319–1323.

[215] M. Carmack, M. Behforouz, G. A. Berchtold, S. M. Berkowitz, D. Wiesler, R. Barone, "The willgerodt-kindler reactions. **6** . Isomerization of the carbonyl group in alkanones and cycloalkanones" *J. Heterocycl. Chem.* **1989**, *26*, 1305–1318.

[216] J. H. Poupaert, S. Duarte, E. Colacino, P. Depreux, C. R. McCurdy, D. L. Lambert, "Willgerodt-Kindler's Microwave-Enhanced Synthesis of Thioamide Derivatives" *Phosphorus Sulfur Silicon Relat. Elem.* **2004**, *179*, 1959–1973.

[217] J. H. Poupaert, K. Bouinidane, M. Renard, D. M. Lambert, M. Isa, "Base Catalysis in the Willgerodt-Kindler Reaction" *Org. Prep. Proced. Int.* **2001**, *33*, 335–340.

[218] T. B. Nguyen, P. Retailleau, "Elemental Sulfur-Promoted Oxidative Rearranging Coupling between o-Aminophenols and Ketones: A Synthesis of 2-Alkyl benzoxazoles under Mild Conditions" *Org. Lett.* **2017**, *19*, 3887–3890.

[219] A. Y. Solovyev, D. A. Androsov, D. C. Neckers, "One-Pot Synthesis of Substituted 2-Aminobenzo[*b*]thiophenes" *J. Org. Chem.* **2007**, *72*, 3122–3124.

[220] A. Rais, H. Ankati, E. Biehl, "Preparation of 5-nitro-2-amino[*b*]thiophenes and 1-(2-amino-5-nitrophenyl)ethanones *via* microwave irradiation" *J. Heterocycl. Chem.* **2009**, *46*, 599–602.

[221] D. A. Androsov, A. Y. Solovyev, M. L. Petrov, R. J. Butcher, J. P. Jasinski, "A convenient approach towards 2- and 3-aminobenzo[b]thiophenes" *Tetrahedron* **2010**, *66*, 2474–2485.

[222] F. Asinger, M. Thiel, "Einfache Synthesen und chemisches Verhalten neuer heterocyclischer Ringsysteme" *Angew. Chem.* **1958**, *70*, 667–683.

[223] N. Griboura, K. Gatzonas, C. G. Neochoritis, "Still Relevant Today: The Asinger Multicomponent Reaction" *ChemMedChem* **2021**, *16*, 1997–2020.

[224] Y. Huang, A. Dömling, "The Gewald multicomponent reaction" *Mol. Divers.* **2011**, *15*, 3–33.

[225] K. Gewald, E. Schinke, H. Böttcher, “Heterocyclen aus CH-aciden Nitrilen, VIII. 2-Amino-thiophene aus methylenaktiven Nitrilen, Carbonylverbindungen und Schwefel” *Chem. Ber.* **1966**, *99*, 94–100.

[226] J. Sharma, P. A. Champagne, “Mechanisms of the Gewald Synthesis of 2-Aminothiophenes from Elemental Sulfur” *J. Org. Chem.* **2024**, *89*, 9609–9619.

[227] T. T. T. Nguyen, V. A. Le, P. Retailleau, T. B. Nguyen, “Access to 2-Amino-3-Arylthiophenes by Base-Catalyzed Redox Condensation Reaction Between Arylacetonitriles, Chalcones, and Elemental Sulfur” *Adv. Synth. Catal.* **2020**, *362*, 160–165.

[228] T. B. Nguyen, D. H. Mac, P. Retailleau, “Base-Catalyzed Three-Component Reaction of α-Cyanoacetates with Chalcones and Elemental Sulfur: Access to 2-Aminothiophenes Unobtainable via the Gewald Reaction” *J. Org. Chem.* **2021**, *86*, 9418–9427.

[229] L. Zheng, G. Liu, X. Zou, Y. Zhong, L. Deng, Y. Wu, B. Yang, Y. Wang, W. Guo, “DBU-Promoted Three-Component Cascade Annulations to Access Multiply Substituted 3-Cyano-thiophenes” *Asian J. Org. Chem.* **2022**, *11*, e202200394.

[230] N. D. Lai, T. T. Nguyen, N. N. H. Nguyen, P. Retailleau, D. H. Mac, T. B. Nguyen, “Direct access to 2-aryl-3-cyanothiophenes by a base-catalyzed one-pot two-step three-component reaction of chalcones with benzoylacetonitriles and elemental sulfur” *Org. Chem. Front.* **2022**, *9*, 3163–3168.

[231] M. Adib, S. Rajai-Daryasarei, R. Pashazadeh, M. Jahani, M. Amanlou, “Reaction between Chalcones, 1,3-Dicarbonyl Compounds, and Elemental Sulfur: A One-Pot Three-Component Synthesis of Substituted Thiophenes” *Synlett* **2018**, *29*, 1583–1588.

[232] A. M. Shestopalov, K. G. Nikishin, A. V. Gromova, L. A. Rodinovskaya, “One-pot synthesis of 4,6-diaryl-3-cyanopyridine-2(1H)-thiones and their transformation to substituted thieno[2,3-b;4,5-b]dipyridines and pyrido[3",2":4,5]thieno[3,2-d]pyrimidines” *Russ. Chem. Bull.* **2003**, *52*, 2203–2206.

[233] B. N. Nguyen, M. H. Tran, T. T. T. Bui, D. H. Mac, V. P. Pham, P. Retailleau, T. B. Nguyen, “Sulfur-Promoted Oxidative Condensation of Chalcones with Unsubstituted Cyanoacetamide in DMSO: Access to 3-Cyanopyrid-2-ones” *J. Org. Chem.* **2023**, *88*, 11197–11204.

[234] C. N. Nguyen, D. T. Nguyen, H. A. Tran, D. H. Mac, T. T. T. Nguyen, P. Retailleau, T. B. Nguyen, “Base- and sulfur-promoted oxidative lactonization of chalcone-acetate Michael adducts: access to pyran-2-ones” *Org. Biomol. Chem.* **2024**, *22*, 3871–3875.

[235] V. P. Nguyen, N. N. H. Nguyen, N. D. Lai, D. H. Mac, P. Retailleau, T. B. Nguyen, "Sulfur-Promoted Oxidative Cyclization of Pentan-1-ones: Direct Access to Tetrasubstituted Furans from Deoxybenzoins and Chalcones" *Org. Lett.* **2023**, *25*, 6419–6423.

[236] F. H. McMillan, "Conversion of Benzylamine to N-Substituted Thiobenzamides" *J. Am. Chem. Soc.* **1948**, *70*, 868–869.

[237] K. Aghapoor, H. R. Darabi, K. Tabar-Heydar, "The Different, but Interesting Behaviors of Benzyl Systems in the Willgerodt-Kindler Reaction under Solvent-Free Conditions" *Phosphorus Sulfur Silicon Relat. Elem.* **2002**, *177*, 1183–1187.

[238] T. B. Nguyen, L. Ermolenko, A. Al-Mourabit, "Efficient and Selective Multicomponent Oxidative Coupling of Two Different Aliphatic Primary Amines into Thioamides by Elemental Sulfur" *Org. Lett.* **2012**, *14*, 4274–4277.

[239] J. Zhou, S. Wang, Y. Lu, L. Li, W. Duan, Q. Wang, H. Wang, W. Wei, "Solvent-driven C(sp^3)–H thiocarbonylation of benzylamine derivatives under catalyst-free conditions" *Green Chem.* **2021**, *23*, 767–773.

[240] T. B. Nguyen, L. Ermolenko, A. Al-Mourabit, "Nitro-Methyl Redox Coupling: Efficient Approach to 2-Hetarylbenzothiazoles from 2-Halonitroarene, Methylhetarene, and Elemental Sulfur" *Org. Lett.* **2013**, *15*, 4218–4221.

[241] H. Xie, J. Cai, Z. Wang, H. Huang, G.-J. Deng, "A Three-Component Approach to 3,5-Diaryl-1,2,4-thiadiazoles under Transition-Metal-Free Conditions" *Org. Lett.* **2016**, *18*, 2196–2199.

[242] W. Thiel, R. Mayer, "Dithiocarbonsäuren, Dithiocarbonsäureester oder Thiocarbonsäureamide aus methylenaktiven Chlormethylverbindungen und Schwefel" *J. Prakt. Chem.* **1989**, *331*, 243–262.

[243] H. Jin, X. Chen, C. Qian, X. Ge, S. Zhou, "Transition-Metal-Free, General Construction of Thioamides from Chlorohydrocarbon, Amide and Elemental Sulfur" *Eur. J. Org. Chem.* **2021**, *2021*, 3403–3406.

[244] T. B. Nguyen, P. Retailleau, "Sulfur-Promoted DABCO-Catalyzed Oxidative Trimerization of Phenylacetonitriles" *J. Org. Chem.* **2019**, *84*, 5907–5912.

[245] M. Carmack, D. F. DeTar, "The Willgerodt and Kindler Reactions. III. Amides from Acetylenes and Olefins; Studies Relating to the Reaction Mechanisms" *J. Am. Chem. Soc.* **1946**, *68*, 2029–2033.

[246] D. B. Pattison, M. Carmack, "The Willgerodt Reaction. IV. Acetylenes, Olefins, and Tertiary Carbinols" *J. Am. Chem. Soc.* **1946**, *68*, 2033–2035.

[247] T. B. Nguyen, M. Q. Tran, L. Ermolenko, A. Al-Mourabit, "Three-Component Reaction between Alkynes, Elemental Sulfur, and Aliphatic Amines: A General, Straightforward, and Atom Economical Approach to Thioamides" *Org. Lett.* **2014**, *16*, 310–313.

[248] M. Hang Nguyen, H. Sam Nguyen, L. Anh Nguyen, B. Ngoc Nguyen, H. Thuong Cao, D. Hung Mac, T. Binh Nguyen, "Base-Catalyzed Synthesis of *N* -Aryl Thioacetamides from Multicomponent Reaction of Phenylacetylenes, Sulfur and Anilines" *Eur. J. Org. Chem.* **2024**, *27*, e202301319.

[249] G. Zhang, H. Yi, H. Chen, C. Bian, C. Liu, A. Lei, "Trisulfur Radical Anion as the Key Intermediate for the Synthesis of Thiophene via the Interaction between Elemental Sulfur and NaO *t* Bu" *Org. Lett.* **2014**, *16*, 6156–6159.

[250] J. Tang, X. Zhao, "Synthesis of 2,5-disubstituted thiophenes via metal-free sulfur heterocyclization of 1,3-diynes with sodium hydrosulfide" *RSC Adv.* **2012**, *2*, 5488.

[251] L. Cheng, M. Wang, Y. Gu, P. He, Z. Wang, Z. Zhuang, L. Kong, Y. Li, "Synthesis of 1,4-dithiins and 1,4-diselenins from alkynes and elemental sulfur/selenium under transition metal-free conditions with high regioselectivity" *Org. Chem. Front.* **2023**, *10*, 2708–2713.

[252] K. S. Choi, I. Akiyama, M. Hoshino, J. Nakayama, "A Convenient Synthesis of 1,2-Dithietes and 1,2-Dithioxo Compounds Stabilized by Buttressing and Resonance Effects, Respectively, by Sulfuration of Alkynes with Elemental Sulfur" *Bull. Chem. Soc. Jpn.* **1993**, *66*, 623–629.

[253] J. Nakayama, R. Yomoda, M. Hoshino, "Reactions of Elemental Sulfur and Selenium with Some Asetylenic Compounds. Formation of Thiophenes and Selemophenes" *Heterocycles* **1987**, *26*, 2215.

[254] H. R. Darabi, K. Aghapoor, K. Tabar-Heydar, M. Nooshabadi, "Synthesis of Phenylthioacetomorpholide: Effect of Substrate on the Willgerodt-Kindler Reaction" *Phosphorus Sulfur Silicon Relat. Elem.* **2002**, *177*, 1189–1192.

[255] L. Liu, Z. Guo, K. Xu, S. Hui, X. Zhao, Y. Wu, "Transition-metal-free cleavage of C–C double bonds: a three-component reaction of aromatic alkenes with S_8 and amides towards aryl thioamides" *Org. Chem. Front.* **2018**, *5*, 3315–3318.

[256] P. Zhang, W. Chen, M. Liu, H. Wu, "Base-Controlled Three Component Reactions of Amines, Elemental Sulfur, and Styrenes: Synthesis of Thioamides under Metal-Free Conditions" *J. Org. Chem.* **2018**, *83*, 14269–14276.

[257] T. Mizuno, M. Matsumoto, I. Nishiguchi, T. Hirashima, "Facile synthesis of urea derivatives under mild conditions" *Heteroatom Chem.* **1993**, *4*, 455–458.

[258] T. Mizuno, T. Daigaku, I. Nishiguchi, “Reaction of thiolates with carbon monoxide” *Tetrahedron Lett.* **1995**, *36*, 1533–1536.

[259] T. Mizuno, J. Takahashi, A. Ogawa, “Facile S-alkyl thiocarbamate synthesis by a novel DBU-assisted carbonylation of amines with carbon monoxide and sulfur” *Tetrahedron* **2003**, *59*, 1327–1331.

[260] T. Mizuno, T. Iwai, Y. Ishino, “Solvent-assisted thiocarboxylation of amines and alcohols with carbon monoxide and sulfur under mild conditions” *Tetrahedron* **2005**, *61*, 9157–9163.

[261] T. Mizuno, M. Mihara, T. Iwai, T. Ito, Y. Ishino, “Practical Synthesis of Urea Derivatives from Primary Amines, Carbon Monoxide, Sulfur, and Oxygen under Mild Conditions” *Synthesis* **2006**, *2006*, 2825–2830.

[262] M. Lipp, F. Dallacker, I. M. Z. Köcker, “Über die Addition von Schwefel und Selen an Isonitrile” *Monatsh. Chem.* **1959**, *90*, 41–48.

[263] T. Nguyen, L. Ermolenko, A. Al-Mourabit, “Three-Component Reaction between Isocyanides, Aliphatic Amines and Elemental Sulfur: Preparation of Thioureas under Mild Conditions with Complete- Atom Economy” *Synthesis* **2014**, *46*, 3172–3179.

[264] A. Németh, P. Ábrányi-Balogh, “Recent Advances in the Synthesis of Isothiocyanates Using Elemental Sulfur” *Catalysts* **2021**, *11*, 1081.

[265] A. G. Németh, G. M. Keserű, P. Ábrányi-Balogh, “A novel three-component reaction between isocyanides, alcohols or thiols and elemental sulfur: a mild, catalyst-free approach towards *O* -thiocarbamates and dithiocarbamates” *Beilstein J. Org. Chem.* **2019**, *15*, 1523–1533.

[266] R. Nickisch, P. Conen, S. M. Gabrielsen, M. A. R. Meier, “A more sustainable isothiocyanate synthesis by amine catalyzed sulfurization of isocyanides with elemental sulfur” *RSC Adv.* **2021**, *11*, 3134–3142.

[267] J. H. Boyer, V. T. Ramakrishnan, “Sulfurization of isocyanides” *J. Org. Chem.* **1972**, *37*, 1360–1364.

[268] W. Bao, C. Chen, N. Yi, J. Jiang, Z. Zeng, W. Deng, Z. Peng, J. Xiang, “Synthesis of 2-Amino-1,3,4-oxadiazoles through Elemental Sulfur Promoted Cyclization of Hydrazides with Isocyanides” *Chin. J. Chem.* **2017**, *35*, 1611–1618.

[269] R. Sato, S. Takizawa, S. Oae, “Reaction of Aromatic Nitro Compounds with Elemental Sulfur in Liquid Ammonia and Amines” *Phosphorus Sulfur Relat. Elem.* **1979**, *7*, 229–234.

[270] K. Niknam, A. R. Kiasat, F. Kazemi, A. Hossieni, "Efficient Reduction of Nitroarenes to the Corresponding Anilines with Sulfur in Basic Media under Solvent-Free Conditions" *Phosphorus Sulfur Relat. Elem.* **2003**, *178*, 1385–1389.

[271] M. A. McLaughlin, D. M. Barnes, "A practical and selective reduction of nitroarenes using elemental sulfur and mild base" *Tetrahedron Lett.* **2006**, *47*, 9095–9097.

[272] T. B. Nguyen, L. Ermolenko, P. Retailleau, A. Al-Mourabit, "Elemental Sulfur Disproportionation in the Redox Condensation Reaction between *o* -Halonitrobenzenes and Benzylamines" *Angew. Chem. Int. Ed.* **2014**, *53*, 13808–13812.

[273] A. H. Romero, H. Cerecetto, "A Common, Facile and Eco-Friendly Method for the Reduction of Nitroarenes, Selective Reduction of Poly-Nitroarenes and Deoxygenation of *N* -Oxide Containing Heteroarenes Using Elemental Sulfur" *Eur. J. Org. Chem.* **2020**, *2020*, 1853–1865.

[274] D. A. Boyd, "Sulfur and Its Role In Modern Materials Science" *Angew. Chem. Int. Ed.* **2016**, *55*, 15486–15502.

[275] H. Mutlu, E. B. Ceper, X. Li, J. Yang, W. Dong, M. M. Ozmen, P. Theato, "Sulfur Chemistry in Polymer and Materials Science" *Macromol. Rapid Commun.* **2019**, *40*, 1800650.

[276] S. Afonso, H. Mutlu, "The Fusion of Elemental Sulfur With Waste Cooking Oil-Based Derivatives: Beyond Renewability" *Eur. J. Lipid Sci. Tech.* **2025**, e70018.

[277] C. W. Schmitt, L. J. Dodd, J. K. Walz, L. Deterding, P. Lott, A. P. Grimm, M. P. Shaver, T. Hasell, P. Théato, "A critical review on the sustainability of inverse vulcanised polymers" *RSC Sustainability* **2025**, *3*, 4190–4227.

[278] C. Guise-Richardson, "Redefining Vulcanization: Charles Goodyear, Patents, and Industrial Control, 1834-1865" *Technol Cult.* **2010**, *51*, 357–387.

[279] M. R. Krejsa, J. L. Koenig, "A Review of Sulfur Crosslinking Fundamentals for Accelerated and Unaccelerated Vulcanization" *Rubber Chem. Technol.* **1993**, *66*, 376–410.

[280] Q. Lian, Y. Li, K. Li, J. Cheng, J. Zhang, "Insights into the Vulcanization Mechanism through a Simple and Facile Approach to the Sulfur Cleavage Behavior" *Macromolecules* **2017**, *50*, 803–810.

[281] M. Akiba, "Vulcanization and crosslinking in elastomers" *Prog. Polym. Sci.* **1997**, *22*, 475–521.

[282] M. M. Coleman, J. R. Shelton, J. L. Koenig, "Sulfur Vulcanization of Hydrocarbon Diene Elastomers" *Ind. Eng. Chem. Prod. Res. Develop.* **1974**, *13*, 154–166.

[283] G. Heideman, R. N. Datta, J. W. M. Noordermeer, B. Van Baarle, "Activators in Accelerated Sulfur Vulcanization" *Rubber Chem. Technol.* **2004**, *77*, 512–541.

[284] J. Lim, J. Pyun, K. Char, "Recent Approaches for the Direct Use of Elemental Sulfur in the Synthesis and Processing of Advanced Materials" *Angew. Chem. Int. Ed.* **2015**, *54*, 3249–3258.

[285] J. H. Hwang, J. M. Lee, J. H. Seo, G. Y. Noh, W. Byun, S. Kim, W. Lee, S. Park, D.-G. Kim, Y. S. Kim, "Inverse vulcanization of elemental sulfur catalyzed by trialkyl amines" *Green Chem.* **2023**, *25*, 4641–4646.

[286] Y. Zhang, N. G. Pavlopoulos, T. S. Kleine, M. Karayilan, R. S. Glass, K. Char, J. Pyun, "Nucleophilic Activation of Elemental Sulfur for Inverse Vulcanization and Dynamic Covalent Polymerizations" *J. Polym. Sci. A Polym. Chem.* **2019**, *57*, 7–12.

[287] X. Wu, J. A. Smith, S. Petcher, B. Zhang, D. J. Parker, J. M. Griffin, T. Hasell, "Catalytic inverse vulcanization" *Nat. Commun.* **2019**, *10*, 647.

[288] J. Jia, J. Liu, Z.-Q. Wang, T. Liu, P. Yan, X.-Q. Gong, C. Zhao, L. Chen, C. Miao, W. Zhao, S. Cai, X.-C. Wang, A. I. Cooper, X. Wu, T. Hasell, Z.-J. Quan, "Photoinduced inverse vulcanization" *Nat. Chem.* **2022**, *14*, 1249–1257.

[289] P. Yan, W. Zhao, F. McBride, D. Cai, J. Dale, V. Hanna, T. Hasell, "Mechanochemical synthesis of inverse vulcanized polymers" *Nat. Commun.* **2022**, *13*, 4824.

[290] A. D. Tikoalu, N. A. Lundquist, J. M. Chalker, "Mercury Sorbents Made By Inverse Vulcanization of Sustainable Triglycerides: The Plant Oil Structure Influences the Rate of Mercury Removal from Water" *Adv. Sustainable Syst.* **2020**, *4*, 1900111.

[291] M. J. H. Worthington, R. L. Kucera, I. S. Albuquerque, C. T. Gibson, A. Sibley, A. D. Slattery, J. A. Campbell, S. F. K. Alboaiji, K. A. Muller, J. Young, N. Adamson, J. R. Gascooke, D. Jampaiah, Y. M. Sabri, S. K. Bhargava, S. J. Ippolito, D. A. Lewis, J. S. Quinton, A. V. Ellis, A. Johs, G. J. L. Bernardes, J. M. Chalker, "Laying Waste to Mercury: Inexpensive Sorbents Made from Sulfur and Recycled Cooking Oils" *Chem. Eur. J.* **2017**, *23*, 16219–16230.

[292] M. P. Crockett, A. M. Evans, M. J. H. Worthington, I. S. Albuquerque, A. D. Slattery, C. T. Gibson, J. A. Campbell, D. A. Lewis, G. J. L. Bernardes, J. M. Chalker, "Sulfur-Limonene Polysulfide: A Material Synthesized Entirely from Industrial By-Products and Its Use in Removing Toxic Metals from Water and Soil" *Angew. Chem. Int. Ed.* **2016**, *55*, 1714–1718.

[293] T. Sehn, J. Fanelli, L. Wahl, M. A. R. Meier, "High sulfur content composite materials from renewable fatty acid cellulose esters (FACEs) *via* inverse vulcanization" *RSC Sustainability* **2025**, *3*, 291–299.

[294] M. S. Karunarathna, M. K. Lauer, T. Thiounn, R. C. Smith, A. G. Tennyson, "Valorisation of waste to yield recyclable composites of elemental sulfur and lignin" *J. Mater. Chem. A* **2019**, *7*, 15683–15690.

[295] J. Pyun, R. A. Norwood, "Infrared plastic optics and photonic devices using chalcogenide hybrid inorganic/organic polymers via inverse vulcanization of elemental sulfur" *Prog. Polym. Sci.* **2024**, *156*, 101865.

[296] Z. W. Seh, Y. Sun, Q. Zhang, Y. Cui, "Designing high-energy lithium–sulfur batteries" *Chem. Soc. Rev.* **2016**, *45*, 5605–5634.

[297] H. Shen, B. Zheng, H. Zhang, "A Decade Development of Inverse Vulcanization Towards Green and Sustainable Practices" *Polym. Rev.* **2024**, *64*, 1211–1266.

[298] S. Penczek, R. Ślazak, A. Duda, "Anionic copolymerisation of elemental sulphur" *Nature* **1978**, *273*, 738–739.

[299] A. Duda, S. Penczek, "Anionic copolymerisation of elemental sulfur with 2,2-dimethylthiirane" *Makromol. Chem.* **1980**, *181*, 995–1001.

[300] A. Duda, S. Penczek, "Anionic copolymerization of elemental sulfur with propylene sulfide" *Macromolecules* **1982**, *15*, 36–40.

[301] T. Sehn, B. Huber, J. Fanelli, H. Mutlu, "Straightforward synthesis of aliphatic polydithiocarbonates from commercially available starting materials" *Polym. Chem.* **2022**, *13*, 5965–5973.

[302] C. Gallizioli, D. Battke, H. Schlaad, P. Deglmann, A. J. Plajer, "Ring-Opening Terpolymerisation of Elemental Sulfur Waste with Propylene Oxide and Carbon Disulfide via Lithium Catalysis" *Angew. Chem. Int. Ed.* **2024**, *63*, e202319810.

[303] C. Gallizioli, P. Deglmann, A. J. Plajer, "Kinetically Enhanced Access to a Dynamic Polyester Platform via Sequence Selective Terpolymerisation of Elemental Sulphur" *Angew. Chem. Int. Ed.* **2025**, *64*, e202501337.

[304] Y. Kawai, T. Kanbara, K. Hasegawa, "Preparation of polythioamides from dialdehydes and 4,4'-trimethylenedipiperidine with sulfur by the Willgerodt-Kindler reaction" *J. Polym. Sci. A Polym. Chem.* **1999**, *37*, 1737–1740.

[305] T. Kanbara, Y. Kawai, K. Hasegawa, H. Morita, T. Yamamoto, "Preparation of polythioamides from dialdehydes and diamines with sulfur by the Willgerodt–Kindler type reaction" *J. Polym. Sci. A Polym. Chem.* **2001**, *39*, 3739–3750.

[306] W. Li, X. Wu, Z. Zhao, A. Qin, R. Hu, B. Z. Tang, "Catalyst-Free, Atom-Economic, Multicomponent Polymerizations of Aromatic Diynes, Elemental Sulfur, and Aliphatic Diamines toward Luminescent Polythioamides" *Macromolecules* **2015**, *48*, 7747–7754.

[307] L. Zhang, Y. Hu, R. Hu, B. Z. Tang, "Room temperature synthesis of polythioamides from multicomponent polymerization of sulfur, pyridine-activated alkyne, and amines" *Chem. Commun.* **2022**, *58*, 1994–1997.

[308] W. Cao, F. Dai, R. Hu, B. Z. Tang, "Economic Sulfur Conversion to Functional Polythioamides through Catalyst-Free Multicomponent Polymerizations of Sulfur, Acids, and Amines" *J. Am. Chem. Soc.* **2020**, *142*, 978–986.

[309] Z. Sun, H. Huang, L. Li, L. Liu, Y. Chen, "Polythioamides of High Refractive Index by Direct Polymerization of Aliphatic Primary Diamines in the Presence of Elemental Sulfur" *Macromolecules* **2017**, *50*, 8505–8511.

[310] P. Liao, J. Huang, Y. Yan, B. Z. Tang, "Clusterization-triggered emission (CTE): one for all, all for one" *Mater. Chem. Front.* **2021**, *5*, 6693–6717.

[311] T. Tian, R. Hu, B. Z. Tang, "Room Temperature One-Step Conversion from Elemental Sulfur to Functional Polythioureas through Catalyst-Free Multicomponent Polymerizations" *J. Am. Chem. Soc.* **2018**, *140*, 6156–6163.

[312] J. Zhang, Q. Zang, F. Yang, H. Zhang, J. Z. Sun, B. Z. Tang, "Sulfur Conversion to Multifunctional Poly(*O* -thiocarbamate)s through Multicomponent Polymerizations of Sulfur, Diols, and Diisocyanides" *J. Am. Chem. Soc.* **2021**, *143*, 3944–3950.

[313] R. Nickisch, P. Conen, M. A. R. Meier, "Polythiosemicarbazones by Condensation of Dithiosemicarbazides and Dialdehydes" *Macromolecules* **2022**, *55*, 3267–3275.

[314] R. Nickisch, W. M. De Vos, M. A. R. Meier, M. I. Baig, "Removal of Transition-Metal Ions by Metal-Complexing Polythiosemicarbazone Membranes" *ACS Appl. Polym. Mater.* **2023**, *5*, 7240–7251.

[315] Y. Yang, R. Hu, B. Z. Tang, "Exploration of Poly(thiazole-2-thione) Structures from Multicomponent Polymerizations of Elemental Sulfur, Dichalcones, and Diisocyanides" *Macromolecules* **2025**, *58*, 6577–6589.

[316] Y. Huang, Y. Yu, R. Hu, B. Z. Tang, "Multicomponent Polymerizations of Elemental Sulfur, CH_2Cl_2 , and Aromatic Amines toward Chemically Recyclable Functional Aromatic Polythioureas" *J. Am. Chem. Soc.* **2024**, *146*, 14685–14696.

[317] R. Williams, W. P. Jencks, F. H. Westheimer, "Bordwell pKa Table," can be found under https://organicchemistrydata.org/hansreich/resources/pka/pka_data/pka-compilation-williams.pdf, (accessed 07.10.2025)

[318] M. C. Stuparu, A. Khan, "Thiol-epoxy 'click' chemistry: Application in preparation and postpolymerization modification of polymers" *J. Polym. Sci. A Polym. Chem.* **2016**, *54*, 3057–3070.

[319] A. Khan, “Thiol-epoxy ‘click’ reaction in polymer synthesis” *Prog. Polym. Sci.* **2025**, *169*, 102022.

[320] A. Khan, “Thiol-epoxy ‘click’ chemistry: a focus on molecular attributes in the context of polymer chemistry” *Chem. Commun.* **2023**, *59*, 11028–11044.

[321] S. De, A. Khan, “Efficient synthesis of multifunctional polymers via thiol–epoxy ‘click’ chemistry” *Chem. Commun.* **2012**, *48*, 3130.

[322] D. Guzmán, X. Ramis, X. Fernández-Francos, A. Serra, “New catalysts for diglycidyl ether of bisphenol A curing based on thiol–epoxy click reaction” *European Polymer Journal* **2014**, *59*, 377–386.

[323] H. Yeo, A. Khan, “Photoinduced Proton-Transfer Polymerization: A Practical Synthetic Tool for Soft Lithography Applications” *J. Am. Chem. Soc.* **2020**, *142*, 3479–3488.

[324] Y. Yoshida, K. Ohnaka, T. Endo, “Reprocessable Aliphatic Polydithiourethanes Based on the Reversible Addition Reaction of Diisothiocyanates and Dithiols” *Macromolecules* **2019**, *52*, 6080–6087.

[325] F. Gamardella, S. Muñoz, S. De La Flor, X. Ramis, A. Serra, “Recyclable Organocatalyzed Poly(Thiourethane) Covalent Adaptable Networks” *Polymers* **2020**, *12*, 2913.

[326] C.-J. Fan, Z.-B. Wen, Z.-Y. Xu, Y. Xiao, D. Wu, K.-K. Yang, Y.-Z. Wang, “Adaptable Strategy to Fabricate Self-Healable and Reprocessable Poly(thiourethane-urethane) Elastomers via Reversible Thiol–Isocyanate Click Chemistry” *Macromolecules* **2020**, *53*, 4284–4293.

[327] J. Shin, J. Lee, H. M. Jeong, “Properties of polythiourethanes prepared by thiol–isocyanate click reaction” *J. Appl. Polym. Sci.* **2018**, *135*, 46070.

[328] D. P. Nair, M. Podgórski, S. Chatani, T. Gong, W. Xi, C. R. Fenoli, C. N. Bowman, “The Thiol-Michael Addition Click Reaction: A Powerful and Widely Used Tool in Materials Chemistry” *Chem. Mater.* **2014**, *26*, 724–744.

[329] D. Berne, V. Ladmiral, E. Leclerc, S. Caillol, “Thia-Michael Reaction: The Route to Promising Covalent Adaptable Networks” *Polymers* **2022**, *14*, 4457.

[330] B. D. Mather, K. Viswanathan, K. M. Miller, T. E. Long, “Michael addition reactions in macromolecular design for emerging technologies” *Prog. Polym. Sci.* **2006**, *31*, 487–531.

[331] J. M. J. M. Ravasco, H. Faustino, A. Trindade, P. M. P. Gois, “Bioconjugation with Maleimides: A Useful Tool for Chemical Biology” *Chem. Eur. J.* **2019**, *25*, 43–59.

[332] M. Winkler, Y. S. Raupp, L. A. M. Köhl, H. E. Wagner, M. A. R. Meier, "Modified Poly(ε-caprolactone)s: An Efficient and Renewable Access via Thia-Michael Addition and Baeyer–Villiger Oxidation" *Macromolecules* **2014**, *47*, 2842–2846.

[333] A. B. Lowe, "Thiol-ene 'click' reactions and recent applications in polymer and materials synthesis" *Polym. Chem.* **2010**, *1*, 17–36.

[334] F. Dénès, M. Pichowicz, G. Povie, P. Renaud, "Thiyl Radicals in Organic Synthesis" *Chem. Rev.* **2014**, *114*, 2587–2693.

[335] T. Posner, "Beiträge zur Kenntniss der ungesättigten Verbindungen. II. Ueber die Addition von Mercaptanen an ungesättigte Kohlenwasserstoffe" *Ber. Dtsch. Chem. Ges.* **1905**, *38*, 646–657.

[336] K. Griesbaum, "Problems and Possibilities of the Free-Radical Addition of Thiols to Unsaturated Compounds" *Angew. Chem. Int. Ed. Engl.* **1970**, *9*, 273–287.

[337] C. M. Q. Le, F. Morlet-Savary, A. Chemtob, "Role of thiol oxidation by air in the mechanism of the self-initiated thermal thiol–ene polymerization" *Polym. Chem.* **2021**, *12*, 6594–6605.

[338] U. Biermann, W. Butte, R. Koch, P. A. Fokou, O. Türünç, M. A. R. Meier, J. O. Metzger, "Initiation of Radical Chain Reactions of Thiol Compounds and Alkenes without any Added Initiator: Thiol-Catalyzed *cis* / *trans* Isomerization of Methyl Oleate" *Chem. Eur. J.* **2012**, *18*, 8201–8207.

[339] H. Mutlu, A. N. Parvulescu, P. C. A. Bruijnincx, B. M. Weckhuysen, M. A. R. Meier, "On the Polymerization Behavior of Telomers: Metathesis versus Thiol–Ene Chemistry" *Macromolecules* **2012**, *45*, 1866–1878.

[340] T. M. Roper, C. A. Guymon, E. S. Jönsson, C. E. Hoyle, "Influence of the alkene structure on the mechanism and kinetics of thiol–alkene photopolymerizations with real-time infrared spectroscopy" *J. Polym. Sci. A Polym. Chem.* **2004**, *42*, 6283–6298.

[341] B. H. Northrop, R. N. Coffey, "Thiol–Ene Click Chemistry: Computational and Kinetic Analysis of the Influence of Alkene Functionality" *J. Am. Chem. Soc.* **2012**, *134*, 13804–13817.

[342] K. F. Long, N. J. Bongiardina, P. Mayordomo, M. J. Olin, A. D. Ortega, C. N. Bowman, "Effects of 1°, 2°, and 3° Thiols on Thiol–Ene Reactions: Polymerization Kinetics and Mechanical Behavior" *Macromolecules* **2020**, *53*, 5805–5815.

[343] Q. Wang, H. Cui, X. Wang, Z. Hu, P. Tao, M. Li, J. Wang, Y. Tang, H. Xu, X. He, "Exceptional Light Sensitivity by Thiol–Ene Click Lithography" *J. Am. Chem. Soc.* **2023**, *145*, 3064–3074.

[344] L. Zhang, N. Vilà, T. Klein, G.-W. Kohring, I. Mazurenko, A. Walcarius, M. Etienne, "Immobilization of Cysteine-Tagged Proteins on Electrode Surfaces by Thiol–Ene Click Chemistry" *ACS Appl. Mater. Interfaces* **2016**, *8*, 17591–17598.

[345] C. Resetco, B. Hendriks, N. Badi, F. Du Prez, "Thiol–ene chemistry for polymer coatings and surface modification – building in sustainability and performance" *Mater. Horiz.* **2017**, *4*, 1041–1053.

[346] A. Llevot, S. O. Steinmüller, B. Bitterer, B. Ridder, J. Berson, S. Walheim, T. Schimmel, S. Bräse, F. Scheiba, M. A. R. Meier, "Sequence-controlled molecular layers on surfaces by thiol–ene chemistry: synthesis and multitechnique characterization" *Polym. Chem.* **2017**, *8*, 5824–5828.

[347] T. O. Machado, C. Sayer, P. H. H. Araujo, "Thiol-ene polymerisation: A promising technique to obtain novel biomaterials" *Eur. Polym. J.* **2017**, *86*, 200–215.

[348] L. Filippi, M. A. R. Meier, "Fully Renewable Non-Isocyanate Polyurethanes via the Lossen Rearrangement" *Macromol. Rapid Commun.* **2021**, *42*, 2000440.

[349] L. Breloy, C. A. Ouarabi, A. Brosseau, P. Dubot, V. Brezova, S. Abbad Andaloussi, J.-P. Malval, D.-L. Versace, "β-Carotene/Limonene Derivatives/Eugenol: Green Synthesis of Antibacterial Coatings under Visible-Light Exposure" *ACS Sustainable Chem. Eng.* **2019**, *7*, 19591–19604.

[350] R. Acosta Ortiz, R. S. Sánchez Huerta, A. S. Ledezma Pérez, A. E. García Valdez, "Synthesis of a Curing Agent Derived from Limonene and the Study of Its Performance to Polymerize a Biobased Epoxy Resin Using the Epoxy/Thiol-Ene Photopolymerization Technique" *Polymers* **2022**, *14*, 2192.

[351] K. Ma, S. Zhao, H. Zhao, Y. Liu, Y. Fu, C. Pang, "Biobased Thiol-ene Networks with High Optical Transparency and Abbe Number Derived from Citric Acid" *Macromolecules* **2024**, *57*, 7614–7623.

[352] E. A. Prebihalo, M. Johnson, T. M. Reineke, "Bio-Based Thiol–ene Network Thermosets from Isosorbide and Terpenes" *ACS Macro Lett.* **2024**, *13*, 586–591.

[353] C. Li, M. Johansson, R. J. Sablong, C. E. Koning, "High performance thiol-ene thermosets based on fully bio-based poly(limonene carbonate)s" *Eur. Polym. J.* **2017**, *96*, 337–349.

[354] D. A. Echeverri, H. C. Inciarte, N. Cortés, D. A. Estenoz, M. L. Polo, L. A. Rios, "Synthesis of a renewable polyamine from canola oil by photocatalyzed thiol-ene addition of cysteamine under green conditions" *J. Appl. Polym. Sci.* **2023**, *140*, e54036.

[355] J. Justynska, Z. Hordyjewicz, H. Schlaad, "Toward a toolbox of functional block copolymers via free-radical addition of mercaptans" *Polymer* **2005**, *46*, 12057–12064.

[356] A. B. Lowe, C. E. Hoyle, C. N. Bowman, “Thiol-yne click chemistry: A powerful and versatile methodology for materials synthesis” *J. Mater. Chem.* **2010**, *20*, 4745.

[357] B. Yao, J. Sun, A. Qin, B. Z. Tang, “Thiol-yne click polymerization” *Chin. Sci. Bull.* **2013**, *58*, 2711–2718.

[358] B. D. Fairbanks, T. F. Scott, C. J. Kloxin, K. S. Anseth, C. N. Bowman, “Thiol−Yne Photopolymerizations: Novel Mechanism, Kinetics, and Step-Growth Formation of Highly Cross-Linked Networks” *Macromolecules* **2009**, *42*, 211–217.

[359] O. Türünç, M. A. R. Meier, “A novel polymerization approach via thiol-yne addition” *J. Polym. Sci. A Polym. Chem.* **2012**, *50*, 1689–1695.

[360] Y. Dong, J. W. Y. Lam, A. Qin, J. Liu, Z. Li, B. Z. Tang, J. Sun, H. S. Kwok, “Aggregation-induced emissions of tetraphenylethene derivatives and their utilities as chemical vapor sensors and in organic light-emitting diodes” *Appl. Phys. Lett.* **2007**, *91*, 011111.

[361] K. Müllen, U. Scherf, “Conjugated Polymers: Where We Come From, Where We Stand, and Where We Might Go” *Macromol. Chem. Phys.* **2023**, *224*, 2200337.

[362] J. Mei, N. L. C. Leung, R. T. K. Kwok, J. W. Y. Lam, B. Z. Tang, “Aggregation-Induced Emission: Together We Shine, United We Soar!” *Chem. Rev.* **2015**, *115*, 11718–11940.

[363] J. Mei, Y. Hong, J. W. Y. Lam, A. Qin, Y. Tang, B. Z. Tang, “Aggregation-Induced Emission: The Whole Is More Brilliant than the Parts” *Adv. Mater.* **2014**, *26*, 5429–5479.

[364] J. Luo, Z. Xie, J. W. Y. Lam, L. Cheng, B. Z. Tang, H. Chen, C. Qiu, H. S. Kwok, X. Zhan, Y. Liu, D. Zhu, “Aggregation-induced emission of 1-methyl-1,2,3,4,5-pentaphenylsilole” *Chem. Commun.* **2001**, 1740–1741.

[365] H. Wang, E. Zhao, J. W. Y. Lam, B. Z. Tang, “AIE luminogens: emission brightened by aggregation” *Mater. Today* **2015**, *18*, 365–377.

[366] J.-B. Xiong, H.-T. Feng, J.-P. Sun, W.-Z. Xie, D. Yang, M. Liu, Y.-S. Zheng, “The Fixed Propeller-Like Conformation of Tetraphenylethylene that Reveals Aggregation-Induced Emission Effect, Chiral Recognition, and Enhanced Chiroptical Property” *J. Am. Chem. Soc.* **2016**, *138*, 11469–11472.

[367] G.-F. Zhang, Z.-Q. Chen, M. P. Aldred, Z. Hu, T. Chen, Z. Huang, X. Meng, M.-Q. Zhu, “Direct validation of the restriction of intramolecular rotation hypothesis via the synthesis of novel ortho-methyl substituted tetraphenylethenes and their application in cell imaging” *Chem. Commun.* **2014**, *50*, 12058–12060.

[368] S. Suzuki, S. Sasaki, A. S. Sairi, R. Iwai, B. Z. Tang, G. Konishi, "Principles of Aggregation-Induced Emission: Design of Deactivation Pathways for Advanced AIEgens and Applications" *Angew Chem Int Ed* **2020**, *59*, 9856–9867.

[369] Y. Chen, J. W. Y. Lam, R. T. K. Kwok, B. Liu, B. Z. Tang, "Aggregation-induced emission: fundamental understanding and future developments" *Mater. Horiz.* **2019**, *6*, 428–433.

[370] Y. Xie, Z. Li, "Recent Advances in the *Z* / *E* Isomers of Tetraphenylethene Derivatives: Stereoselective Synthesis, AIE Mechanism, Photophysical Properties, and Application as Chemical Probes" *Chem. Asian J.* **2019**, *14*, 2524–2541.

[371] S. Doose, H. Neuweiler, M. Sauer, "Fluorescence Quenching by Photoinduced Electron Transfer: A Reporter for Conformational Dynamics of Macromolecules" *ChemPhysChem* **2009**, *10*, 1389–1398.

[372] Q. Peng, Z. Shuai, "Molecular mechanism of aggregation-induced emission" *Aggregate* **2021**, *2*, e91.

[373] B. Wang, Y. Liu, X. Chen, X.-T. Liu, Z. Liu, C. Lu, "Aggregation-induced emission-active supramolecular polymers: from controlled preparation to applications" *Chem. Soc. Rev.* **2024**, *53*, 10189–10215.

[374] R. Hu, N. L. C. Leung, B. Z. Tang, "AIE macromolecules: syntheses, structures and functionalities" *Chem. Soc. Rev.* **2014**, *43*, 4494–4562.

[375] W. Wu, S. Ye, R. Tang, L. Huang, Q. Li, G. Yu, Y. Liu, J. Qin, Z. Li, "New tetraphenylethylene-containing conjugated polymers: Facile synthesis, aggregation-induced emission enhanced characteristics and application as explosive chemsensors and PLEDs" *Polymer* **2012**, *53*, 3163–3171.

[376] R. Hu, Y. Kang, B. Z. Tang, "Recent advances in AIE polymers" *Polym. J.* **2016**, *48*, 359–370.

[377] A. Qin, J. W. Y. Lam, B. Z. Tang, "Luminogenic polymers with aggregation-induced emission characteristics" *Prog. Polym. Sci.* **2012**, *37*, 182–209.

[378] R. Hu, A. Qin, B. Z. Tang, "AIE polymers: Synthesis and applications" *Prog. Polym. Sci.* **2020**, *100*, 101176.

[379] G. Hong, X. Gan, C. Leonhardt, Z. Zhang, J. Seibert, J. M. Busch, S. Bräse, "A Brief History of OLEDs—Emitter Development and Industry Milestones" *Adv. Mater.* **2021**, *33*, 2005630.

[380] M. Godumala, S. Choi, M. J. Cho, D. H. Choi, "Thermally activated delayed fluorescence blue dopants and hosts: from the design strategy to organic light-emitting diode applications" *J. Mater. Chem. C* **2016**, *4*, 11355–11381.

[381] W. Z. Yuan, P. Lu, S. Chen, J. W. Y. Lam, Z. Wang, Y. Liu, H. S. Kwok, Y. Ma, B. Z. Tang, "Changing the Behavior of Chromophores from Aggregation-Caused Quenching to Aggregation-Induced Emission: Development of Highly Efficient Light Emitters in the Solid State" *Adv. Mater.* **2010**, *22*, 2159–2163.

[382] D. Harshini, P. Devibala, V. M. Angela, S. Nagarajan, "Approaches for Fabricating Tri- and Tetraphenylethene-Based Blue Organic Light-Emitting Diodes Using Donor–Acceptor and Non-Donor–Acceptor Molecular Architectures" *Phys. Status Solidi RRL* **2022**, *16*, 2200206.

[383] S. Kuppusamy, M. Ghasemi, E. U. Rashid, D. Volyniuk, O. Bezvikonnyi, K. Kaur, J. Simokaitiene, A. Bucinskas, M. Stanitska, O. Navozenko, J. V. Grazulevicius, "Tetraphenyl ethylene derivatives exhibiting aggregation induced emission enhancement for OLEDs and optical sensors of nitroaromatic explosives" *Opt. Mater.* **2025**, *163*, 116988.

[384] Z. Zhao, J. W. Y. Lam, B. Z. Tang, "Tetraphenylethene: a versatile AIE building block for the construction of efficient luminescent materials for organic light-emitting diodes" *J. Mater. Chem.* **2012**, *22*, 23726.

[385] A. Islam, D. Zhang, R. Peng, R. Yang, L. Hong, W. Song, Q. Wei, L. Duan, Z. Ge, "Non-Doped Sky-Blue OLEDs Based on Simple Structured AIE Emitters with High Efficiencies at Low Driven Voltages" *Chem. Asian J.* **2017**, *12*, 2189–2196.

[386] Q. Wei, N. Fei, A. Islam, T. Lei, L. Hong, R. Peng, X. Fan, L. Chen, P. Gao, Z. Ge, "Small-Molecule Emitters with High Quantum Efficiency: Mechanisms, Structures, and Applications in OLED Devices" *Adv. Opt. Mater.* **2018**, *6*, 1800512.

[387] G. Lyu, J. Kendall, I. Meazzini, E. Preis, S. Bayseç, U. Scherf, S. Clément, R. C. Evans, "Luminescent Solar Concentrators Based on Energy Transfer from an Aggregation-Induced Emitter Conjugated Polymer" *ACS Appl. Polym. Mater.* **2019**, *1*, 3039–3047.

[388] Y. Yang, Q. Pei, "Poly(1,4-phenylene-1,2-diphenylvinylene) and tris(8-quinolinolato)aluminum bilayer light-emitting diodes" *Polym. Adv. Technol.* **1997**, *8*, 431–436.

[389] S. W. Phang, R. Daik, M. H. Abdullah, "Poly(4,4′-diphenylene diphenylvinylene) as a non-magnetic microwave absorbing conjugated polymer" *Thin Solid Films* **2005**, *477*, 125–130.

[390] X. Wang, J. Hu, T. Liu, G. Zhang, S. Liu, "Highly sensitive and selective fluorometric off–on K+ probe constructed via host–guest molecular recognition and aggregation-induced emission" *J. Mater. Chem.* **2012**, *22*, 8622.

[391] D. D. La, S. V. Bhosale, L. A. Jones, S. V. Bhosale, "Tetraphenylethylene-Based AIE-Active Probes for Sensing Applications" *ACS Appl. Mater. Interfaces* **2018**, *10*, 12189–12216.

[392] Y. Huang, G. Zhang, R. Zhao, D. Zhang, "Tetraphenylethene-Based *cis/trans* Isomers for Targeted Fluorescence Sensing and Biomedical Applications" *Chem. Eur. J.* **2023**, *29*, e202300539.

[393] P. Alam, N. L. C. Leung, J. Zhang, R. T. K. Kwok, J. W. Y. Lam, B. Z. Tang, "AIE-based luminescence probes for metal ion detection" *Coord. Chem. Rev.* **2021**, *429*, 213693.

[394] W. Dong, Y. Pan, M. Fritsch, U. Scherf, "High sensitivity sensing of nitroaromatic explosive vapors based on polytriphenylamines with AIE-active tetraphenylethylene side groups" *J. Polym. Sci. A Polym. Chem.* **2015**, *53*, 1753–1761.

[395] S. Baysec, E. Preis, S. Allard, U. Scherf, "Very High Solid State Photoluminescence Quantum Yields of Poly(tetraphenylethylene) Derivatives" *Macromol. Rapid Commun.* **2016**, *37*, 1802–1806.

[396] A. C. B. Rodrigues, I. S. Geisler, P. Klein, J. Pina, F. J. H. Neuhaus, E. Dreher, C. W. Lehmann, U. Scherf, J. S. Seixas De Melo, "Designing highly fluorescent, arylated poly(phenylene vinylene)s of intrinsic microporosity" *J. Mater. Chem. C* **2020**, *8*, 2248–2257.

[397] H. Zhou, M. H. Chua, B. Z. Tang, J. Xu, "Aggregation-induced emission (AIE)-active polymers for explosive detection" *Polym. Chem.* **2019**, *10*, 3822–3840.

[398] F. S. Mehamod, R. Daik, M. Ahmad, "The potential application of poly(1,4-phenylene diphenylvinylene), p-PDV for oxygen detection based on fluorescence quenching" *Sens. Actuators B Chem.* **2003**, *96*, 537–540.

[399] V. Hariprasad, K. S. Keremane, P. Naik, D. D. Babu, S. M. Shivashankar, "Tetraphenylethylene (TPE)-Based AIE Luminogens: Recent Advances in Bioimaging Applications" *Photochem* **2025**, *5*, 23.

[400] M. Gao, B. Z. Tang, "AIE-based cancer theranostics" *Coord. Chem. Rev.* **2020**, *402*, 213076.

[401] K. S. Sharath Kumar, Y. R. Girish, M. Ashrafizadeh, S. Mirzaei, K. P. Rakesh, M. Hossein Gholami, A. Zabolian, K. Hushmandi, G. Orive, F. B. Kadumudi, A. Dolatshahi-Pirouz, V. K. Thakur, A. Zarrabi, P. Makvandi, K. S. Rangappa, "AIE-featured tetraphenylethylene nanoarchitectures in biomedical application: Bioimaging, drug delivery and disease treatment" *Coord. Chem. Rev.* **2021**, *447*, 214135.

[402] Q. Zhao, Y. Chen, M. Sun, X.-J. Wu, Y. Liu, "Construction and drug delivery of a fluorescent TPE-bridged cyclodextrin/hyaluronic acid supramolecular assembly" *RSC Adv.* **2016**, *6*, 50673–50679.

[403] J. Ma, Y. Gu, D. Ma, W. Lu, J. Qiu, "Insights into AIE materials: A focus on biomedical applications of fluorescence" *Front. Chem.* **2022**, *10*, 985578.

[404] A. B. Flynn, W. W. Ogilvie, "Stereocontrolled Synthesis of Tetrasubstituted Olefins" *Chem. Rev.* **2007**, *107*, 4698–4745.

[405] M. Zhang, W. Zhao, "Stereodefined tetraarylethylenes: Synthesis and applications" *Aggregate* **2021**, *2*, e60.

[406] A. Bongso, R. Roswanda, Y. M. Syah, "Recent advances of carbonyl olefination *via* McMurry coupling reaction" *RSC Adv.* **2022**, *12*, 15885–15909.

[407] X.-F. Duan, J. Zeng, J.-W. Lü, Z.-B. Zhang, "A Facile Synthesis of Tetraarylethenes via Cross McMurry Coupling between Diaryl Ketones" *Synthesis* **2007**, *2007*, 713–718.

[408] J. Wang, J. Mei, R. Hu, J. Z. Sun, A. Qin, B. Z. Tang, "Click Synthesis, Aggregation-Induced Emission, *E* / *Z* Isomerization, Self-Organization, and Multiple Chromisms of Pure Stereoisomers of a Tetraphenylethene-Cored Luminogen" *J. Am. Chem. Soc.* **2012**, *134*, 9956–9966.

[409] X.-F. Duan, J. Zeng, J.-W. Lü, Z.-B. Zhang, "Insights into the General and Efficient Cross McMurry Reactions between Ketones" *J. Org. Chem.* **2006**, *71*, 9873–9876.

[410] M. Banerjee, S. J. Emond, S. V. Lindeman, R. Rathore, "Practical Synthesis of Unsymmetrical Tetraarylethylenes and Their Application for the Preparation of [Triphenylethylene−Spacer−Triphenylethylene] Triads" *J. Org. Chem.* **2007**, *72*, 8054–8061.

[411] W. Wang, T. Lin, M. Wang, T.-X. Liu, L. Ren, D. Chen, S. Huang, "Aggregation Emission Properties of Oligomers Based on Tetraphenylethylene" *J. Phys. Chem. B* **2010**, *114*, 5983–5988.

[412] Y. Wang, I. Zhang, B. Yu, X. Fang, X. Su, Y.-M. Zhang, T. Zhang, B. Yang, M. Li, S. X.-A. Zhang, "Full-color tunable mechanofluorochromism and excitation-dependent emissions of single-arm extended tetraphenylethylenes" *J. Mater. Chem. C* **2015**, *3*, 12328–12334.

[413] C. Zhou, D. E. Emrich, R. C. Larock, "An Efficient, Regio- and Stereoselective Palladium-Catalyzed Route to Tetrasubstituted Olefins" *Org. Lett.* **2003**, *5*, 1579–1582.

[414] C. Zhou, R. C. Larock, "Regio- and Stereoselective Route to Tetrasubstituted Olefins by the Palladium-Catalyzed Three-Component Coupling of Aryl Iodides, Internal Alkynes, and Arylboronic Acids" *J. Org. Chem.* **2005**, *70*, 3765–3777.

[415] V. Kotek, H. Dvořáková, T. Tobrman, "Modular and Highly Stereoselective Approach to All-Carbon Tetrasubstituted Alkenes" *Org. Lett.* **2015**, *17*, 608–611.

[416] F. Cacialli, R. Daik, P. Dounis, W. J. Feast, R. H. Friend, N. D. Haylett, C. P. Jarrett, C. Schoenenberger, J. A. Stephens, G. Widawski, "Recent developments in the controlled synthesis and manipulation of electroactive organic polymers" *Philos. Trans. R. Soc. A* **1997**, *355*, 707–714.

[417] F. Cacialli, R. Daik, W. J. Feast, R. H. Friend, C. Lartigau, "Synthesis and properties of poly(arylene vinylene)s with controlled structures" *Opt. Mater.* **1999**, *12*, 315–319.

[418] K. Nakagawa, I. Tomita, "Synthesis of Wholly Aromatic Polymers Possessing Tetra-aryl-substituted Vinylene Units by Palladium-catalyzed Three-component Coupling Polymerization" *Chem. Lett.* **2007**, *36*, 638–639.

[419] H. Höurhold, J. Gottschaldt, J. Opfermann, "Untersuchungen über Poly(arylenvinylen)e. XVII [1]. Poly(1,4-phenylen-1,2-diphenylvinylen)" *J. Prakt. Chem.* **1977**, *319*, 611–621.

[420] H. -H. Hörhold, D. Raabe, "Untersuchungen über Poly(arylenvinylen)e. 21. Mitteilung. Synthese von Poly(arylen-1,2-diphenylvinylen)en durch Dehalogenierungspolykondensation von Bis(α,α-dichlorbenzyl)aromaten" *Acta Polym.* **1979**, *30*, 86–92.

[421] D. Raabe, H. -H. Hörhold, "Investigation of poly(arylene vinylenes), 39. Synthesis of functionalized poly(1,4-phenylene-1,2-diphenylvinylenes) by dehydrochlorination of unsymmetric p-xylene dichlorides" *Acta Polym.* **1992**, *43*, 275–278.

[422] P. Conen, R. Nickisch, M. A. R. Meier, "Synthesis of highly substituted alkenes by sulfur-mediated olefination of N-tosylhydrazones" *Commun. Chem.* **2023**, *6*, 255.

[423] R. Nickisch, "Activation of Elemental Sulfur via Multicomponent Reactions for more Sustainable Organocatalysts and Sulfur-containing Polymers", Dissertation, Karlsruhe Institute of Technology (KIT), **2023**

[424] P. Conen, "Investigation of a Novel Bamford-Stevens-Type Olefination Reaction", Master Thesis, Karlsruhe Institute of Technology (KIT), **2022**.

[425] M. Ghavre, "Bamford-Stevens and Shapiro Reactions in Organic Synthesis" *Asian J. Org. Chem.* **2020**, *9*, 1901–1923.

[426] X. Zhang, P. Sivaguru, Y. Pan, N. Wang, W. Zhang, X. Bi, "The Carbene Chemistry of *N* -Sulfonyl Hydrazones: The Past, Present, and Future" *Chem. Rev.* **2025**, *125*, 1049–1190.

[427] G. Mlostoń, R. Jasiński, K. Kula, H. Heimgartner, "A DFT Study on the Barton–Kellogg Reaction – The Molecular Mechanism of the Formation of Thiiranes in the Reaction

between Diphenyldiazomethane and Diaryl Thioketones" *Eur. J. Org. Chem.* **2020**, *2020*, 176–182.

[428] J. M. Burns, T. Clark, C. M. Williams, "Comprehensive Computational Investigation of the Barton–Kellogg Reaction for Both Alkyl and Aryl Systems" *J. Org. Chem.* **2021**, *86*, 7515–7528.

[429] D. H. R. Barton, B. J. Willis, "Olefin synthesis by two-fold extrusion processes. Part 1. Preliminary experiments" *J. Chem. Soc., Perkin Trans. 1* **1972**, 305.

[430] G. Mlostoń, H. Heimgartner, "Reactions of thiocarbonyl compounds with electrophilic and nucleophilic carbenes as well as with their metal complexes" *J. Sulfur Chem.* **2020**, *41*, 672–700.

[431] R. Huisgen, "From Thiiranes to Thiocarbonyl *S* -Sulfides; Recent Results" *Phosphorus Sulfur Silicon Relat. Elem.* **1989**, *43*, 63–94.

[432] F. G. Erko, L. Cseh, J. Berthet, G. H. Mehl, S. Delbaere, "Synthesis and photochromic properties of a bis(diarylethene)-naphthopyran hybrid" *Dyes Pigm.* **2015**, *115*, 102–109.

[433] L.-S. Tan, Z. Yu, *Bis(Aniline) Compounds Containing Multiple Substituents with Carbon-Carbon Triple-Bonded Groups*, **2021**, US10988437B1.

[434] S. M. Gannon, J. G. Krause, "Phase-Transfer Permanganate Oxidation of Unfunctionalized Benzylic Positions" *Synthesis* **2002**, *1987*, 915–917.

[435] I. Simsek Turan, F. Pir Cakmak, F. Sozmen, "Highly selective fluoride sensing via chromogenic aggregation of a silyloxy-functionalized tetraphenylethylene (TPE) derivative" *Tetrahedron Lett.* **2014**, *55*, 456–459.

[436] X. Hu, Q. Chen, J. Wang, Q. Cheng, C. Yan, J. Cao, Y. He, B. Han, "Tetraphenylethylene-based Glycoconjugate as a Fluorescence 'Turn-On' Sensor for Cholera Toxin" *Chem. Asian J.* **2011**, *6*, 2376–2381.

[437] E. Liang, F. Su, Y. Liang, G. Wang, W. Xu, S. Li, C. Yang, J. Tang, N. Zhou, "Dissipative aggregation-induced emission behaviour of an amino-functionalized tetraphenylethene using a pH oscillator" *Chem. Commun.* **2020**, *56*, 15169–15172.

[438] N. Akhtar, O. Biswas, D. Manna, "Stimuli-responsive transmembrane anion transport by AIE-active fluorescent probes" *Org. Biomol. Chem.* **2021**, *19*, 7446–7459.

[439] N. H. Kim, D. Kim, "Identification of the donor-substitution effect of tetraphenylethylene AIEgen: Synthesis, photophysical property analysis, and bioimaging applications" *Dyes Pigm.* **2022**, *199*, 110098.

[440] P. Conen, F. J. O. Niedermaier, S. Abou El Mirate, M. A. R. Meier, "A Novel Synthesis Strategy for Poly(Arylene-Vinylene) Derivatives by Elemental Sulfur-Mediated Polyolefination" *Macromol. Rapid Commun.* **2025**, 2500166.

[441] Y. Hong, J. W. Y. Lam, B. Z. Tang, "Aggregation-induced emission" *Chem. Soc. Rev.* **2011**, *40*, 5361.

[442] H. Wang, Q. Li, P. Alam, H. Bai, V. Bhalla, M. R. Bryce, M. Cao, C. Chen, S. Chen, X. Chen, Y. Chen, Z. Chen, D. Dang, D. Ding, S. Ding, Y. Duo, M. Gao, W. He, X. He, X. Hong, Y. Hong, J.-J. Hu, R. Hu, X. Huang, T. D. James, X. Jiang, G. Konishi, R. T. K. Kwok, J. W. Y. Lam, C. Li, H. Li, K. Li, N. Li, W.-J. Li, Y. Li, X.-J. Liang, Y. Liang, B. Liu, G. Liu, X. Liu, X. Lou, X.-Y. Lou, L. Luo, P. R. McGonigal, Z.-W. Mao, G. Niu, T. C. Owyong, A. Pucci, J. Qian, A. Qin, Z. Qiu, A. L. Rogach, B. Situ, K. Tanaka, Y. Tang, B. Wang, D. Wang, J. Wang, W. Wang, W.-X. Wang, W.-J. Wang, X. Wang, Y.-F. Wang, S. Wu, Y. Wu, Y. Xiong, R. Xu, C. Yan, S. Yan, H.-B. Yang, L.-L. Yang, M. Yang, Y.-W. Yang, J. Yoon, S.-Q. Zang, J. Zhang, P. Zhang, T. Zhang, X. Zhang, X. Zhang, N. Zhao, Z. Zhao, J. Zheng, L. Zheng, Z. Zheng, M.-Q. Zhu, W.-H. Zhu, H. Zou, B. Z. Tang, "Aggregation-Induced Emission (AIE), Life and Health" *ACS Nano* **2023**, *17*, 14347–14405.

[443] Y. Duo, L. Han, Y. Yang, Z. Wang, L. Wang, J. Chen, Z. Xiang, J. Yoon, G. Luo, B. Z. Tang, "Aggregation-Induced Emission Luminogen: Role in Biopsy for Precision Medicine" *Chem. Rev.* **2024**, *124*, 11242–11347.

[444] M. H. Chua, K. L. O. Chin, X. J. Loh, Q. Zhu, J. Xu, "Aggregation-Induced Emission-Active Nanostructures: Beyond Biomedical Applications" *ACS Nano* **2023**, *17*, 1845–1878.

[445] W. Zhao, E. M. Carreira, "Synthesis and Photochromism of Novel Phenylene-Linked Photochromic Bispyrans" *Org. Lett.* **2006**, *8*, 99–102.

[446] Z. Liu, K. Raveendra Babu, F. Wang, Y. Yang, X. Bi, "Influence of sulfonyl substituents on the decomposition of *N* -sulfonylhydrazones at room temperature" *Org. Chem. Front.* **2019**, *6*, 121–124.

[447] Z. Liu, P. Sivaguru, G. Zanoni, X. Bi, "*N* -Triftosylhydrazones: A New Chapter for Diazo-Based Carbene Chemistry" *Acc. Chem. Res.* **2022**, *55*, 1763–1781.

[448] A. G. Myers, B. Zheng, M. Movassaghi, "Preparation of the Reagent *o* -Nitrobenzenesulfonylhydrazide" *J. Org. Chem.* **1997**, *62*, 7507–7507.

[449] I. S. Geisler, "Design and Synthesis of Luminescent Poly(Arylene Vinylene)s and Poly(Arylene Enthynylene)s", Dissertation, Bergische Universität Wuppertal, **2021**.

[450] D. M. Johansson, M. Theander, O. Inganäs, M. R. Andersson, "A convenient synthetic route to poly(p-phenylene-1,2-diphenylvinylenes)" *Synthetic Met.* **2000**, *113*, 293–297.

[451] P. Conen, F. C. M. Scheelje, R. Häusl, M. A. R. Meier, "Synthesis of Novel Vegetable Oil-derived Polythiols and their Thermosets" *ACS Sustainable Chem. Eng.* **2025**, accepted.

[452] L. J. Bartlewski, P. Conen, Q. Cai, M. Bürk, D. Armspach, M. A. R. Meier, "A more sustainable two-step synthesis of alkylated β-cyclodextrin *via* acetylation and $GaBr_3$ -catalyzed reduction" *RSC Sustainability* **2025**, *3*, 4126.

[453] S. C. Ligon-Auer, M. Schwentenwein, C. Gorsche, J. Stampfl, R. Liska, "Toughening of photo-curable polymer networks: a review" *Polym. Chem.* **2016**, *7*, 257–286.

[454] D. Guzmán, B. Mateu, X. Fernández-Francos, X. Ramis, A. Serra, "Novel thermal curing of cycloaliphatic resins by thiol-epoxy click process with several multifunctional thiols: Thermal curing of cycloaliphatic resins by click process" *Polym. Int.* **2017**, *66*, 1697–1707.

[455] J. Anthony Dicks, C. Woolard, "Thiol-X Chemistry: A Skeleton Key Unlocking Advanced Polymers in Additive Manufacturing" *Macromol. Mater. Eng.* **2025**, *310*, 2400445.

[456] S.-M. Hong, O. Y. Kim, S.-H. Hwang, "Chemistry of Polythiols and Their Industrial Applications" *Materials* **2024**, *17*, 1343.

[457] A. Zhang, H. Yan, J. Wang, C. Lv, W. Wang, Z. Zhang, W. Lu, T. Li, Q. Li, "Separation of Water and 3-Mercaptopropionic Acid Using Four Solvents: Liquid–Liquid Equilibrium Measurements, Thermodynamic Simulations, and Quantum Chemical Calculations" *J. Chem. Eng. Data* **2023**, *68*, 2676–2685.

[458] J. F. Brazdil in *Ullmann's Encyclopedia of Industrial Chemistry* (Ed.: Wiley-VCH Verlag GmbH & Co. KGaA), Wiley-VCH, Weinheim, Germany, **2012**, p. a01_177.pub3.

[459] F. C. M. Scheelje, M. A. R. Meier, "Non-isocyanate polyurethanes synthesized from terpenes using thiourea organocatalysis and thiol-ene-chemistry" *Commun. Chem.* **2023**, *6*, 239.

[460] C. S. Marvel, L. E. Olson, "Polyalkylene sulfides. XIII. Polymers from 4-vinyl-1-cyclohexene and *d* -limonene" *J. Polym. Sci.* **1957**, *26*, 23–28.

[461] M. Firdaus, M. A. R. Meier, U. Biermann, J. O. Metzger, "Renewable co-polymers derived from castor oil and limonene" *Eur. J. Lipid Sci. Technol.* **2014**, *116*, 31–36.

[462] R. Acosta Ortiz, E. Adeligna Obregón Blandón, R. Guerrero Santos, "Synthesis of Novel Hexathiolated Squalene and Its Thiol-Ene Photopolymerization with Unsaturated Monomers" *Green Sustainable Chem.* **2012**, *02*, 62–70.

[463] P. S. Löser, A. Lamouroux, M. A. R. Meier, A. Llevot, "A proof-of-concept study on a fully biobased and degradable polymer network based on vanillin and myrcene" *Polym. Chem.* **2024**, *15*, 2240–2252.

[464] J. Yan, S. Ariyasivam, D. Weerasinghe, J. He, B. Chisholm, Z. Chen, D. Webster, "Thiourethane thermoset coatings from bio-based thiols" *Polym. Int.* **2012**, *61*, 602–608.

[465] M. Ionescu, D. Radojčić, X. Wan, Z. S. Petrović, T. A. Upshaw, "Functionalized vegetable oils as precursors for polymers by thiol-ene reaction" *Eur. Polym. J.* **2015**, *67*, 439–448.

[466] G. Biresaw, J. C. Lansing, G. B. Bantchev, R. E. Murray, R. E. Harry-O'Kuru, "Chemical, Physical and Tribological Investigation of Polymercaptanized Soybean Oil" *Tribol. Lett.* **2017**, *65*, 87.

[467] S.-S. Kim, H. Ha, C. J. Ellison, "Soybean Oil-Based Thermoset Films and Fibers with High Biobased Carbon Content via Thiol–Ene Photopolymerization" *ACS Sustainable Chem. Eng.* **2018**, *6*, 8364–8373.

[468] G. B. Bantchev, K. E. Vermillion, J. C. Lansing, G. Biresaw, "Heat- and light-induced thiol-ene oligomerization of soybean oil-based polymercaptan" *J. Appl. Polym. Sci.* **2018**, *135*, 46150.

[469] M. E. Duarte, B. Huber, P. Theato, H. Mutlu, "The unrevealed potential of elemental sulfur for the synthesis of high sulfur content bio-based aliphatic polyesters" *Polym. Chem.* **2020**, *11*, 241–248.

[470] U. Biermann, J. O. Metzger, "Synthesis of Ethers by $GaBr_3$ -Catalyzed Reduction of Carboxylic Acid Esters and Lactones by Siloxanes" *ChemSusChem* **2014**, *7*, 644–649.

[471] U. Biermann, J. O. Metzger, "Reduction of high oleic sunflower oil to glyceryl trioleyl ether" *Eur. J. Lipid Sci. Tech.* **2014**, *116*, 74–79.

[472] P. Dannecker, U. Biermann, M. von Czapiewski, J. O. Metzger, M. A. R. Meier, "Renewable Polyethers via $GaBr_3$ -Catalyzed Reduction of Polyesters" *Angew. Chem. Int. Ed.* **2018**, *57*, 8775–8779.

[473] M. Rhein, S. Zarbakhsh, M. A. R. Meier, "Further Insights into the Catalytic Reduction of Aliphatic Polyesters to Polyethers" *Macromol. Chem. Phys.* **2023**, *224*, 2200289.

[474] M. Desroches, S. Caillol, V. Lapinte, R. Auvergne, B. Boutevin, "Synthesis of Biobased Polyols by Thiol−Ene Coupling from Vegetable Oils" *Macromolecules* **2011**, *44*, 2489–2500.

[475] T. Hayashi, A. Kazlauciunas, P. D. Thornton, "Dye conjugation to linseed oil by highly-effective thiol-ene coupling and subsequent esterification reactions" *Dyes Pigm.* **2015**, *123*, 304–316.

[476] D. Castejón, I. Mateos-Aparicio, M. D. Molero, M. I. Cambero, A. Herrera, "Evaluation and Optimization of the Analysis of Fatty Acid Types in Edible Oils by 1H-NMR" *Food Anal. Method.* **2014**, *7*, 1285–1297.

[477] O. Türünç, M. Firdaus, G. Klein, M. A. R. Meier, "Fatty acid derived renewable polyamides via thiol–ene additions" *Green Chem.* **2012**, *14*, 2577.

[478] X. Mao, Q. Xie, Y. Duan, S. Yu, Y. Nie, "Pyrolysis of Methyl Ricinoleate: Distribution and Characteristics of Fast and Slow Pyrolysis Products" *Materials* **2022**, *15*, 1565.

[479] M. Winnacker, B. Rieger, "Biobased Polyamides: Recent Advances in Basic and Applied Research" *Macromol. Rapid Commun.* **2016**, *37*, 1391–1413.

[480] H. C. Inciarte, N. Cortés, D. A. Echeverri, L. A. Rios, "A fully bio-based monomer derived from undecylenic acid, glycerol, and CO_2 useful for the synthesis of polyhydroxyurethanes" *J. Appl. Polym. Sci.* **2024**, *141*, e54831.

[481] N. Sakai, T. Moriya, K. Fujii, T. Konakahara, "Direct Reduction of Esters toEthers with an Indium(III) Bromide/TriethylsilaneCatalytic System" *Synthesis* **2008**, *2008*, 3533–3536.

[482] B. Rupasinghe, J. C. Furgal, "Degradation of silicone-based materials as a driving force for recyclability" *Polym. Int.* **2022**, *71*, 521–531.

[483] G. Ducom, B. Laubie, A. Ohannessian, C. Chottier, P. Germain, V. Chatain, "Hydrolysis of polydimethylsiloxane fluids in controlled aqueous solutions" *Water Sci. Technol.* **2013**, *68*, 813–820.

[484] Örn, Anton, Degradation Studies on Polydimethylsiloxane, Master Thesis, Abo Akademi University, **2019**.

[485] N. Sakai, T. Moriya, T. Konakahara, "An Efficient One-Pot Synthesis of Unsymmetrical Ethers: A Directly Reductive Deoxygenation of Esters Using an $InBr_3$ /Et_3 SiH Catalytic System" *J. Org. Chem.* **2007**, *72*, 5920–5922.

[486] J. C. Kang, R. A. Kornfeld, R. H. Newman, W. R. Johnson, "Copyrolysis of carbohydrates and sulfur compounds. 1. Formation of thioacetic acid and its decomposition to carbonyl sulfide" *J. Agric. Food Chem.* **1980**, *28*, 992–997.

[487] R. Taylor, "The mechanism of thermal elimination. Part 14. Pyrolysis of diacetamide, 2-acetoxypyridine, diacetyl sulphide, and thioacetic acid: possible involvement of enol forms in gas-phase eliminations" *J. Chem. Soc., Perkin Trans. 2* **1983**, 89.

[488] F. G. Bordwell, W. A. Hewett, "The Free Radical Addition of Thiolacetic Acid to Some Cyclic Olefins" *J. Am. Chem. Soc.* **1957**, *79*, 3493–3496.

[489] S. A. Svarovsky, Z. Szekely, J. J. Barchi, "Synthesis of gold nanoparticles bearing the Thomsen–Friedenreich disaccharide: a new multivalent presentation of an important tumor antigen" *Tetrahedron: Asymmetry* **2005**, *16*, 587–598.

[490] Y. Mi, P. Liang, Z. Yang, D. Wang, W. He, H. Cao, H. Yang, "Synthesis and co-assembly of gold nanoparticles functionalized by a pyrene–thiol derivative" *RSC Adv.* **2015**, *5*, 140–145.

[491] P. Dannecker, U. Biermann, A. Sink, F. R. Bloesser, J. O. Metzger, M. A. R. Meier, "Fatty Acid–Derived Aliphatic Long Chain Polyethers by a Combination of Catalytic Ester Reduction and ADMET or Thiol-Ene Polymerization" *Macromol Chem. Phys.* **2019**, *220*, 1800440.

[492] K. A. Waibel, R. Nickisch, N. Möhl, R. Seim, M. A. R. Meier, "A more sustainable and highly practicable synthesis of aliphatic isocyanides" *Green Chem.* **2020**, *22*, 933–941.

[493] R.-J. Van Putten, J. C. Van Der Waal, E. De Jong, C. B. Rasrendra, H. J. Heeres, J. G. De Vries, "Hydroxymethylfurfural, A Versatile Platform Chemical Made from Renewable Resources" *Chem. Rev.* **2013**, *113*, 1499–1597.

[494] X. Wang, S. Gao, J. Wang, S. Xu, H. Li, K. Chen, P. Ouyang, "The production of biobased diamines from renewable carbon sources: Current advances and perspectives" *Chin. J. Chem. Eng.* **2021**, *30*, 4–13.

[495] A. B. Dros, O. Larue, A. Reimond, F. De Campo, M. Pera-Titus, "Hexamethylenediamine (HMDA) from fossil- vs. bio-based routes: an economic and life cycle assessment comparative study" *Green Chem.* **2015**, *17*, 4760–4772.

[496] P. Nad, S. Goswami, H. K. Kisan, A. Mukherjee, "Unlocking the Potential of Tris(Pentafluorophenyl)Borane in Reductive Desulfurization of Thioamides With Silane" *Chem. Eur. J.* **2025**, *31*, e202500738.

[497] M. Saito, S. Murakami, T. Nanjo, Y. Kobayashi, Y. Takemoto, "Mild and Chemoselective Thioacylation of Amines Enabled by the Nucleophilic Activation of Elemental Sulfur" *J. Am. Chem. Soc.* **2020**, *142*, 8130–8135.

[498] C. G. S. Lima, J. L. Monteiro, T. de Melo Lima, M. Weber Paixão, A. G. Corrêa, "Angelica Lactones: From Biomass-Derived Platform Chemicals to Value-Added Products" *ChemSusChem* **2018**, *11*, 25–47.

[499] A. Moutayakine, S. Meninno, A. Lattanzi, "Organo-, Metal-, and Enzyme-Mediated Stereoselective Transformations of α-Angelica Lactone" *ChemCatChem* **2025**, *17*, e202500060

[500] J. B. Jones, J. M. Young, “CARCINOGENICITY OF LACTONES: I. THE REACTION OF 4-METHYLBUTENO- AND 4-METHYLBUTANO-γ-LACTONES WITH PRIMARY AMINES” *Can. J. Chem.* **1966**, *44*, 1059–1068.

[501] A. Queen, Studies on Pyrrole Derivatives, Master Thesis, Durham University, **1958**.

[502] E. E. Sergeev, L. L. Gogin, T. B. Khlebnikova, E. G. Zhizhina, Z. P. Pai, “Methods for the Catalytic Synthesis of Piperazine” *Catal. Ind.* **2022**, *14*, 218–230.

[503] C. G. Sanz, K. A. Dias, R. P. Bacil, R. A. M. Serafim, L. H. Andrade, E. I. Ferreira, S. H. P. Serrano, “Electrochemical characterization of para- and meta-nitro substituents in aqueous media of new antichagasic pharmaceutical leaders” *Electrochim. Acta* **2021**, *368*, 137582.